The Dynamics of Open–Ocean Plankton Ecosystem Models

Andrew Yool

Submitted for the degree of :
Doctor of Philosophy

Department of Biological Sciences
University of Warwick
Coventry CV4 7AL
England, UNITED KINGDOM

September 1997

For my parents.

Contents

List of Figures

List of Tables

Acknowledgements

Friends help you move. Real friends help you move bodies.
The very best friends help you bury them, then forget where.
– Anonymous

Although I would like to be able to claim the entire credit (or take the full blame) for this thesis, both it, and the research described within it, could not have been completed without the help and support of many friends and colleagues. I would like to thank them all for their assistance and patience with me during my time at Warwick. However, I would like to give special mention to the following, all of whom bore more than their fair share of my difficulties.

In the first instance, I would like to be able to thank my supervisor, Professor Jacquie McGlade. I cannot say enough good things about my time working under her. I was lucky to get her supervision and am pleased to say that no one could have been a better supervisor.

I would also like to acknowledge the support of Graham Medley. His generous proof–reading and discussion of my research much improved its final form in this thesis, and his morale–boosting proved crucial to its completion.

The problems tackled and the approaches used during my research greatly benefited from discussions with Matt Keeling, Martin Bees and, especially, Andy Edwards. As well as correcting the trajectory of my work for (glaring) mathematical misunderstandings, their confidence in my ability not to get things completely wrong raised me up from several spiral sinks of despondency. Matt also served as the primary filter for my raw and untreated first drafts (give that man a medal).

The persuasions and prejudices of my plankton compatriots, Steve Emsley and Mahk Baird made for many interesting (and several drunken) discussions, and were helpful on many occasions in guiding (or stifling) my research. I have more than high hopes for their own research (although their results may dash my own!).

I would like to thank (Brother) John Edmunds for his interest in (*i.e.* "Have you finished yet?"), and support of my work. Additionally, I am very grateful to him for the opportunity to "try my hand" in

the field of prion evolution (Lamarck lives!). My thanks also to Chris ("Butch") O'Callaghan for his sterling assistance with several of the more statistical aspects of my research (as well as his unflagging support/opposition to all things empirical/theoretical).

During my spell as a microbiologist, the patience and assistance of Julie Scanlan and *Synechococcus* sp. were invaluable. Anne Marie Gearhart, Minus van Baalen, Adam Ward, James Cole, Jack Cohen and Esme Fryer also provided much–needed advice, ideas and moral support in more than generous amounts. I am especially indebted to Anne for not murdering me (not a court in the land would convict her).

The help of Susan Taylor, though not obviously visible in this thesis, was considerable and very gratefully received. In addition to assistance with all manner of administrative minutiae, I am indebted to her for all of the morale–boosting, flattering and humour she injected into my time at Warwick (even if she did name the puffer fish after me).

In addition to those already mentioned, I am also grateful to many other EAMG denizens for making my time, particularly that of my final year, pass much more happily than it otherwise should have done. I suppose it could be argued that they delayed my final submission. Thank you Joël, Alan, Martin, E.J., Bindi, Lisa, Sarah and Ben.

I would particularly like to acknowledge the contribution to my research made by the "*Mathematical Modelling of Plankton Population Dynamics*" symposium, held at the Isaac Newton Institute in Cambridge during the summer of 1996. The running of the symposium by Dr. Mike Fasham, Professor John Brindley and Dr. Trevor Platt (as well as the Institute's staff) made it a wholly beneficial experience. During the symposium I was fortunate to receive advice and suggestions on my research from Dr. Fasham (Chapters 3 and 5), Professor Brindley (Chapters 3 and 4), Dr. Ian Totterdell (Chapter 3), Dr. Igor Mezić (Chapter 5) and Dr. Arnold Taylor (Chapter 6).

Finally, I would like to single out Andrew Morris, Alex Mant and Ian Rose for their friendship and encouragement (not to mention the loan of Alex's bicycle) during my time at Warwick. I *really* don't know what I would have done without them.

This research was supported by a grant from the BBSRC (formerly SERC) and one other anonymous government agency.

Declaration

This thesis is the result of original research conducted by myself unless stated in the text or acknowledgements. The research was carried out under the supervision of Professor J. M. McGlade at the University of Warwick. All sources of information used have been specifically acknowledged. Individuals who provided data sets have been fully acknowledged.

No part of this thesis has been submitted for a degree at any other university.

Abbreviations

CA	Cellular Automata
CML	Coupled Map Lattice
CPR	Continuous Plankton Recorder
DCM	Deep Chlorophyll Maximum
DIN	Dissolved Inorganic Nitrogen
DOM	Dissolved Organic Matter
DON	Dissolved Organic Nitrogen
DVM	Diel Vertical Migration
GCM	General Circulation Model
HNLC	High Nutrient, Low Chlorophyll (region)
IBM	Individual Based Model
IPS	Interacting Particle System
MC	Monte Carlo (simulation)
M–M	Michaelis–Menten (function)
NPP	Net Primary Productivity
ODE	Ordinary Differential Equation
OWS	Ocean Weather Station/Ship
PAR	Photosynthetically Active Radition
PDE	Partial Differential Equation
P–I	Photosynthesis–Irradiance (curve)
PN	Phytoplankton–Nutrient (model)
PON	Particulate Organic Nitrogen
PS	Photosynthesis
PZ	Phytoplankton–Zooplankton (model)
RDE	Reaction–Diffusion Equation
ZPD	Zooplankton–Phytoplankton–Detritus (model)
ZPN	Zooplankton–Phytoplankton–Nutrient (model)
ZPND	Zooplankton–Phytoplankton–Nutrient–Detritus (model)

Unit conversion

Mass and moles

$$
\begin{aligned}
1\,\text{mol C} &= 12.0\,\text{g C} \\
1\,\text{mol N} &= 14.0\,\text{g N} \\
1\,\text{mol chl. a} &= 893.5\,\text{g chl. a}
\end{aligned}
$$

Standard biological conversions

$$
\begin{aligned}
1\,\text{mol N} &: 6.625\,\text{mol C} \\
1\,\text{g chl.} &: 50\,\text{g C} \\
1\,\text{mol N} &: 1.59\,\text{g chl.}
\end{aligned}
$$

Standard oceanographic measures

$$
\begin{aligned}
1\,\text{g C m}^{-3} &= 12.579\,\text{mmol N m}^{-3} \\
1\,\text{mg chl. m}^{-3} &= 0.629\,\text{mmol N m}^{-3} \\
1\,\text{mmol C m}^{-3} &= 0.151\,\text{mmol N m}^{-3} \\
1\,\text{mM N m}^{-3} &\equiv 1\,\text{mmol N m}^{-3} \\
1\,\text{mg at. N m}^{-3} &\equiv 1\,\text{mmol N m}^{-3}
\end{aligned}
$$

Summary

In contributing around 40% of total annual primary productivity, the plankton ecosystems of the world ocean play a significant part in the global cycle of carbon. The formulation of dynamic models of plankton ecology is one facet of the study of this cycle, and though much progress has been made, considerable uncertainty still surrounds many aspects of their construction. This thesis focuses on one such plankton model, the nitrogen mixed–layer ecosystem model of Fasham (1993), and several investigations of its structure and parameterisation have been undertaken.

In the first of these the importance of the model's structure has been studied by rationally reducing the full seven compartment form of the model to a simple phytoplankton–zooplankton ecology, and then gradually re–assembling it. This work found the presence of detritus key to the success of the reduced models, while also finding bacteria to be a mostly redundant component of the full model.

A notable feature of modelled summers at OWS "India" in the North Atlantic (and tentatively in data from this location) is the occurrence of predator–prey oscillations. Since such behaviour has consequences for tests of the model, these oscillations were investigated numerically to establish their true nature. Although it was found that they were really transients towards a stable fixed point, further explorations of the parameter space of the model located regions in which stable limit cycle behaviour occurred, and these regions suggested situations under which oscillatory behaviour might be observed in the real world.

Of particular importance in the construction of models is the assignment of parameter values. As estimating most of these requires difficult or time–consuming experiments, knowing which parameters most strongly influence model behaviour can optimise the development of a model. To this end, a sensitivity study of the model was performed, primarily using stochastic techniques. This study found that phytoplankton photosynthesis and zooplankton grazing parameters topped the rankings of parameter sensitivity. Further work explored the sensitivity technique known as stochastic parameters (Kremer, 1983).

Finally, a variant of the Fasham (1993) model in which vertical space was represented by two communicating layers was constructed, and several facets of its behaviour explored. The importance of latitude and zooplankton migration, as well as the properties of Taylor (1988) were examined, with particular emphasis on the significance of any DCM that formed in the model solutions.

Throughout the thesis results are related to the literature and, where possible, to data. Most sections, however, refer to comparisons between models or parts of models, but the analysis always aims to place results in context within plankton modelling.

If I have not seen as far as others, it is because giants were standing on my shoulders.

– Hal Abelson

Chapter 1

Introduction

OCEAN, *n. A body of water occupying about two-thirds of a world made for man – who has no gills.*

– Ambrose Bierce (1842–1914)

1.1 Opening remarks

This thesis is structured into seven chapters : two introductory chapters, the first a general introduction, the second an introduction to the specific plankton model used; four chapters of research examining distinct problems; and a final conclusions and discussion chapter. Each research chapter opens with a short introduction to the appropriate subject matter, and closes with a full discussion of the results. The final chapter aims to both summarise the thesis and to place the work it contains into context within the field of plankton modelling.

This general introduction is broken into a number of different sections. The chapter begins with brief rationale to outline the importance of plankton ecosystems to global biogeochemical cycles. This is followed by a biological and physical introduction to plankton systems, which includes a description the types of organisms encountered in such systems and modelled in this thesis. The chapter is then concluded by an introduction to mathematical and ecological modelling in general, and plankton modelling in particular.

All abbreviations used in the text are listed in the preamble preceding this chapter. A table of the model currency units and their standard conversions to other currencies is also included in this section. Throughout almost all of the thesis a standard currency is used (mmol N m^{-3}), but at several points where research is compared with other work or measurements, the currencies favoured by such work are used and these conversion measures applied.

1.2 Rationale

The work contained within this thesis deals entirely with open–ocean plankton ecosystems. The world ocean covers approximately 70% of the earth's surface, and the photosynthetic organisms within it are responsible for 40% of the annual, global total of net primary production (Raven, 1995). Consequently, these ecosystems play an important role in regulating fluxes of key constituents in the biosphere.

Photosynthesis (PS) uses carbon dioxide (CO_2) as its raw material. Over the past two decades, the scientific community has become concerned about the level of CO_2 in the atmosphere because of its rise in concentration due to the actions of human civilisation (particularly the combustion of carbon–rich fossil fuels and the concurrent clearance of large tracts of forested land). This interest principally stems from the activity of CO_2 in the atmosphere as a so–called "greenhouse gas".

Greenhouse gases (of which CO_2 is only one; others include methane, ozone, dinitrogen oxide, chlorofluorocarbons and water vapour) influence the thermal balance of the earth's atmosphere by being transparent to shorter wavelength, visible electromagnetic radiation (like that from the sun), but opaque to longer wavelength, infra–red radiation (like that which is re–radiated by the earth). This essentially allows these gases to "trap" thermal energy in the atmosphere, and to warm the surface of the earth. This effect has been a feature of the atmosphere for billions of years, and in the past the concentrations of greenhouse gases have been considerably different to those at present (both upwards and downwards). Past variations in the CO_2 level of the atmosphere have been associated with climate change (Adams *et al.*, 1990) and this, plus the fact that the anthropogenic changes to the atmosphere at present are occurring at rates considerably faster than the natural rates measured from ice–core records (Watson & Maddock, 1991), suggests to most researchers that increasing atmospheric CO_2 is likely to substantially affect both the natural biosphere and human activity.

While there are many possible consequences that global warming through an enhanced greenhouse effect may result in, changes to sea–level, weather patterns, ocean circulation, species distribution and the geographical range of diseases such as malaria, are perceived as being particularly important (McGlade, 1990). For example, in the context of plankton systems, Roemmich & McGowan (1995) report that, concurrent with a 1.5°C rise in surface water temperatures (probably caused by greenhouse warming), zooplankton populations in the California Current have fallen by 80% over a period of 40 years (they suggest that the mechanism is a shallower mixed layer and reduced phytoplankton production). Lashof (1991) draws attention to several potential pathways of positive feedbacks which may occur as a result of global warming (*e.g.* increases in atmospheric water vapour, decreases in reflective snow and ice, methane from wetlands, *et cetera*). Hardin (1985) underlines the potential (if less likely) significance of such positive feedbacks by contrasting the relatively mild climate of the earth at present with that of its

sister planet, Venus, apparently a victim of an over–active greenhouse effect.

Given the potential for climate change to elicit large–scale changes in the biosphere, researchers are interested in mechanisms which control or affect the quantity of CO_2 in the atmosphere. For obvious reasons, mechanisms which promote "carbon burial" (the removal of CO_2 from the atmosphere to long–term sinks) are of particular interest. A major carbon burial ($\simeq$80% of the total) route is via the silicate–carbonate loop, whereby weathering of silicate rocks results in the formation of carbonates which are subsequently buried by natural geological processes (Worsley, Nance & Moody, 1991). The remaining carbon burial occurs via biological activity (*i.e.* organic material which is not oxidised and is buried geologically).

In this context, plankton systems are important, since a fraction of their annual production is exported to the deep ocean where it may ultimately be buried (Adams *et al.*, 1990). Raven (1995) estimates that 0.3% of annual marine production is preserved in deep ocean sediments by this mechanism. While terrestrial production may also bury carbon, the carbon it consumes comes mostly from the atmosphere. Since almost all (98.5%; Sarmiento & Orr, 1991) of the global carbon pool exists in the ocean (partially as dissolved CO_2, but mostly as bicarbonate, HCO_3^-), any removal of CO_2 directly from the atmosphere by, for instance, terrestrial primary production[1], may merely shift the ocean–atmosphere equilibrium and lead to the replacement of the removed atmospheric CO_2 by oceanic CO_2. Consequently, the direct removal of carbon from the oceans by plankton systems is of interest to researchers. Note though that there is still uncertainty about the potential importance of this carbon sink (Fasham, 1993, outlines several of the major gaps in understanding).

An important issue here is whether or not an increase in atmospheric CO_2 would lead to an increase in aquatic photosynthesis (as it appears to do for terrestrial photosynthesis; Wilsey, 1996). It is commonly assumed that planktonic primary production is not limited by carbon availability (because of the high concentration of HCO_3^- ions), and thus an increase in CO_2 would not lead to an increase in production. While this does appear generally correct (Raven, 1994), there is evidence (Riebesell, Wolf–Gladrow & Smetacek, 1993; Hein & Sand–Jensen, 1997) that in some cases primary production by plankton can be limited by CO_2 availability and may rise with its increasing concentration (since HCO_3^- needs to be converted to CO_2 before it can be used by the photosynthetic enzyme RuBisCO[2]).

In relation to a limitation on primary production, and of recent interest, is the suggestion by Martin & Fitzwater (1988) that plankton in certain regions of the world ocean are growth–limited by the lack of availability of iron (which is an important micro–nutrient in certain photosynthetic and nutrient re-

[1] The planting of forests with the intention of removing CO_2 from the atmosphere is commonly proposed as a measure to counter the greenhouse effect. As indicated here, this measure may be significantly less effective than believed by its proponents.

[2] Ribulose 1,5–bisphosphate carboxylase–oxygenase : probably the most common enzyme on the face of the earth (J. A. Raven, University of Dundee, pers. comm.)

ductive enzymes; Geider & LaRoche, 1994). While this suggestion has been vindicated by large scale experiments in the Pacific ocean (Behrenfeld *et al.*, 1996), and modelling work has suggested iron–fertilisation of the oceans may produce an impact on atmospheric CO_2 (Peng & Broecker, 1991), other researchers (Fuhrman & Capone, 1991) urge caution over such results because of the potential side–effects of such "climate–engineering" (particularly the release of dinitrogen oxide, a greenhouse gas 290 times as powerful as CO_2).

In summary, given the potential significance of global warming, and the importance of plankton ecosystems in influencing the global carbon cycle, understanding the physical and biological dynamics which govern plankton communities is a key step towards improving our understanding of the processes which may ultimately weigh heavily on the fate of human civilisation.

1.3 What are plankton?

Essentially, plankton are communities or populations of organisms whose powers of locomotion are insufficient to prevent them from being transported passively by their surrounding medium (Omori & Ikeda, 1992).

Although the term is usually confined to microscopic organisms in open water (or pelagic) habitats, it applies additionally to both organisms of much greater size, and to organisms that occupy quite different habitats. Macroscopic coelenterates (such as jellyfish or *Physalia* sp., the Portuguese man–of–war[3]) and algae (such as pelagic *Sargassum* sp.) provide examples of larger organisms whose movement is largely determined by the water currents they find themselves in. And in terrestrial ecology, certain insects are occasionally referred to as *aerial plankton*. This term is arguably justified since their relatively weak flying leads to their dispersal being strongly governed by the wind (Russell & Wilson, 1996).

However, using the above definition of plankton, and given strong enough movement of the medium (*e.g.* rapid water currents or gale–force winds), almost anything will become plankton. For example, an early sequence in the film "The Wizard of Oz" illustrates vividly a Kansas farm building becoming a temporary, aerial plankter. The distinction between planktonic species and non–planktonic species is further blurred by organisms, such as fish, which graduate from the plankton to the *nekton* (organisms whose locomotory abilities are sufficient to allow them to avoid being passively transported) as they grow to adulthood.

In this thesis, however, the plankton under consideration are microscopic and aquatic. More specifically, they are confined to the pelagic environment of the open ocean. This environment can be a relatively

[3]Portuguese men–of–war provide a particularly interesting example of plankton since their dispersal is controlled both by water currents and by wind (through means of a gas–filled sac which protrudes from the water).

productive one, and has the advantage of being comparatively isolated from the confounding influences (*e.g.* rivers, tides, the sea floor, *et cetera*) of shallower coastal environments.

1.4 Plankton assemblages

The planktonic assemblages of aquatic systems contain representatives of every major living group. Although phylogeny and traditional taxonomy (Hoek, Mann & Jahns, 1995, and Barnes, 1986, provide excellent botanical and zoological overviews respectively) are an important source of information about individual plankton species, the complex mix of species in plankton ecosystems is usually less finely treated in most matters of ecology. Species are typically grouped into classes based on their size, trophic position or coarse phylogenetic/functional group.

1.4.1 Classification by size

Although there are few firm gradations (the distinction between prokaryotic bacteria and more complex eukaryotic cells provides a rare example), one of the principal characters used to classify members of the plankton is their size. To some degree this has a historical basis, since plankton groups have often only been discovered and quantified as more and more accurate techniques have become available. Table 1.1 presents an example of size–based classification. Note that while the organisms at the top and bottom of the table are separated by 5 orders of magnitude in diameter or length, in volumetric terms they may be separated by up to 15 orders of magnitude.

In terrestrial ecosystems, ecological pathways between organisms are often unrelated to their size. For example, dominant photosynthetic organisms such as trees are usually grazed by organisms across a wide range of size, from insects through to elephants. Similarly, although usually not as starkly, predatory organisms often feed on sizes of prey above and below their own size. This is partially because gravity dominates terrestrial systems and the medium (air) is relatively non–viscous. Phototrophs to be grazed, or felled prey to be consumed, consequently remain broadly in one place, allowing the consumer to ingest them at leisure.

By contrast, in an aquatic environment, the viscosity of the medium makes it much more difficult to move through it, and much easier for organisms to find themselves carried passively through it. This is particularly true of smaller organisms, and this physical phenomenon is often described by a ratio known as the Reynolds number (see later). As a result, often neither predator nor prey are static, and "felled" prey are unlikely to remain long at a constant depth even in a still water column. Consequently, predators (or grazers) tend to only consume other organisms of smaller size, since these organisms can be ingested directly. This is sometimes referred to as *gape–limitation*, since consumption of organisms is restricted to those organisms that a consumer can fit into its mouth (Hairston & Hairston, 1993). This situation is further entrenched in pelagic situations by selective pressures on active consumers to

Group	Diameter	Major organisms
Ultrananoplankton	< 2 μm	Prokaryotic plankton
Nanoplankton	2 – 20 μm	Fungi, small phytoplankton and protistan zooplankton
Microplankton	20 – 200 μm	Most phytoplankton and protistan microzooplankton, juvenile metazoan mesozooplankton
Mesoplankton	200 μm – 2 mm	Metazoan zooplankton (*e.g.* copepods, appendicularians, cladocerans)
Macroplankton	2 – 20 mm	Metazoan zooplankton (*e.g.* copepods, euphausiids, pteropods)
Megaloplankton	> 20 mm	Metazoan zooplankton (*e.g.* euphausiids, cephalopods, scyphozoans, thaliaceans)

Table 1.1: A grouping of planktonic organisms based on classification by size. Note that with increasing size, each group covers a range one order of magnitude greater than the previous group. See later text for details about named example organisms. The latter three groups are often referred to as *net plankton* since they can be accurately quantified by sampling with nets. The former three groups are usually sampled by means of water bottles. After Omori & Ikeda (1992).

be streamlined so that locomotion (*i.e.* when chasing prey) through the medium may be more efficient. These pressures tend to prevent the evolution of grasping structures which could otherwise be used to hold prey in one place while they were consumed.

Reynolds numbers (Re) are often used to quantify the importance of forces due to the viscosity in a given medium. The number is a ratio of the inertial to viscous forces acting on an object. The inertial force here is the force which was required to accelerate the object to the velocity at which it is travelling. The ratio is calculated by dividing the velocity of the object, u, times its typical dimension, d, by the kinematic viscosity of the medium, ν :

$$Re = \frac{ud}{\nu} \tag{1.1}$$

The typical dimension here may be the width or length of an organism around which the fluid flow is occurring. Smaller organisms (those with a lower typical dimension) are more affected than larger ones by the viscosity of the medium, and are therefore more liable to have their movements disrupted by movement of the medium (Mann & Lazier, 1991).

The dominance of different size and lifestyle (attached versus free) classes of photosynthetic organisms in aquatic environments is reviewed by Raven (1995). He concludes that microscopic organisms dominate the pelagic environment through factors such as their smaller boundary layers (which affect nutrient

uptake) and their better performance at lower irradiances (since they have a higher relative photon absorption than larger plants, and have less non–photosynthetic tissues to "waste" energy on). Furthermore, since the sea floor in the open ocean is normally much deeper than 270 m (the deepest recorded instance of net photosynthesis occurring is from a seamount at 268 m below the surface of the ocean; Littler *et al.*, 1985), attached macroscopic organisms (which can dominate shallower waters) are excluded from the competition.

1.4.2 Classification by trophic position

A common way in which planktonic species assemblages are studied is by grouping the various species present into several groups of broadly similar functionality. This can simplify both the measurement and analysis of ecosystems. It is also particularly appealing to modellers (*e.g.* see Totterdell *et al.*, 1993) since it allows them to represent the system in question by a relatively small number of variables. The following sections aim to briefly outline the major characteristics of the three broad ecological groups distinguished in the models in later chapters.

Phytoplankton

Phytoplankton form the base of the majority of pelagic marine ecosystems. As photoautotrophs they derive the energy they use from solar irradiation they absorb using their photosynthetic pigments (of which there are many different ones). This energy is trapped in organic carbon compounds and then used by the photoplankton cells for their various metabolic processes, including cell reproduction. As well as their requirements for irradiance and inorganic carbon (CO_2 or HCO_3^-), phytoplankton cells also utilise a number of inorganic nutrients and trace substances which they usually uptake directly from the surrounding medium. These nutrients are used for many cellular processes including DNA replication (phosphates), amino acid synthesis (nitrogen nutrients), enzyme co–factors (iron, zinc, manganese), cell walls/coverings (silicate, calcium carbonate), *et cetera*.

Phytoplankton are often motile and may use this to position themselves more favourably within the water column with respect to irradiance or nutrients. Alternatively, they may use motility to "shear off" the boundary layer of fluid surrounding them to facilitate nutrient uptake. Since the turbulence of the mixed layer environment restricts the control of cells over their position within it, this latter role for motility is likely to be the more significant one, at least while the water column is subject to vigorous mixing.

As in terrestrial ecosystems, photoautotrophs in the ocean also often attempt to protect themselves from herbivorous grazers. Poulet *et al.* (1994) and Haney, Sasner & Ikawa (1995) describe chemical interference of zooplankton grazers by their phytoplankton prey. In the former case this occurs through disruption of the developmental processes of the zooplankton grazer, and in the latter case by interference with the feeding mechanisms of the grazers. Jurgens & Gude (1994) describe the use of cell size

by bacterioplankton to evade their grazers. The formation of long chains or complexes of diatom cells (*e.g. Chaetoceros* sp., *Skeletonema costatum*), as well as the long spines which are characteristic of many diatom and dinoflagellates may at least partially serve the same function (Newell & Newell, 1963; Hoek, Mann & Jahns, 1995).

While the statements above are generally true across the species regarded as phytoplankton, there are several major groups of phytoplankton whose differences merit separate discussion. Although the models considered in this thesis do not distinguish these groups, it is not uncommon for models of specific situations to do so, and it may be inevitable for any model which aims to be "robust" across the world ocean (see later). This latter point is strengthened by the suggestion of Williams *et al.* (1981) (based on observations of the wide distribution of diatom species) that the probability of finding any species of phytoplankton anywhere in the world ocean is non–zero (*i.e.* unlike terrestrial plants, phytoplankton are not confined to specific geographical locales).

An initial distinction is between photosynthetic prokaryotes and eukaryotes. The former are bacteria with relatively simpler cell structure and usually much smaller size. Eukaryotes are usually larger and have a cell structure characterised by the possession of a cell nucleus and organelles (themselves formerly symbiotic bacteria – or even other eukaryotes). Until fairly recently, prokaryotes in the oceans were believed to be almost exclusively eubacteria ("modern" bacteria). However, a survey of the coastal waters off of Antarctica (DeLong *et al.*, 1994) revealed that up to 34% of the prokaryote biomass was actually made up of archaebacteria[4], a group of bacteria hitherto believed to be of very limited importance globally. While the full ecological importance of this discovery is yet unclear, it does indicate that knowledge of the ocean ecosystems is still very much incomplete.

Although the importance to primary production of the archaebacteria is uncertain, the eubacteria known as cyanobacteria (Kingdom **Eubacteria**, Division **Cyanophyta**) are of well known importance globally (Waterbury *et al.*, 1986, provide a detailed overview of the distribution and importance of the genera *Synechococcus* in the world ocean; Campbell, Nolla & Vaulot, 1994). Around 2000 species have been described, although on the whole they are a freshwater group (where they can be responsible for toxic blooms). In the oceans their principal importance lies with their fast growth rates and their trophic position as members of the microbial loop (*i.e.* as prey for microzooplankton). McManus & Dawson (1994) additionally found that cyanobacterial assemblages consistently dominated subsurface communities of phytoplankton in the tropical Atlantic.

One of the most important eukaryote groups are the diatoms (Kingdom **Eukaryota**, Division **Het-**

[4]Although the division of living organisms into the five kingdoms (bacteria, protozoa, animals, plants and fungi) is a commonly used approach, the evolutionary distances involved make the division of all living organisms into archaebacteria, eubacteria and eukaryotes a much more reasonable one, and this approach has been used here. Hoek, Mann & Jahns (1995) use this scheme in their overview of the algae.

erokontophyta, Class **Bascillariophyceae**). These algae are distinguished primarily by their possession of a unique silica cell wall which takes the form of two overlapping valves, or *frustules*. It is estimated that there are more than 100,000 species in the class (Hoek, Mann & Jahns, 1995)[5] and that together their marine planktonic representatives are responsible for around a half of the total amount of marine primary productivity (*i.e.* 20% of the global annual primary production; Thain & Hickman, 1994). In work using mesocosms (large enclosed volumes of seawater situated in the field), Egge & Aksnes (1992) found that so long as the nutrient silicate (which diatoms use to build their "cheaper" silica cell walls) remained above a certain concentration, diatoms were always able to dominate the phytoplankton assemblage. This would accord with their dominance in spring blooms of certain regions when silicate is plentiful. However, silicate (unlike nitrogen nutrients) is not regenerated efficiently by higher trophic levels, and diatoms usually lose dominance relatively quickly as a consequence and have to wait until mixing deepens sufficiently to re–introduce silicate to the photic zone (Dugdale, Wilkerson & Minas, 1995). This waiting may occur in deeper waters which are reached by the diatoms either as fast sinking resting spores (Hoek, Mann & Jahns, 1995) or as large aggregates of cells (*e.g.* Crocker & Passow, 1995). Deep mixing prior to the spring bloom re–introduces both these sunken cells and silicate to the mixed layer[6].

Another important group of eukaryotic phytoplankton are the coccolithophores (Kingdom **Eukaryota**, Division **Prymnesiophyta**). They are distinguished by their production of organic scales covered in a layer of calcite ($CaCO_3$). These are important in the biogeochemical cycle of carbon, since the production of the scales uses HCO_3^- and consequently increases the concentration of dissolved CO_2. The coccolithophores (of which the species *Emiliania huxleyi* is probably the most well–known) are also important because of the changes they can induce in the local optical environment (Balch, Kilpatrick & Trees, 1996; Balch *et al.*, 1996). These changes affect both other phytoplankton and the heating of the surface waters of the ocean.

The dinoflagellates (Kingdom **Eukaryota**, Division **Dinophyta**) are an interesting and important group with around 2000 extant species (and a rich fossil record of extinct species). They typically possess two flagella (perpendicular to one another) and are often distinguished by the complex "armour" which covers them. This may be very ornate and is believed to aid in either reducing their sinking rate or deterring grazers (or both). Although they have relatively slower growth rates (Tang, 1996), they can form a major component of the phytoplankton assemblage (Pierce & Turner, 1994a; Bralewska & Witek, 1995). Usually their dominance in assemblages occurs in the summer after that of the diatoms, and some species prefer the more stable vertical water column which occurs during these months (Thomas, Vernet & Gibson, 1995, find that turbulence inhibits the division of certain species). Additionally they can also be a major component of the microzooplankton assemblage (Bralewska & Witek, 1995), either as facultative

[5] Thain & Hickman (1994) cite a much lower estimate of around 10,000 species.

[6] Very recent work by Dugdale & Wilkerson (1998) has linked silicate limitation of diatoms to the phenomenon of High Nutrient, Low Chlorophyll (HNLC) in the eastern equatorial Pacific Ocean.

or obligate heterotrophs (around 50% of dinoflagellates have no photosynthetic apparatus; Hoek, Mann & Jahns, 1995). This "split personality" behaviour of dinoflagellates illustrates the difficulty of modelling large numbers of disparate species with a few functional groups. For instance, in a particularly extreme example, the heterotrophic dinoflagellate *Protoperidinium divergens* even consumes the juvenile stages of copepods (Jeong, 1994). Raven (1997) reviews the importance of such heterotrophy in phototrophs (both for nutrient and autotrophic symbiont acquisition; see also Arenovski, Lin Lim & Caron, 1995). Interestingly, as well as indulging in the capture of other algae for their photosynthetic capability, dinoflagellates themselves are often popular targets for symbiosis with larger organisms (*e.g.* corals; where they are found in the tissues known as *zooxanthellae*). They are additionally important because of their role in toxic blooms (often referred to as *red tides* because of their colour) which may affect coastal fisheries (Tilstone, Figueiras & Fraga, 1994; Anderson, 1997).

Zooplankton

Similarly to the phytoplankton, the assemblage which makes up zooplankton is also a complex mixture of different and distinct species and phylogenetic groups. Unlike the phytoplankton though, where almost all of its members share a common trophic position as autotrophs, zooplankton species include herbivores, bacterivores, detritivores, carnivores and even cannibals.

Most modelling efforts ignore these subtleties and concentrate on the grazing of phytoplankton biomass. Because of their smaller size, microzooplankton (mostly protistan unicells) graze the smaller fraction of the phytoplankton made up of autotrophic bacteria. They also feed on free–living heterotrophic bacteria. In turn, they are consumed by larger, metazoan (multicellular) zooplankton, which may consume them along with the larger phytoplankton fractions (since their size range overlaps that of eukaryotic phytoplankton). These zooplankton may either be adults or the juveniles of still larger zooplankton fractions (and can be modelled as such). Some of these juveniles (or larval stages) are merely temporary members of the plankton system (*meroplankton*) and graduate to benthic adult stages (*e.g.* many bivalve and gastropod molluscs, barnacles, echinoderms, corals, *et cetera*). These organisms utilise the plankton as a means of dispersal and as a source of food (release of larvae may timed to coincide with events like the spring phytoplankton bloom).

An important ecological consequence of zooplankton grazing of phytoplankton is the fate of the biomass consumed. Phytoplankton are often limited by nutrient availability, and if processes do not replace these nutrients, productivity will cease. As already noted, diatoms suffer quite severely because one of their key nutrients, silicate, is not regenerated efficiently. However, other nutrients, including the nitrogen ones considered by the models in this thesis, are regenerated through the zooplankton or their predators (and also heterotrophic bacteria) (Hutchins & Bruland, 1994, examine the regeneration of trace metals in plankton systems). The production of fast sinking faecal pellets by larger organisms, such as the predators of zooplankton, but also by zooplankton themselves, does however act to remove biomass from the mixed layer without giving it sufficient time to be regenerated. As already indicated, such sinking

fluxes of organic material to the deep ocean are of interest. These processes make higher predators (be they larger zooplankton or nekton) an important component of plankton systems.

Microzooplankton are represented by several major protozoan groups. In addition to the dinoflagellates already met, the foraminiferans (Kingdom **Eukaryota**, Phylum **Rhizopoda**, Class **Granuloreticulosea**, Order **Foraminifera**), ciliates (Kingdom **Eukaryota**, Phylum **Ciliophora**) and tintinnids (a major subdivision of the ciliates) are important groups. The foraminiferans are amoeboids distinguished by their possession of a shell (organic or calcareous) which is usually multichambered. They are entirely heterotrophic and consume their prey by contacting it, then engulfing it. The ciliates are one of the largest groups of protozoans, and have a relatively high degree of organelle development. Their name is derived from the cilia they possess, which are used for locomotion or for feeding. They are heterotrophic, like the foraminiferans, but have a much more specialised feeding apparatus (which often includes a mouth or *cytostome*). Tintinnids are a widely distributed Order of ciliates distinguished by a shell (or *lorica*) which is often composed partially of foreign material (Newell & Newell, 1973; Barnes, 1986). As well as often dominating the ciliate community (Omori & Ikeda, 1992), they can be of significant importance in the microzooplankton link of microbial food webs (Pierce & Turner, 1994b). Note that the juveniles of some of the larger metazoan zooplankton also constitute microzooplankton (*e.g.* copepod nauplius larvae).

The meso– and macrozooplankton are represented by many (if not most) metazoan groups. Probably the most important group are the copepods (Kingdom **Eukaryota**, Phylum **Arthropoda**, Class **Crustacea**, Subclass **Copepoda**). Omori & Ikeda (1992) report that in samples of net plankton from most waters, commonly 80% or more of the individuals caught are copepods. Although clearly ecologically important, they are not commonly familiar since most species are less than 5 mm in length. As a group they include herbivores, omnivores, detritivores and carnivores. While it was formerly thought that they fed by simply sieving water that they were moving through, more recently it has become apparent that feeding is complicated by the viscous effects of water (or even, as in the case of the cladoceran *Daphnia*, the charges on the particles to be consumed; Barnes, 1986), and observations of tethered copepods show that a degree of active capture of particles occurs (Barnes, 1986; Paffenhöfer *et al.*, 1995). Their relatively large size has several important consequences for their life history, some of which have been included in ecological models of zooplankton. Smaller larval stages exist which may feed on different prey (and, in turn, be eaten by different predators). Their relatively larger size permits much greater mobility and this is often manifested in *diel vertical migration* (DVM), where organisms spend different parts of the day at different depths in the water column (there are several proposed reasons for this migration including predator avoidance, food abundance and metabolism control; Loose & Dawidowicz, 1994; DeMeester, Weider & Tollrian, 1995; Williamson *et al.*, 1996). DVM may have important consequences for sinking flux should zooplankton egest consumed material at depth (*e.g.* Atkinson, Ward & Murphy, 1996). Also, some species enter phases of dormancy to tide them through unfavourable conditions (Dahms, 1995).

There are several other important crustacean zooplankton groups, including the cladocerans (*e.g. Daphnia*) and the euphausiids (*e.g.* krill). These share many of the characteristics of copepods. Other important groups include : the molluscan pteropods, heteropods and cephalopods (mostly carnivorous); scyphozoan coelenterates and ctenophores (mostly carnivorous); and the appendicularians and thaliaceans (herbivores, detritivores and omnivores mostly). These latter two groups are considered important because of their production of fast–sinking faecal pellets (Totterdell *et al.*, 1993).

An important issue in zooplankton grazing is how *exactly* the zooplankton graze. At the level of unicells, phagocytosis (where one cell entirely engulfs another) is one such procedure used. It requires direct contact between the prey and the predator cells (see Davidson, Cunningham & Flynn, 1995, for a detailed study of one such system). As the ciliates illustrate though, grazing even in unicells can be more complicated than mere phagocytosis. Because of their size and (normally) more complex anatomy, multicellular metazoans have many more different approaches to food acquisition. Some also rely on passive contact (*e.g.* the coelenterates and ctenophores; the former use poisoned barbs to immobilise prey, the latter adhesive compounds), while some actively hunt (*e.g.* some euphausiids, polychaete annelids). The appendicularians feed uniquely by using a gelatinous casing which is secreted around their bodies. Water is pumped through this casing to a filter where small plankton are trapped then consumed (since the casing becomes clogged, it is replaced regularly – sometimes as frequently as every few hours). The thaliaceans use a feeding technique not dissimilar to that used by benthic molluscs. A continuously generated mucus net traps particles in the water and is drawn constantly into the organism's mouth. In a related issue, Rothschild & Osborn (1988) have suggested that the role of turbulence should be considered in all feeding interactions. As well as directly affecting contact rates between organisms, they suggest that organisms may take advantage of turbulent energy rather than use their own metabolic energy to capture prey.

Heterotrophic bacteria

In addition to the autotrophic bacteria already classified here as phytoplankton, large assemblages of heterotrophic bacteria occur in the ocean. These are broadly classified as either "free" or "attached" bacteria (Totterdell *et al.*, 1993). The former are those bacteria which exist freely in the plankton and derive energy from dissolved organic material (DOM) there (Zweifel, Norrman & Hagström, 1993). The latter are those which associate with particulate detrital material in the water column and degrade this to derive energy and material for growth. The majority of bacteria appear to be in the former group (Azam *et al.*, 1983), although as yet the precise ecological significance of free bacteria is not entirely understood (Fasham, 1993). However, they do play an important role in the regeneration of nutrients (Lee & Fisher, 1994). In addition to utilising DOM for its energy content, heterotrophic bacteria also utilise ammonium or other organic nitrogen sources to provide nitrogen for amino acid synthesis.

In addition to losses incurred due to grazing by microzooplankton, heterotrophic (and autotrophic) bacteria also suffer losses due to the activity of viruses (or *phages*). Suttle (1994) found that up to 20%

of marine heterotrophic bacteria were infected at any given time and that this led to a comparable daily loss rate of cells to lysis. Weinbauer & Peduzzi (1995) found that loss to viruses could be more significant than loss to microzooplankton (nanoflagellates) in certain situations. However, as Murray (1995) points out, bacteria can also destroy viruses which affect other organisms, and suggests that the excretion of DOM by phytoplankton may aim to support a virus–killing population of heterotrophic bacteria.

1.4.3 Model biology

The three trophic levels described here are those used in Fasham's (1993) model of the open–ocean plankton ecosystem. This model forms the basis of this thesis. As the absence of familiar aquatic animals such as fish and whales implies, the biology represented in the model is a (severe) truncation of real biology in the world ocean. However, although these macroscopic ocean inhabitants have a major role in the economic use of the ocean, their absence (at least in terms of explicit representation in models) is of limited significance to the problems (*e.g.* predicting biological production or carbon flux to the deep ocean) addressed by such models.

As is discussed more fully in Chapter 2, there is some variety in the level of detail in biological models of the ocean. Although reducing the entirety of ocean biology to three compartments (or *state variables*) may appear extreme, many models use even fewer. Kremer (1983), Taylor (1988) and Taylor *et al.* (1991), for instance, all use models in which the biology is reduced to only a phytoplankton compartment. Phytoplankton–Zooplankton (PZ) and Zooplankton–Phytoplankton–Nutrient (ZPN) models, which expand upon the earlier models by modelling both phytoplankton and their grazers, are also a common choice. Beyond the likes of the Fasham (1993) model, several models include multiple types of phytoplankton and zooplankton to model situations in which appropriate data are available (*e.g.* Kremer & Nixon, 1978; Andersen, Nival & Harris, 1987).

Ultimately, extreme biological detail may be required in a model if it is to accurately capture the behaviour of plankton ecosystems (*e.g.* in the "globally robust" models imagined by Fasham, 1993). However, as Totterdell *et al.* (1993) discuss, increasing model complexity quickly leads to trade–offs against model tractability (*e.g.* determining analytical solutions; simulation in General Circulation Models, GCMs) and ease of understanding. Chapter 3 explores some issues of model complexity during the deconstruction then reconstruction of the Fasham (1993) model.

1.5 Ocean physics

In addition to purely biological interactions, most organisms in the ocean are also profoundly influenced by the physics of the medium they inhabit. This influence operates on many different scales, from the forces and factors affecting a single cell up to those which control the biological productivity of ocean basins.

1.5.1 Irradiance and ocean heating

The upper ocean is warmed by radiation from the sun. This takes the form of mostly shorter wavelength radiation in the visible and infra–red regions of the electromagnetic spectrum. The quantity of radiation reaching the top of the earth's atmosphere varies predictably with both latitude and season since both of these parameters affect the angle of a given position on earth relative to the incident solar radiation (Brock, 1981, presents a series of standard astronomical formulae which can calculate the spatial and temporal patterns of irradiance across the earth; see also Chapter 2). Correcting this radiation flux to account for the effects of the atmosphere is considerably more complicated (Chapter 2 describes the empirical correction algorithm used in this thesis). Even after penetrating the earth's atmosphere, some of the radiation which reaches the surface is lost by reflection at the surface of the ocean (this is obviously particularly high when the ocean surface is covered in sea ice and this is especially significant seasonally in the Southern Ocean around Antarctica).

Once radiation has penetrated the ocean's surface it is attenuated down the water column as it is absorbed by both the water itself, and by material within the water column (including the organisms there). The rate of attenuation is variable with the wavelength of the radiation, and for a given wavelength, λ, can be described by the following equation :

$$I_z = I_0 \exp\{-\alpha_\lambda z\}, \tag{1.2}$$

where I_z is the intensity of irradiance of at depth z, given the intensity of irradiance just below the water's surface, I_0, and the attenuation coefficient for irradiance of wavelength λ, α_λ (assuming that α_λ is constant down the water column) (Mann & Lazier, 1991). The attenuation coefficient is variable between different wavelengths. For longer wavelength radiation such as infra–red, the coefficient can be as high as 20 m^{-1} (*i.e.* by a depth of only 1 m, $\gg 99\%$ of the radiation has already been absorbed). The action spectrum of chlorophyll *a* (the major photosynthetic pigment used by most photoautotrophs) shows that shorter wavelengths of radiation are favoured, and the attenuation coefficients of water at these wavelengths are considerably smaller (visible red and blue wavelengths have coefficients of around 0.4 and 0.004 m^{-1} respectively). However, even with these lower attenuation coefficients, the majority of radiation which enters the water column is absorbed within the first 10 m.

1.5.2 Vertical structure and mixing

One might expect that this pattern of absorption would lead to a similar thermal profile in the water column, as the energy of the absorbed photons is transformed to thermal energy. However, as measurements of the vertical profile of temperature reveal, processes which mix the water column normally disrupt the pattern of energy dissipation. These processes include stirring by the wind and convection generated by the loss of heat at the surface of the water. This leads to the generation of a so–called *mixed layer* at the surface of the ocean with a relatively homogeneous thermal structure. This layer overlies cooler water, and between the two layers there is a region known as the *thermocline* across which

the temperature changes from the relatively higher surface temperatures to the lower deeper ones.

The thermal difference between the mixed layer and the deeper ocean leads directly to differences in the density of the layers. Deeper water is cooler and denser, while mixed layer water is warmer and lighter. The layers are then also separated by a region across which density changes, the so–called *pycnocline*. This tends to reduce interchange between the layers since when denser parcels of water from below the pycnocline try to mix into the mixed layer, they tend to sink out, while the reverse happens when lighter parcels of water from the mixed layer try to mix into the deep ocean. Consequently the layers become relatively isolated, with the isolation increasing with the density difference between the two layers. Since the irradiance used by phytoplankton is mostly confined to the mixed layer (the region in which irradiance is sufficient to promote net phytoplankton growth is sometimes known as the *photic zone*), but their nutrients are replenished from the deep ocean, the reduced communication between the surface and deeper ocean layers has interesting biological consequences.

The depth of the mixed layer (and thus the extent of the thermocline) varies with wind and solar forcing. The more energy transferred to the ocean by winds, the greater the turbulence and the deeper the resulting mixed layer. However, the effects of wind mixing can be countered by the increased buoyancy caused by solar heating of the surface waters (although this is obviously affected by the diel nature of the solar forcing). Taylor & Stephens (1993) examine the influence of mixing and the stabilisation of a shallow mixed layer on the timing of the spring phytoplankton bloom.

The mixing described above takes place mostly as a result of the turbulence introduced into the ocean system by instability mechanisms which affect large scale water motions (of which the breaking of the surface waves generated by wind action across the ocean surface is an example). Turbulence itself, despite its appearance as random water movement, is a complex phenomenon produced by the dissipation of kinetic energy to smaller and smaller scales. This process is known as the *energy cascade* (Henderson–Sellers & Robinson, 1986). The kinetic energy is continually transferred to smaller scales until the viscosity of the water itself interferes with the process by resisting the shear caused by the smallest eddies. This restricts eddies to minimum sizes of just a few millimetres. As a consequence, organisms with a typical dimension of less than 1 mm are forced to rely on molecular diffusion to supply them with nutrients or rid them of their waste products. Unless, that is, they resort to strategies such as sinking (potentially dangerous for a phytoplankton cell wishing to remain in the photic zone) or swimming to "shear away" the boundary layer of stationary medium which surrounds them.

In addition to mixing via the turbulent dissipation of kinetic energy, the mixed layer is also affected by a process known as Langmuir circulation. Above a wind speed of around 3 m s^{-1}, this produces coherent horizontal "rolls" which line up in the same direction as the wind. The rolls can be up to 200 m in diameter, and are often identified from the debris which occurs on the sea surface where two rolls converge (pairs of neighbouring rolls rotate in opposite directions) (Barstow, 1983). As well as providing

another mechanism to mix the surface waters, work has found that cross–sectional heterogeneity in the rolls occurs, causing certain regions to disperse plankton rapidly, and other regions to hold them for long periods of time (Bees, Mezić & McGlade, 1997).

Mann & Lazier (1991) provide a more thorough treatment of the issues sketched above.

1.5.3 Large scale ocean circulation

The previous section briefly described some of the physical phenomena which affect plankton systems at the small (individual organism) and medium (mixed layer) scale. The models used in this thesis are applied at the medium scale, but are often applied (*e.g.* Fasham *et al.*, 1993; Sarmiento *et al.*, 1993) at a larger scale (*e.g.* ocean basin). To put such related work in context, this short section outlines some of the physical processes in operation at such scales.

The earth's atmosphere receives energy from direct, reflected and re–emitted irradiance. This energy manifests itself in the movement of air in response to its thermal state. Since the earth does not receive irradiance evenly over its surface (the poles receive considerably less irradiance per unit surface area than the equatorial region), the heating of the atmosphere is similarly uneven. Since warm air rises, one might expect that this skewed distribution of solar heating would be resolved simply by the movement of warmer, lighter equatorial air over cooler, denser polar air. However, the rotation of the earth

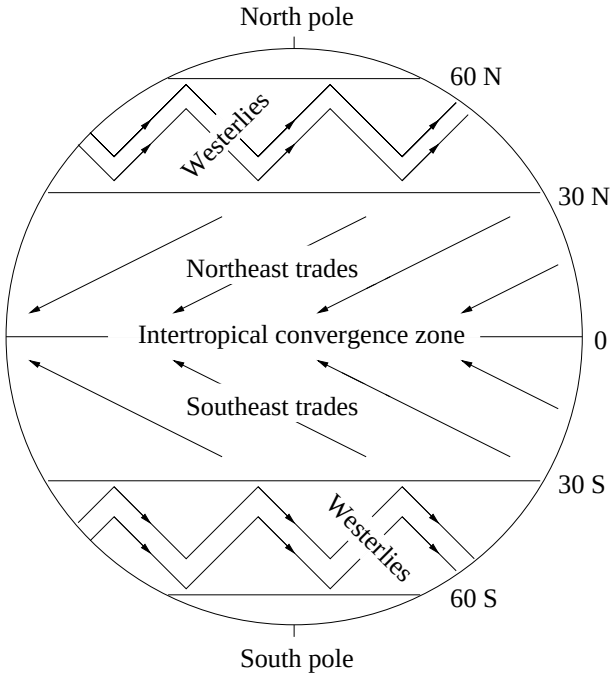

Figure 1.1: Trade and westerly wind systems in the northern and southern hemispheres of the earth. The jagged appearance of the westerlies represents their meanderings which lead to the formation of Rossby waves (see text). After Mann & Lazier (1991).

complicates the picture, leading to the formation of two major wind systems : the trade winds and the westerlies (see figure 1.1).

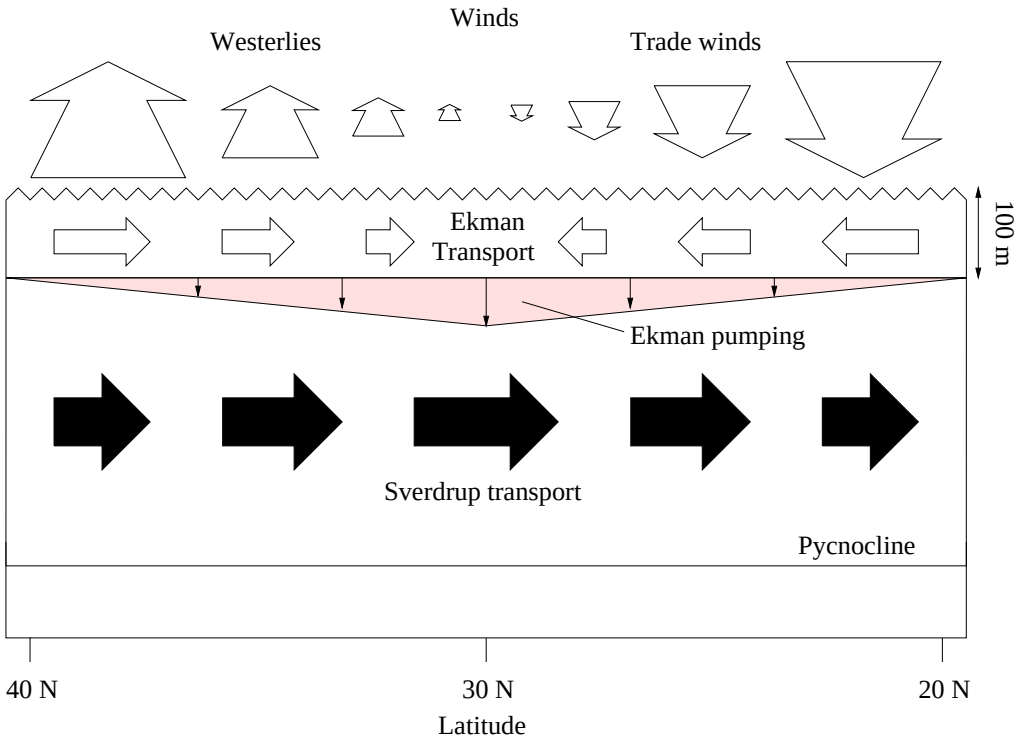

Figure 1.2: Diagrammatic representation of the processes of Ekman and Sverdrup transport (in the northern hemisphere). Ekman transport of surface water (< 100 m) north and south towards 30° is caused by the action of the trade and westerly winds (out of and into the page respectively) on the surface of the ocean. This water movement causes water to be "pumped" downwards where Ekman transport converges. This in turn leads to the process of Sverdrup transport of deeper water (up to 1000 m) towards the equator (see text for more details). After Mann & Lazier (1991).

The trade winds arise in the manner already suggested, namely warmer, equatorial air rises up and moves polewards, and is replaced by cooler, denser air from the subtropics. Because of the Coriolis effect[7], the flows of air from the subtropics to the equator are deflected to the west, generating the northeast and southeast trade winds (these are named after the direction from which they come). The rising equatorial air cools as it moves towards the poles and descends in the subtropics ($\sim 30°$ N/S). This circular pattern of air flow, where equatorial air is replaced by subtropical air, which it then replaces itself, creates convection cells which are known as Hadley cells. Since these cells essentially retain the thermal energy supplied to the tropics within the tropics and subtropics, this creates a thermal (and thus pressure) gradient between latitude 30° and the poles. This gradient gives rise to strong westerly

[7] The Coriolis effect is a consequence of the earth's rotation on its axis, and affects the movement of bodies of air and water over the earth's surface. In the context of the oceans, it is responsible for why, relative to the surface of the earth, a moving body of water veers to the right in the northern hemisphere, and to the left in the southern hemisphere.

winds which are perpendicular the pressure gradient, and flow continuously around the earth. These winds vary in strength with altitude (the jet–stream marks their maximum) and also meander north and south. This meandering produces waves (around 10000 km long) known as Rossby waves. These have periods of around a month and are responsible for shifting weather patterns in the mid–latitudes.

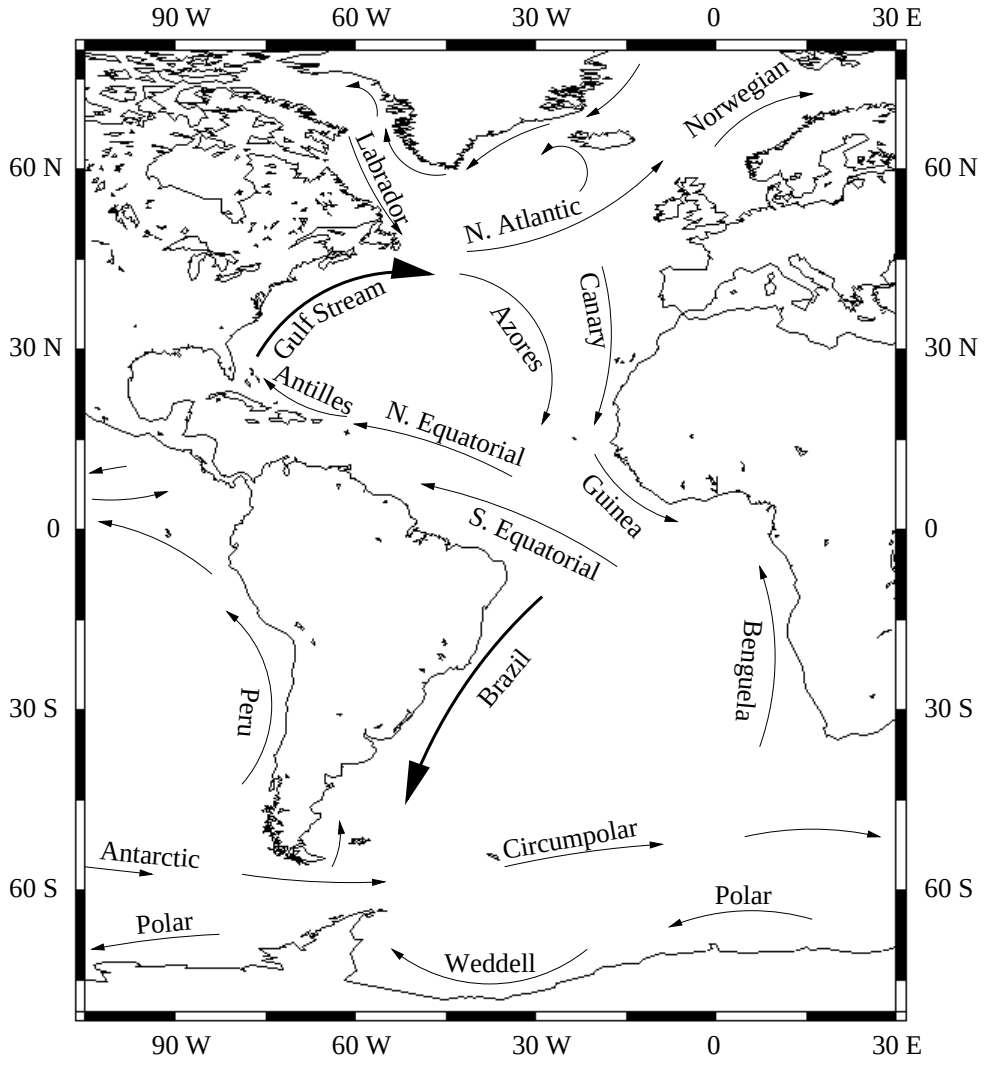

Figure 1.3: The major surface currents of the northern and southern Atlantic ocean. Western boundary currents (the Gulf Stream and the Brazil current) are emphasised. Note the circular pattern of flows in the northern and southern regions. After Mann & Lazier (1991).

The trade winds and the westerlies play an important role in the generation of surface and deeper layer flows within the ocean. Moving in opposite directions at lower and higher latitudes respectively, they generate stress on the ocean's surface which, in combination with the Coriolis force, leads to the transport of water in the upper layer of the ocean. The interaction between the wind stress and the Coriolis force acts to produce water movement to the right of the wind. Consequently, surface water on the poleward side of the subtropics ($> 30°$) moves towards the equator, while water on the equatorial side of the subtropics ($< 30°$) moves towards the poles. These water movements are known as Ekman transport. Since

these movements are opposite to one another, the moving water has to go somewhere, leading to a region of downwelling water at the subtropics (this downwelling is known as Ekman pumping). The ocean layer beneath the surface wind–driven layer compensates for the downward Ekman pumping with a horizontal flow towards the equator (see figure 1.2). Although the surface flows are in opposite directions and head towards the subtropics, this deeper flow, known as Sverdrup transport, is equatorial. The net effect of this wind–driven circulation is an equatorial pattern of water circulation. The Californian, Canary, Peruvian, and Benguelan currents are examples of this circulation pattern. However, these currents only complete half the full circulation required. The patterns are completed by flow parallel to the equator and by relatively stronger flow at the westward boundaries of the ocean basins (the Gulf stream and the Brazil current are these western flows in the northern and southern Atlantic ocean respectively). These currents close the circular patterns of surface flow in the main ocean basins (see figure 1.3[8]). These patterns are known as *gyres*, and play significant roles in dissipating inertia and thermal energy through the oceans. In the case of the Gulf Stream, some of this energy is dissipated by occasional meanderings which break off into separate rings (the Ring Group, 1981, followed the evolution of ring "Bob" across the course of its seven month life).

Again, the processes outlined here are comprehensively discussed by Mann & Lazier (1991) and Henderson–Sellers & Robinson (1986).

1.5.4 Model physics

The models considered in this thesis take a considerably simpler view of the structure of the ocean. In the first instance, horizontal space is not considered at all (although many other models do treat its importance at different scales). Vertical space is represented, but in an implicit manner. Most of the models consider only the region of the ocean from the surface of the ocean to the top of the thermocline. Below this is the so–called *deep ocean* which is assumed to play a relatively minor role in the biological dynamics of the ocean, and acts only to re–mineralise organic material back to inorganic nutrient. Figure 1.4 shows a diagrammatic representation of the system.

The actions of the sun and wind on the modelled vertical section are assumed to mix it homogeneously down its entire depth. The components of the biological model are thus represented by an average concentration within the layer. Since neither the patterns of wind or solar forcing are constant across the year, neither is the depth of mixing. In the models here, the seasonal pattern of mixing is (again) represented implicitly using measurements from geographical locations of interest.

Some models (*e.g.* Taylor, 1988; Taylor *et al.*, 1991; Ross, Gurney & Heath, 1994) assume a slightly more realistic representation of the water column in which the thermocline layer (*i.e.* the region between the mixed layer and the deep ocean across which the temperature changes between that of its

[8]The coastline map of figure 1.3 was created using the web utility "Online Map Creation". This utility was written by Martin Weinelt, and is available at `http://www.aquarius.geomar.de/omc`.

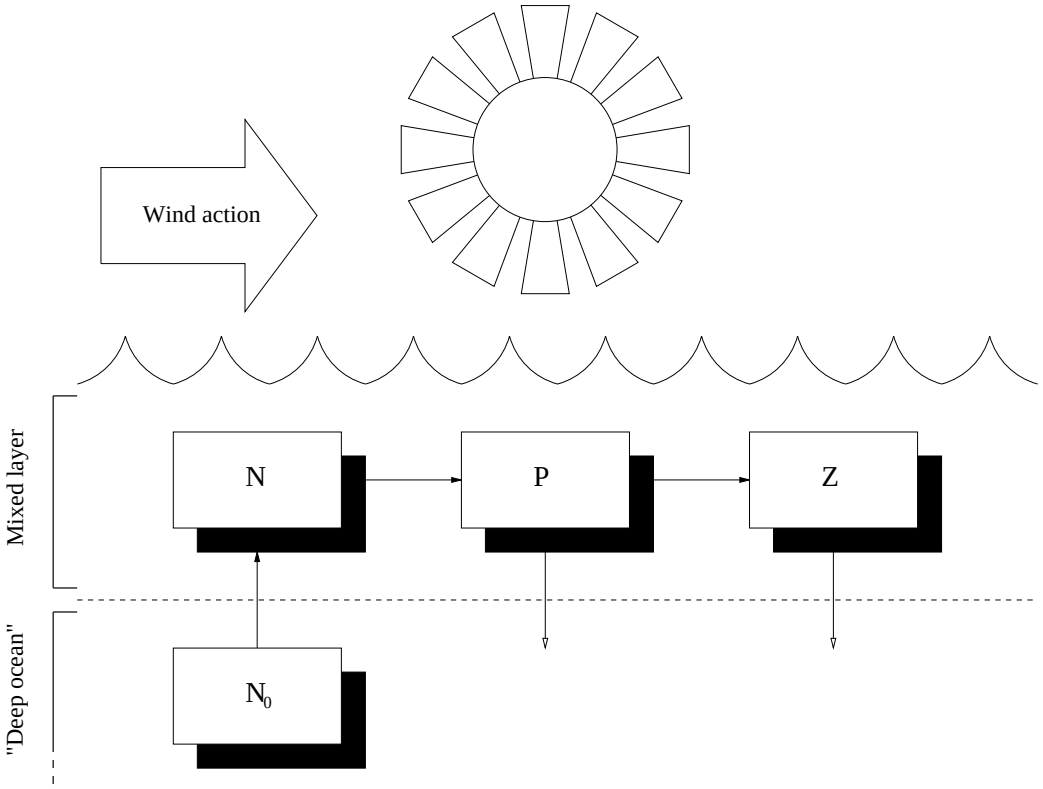

Figure 1.4: Diagrammatic representation of the modelled physical and biological system.

two sandwiching layers) is represented explicitly. Chapter 6 uses this approach as well and some of the advantages and problems associated with this approach are discussed there.

1.6 Studying plankton systems

A crucial aspect in the study of plankton systems which has been neglected so far is the way in which the systems are actually studied. While this thesis is a modelling one and uses no methods or techniques to obtain measurements from the real world, it does use data which has been collected from there, and that data has been collected in a number of different ways. This brief section introduces some of the ways in which data are gathered. Newell & Newell (1973), Stein (1973) and Omori & Ikeda (1992) provide more detailed accounts of some of the techniques outlined here.

In addition to the actual techniques and mechanisms used to sample the ocean, there is a large body of information regarding appropriate spatial and temporal scales at which sampling should occur (see Omori & Ikeda, 1992). For example, if zooplankton under study undergo DVM, any sampling of their biomass needs to account for this if it is to be accurate. Similarly, in coastal regions the timing of tidal

events may strongly affect sampling results and care should be taken to ensure that sampling does not falsely report the true distribution and abundance of organisms. There is also a considerable body of taxonomic information which identifies and describes biological species. Again, after Williams *et al.* (1981), as plankton species can potentially be found in any part of the world ocean, this can be an important consideration.

1.6.1 Plankton measurements

There are a number of different ways to quantify plankton densities in the ocean. For medium to large species or groups (*e.g.* mesozooplankton), it is common to sample with netting. In addition to mesh size differences, there are several different shapes of nets, and there are several different patterns by which the nets can be towed through the water (see Omori & Ikeda, 1992). Nets have the advantage of sampling a large volume of water (which may be necessary if the plankton fraction of interest is comparatively rare), but only allow an average density to be obtained (which may even be an underestimate if net avoidance by the organisms in question is an issue). In trophic level studies, where trapped zooplankton are examined for the contents of their digestive tracts, the phenomenon of *net feeding* (where trapped zooplankton ingest unrepresentative prey that happen to coincide in the net) may also complicate measurements.

Microzooplankton and smaller fractions, are generally sampled using bottles. These avoid the problem of net clogging, and may be used to sample only at specific depths. After the sample is taken, biomass or identification of different fractions may be made following filtration to separate different size classes. There are many different techniques for quantifying biomass. Flow cytometry, for instance, allows the determination of both cell numbers and cell volumes from very small sample volumes (and, potentially, some degree of taxonomic distinction; C. S. Dow, University of Warwick, pers. comm.). Alternatively, samples may be used in experiments to measure properties such as photosynthesis, grazing, or the uptake or production of substances of interest. In the case of bacteria, epifluorescent microscopy can be used to distinguish different types of bacteria (*e.g.* autotrophic versus heterotrophic).

Another commonly used sampling mechanism is the so–called continuous plankton recorder (CPR). These devices are generally used to sample phytoplankton across large transects. They are towed behind vessels either at a fixed depth, or across a vertical range as they are towed. Often a silk screen is used to trap planktonic organisms as the device is towed. The screen is slowly wound and stored so that organisms caught at different times are trapped on a different section of the silk. The silk may then be rolled up in a bath of preservative and examined later, usually for chlorophyll content. If the rate of the screen movement is tied to the rate of passage through the water, comparable lengths of the screen will allow comparison of comparable volumes of water, and a spatial transect of chlorophyll can be constructed. Variants of such devices can be used to measure different fractions of the plankton. Hays, Warner & LeFevre (1996), for instance, examined CPR data for 7 copepod taxa to determine their long–term patterns of DVM.

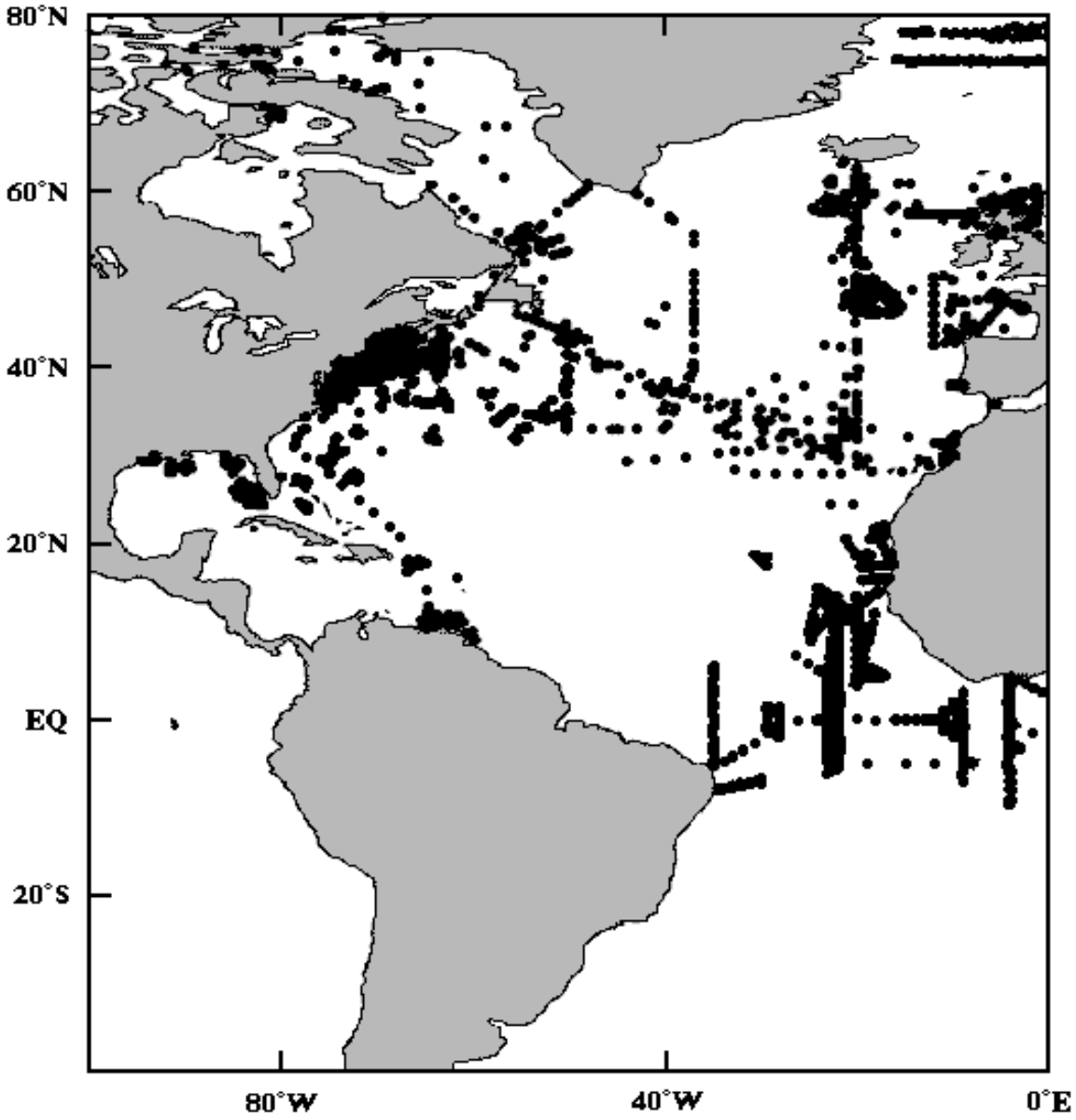

Figure 1.5: Sampling sites in the North Atlantic from the World Ocean Optics Database (WOOD). Black circles represent sampled locations. Map courtesy of the WOOD.

1.6.2 Shipboard, cruise and marine stations

Traditionally, research cruises, ships–of–fortune and marine stations have provided data. Research cruises typically visit an ocean region of interest, then over a period of time and/or space sample the region in question. Measurements or observations made will depend on the "mission" at hand, but generally cruises provide a body of detailed data. The recent (1987–1992) Biogeochemical Ocean Flux Study (BOFS) cruises, for instance, collected data which included : Conductivity–Temperature–Depth (CTD) data of temperature, attenuation, salinity, irradiance, and chlorophyll; nutrient concentrations; zooplankton biomass; phytoplankton species; primary productivity; and sinking flux measurements from

sediment traps (Lowry, Machin & Cramer, 1994).

So–called ships–of–fortune are usually commercial vessels to which scientific instruments (*e.g.* the CPR) are attached. Although there is no opportunity to control the transect sampled, the frequency of such vessels, as well as their consistency of route, makes them a valuable source of data.

Marine stations share the sampling bandwidth capabilities of research cruises, but confine themselves to measurements in their immediate vicinity. While this does allow the generation of large, temporal data sets from particular locations (*e.g.* OWS "India"), stations cannot easily provide information about spatial components to their data.

Figure 1.5 shows the locations of cruises and ocean stations in the North Atlantic Ocean (dating from the early 1960s). The map originates from the World Ocean Optics Database[9] which contains data from cruises or stations where measurements related to ocean optics were made. As is clear from the figure, sampling is heterogeneous and predominantly coastal or near–coastal (particularly the eastern seaboard off the U.S.A. and the North Sea), although there are several obvious transect studies. The southern, central region of the North Atlantic is more sparsely sampled, partially reflecting the lower biological productivity (and hence reduced research interest) of this region. Although not shown here, the seasonal pattern of sampling is also heterogeneous, with the majority of cruises occurring during the period from the late spring to the early autumn. This temporal window is not (yet) wide enough to provide much information on the over–wintering behaviour of phytoplankton and zooplankton (Totterdell *et al.*, 1993).

1.6.3 Remote sensing platforms

With the advent of earth–orbiting satellites, the opportunity has arisen to collect synoptic data from the oceans with superb spatial and temporal coverage. Depending upon the orbital parameters of the satellite (altitude; polar versus equatorial orbit), coverage can vary from a constant field of view of a given area (geostationary satellites), to periodic views of much greater areas (polar orbiting satellites). In addition to the spatial and temporal aspects to the coverage provided by a satellite, the information produced also depends on the region of the electromagnetic spectrum measured. Cole (1997) summarises the uses of different regions of the spectrum :

- **Visible sensor**

  Produces colour maps which may be used to derive chlorophyll concentration or water turbidity. These may then be used to calculate photosynthesis, sediment load, track pollution, classify habitats or study ocean circulation patterns.

[9] The WOOD is administered by Jeffrey Smart and is available at `http://wood.jhuapl.edu/`. The WOOD is funded by the Office of Naval Research's Ocean Optics Programme.

- **Infra–red sensor**

  Produces sea–surface temperature (SST) maps. These may be used again to study ocean circulation or to classify habitats. They may also be used (*e.g.* Cole, 1997) as an indicator for upwelling activity.

- **Microwave sensor**

  Produces maps of sea ice distribution. These may be used in climate change studies or to warn shipping.

- **Radar altimetry**

  May be used to produce maps of sea level, wave height or sea roughness. These may be used to identify ocean currents and eddies, or again for shipping.

Visible sensors usually make use of reflected solar radiation. With respect to the oceans, this may either be reflected from the ocean's surface or from deeper horizons within the water column. Infra–red and microwave sensors normally make use of radiation re–emitted from the earth, and radar sensors detect the backscatter of radiation emitted usually by the satellite itself. In the context of plankton studies, most interest lies in using visible radiation sensors which can detect ocean colour (although information from other wavebands often helps in the processing of ocean colour results). These sensors are used to estimate the concentration of phytoplankton pigments, and ultimately these estimates may be used to calculate primary productivity. Platt, Sathyendranath & Longhurst (1995) provide an overview of the methods used to estimate productivity from ocean colour.

In spite of the advantages satellites offer in terms of spatio–temporal coverage, they have a number of limitations. An obvious one of these is the confounding influence of cloud cover, which affects both visible and infra–red radiation. With respect to using ocean colour as a proxy for phytoplankton pigment concentration, there are also problems associated with the vertical distribution of phytoplankton in the water column (*i.e.* is surface chlorophyll representative of its vertical distribution?). Platt, Sathyendranath & Longhurst (1995) and Hoepffner, Barker, Nykjaer, Estrada & Schlittenhardt (1994) describe techniques for accounting for such problems (*e.g.* the division of the ocean into *provinces* which show common seasonal patterns of vertical phytoplankton distribution).

1.7 Why model?

> *I am never content until I have constructed a mechanical model of the subject I am studying. If I succeed in making one, I understand; otherwise I do not.*
>
> – Lord Kelvin

Although often not stated explicitly (for instance, as in the field of molecular biology), the principle aim of science is to construct models of the world. By incorporating and summarising our knowledge, mod-

els are built to capture the essence of particular systems. Ideally, these models allow us to understand what we can observe of the system, and occasionally can be used to predict what the system may do in the future. The former feature of models is particularly valuable in directing research agendas and highlighting areas of relative ignorance.

Models may take many forms, from simple, qualitative descriptions of a system, through to complex, quantitative forms. In the quantitative sciences, where models are normally verified against measurements of the real world, it is essential for models to be quantitative. Mathematics has thus become a powerful tool, both in formulating models from knowledge about a system, and exploring the constructed model to determine if it has any features which make it either testable or unrealistic.

In the case of physics, mathematics has been applied to problems for centuries, and has been remarkably successful in both describing and predicting systems (*e.g.* Newtonian mechanics, thermodynamics). Indeed, until the advent of quantum mechanics, viewing the world as an elaborate machine governed entirely by deterministic mathematical laws was commonplace. Note though, that even if the universe were entirely deterministic, the existence of chaotic systems would render it difficult to make reliable predictions in practice. Nonetheless, even with the apparent stochasticity introduced into the universe by quantum mechanics, physics has been very successful in describing and predicting the behaviour of phenomena.

However, the application of mathematics to biological systems has, historically, been considerably less successful (at least in terms of producing a theoretical backbone to the subject). Systems which biologists study are usually considerably more complex (*e.g.* because of their heterogeneity) than those studied by physicists, and not obviously amenable to being reduced to a small number of important components. In sub–organism level systems, the objects under study (even the smallest of them) are usually highly complex, being made of thousands of parts (molecular and multi–molecular), and mixing matter, energy and information in ways which make it difficult to tease out exactly what is going on. In multi–organism systems (such as the plankton ones in this thesis) additional complexity enters through variety in the individual organisms, in their interactions with their physical environment and in their interactions with one another.

Partially because of this, biologists have traditionally studied nature in a mostly qualitative way. For instance, a substantial fraction of ecological research has involved determining detailed food webs to describe the trophic relationships between species in particular ecosystems (see Begon, Harper & Townsend, 1986, for examples). Where numerical approaches have been used, they have been typically statistical or have ignored the dynamics of interacting organisms. Such studies, while useful in their own right and providing foundations for other research, do not usually lend themselves to the kinds of predictions which ecologists are increasingly asked to make. Forecasting the consequences of many of the impacts of human civilisation on the earth's ecology requires ecologists to extrapolate to situations outside of

their empirical data. This forces ecologists to develop more accurate theoretical models, and necessitates confronting the complexity of biological systems.

Biological modellers are usually forced to handle this complexity by stripping the system to be modelled down to its bare essentials[10], making many empirical assumptions about how these essential components interact and then extensively modifying the model *ad hoc* to fit with observations made of the real system. There are notable exceptions to this broad categorisation, where the systems studied are sufficiently simple that the base physics underlying them can be incorporated into the models (Alexander, 1995; Murray, 1989; Bees & Hill, 1997), but as yet these approaches are confined to relatively narrow areas of biology.

1.7.1 Historical background

The clergyman Thomas Malthus was one of the first[11] people to frame a biological problem in terms of mathematics. His 1798 work, *An Essay on the Principle of Population*, described how human population growth beyond the limit of sustenance is checked by famine, disease and warfare. Although his public policy suggestions based on these observations were (and still are) widely misunderstood and attacked, his influence on biology continues to this day (Hardin, 1968, 1993; Yool, 1994; Mogie, 1996).

During the nineteenth century there were further attempts to apply mathematical techniques to biological problems (including the development of statistics, a discipline with firm roots in biology), but it was not really until the twentieth century that major efforts were expended.

1.7.2 The Lotka–Volterra model

One of the earliest, and most well–known, ecological models is the predator–prey model of Lotka (1925) and Volterra (1926). Vito Volterra originally built the model to describe the predator–prey interactions of fish species. He had been asked to do so by his prospective son–in–law, Humberto D'Ancona, who was a biologist studying fish populations in the Adriatic Sea. Fishing activity in the sea was (understandably) curtailed by the First World War, and fish populations had been able to return to a more natural, but counter–intuitive, equilibrium where the proportion of predators (sharks) to prey was much greater[12]. Alfred Lotka, who was a biologist and an actuary, independently produced the same model. The model takes the form of a pair of coupled ordinary differential equations (ODEs) with four simple terms representing intra– and inter–specific processes.

$$\frac{dN}{dt} = N(a - bP) \tag{1.3}$$

[10] Or, more accurately, what are perceived as the system's bare essentials. Frequently, the "bare essentials" are those parts of a system which are most easily measured or which have the greatest practical value.

[11] Daniel Bernoulli's mathematical evaluation of the treatment of smallpox by vaccination predates Malthus' work by almost 40 years (Anderson & May, 1991). However, his efforts are largely over–shadowed by those of Malthus probably because of the controversy (and resultant persistence) of Malthus' work.

[12] As Sigmund (1993) amusingly remarked, "Why should the war favour sharks? It couldn't just be the *Zeitgeist*, surely."

$$\frac{dP}{dt} = P(cbN - d) \tag{1.4}$$

Prey (N), are born at a constant rate, a, and are consumed by predators (P) at rate b, which is modified by the predator density. Predators increase in number through consuming prey, where the constant c either relates to transfer efficiency (*i.e.* how much of a prey's biomass/energy can be used by the predator) or some other conversion measure (*i.e.* how many prey need to be eaten to make a new predator). And they die (*i.e.* through natural mortality or predation) at a constant rate, d.

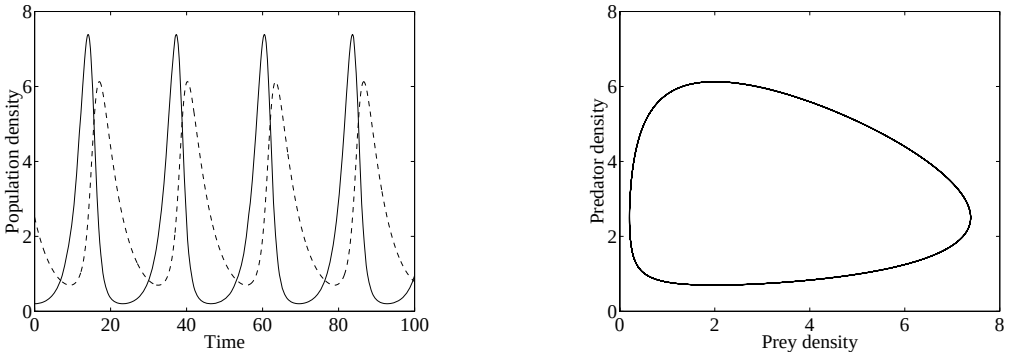

Figure 1.6: A time series (left) and phase portrait (right) of a Lotka–Volterra model simulation. Prey are represented by the solid line in the time series, predators by the dashed line. Motion around the orbit shown in the phase portrait is anti–clockwise, with predator density rising after that of the prey.

Figure 1.6 shows a typical result from the Lotka–Volterra model. Predator populations "chase" prey ones through time, creating oscillations in both populations. These oscillations trace an egg–shaped cycle in predator–prey space, with each orbit of the cycle taking the populations of both species back through their initial conditions. The position and shape of this cycle (assuming constant parameter values) depends critically on the initial populations of both modelled species. This is because the model is *neutrally stable*, with each combination of initial conditions producing a slightly different cycle. This is quite unlike most cyclic systems, including those described later in this thesis, where the same cycle is produced irrespective of the initial conditions (*i.e. globally attracting* cycles).

As such though, the Lotka–Volterra model contains several assumptions which are unrealistic for most natural populations. Amongst these are the assumptions that both the prey growth and predator death terms are density independent. Since in most real–life situations, prey population growth is likely to be limited by food availability, and predator mortality is liable to vary with the density of higher predators, both prey food availability and higher predator density are likely to be strongly dependent on the density of prey and predators respectively. Modifying the equations to those below, where prey growth is now density dependent (with K as the maximum possible prey density, or *carrying capacity*), changes the model system so that instead of neutrally–stable cycles, only a stable fixed point exists. This stable

fixed point attracts trajectories from all initial conditions to its location in model phase space.

$$\frac{dN}{dt} = N(a(1-\frac{N}{K}) - bP) \quad (1.5)$$

$$\frac{dP}{dt} = P(cbN - d) \quad (1.6)$$

Despite the simplicity of the Lotka–Volterra model, it is still a popular one amongst modellers. The particular Lotka–Volterra model detailed here is by no means the only one, and the term "Lotka–Volterra model" is applied across a wide range of simple predator–prey or two species competition models. May (1974) and Begon, Harper & Townsend (1986) review the model and some of its variants, and discuss modifications to the basic form, as well as their outcomes (*e.g.* the construction of n species versions of the Lotka–Volterra model).

1.7.3 Mathematical considerations

Again despite its relative simplicity, the Lotka–Volterra model illustrates several major, and often unstated, assumptions of many ecological models. Since some of these bear on the plankton models in this thesis they are discussed below.

- **Discrete versus continuous populations**

  Both predator and prey populations are described by continuous state variables, while in reality biological populations consist of discrete individuals. This discreteness problem is overcome by essentially assuming that the populations of predators and prey are sufficiently large that a continuous variable can adequately describe them : the so–called *continuity assumption*. The assumption breaks down where the populations to be modelled are low, or where the continuously modelled population tends to vanishingly small values. This latter feature of continuous models can create so–called *nanopeople* (D. A. Rand, University of Warwick, pers. comm.), model populations so small that when considered in terms of the numbers of individuals they represent, they actually constitute fractions of individuals. When this occurs, the problem is not so much in the low densities *per se*, but rather in ignoring the stochastic effects which become important when densities are low (*i.e.* populations at extremely low densities risk extinction by minor events affecting individuals).

- **Determinism**

  It is assumed that the system under study can be modelled by deterministic rules. While individual events may occur stochastically, models can assume that large enough numbers of events can be described by deterministic statements based on average behaviour (this is related to the issue of discrete versus continuous populations)[13]. Researchers have found that certain situations (*e.g.* Hendry & McGlade, 1995; Keeling, 1995) are best described by models which incorporate some degree of stochasticity.

[13] In a directly physical example, while the behaviour of an individual electron in the famous double–slit experiment may be stochastic and entirely unpredictable, the behaviour of large numbers of them may be described almost perfectly by the deterministic theories of quantum mechanics.

- **Homogeneous mixing**

  Populations are assumed to be sufficiently well mixed (*e.g.* either by physical processes or by the active movement of individuals within the population) that they can be adequately represented by a single population at an average density. So–called "patch" models or models in which space (or some other dimension over which populations are heterogeneous; *e.g.* age, size, disease susceptibility) is explicitly included provide alternatives (Keeling, 1995, and Morris, 1997, provide multiple examples of spatial cellular automata, coupled map lattices and reaction–diffusion systems).

- **Averaged rate processes**

  Processes (such as birth, death or decay) are assumed to be adequately described by an average rate. A process, for example, which is known to take an average of 10 days to occur, is commonly modelled as a constant rate of 0.1 d^{-1} (Keeling & Grenfell, 1997). This approach is again strongly tied to the continuity assumption.

- **Closed system**

  The modelled system is assumed to represent the "entire world". Factors in the real world whose effects are believed to be insignificant compared to the effects of the modelled components upon one another are entirely ignored. The model is therefore a truncation of the real world.

- **Identical inhabitants**

  In addition to assuming that populations can be described by a continuous variable, ecological models usually assume that all individuals in those populations are identical, or at least have no differences of any consequence to the situation under consideration. Evolutionary models, where populations may be broken into multiple sub–populations based on their genetics (or rather the phenotypic effects of their genetics), are an alternative (Keeling & Rand, 1995).

In the case of the plankton systems studied in this thesis, good cases can be made for assuming each of these in models. Table 1.2, for instance, summarises literature data collected on the densities of several major plankton groups from various locations and at various times of the year. Densities of bacterioplankton (table entries 1–6), protistan phyto– and zooplankton (table entries 7–10) and metazoan mesozooplankton (table entries 11–12) are listed. Although mesozooplankton can often fall to winter densities as low as tens of individuals per cubic metre or less, in the plankton models considered in this thesis, mesozooplankton are only the largest organisms represented by the zooplankton compartment. These population sizes are sufficiently high for the continuity assumption to apply.

The physical environment in which open–ocean plankton systems exist is one in which the surface waters are mixed both by currents within the water itself, and by the action of wind over the surface of the ocean. Wind mixing can be particularly strong, often mixing up to depths of hundreds of metres. Although mixing can create vertical structures, such as Langmuir cells (Bees, Mezić & McGlade, 1997), which may partition plankton, mixing generally acts to homogenise the surface waters to the top of the

Source	Region	Group	Details	Density	
1	Eastern S. Pacific	*Synechococcus* sp.	Bloom maximum	90	$\times 10^9$
1	Central N. Atlantic	*Synechococcus* sp.	Summer depth range	0.1 – 75	$\times 10^9$
1	Sargasso Sea	*Synechococcus* sp.	Autumn depth range	0.1 – 10	$\times 10^9$
2	Equatorial Pacific	*Synechococcus* sp.	HNLC surface waters	10	$\times 10^9$
3	Baltic Sea	Bacterioplankton	Spring–autumn range	0.6 – 2.4	$\times 10^{12}$
4	Buzzards Bay, USA	Bacterioplankton	Annual range	0.3 – 10.9	$\times 10^{12}$
5	Western S. Atlantic	*E. huxleyi*	Spring bloom range	0.2 – 609	$\times 10^6$
6	Central N. Atlantic	*E. huxleyi*	Early summer range	0.03 – 20	$\times 10^9$
7	Buzzards Bay, USA	Dinoflagellates	Annual range	0.5 – 225	$\times 10^6$
8	Buzzards Bay, USA	Tintinnids	Mean annual range	0.4 – 1.2	$\times 10^6$
9	Suruga Bay, Japan	Mesozooplankton	Annual range	0.02 – 4	$\times 10^3$
10	California Current	Mesozooplankton	Early summer range	0 – 2	$\times 10^3$

Table 1.2: Observed ranges of densities for several plankton groups from the literature. Densities measured in cells m^{-3}. Mesozooplankton densities in individuals m^{-3}. Sources : 1. Waterbury *et al.* (1986); 2. Wells, Price & Bruland (1994); 3. Zweifel, Norrman & Hagström (1993); 4. Turner & Borkman (1993); 5. Gayoso (1995); 6. Balch *et al.* (1996); 7. Pierce & Turner (1994a); 8. Pierce & Turner (1994b); 9. Omori & Ikeda (1992); 10. Huntley *et al.* (1995). See text for further details.

seasonal thermocline. As such, the assumption of plankton as evenly mixed through the surface mixed layer is not unreasonable.

The biological processes considered by most plankton models usually occur over time scales ranging from hours up to days. While seasonal cycles and certain biological phenomena occur over obviously longer periods (*e.g.* the duration of the planktivorous Blue Whale's gestation is approximately one year), processes key to the models used in this thesis (cell division, nutrient uptake, grazing, excretion, decomposition, sinking) occur over relatively short periods of time (minutes to hours) and are usually assumed to be adequately represented by exponential rates.

The assumption of identical inhabitants is perhaps the least defensible in the case of the models used in this thesis. The three biological state variables (phytoplankton, zooplankton and bacteria) used by Fasham (1993), are intended to cover a size spectrum of organisms from prokaryotes up to metazoans (approximately 1 μm $\rightarrow$ 1 mm), and a trophic spectrum which includes photosynthetic autotrophs, detritivores, grazers, cannibals, and predators (and frequently organisms which indulge in more than one of these lifestyles). The continuous range of size (which encompasses differences in uptake rates, locomotory ability, vulnerability, *et cetera*) and the variety in life history, nutrient requirement, prey

preference, and behaviour further complicates attempts to describe plankton systems with a small number of functional groups. However, modellers have found that even simple models, which parameterise only the most important ecological processes (*e.g.* photosynthesis, nutrient limitation, grazing, regeneration), can relatively successfully predict certain key features of plankton dynamics (*e.g.* spring blooms – Taylor *et al.*, 1991; recurrent red tide events – Truscott & Brindley, 1994). Some researchers have found the creation of multiple nutrient, phytoplankton or zooplankton compartments necessary to more accurately capture certain features of data (Kremer & Nixon, 1978; Andersen, Nival & Harris, 1987), but the success of simpler models suggests that they still have a role to play in plankton modelling.

1.7.4 The rise of computational power

As already stated, the Lotka–Volterra model introduced earlier is somewhat unrealistic because of several of the assumptions made in its formulation. Although such assumptions may be made where knowledge of the system in question is poor, the avoidance of more realistic (and complicated) forms does allow the model to be rigorously analysed by mathematical techniques.

In the time of Lotka and Volterra, this was an important consideration, since understanding a model depended on being able to deduce its behaviour through analysis. In the latter half of this century, however, the appearance of digital computers, as well as their (so far) relentless rise in processing power, has permitted researchers to formulate models without regard for their analytical solubility. Numerical simulation of these models to examine their behaviour has become commonplace. While simulation is less powerful than rigorous analysis in terms of understanding model behaviour, it does permit the examination of systems which were hitherto intractable for all practical purposes (*e.g.* complex ordinary or partial differential equations, individual based models, spatially–extended systems). The work contained in this thesis, for instance, has relied almost entirely upon numerical solutions of ODE models of the plankton ecosystem.

1.7.5 Plankton modelling

The modelling of plankton populations has a history stretching back to the work of Gordon Riley in the 1940s. Riley, in common with many of his contemporaries in biological oceanography, was interested in the phenomenon of the spring phytoplankton bloom. Using the ideas of Gran about the stabilisation of the surface waters in spring, he produced a quantitative model of the phytoplankton dynamics in the North Atlantic (Riley, Stommel & Bumpus, 1949). This work was expanded later by Sverdrup (1953), but remains the basis of models of the spring phytoplankton bloom (including those in this thesis). Mann & Lazier (1991) and Fasham (1993) provide some further background to the origins of plankton modelling.

Latter–day modelling efforts address plankton behaviour across the full range of space and/or time. There is also a substantial body of more abstract theoretical work (*e.g.* Bascompte, Solé & Valls, 1992;

Malchow, 1994; Truscott & Brindley, 1994; Rose, 1998), which explores processes from a mathematical perspective. The work in this thesis focuses on non–spatial models, and their behaviour across annual cycles of physical forcing. In contrast, other work (*e.g.* Davidson, Cunningham & Flynn, 1993; Davidson & Cunningham, 1996) has focussed on resolving behaviour at the shorter time scales of hours to days.

As indicated, there is also work which additionally focuses on spatial elements of plankton dynamics. Again, such work covers a wide range of scales, from metres to kilometres (*e.g.* Pascual, 1993; Malchow, 1994; Bees, Mezić & McGlade, 1997), all the way to full ocean basin simulations in general circulation models (GCMs) (*e.g.* Wroblewski, 1989; Sarmiento *et al.*, 1993). Recently there has been the appearance of models in which the life histories of individual plankters are followed in both space and time (Woods & Barkmann, 1995).

The different models outlined above are often used to answer research questions which cannot be settled, or reasonably addressed, from observations. For instance, large scale GCM simulations are normally concerned with estimating total oceanic productivity over the ocean basin in question. Models at the smaller end of the spatial scale are often used to predict the consequences to plankton population dynamics of small to medium scale physical processes such as diffusion[14], advection or Langmuir circulation. Models (usually non–spatial ones similar to those in this thesis) are also commonly used to examine specific ecological questions. For example, several researchers have investigated the occurrence of so–called "High Nutrient, Low Chlorophyll" (HNLC) regions. Since nutrients normally limit phytoplankton growth, these regions (where nutrients, for no obvious reason, go unused by phytoplankton) have long been considered anomalous, and have attracted several modelling studies (Evans & Parslow, 1985; Frost, 1987; Steele & Henderson, 1992; Fasham, 1995) which attempt to explicate them.

The research in this thesis centres around the nitrogen ecosystem model of the oceanic mixed layer described by Fasham (1993) . This model is described, mathematically and ecologically, in Chapter 2. The chapter also aims to place this model into context within plankton modelling by comparing it with several other plankton models.

1.8 Summary

This chapter has attempted to lay a foundation for the biology and physics which underlie the models that form the basis of this thesis. Additionally, sections have aimed to explain (and defend) the simplifications of this foundation by models. Models are, by definition, abstractions of reality.

[14] The term "diffusion" is often used to describe processes such as active swimming, advection and wind–mixing which, as far as modelling is concerned, are analogous to true molecular diffusion.

Chapter 2

Introducing the Fasham (1993) model

Give me four parameters and I'll draw you an elephant. Give me five, and I'll waggle its trunk.

– Linus Pauling (1901–1994)

2.1 Introduction

The Fasham (1993) model of the marine ecosystem is one of several which aim to describe the seasonal dynamics of the open–ocean planktonic ecosystem of the North Atlantic (Wroblewski, 1989; Taylor *et al.*, 1991; Bauer *et al.*, 1993; Taylor *et al.*, 1993; Dadou *et al.*, 1996). Although originally proposed in Fasham, Ducklow & McKelvie (1990), several refinements (primarily changes to the functional responses of plankton mortality and predation) have subsequently been made, leading to the choice of Fasham (1993) as the model upon which the research detailed in this thesis is based.

Although the model has several failings, some of which have been addressed in subsequent papers (Fasham, 1995; Fasham & Evans, 1995), it has several features which recommend it :

(i) It is a relatively detailed model of the ecosystem, incorporating the most important biotic compartments plus several abiotic and detritus compartments;

(ii) It takes account of two of the more significant physical aspects of the ocean, vertical mixing and solar irradiance;

(iii) Despite having seven compartments and around thirty parameters (many of which have not been evaluated in the field or by experimental work, and some of which cannot reasonably be estimated at all), it is still simpler than some of the more detailed ecosystem models (Kremer & Nixon, 1978; Taylor *et al.*, 1993).

In this chapter, the Fasham (1993) model is introduced. Each of the model's seven equations and their derivations are detailed. The model is also compared with several other popular plankton models. This comparison is important because the paucity of data and the lack of any mechanistic theories underlying the ecological interactions under study, often makes the choice of model appear more a case of personal preference than objective merit. Steele and Henderson (1992) recently underlined this in a review of the various predation terms used by modellers to "close" models.

2.2 Model equations

The Fasham (1993) model describes the open–ocean plankton ecosystem with seven coupled ordinary differential equations (ODEs). These describe the time–evolution of mixed layer concentrations of phytoplankton (P), zooplankton (Z), bacteria (B), detritus or particulate organic nitrogen (D), nitrate (N_n), ammonium (N_r), and dissolved organic nitrogen (N_d). The mixed layer has a depth of M.

$$\begin{aligned}
\frac{dP}{dt} &= (1-\gamma)\sigma(t,M,P,N_n,N_r)P - G_1 - \frac{\mu_1 P^2}{k_5+P} - \frac{(m+h^+(t))P}{M} \\
&= growth - grazing\,loss - natural\,mortality - mixing\,and\,dilution
\end{aligned}$$

$$\begin{aligned}
\frac{dZ}{dt} &= \beta_1 G_1 + \beta_2 G_2 + \beta_3 G_3 - \frac{\mu_2 Z^2}{k_6+Z} - \frac{h(t)Z}{M} \\
&= grazed\,P + grazed\,B + grazed\,D - predation - dilution\,and\,concentration
\end{aligned}$$

$$\begin{aligned}
\frac{dB}{dt} &= U_1 + U_2 - G_2 - \mu_3 B - \frac{(m+h^+(t))B}{M} \\
&= DON\,uptake + ammonium\,uptake - grazing\,loss - excretion - mixing\,and\,dilution
\end{aligned}$$

$$\begin{aligned}
\frac{dD}{dt} &= (1-\beta_1)G_1 + (1-\beta_2)G_2 - \beta_3 G_3 - \mu_4 D + \frac{\mu_1 P^2}{k_5+P} - \frac{(m+V+h^+(t))D}{M} \\
&= lost\,grazed\,P + lost\,grazed\,B - grazing\,loss - breakdown + P\,mortality \\
&\quad - mixing,\,dilution\,and\,sinking
\end{aligned}$$

$$\begin{aligned}
\frac{dN_n}{dt} &= -J(t,M,P)Q_1(N_n,N_r)P + \frac{(m+h^+(t))}{M}(N_0 - N_n) \\
&= -loss\,to\,P\,growth + entrainment\,from\,the\,deep\,ocean
\end{aligned}$$

$$\begin{aligned}
\frac{dN_r}{dt} &= -J(t,M,P)Q_2(N_r)P - U_2 + \mu_3 B + \frac{\epsilon\mu_2 Z^2}{k_6+Z} - \frac{(m+h^+(t))N_r}{M} \\
&= -loss\,to\,P\,growth - loss\,to\,B\,growth + B\,excretion + Z\,mortality \\
&\quad - mixing\,and\,dilution
\end{aligned}$$

$$\begin{aligned}
\frac{dN_d}{dt} &= \gamma\sigma(t,M,P,N_n,N_r)P + \mu_4 D + \frac{\delta\mu_2 Z^2}{k_6+Z} - U_1 - \frac{(m+h^+(t))N_d}{M} \\
&= exuded\,photosynthate + D\,breakdown + Z\,mortality - loss\,to\,B\,growth \\
&\quad - mixing\,and\,dilution
\end{aligned}$$

The coupling between the equations takes the form of flows of the model currency, nitrogen, between the compartments (currency is expressed here in volumetric terms, mmol N m^{-3}). These flows represent biological and physical processes such as grazing, nutrient uptake and mixing. Table 2.1 lists the defini-

Function	Ecological process	Definition
σ	Phytoplankton growth	$J(t,M,P)Q(N_n,N_r)$
$J(t,M,P)$	Light–limited phytoplankton growth	$\frac{1}{M}\int_0^M F(I_0(t)\exp\{-(k_w+k_cP)z\})\,dz$
$F(I)$	Photosynthesis–irradiance curve	$\frac{V_p\alpha I}{\sqrt{({V_p}^2+\alpha^2I^2)}}$
$Q(N_n,N_r)$	Nutrient–limited phytoplankton growth	$Q_1(N_n,N_r)+Q_2(N_r)$
$Q_1(N_n,N_r)$	Nitrate limitation	$\frac{N_n\exp\{-\psi N_r\}}{k_1+N_n}$
$Q_2(N_r)$	Ammonium limitation	$\frac{N_r}{k_2+N_r}$
G_1	Zooplankton grazing on phytoplankton	$\frac{gp_1P^2Z}{k_3(p_1P+p_2B+p_3D)+p_1P^2+p_2B^2+p_3D^2}$
G_2	Zooplankton grazing on bacteria	$\frac{gp_2B^2Z}{k_3(p_1P+p_2B+p_3D)+p_1P^2+p_2B^2+p_3D^2}$
G_3	Zooplankton grazing on detritus	$\frac{gp_3D^2Z}{k_3(p_1P+p_2B+p_3D)+p_1P^2+p_2B^2+p_3D^2}$
S	Most limiting bacterial growth substrate	$\min(N_r,\,\eta N_d)$
U_1	Bacterial uptake of DON	$\frac{V_bBN_d}{k_4+S+N_d}$
U_2	Bacterial uptake of ammonium	$\frac{V_bBS}{k_4+S+N_d}$

Table 2.1: Model functions, their definitions and a description of the ecological processes concerned.

tions and decriptions of the ecological processes not defined explicitly in the equations given previously. Table 2.2 lists all of the model parameters, their definitions and units, and their baseline values from Fasham (1993). Two of the model parameters, V_p and N_0, are given two values in the table. These refer to two geographical locations in the North Atlantic ocean at which the model was simulated by Fasham (1993) : Ocean Weather Station (OWS) "India" (59° N, 19° W) and Bermuda Station "S" (30° 10' N, 64° 30' W). Parameters marked with an asterisk are those which were either used to "fine–tune" the model, or for which there were no good estimates (or even both).

Often a series of essentially similar processes are summed into a single term to reduce model complexity. For example, the natural mortality term for phytoplankton represents a series of loss processes including viral mortality, cell starvation and natural cell death.

The choice of nitrogen as model currency reflects its position as the most limiting major nutrient. Whilst

this is not beyond dispute, especially with respect to recent interest in micronutrients such as iron (Martin & Fitzwater, 1988; Fasham, 1995; Behrenfeld *et al.*, 1996), it is generally accepted, at least within the context of the North Atlantic.

The mixed layer is assumed to be sufficiently well mixed that the model components can be represented by a constant, homogeneous concentration throughout it (*i.e.* that physical mixing processes occur at rates which are fast when compared to the growth rates of the biological components of the model). Consequently, vertical space is represented only implicitly in the phytoplankton light–limited growth term and in the loss of material through mixing with the deep ocean. Although entirely ignored here, horizontal space has been introduced into the Fasham (1993) model in more recent work (Fasham *et al.*, 1993; Sarmiento *et al.*, 1993).

In addition to the interactions between the equations, all of the compartments are forced by one or both of the two forcing functions : the annual cycles of mixed–layer depth and solar irradiance. Values of these are interpolated from data and calculated using standard astronomical formulae respectively.

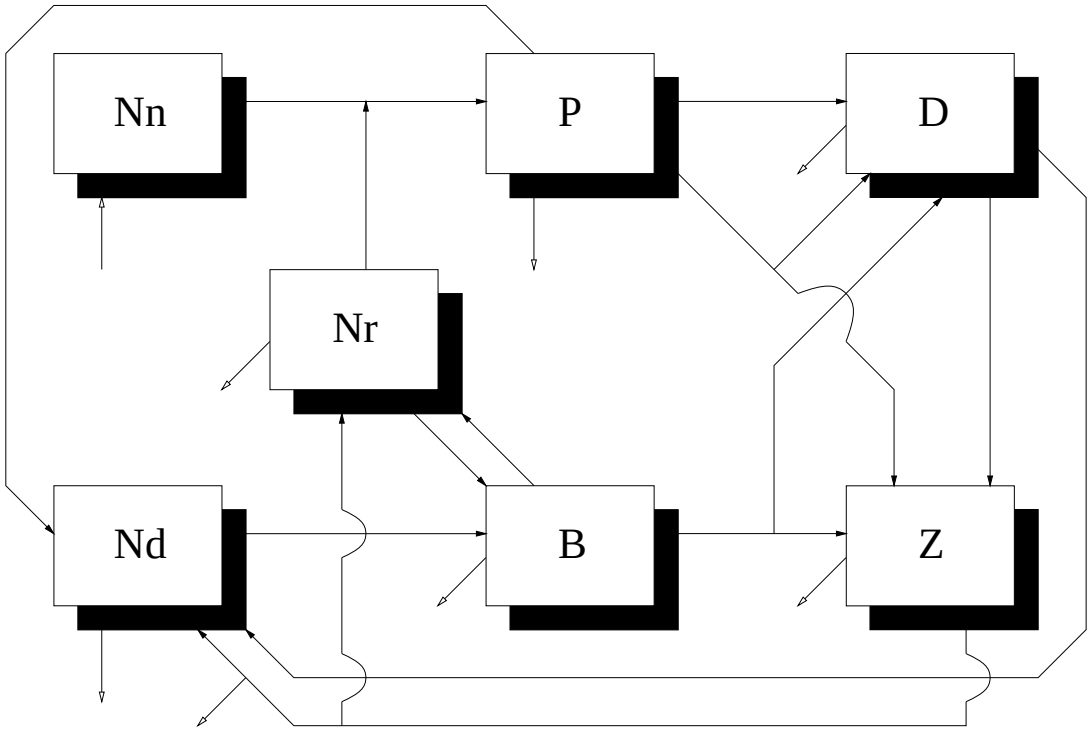

Figure 2.1: Diagrammatic representation of the Fasham (1993) model. All pathways between compartments have been shown. Empty arrow–headed flows represent flows into or out of the modelled mixed–layer system

Figure 2.1 illustrates the basic structure of the full ecosystem model. The seven compartments are linked by various ecological and chemical pathways. The model is non–conservative (unlike the ZPN model

Symbol		Parameter	Value	Units
C		Cloudiness	4	oktas
a		Air–water albedo	0.05	
λ		Ratio of PAR to total irradiance	0.43	
k_w		Attenuation coefficient of downwelling irradiance	0.04	m^{-1}
k_c		Phytoplankton self–shading coefficient	0.03	m^2 (mmol N)$^{-1}$
V_p		Phytoplankton maximum growth rate (India)	1.25	d^{-1}
V_p		Phytoplankton maximum growth rate (Bermuda)	2.90	d^{-1}
α		Initial slope of P–I curve	0.025	(W m^{-2})$^{-1}$ d^{-1}
γ		Phytoplankton exudation fraction	0.05	
ψ		Nitrate uptake ammonium inhibition parameter	1.5	(mmol N m^{-3})$^{-1}$
k_1		Nitrate uptake half–saturation constant	0.5	mmol N m^{-3}
k_2		Ammonium uptake half–saturation constant	0.5	mmol N m^{-3}
k_3		Zooplankton feeding half–saturation constant	1.0	mmol N m^{-3}
k_4		Bacterial half–saturation uptake constant	0.5	mmol N m^{-3}
k_5	*	Phytoplankton mortality half–saturation constant	0.2	mmol N m^{-3}
k_6	*	Zooplankton loss rate half–saturation constant	0.2	mmol N m^{-3}
μ_1	*	Phytoplankton maximum mortality	0.05	d^{-1}
μ_2	*	Zooplankton maximum loss rate	0.325	d^{-1}
μ_3	*	Bacterial excretion rate	0.05	d^{-1}
μ_4		Detrital breakdown rate	0.05	d^{-1}
$\beta_{1,2,3}$		Zooplankton feeding efficiencies	0.75	
$p_{1,2,3}$	*	Zooplankton feeding preferences	0.50, 0.25, 0.25	
g		Zooplankton maximum ingestion rate	1.0	d^{-1}
ϵ	*	Fraction of zooplankton losses going to ammonium	0.70	
δ	*	Fraction of zooplankton losses going to DON	0.20	
V_b		Bacterial maximum uptake rate	2.0	d^{-1}
η		Ratio of ammonium:DON uptake for bacteria	0.6	
V	*	Detrital sinking rate	10	m d^{-1}
N_0		Subthermocline nitrate concentration (India)	12	mmol N m^{-3}
N_0		Subthermocline nitrate concentration (Bermuda)	2	mmol N m^{-3}
m	*	Cross–thermocline mixing rate	0.01	m d^{-1}

Table 2.2: The model parameters and their values as used in Fasham (1993). Parameters which were used to "fine–tune" the model and/or there are no good estimates for are marked with an asterisk.

of Wroblewski, 1989), and nitrogen can enter or leave the modelled mixed layer via a number of flow routes. These are indicated on the flow diagram by empty arrow–headed flows.

The following sections describe the seven equations and the two forcing functions used in the model.

2.2.1 Phytoplankton

The terms in this equation encompass, respectively, phytoplankton growth, phytoplankton loss to grazing zooplankton, natural mortality and a mixing/dilution loss. Terminology follows that set in Fasham (1993) and summarised in tables 2.1 and 2.2.

$$\frac{dP}{dt} = (1-\gamma)\sigma(t, M, P, N_n, N_r)P - G_1 - \frac{\mu_1 P^2}{k_5 + P} - \frac{(m + h^+(t))P}{M} \tag{2.1}$$

where,

$$\sigma = J(t, M, P)Q(N_n, N_r) \tag{2.2}$$

Phytoplankton growth, σ, is limited by both irradiance, I, and nutrient availability. It is described by a multiplicative relationship between the maximum possible growth in the given depth–integrated irradiance field, J, and the limitation imposed by the ambient nutrient concentrations, Q.

$$J(t, M, P) = 2\frac{1}{M}\int_0^{\tau}\int_0^{M} F(I_0(t)\exp\{-(k_w + k_c P)z\})\,dz\,dt \tag{2.3}$$

where,

$$F(I) = \frac{V_p \alpha I}{\sqrt{({V_p}^2 + \alpha^2 I^2)}} \tag{2.4}$$

Maximum possible irradiance–limited growth, J, is calculated by integrating surface irradiance both down through the water column (dz) to the top of the thermocline, and through the day (dt; where τ takes the value half of the day length). $I_0(t)$ is the quantity of irradiance just below the surface of the ocean.

Depth–integration attenuates the irradiance exponentially due to absorption by the photosynthetic pigments of the phytoplankton, k_c, and by the sea water itself, k_w. Although ignored in this model, particulate material present in sea water (including particulate organic material) plays a significant role in the submarine absorption of radiation (Garver *et al.*, 1994). Both k_w and k_c were assigned average values inside the ranges measured in the field. Note that irradiance is not spectrally resolved here, and is essentially treated as if it consists only of photons which are attenuatated at some average rate down the water column (*i.e.* k_w is assigned a value of 0.04 m^{-1} which falls between the comparable values of 0.4 and 0.004 m^{-1} for red and blue light respectively). Since vertical space is not represented explicitly in this model, the mixed layer is assumed to be sufficiently homogeneous for the phytoplankton (as well as the other model compartments) to have a uniform vertical distribution. Figure 2.2 shows the modelled decline of irradiance with depth for a water column at OWS "India" during the spring bloom. By a depth of 10 m, irradiance has already fallen to less than 50% of that at the surface.

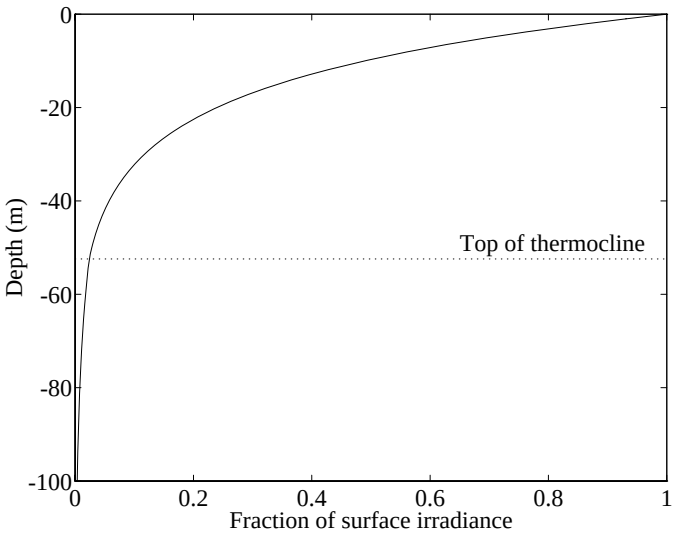

Figure 2.2: Modelled attenuation of irradiance with depth for a water column at OWS "India" during a simulated spring bloom (day 143). The top of the thermocline (and bottom of the mixed layer) on this day is marked. Above this, attenuation of irradiance is a combination of absorption by sea water itself and by the photosynthetic pigments of the phytoplankton.

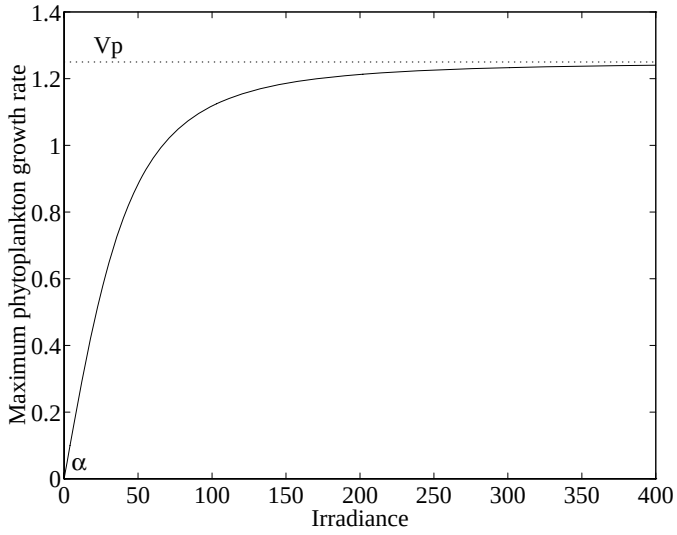

Figure 2.3: The photosynthesis–irradiance (or P–I) curve used in this model. The shape of the curve is controlled here by two parameters; V_p, the maximum phytoplankton growth rate, and α, the initial slope of the curve. Irradiance in W m^{-2}, growth rate in d^{-1}.

Given the submarine irradiance field, a standard empirical function, $F(I)$, is used to describe the photosynthesis–irradiance (P–I) curve. This uses the maximum phytoplankton growth rate, V_p, and the initial slope of the P–I curve, α, together with irradiance to calculate growth. Figure 2.3 illustrates

this relationship of maximum phytoplankton growth to irradiance for OWS "India" parameter values.

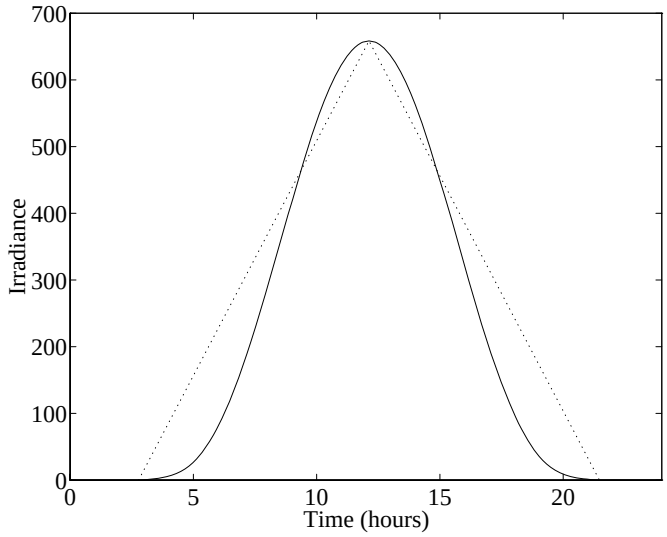

Figure 2.4: The pattern of sea–surface irradiance calculated for day 173 (mid–summers day) of an OWS "India" simulation (solid), and that assumed by the analytical equation derived by Evans & Parslow (1985) (dotted). Irradiance in W m^{-2}.

Drawing on a large number of studies, Eppley (1972) derived the following empirical relationship between maximum phytoplankton growth and temperature,

$$V_p = 0.6\,(1.066)^T \tag{2.5}$$

where T is the temperature in degrees Celsius. This equation was used by Fasham (1993) to determine average values of V_p across the year for both OWS "India" and Bermuda Station "S". The parameter α was assigned the average of measurements made by Trevor Platt's group (Bedford Institute of Oceanography, Dartmouth, Nova Scotia, Canada) in the Sargasso Sea (Bermuda Station "S" shares the physical and biological characteristics found in the Sargasso Sea).

In Fasham (1993), light–limited growth is integrated analytically, both down the water column and through the day, using a formulation derived by Evans & Parslow (1985). This formulation assumes that irradiance, $I_0(t)$, forms a triangular shape, rising linearly from 0 at dawn to a maximum at noon and then declining to 0 at dusk. It also assumes that, through a given day, the phytoplankton population remains constant. Figure 2.4 illustrates a single day's approximated pattern of sea–surface irradiance and the irradiance assumption used in the analytical form. (The work in this thesis makes use of a slightly modified version of this integral. Full details of the approach used are described in Chapter 3).

Nitrogenous nutrients are represented in this model by both nitrate (NO_3^-) and ammonium (NH_4^+). In both cases the basic Michaelis–Menten functional form is adopted for uptake kinetics. This form is hy-

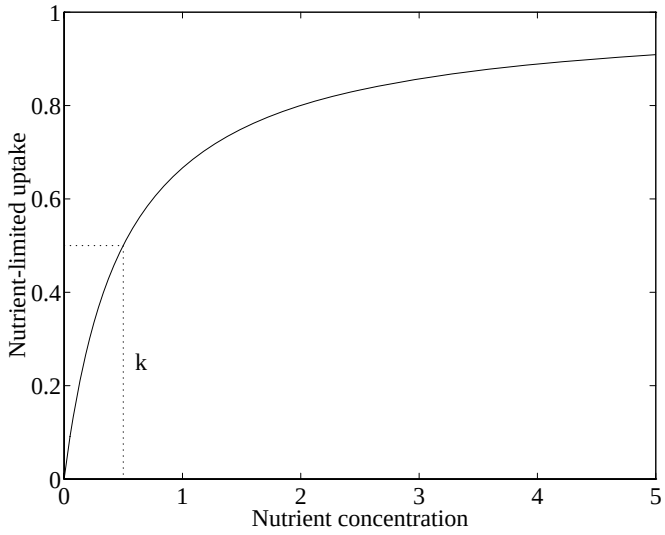

Figure 2.5: The Michaelis–Menten curve for uptake of a nutrient with a half–saturation constant, k, of 0.5 mmol N m^{-3} (solid). The dotted lines mark uptake of half the maximum rate at the specified value of k. Concentration in mmol N m^{-3}.

perbolic and requires a half–saturation term (k_1 and k_2 for nitrate and ammonium respectively) which specifies the concentration of nutrient at which uptake is half the maximum rate. Figure 2.5 illustrates a standard Michaelis–Menten curve.

However, for energetic reasons related to the charge of these ionic species, ammonium is taken up preferrentially by phytoplankton, and a phenomenon of ammonium inhibition of nitrate uptake has been observed (Dortch, 1990, provides an exhaustive review of the phenomenon, although she concludes that it is a much smaller effect than is commonly believed). This effect is taken account of by limiting nitrate uptake with a negative exponential of ammonium concentration (modified by the coefficient, ψ). The nutrient–limitation part of phytoplankton growth then looks as follows,

$$Q(N_n, N_r) = Q_1(N_n, N_r) + Q_2(N_r) = \frac{N_n \exp\{-\psi N_r\}}{k_1 + N_n} + \frac{N_r}{k_2 + N_r} \tag{2.6}$$

The half–saturation constants assigned by Fasham (1993) fall within the observed range, although recent work by Harrison, Harris & Irwin (1996) measured half–saturation constants an order of magnitude smaller than had previously been calculated ($k_1 \simeq 0.023$, $k_2 \simeq 0.032$). The parameter ψ was assigned a value based on the estimates of Wroblewski (1977).

Fasham (1995) examined this choice of formulation, and found that it could be more adequately replaced by an uptake model in which ammonium inhibition is only implicitly parameterised (by means of a considerably lower k_2 value). This form is not reproduced here, but the significance of this choice is examined in Chapter 3. More recent work by Flynn, Fasham & Hipkin (1997) includes an explicit compartment for intracellular glutamine (an early product of nitrogen after its assimilation into a cell),

and uses this compartment in modelling the interaction between nitrate and ammonium uptake.

The two nutrient limitation terms in equation 2.6 are added together to give total nutrient limitation. A popular alternative to this, is to set total nutrient limitation to that of the most limiting nutrient (Kremer & Nixon, 1978; Andersen *et al.*, 1987). O'Neill *et al.* (1989) provide an overview of the issue of multiple nutrient limitation in ecological models.

Phytoplankton exude a fraction of their net production as dissolved organic material. The amount varies in space and time and by species, and estimates of the percentage of primary production exuded range up to 70% (Moloney & Field, 1991). However, despite the potential significance of exudation, the reasons for it are not entirely clear. Several suggestions have been made including exudation as a means to regulate cell osmotic potential, to ensure the correct stoichiometric ratios of different elements without "switching off" the photosynthetic apparatus, and to establish a local bacterial community. This last hypothesis suggests that a local bacterial population may aid phytoplankton growth by regenerating trace elements, or reducing phytoplankton viral mortality by acting as an alternative adsorbing surface for viral particles (Murray, 1995). In this model, a constant fraction of DON exudation, γ, is assumed to be exuded. Fasham (1993) assigned γ a conservative estimate of 5% based partially on the measured values of γ.

As stated previously, the phytoplankton natural mortality term is really a hybrid of several loss processes. These include viral mortality, cell death due to an imbalance in respiration and photosynthesis and general cell death due to senescence and accidents. In Fasham, Ducklow & McKelvie (1990) (and many other models), this term is assigned a linear form. However, the term has been made non–linear here since disease mortality is likely to be density dependent, and because the corresponding zooplankton mortality term is similarly of Michaelis–Menten type (it includes predation losses, also likely to be density dependent). Since estimates of natural phytoplankton mortality are exceedingly rare, the values of the parameters μ_1 and k_5 used here were tuned by Fasham (1993) to better estimate annual net primary production.

As described in the later section on the mixed layer dynamics, the final term controls phytoplankton losses due to mixing out of the upper mixed layer and dilution by entrainment of formerly subthermocline waters when the mixed layer deepens.

2.2.2 Zooplankton

The terms in this equation encompass, respectively, grazing on phytoplankton, grazing on bacteria, grazing on detritus, predation/excretion losses and a dilution/concentration term.

$$\frac{dZ}{dt} = \beta_1 G_1 + \beta_2 G_2 + \beta_3 G_3 - \frac{\mu_2 Z^2}{k_6 + Z} - \frac{h(t)Z}{M} \tag{2.7}$$

where,

$$G_1 = \frac{gp_1P^2Z}{k_3(p_1P + p_2B + p_3D) + p_1P^2 + p_2B^2 + p_3D^2} \tag{2.8}$$

(there are analogous expressions for G_2 and G_3; see table 2.1)

As with the phytoplankton compartment, the zooplankton compartment attempts to model a diverse range of species (from many different phyla) with a single ODE. The equation above describes an organism which is a combination of herbivore, bacteriovore and detritivore. Although there is evidence that protistan microzooplankton can be of considerable importance (Burkill *et al.*,1993, found that microzooplankton grazing of phytoplankton was more than an order of magnitude higher than that of copepod mesozooplankton), Fasham (1993) assumed a more copepod–like herbivorous zooplankter and based parameter values appropriately (Evans & Parslow, 1985; and references therein).

The grazing terms used here (G_1, G_2 and G_3) are an adapted form of the Michaelis–Menten equation. The derivation below shows how this form was arrived at and how, in principle, it can be extended for n prey species.

$$\begin{aligned} Grazed &= \frac{gZF}{k_3 + F} \\ F &= p_1^*X_1 + p_2^*X_2 + \ldots + p_n^*X_n \end{aligned}$$

then,

$$\begin{aligned} Grazed &= \frac{gZ(p_1^*X_1 + p_2^*X_2 + \ldots + p_n^*X_n)}{k_3 + p_1^*X_1 + p_2^*X_2 + \ldots + p_n^*X_n} \\ Grazed &= \frac{gZp_1^*X_1}{k_3 + p_1^*X_1 + p_2^*X_2 + \ldots + p_n^*X_n} + \frac{gZp_2^*X_2}{k_3 + p_1^*X_1 + p_2^*X_2 + \ldots + p_n^*X_n} + \ldots + \\ &\quad \frac{gZp_n^*X_n}{k_3 + p_1^*X_1 + p_2^*X_2 + \ldots + p_n^*X_n} \end{aligned}$$

At this point then, from an initial Michaelis–Menten form, for each prey species (X_x) there is a term to describe the grazing pressure exerted on it. This term is related to the feeding preference (p_x^*) the zooplankton (Z) have for the item, and the quantities of alternate prey (F is total available food, scaled with feeding preferences). The g and k_3 terms define the maximum grazing rate and the half–saturation constant of grazing respectively.

As already pointed out, the zooplankton compartment was created to encompass a wide variety of zooplankton species. In order to parameterise the changing composition of the zooplankton compartment, and consequently its changing feeding preferences, the feeding preferences were allowed to vary with food availability.

$$p_1^* = \frac{p_1X_1}{p_1X_1 + p_2X_2 + \ldots + p_nX_n}$$

Where p_x is a nominal preference value (*i.e.* the parameter listed in the parameter values table). Substituting this into the *Grazed* equation above yields the final form used in the models.

$$Grazed = \frac{gZ\left(\frac{p_1X_1}{p_1X_1 + p_2X_2 + \ldots + p_nX_n}X_1 + \ldots + \frac{p_nX_n}{p_1X_1 + p_2X_2 + \ldots + p_nX_n}X_n\right)}{k_3 + \frac{p_1X_1}{p_1X_1 + p_2X_2 + \ldots + p_nX_n}X_1 + \ldots + \frac{p_nX_n}{p_1X_1 + p_2X_2 + \ldots + p_nX_n}X_n}$$

$$Grazed = \frac{gZp_1X_1^2}{k_3(p_1X_1 + p_2X_2 + \ldots + p_nX_n) + p_1X_1^2 + p_2X_2^2 + \ldots + p_nX_n^2} + \ldots + \frac{gZp_nX_n^2}{k_3(p_1X_1 + p_2X_2 + \ldots + p_nX_n) + p_1X_1^2 + p_2X_2^2 + \ldots + p_nX_n^2}$$

Such a form "switches" the zooplankton compartment between prey types and attempts to mimic the seasonally changing nature of the zooplankton species assemblage.

To account for zooplankton assimilation/feeding inefficiency, constant fractions (β_1, β_2 and β_3) of material ingested were assimilated, with the remainder lost to the detritus compartment. The assimilation efficiency was assumed constant between the three prey types and assigned a value from measurements.

Excretion and predation are combined here in a single loss term. This term is also of Michaelis–Menten form and it acts partly as a closure term for the system since predation exports nitrogen to unmodelled higher predators. A fraction of this flow into predators finds itself ultimately in faecal pellets or dead organisms which sink out of the mixed layer. The remainder is returned to the modelled system as ammonium and DON. The allocation between these compartments is dictated by the constant fractions ϵ and δ respectively.

The form of system closure has attracted considerable attention in recent years (Steele & Henderson, 1992; Fasham, 1995; Edwards, 1997), but observationally and experimentally the best choice of term is, at this time, unclear. For this reason, the zooplankton loss parameters, μ_2 and k_6, were used by Fasham (1993) to "fine–tune" the model so that summer nitrate levels fell within the observed range.

Finally, as described more fully later, zooplankton are assumed here to be capable of migrating and remaining in the mixed layer even during its shallowing and deepening. The final term ensures this by concentrating and diluting them appropriately.

2.2.3 Bacteria

The terms in this equation encompass, respectively, DON uptake, ammonium uptake, loss to zooplankton grazing, excretion and a mixing/dilution loss.

$$\frac{dB}{dt} = U_1 + U_2 - G_2 - \mu_3 B - \frac{(m + h^+(t))B}{M} \tag{2.9}$$

where,

$$U_1 = \frac{V_b B N_d}{k_4 + S + N_d} \tag{2.10}$$

and,

$$U_2 = \frac{V_b B S}{k_4 + S + N_d} \tag{2.11}$$

where,

$$S = \min(N_r, \eta N_d) \tag{2.12}$$

Bacteria here utilise both DON and ammonium as growth substrates. As mentioned in Chapter 1, heterotrophic bacteria are also involved in the decay of detritus. However, the bacteria considered here are free bacteria and are not associated with detritus, hence the assignment of growth substrates here (the breakdown term in the detritus equation may be seen as an implicit representation of attached bacteria).

The uptake of DON and ammonium here is controlled again by Michaelis–Menten terms. However, these terms are somewhat different here since bacterial growth requires both substrates for different metabolic purposes. While dissolved organic material contains nitrogen, heterotrophic bacteria (which this compartment represents) utilise DON as a source of carbon (for their energetic requirements). Ammonium is thought to be mostly used as a source of nitrogen for protein synthesis. Consequently, both have to be acquired for normal bacterial growth.

To account for this, the uptake of both substrates is related to the concentration of the most–limiting substrate, S. This is quite different to the situation in the phytoplankton compartment where uptake rates of nitrate and ammonium are (mostly) independent, since both substrates are used interchangeably for similar metabolic purposes.

The concentration of DON is modified by the coefficient η to ensure that a constant bacterial C:N ratio is maintained, and to account for the efficiencies of carbon and nitrogen metabolism. Fasham (1993) assumed that the gross growth efficiencies were the same for carbon and nitrogen, and used estimates of the C:N ratios of DON and bacteria to determine a value for η. The maximum rate of bacterial growth, V_b, was chosen as typical of oceanic bacteria.

Unlike the comparable terms in the phytoplankton and zooplankton equations, bacterial excretion and loss is modelled here as a constant, linear rate, μ_3. Since bacteria are subject to similar loss and mortality processes, it is arguable that their loss terms should be modelled similarly. Bacterial viruses (also known as *phages*), for instance, are known to often play an important role in these dynamics (Suttle, 1994; Weinbauer & Peduzzi, 1995). However, for simplicity a linear rate was chosen and this has been retained here. Since reliable estimates of μ_3 were unavailable, Fasham (1993) varied μ_3 until simulated bacterial growth efficiencies were obtained that were comparable with measurements.

As in the phytoplankton equation, bacteria are assumed to be unable to prevent their loss from the mixed layer and the final term accounts for detrainment losses, mixing out and dilution.

2.2.4 Detritus (particulate organic nitrogen)

The terms in this equation encompass, respectively, inputs from the inefficiency of zooplankton grazing on phytoplankton and bacteria, loss to zooplankton grazing, breakdown to soluble compounds, inputs

of dead phytoplankton cells and mixing/dilution/sinking.

$$\frac{dD}{dt} = (1-\beta_1)G_1 + (1-\beta_2)G_2 - \beta_3 G_3 - \mu_4 D + \frac{\mu_1 P^2}{k_5 + P} - \frac{(m + V + h^+(t))D}{M} \tag{2.13}$$

The majority of these terms have been defined in previous equations and the reader is directed back to earlier sections for their derivation and biological meaning.

Zooplankton feeding inefficiency ("sloppy feeding" and digestive inefficiencies) account for the majority of sources for detritus. The zooplankton graze detritus as well, and this inefficiency extends here (hence why zooplankton only graze $\beta_3 G_3$).

Detritus breaks down to DON at a constant rate, μ_4. The linear form of this rate is less objectionable here since detritus is not subject to the density dependent effects (viral infection, predation) which afflict the previous three compartments. The rate was chosen within the range of observations, and gives a reasonable estimate of bacterial production.

The nature of the inputs to the detrital compartment mean that it consists of relatively large particles of material (aggregated cells, faecal pellets, *et cetera*). These larger particles are assumed to sink out of the mixed layer, and the final sinking/mixing/dilution loss term is modified to incorporate a sinking velocity, V. Choosing a value for this process is complicated by differently–sized particles sinking at different velocities, and by the difficulty in separating living particles from detrital ones when measurements are made. Using a regression of particle flux against particle density data (*i.e.* how much sinks out versus how much there is in the water column), Fasham estimated a sinking velocity of 4 m d^{-1}. This estimate was used to suggest an appropriate magnitude for the parameter, and then a value was chosen on the basis of model performance.

As indicated in Chapter 1, sinking fluxes out of the mixed layer are of interest biogeochemically since some of the material lost in this way is ultimately buried geologically.

2.2.5 Nitrate

The terms in this equation encompass, respectively, losses due to phytoplankton uptake and entrainment/mixing gains.

$$\frac{dN_n}{dt} = -J(t, M, P)Q_1(N_n, N_r)P + \frac{(m + h^+(t))}{M}(N_0 - N_n) \tag{2.14}$$

Nitrate is assumed in the model to be at non–zero concentrations below the thermocline. All other model state variables are assumed to return to nitrate through chemical and biological degradation and are set to zero concentration below the mixed layer. The actual value of deep nitrate is strongly related to latitude (Strass & Woods, 1991).

Although in Fasham (1993) and in this work, the subthermocline concentration, N_0, has been assumed to be constant with time and mixed–layer depth, other authors (Frost, 1987; Fasham, 1995) have considered more realistic formulations.

2.2.6 Ammonium

The terms in this equation encompass, respectively, losses due to phytoplankton uptake, losses due to bacterial uptake, bacterial excretion, zooplankton inputs and a mixing/dilution loss.

$$\frac{dN_r}{dt} = -J(t,M,P)Q_2(N_r)P - U_2 + \mu_3 B + \frac{\epsilon\mu_2 Z^2}{k_6+Z} - \frac{(m+h^+(t))N_r}{M} \tag{2.15}$$

As such, the terms here represent the origins or end points of flows of nitrogen described in previous equations.

2.2.7 Dissolved organic nitrogen (DON)

The terms in this equation encompass, respectively, phytoplankton exudation, detrital breakdown, zooplankton inputs, losses due to bacterial uptake and a mixing/dilution loss.

$$\frac{dN_d}{dt} = \gamma\sigma(t,M,P,N_n,N_r)P + \mu_4 D + \frac{\delta\mu_2 Z^2}{k_6+Z} - U_1 - \frac{(m+h^+(t))N_d}{M} \tag{2.16}$$

Similarly to the ammonium equation, the terms here refer to flows described in previous equations.

2.3 Forcing functions

In addition to the dynamical behaviour of the model, Fasham (1993) uses two forcing functions to drive the system. Both represent physical processes which are, it is assumed, unaffected by the biological dynamics of the upper mixed layer. Lovelock (1989) suggests a mechanism whereby marine phytoplankton may influence cloud seeding patterns (and thus sea surface irradiance) through the release of dimethyl sulphide (DMS) (see also Liss *et al.*, 1997). Sathyendranath *et al.* (1991) and Kahru, Leppanen & Rud (1993) discuss how the absorption of solar radiation by phytoplankton pigments can influence sea surface temperatures (and thus the water column stability to mixing). However, processes such as these are ignored here (though both relate to the forcing processes used in the model). All models in the thesis use both forcing functions as described below.

2.3.1 Solar irradiance

The following astronomical formulae (Brock, 1981) calculate irradiance at the top of the atmosphere for any given time and latitude.

declination of Earth, $D1$

$$D1 = 0.409230\sin\left(\frac{2\pi(284+day)}{365}\right) \tag{2.17}$$

radius vector of Earth, $R1$

$$R1 = \frac{1}{\sqrt{(1 + 0.033\cos(\frac{2\pi day}{365}))}} \tag{2.18}$$

hour angle, $W2$

$$W2 = (hour - 12)\frac{\pi}{12} \tag{2.19}$$

zenith angle, Z

$$Z = \arccos(\sin(D1)\sin(latitude) + \cos(D1)\cos(latitude)\cos(W2)) \tag{2.20}$$

irradiance at the top of the atmosphere, I_{top}

$$I_{top} = \frac{I\Theta}{R1^2}\cos(Z) \tag{2.21}$$

The solar constant, $I\Theta$, has a value of 1353 W m^{-2}. All angles, including *latitude*, are in radians. Time enters as both days after January the 1st, *day*, and hours after midnight, *hour*.

Once irradiance at the top of the atmosphere has been calculated it is then necessary to determine the atmospheric transmittance in order to calculate sea surface irradiance. This procedure is complicated considerably by the properties of the atmosphere (*e.g.* clouds, aerosols, gaseous composition). Several formulae have been derived to perform this (Reed, 1977; Smith & Dobson, 1984; Evans & Parslow, 1985; Dobson & Smith, 1988; Bauer *et al.*, 1993), but following Fasham (1993), Smith & Dobson (1984) was used. Although not used in the work detailed in this thesis, these other cloud algorithms (except Bauer *et al.*, 1993) were written into the programs used to simulate the model and can be found in Appendix A-2.4. The different cloud algorithms (again, except Bauer *et al.*, 1993) use the standard ground–based meteorological unit, the *okta*, to quantify cloud cover. This unit is a somewhat qualitative unit which divides cloud cover into eighths of the sky. An entirely cloud–free sky rates 0 oktas, whilst total cloud cover rates 8 oktas. The actual density of the cloud cover (*i.e.* are the clouds thick? is there more than one layer of cloud?) is not considered.

Given cloud cover in oktas[1], the algorithm devised by Smith and Dobson (1984) uses one of two empirical formulae to determine the fraction of incoming irradiance, which reaches the sea surface.

If cloud cover, C, is greater than 5 oktas,

$$C_F = S(cld_{(1,C)} + (cld_{(2,C)}S)) \tag{2.22}$$

Otherwise, where cloud cover, C, is less than or equal to 5 oktas,

$$C_F = \left(cld_{(2,C)} + S\exp\frac{-cld_{(1,0)}}{S}\left(\frac{C}{8}\exp\frac{-cld_{(1,C)}}{S} + 1.0 - \frac{C}{8}\right)\right) \tag{2.23}$$

where,

$$S = \sin(\frac{\pi}{2} - Z) \tag{2.24}$$

[1] All of the work presented in this thesis assumes an average cloud cover of 4 oktas.

and,

Array i	**Array** j								
	$cld_{(i,0)}$	$cld_{(i,1)}$	$cld_{(i,2)}$	$cld_{(i,3)}$	$cld_{(i,4)}$	$cld_{(i,5)}$	$cld_{(i,6)}$	$cld_{(i,7)}$	$cld_{(i,8)}$
$cld_{(1,j)}$	0.240	0.070	-0.010	0.055	0.070	0.090	0.310	0.235	0.103
$cld_{(2,j)}$	0.0520	0.0525	0.0430	0.0395	0.0375	0.0345	0.439	0.388	0.296

Substitution of the relevant values from the array into the algorithm produces an estimate of the fraction of the irradiance incident at the top of the atmosphere which makes it to the sea surface.

$$I_{ss} = C_F I_{top} \tag{2.25}$$

More recent work by Bauer *et al.* (1993), compared data from remotely–sensed satellite images with ship–based readings, to determine a robust empirical algorithm for determining sea surface irradiance given cloud cover. Although this algorithm is not used here, it allows the calculation of spatio–temporal maps of estimated sea surface irradiance which may be used in more detailed spatial simulations.

Irradiance reaching the sea surface, I_{ss}, is then further corrected to account for air–surface albedo, a, and the ratio of photosynthetically active radiation (PAR) to total radiation, λ, such that irradiance just below the surface of the water, I_0, can be given as :

$$I_0 = \lambda(1-a)I_{ss} \tag{2.26}$$

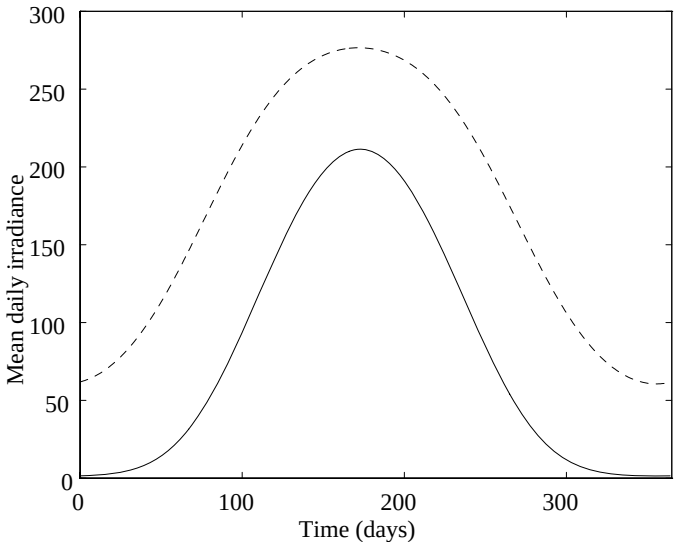

Figure 2.6: Annual cycles of mean daily sea surface irradiance at OWS "India" (solid line) and Bermuda Station "S" (dashed line). The Smith & Dobson (1984) atmospheric transmittance model is used, with a cloud cover of 4 oktas. Irradiance in W m^{-2}.

Figure 2.6 shows simulated annual cycles of mean daily sea surface irradiance at OWS "India" and at Bermuda Station "S". While both show the same sinusoidal curve across the year, the predicted irradiance at OWS "India" during the winter falls to extremely low daily averages. (The consequences of this for the modelled biology become clear in Chapter 3).

2.3.2 Mixed layer depth

Unlike the solar forcing detailed above, the dynamics of the mixed layer are modelled entirely empirically. Table 2.3 lists the monthly averages of mixed–layer depth compiled by Levitus (1982) for the locations of OWS "India" and Bermuda Station "S".

Day	OWS "India"	Bermuda Station
1	368	103
16	440	110
46	529	155
75	571	196
105	360	50
136	57	25
166	36	19
197	28	19
228	31	19
258	50	25
289	70	38
319	323	55
350	296	81
366	368	103

Table 2.3: Monthly averages of mixed–layer depth determined by Levitus (1982) for OWS "India" and Bermuda Station "S". Day 1 (and day 366) is January the 1st. Mixed–layer depth is in metres. (Data courtesy of Dr. Mike Fasham).

These data were linearly interpolated to generate values of mixed–layer depth on intermediate days, and figure 2.7 shows the resulting seasonal cycles of mixed–layer depth at OWS "India" and Bermuda Station "S". Daily values of mixed layer depth are then used to specify the rate of change, $h(t)$, in depth.

$$\frac{dM}{dt} = h(t) \tag{2.27}$$

Since a linear interpolation was used, the annual cycle of $h(t)$ assumes a stepwise shape. Non–motile entities (phytoplankton, bacteria, detritus, DON, and inorganic nitrogen here) are detrained from the

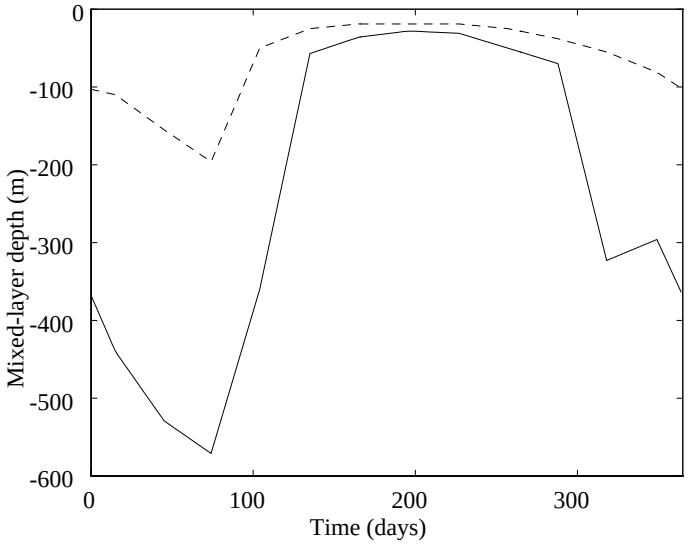

Figure 2.7: Annual cycles of mixed–layer depth at OWS "India" (solid line) and Bermuda Station "S" (dashed line).

mixed layer when it shallows, and diluted with sub–thermocline waters when it deepens. As a volumetric model, this can be described by defining a second rate variable :

$$h^+(t) = \max(h(t), 0) \tag{2.28}$$

For example, when the mixed layer is shallowing, $h(t)$ is negative and $h^+(t)$ is zero. By substituting this into the phytoplankton equation, the concentration of phytoplankton remains constant since detrainment, whilst reducing total phytoplankton biomass in the mixed layer, does not alter its concentration. By contrast, in the case of a deepening mixed layer, $h^+(t) = h(t)$, and the concentration of phytoplankton falls. Here, subthermocline water (which is assumed to contain no phytoplankton cells) is introduced into the mixed layer, increasing the volume of the mixed layer and consequently reducing phytoplankton concentration, although **not** reducing their total biomass.

Motile entities on the other hand (zooplankton here), may be assumed to be capable of tracking these depth changes, and consequently, whilst still diluted by a deepening mixed layer, actively concentrate in a shallowing one. As such, the original $h(t)$ formulation is suitable.

2.4 Comparison with other models

As previously indicated, the Fasham (1993) model is only one of many which aim to capture the dynamics of plankton ecosystems. The various attempts fall across a continuum whose extremes can be broadly described by two approaches. At one extreme there are models, usually very complex models, which aim to faithfully (and quantitatively) represent the measured biological and physical processes occurring in the specific ecosystem in question. At the other extreme, there are models, usually much simpler models, which instead try to capture or explore the dynamics of key ecological pathways or relationships.

Models at the former extreme tend to contain considerable biological and physical detail, are often built by ecologists familiar with the system, and usually are examined solely through numerical methods. While such models often compare favourably with particular data, it is usually very difficult to derive any general understanding of the model's behaviour which could aid its application in a different situation (*i.e.* the model begins to become as complicated as the situation under study). One of the best examples of this is the Narragansett Bay model from the monograph by Kremer & Nixon (1978). Woods & Barkmann's (1995) individual–based model (IBM) of zooplankton production in the North Atlantic (which uses the Lagrangian Ensemble method to track discrete plankton particles in a 3–dimensional volume) provides another example.

Models at the latter extreme usually focus on a subset of the ecological processes perceived to be the most important, and use the resulting model to establish the range of qualitative behaviour it can produce. This simplicity may allow analytical solutions to be derived, which may lead consequently to the generality of results across new or specific situations. There are many examples of such models (Bascompte, Solé & Valls, 1992; Beltrami & Carroll, 1994; Malchow, 1994; Truscott & Brindley, 1994). However, because they normally ignore, or at best only implicitly include many biological and physical aspects of plankton systems, they are usually less useful for making quantitative predictions to compare with data.

The Fasham (1993) model falls between the two extremes of models. Although it does model seven state variables, much of the complexity of the real ecosystem (*e.g.* different phytoplankton and zooplankton sizes and classes, non–nitrogenous nutrient limitation) has been sacrificed to study key processes such as phytoplankton production and the sinking flux from the mixed layer. Equally, it introduces a relatively complex representation of the regeneration pathways in the ocean ecosystem.

Although the two extremes of approach create a continuum of models with different structures and different aims, the models are all intended to represent the same systems and share key biological and physical processes. As such, certain pathways can be compared and contrasted between models. In

Mortality term	**Function**
Constant	$\frac{dX}{dt} = \ldots - (\mu)X$
Linear	$\frac{dX}{dt} = \ldots - (\mu X)X$
Rectilinear	$\frac{dX}{dt} = \ldots - (\mu X)X$ **or** $\frac{dX}{dt} = \ldots - (\mu)X$
Michaelis–Menten	$\frac{dX}{dt} = \ldots - \left(\frac{\mu X}{(k+X)}\right)X$
Sigmoid	$\frac{dX}{dt} = \ldots - \left(\frac{\mu X^2}{(k^2+X^2)}\right)X$
Ivlev	$\frac{dX}{dt} = \ldots - (\mu(1 - \exp\{-I_v X\}))X$
Ivlev with refuge	$\frac{dX}{dt} = \ldots - (\mu(1 - \exp\{-I_v(X - X_{min})\}))X$

Table 2.4: Common functional forms used in plankton models. All are presented here as loss processes for the state variable X. The parameters are : μ, loss rate; k, loss rate half–saturation constant; I_v, Ivlev constant; X_{min}, "refuge" concentration.

this section, the modelling approaches used in Fasham (1993) are compared with those taken by other modellers. The section aims to underline that the formulation of the plankton ecosystem used in the Fasham (1993) model is by no means the only one. In later chapters the functional forms of some of the processes discussed here are examined to assess their significance.

The full list of models examined is as follows :

1. Fasham (1993); 2. Kremer & Nixon (1978); 3. Steele & Henderson (1981); 4. Kremer (1983); 5. Evans & Parslow (1985); 6. Andersen, Nival & Harris (1987); 7. Frost (1987); 8. Taylor (1988); 9. Wroblewski (1989); 10. Fasham, Ducklow & McKelvie (1990); 11. Moloney & Field (1991); 12. Taylor *et al.* (1991); 13. Bascompte, Solé & Valls (1992); 14. Beltrami & Carroll (1994); 15. Malchow (1994); 16. Ross, Gurney & Heath (1994); 17. Truscott & Brindley (1994); 18. Fasham (1995); 19. Mosekilde (1996).

The models are first classified by their crude structure (*i.e.* simple or complex), and then their handling of several key pathways is listed. Tables 2.5 and 2.6 contains lists of six model descriptions or shared properties for 18 other plankton models (as well as the Fasham, 1993, model itself).

Table 2.4 contains a list of common functional forms used in the models examined. In each case the form is presented as a loss term for the state variable X. The rectilinear, Michaelis–Menten (M–M) and sigmoid terms are also often referred to as types I, II and III respectively (additionally, the Michaelis–Menten term is also often referred to as a "hyperbolic" response curve). The rectilinear form consists

of two functions, a linear one which is used below a certain concentration of X, and a constant one which is used when X is above this concentration. The final term on the table is an Ivlev one, but with a "refuge" (in principle, any of the other functional forms could also have a "refuge"). In the context here, a "refuge" is a concentration (X_{min} here) of X below which it is not depleted by the loss process in question. Ecologically, such a "refuge" may exist where a predator ceases feeding on prey when their concentration has dropped below a certain density (such a cessation may allow a predator to save resources which would otherwise be wasted on active searching for scarce prey).

All bar two of the models use differential equations to describe the plankton systems in question. Frost (1987) and Bascompte, Solé & Valls (1992) instead use difference equations to model the day by day evolution of the populations they study. Of the differential equation models, several have an explicit spatial element. To model the Narragansett Bay system, Kremer & Nixon (1978) divided the bay into 8 geographical regions, each of which was simulated as a distinct series of ODEs. Information about the rates of water flow between these 8 regions was then used to link the modelled plankton systems within them together. Using a similar (but much larger scale) approach, Wroblewski (1989) embedded a zooplankton–phytoplankton–nutrient (ZPN) model within a general circulation model (GCM) of the North Atlantic ocean (a similar approach was used by Fasham *et al.*, 1993, and Sarmiento *et al.*, 1993). Malchow (1994)[2], by contrast, modelled the behaviour of diffusing phytoplankton and zooplankton at a smaller scale. Malchow's (1994) model also explicitly resolved vertical space. Taylor (1988), Taylor *et al.* (1991) and Ross, Gurney & Heath (1994) also included vertical resolution in the form of two communicating layers (the mixed layer and a thermocline layer between it and the deep ocean).

2.4.1 Model structures

All of the models examined here have a phytoplankton compartment. This makes sense since almost all of the energy which flows through the plankton ecosystem enters it via the photosynthetic processes of the phytoplankton. Inputs of organic material from rivers, terrestrial run–off and upwelling events can provide alternative sources of energy (Sarmiento & Sundquist, 1992, estimate that inputs to the ocean of organic carbon from terrestrial sources are up to 0.5 Gt C y^{-1} – global marine net primary productivity is estimated at 30 Gt C y^{-1} by comparison). After this foundation compartment, modellers diverge in two obvious directions, towards nutrients or towards herbivores.

Although most of the models on the list have more than two model compartments (and several have many more), more than a third of the list consists of models which are either phytoplankton–nutrient (PN) or phytoplankton–zooplankton (PZ) models. As would be expected, the models which favour nutrient over zooplankton (or vice versa) usually address different questions. For example, Taylor (1988) and Taylor *et al.* (1991) are both primarily concerned with the phytoplankton–nutrient interaction in models which represent the ocean as two vertical layers rather than the single layer here. Both are interested in the effects of having the phytoplankton in the deeper layer control the nutrient flux to the shallower layer,

[2]Curiously, Malchow (1994) is a carbon–copy of Malchow (1993).

Model	Type	Phytoplankton growth limitation	
		Irradiance limitation	Nutrient limitation
1	**Complex**	**Depth–integrated**	**M–M, multiple, additive**
2	Complex	Complex	M–M, multiple, most–limiting
3	ZPN	Complex	M–M
4	PN	Complex	M–M, multiple, most–limiting
5	ZPN	Depth–integrated	M–M
6	Complex	M–M	M–M, multiple, multiplicative
7	ZPN	Depth–integrated	M–M
8	PN	Simple	M–M
9	ZPN	Depth–integrated	M–M
10	Complex	Depth–integrated	M–M, multiple, additive
11	Complex	–	M–M
12	PN	M–M	M–M
13	PZ	No explicit I or N limitation, implicit rK form	
14	PZ	No explicit I or N limitation, implicit rK form	
15	PZ	–	M–M, fixed N
16	Complex	Complex	M–M, with quotas
17	PZ	No explicit I or N limitation, implicit rK form	
18	Complex	Depth–integrated	M–M, multiple, multiplicative
19	Complex	Simple	M–M

Table 2.5: Model structures and phytoplankton growth limitation terms for a range of plankton models from the literature. Complex models are those with a structure more detailed than zooplankton–phytoplankton–nutrient–detritus (ZPND). The expression "implicit rK form" refers to processes which relate population growth to a constant rate, r, and a population carrying capacity, K. See the text for further details regarding specific irradiance and nutrient limitation terms.

while the phytoplankton in the shallower layer control the irradiance flux to the deeper layer (Chapter 6 examines a similar model based around the Fasham, 1993, model). By contrast, Bascompte, Solé & Valls (1992), Malchow (1994) and Truscott & Brindley (1994) are interested in the effects of grazer control on phytoplankton populations. Although Malchow (1994) also investigates the role of nutrients and higher

Model	Zooplankton grazing	Phytoplankton losses	Zooplankton losses
1	**M–M, with preferences**	**M–M**	**M–M**
2	Ivlev, with refuge	Constant	Explicit C, Ivlev
3	Sigmoid	Constant	Linear
4	–	Constant	–
5	M–M, with refuge	Constant	Constant
6	Ivlev, with preferences	Rectilinear	Explicit C, Ivlev
7	M–M, with refuge	–	Explicit C, M–M
8	–	Constant	–
9	Ivlev	Constant	Constant
10	M–M, with preferences	Constant	Constant
11	M–M, with refuge	Constant	Explicit C, M–M, with refuge
12	–	Constant, seasonal	–
13	Constant	–	–
14	Constant	Constant, plus infection	Constant
15	M–M	Linear	Sigmoid, and Constant
16	M–M, with migrating Z	Constant	Explicit C, M–M
17	Sigmoid	Constant	Constant
18	Sigmoid	Constant	Explicit C, Sigmoid
19	M–M, with preferences	Constant	Explicit C, M–M

Table 2.6: Zooplankton grazing, phytoplankton loss and zooplankton loss terms for a range of plankton models from the literature. The expression "Explicit C" refers to models in which zooplankton are grazed by explicitly modelled higher predators. See the text for further details regarding specific terms.

predation on this interaction, these latter processes are treated implicitly so that the key interaction, that between phytoplankton and zooplankton, dominates the study.

Of the remaining models examined, most have been described here as "complex", but four are ZPN models. This class of models is a popular one, since it allows researchers to study both top–down (zoo-

plankton) and bottom–up (nutrient) control of phytoplankton populations. The role of implicit higher predation in shifting this balance has been examined by Steele & Henderson (1992) using ZPN models (this work has not been included in the list since it studies several different models). Another advantage ZPN models offer over simpler PN or PZ models, is that explicit regenerative pathways are easier to parameterise. Regeneration is not an issue at all in PZ models, and is complicated in PN models by the difficulty in creating plausible phytoplankton loss processes in the absence of grazer control. By building a loop of interacting model compartments, ZPN models are the first to come close to fully modelling plankton systems.

The remaining models are all classed as "complex" models. All of them attempt to model more complete ecosystems. Some of them (Kremer & Nixon, 1978; Andersen, Nival & Harris, 1987; Ross, Gurney & Heath, 1994) aim to model very specific plankton systems, usually in response to the availability of detailed time series data for those systems. The others, of which the Fasham (1993) model is an example, while still aiming to successfully model complete ecosystems, try to do so with more generic models, and often compare these models to data sets from quite geographically distinct areas (Fasham, Ducklow & McKelvie, 1990; Fasham, 1995).

A feature of all of the more complex models, is their use of detritus or particulate/dissolved organic compartments to further parameterise the regeneration of dead or excreted organic material to the inorganic nutrients which phytoplankton can utilise. Several of the models (Kremer & Nixon, 1978; Andersen, Nival & Harris, 1987; Moloney & Field, 1991) introduce further complexity through multiple nutrient, phytoplankton or zooplankton classes. Kremer & Nixon (1978) split the zooplankton compartment (which explicitly represents copepod species) into age classes for different developmental stages (which feed on different prey and which are consumed by different predators). While such approaches clearly make good ecological sense (as Chapter 1 outlined, there are many different types of each of these trophic classes), other models (Fasham, 1993; Ross, Gurney & Heath, 1994; Fasham, 1995) have resisted this approach, mostly because of the (unwanted) parameter and functional requirements such additions make (for instance, Kremer & Nixon's model requires more than 50 physiological coefficients). Fasham (1995), in particular, through use of a single phytoplankton–single zooplankton model, draws attention to the need to add further levels of such complexity only when they are absolutely necessary (Kremer & Nixon, 1978, explore and discuss the importance of multiple phytoplankton types in their detailed estuarine model).

2.4.2 Phytoplankton limitation

Since phytoplankton form the basis of all of the models discussed here, one of the uniting features of the models is their need to represent the processes by which phytoplankton grow, and the limitations placed upon this growth.

Almost all of the models on the list restrict phytoplankton growth through either irradiance or nutrient limitation (usually both). However, several models use more implicit methods to limit phytoplankton densities. Truscott & Brindley's (1994) PZ model provides a good example of such a model. Phytoplankton growth is controlled by the following term :

$$\frac{dP}{dt} = rP\left(1 - \frac{P}{K}\right) \tag{2.29}$$

A constant growth rate, r, increases phytoplankton density towards a carrying capacity, K. At this density, phytoplankton population growth ceases. Since the model is concerned with the phytoplankton–zooplankton interaction (specifically the occurrence of bloom phenomena), the exact mechanism for the cessation of growth is not of interest (*e.g.* nutrient limitation? self–shading?). Bascompte, Solé & Valls (1992) and Beltrami & Carroll (1994) use very similar implicit functions to limit phytoplankton growth.

Irradiance limited growth

Although most of the plankton models have an irradiance–limited step to phytoplankton growth, there are differences as to how this step is implemented. The Fasham (1993) model builds upon previous models (Evans & Parslow, 1985; Fasham, Ducklow & McKelvie, 1990) and uses a standard P–I growth curve, and then explicitly integrates this curve through the submarine light field down the water column. Similar approaches are used by the ZPN models of Frost (1987) and Wroblewski (1989).

There are as many variants to this process as there are models. While considering mixed–layer depth in their formulation, Steele & Henderson (1981) do so in an implicit fashion which assumes that this depth is invariant, and then scales certain model parameters appropriately (and non–transparently). Taylor *et al.* (1991) consider different colours of downwelling irradiance, and calculate the fractions of this irradiance which penetrate to the middle of each of the two modelled ocean layers. The calculated light is then used in a Michaelis–Menten term to determine the maximum light–limited growth rate. Andersen, Nival & Harris (1987) use a similar Michaelis–Menten term, but consider only irradiance at the surface of the water (like Steele & Henderson, 1981, they are only concerned with a relatively shallow, enclosed ecosystem). Kremer & Nixon (1978) use the ratio of incident to optimum light, and integrate it across both the day and down the water column. Additionally, the phytoplankton acclimate (via an optimum light parameter) to the ambient light conditions using a weighted average of the light conditions of the previous three days.

In constrast, neither Moloney & Field (1991) nor Malchow (1994) include an element of light limitation. Both tie growth to nutrient availability (although in the latter model, nutrients are fixed at a constant concentration).

Nutrient limited growth

With the exception of the three PZ models mentioned previously, all of the models examined (even the fixed nutrient PZ model of Malchow, 1994) include nutrient–limitation in their formulations of phy-

toplankton growth. And in every case, the Michaelis–Menten form of limitation is used (which, as described previously, makes use of a half–saturation constant of nutrient uptake). However, although there is constancy between models on this choice of term, there are several minor variants in its use.

While most of the models examined consider only a single limiting nutrient, Fasham (1993) considers phytoplankton to be limited by two nitrogenous nutrients, nitrate and ammonium. Kremer & Nixon (1978) go even further, with growth limited by three different nutrients, nitrogen, phosphorus (as phosphate) and silicon (as silicate). As illustrated by both of these cases (and in the other examples of multiple nutrient limited models), while Michaelis–Menten terms govern the limitation of each of the nutrients, the interaction between the different limitations can be very different. Fasham (1993) considers the limitation as additive, so that total nutrient limitation is the sum of the two Michaelis–Menten terms. However, other models (Andersen, Nival & Harris, 1987; Fasham, 1995) favour a multiplicative relationship (where total limitation is the product of individual limitations), and yet others favour a "most–limiting" relationship (where nutrient limited growth is determined by the most limiting nutrient; also known as Liebig's law).

The choice between these different forms is unclear since each has different theoretical advantages and disadvantages (see O'Neill *et al.*, 1989). Chapter 3 includes a comparison of the form used in Fasham (1993) with the multiplicative form used by Fasham (1995).

2.4.3 Phytoplankton losses

Another major set of ecological pathways most plankton models share are those which deal with phytoplankton losses. All of the models examined have such processes (phytoplankton biomass has got to go somewhere after all), although, as with irradiance–limitation, there can be considerable variation in the choice of formulation between models.

For the purposes of this section, the losses have been divided into those which relate explicitly to consumption by zooplankton, and those which either represent other sources of mortality (or loss) or are used to represent phytoplankton mortality in general (this latter qualification applies to the three PN models on the list).

Zooplankton grazing

Of the models examined, almost half use a Michaelis–Menten term as the functional form of zooplankton grazing. Of the remainder, all bar two use other curved functional forms (sigmoidal, Ivlev). The two which do not use a curved response (Bascompte, Solé & Valls, 1992; and Beltrami & Carroll, 1994) are simple PZ models whose interests lie in other facets of their behaviour (chaotic behaviour and viral dynamics respectively).

Eccleston–Parry & Leadbeater (1994) review the growth response of microzooplankton against the concentration of their picoplanktonic prey. Their results support the description of the grazing rates of these microzooplankton by a Michaelis–Menten relationship. In direct observations of the feeding behaviour of individual copepods, Paffenhöfer *et al.* (1995) found a rectilinear–like response of cell capture rate against cell concentration.

Curved responses such as the Michaelis–Menten, Ivlev and sigmoid forms, are used throughout ecology to represent processes, such as grazing, which are density–dependent and saturate to a constant rate with increasing density of some model component. In the case of the Michaelis–Menten and Ivlev forms, as prey density increases, predators (zooplankton here) become "satiated" and show an increasingly invariant specific rate of consumption with rising prey. This "satiation" may represent a number of different ecological processes. The sigmoidal form is broadly similar, but produces a decrease in the zooplankton grazing rate at low phytoplankton densities. In a later section of Chapter 4, the significance of the choice of different functional forms for predation on zooplankton is examined, and the ecological rationale behind different forms is more fully discussed.

Aside from the choice of the curved response used by the model zooplankton to graze the model phytoplankton, there are several other variations in the terms used. Several include a "refuge" for phytoplankton which acts to prevent grazing on them when their concentration falls below a specified value. This may parameterise a grazer which ceases to actively search for food when the energy expended doing so exceeds the gains from phytoplankton captured.

Another variation between the grazing terms enters where the zooplankton consume more than one prey species. Fasham (1993), Fasham, Ducklow & McKelvie (1990) and Mosekilde (1996) all use a preference system where prey at a higher density are given preference over prey at lower density (this is further skewed by Fasham, 1993, where the phytoplankton are further favoured by parameterisation). The model of Andersen, Nival & Harris (1987) does not use a preference system for dealing with multiple prey, but instead uses parameters to assign prey different capture efficiencies (which are independent of prey density).

Ross, Gurney & Heath (1994) model a two layer system in which a single zooplankton compartment grazes phytoplankton in both layers. A simple function, based on the ratio of phytoplankton in the two layers, is used by the zooplankton to divide their time between these two layers.

Other losses

Aside from losses due to the activity of zooplankton grazers, most model phytoplankton usually have additional losses to other processes. These losses are incurred through ecological pathways such as cell starvation, metabolic processes such as respiration, cells sinking out of the modelled mixed layer, viral infection, natural cell death and even accidents. Usually though, models only include an explicit subset

of these processes (Steele & Henderson, 1981, have a respiration and sinking loss terms; Andersen, Nival & Harris, 1987, use a rate which varies with nutrient starvation), or use a single term which implicitly includes several processes (Fasham, 1993; Mosekilde, 1996).

Almost all of the models examined use a constant function to include loss processes, but a few others use different forms (Fasham, 1993; Andersen, Nival & Harris, 1987; Malchow, 1994). Since the loss processes identified above are mostly independent of cell density, the use of a constant form makes sense. However, some processes are almost certainly density dependent. Suttle & Chan (1994), for instance, report results from a field survey of infective cyanophages which suggest that efficient propagation of the phages is dependent on the density of their hosts, *Synechococcus* cyanobacteria. In their PZ model of viral dynamics, Beltrami & Carroll (1994) explicitly include viral infection through an infected (and infectious) phytoplankton compartment.

Of the models which use a non–constant form, the processes represented by the Michaelis–Menten term in Fasham's (1993) model are somewhat ambiguous, since the term was chosen to match with the comparable one in the zooplankton equation, and then the values of its parameters were used to "fine–tune" the model. Andersen, Nival & Harris (1987) chose a rectilinear response to parameterise the effect of nutrient starvation on phytoplankton. Malchow (1994) used a linear form to parameterise the competitive consequences of high phytoplankton density (although the exact nature of this competition is not made explicit).

As already pointed out, several of the models examined are PN models and their phytoplankton (obviously) have no explicit losses to zooplankton (Kremer, 1983; Taylor, 1988; Taylor *et al.*, 1991). Since their phytoplankton loss terms then include both grazing and other loss terms, their losses have been included in this category. Despite the use of density dependent responses in almost all of the models in which zooplankton grazing is explicit, all three of the PN models use a constant form for phytoplankton loss. Taylor *et al.* (1991) augment this form by allowing the constant rate to vary seasonally.

2.4.4 Zooplankton losses

Around half of the models examined include an explicit carnivore compartment which feeds on zooplankton (labelled "Explicit C" in table 2.6). Of those, all use a curved functional response to describe the relationship. Fasham (1995) examined the significance of an explicit carnivore compartment, and found that when a sigmoidal functional form was used to represent the functional response of these carnivores, a linear form for zooplankton loss was a good parameterisation of this when the carnivores were treated only implicitly. Since an implicit carnivore requires fewer parameters to represent it, this approach has some merit.

Of the remaining models, a mixture of functional forms are used, with the constant form being the most

Symbol	Value	Units	Range in literature minimum		maximum	
C	4	oktas	*4*	*(1)*	7	(5)
a	0.05		–		–	
λ	0.43		–		–	
k_w	0.04	m^{-1}	0.03	(12)	0.20	(3)
k_c	0.03	m^2 (mmol N)$^{-1}$	*0.03*	*(1)*	0.12	(5)
V_p	1.25	d^{-1}	0.62	(8)	3.0	(6)
α	0.025	(W m^{-2})$^{-1}$ d^{-1}	*0.025*	*(1)*	0.140	(18)
γ	0.05		0.05	(10)	0.15	(11)
ψ	1.5	(mmol N m^{-3})$^{-1}$	–		–	
k_1	0.5	mmol N m^{-3}	0.0005	(11)	3.86	(11)
k_2	0.5	mmol N m^{-3}	0.01	(18)	*0.5*	*(1)*
k_3	1.0	mmol N m^{-3}	1.00	(5)	1.89	(16)
k_4	0.5	mmol N m^{-3}	0.0005	(11)	14.30	(19)
k_5	0.2	mmol N m^{-3}	–		–	
k_6	0.2	mmol N m^{-3}	*0.2*	*(1)*	5.03	(16)
μ_1	0.05	d^{-1}	0.05	(12)	0.20	(12)
μ_2	0.30	d^{-1}	0.04	(9)	15.0	(16)
μ_3	0.05	d^{-1}	*0.05*	*(1)*	0.9	(19)
μ_4	0.05	d^{-1}	0.009	(19)	0.18	(*)
$\beta_{1,2,3}$	0.75		0.25	(3)	0.9	(6)
$p_{1,2,3}$	0.50, 0.25, 0.25		–		–	
g	1.0	d^{-1}	0.5	(9)	1.0	(18)
$(\epsilon + \delta)$	0.90		0.0	(3)	1.0	(9)
V_b	2.0	d^{-1}	*2.0*	*(1)*	6.6	(11)
η	0.6		–		–	
V	10	m d^{-1}	0.009	(19)	*10.0*	*(1)*
N_0	12	mmol N m^{-3}	geographically variable			
m	0.01	m d^{-1}	*0.01*	*(1)*	3.0	(5)

Table 2.7: Baseline parameter values from Fasham (1993) and ranges of values of the model parameters from a sample of the modelling literature. Dashes mark those parameters for which no comparable values could be found in the literature. Where the value used in Fasham (1993) is at the extreme of a range of values from other papers, it has been marked with *emphasis*. Abbreviations for literature sources are listed in the text. (*) indicates a value of μ_4 obtained from Jones & Henderson (1986).

popular. Malchow (1994) uses two terms to represent zooplankton loss processes : a constant term for respiration and general mortality, and a sigmoidal term for predation losses. Fasham's (1993) model is unique in its use of the Michaelis–Menten form, although Steele & Henderson's (1981) model is similarly unique in its use of the linear form.

Steele & Henderson (1992) have drawn attention to the importance of the choice of this zooplankton loss term, and the consequences of different forms on model behaviour. In Chapter 4 this issue is explored using versions of the Fasham (1993) model incorporating different zooplankton loss terms.

2.4.5 Model parameters

One aspect not touched upon so far is that of the choice of values for the parameters in the models examined. Table 2.7 lists the parameters used in Fasham's (1993) model, their baseline values (for OWS "India"), and the range of values found across the models examined in this section. For each parameter the modelling literature maximum and minimum are shown, together with a reference to the model from which the value was obtained. No comparable values were found for several parameters (a, λ, ψ, k_5, $p_{1,2,3}$ and η), but where values were found a range was shown (even if one of its extremes was from Fasham's model itself).

2.5 Summary

This chapter has aimed primarily to introduce and describe the focus of this thesis, the Fasham (1993) model. Since this model is only one of many which are used in studies of plankton ecosystems, the chapter has additionally compared Fasham's model to a sample of these other models, to draw attention to the wide variety in both the structures of these models, and the choices of functional responses used in them. This variety partially reflects ignorance about the nature of the pathways, but also often the simplification of models so that they remain analytically tractable.

Although there is considerable variety in the terms chosen for four of the shared model pathways, all of the models which include nutrients (and even in the model of Malchow, 1994, in which nutrients are only implicitly represented) use the Michaelis–Menten term for nutrient uptake. Similarly, the losses of phytoplankton and zooplankton to higher trophic levels, while differing in the exact form used, mostly agree on the representation of these processes by curved responses. However, there are still marked differences between key model processes, like irradiance limitation of phytoplankton growth. Some researchers have explored the significance of some of these differences (Steele & Henderson, 1992; Fasham, 1995; Haney & Jackson, 1996; Edwards, 1997), and several later sections in this thesis address such issues.

Chapter 3

Reducing the Fasham (1993) model

Everything should be made as simple as possible, but no simpler.

– Albert Einstein (1879–1955)

3.1 Introduction

As raised in Chapter 2, the relatively large size of the Fasham (1993) model is in contrast to the many simpler models which are used by other researchers in explorations of plankton dynamics (Steele & Henderson, 1981; Bascompte *et al.*, 1992; Malchow, 1993, 1994; Truscott & Brindley, 1994). While this greater size reflects the difference in the aims of these models (*qualitative* versus *quantitative* explanations), it does complicate any analytical examinations of the Fasham (1993) model and restricts its study to numerical solutions. Furthermore, attempts to validate the model are limited by a lack of measurements for most of the state variables. The inclusion of compartments for which data are unavailable or limited is debatable on both theoretical and empirical grounds, but it does provide a research agenda.

This chapter describes a reduction of the full seven compartment model to the simplest form often favoured in such work, a phytoplankton-zooplankton (PZ) model, and then its gradual reassembly to the full form. The aim is to determine whether a minimum model, which accurately describes the dynamics of the full model, can be reconstructed. Such a reduced model may be more easily (and usefully) integrated in future work, whilst still retaining the behaviour of the full model. In particular, such a model may be more amenable to analysis, or may be more efficiently incorporated into a GCM. Additionally, the removal and replacement of model pathways may indicate which ones are the most (or least) crucial. This latter "spin–off" may assist future modelling or observational programmes by suggesting where efforts may be most fruitfully applied.

3.2 Methodology

3.2.1 Reducing the Fasham (1993) model

Since it was not clear that the full model could be reduced to only a single compartment, the reduction was achieved by first removing five of the model compartments. The connections (ecological pathways) between the two remaining compartments were maintained, but connections to other compartments were either ignored (*i.e.* where they became meaningless in the context of the reduced form) or were modified to compensate for the loss of model complexity (*i.e.* where the connections retained some functional meaning in the reduced model).

Following this, compartments were reinstated one at a time until models of up to six compartments were obtained. The details of all of these reduced forms follow this section.

In principle, such a seven compartment model could be reduced to smaller models in many different and distinct ways. However, in the process of reducing and rebuilding the various models described below, four general rules were applied to provide a consistent framework.

(i) *Biology is important.* The nitrogen dynamics of interest in biogeochemical models are driven by biological processes (principally the trapping of solar energy by autotrophic phytoplankton), so it is crucial that a biological foundation is adhered to;

(ii) *Reconstruction via major flows.* When the model is reconstructed, most attention should be paid to the ecological pathways with the greatest annual throughput of nitrogen;

(iii) *Sensible reconstruction only.* It is possible to rebuild models composed of inappropriate compartments (*e.g.* zooplankton and detritus only). However, in each of the reduced forms described below, consideration was given to the biological realism and potential usefulness of the reduced form;

(iv) *Parameters stay constant.* It is possible that by manipulation of a combination of model parameters, to perhaps unrealistic values, reduced models could be "coaxed" into behaving like the full model. However, since parameters were originally assigned values from the biological literature (where possible), this would undermine the original aim of this study, as well as perhaps reducing the mechanistic integrity of the models. For these reasons, parameters were not allowed to vary from their values in Fasham (1993) unless absolutely necessary.

The following sections detail the reduced model equations as well as the thinking behind their formulation. Where specific ecological pathways (*e.g.* phytoplankton growth terms and zooplankton grazing terms) are duplicated between reduced forms, a full description is given only at the first occurrence of the pathway.

Two compartment models

In the first instance, the full model was reduced to a two compartment equivalent. Although there are examples in the literature of phytoplankton–nutrient models (Taylor, 1988; Taylor *et al.*, 1991), more common are two compartment models based on a phytoplankton–zooplankton ecology (Steele & Henderson, 1981; Bascompte *et al.*, 1992; Malchow, 1993, 1994; Truscott & Brindley, 1994). Whilst such a system immediately neglects any nutrient–limitation of phytoplankton growth, such a limitation is not necessarily important and is clearly, at least in the case of the macro–nutrients used here, less important in certain oceanic environments (Behrenfeld *et al.*, 1996). Additionally, while it is relatively easy to remove nutrient limitation from the full model (by limiting phytoplankton growth by irradiance only), it is less clear how the zooplankton compartment could be replaced by an implicit grazing loss function. For these reasons the first reduced model was a PZ ecology.

Model 2c

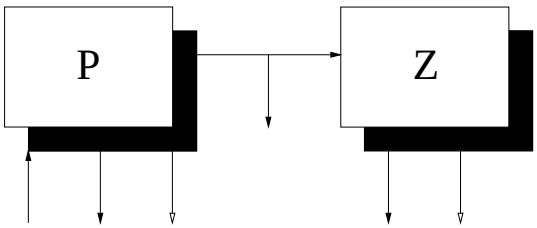

Figure 3.1: Model 2c, a two compartment PZ system. In this, and all following schematic diagrams of reduced systems, all pathways between compartments have been shown. Empty arrow–headed flows represent flows into or out of the model mixed–layer system. Solid–headed flows out of compartments which appear to lead nowhere represent flows into the mixed layer itself. Usually they represent ecological pathways which the reduced model does not consider.

The following equations describe a two compartment version of Fasham (1993).

$$\frac{dP}{dt} = (1-\gamma)\sigma_b(t,M,P)P - G_{1b} - \frac{\mu_1 P^2}{k_5+P} - \frac{(m+h^+(t))P}{M} \tag{3.1}$$

$$\frac{dZ}{dt} = \beta_1 G_{1b} - \frac{\mu_2 Z^2}{k_6+Z} - \frac{h(t)Z}{M} \tag{3.2}$$

where,

$$\sigma_b = J(t,M,P)$$

$$G_{1b} = \frac{gPZ}{k_3+P}$$

Since nutrients are not included in this model, it is assumed that phytoplankton are only light limited (*i.e.* it is implicitly assumed that nitrogen supply is never limiting). Consequently, the σ term collapses to that above. The remainder of the phytoplankton equation retains the same form to that of the full

model.

When modified to account for only a single prey item, the zooplankton grazing term (Equation 2.8) collapses to the hyperbolic (Holling type II) form shown above (see derivation in Chapter 2). As well as losing the multiple food types directly, this term also loses the (now redundant) prey–switching modifications present in the original form. The remainder of the zooplankton equation remains the same as the full model.

Note that this new grazing term is denoted G_{1b}, with the subscript b to distinguish it from the normal form of the grazing term, G_1. This form of subscripting is continued throughout the descriptions of the reduced models wherever a new form of a term (*e.g.* grazing, phytoplankton growth, bacterial uptake, *et cetera*) is introduced.

As can be seen from the diagram above, several flows from the two compartment system no longer enter other compartments. In the case of this model, where nitrogen is assumed to be non–limiting, this has no consequences. However, in larger models where there are more feedbacks in the ecology, the fate of these flows is more significant.

Three compartment models

The majority of three compartment plankton models add nutrient to the basic PZ ecology to allow nutrient limitation to be studied (Steele & Henderson, 1981; Evans & Parslow, 1985; Frost, 1987; Wroblewski, 1989; Fasham, 1995; Edwards & Brindley, 1996). In the work presented here, three reconstructions address different approaches to the addition of a third compartment. Two are described directly following this, the third in a later section on implicit modelling of nitrate.

Model 3c

The following equations describe a three compartment version of Fasham (1993). This system adds a general nutrient compartment to the basic PZ ecology.

$$\frac{dP}{dt} = (1-\gamma)\sigma_c(t,M,P,N)P - G_{1b} - \frac{\mu_1 P^2}{k_5+P} - \frac{(m+h^+(t))P}{M} \tag{3.3}$$

$$\frac{dZ}{dt} = \beta_1 G_{1b} - \frac{\mu_2 Z^2}{k_6+Z} - \frac{h(t)Z}{M} \tag{3.4}$$

$$\frac{dN}{dt} = -(1-\gamma)\sigma_c(t,M,P,N)P + (1-\beta_1)G_{1b} + \frac{\mu_1 P^2}{k_5+P} + (\epsilon+\delta)\frac{\mu_2 Z^2}{k_6+Z} + \frac{(m+h^+(t))}{M}(N_0-N) \tag{3.5}$$

where,

$$\sigma_c = J(t,M,P)Q_b(N)$$

$$Q_b(N) = \frac{N}{k_1+N}$$

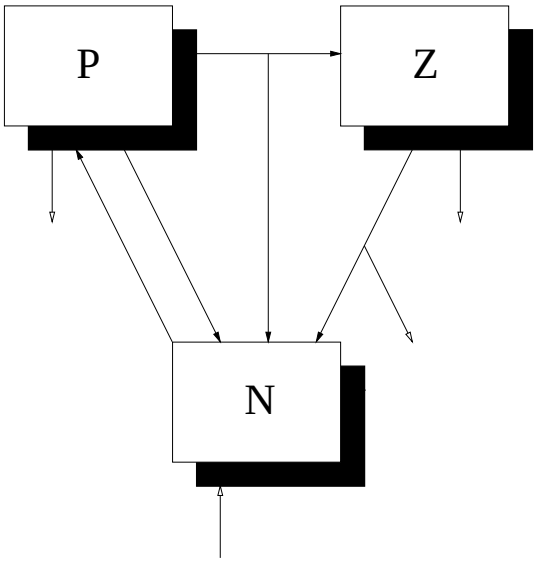

Figure 3.2: Model 3c, a three compartment ZPN system.

With the addition of a general nutrient compartment, the σ_c term now includes nutrient limitation. The general nutrient is assumed to comprise both nitrate and ammonium, so flows which previously returned via regeneration to ammonium now return directly to the general nutrient compartment.

Similarly, phytoplankton uptake of nutrient is a single flow from the general nutrient pool. Because there is no distinction between the two base nitrogen nutrients, the inhibition of nitrate uptake due to ammonium is ignored. Nutrient uptake is represented instead as a single Michaelis–Menten term. Since the half–saturation constants for nitrate and ammonium uptake are the same in the full model, k_1 is arbitrarily used here. The remainder of the phytoplankton equation remains the same as 2c.

The zooplankton equation remains the same as in 2c as its only direct interaction with other compartments is through grazing on phytoplankton.

The nutrient equation primarily acts as a source for the phytoplankton growth and a sink to zooplankton mortality. However, since several other flows, notably those into the detrital compartment, are relatively substantial, it has been assumed here that the breakdown and regeneration processes are sufficiently fast to return organic nitrogen (dissolved and particulate) instantaneously back to inorganic nutrient.

Model 3c2

The following equations describe a second three compartment version of Fasham (1993). This system adds a detritus compartment to the basic PZ ecology.

$$\frac{dP}{dt} = (1-\gamma)\sigma_b(t,M,P)P - G_{1c} - \frac{\mu_1 P^2}{k_5+P} - \frac{(m+h^+(t))P}{M} \tag{3.6}$$

$$\frac{dZ}{dt} = \beta_1 G_{1c} + \beta_2 G_{2c} - \frac{\mu_2 Z^2}{k_6+Z} - \frac{h(t)Z}{M} \tag{3.7}$$

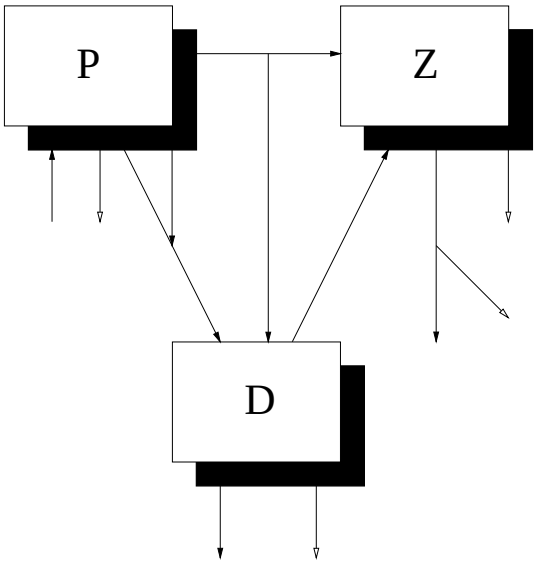

Figure 3.3: Model 3c2, a three compartment ZPD system.

$$\frac{dD}{dt} = (1-\beta_1)G_{1c} - \beta_2 G_{2c} - \mu_4 D + \frac{\mu_1 P^2}{k_5 + P} - \frac{(m + V + h^+(t))D}{M} \tag{3.8}$$

where,

$$G_{1c} = \frac{g p_{1b} P^2 Z}{k_3(p_{1b}P + p_{2b}D) + p_{1b}P^2 + p_{2b}D^2}$$

$$G_{2c} = \frac{g p_{2b} D^2 Z}{k_3(p_{1b}P + p_{2b}D) + p_{1b}P^2 + p_{2b}D^2}$$

With this model an attempt was made to break away from traditional three compartment ZPN models by putting a detrital compartment in before that of nutrient. As with the two compartment version detailed above, phytoplankton are assumed to never suffer nutrient limitation. Growth is only light limited.

The grazing term of the zooplankton equation is now modified to account for the presence of detritus as a secondary prey item (see the derivation in Chapter 2). In the full model, where there are three prey species, the zooplankton were assigned nominal preferences for each ($p_1 = 0.50$, $p_2 = p_3 = 0.25$). In the absence of any information to select these preferences for a two prey species model, they have been assigned equal value ($p_{1b} = p_{2b} = 0.50$). This choice of preferences is used for all of the reduced forms which have two prey species for zooplankton. Other than the addition of the grazing term for detritus, the zooplankton equation remains the same as model 2c.

The detrital equation retains most of its terms from the full model. The only absence is that from zooplankton feeding inefficiency on bacterial populations.

As with the 2c model, flows which exit the modelled compartments bound for unmodelled compartments are ignored because nutrients are not limiting.

Four compartment models

Increasing the complexity of the modelled ecosystem can be achieved in a number of different ways. An increase to four compartments presents a number of possibilities.

In the first case, which compartment should be "resurrected"? In model 3c above, the potential for "short–circuiting" nitrogen flows by assuming instantaneous regeneration of organic nitrogen to inorganic forms was raised. In this context, the next model element added should probably act as some sort of "buffer" to re–introduce regeneration lags.

Ammonium is probably too directly usable to qualify, and DON is not really representative of the bulk of the outflows from phytoplankton and zooplankton compartments (mostly whole dead organisms, parts of organisms or excretory/faecal material). The addition of bacteria as the fourth compartment would be difficult, primarily because they would lack a heterotrophic substrate for growth, but also because their ecological "role" of recycler would be entirely absent.

In the first instance then, two models were constructed which added detritus to the ZPN system. A third model is described in the later section on implicit modelling of nitrate.

Model 4c

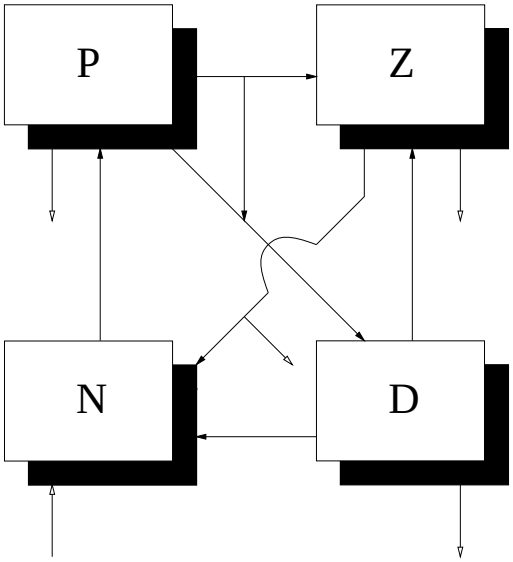

Figure 3.4: Model 4c, a four compartment ZPND system.

The following equations describe a four compartment version of Fasham (1993). This system includes both a general nutrient and a detritus compartment.

$$\frac{dP}{dt} = (1-\gamma)\sigma_c(t,M,P,N)P - G_{1c} - \frac{\mu_1 P^2}{k_5+P} - \frac{(m+h^+(t))P}{M} \tag{3.9}$$

$$\frac{dZ}{dt} = \beta_1 G_{1c} + \beta_2 G_{2c} - \frac{\mu_2 Z^2}{k_6 + Z} - \frac{h(t)Z}{M} \tag{3.10}$$

$$\frac{dD}{dt} = (1-\beta_1)G_{1c} - \beta_2 G_{2c} - \mu_4 D + \frac{\mu_1 P^2}{k_5 + P} - \frac{(m + V + h^+(t))D}{M} \tag{3.11}$$

$$\frac{dN}{dt} = -(1-\gamma)\sigma_c(t,M,P,N)P + \frac{(\epsilon+\delta)\mu_2 Z^2}{k_6+Z} + \mu_4 D + \frac{(m+h^+(t))}{M}(N_0 - N) \tag{3.12}$$

The equations remain similar to those described for previous models. Phytoplankton are again limited by the single general nutrient, whilst zooplankton and detritus equations remain identical to that described for model 3c2.

Unlike model 3c, instantaneous regeneration to nutrient only occurs for flows of DON. Flows of particulate organic nitrogen enter the detrital compartment directly.

Model 4c2

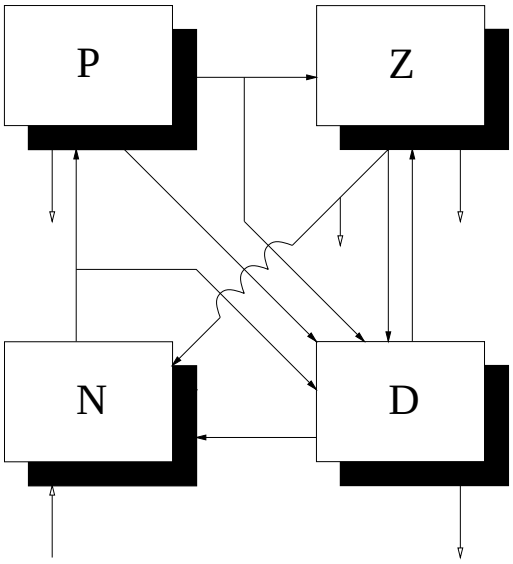

Figure 3.5: Model 4c2, a four compartment ZPND system.

The following equations describe a second four compartment version of Fasham (1993). This system also includes nutrient and detrital compartments.

$$\frac{dP}{dt} = (1-\gamma)\sigma_c(t,M,P,N)P - G_{1c} - \frac{\mu_1 P^2}{k_5+P} - \frac{(m+h^+(t))P}{M} \tag{3.13}$$

$$\frac{dZ}{dt} = \beta_1 G_{1c} + \beta_2 G_{2c} - \frac{\mu_2 Z^2}{k_6+Z} - \frac{h(t)Z}{M} \tag{3.14}$$

$$\frac{dD}{dt} = (1-\beta_1)G_{1c} - \beta_2 G_{2c} - \mu_4 D + \gamma\sigma_c(t,M,P,N)P + \frac{\mu_1 P^2}{k_5+P} + \frac{\delta\mu_2 Z^2}{k_6+Z} - \frac{(m+V+h^+(t))D}{M} \tag{3.15}$$

$$\frac{dN}{dt} = -\sigma_c(t,M,P,N)P + \frac{\epsilon\mu_2 Z^2}{k_6+Z} + \mu_4 D + \frac{(m+h^+(t))}{M}(N_0 - N) \tag{3.16}$$

The equations for model 4c2 differ from those of 4c only in the flow of DON. In model 4c, DON was assumed to be instantaneously regenerated to inorganic nutrient. In this model, DON flows into the detritus compartment together with particulate organic nitrogen. Whilst this does permit DON to sink out of the mixed layer, it also allows its regeneration to be a rate limited process.

However, this regeneration of detritus to nutrient introduces a complication. In the full model, detrital breakdown produces DON which is regenerated by bacteria to ammonium. As any DON produced in this model now flows into detritus, detrital breakdown itself should flow back into the detrital compartment (*i.e.* not a flow at all). This has been "resolved" by effectively introducing a new pathway allowing the detritus to be regenerated as general nutrient. For simplicity, the rate of this regeneration has been set to μ_4, the standard value for detrital breakdown.

Five and six compartment models

Since one of the principal reasons for reducing the size of the full model was to facilitate its use in future work, models of five or more compartments are obviously of less value in this aim. However, should it not prove possible to replicate the behaviour of the full model in the reduced forms so far described, the construction of larger models which restore more of the ecological pathways may be useful in identifying weaknesses of the reduced forms or possible key flows in the full form.

To this end, seven models with five or six compartments have been constructed. Two are described in the section on implicit modelling of nitrate.

Model 5c

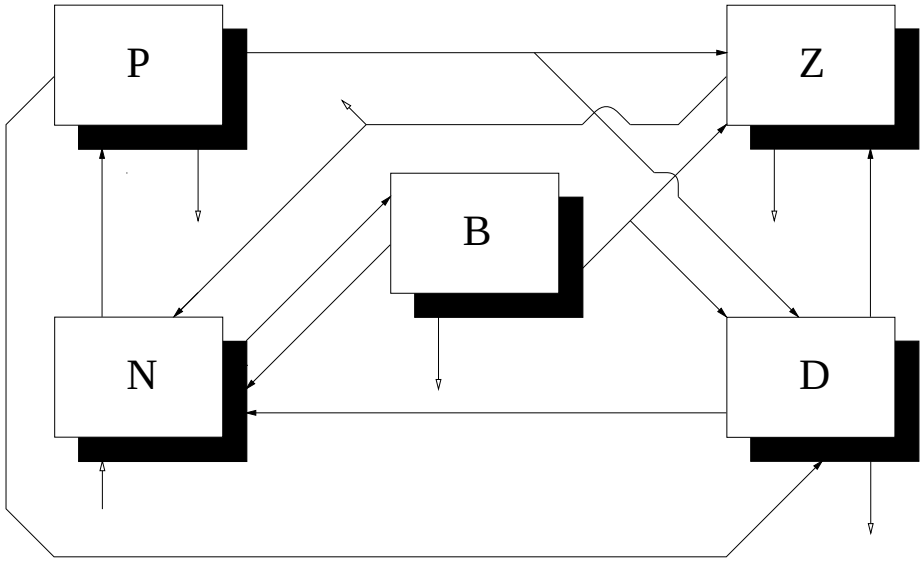

Figure 3.6: Model 5c, a five compartment system.

The following equations describe a five compartment version of Fasham (1993). This system adds a bacteria compartment.

$$\frac{dP}{dt} = (1-\gamma)\sigma_c(t,M,P,N)P - G_1 - \frac{\mu_1 P^2}{k_5+P} - \frac{(m+h^+(t))P}{M} \tag{3.17}$$

$$\frac{dZ}{dt} = \beta_1 G_1 + \beta_2 G_2 + \beta_3 G_3 - \frac{\mu_2 Z^2}{k_6+Z} - \frac{h(t)Z}{M} \tag{3.18}$$

$$\frac{dB}{dt} = U_{1b} - G_2 - \mu_3 B - \frac{(m+h^+(t))B}{M} \tag{3.19}$$

$$\frac{dD}{dt} = (1-\beta_1)G_1 + (1-\beta_2)G_2 - \beta_3 G_3 - \mu_4 D + \frac{\mu_1 P^2}{k_5+P} - \frac{(m+V+h^+(t))D}{M} \tag{3.20}$$

$$\frac{dN}{dt} = -(1-\gamma)\sigma_c(t,M,P,N)P + \frac{(\epsilon+\delta)\mu_2 Z^2}{k_6+Z} - U_{1b} + \mu_3 B + \mu_4 D + \frac{(m+h^+(t))}{M}(N_0 - N) \tag{3.21}$$

where,

$$U_{1b} = \frac{V_b B N}{k_4+N}$$

This model retains the basic structure of model 4c but adds a compartment to represent bacteria. This addition provides a third prey species for zooplankton.

Since DON is assumed to decay instantaneously to inorganic nutrient and DON flows enter this compartment directly, bacteria uptake their substrate solely from the nutrient compartment. As such this places them in direct conflict with phytoplankton for nutrients. This may have consequences for model behaviour. However, because bacteria also excrete ammonium (which flows into the general nutrient compartment), the significance of this feature of the model is unclear.

Model 5c2

The following equations describe a second five compartment version of Fasham (1993). This system also adds a bacteria compartment.

$$\frac{dP}{dt} = (1-\gamma)\sigma_c(t,M,P,N)P - G_1 - \frac{\mu_1 P^2}{k_5+P} - \frac{(m+h^+(t))P}{M} \tag{3.22}$$

$$\frac{dZ}{dt} = \beta_1 G_1 + \beta_2 G_2 + \beta_3 G_3 - \frac{\mu_2 Z^2}{k_6+Z} - \frac{h(t)Z}{M} \tag{3.23}$$

$$\frac{dB}{dt} = U_{1c} + U_{2c} - G_2 - \mu_3 B - \frac{(m+h^+(t))B}{M} \tag{3.24}$$

$$\frac{dD}{dt} = (1-\beta_1)G_1 + (1-\beta_2)G_2 - \beta_3 G_3 - U_{1c} + \frac{\delta\mu_2 Z^2}{k_6+Z} + \gamma\sigma_c(t,M,P,N)P + \frac{\mu_1 P^2}{k_5+P} - \frac{(m+V+h^+(t))D}{M} \tag{3.25}$$

$$\frac{dN}{dt} = -\sigma(t,M,P,N)P + \frac{\epsilon\mu_2 Z^2}{k_6+Z} - U_{2c} + \mu_3 B + \frac{(m+h^+(t))}{M}(N_0 - N) \tag{3.26}$$

where,

$$U_{1c} = \frac{V_b B D}{k_4+S_c+D}$$

$$U_{2c} = \frac{V_b B S_c}{k_4+S_c+D}$$

$$S_c = \min(N, \eta D)$$

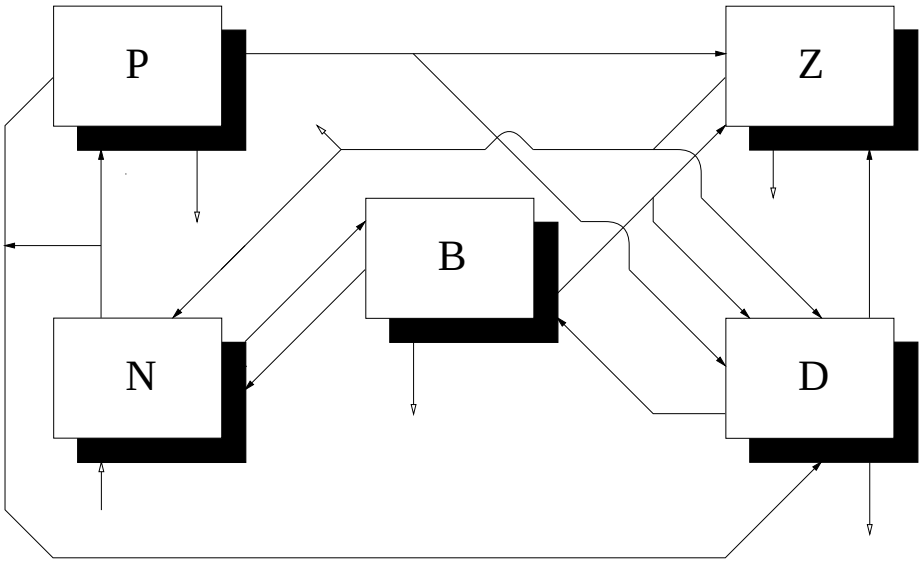

Figure 3.7: Model 5c2, a five compartment system.

Following the lead of model 5c, this model takes its basic structure from model 4c2 and adds a bacterial compartment. As above, this adds a third prey species for zooplankton.

Since DON flows in this model enter the detrital compartment, bacteria here use detritus as a growth substrate analogously to their use of DON in the full model. Ecologically this is not (at a first glance) unreasonable, since particulate organic material is degraded by attached bacteria (see Chapter 1). However, since the bacteria in the full model mainly represent free bacteria, this pathway is questionable, but its consequences unclear. General nutrient is used by the bacteria as a replacement for ammonium, and is both absorbed and excreted.

As in model 4c2, there is a new pathway to allow the decay of detritus to inorganic nutrient.

Model 5c3

The following equations describe a third five compartment version of Fasham (1993). This system adds an ammonium compartment.

$$\frac{dP}{dt} = (1-\gamma)\sigma(t,M,P,N_n,N_r)P - G_{1c} - \frac{\mu_1 P^2}{k_5+P} - \frac{(m+h^+(t))P}{M} \tag{3.27}$$

$$\frac{dZ}{dt} = \beta_1 G_{1c} + \beta_2 G_{2c} - \frac{\mu_2 Z^2}{k_6+Z} - \frac{h(t)Z}{M} \tag{3.28}$$

$$\frac{dD}{dt} = (1-\beta_1)G_{1c} - \beta_2 G_{2c} - \mu_4 D + \gamma\sigma(t,M,P,N_n,N_r)P + \frac{\mu_1 P^2}{k_5+P} + \frac{\delta\mu_2 Z^2}{k_6+Z} - \frac{(m+V+h^+(t))D}{M} \tag{3.29}$$

$$\frac{dN_n}{dt} = -J(t,M,P)Q_1(N_n,N_r)P + \frac{(m+h^+(t))}{M}(N_0-N_n) \tag{3.30}$$

$$\frac{dN_r}{dt} = -J(t,M,P)Q_2(N_r)P + \mu_4 D + \frac{\epsilon\mu_2 Z^2}{k_6+Z} - \frac{(m+h^+(t))N_r}{M} \tag{3.31}$$

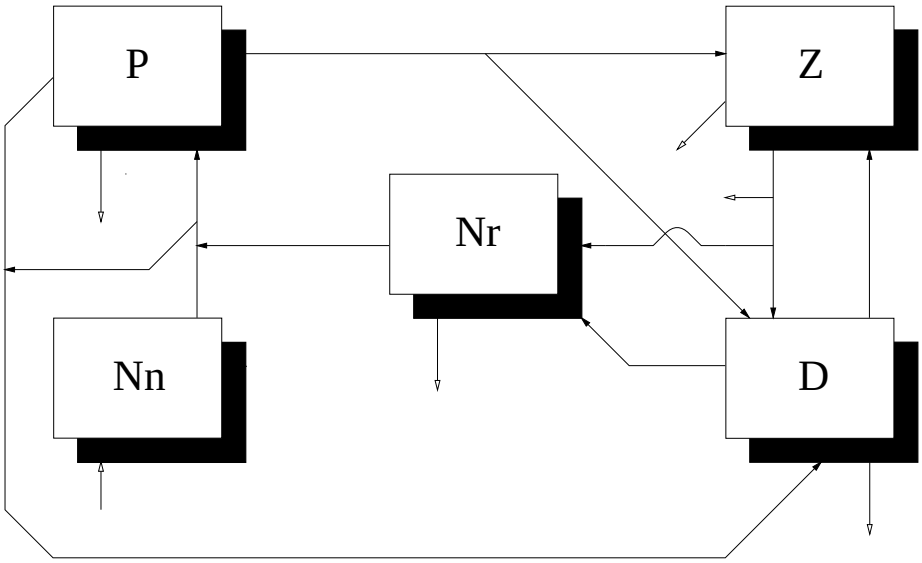

Figure 3.8: Model 5c3, a five compartment system.

where,

$$\sigma = J(t, M, P)Q(N_n, N_r)$$

This third five compartment model builds again on model 4c2, but adds an ammonium compartment and replaces the general nutrient compartment with nitrate.

The phytoplankton equation is modified to uptake from both base nutrients, and recycled nitrogen from zooplankton and detritus now returns to ammonium. As described previously, the detrital compartment has an additional flow to allow its breakdown to usable ammonium.

The presence of both base nitrogen nutrients allows this model to determine the f–ratio of phytoplankton production. This ratio is the fraction of "new" primary production (that which involves nitrate) to total primary production. Since nitrate is normally introduced into the mixed layer by physical processes such as mixing or entrainment, production using it is called "new" production. By contrast, ammonium is normally recycled into the mixed layer by the activities of zooplankton and bacteria within the layer, and production using it is described as "regenerated" production. The f–ratio is a useful measure which provides insight into the patterns of nitrogen flow in an ecosystem. Here it also provides another yardstick against which the reduced models can be compared to the full model.

Model 6c

The following equations describe a six compartment version of Fasham (1993). This system adds an ammonium compartment.

$$\frac{dP}{dt} = (1-\gamma)\sigma(t, M, P, N_n, N_r)P - G_1 - \frac{\mu_1 P^2}{k_5 + P} - \frac{(m + h^+(t))P}{M} \tag{3.32}$$

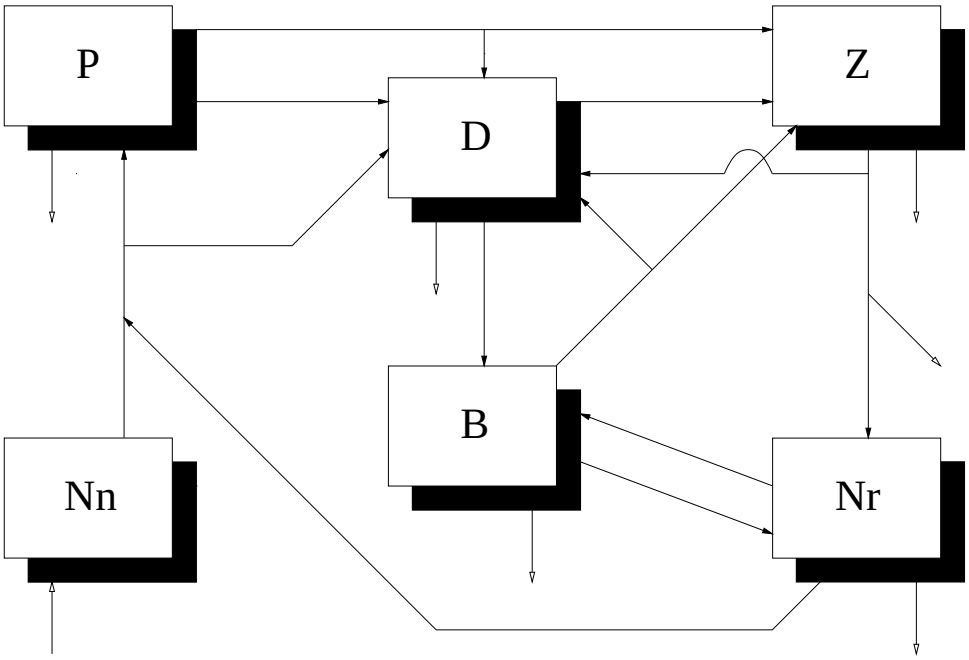

Figure 3.9: Model 6c, a six compartment system.

$$\frac{dZ}{dt} = \beta_1 G_1 + \beta_2 G_2 + \beta_3 G_3 - \frac{\mu_2 Z^2}{k_6 + Z} - \frac{h(t)Z}{M} \tag{3.33}$$

$$\frac{dB}{dt} = U_{1d} + U_{2d} - G_2 - \mu_3 B - \frac{(m + h^+(t))B}{M} \tag{3.34}$$

$$\frac{dD}{dt} = (1-\beta_1)G_1 + (1-\beta_2)G_2 - \beta_3 G_3 - U_{1d} + \gamma\sigma(t,M,P,N)P + \frac{\mu_1 P^2}{k_5 + P} + \frac{\delta\mu_2 Z^2}{k_6 + Z} - \frac{(m + V + h^+(t))D}{M} \tag{3.35}$$

$$\frac{dN_n}{dt} = -J(t,M,P)Q_1(N_n,N_r)P + \frac{(m + h^+(t))}{M}(N_0 - N_n) \tag{3.36}$$

$$\frac{dN_r}{dt} = -J(t,M,P)Q_2(N_r)P - U_{2d} + \mu_3 B + \frac{\epsilon\mu_2 Z^2}{k_6 + Z} - \frac{(m + h^+(t))N_r}{M} \tag{3.37}$$

where,

$$\begin{aligned} \sigma &= J(t,M,P)Q(N_n,N_r) \\ U_{1d} &= \frac{V_b B D}{k_4 + S_d + D} \\ U_{2d} &= \frac{V_b B S_d}{k_4 + S_d + D} \\ S_d &= \min(N_r, \eta D) \end{aligned}$$

This model takes model 5c2 as its basis and adds an ammonium compartment. This addition allows the split of the general nutrient compartment into nitrate and ammonium, as described for model 5c3 above.

This split has the same consequences for phytoplankton and zooplankton already described. Bacteria now use this ammonium, rather than general nutrient, as a growth substrate together with detritus. The detrital compartment retains its new breakdown pathway to return organic nitrogen to ammonium.

Model 6c2

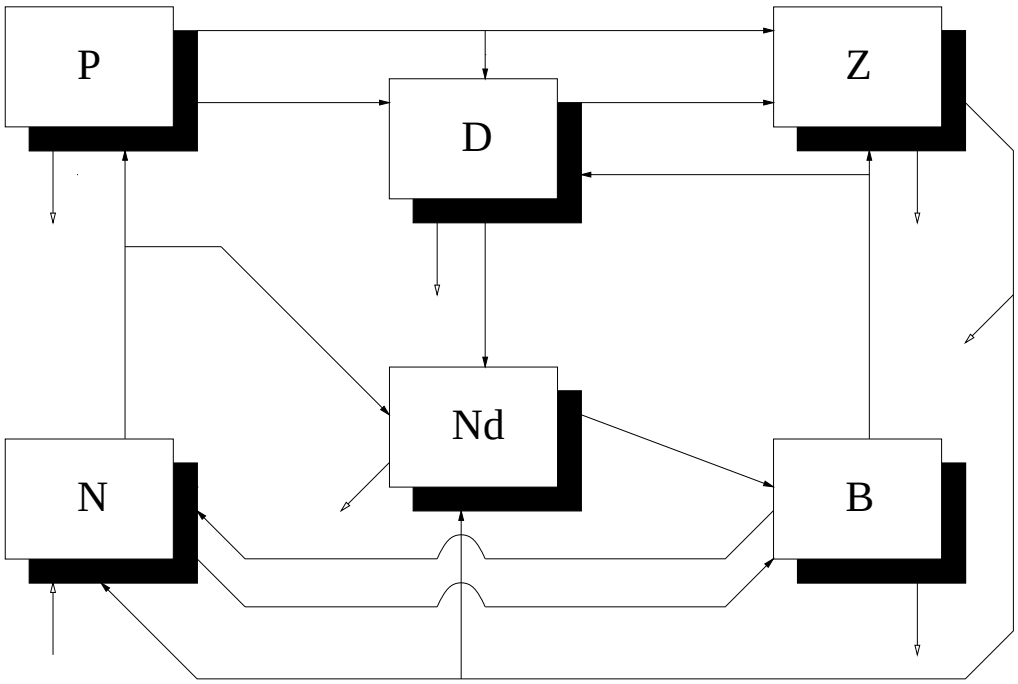

Figure 3.10: Model 6c2, a six compartment system.

The following equations describe a second six compartment version of Fasham (1993). This system adds a dissolved organic nitrogen compartment.

$$\frac{dP}{dt} = (1-\gamma)\sigma_c(t,M,P,N)P - G_1 - \frac{\mu_1 P^2}{k_5+P} - \frac{(m+h^+(t))P}{M} \tag{3.38}$$

$$\frac{dZ}{dt} = \beta_1 G_1 + \beta_2 G_2 + \beta_3 G_3 - \frac{\mu_2 Z^2}{k_6+Z} - \frac{h(t)Z}{M} \tag{3.39}$$

$$\frac{dB}{dt} = U_{1e} + U_{2e} - G_2 - \mu_3 B - \frac{(m+h^+(t))B}{M} \tag{3.40}$$

$$\frac{dD}{dt} = (1-\beta_1)G_1 + (1-\beta_2)G_2 - \beta_3 G_3 - \mu_4 D + \frac{\mu_1 P^2}{k_5+P} - \frac{(m+V+h^+(t))D}{M} \tag{3.41}$$

$$\frac{dN}{dt} = -\sigma_c(t,M,P,N)P - U_{2e} + \mu_3 B + \frac{\epsilon\mu_2 Z^2}{k_6+Z} + \frac{(m+h^+(t))}{M}(N_0 - N) \tag{3.42}$$

$$\frac{dN_d}{dt} = \gamma\sigma(t,M,P,N)P + \mu_4 D + \frac{\delta\mu_2 Z^2}{k_6+Z} - U_{1e} - \frac{(m+h^+(t))N_d}{M} \tag{3.43}$$

where,

$$U_{1e} = \frac{V_b B N_d}{k_4 + S_e + N_d}$$

$$
\begin{aligned}
U_{2e} &= \frac{V_b B S_e}{k_4 + S_e + N_d} \\
S_e &= \min(N, \eta N_d)
\end{aligned}
$$

This model essentially takes model 5c as its basis and adds a DON compartment. This redirects several flows which previously entered detritus.

The attention of bacteria is now split between general nutrient and DON for growth substrate. The detrital compartment no longer needs the new pathway to allow decay into base nitrogen nutrients.

3.2.2 Modelling nitrate implicitly

In the work here, the major aim has been to examine reduced models to determine the minimum size of model required to study the more complex plankton ecosystems that the models of Fasham, Ducklow & McKelvie (1990) and Fasham (1993) were built to study.

One of the ways in which such models could be made would be to represent compartments or processes of the full model implicitly (in a not dissimilar way, the full model represents many processes from reality implicitly). In some of the models already described this has been done (recycling elements have been replaced by simple rates or allowed to become instantaneous).

In the following four models the general nutrient compartment has been replaced by an implicit nitrate compartment and an explicit ammonium compartment. The aim being to examine the usefulness of an implicit compartment, but also to predict the f–ratio (which depends more on the concentration of ammonium than the concentration of nitrate).

The nitrate compartment is put back into the four reduced forms as a constant value (N_n^*). In most of the numerical solutions presented here, the value used is that of the annual mean nitrate concentration from solutions using the full model.

Model 3c3

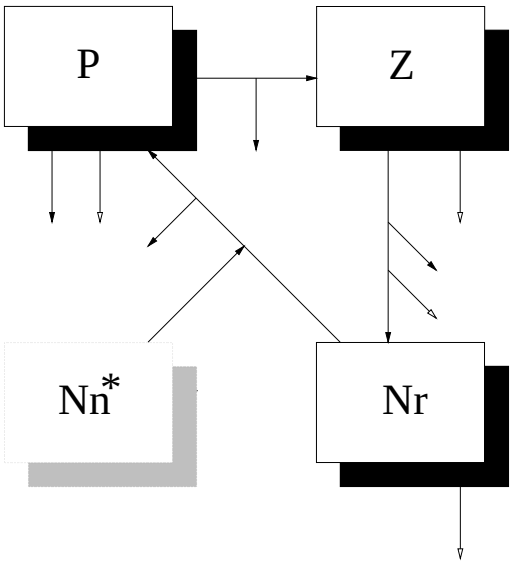

Figure 3.11: Model 3c3, a three compartment system. In this and subsequent schematic diagrams, the shaded N_n^* compartment is modelled only implicitly (see text for details).

The following equations describe a three compartment version of Fasham (1993).

$$\frac{dP}{dt} = (1-\gamma)\sigma_d(t,M,P,N_n^*,N_r)P - G_{1b} - \frac{\mu_1 P^2}{k_5+P} - \frac{(m+h^+(t))P}{M} \tag{3.44}$$

$$\frac{dZ}{dt} = \beta_1 G_{1b} - \frac{\mu_2 Z^2}{k_6+Z} - \frac{h(t)Z}{M} \tag{3.45}$$

$$\frac{dN_r}{dt} = -J(t,M,P)Q_2(N_r)P + \frac{\epsilon\mu_2 Z^2}{k_6+Z} - \frac{(m+h^+(t))N_r}{M} \tag{3.46}$$

where,

$$\begin{aligned} \sigma_d &= J(t,M,P)Q(N_n^*,N_r) \\ Q(N_n^*,N_r) &= Q_1(N_n^*,N_r) + Q_2(N_r) \\ Q_1 &= \frac{N_n^* \exp\{-\psi N_r\}}{k_1+N_n^*} \\ Q_2 &= \frac{N_r}{k_2+N_r} \end{aligned}$$

This three compartment model is based upon model 3c. As already described, the general nutrient compartment has been replaced by an ammonium one, and nitrate is represented implicitly in the phytoplankton nutrient uptake equations.

Since the model is no longer conservative in its treatment of nitrogen flows, and since the f–ratio is of interest, flows into detritus and DON are ignored (similarly to models 2c and 3c2, but dissimilar to model 3c).

Model 4c3

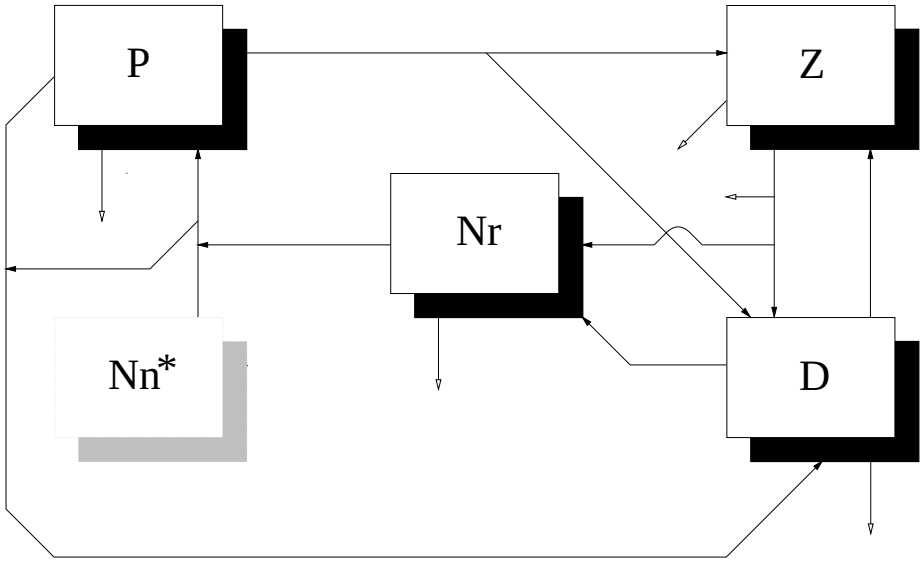

Figure 3.12: Model 4c3, a four compartment system.

The following equations describe a four compartment version of Fasham (1993).

$$\frac{dP}{dt} = (1-\gamma)\sigma_d(t,M,P,N_n^*,N_r)P - G_{1c} - \frac{\mu_1 P^2}{k_5+P} - \frac{(m+h^+(t))P}{M} \tag{3.47}$$

$$\frac{dZ}{dt} = \beta_1 G_{1c} + \beta_2 G_{2c} - \frac{\mu_2 Z^2}{k_6 + Z} - \frac{h(t)Z}{M} \tag{3.48}$$

$$\frac{dD}{dt} = (1-\beta_1)G_{1c} - \beta_2 G_{2c} - \mu_4 D + \gamma\sigma_d(t, M, P, N_n^*, N_r)P + \frac{\mu_1 P^2}{k_5 + P} + \frac{\delta\mu_2 Z^2}{k_6 + Z} - \frac{(m + V + h^+(t))D}{M} \tag{3.49}$$

$$\frac{dN_r}{dt} = -J(t, M, P)Q_2(N_r)P + \frac{\epsilon\mu_2 Z^2}{k_6 + Z} + \mu_4 D - \frac{(m + h^+(t))N_r}{M} \tag{3.50}$$

This four compartment model is based upon model 4c2. As previously, the general nutrient compartment has been replaced by implicit nitrate and an explicit ammonium compartment.

Model 5c4

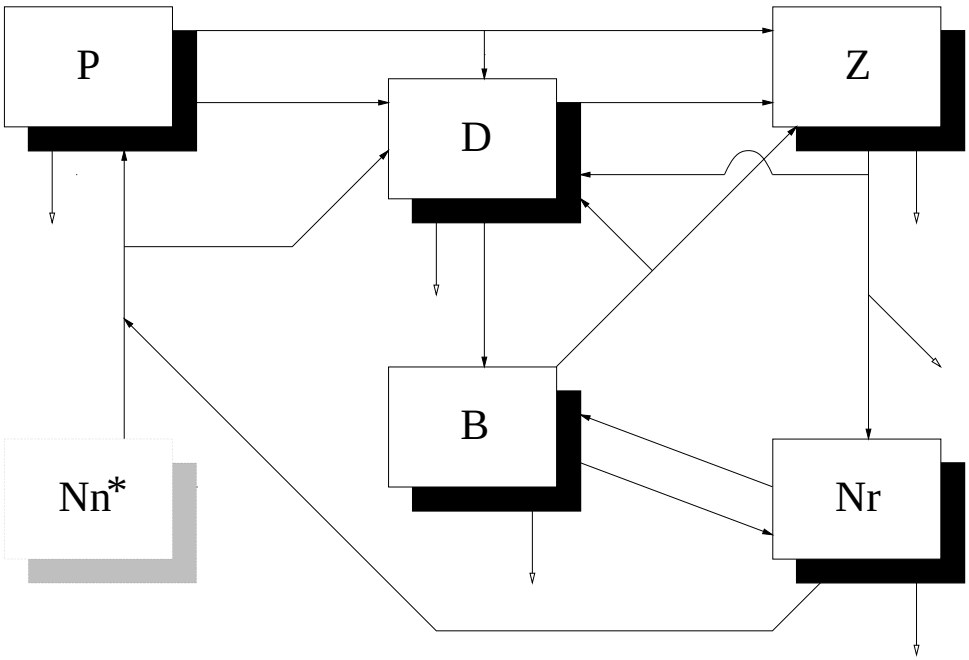

Figure 3.13: Model 5c4, a five compartment system.

The following equations describe a five compartment version of Fasham (1993).

$$\frac{dP}{dt} = (1-\gamma)\sigma_d(t, M, P, N_n, N_r)P - G_1 - \frac{\mu_1 P^2}{k_5 + P} - \frac{(m + h^+(t))P}{M} \tag{3.51}$$

$$\frac{dZ}{dt} = \beta_1 G_1 + \beta_2 G_2 + \beta_3 G_3 - \frac{\mu_2 Z^2}{k_6 + Z} - \frac{h(t)Z}{M} \tag{3.52}$$

$$\frac{dB}{dt} = U_{1d} + U_{2d} - G_2 - \mu_3 B - \frac{(m + h^+(t))B}{M} \tag{3.53}$$

$$\frac{dD}{dt} = (1-\beta_1)G_1 + (1-\beta_2)G_2 - \beta_3 G_3 - U_{1d} + \gamma\sigma_d(t, M, P, N)P + \frac{\mu_1 P^2}{k_5 + P} + \frac{\delta\mu_2 Z^2}{k_6 + Z} - \frac{(m + V + h^+(t))D}{M} \tag{3.54}$$

$$\frac{dN_r}{dt} = -J(t, M, P)Q_2(N_r)P - U_{2d} + \mu_3 B + \frac{\epsilon\mu_2 Z^2}{k_6 + Z} - \frac{(m + h^+(t))N_r}{M} \tag{3.55}$$

This five compartment model is based upon model 6c. The nitrate equation in that model has been removed however, and the occurrence of nitrate in the remainder of the equations replaced by N_n^*.

Model 6c3

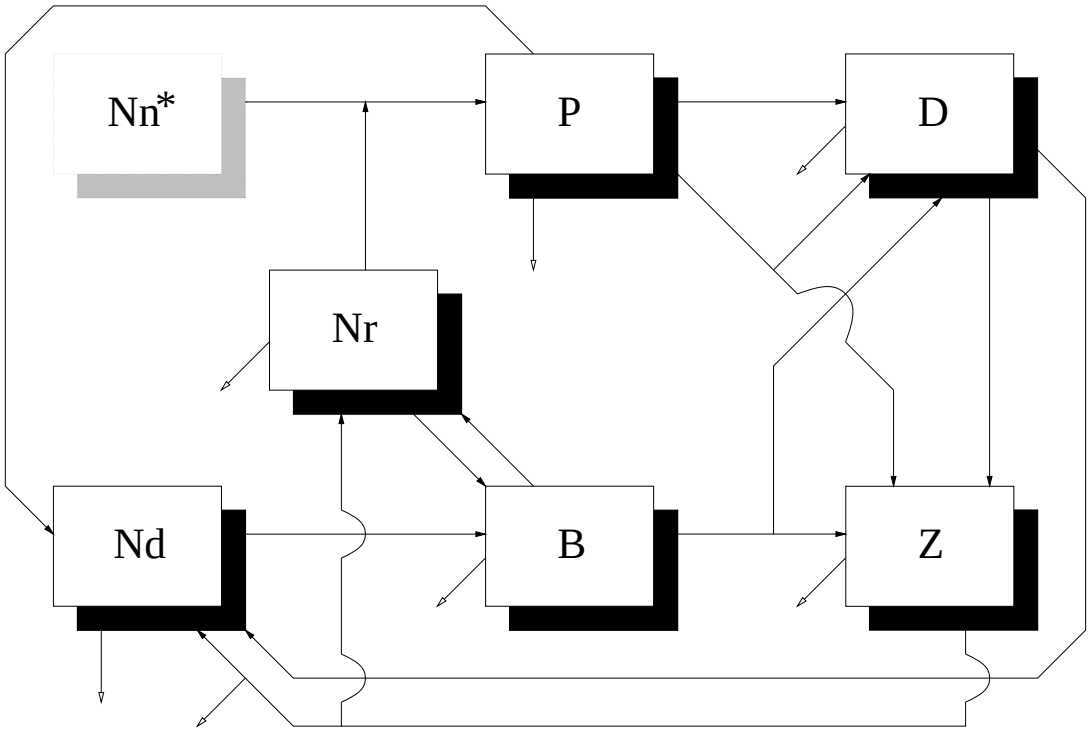

Figure 3.14: Model 6c3, a six compartment system.

The following equations describe a third six compartment version of Fasham (1993).

$$\frac{dP}{dt} = (1-\gamma)\sigma_d(t,M,P,N_n,N_r)P - G_1 - \frac{\mu_1 P^2}{k_5+P} - \frac{(m+h^+(t))P}{M} \tag{3.56}$$

$$\frac{dZ}{dt} = \beta_1 G_1 + \beta_2 G_2 + \beta_3 G_3 - \frac{\mu_2 Z^2}{k_6+Z} - \frac{h(t)Z}{M} \tag{3.57}$$

$$\frac{dB}{dt} = U_1 + U_2 - G_2 - \mu_3 B - \frac{(m+h^+(t))B}{M} \tag{3.58}$$

$$\frac{dD}{dt} = (1-\beta_1)G_1 + (1-\beta_2)G_2 - \beta_3 G_3 - \mu_4 D + \frac{\mu_1 P^2}{k_5+P} - \frac{(m+V+h^+(t))D}{M} \tag{3.59}$$

$$\frac{dN_r}{dt} = -J(t,M,P)Q_2(N_r)P - U_2 + \mu_3 B + \frac{\epsilon\mu_2 Z^2}{k_6+Z} - \frac{(m+h^+(t))N_r}{M} \tag{3.60}$$

$$\frac{dN_d}{dt} = \gamma J(t,M,P)Q(N_n,N_r)P + \mu_4 D + \frac{\delta\mu_2 Z^2}{k_6+Z} - U_1 - \frac{(m+h^+(t))N_d}{M} \tag{3.61}$$

This six compartment model is based directly upon the full model. The nitrate equation in the full model has been removed however, and the occurrence of nitrate in the remainder of the equations replaced by N_n^*.

Table 3.1 presents a summary of the compartments present in each of the fourteen reduced forms. In the final column the number of parameters required for each model is listed. The full model has 33 parameters in total.

Model complexity	**Name**	**P**	**Z**	**B**	**D**	$\mathbf{N}_n$	$\mathbf{N}_r$	$\mathbf{N}_d$	**N**	$\mathbf{N}_n^*$	**Param**
2 compartment	2c	√	√								16
3 compartment	3c	√	√						√		20
	3c2	√	√		√						20
	3c3	√	√				√			√	21
4 compartment	4c	√	√		√				√		25
	4c2	√	√		√				√		25
	4c3	√	√		√		√			√	27
5 compartment	5c	√	√	√	√				√		30
	5c2	√	√	√	√				√		30
	5c3	√	√		√	√	√				27
	5c4	√	√	√	√		√			√	32
6 compartment	6c	√	√	√	√	√	√				32
	6c2	√	√	√	√			√	√		31
	6c3	√	√	√	√		√	√		√	33
Full model		√	√	√	√	√	√	√			33

Table 3.1: A summary table of the compartments present in each of the reduced models. N_n^* is represented implicitly in the models indicated. The **Param** column lists the number of parameters required for each reduced model.

3.2.3 Ammonium inhibition of nitrate uptake

As mentioned in chapter 2, the formulation of ammonium–inhibition of nitrate uptake used in the Fasham (1993) model (and the reduced forms) is by no means the only one.

$$Q(N_n, N_r) = Q_1(N_n, N_r) + Q_2(N_r) = \frac{N_n \exp\{-\psi N_r\}}{k_1 + N_n} + \frac{N_r}{k_2 + N_r} \tag{3.62}$$

In fact, some researchers (A. H. Taylor, Plymouth Marine Laboratory, pers. comm.) have expressed strong reservations about this particular form.

Fasham (1995) examined this form, and found it to be more adequately replaced by an uptake model in which ammonium inhibition is only implicitly parameterised.

$$Q(N_n, N_r) = \frac{\frac{N_n}{k_1} + \frac{N_r}{k_2}}{1 + \frac{N_n}{k_1} + \frac{N_r}{k_2}} \tag{3.63}$$

This form drops direct inhibition by the negative exponential of ammonium and its coefficient,ψ, but compensates for this by reducing the value of k_2 to 0.01. This allows the model phytoplankton to still express a preference for ammonium, but removes the limitation on Q placed on the previous formulation by the negative exponential (which reduced overall nutrient uptake as a result of inhibition of nitrate uptake).

This approach of favouring ammonium uptake by reducing its half–saturation constant is used by many other models (*e.g.* Hofmann & Ambler, 1988; Taylor *et al.*, 1993), but has been criticised in a recent paper which drew together the results of five research cruises in the North Atlantic (Harrison, Harris & Irwin, 1996). One of the results from this paper was that half–saturation constants for nitrate and ammonium should be set to equivalent values (albeit ones up to an order of magnitude lower than those chosen in Fasham, 1993).

However, to examine the possible importance of this alternative formulation, it has been put into a version of the full model so that the significance of this particular facet of the model can be explored. This alternative full model is referred to as the NH_4 model. Some of its results appear alongside those of the reduced models, but a separate discussion appears at the end of the results section.

3.2.4 Model numerical solutions

Mixed–layer depth data was available for both OWS "India" and Bermuda Station "S", and numerical solutions were performed at these locations with all of the reduced models. OWS "India" is at a temperate latitude in the North Atlantic Ocean and has very deep mixing during the winter months. Bermuda Station "S", by contrast, is sub–tropical with considerably shallower mixing, even in the winter months.

Forced solutions were favoured over unforced ones for several reasons. Primarily, the full Fasham (1993) model was originally created to study annual cycles rather than steady state situations. Additionally, since unforced solutions would probably only produce a stable equilibrium (see Chapter 4), distinguishing a "good" model from a "bad" one would be more difficult. Essentially, the dynamics through time, rather than the constant flows between compartments, are of greater interest in this work.

Although the disparity between these two stations provides a not unreasonable sample of the variety of physical forcing the model would likely experience if simulated all over the global ocean, additional solutions under different forcing regimes were performed.

Aside from the differences in receipt of irradiance due to latitude, the two principal differences between OWS "India" and Bermuda Station "S" are the depth of winter mixing already mentioned, and the deep ocean nitrate concentration. The influences these two features have on the seasonal dynamics of the full model were examined by calculating solutions across ranges of mixed layer winter maxima and subthermocline nitrate concentration.

Since these ranges were observed to produce significant qualitative changes in the behaviour of the full model, the reduced models (where appropriate) were similarly examined.

In all of these additional solutions, the models were run with the appropriate differences, but with otherwise OWS "India" settings. In the case of different cycles of mixed–layer depth, a small number of alternative series of mixed–layer depth were generated such that the winter maximum was set to a given value and the rest of the data set scaled around this value. Figure 3.15 shows these new data sets.

Computational details

All of the model solutions described were performed on Sun SPARC stations (IPX, 10 and 20) using programs written in the C language by the author. Several representative programs and subroutines have been included in Appendix A-2. All model output was handled by the visualisation software, MATLAB v5.0 (The MathWorks, Inc., Massachusetts, USA), for analysis and interpretation. Additionally, MATLAB was used to produce all of the graphical output shown.

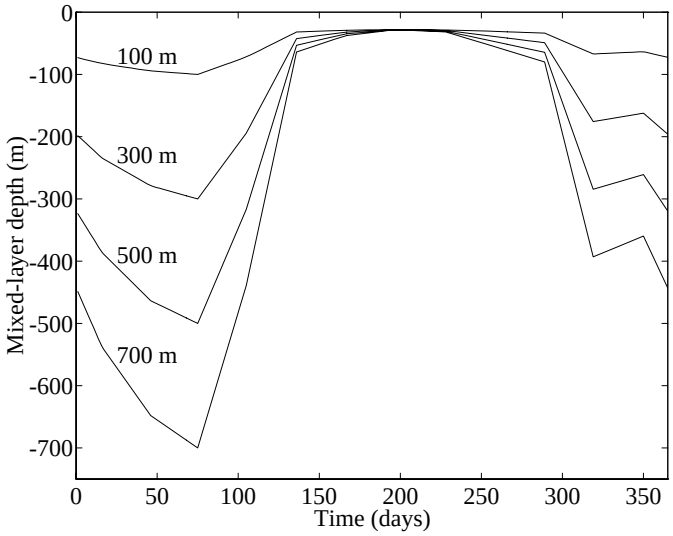

Figure 3.15: Annual mixed–layer depth profiles generated from the OWS "India" data set but re–scaled to new winter maximum depths.

A Runge–Kutta IV scheme (with fixed step–length) was used to perform the numerical integration of the ODEs in this (and later) work. Testing showed that for most cases, a consistent model solution was produced for all step–lengths less than 3 hours (*i.e.* 8 iterations per day). For simplicity, a step–length of 1 hour was used (*i.e.* 24 iterations per day). Model runs where a shorter step–length was required are identified in the text.

Given this step length, it was found that usually within 5 to 10 simulated years, transient behaviour in the model died out (*i.e.* variation between compartment values on the same day of consecutive years was less than 10^{-6} mmol N m^{-3}) and the system produced a consistent annual pattern. In all of the results presented, 50 years were allowed to minimise transient effects. The results shown were then all taken from year 51.

In all solutions, initial conditions for model compartments were set to 0.01 mmol N m^{-3}. The only exceptions were for nitrate or comparable nutrient compartments which were set to the default value for N_0.

Analytical integration of light–limited growth

The model described in Fasham (1993) makes use of an analytical formulation derived by Evans & Parslow (1985) for integrating primary production both down the mixed layer and through the day. In all of the work described in this thesis, this approach has been revised. An analytical function for instantaneous light–limited growth down the water column has been derived, and this function is numerically integrated across the day. This allows the function to more accurately represent the non–linear pattern

of daily irradiance, and to account for changes in the phytoplankton population during the day.

The software package MAPLE V (Waterloo Maple Software, Waterloo, Ontario, Canada) was used to produce the analytical form and the equations below detail the formula derived for depth–integrated production.

Given that irradiance is attenuated with depth due to absorption by water, k_w, and phytoplankton pigments, k_c, irradiance at a given depth, I_z, can be calculated from irradiance just below the surface of the water, I_0, by applying the following equation :

$$I_z = I_0 \exp\{-(k_w + k_c P)z\}$$

A standard function, $F(I)$, is then used to describe the relationship between photosynthesis and irradiance. This takes the form of a curve described by the maximum growth rate, V_p, and the initial slope of the curve, α :

$$F(I) = \frac{V_p \alpha I}{\sqrt{({V_p}^2 + \alpha^2 I^2)}}$$

To produce an equation for instantaneous photosynthesis down a water column, the previous two equations must be combined by integrating them with respect to depth :

$$J(M, P, I_0) = \frac{1}{M} \int_0^M F(I_0 \exp\{-(k_w + k_c P)z\})\, dz$$

This then yields an equation which expresses instantaneous irradiance–limited growth in terms of mixed–layer depth, M, phytoplankton concentration, P, and irradiance just below the surface of the water, I_0 :

$$\begin{aligned} J(M, P, I_0) &= -\frac{1}{M}\left(\frac{\ln\left(\alpha I_0 \exp\{-(k_w + k_c P)M\} + \sqrt{V_p^2 + \alpha^2 I_0^2 (\exp\{-(k_w + k_c P)M\})^2}\right)}{\alpha I_0 (k_w + k_c P)}\right) \\ &\quad + \frac{1}{M}\left(\frac{\ln\left(\alpha I_0 + \sqrt{V_p^2 + \alpha^2 I_0^2}\right)}{\alpha I_0 (k_w + k_c P)}\right) \end{aligned}$$

This function is then just treated in the same manner as other model terms and calculated on an iteration–by–iteration basis during a model run.

3.3 Results

3.3.1 OWS "India" solutions

Figures 3.16 to 3.19 illustrate the seasonal patterns of pairs of the various model compartments produced by the full model and its reduced forms at OWS "India". Where a reduced model lacks both of the compartments, a gap is left in the appropriate position on the figure tableau.

With the exception of model 5c, all of the models capture the basic winter/summer pattern of ecosystem activity observed at OWS "India". Model 5c fails to replicate this pattern for several reasons, primarily because the bacteria are assumed to not be limited by the forcing functions represented in the model. This combines with the bacterial compartment's use of general nutrient as its sole substrate, and allows the bacteria to uptake nutrient at relatively high rates throughout the year. This leads to high bacterial populations all year round, high zooplankton populations, low nutrient concentrations, and resultingly low phytoplankton populations (a combination of low nutrient concentrations and high zooplankton grazing pressure).

Phytoplankton and zooplankton

Figure 3.16 shows the abundances of phytoplankton and zooplankton through an annual cycle. Of particular note in the full model are the cycles of the populations in the summer months following the spring bloom. The significance of such cycles has been examined in recent work by Edwards & Brindley (1996) and Popova *et al.* (1997), and is more fully examined for the Fasham (1993) model in Chapter 4.

Of the reduced models, there are roughly three classes of behaviour. Models which are very similar to the full model (*e.g.* 3c2, 4c, 4c2, 4c3, 5c3, 6c2 and 6c3), models whose summer peaks and troughs are higher and lower respectively than the full model's (*e.g.* 2c, 3c and 3c3), and models where the summer zooplankton peaks are considerably greater than those of the full model (*e.g.* 5c2, 5c4 and 6c).

Bacteria and ammonium

Figure 3.17 shows the abundance of bacteria and the concentration of ammonium through an annual cycle. Gaps exist where models lack both of these compartments.

Only models 6c2 and 6c3 come close to accurately mimicing the full model. However, models 4c3 and 5c3 are only slightly different in their annual patterns of ammonium concentration. As previously, models 5c2, 5c4 and 6c show similar patterns which diverge from the full model. Model 3c3 utterly fails to capture the annual pattern of ammonium observed in the full model.

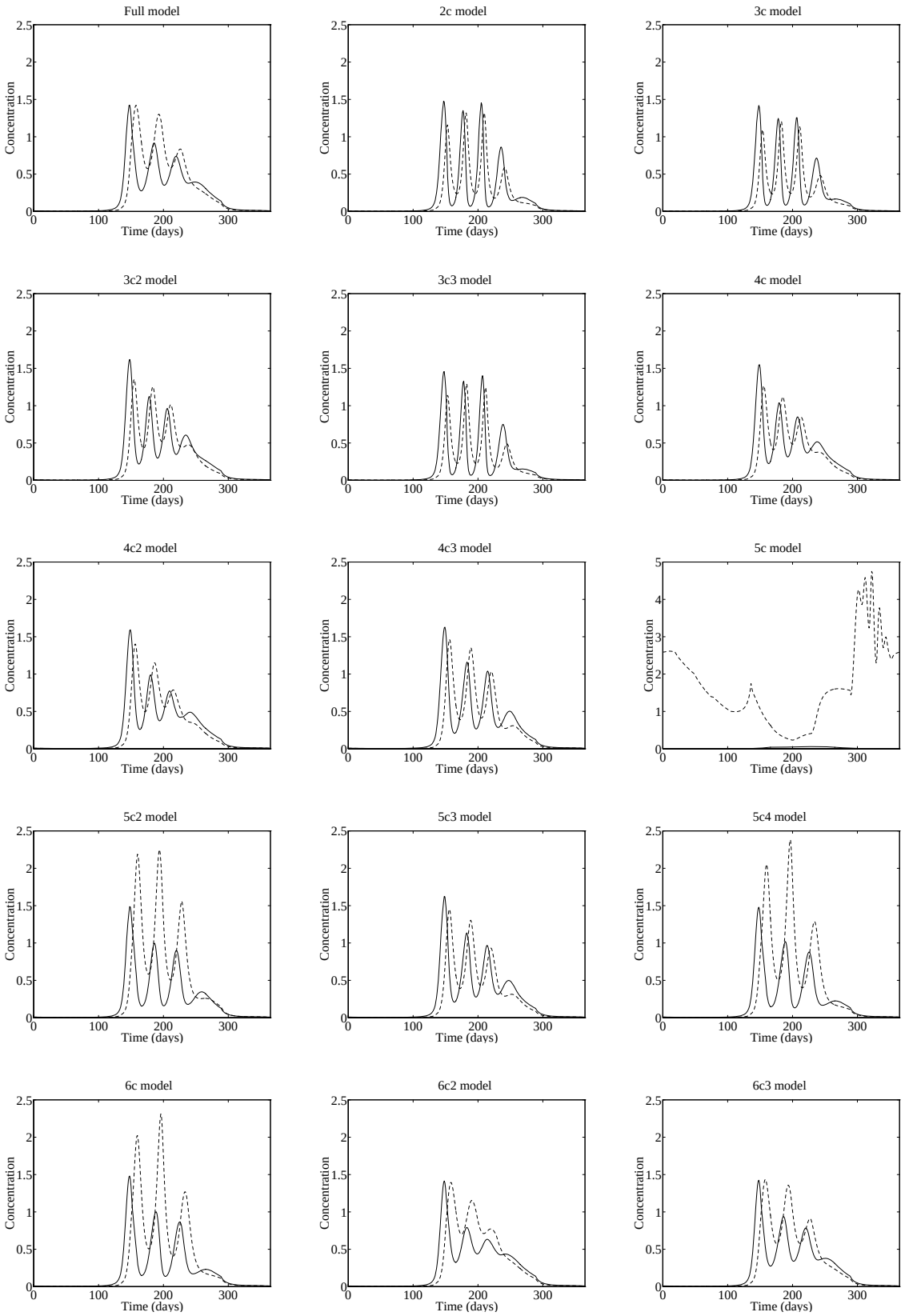

Figure 3.16: Simulated annual cycles of phytoplankton (solid line) and zooplankton (dashed line) at OWS "India" in each of the models. Note the change of scale for model 5c. Concentrations are in mmol N m^{-3}.

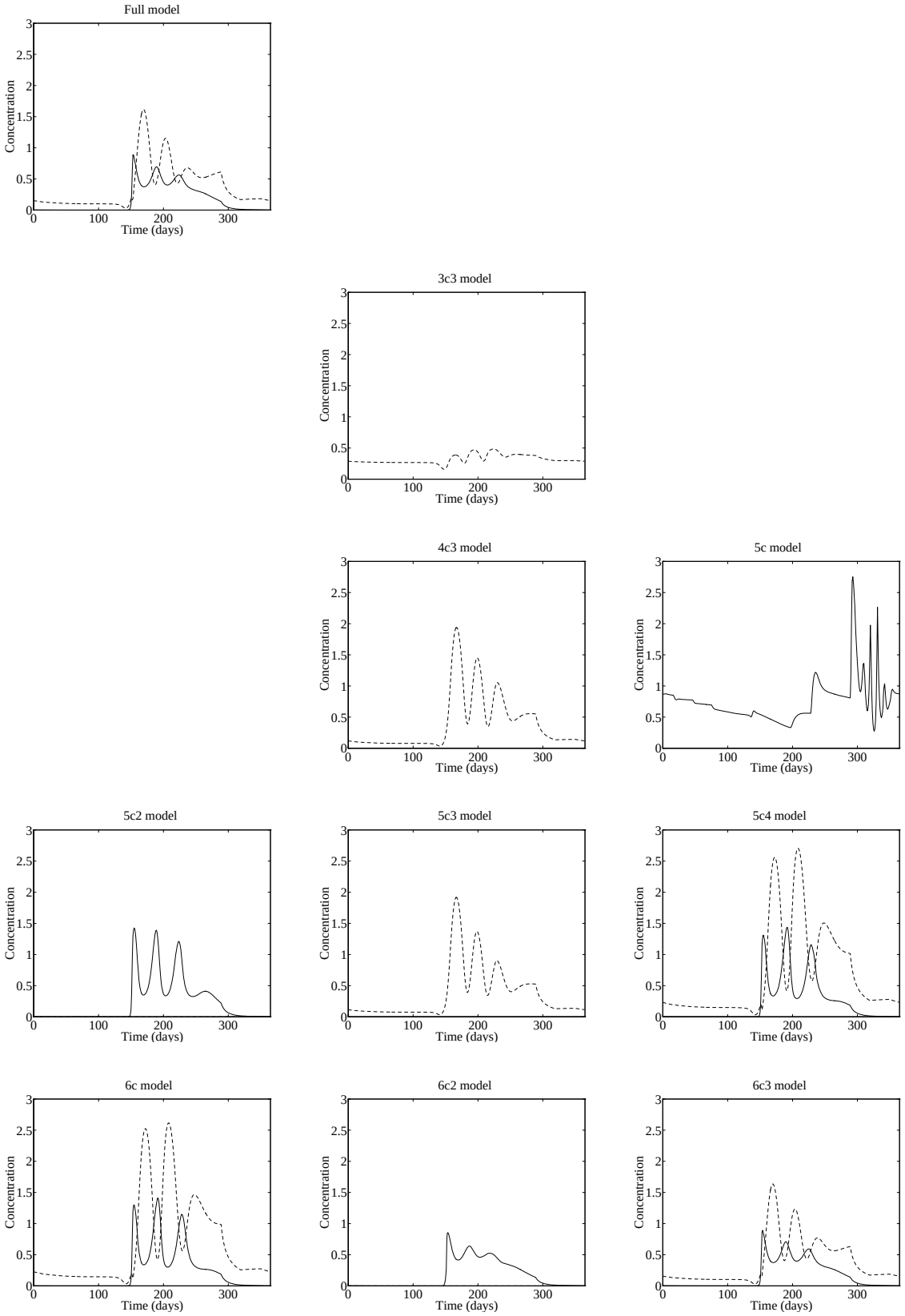

Figure 3.17: Simulated annual cycles of bacteria (solid line) and ammonium (dashed line) at OWS "India" in each of the appropriate models. Concentrations are in mmol N m^{-3}.

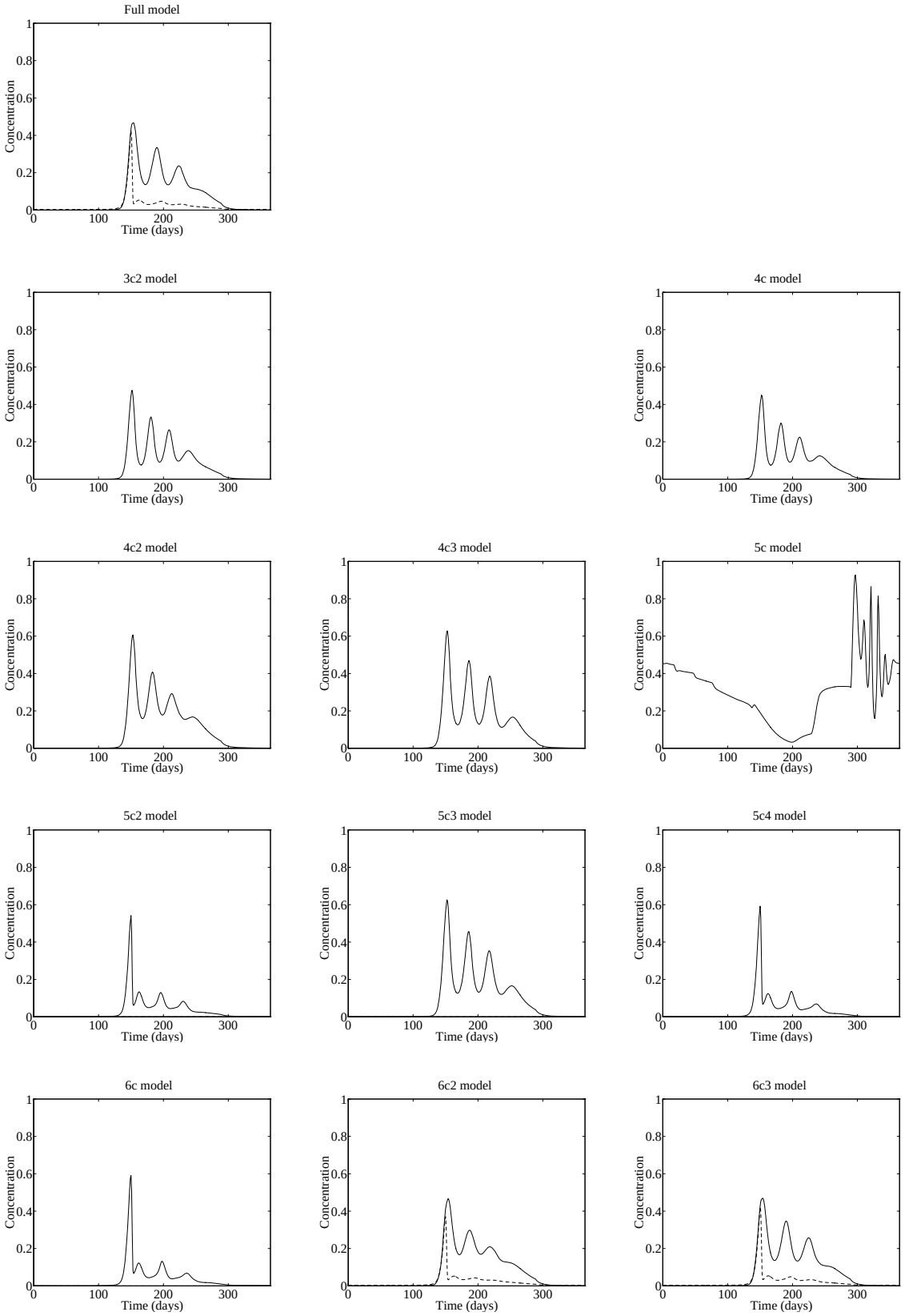

Figure 3.18: Simulated annual cycles of detritus (solid line) and DON (dashed line) at OWS "India" in each of the appropriate models. Concentrations are in mmol N m^{-3}.

Detritus and DON

Figure 3.18 shows the concentrations of detritus and DON through an annual cycle. Because of the relatively tight coupling between detritus and phytoplankton (through natural mortality and zooplankton grazing inefficiency), the pattern of detritus is similar to that of phytoplankton. The pattern of DON shows an early spring spike where concentrations rise before bacterial populations have risen sufficiently to utilise the DON.

Unsurprisingly, most reduced models show seasonal concentrations of detritus which are similar to that of the full model. However, most have slightly more extreme peaks and troughs (*e.g.* models 3c2 and 4c) or slightly more rapid cycles (*e.g.* model 4c2). Models 5c2, 5c4 and 6c show patterns of detritus abundance which are very similar to those of the full model (plus models 6c2 and 6c3) for DON.

Only models 6c2 and 6c3 incorporate DON explicitly, and both capture its annual cycle of abundance well.

Nitrate and total system nitrogen

Figure 3.19 shows the concentrations of nitrate or general nutrient and total system nitrogen across the annual cycle. In the full model, nitrate is depleted from the mixed layer during the productive summer months but recovers to high levels in the unproductive, deeper mixed winter months.

With the exception of model 5c3, all of the reduced models show greater summer nitrate/nutrient levels than the full model. However, this is perhaps unsurprising considering that where a general nutrient compartment exists it receives regenerated flows as well as nitrogen entrainment. Models 4c2 and 6c2 show lower summer nitrate levels and somewhat better agreement with the seasonal pattern than the other reduced forms.

The implicit nitrate models have constant nitrate so are unable to provide information about the cycle of nitrate abundance or total system nitrogen.

Phytoplankton growth limitation

Figure 3.20 shows the pattern of growth limitations placed on the phytoplankton. Maximum irradiance–limited growth is determined from the depth–integrated light field. Nutrient limitation represents combined nitrate and ammonium limitation where appropriate. At OWS "India", growth limitation is most severe in the winter where lack of incident irradiance reduces growth to almost zero. As summer approaches and irradiance increases, this growth limitation is reduced. However, it is still sufficiently severe to exert the greater influence. Nutrient limitation is mild by comparison.

Almost all of the reduced models have a similar pattern of irradiance limitation to the full model. Mod-

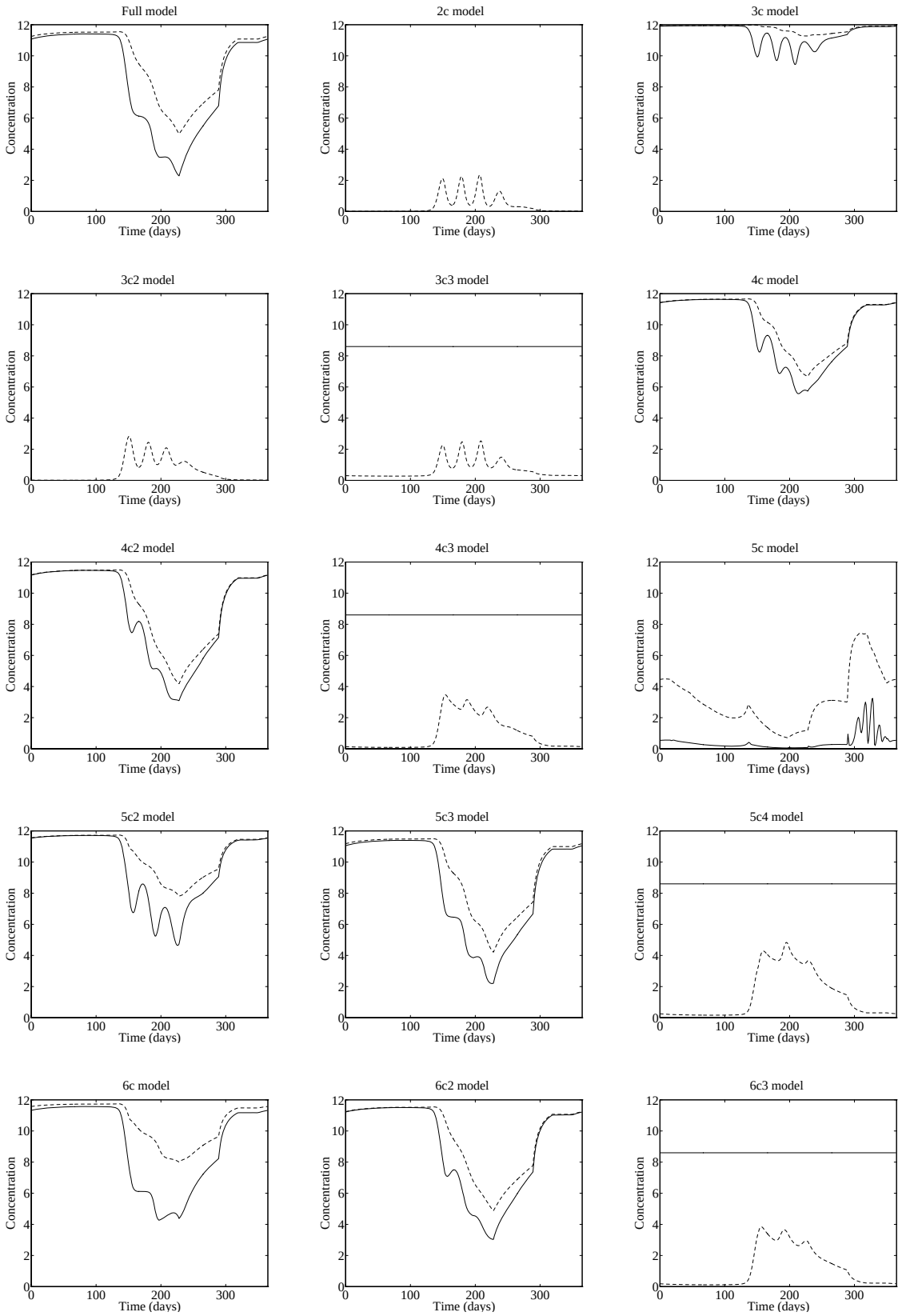

Figure 3.19: Simulated annual cycles of nitrate/nutrient (solid line) and total system nitrogen (dashed line) at OWS "India" in each of the models. Concentrations are in mmol N m^{-3}.

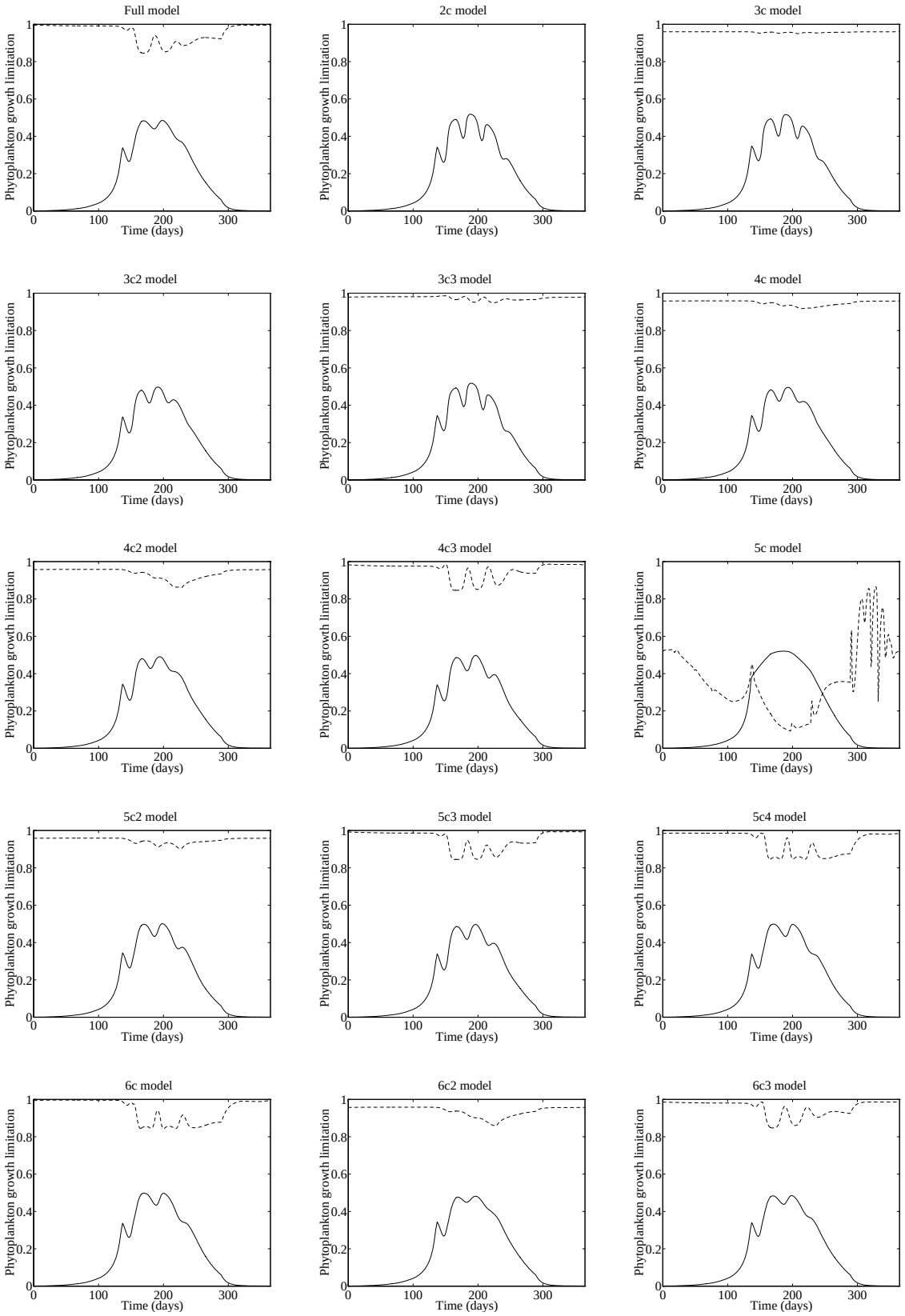

Figure 3.20: Simulated annual cycles of maximum possible phytoplankton growth (solid line) and nutrient limitation (dashed line) at OWS "India" in each of the appropriate models. Maximum growth in d^{-1}, nutrient limitation is non–dimensional.

els 2c, 3c and 3c3 show greater limitation where their phytoplankton populations grow high enough to induce self–shading.

Nutrient limitation is somewhat more haphazard because the models less accurately model nutrients (as seen in Figure 3.19).

Zooplankton mortality rate

Figure 3.21 shows the annual pattern of zooplankton loss rate. Since zooplankton are are their greatest concentration in the summer, their loss rates (through predation) are greatest then too.

The reduced models only perform as well here as they do in modelling zooplankton. Several models (*e.g.* 2c, 3c and 3c3) have significant variation in the summer months as their zooplankton populations undergo extreme fluctuations.

f–ratio

Figure 3.22 shows the annual pattern of the f–ratio. In the winter, when nitrate concentrations are high due to deep mixing and low production, the ratio is close to one. In the summer, when nitrate levels are somewhat reduced and ammonium levels are more significant through regeneration processes, the ratio falls, recovering as winter sets in.

Models 4c3, 5c3 and especially 6c3 compare well with the full model. Model 3c3 unsurprisingly fails to capture the variation across the year. Models 5c4 and 6c have very low troughs in the summer due to high ammonium concentrations generated through regenerative processes.

Note that the annual pattern of the f–ratio for the NH_4 model is also shown in figure 3.22. The results from this model are fully discussed in section 3.3.7.

OWS "India" statistics

Table 3.2 details a series of statistics which quantify particular aspects of the OWS "India" solutions. Net primary productivity quantifies the total amount of nitrogen which is absorbed by phytoplankton across the year (after exudation losses). The quantity is depth–integrated so the units are in an areal measure (*i.e.* m^{-2}. The f–ratio here is the fraction of total annual primary production which comes from "new" (nitrate) production. Note that this is not the mean of the daily f–ratio values (which would be biased by days on which the production was low since these days would carry equal weight to a day on which total production was high). The first two phytoplankton statistics respectively refer to the maximum size of the spring bloom (**P max**), and the day on which this maximum occurs (**P time**). The last two statistics refer to the phytoplankton–zooplankton oscillations which dominate the summer months. A simple MATLAB macro was written to determine the location of turning points in the annual

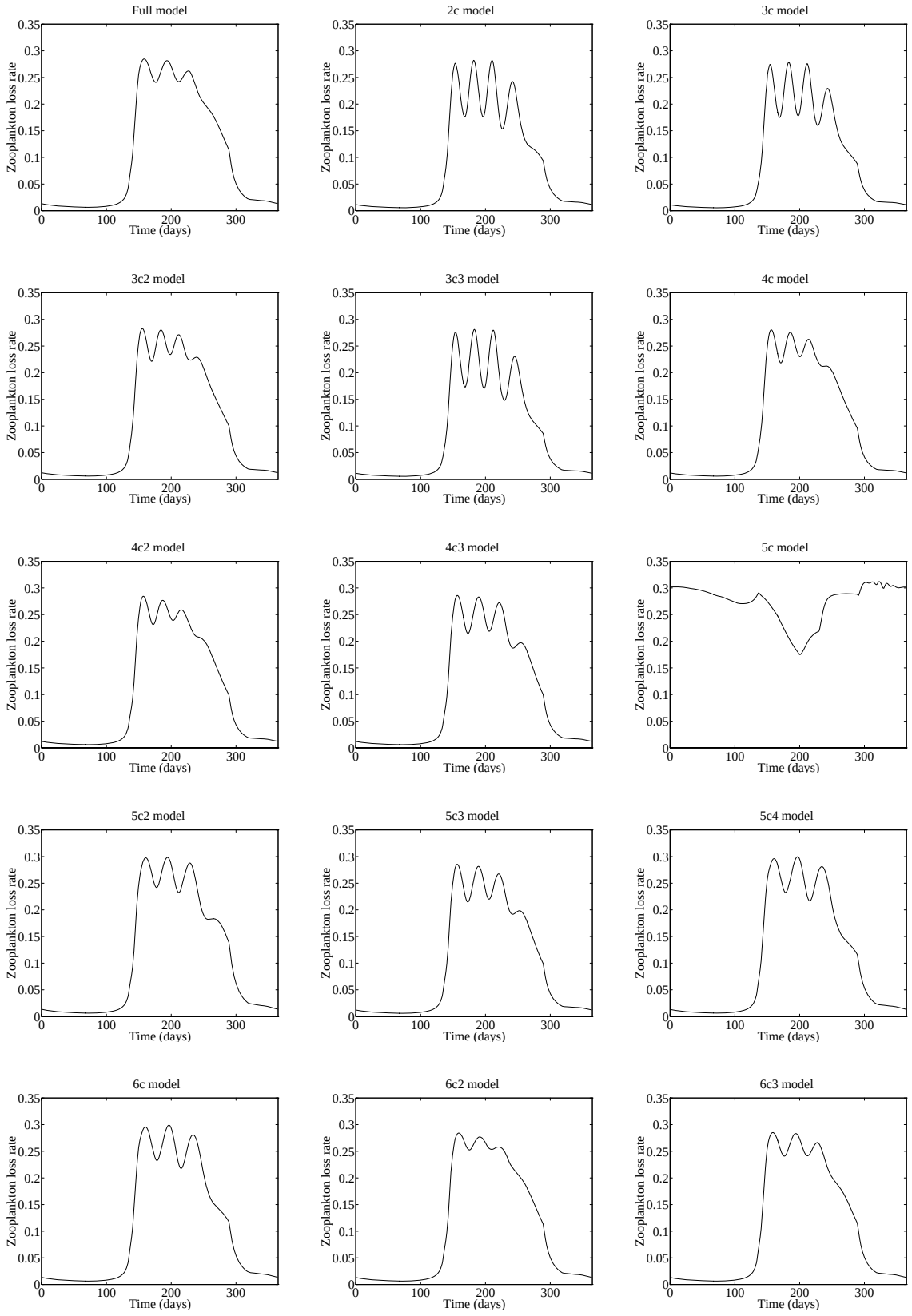

Figure 3.21: Simulated annual cycles of zooplankton daily loss rate at OWS "India" in each of the models.

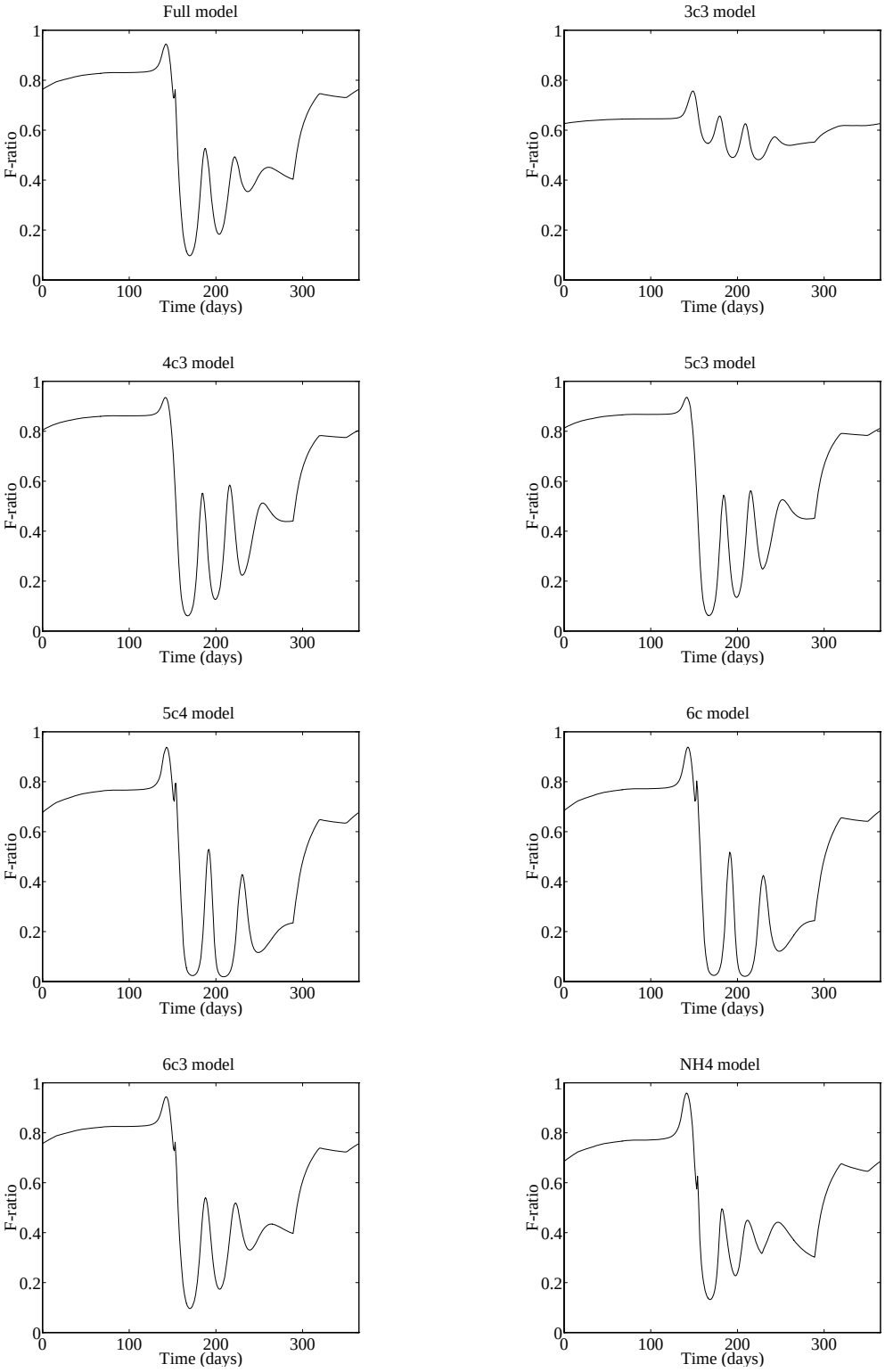

Figure 3.22: Simulated annual cycle of the f–ratio at OWS "India" in each of the appropriate models.

Model	NPP	f–ratio	P max	P time	P peaks	P cycle
Full	0.9402	0.5051	1.4230	148	4	34
2c	0.8688		1.4767	147	4	29
3c	0.8062		1.6656	148	4	30
3c2	1.0948		1.6656	148	4	30
3c3	0.8315	0.6226	1.4572	148	5	30
4c	0.9518		1.5499	149	4	30
4c2	0.9630		1.5937	149	4	31
4c3	0.9755	0.4974	1.6285	149	4	33
5c	0.0176		0.0470	183	3	28
5c2	0.8630		1.4883	148	4	37
5c3	0.9604	0.4995	1.6236	148	4	33
5c4	0.8346	0.4584	1.4799	148	4	39
6c	0.8301	0.4577	1.4805	148	4	39
6c2	0.9410		1.4151	148	4	32
6c3	0.9545	0.5041	1.4247	148	4	34
NH_4	1.0016	0.4668	1.4119	148	3	33

Table 3.2: Model statistics from OWS "India" solutions. **NPP** is total annual net primary productivity (mol N m^{-2} y^{-1}). **f–ratio** is the mean annual f–ratio in the appropriate models. **P max** is the maximum concentration of phytoplankton in the spring bloom (mmol N m^{-3}). **P time** is the day of the year this maximum occurs. **P peaks** is the number of phytoplankton oscillations in the summer months. **P cycle** is the mean period of these oscillations (days).

phytoplankton time series. The number of turning points it found during the summer months (**P peaks**) and the average time between them (**P cycle**) were then calculated.

Since phytoplankton form the key component of the majority of the models here (model 5c provides an exception), net primary productivity essentially provides a measure of the quantity of nitrogen "pumped" around the ecosystem. Most of the models (4c, 4c2, 4c3, 5c3, 6c2 and 6c3 especially) show NPP comparable to that of the full model. However, it is significant that even model 2c, whose dynamics depart radically from the full model's, exhibits NPP close to that of the full model.

The significance of the f–ratio has already been touched upon. Models 6c and 5c4 (which is an implicit nitrate representation of model 6c) can clearly been seen to depart from the average value for the full model. The higher ammonium concentrations of both these models act to shift the annual f–ratio lower.

In the case of model 3c3 (which produces much lower seasonal concentrations of ammonium), the situation is reversed. The remaining models fall within a narrow range around the full model. The results from the NH_4 model are discussed in a later section.

With the much–noted exception of model 5c, the timing and magnitude of the spring bloom is mostly consistent between the full model and its reduced forms.

Although the exact number of phytoplankton peaks counted occasionally varies due to the occurrence of minor peaks, almost all of the reduced models have average oscillation periods comparable to that of the full model. With the exception of models 5c2, 5c4 and 6c (related to their different patterns of zooplankton activity), all of the reduced models have cycles with a period less than the full model. The larger the model however, the longer the period, up to model 6c3 which matches that of the full model.

3.3.2 Bermuda Station "S" solutions

Figures 3.23 to 3.26 illustrate the seasonal patterns of the various model compartments produced by the full model and its reduced forms at Bermuda Station "S". This station contrasts significantly with OWS "India" in its annual pattern of ecosystem activity. Whereas at OWS "India", the summer is the period of greatest production, at Bermuda Station "S", the late spring and early autumn show greater production, with a relatively unproductive summer period.

Also unlike the OWS "India" solutions, several of the models now depart significantly from this pattern of ecosystem activity. Model 5c still refuses to conform, but additionally the implicit nitrate models, as well as those models lacking nutrient limitation, depart fairly radically from the results of the full model.

Phytoplankton and zooplankton

Figure 3.23 shows the abundance of phytoplankton and zooplankton through an annual cycle. Unlike OWS "India" there are no rapid predator–prey oscillations during the summer months.

However, whilst this is true of the full model, models 2c, 3c2 and 3c3 exhibit such cycles through the summer months. In these models, the lack of nutrient limitation (models 2c and 3c2 directly, model 3c3 indirectly) allow the dynamics to be governed by irradiance limitation which is much reduced at Bermuda Station "S".

Of the remaining reduced models, once again there are roughly three classes of behaviour. Models whose behaviour closely follows that of the full model (*e.g.* 4c, 4c2, 5c3 and 6c2), models with low winter populations but high summer populations (*e.g.* 3c, 3c3, 4c3, 5c4 and 6c3), and models with somewhat higher summer phytoplankton populations and significantly higher zooplankton populations (*e.g.* 5c2 and 6c).

Bacteria and ammonium

Figure 3.24 shows the abundance of bacteria and the concentration of ammonium through an annual cycle.

Of the models possessing these compartments, only models 5c3 and 6c2 describe patterns and magnitudes similar to those of the full model. Models 5c2 and 6c whilst getting similar general patterns, have significantly greater magnitudes. The implicit nitrate models almost reverse the patterns found in the full model, with highs in the summer and lows in the winter.

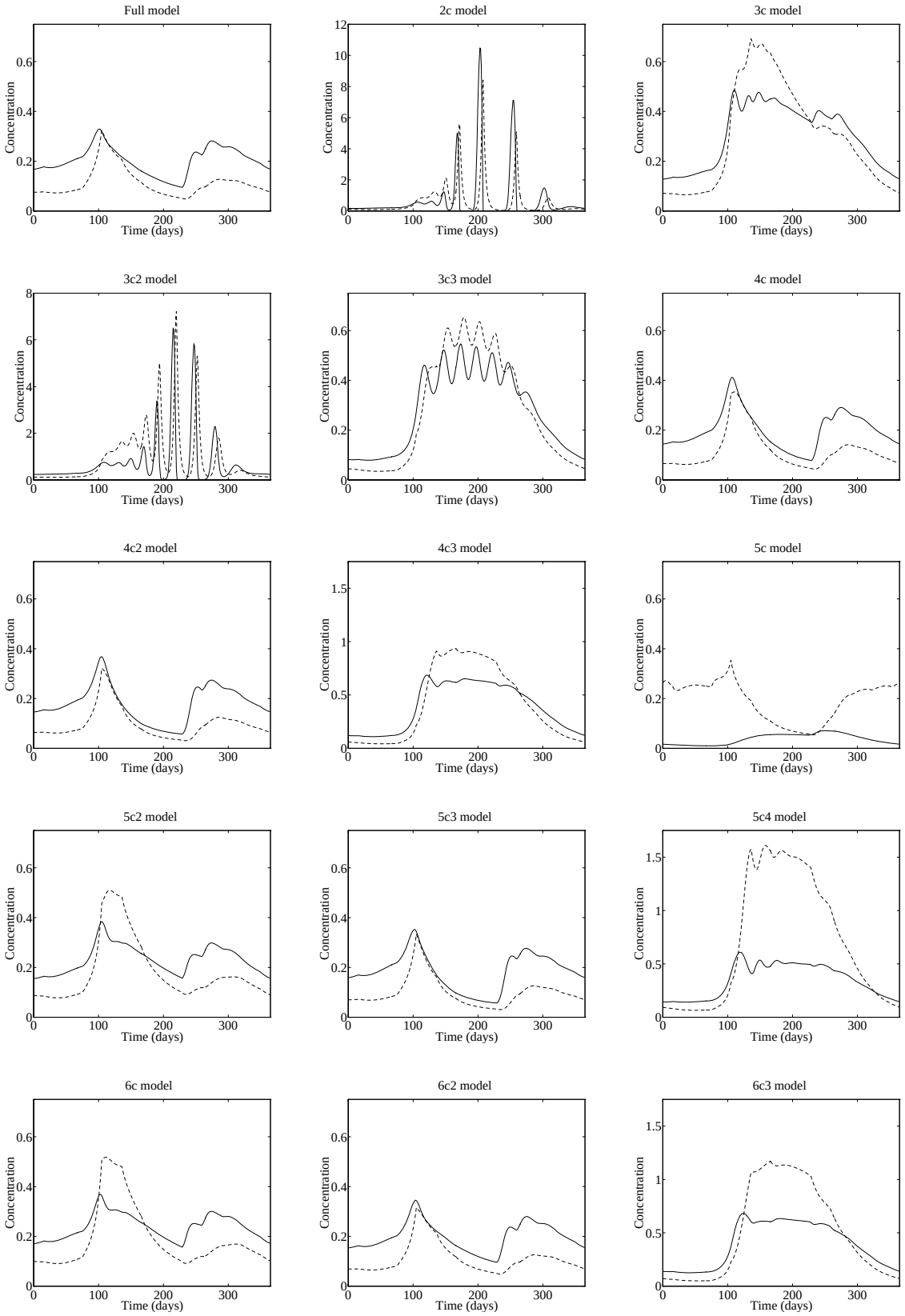

Figure 3.23: Simulated annual cycles of phytoplankton (solid line) and zooplankton (dashed line) at Bermuda Station "S" in each of the models. Note the changes of scale for models 2c, 3c2, 4c3, 5c4 and 6c3. Concentrations are in mmol N m^{-3}.

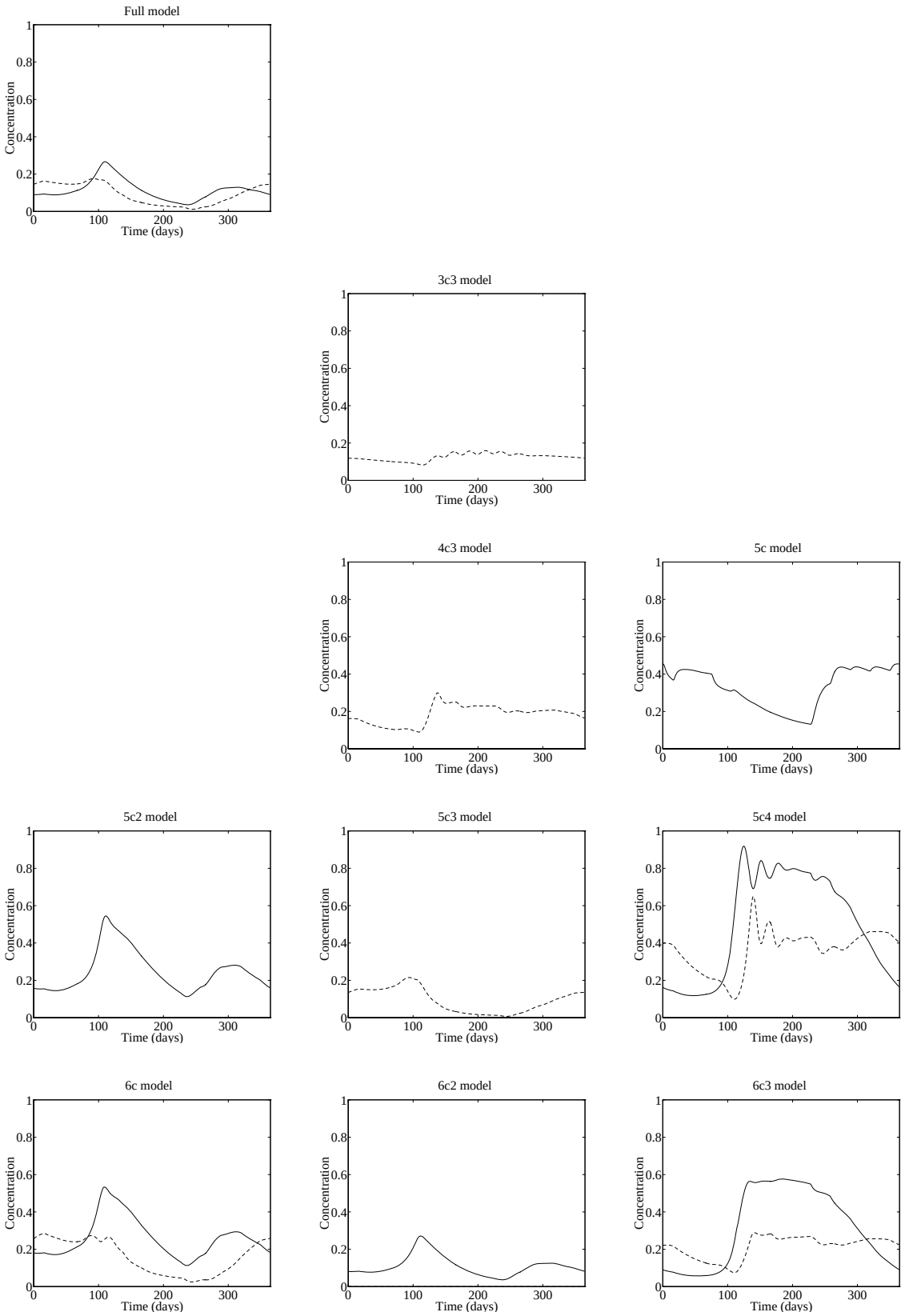

Figure 3.24: Simulated annual cycles of bacteria (solid line) and ammonium (dashed line) at Bermuda Station "S" in each of the appropriate models. Concentrations are in mmol N m^{-3}.

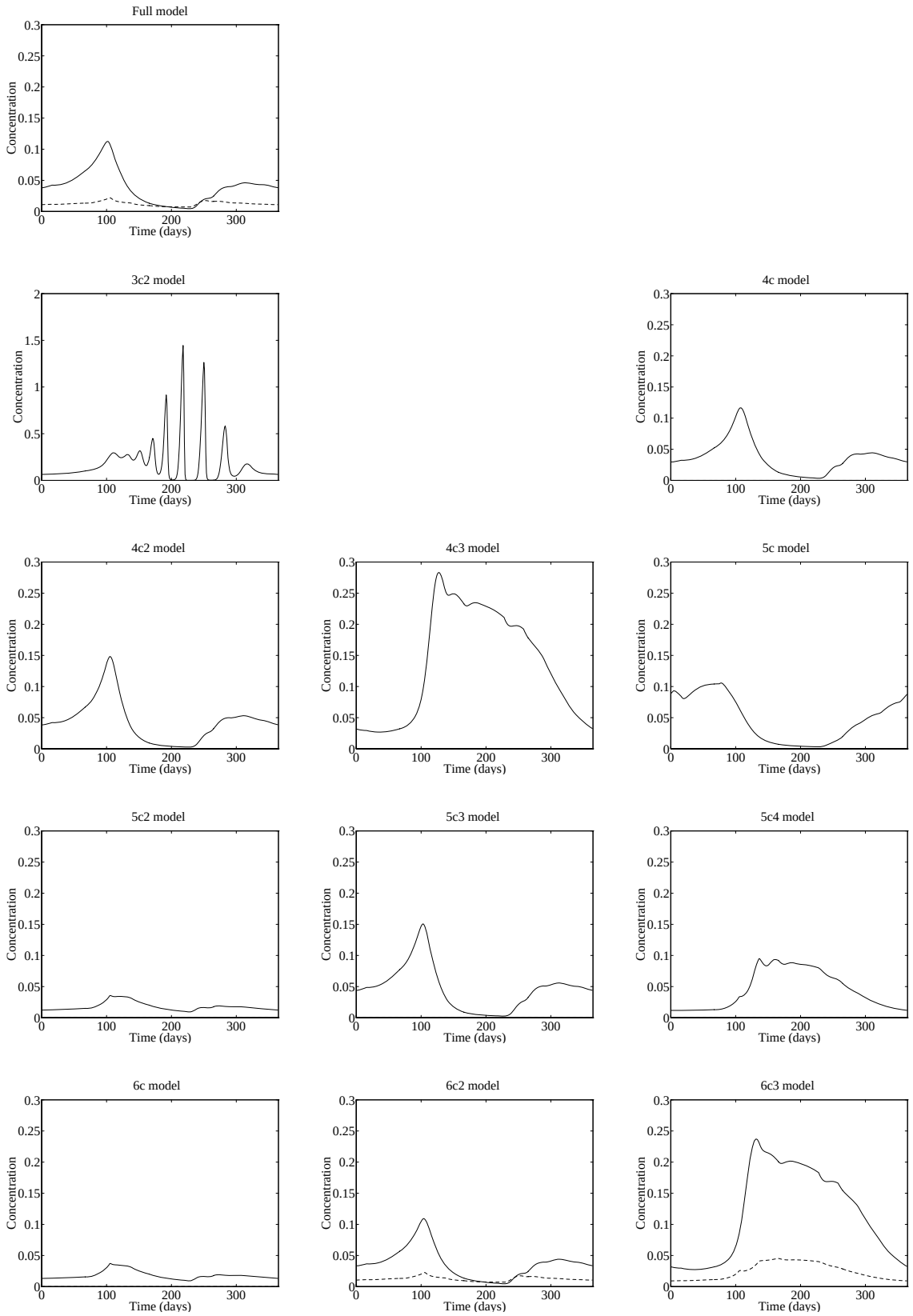

Figure 3.25: Simulated annual cycles of detritus (solid line) and DON (dashed line) at Bermuda Station "S" in each of the appropriate models. Note the change of scale for model 3c2. Concentrations are in mmol N m^{-3}.

Detritus and DON

Figure 3.25 shows the concentrations of detritus and DON through an annual cycle. As with OWS "India", detrital levels are tied strongly to those of phytoplankton. Since bacterial populations at Bermuda Station "S" do not die back in the winter as significantly as those at OWS "India", the spring bloom of phytoplankton production here is not marked by a significant spike of DON. Levels remain fairly constant throughout the year.

Once again, only models 4c, 4c2, 5c3 and 6c2 reproduce the patterns of production observed in the full model. Model 3c2 degenerates into extreme fluctuations which track the summer phytoplankton–zooplankton cycles. Models 5c2 and 6c, as was observed in the OWS "India" solutions, show detrital patterns which resemble the DON patterns of the full model. The implicit nitrate models again show summer–high, winter–low patterns.

Nitrate and total system nitrogen

Figure 3.26 shows the concentrations of nitrate or general nutrient and total system nitrogen across the annual cycle. In the full model, nitrate is depleted rapidly at the onset of the spring bloom and remains low throughout the summer period before recovering slowly in the winter. Unlike OWS "India", where nitrate levels return to values close to those in the subthermocline layer, nitrate levels here remain low because of shallower winter mixing and greater populations of phytoplankton.

The same patterns of similarity to the full model continue here. Models 4c, 4c2, 5c3 and 6c2 follow the full model closely (5c3 particularly because it has a nitrate rather than a general nutrient compartment). Models 5c2 and 6c come closer to the full model here but have much greater total system nitrogen. The implicit nitrate models cannot be used here because of their non–conservative nature.

Phytoplankton growth limitation

Figure 3.27 shows the patterns of growth limitations placed on the phytoplankton. Unlike OWS "India", growth limitation is more severely constrained by nutrient limitation. In the winter, irradiance levels, whilst low, still permit growth. As the season progresses and irradiance rises, nutrients are depleted shortly after the spring bloom and a summer of severe nutrient limitation follows. As the irradiance falls in the winter and the mixed layer deepens, nutrient levels rise again, lowering limitation.

Almost all of the reduced models have the same pattern of irradiance limitation to the full model. Since they lack nutrient limitation, models 2c and 3c2 allow phytoplankton populations to reach levels where self–shading is extreme (although not as extreme as winter irradiance limitation).

Patterns of nutrient limitation are usually similar to those in the full model, although models 5c2 and 6c are not as nutrient limited in the summer months due to higher levels of regenerated ammonium. Model

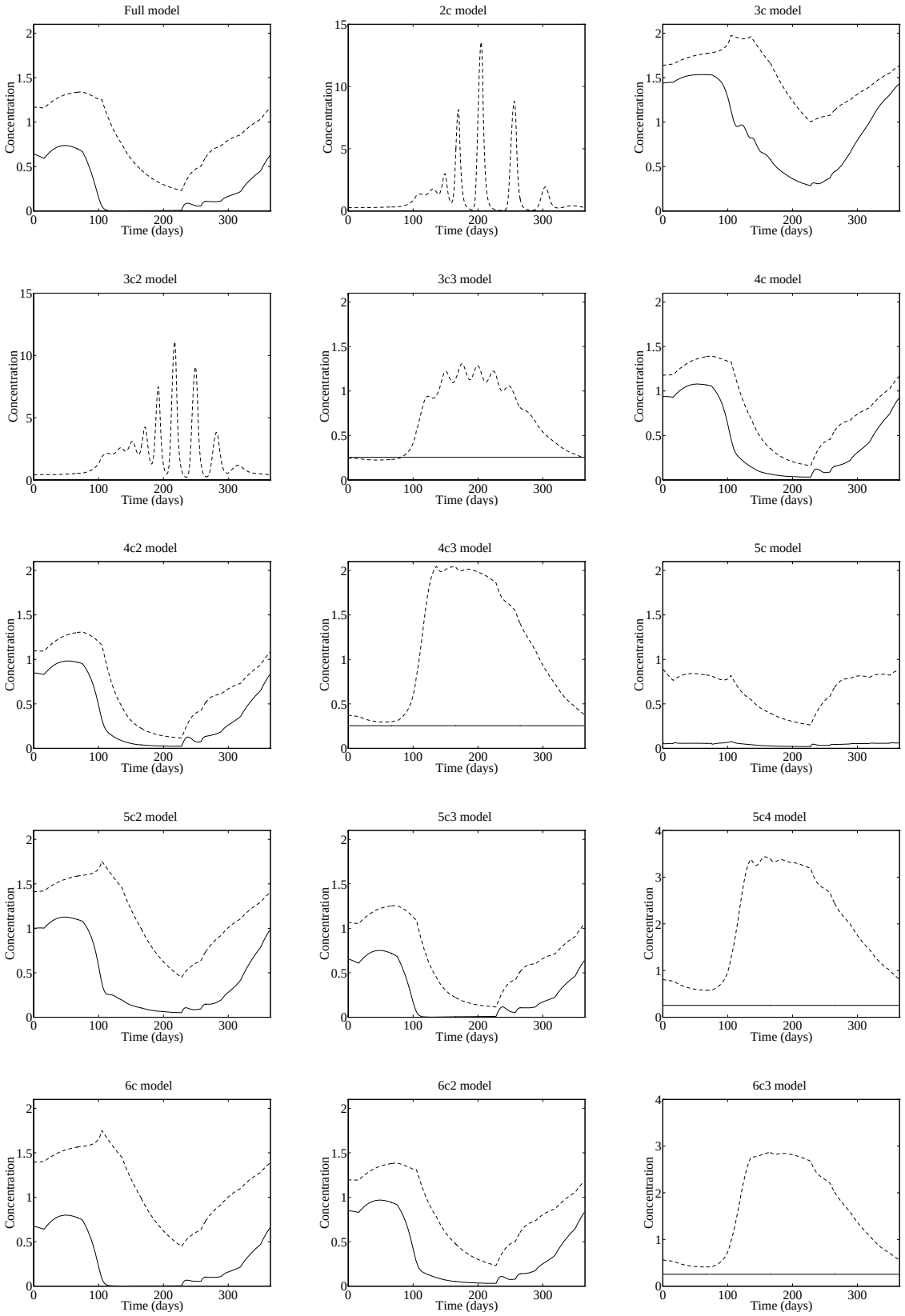

Figure 3.26: Simulated annual cycles of nitrate/nutrient (solid line) and total system nitrogen (dashed line) at Bermuda Station "S" in each of the models. Note the changes of scale for models 2c, 3c2, 5c4 and 6c3. Concentrations are in mmol N m^{-3}.

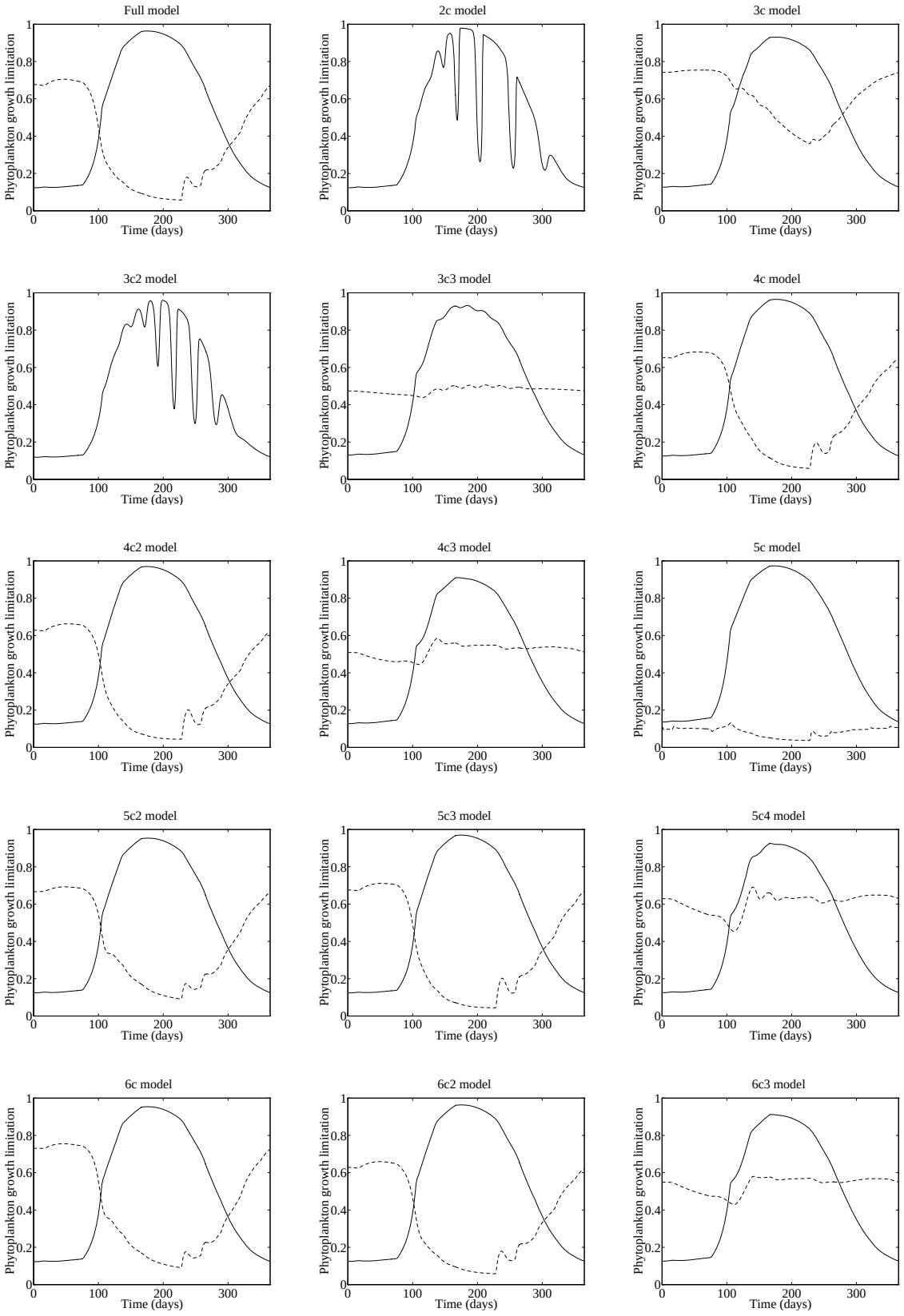

Figure 3.27: Simulated annual cycles of maximum possible phytoplankton growth (solid line) and nutrient limitation (dashed line) at Bermuda Station "S" in each of the appropriate models. Maximum growth in d^{-1}, nutrient limitation is non–dimensional.

3c shows considerably less nutrient limitation in the summer because of instantaneous regeneration to usable nutrient, and consequently this leads to its high summer phytoplankton populations.

The implicit nitrate models comprehensively fail to capture the pattern of nutrient limitation observed in the full model. In an environment such as this one, where the ecosystem rides very closely to nutrient starvation, the existence of a never–ending supply of nutrients (in the form of the implicit nitrate compartment) severely disrupts the normal seasonal patterns.

Zooplankton mortality rate

Figure 3.28 shows the annual pattern of zooplankton loss rate. As already stated, these results are tied very closely to the abundances of zooplankton. Those models which capture zooplankton abundance well also do well with zooplankton loss rate (*e.g.* models 4c, 4c2, 5c3 and 6c2).

f–ratio

Figure 3.29 shows the annual patterns of the f–ratio. As with OWS "India", the winter months have relatively greater amounts of new (nitrate fueled) production, and the summer months higher amounts of regenerated (ammonium fueled) production. Late autumn spikes of new production arise as the deepening mixed layer entrains more nitrate from beneath the thermocline.

None of the reduced models describe the pattern of the full model particularly well. The implicit nitrate models are entirely at sea, with ratios which remain fairly constant throughout most of the year. These are punctuated only in the period from winter to spring where falling ammonium levels increase the f–ratio, only for it to fall following the spring bloom when zooplankton abundance rises sufficiently to provide regenerated ammonium.

Model 5c3 appears to overestimate the significance of new production in the late summer and early autumn, but otherwise shows a similar pattern to the full model. The reason for this overestimation is unclear since otherwise this model agrees relatively well with the full model with respect to nitrate and ammonium concentrations.

Model 6c goes the reverse way and consistently overestimates the significance of regenerated production, leading to the annual pattern of f–ratio being shifted downwards. This pattern is caused by greater abundances of zooplankton which regenerate more nitrogen to ammonium.

Bermuda Station "S" statistics

Table 3.3 details a series of statistics which quantify particular aspects of the Bermuda Station "S" solutions. The definitions here are the same as those already described for OWS "India".

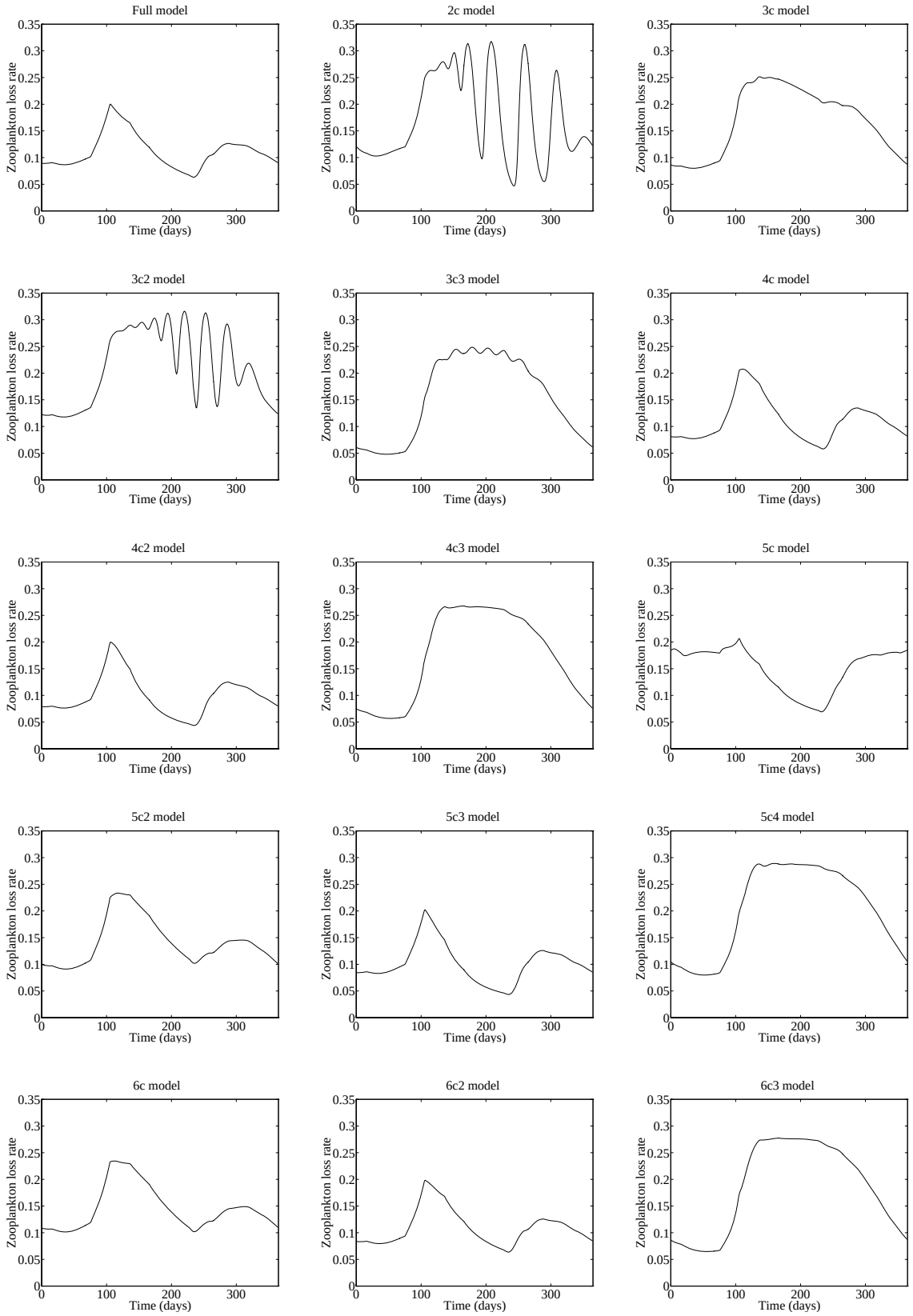

Figure 3.28: Simulated annual cycles of zooplankton daily loss rate at Bermuda Station "S" in each of the models.

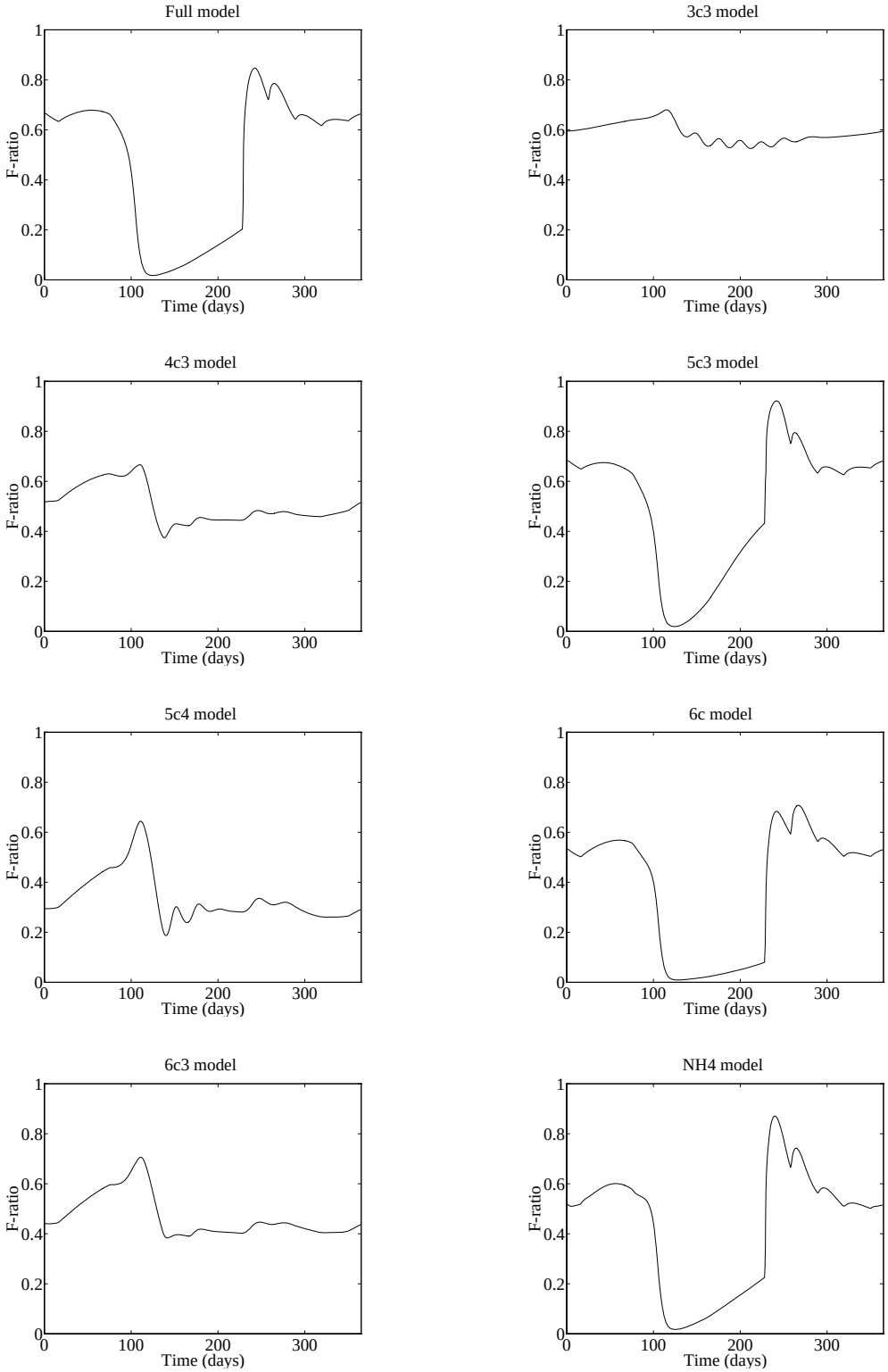

Figure 3.29: Simulated annual cycle of the f–ratio at Bermuda Station "S" in each of the appropriate models.

Model	NPP	f–ratio	P max	P time	P peaks	P cycle
Full	0.5160	0.5599	0.3293	101	5	71
2c	2.7736		0.6315	128	8	34
3c	1.1656		0.4860	110	7	42
3c2	3.4789		0.7957	108	11	30
3c3	0.8821	0.5810	0.4608	117	8	37
4c	0.5578		0.4117	107	4	86
4c2	0.4739		0.3679	104	4	86
4c3	1.3244	0.4834	0.6857	121	5	57
5c	0.0186		0.0709	251	3	40
5c2	0.6016		0.3835	105	6	52
5c3	0.5118	0.5595	0.3526	102	5	71
5c4	1.3736	0.3390	0.6097	119	6	46
6c	0.6563	0.4232	0.3687	103	7	47
6c2	0.4817		0.3452	104	5	71
6c3	1.3685	0.4594	0.6816	124	5	57
NH_4	0.5670	0.4959	0.3519	102	5	71

Table 3.3: Model statistics from Bermuda Station "S" solutions. **NPP** is total annual net primary productivity (mol N m^{-2} y^{-1}). **f–ratio** is the mean annual f–ratio in the appropriate models. **P max** is the maximum concentration of phytoplankton in the spring bloom (mmol N m^{-3}). **P time** is the day of the year this maximum occurs. **P peaks** is the total number of phytoplankton peaks in the annual cycle. **P cycle** is the mean period of time between these peaks (days).

Unlike OWS "India" solutions, Bermuda Station "S" solutions of the reduced models produce a much wider range of NPP (despite the full model producing an NPP lower than that of the comparable OWS "India" solution). The nutrient unlimited (*i.e.* 2c and 3c2) and implicit nitrate models do particularly badly, with NPP being up to six times greater than that of the full model (model 3c2). Models 4c, 4c2, 5c3 and 6c2 once again perform reasonably well, with NPP values within 10% of the full model. Models 5c2 and 6c are somewhat more productive due to their increased regenerative production.

The averaged f–ratio results here are mostly fairly poor, but with model 5c3 coming very close to that found in the full model. Model 3c3 produced a value slightly above that of the full model, but that it also produced one of the worst daily f–ratio traces of the reduced models does not inspire confidence in such averaged measures. Model 6c produces a lower f–ratio due to greater regenerated production caused by higher ammonium concentrations. The remaining implicit nitrate models do unsurprisingly

poorly (model 5c4 particularly).

With the obvious exception of model 5c, every reduced model over–estimates the size of the phytoplankton spring bloom maximum. For models 2c and 3c2, this excess is dwarfed by later predator–prey cycles in the summer. Model 3c's high spring bloom is merely the start of a summer of high phytoplankton abundance. Models 4c, 4c2, 5c3 and 6c2 do increasingly well, as would be expected from earlier reported results. The results of models 5c2 and 6c disguise their failure to produce the summer phytoplankton lows of the full model. And the implicit models, like model 3c, have high spring blooms which continue into high summer abundances.

On the timing of the bloom, all of the models bloom later than the full model. Most only fall a few days late, but several (*e.g.* 2c, 3c and 3c2) from a week to almost a month late. All of the implicit nitrate models fall around 20 days late, although as already described, their spring blooms are of a very different nature to those of the other models.

The numbers of peaks and the periods between them are of less consequence for Bermuda Station "S" since it lacks the rapid predator–prey cycles present in the OWS "India" solutions. However, they still should provide reasonable (if somewhat coarse) system measures so have been included here. Most models have slightly more peaks and somewhat lower periods between them. However, models 5c3 and 6c2 get the number of peaks and their period perfectly the same as the full model. And models 4c and 4c2, despite having shorter periods at OWS "India" now have somewhat longer ones. However, since Bermuda Station "S" has much less well–defined peaks, these results are less interesting and somewhat dubious.

3.3.3 Mixed–layer depth solutions

Figures 3.30 to 3.33 illustrate the results of numerical solutions calculated at four different annual patterns of mixed–layer depth. For comparison, the top row of each Figure shows the results obtained using the full model.

With the exception of model 6c2, none of the reduced models do very well at emulating the full model at shallow mixed–layer depths. Models 4c2 and 5c3 come close to emulating the asymmetrical oscillations of the full model. However, most produce a series of fairly symmetrical predator–prey cycles through the spring bloom into the summer (*e.g.* models 2c, 3c, 3c2, 5c2, 6c). This is particularly true of all the implicit nitrate models.

However, as the seasonal patterns of mixed–layer depth become deeper, a few more of the models come closer to emulating the full model's annual patterns. This is especially true of the implicit nitrate model, 6c3, although models 3c2, 4c and 4c3 show a similarly improved performance as mixed layers become deeper. In the cases of models 3c2, 4c3 and 6c3, this is due to nutrient limitation becoming less important, and thus allowing these models to more accurately emulate the full model.

Models 2c, 3c, and 3c3 never do well, and always degenerate into extreme summer predator–prey cycles. Models 5c2, 5c4 and 6c show the same higher zooplankton populations already found with these models. Model 5c, as ever, performs very badly in all seasonal cycles.

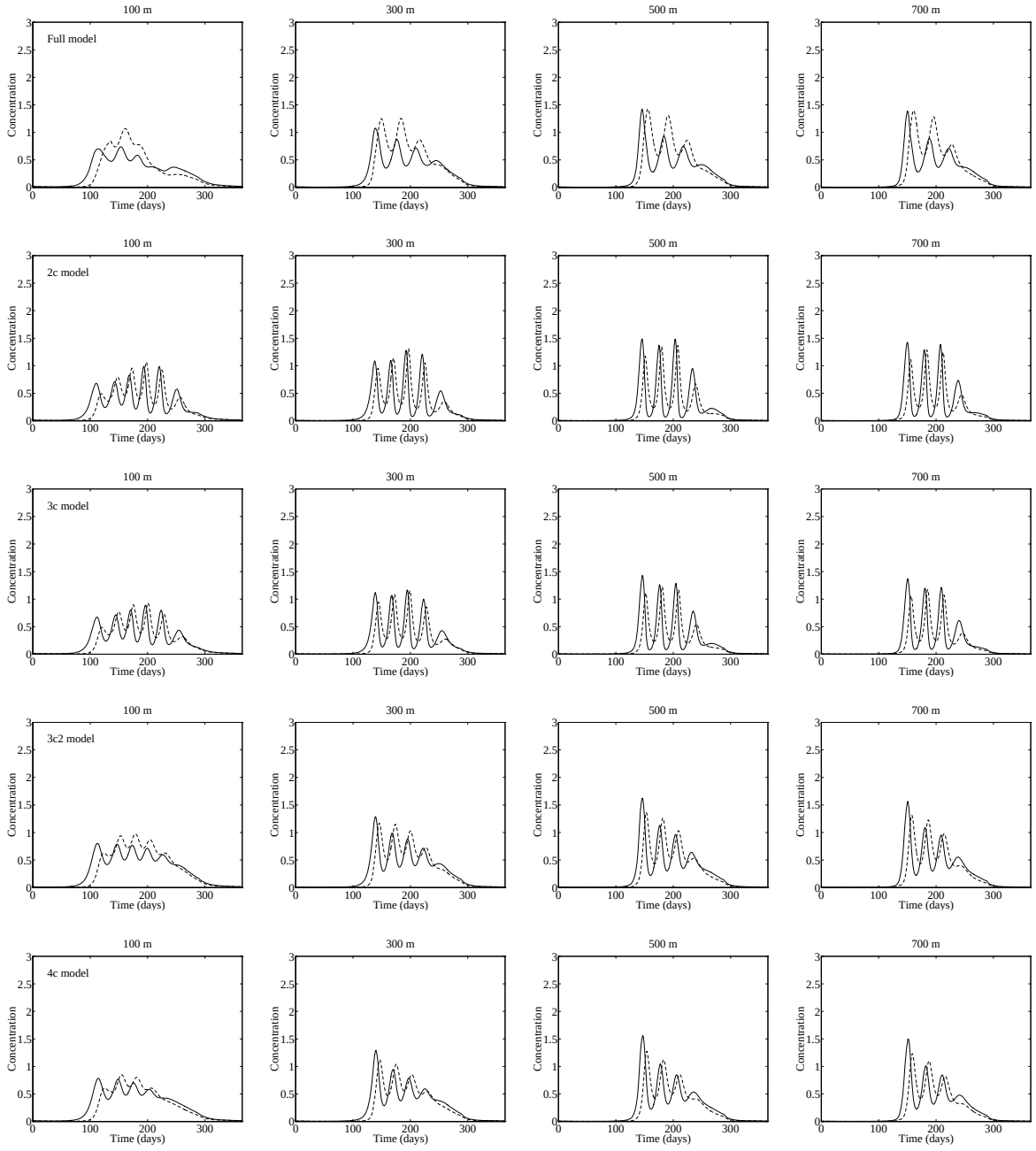

Figure 3.30: Simulated annual cycles of phytoplankton (solid line) and zooplankton (dashed line) at OWS "India" under a range of mixed-layer depth regimes. Concentrations are in mmol N m^{-3}.

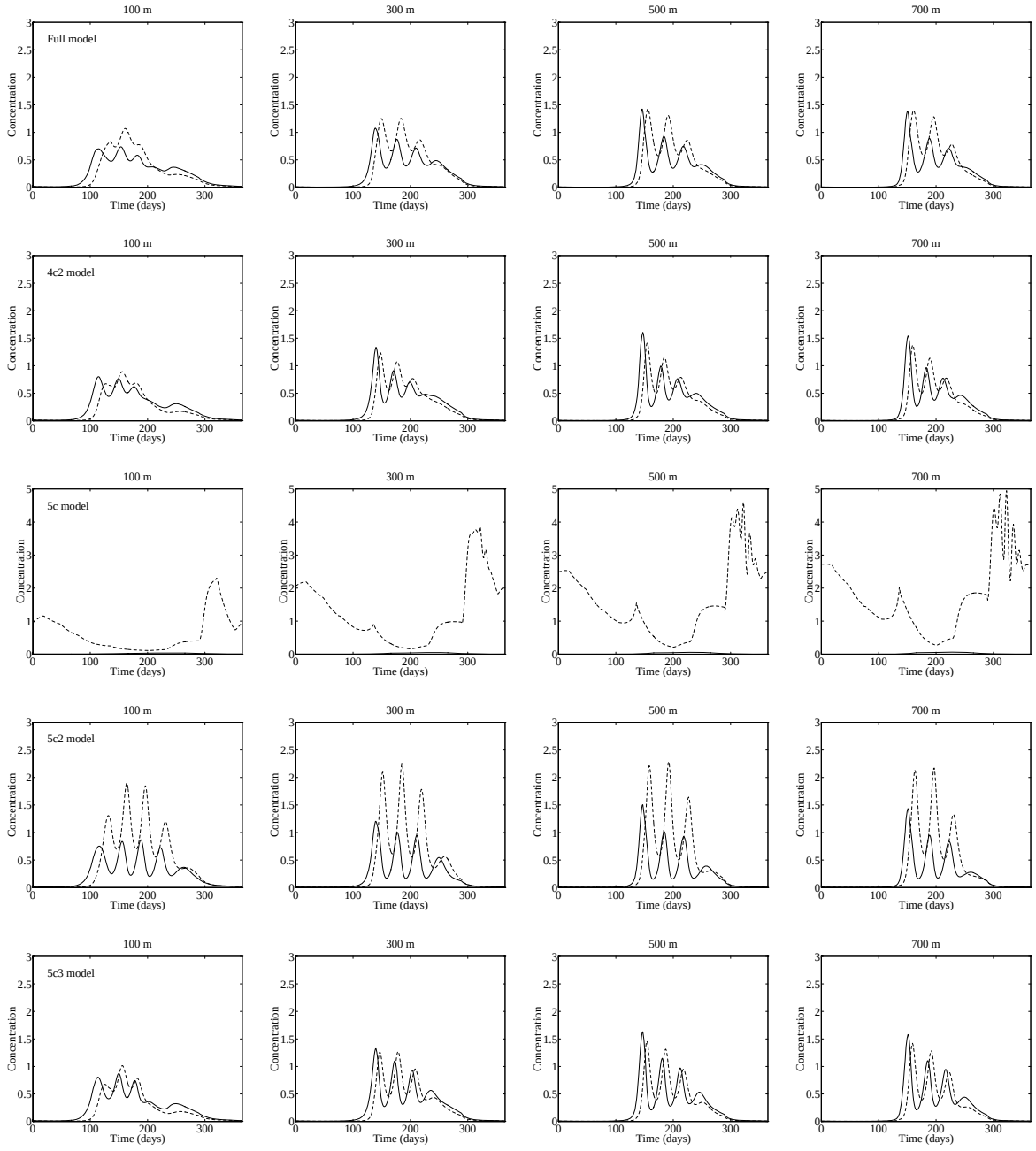

Figure 3.31: Simulated annual cycles of phytoplankton (solid line) and zooplankton (dashed line) at OWS "India" under a range of mixed-layer depth regimes. Note the change of scale for model 5c. Concentrations are in mmol N m^{-3}.

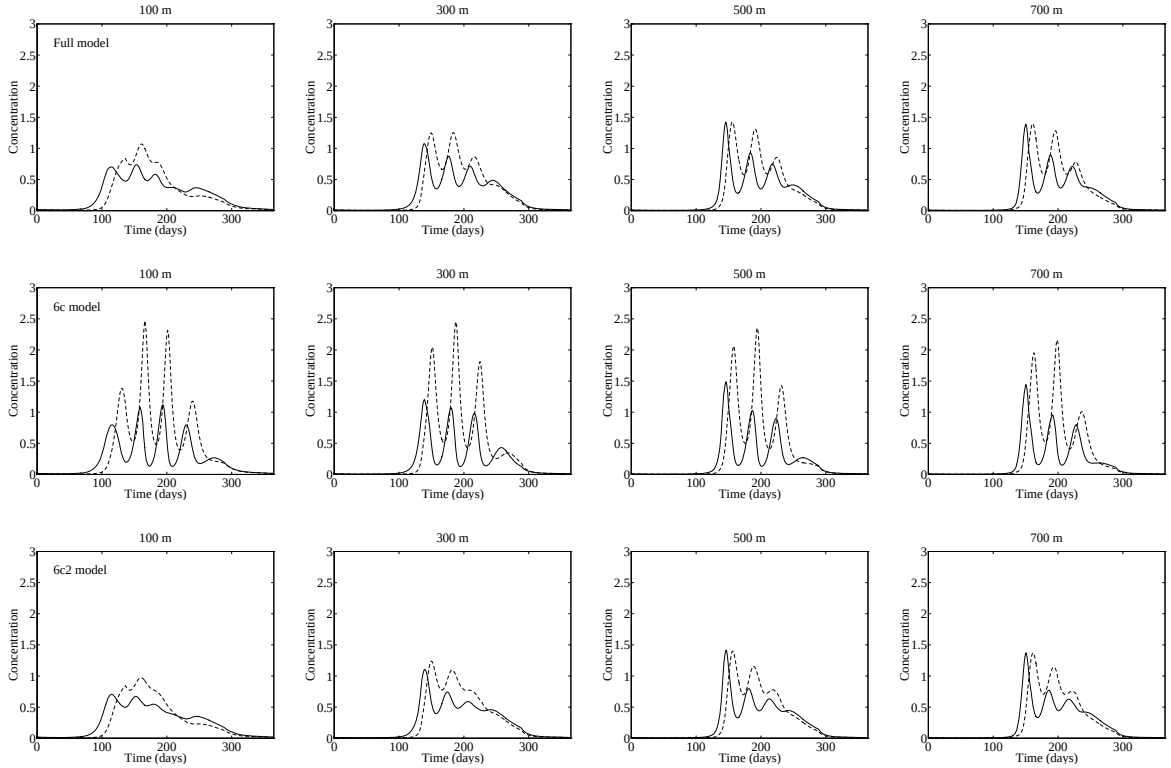

Figure 3.32: Simulated annual cycles of phytoplankton (solid line) and zooplankton (dashed line) at OWS "India" under a range of mixed-layer depth regimes. Concentrations are in mmol N m^{-3}.

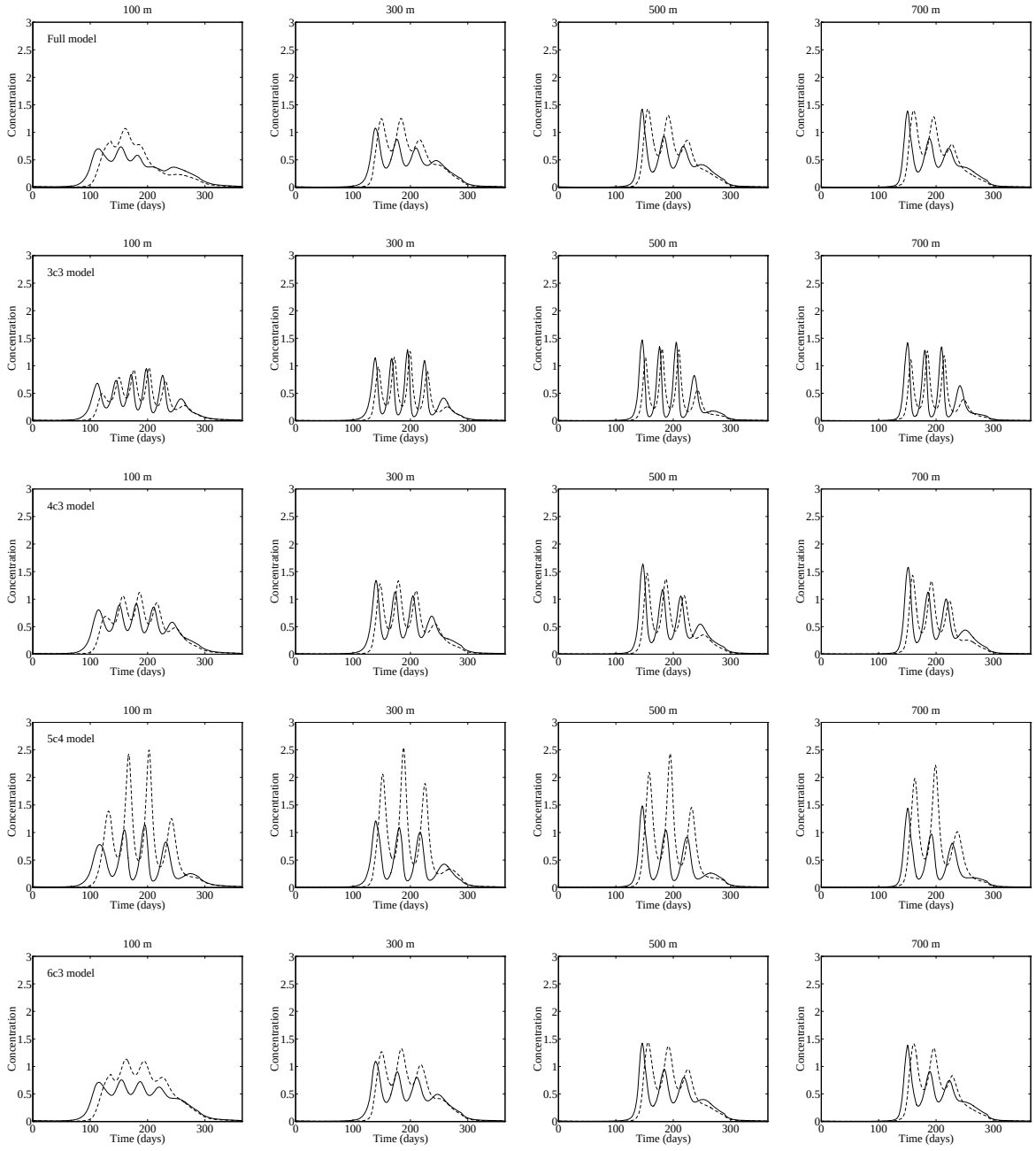

Figure 3.33: Simulated annual cycles of phytoplankton (solid line) and zooplankton (dashed line) at OWS "India" under a range of mixed-layer depth regimes. Concentrations are in mmol N m^{-3}.

3.3.4 Sub–thermocline nitrate solutions

Figures 3.34 to 3.37 illustrate the results of numerical solution calculated at four different subthermocline nitrate or general nutrient concentrations. As previously, for comparison purposes, the top row of each figure shows the results of the full model solutions. Note that models 2c and 3c2 do not appear here since they do not have a subthermocline nutrient reservoir.

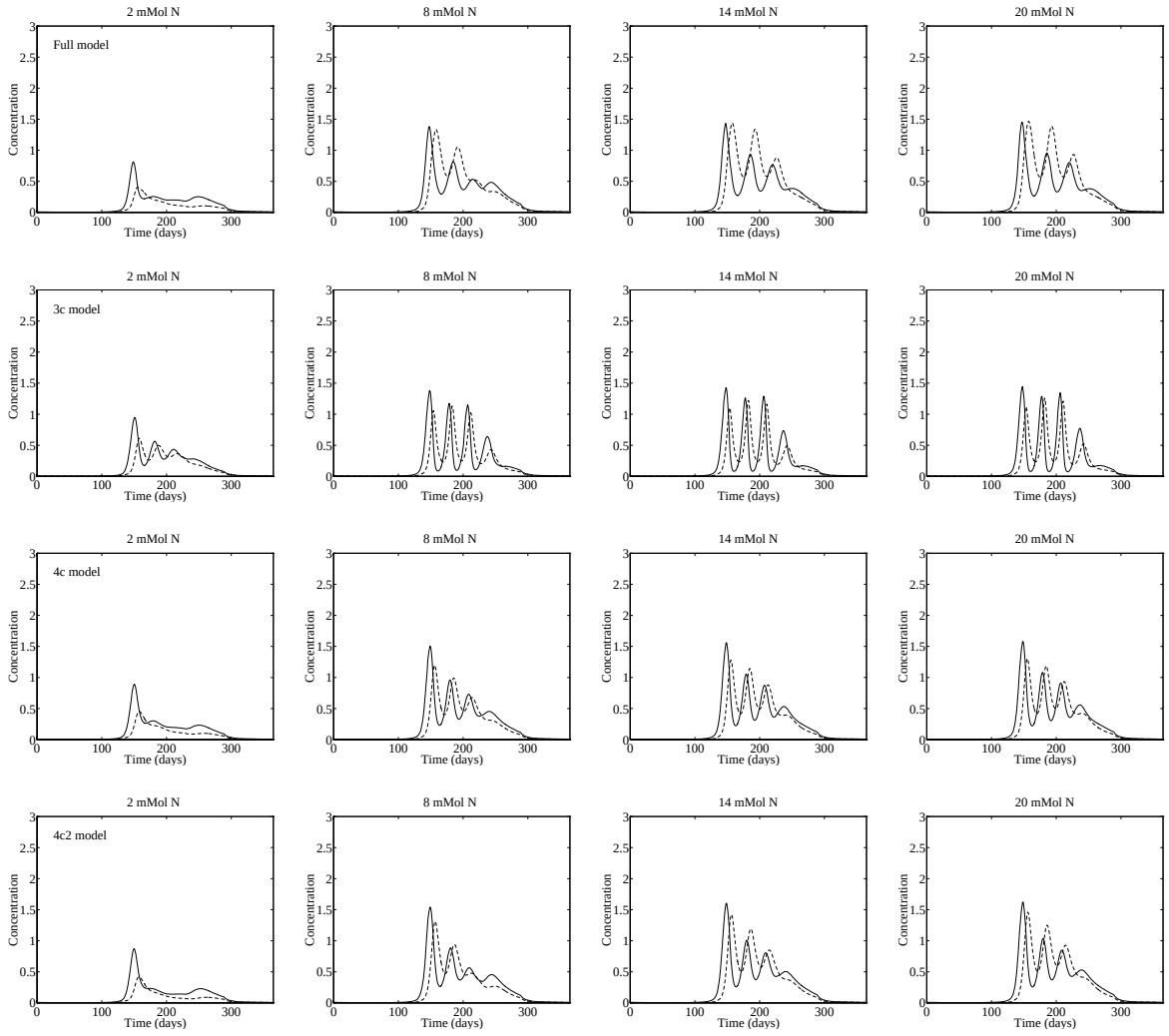

Figure 3.34: Simulated annual cycles of phytoplankton (solid line) and zooplankton (dashed line) at OWS "India" under a range of subthermocline nitrate/nutrient concentrations. Concentrations are in mmol N m^{-3}.

Unsurprisingly, almost all of the models do well at emulating the full model at low nutrient concentrations. Since a shortage of nutrients constricts all activity in the model, excesses in behaviour of the reduced forms are curbed. Model 3c however, because of its instantaneous regeneration of detritus *et cetera* to nutrient, retains more nitrogen in the mixed layer and exhibits slightly greater activity in the summer. As was observed with the similarly nutrient–starved Bermuda Station "S" solutions, the implicit

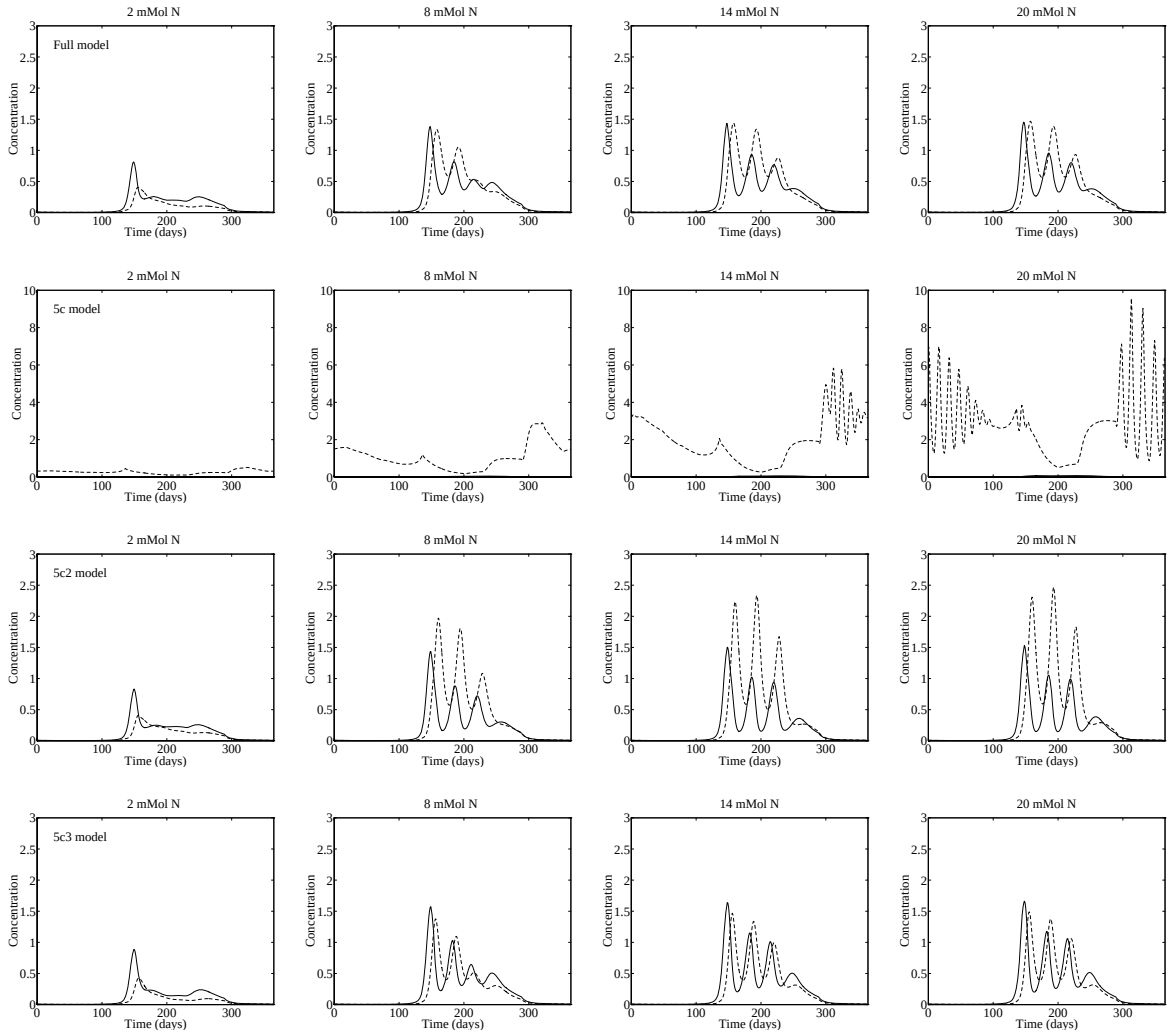

Figure 3.35: Simulated annual cycles of phytoplankton (solid line) and zooplankton (dashed line) at OWS "India" under a range of subthermocline nitrate/nutrient concentrations. Note the change of scale for model 5c. Concentrations are in mmol N m^{-3}.

nitrate models all have much greater phytoplankton production because nitrate supply remains constant.

As the concentration of nutrient below the thermocline is increased the results drift back to those found for solutions at OWS "India". Models 3c and 3c3 return to the more extreme and pronounced summer blooms. Models 4c, 4c2 and 5c3 do well, but still exhibit the slightly more rapid predator–prey cycles in the summer. Models 5c2, 6c and 5c4 begin to show the much higher zooplankton populations and more extreme summer oscillations seen at OWS "India". Model 4c3 becomes more like model 5c3 (its explicit nitrate counterpart) as nitrate levels rise to non–limiting concentrations. Similarly, model 6c3 becomes more and more like the full model (its explicit counterpart) as nitrate levels become saturating.

Interestingly, model 6c2, whilst very similar to the full model at lower subthermocline nitrate concentrations (around those at OWS "India" and lower), departs more and more significantly in the summer as nitrate levels become higher. Principally, the summer zooplankton populations are somewhat higher and

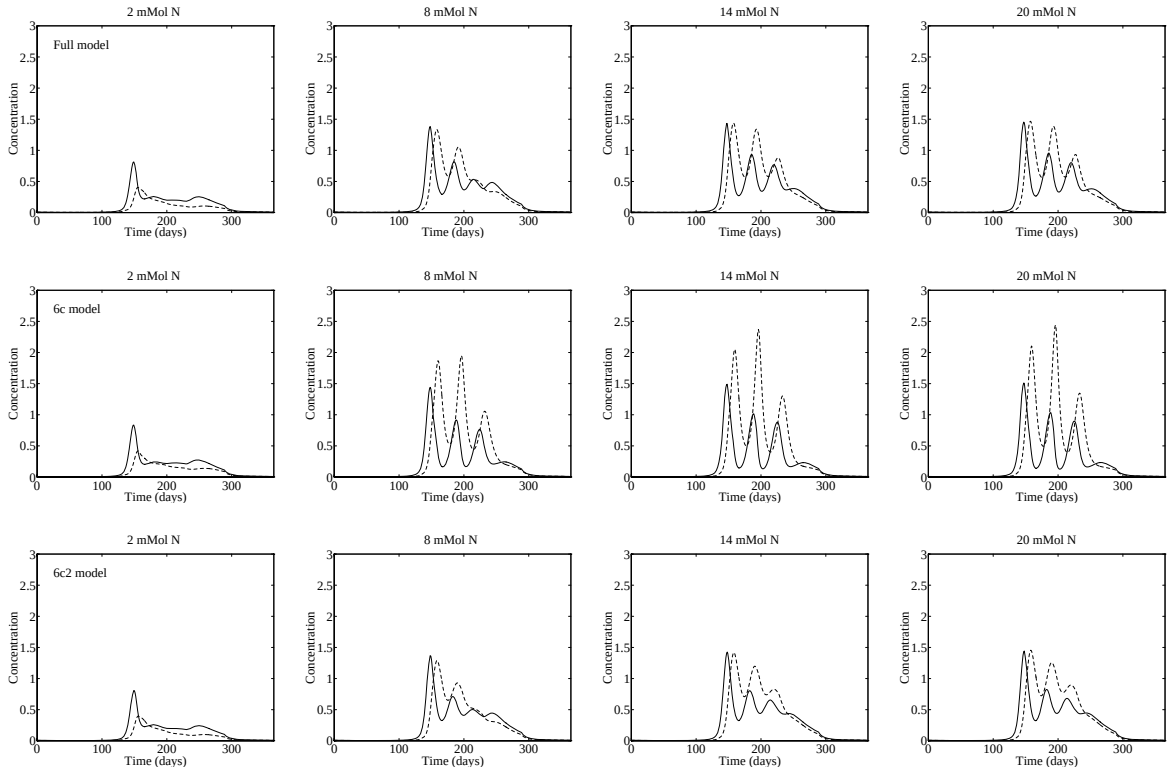

Figure 3.36: Simulated annual cycles of phytoplankton (solid line) and zooplankton (dashed line) at OWS "India" under a range of subthermocline nitrate/nutrient concentrations. Concentrations are in mmol N m^{-3}.

show less extreme oscillations than the full model. Examination of the data from the other compartments does not give much information as to the cause of this.

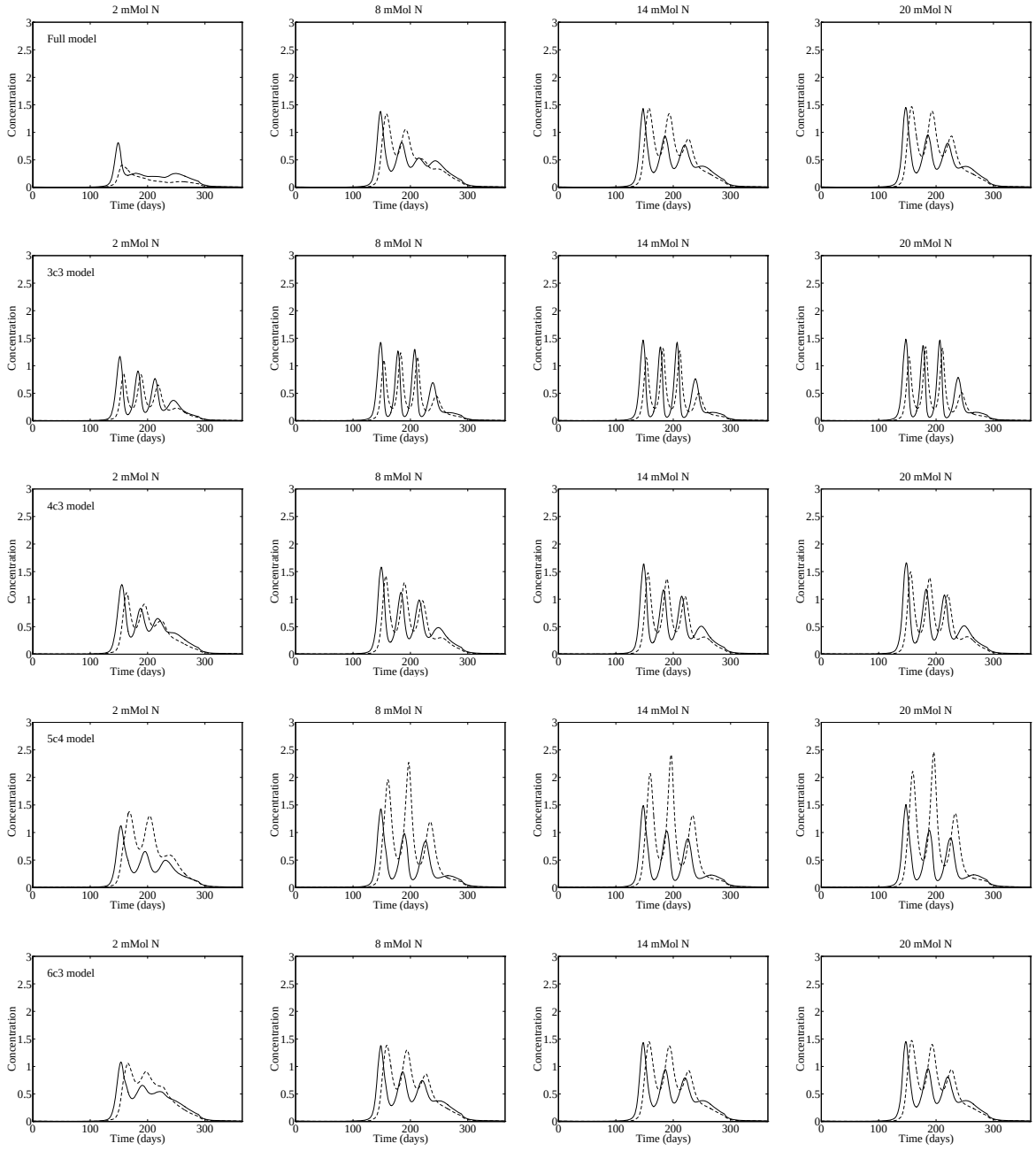

Figure 3.37: Simulated annual cycles of phytoplankton (solid line) and zooplankton (dashed line) at OWS "India" under a range of subthermocline nitrate/nutrient concentrations. Concentrations are in mmol N m^{-3}.

3.3.5 Annual nitrogen flow results

Figures 3.38 to 3.53 show the total annual networks of nitrogen flows for the full model and its reduced forms. All results are derived from solutions determined at OWS "India" except for Figure 3.39 which presents the results from the full model solution at Bermuda Station "S". Figure 3.59 shows the results from an OWS "India" solution of the full model using the nutrient uptake model described in equation 3.63.

OWS "India" versus Bermuda Station "S"

The most significant difference in the flow networks produced from OWS "India" and Bermuda Station "S" solutions is the initial flux of nitrogen from inorganic nutrients to phytoplankton (gross primary production). This flux is essentially the "pump" of the system with every other compartment (excepting nitrate) depending on phytoplankton to fuel them (unsurprising since phototrophs are, for most ecological systems, the only possible source of energy).

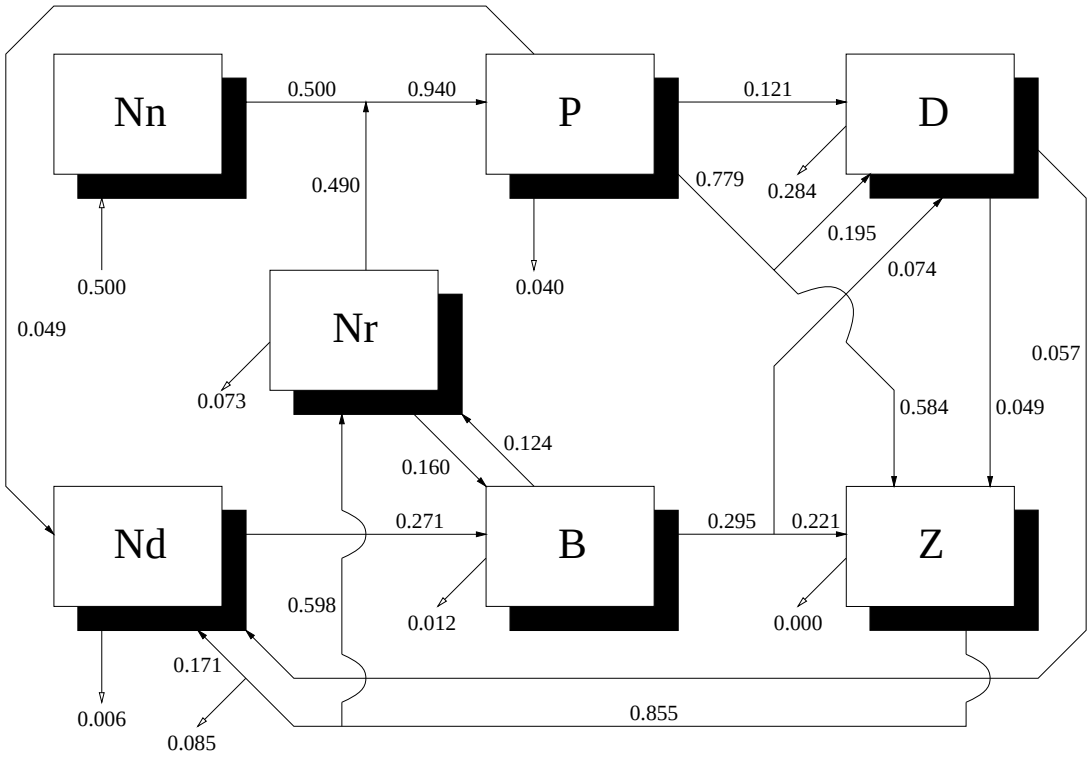

Figure 3.38: Annual nitrogen flows (mol N m^{-2} y^{-1}) at OWS "India" of the Fasham (1993) model.

OWS "India" has a gross primary production almost double that of Bermuda Station "S" despite having a phytoplankton population severely constrained by irradiance levels in the winter. As stated already, low productivity at Bermuda Station "S" is due to reduced availability of subthermocline nitrate, itself

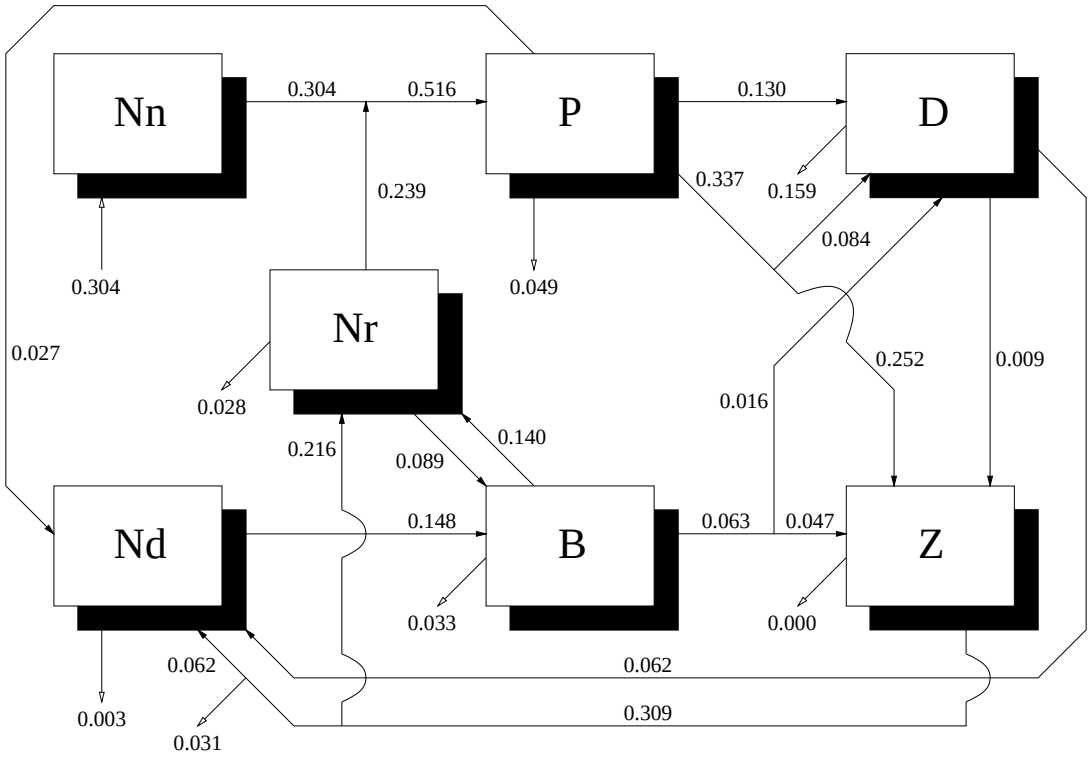

Figure 3.39: Annual nitrogen flows (mol N m^{-2} y^{-1}) at Bermuda Station "S" of the Fasham (1993) model.

due to shallower winter mixing.

Since phytoplankton populations are less limited by irradiance in the winter at Bermuda Station "S", populations remain at comparably high values year round. Due to the lower availability of nitrate however, the populations never attain the concentrations found at OWS "India" in the spring and summer. As a consequence, a lower zooplankton population is supported and a greater fraction of phytoplankton finds its way directly into detritus.

The generally lower concentrations of compartments at Bermuda Station "S" reduces the importance of zooplankton (because of the Michaelis–Menten form of zooplankton grazing) at this location. And relatively greater fractions (indeed, usually greater actual quantities) of phytoplankton, bacteria and detritus are lost due to detrainment.

Interestingly, despite quite different systemic throughputs of nitrogen, both locations have the same ratio of bacterial to phytoplankton production (where production is quantified purely in nitrogen flux terms). Another interesting result is that whilst Bermuda Station "S" has a considerably lower daily average f–ratio than OWS "India", when annual nitrogen flows from ammonium and nitrate are considered, the situation is reversed and Bermuda Station "S" has the greater f–ratio (although the difference is not

quite as extreme as seen in the daily averages).

Reduced model nitrogen flows

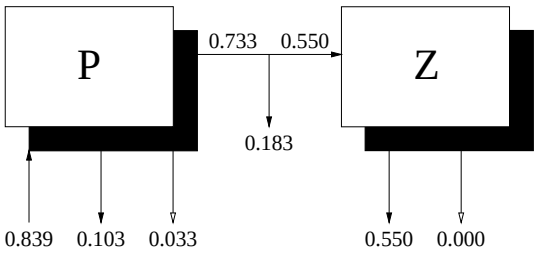

Figure 3.40: Annual nitrogen flows (mol N m^{-2} y^{-1}) at OWS "India" of model 2c.

Figure 3.40 shows the network of nitrogen flows for model 2c. As stated earlier, solid headed arrows relate to flows to other compartments, and empty headed arrows to flows that leave the upper mixed layer. Those solid headed arrows which appear to "go nowhere" are flows which previously entered compartments not modelled here. Since this model is non–conservative, the loss of nitrogen through these pathways is not important to this model.

Interestingly, despite showing quite different dynamical behaviour to the full model, model 2c's annual nitrogen flows are not too dissimilar. Surprisingly even, considering the more extreme behaviour of the model, the flows are even somewhat lower than that of the full model.

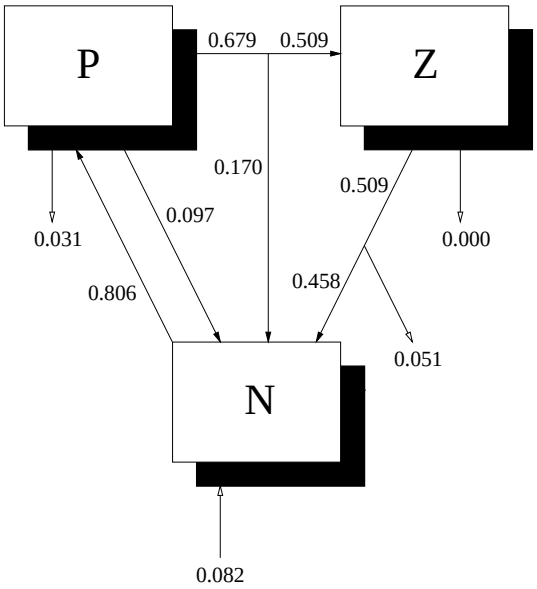

Figure 3.41: Annual nitrogen flows (mol N m^{-2} y^{-1}) at OWS "India" of model 3c.

Figure 3.41 shows the network of flows for model 3c. Curiously, despite having an extra layer of com-

plexity, model 3c is further off from the full model than model 2c, having even lower flows. Additionally, the instantaneous regeneration of dead organic material to general nutrient reduces system loss through sinking or detrainment and consequently very little nutrient is entrained.

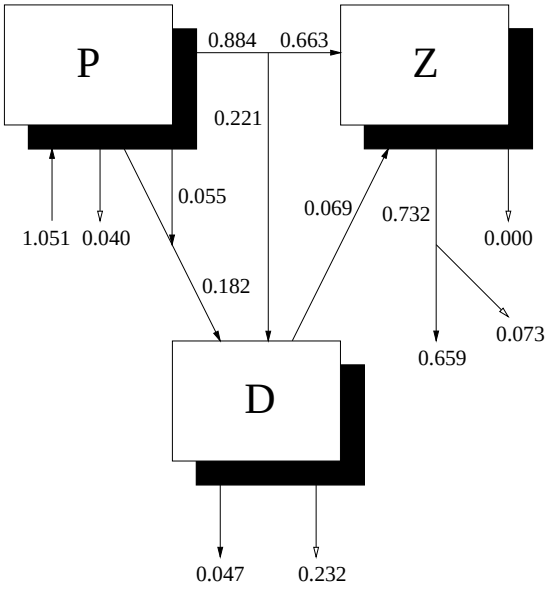

Figure 3.42: Annual nitrogen flows (mol N m^{-2} y^{-1}) at OWS "India" of model 3c2.

Figure 3.42 shows the network of flows for model 3c2. Although sharing growth limitation with model 2c, higher average phytoplankton populations lead to greater primary production than both 2c and the full model. Fewer flows into the new detritus compartment lead to slightly reduced flows out of it compared to the full model. Otherwise, most of the flows are reasonably close to those of the full model.

Figure 3.43 shows the network of flows for model 3c3. Despite the added complexity of another compartment plus an implicit representation of nitrate, the flows are very similar to those of model 2c (agreeing with the results found for the mixed–layer depth solutions).

Figure 3.44 shows the network of flows for model 4c. Once again, flows are not very dissimilar from those of the full model. For the same reasons as model 3c, nutrient entrainment is reduced, although by nowhere near the same magnitude. Noticeably, the new ecological pathway from detritus to general nutrient (introduced to represent regenerative processes) has a very low annual flux.

Figure 3.45 shows the network of flows for model 4c2. The pattern of flows here is similar to that in model 4c, and somewhat closer to that in the full model. The diversion of DON outputs into the detritus compartment (mostly zooplankton mortality) leads to higher detrital concentrations and somewhat greater detrital sinking and grazing fluxes (particularly grazing). The diversion also forces greater entrainment of subthermocline nutrient, although the quantity is still lower than that of the full model.

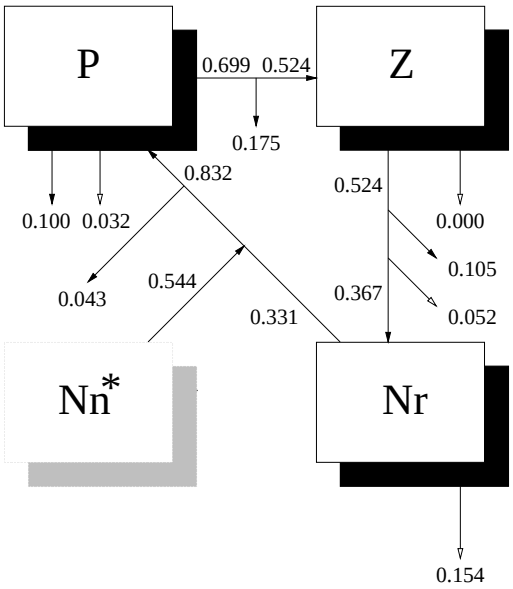

Figure 3.43: Annual nitrogen flows (mol N m^{-2} y^{-1}) at OWS "India" of model 3c3.

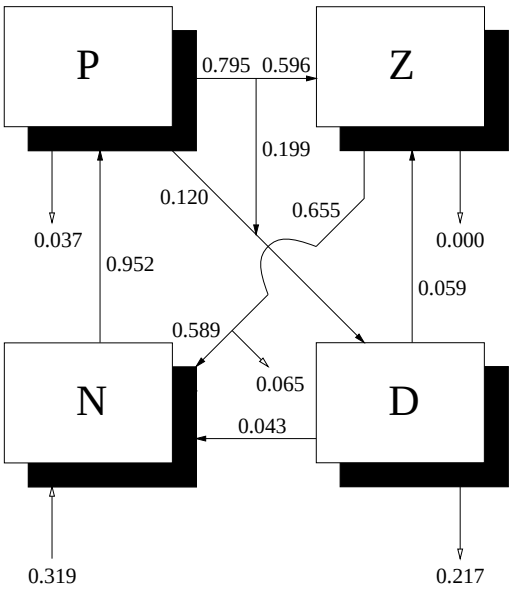

Figure 3.44: Annual nitrogen flows (mol N m^{-2} y^{-1}) at OWS "India" of model 4c.

Figure 3.46 shows the network of flows for model 4c3. Since this model shares the same DON pathways as model 4c2, the nitrogen fluxes are very similar. Production is slightly greater and this is reflected in all of the flows.

Figure 3.47 shows the network of flows for model 5c. The network clearly illustrates what has already been suggested about this model. The phytoplankton compartment is withered to almost nothing, whilst the bacterial compartment has swollen with a massive annual throughput of nitrogen. Although a major regenerative artery running between B–Z–N has been established, entrainment from beneath the ther-

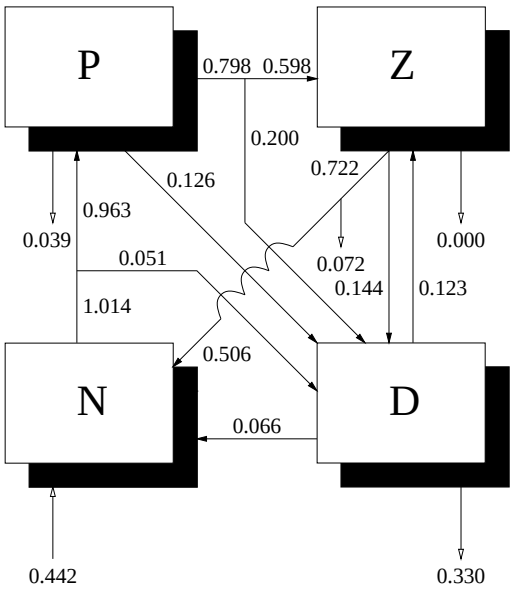

Figure 3.45: Annual nitrogen flows (mol N m^{-2} y^{-1}) at OWS "India" of model 4c2.

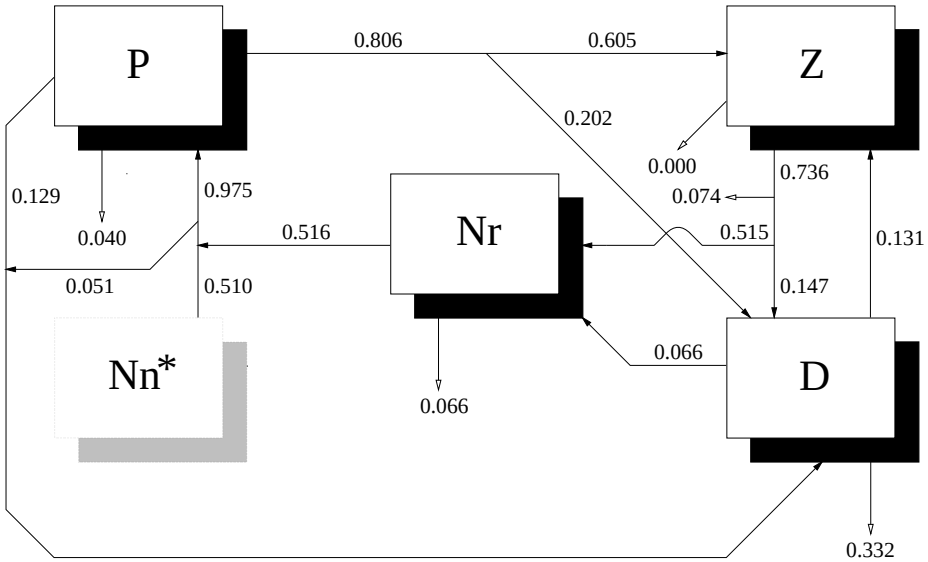

Figure 3.46: Annual nitrogen flows (mol N m^{-2} y^{-1}) at OWS "India" of model 4c3.

mocline is also an order of magnitude greater than that in the full model. The detrital compartment, through feeding inefficiency by the zooplankton, has also become a significant artery for nitrogen flow, although most quickly returns to zooplankton through grazing.

Figure 3.48 shows the network of flows for model 5c2. Although primary production is comparable (but low) to that from other models and the full model, most of the other pathways are significantly different from those of the full model. The "plumbing in" of the bacterial compartment whilst not leading to a disaster of the magnitude model 5c presents, still allows the bacteria access to the general nutrient

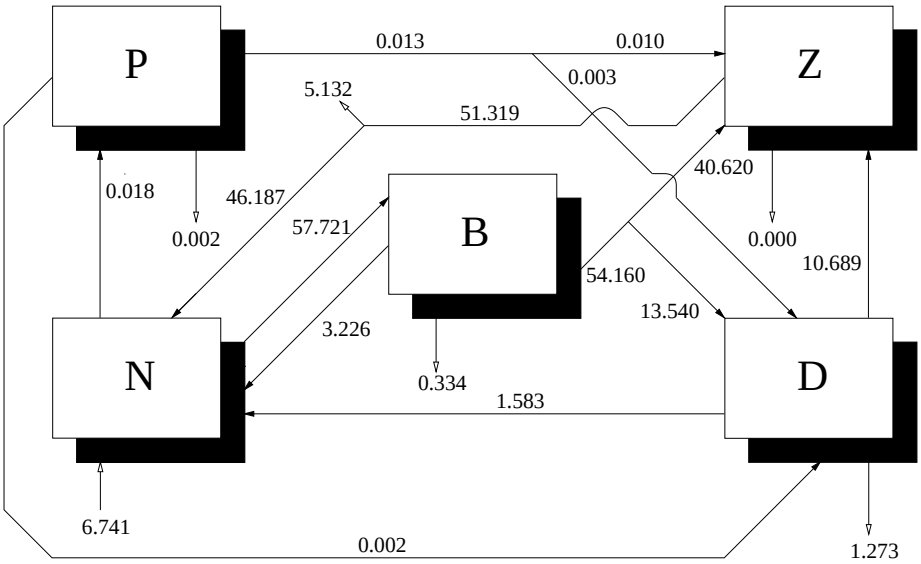

Figure 3.47: Annual nitrogen flows (mol N m^{-2} y^{-1}) at OWS "India" of model 5c.

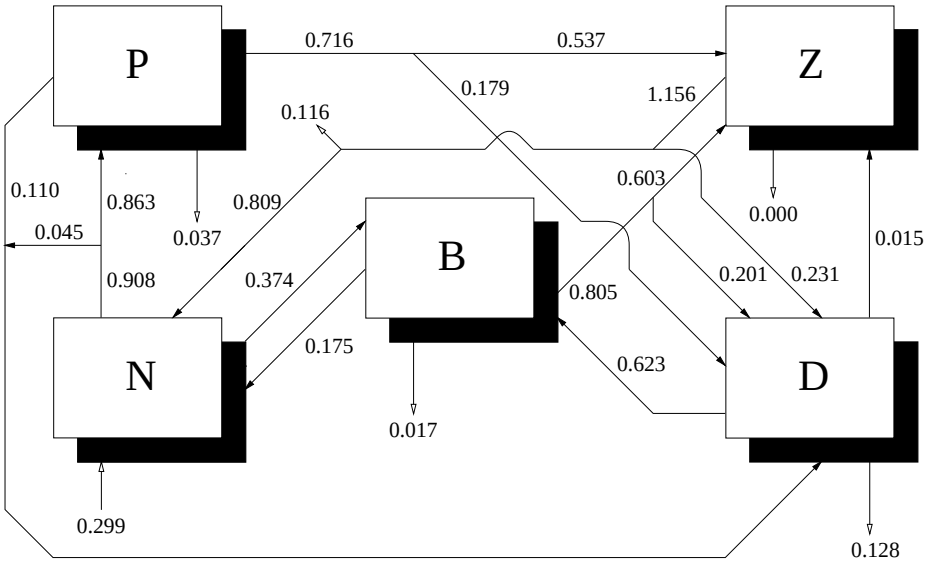

Figure 3.48: Annual nitrogen flows (mol N m^{-2} y^{-1}) at OWS "India" of model 5c2.

compartment. This is combined with access to the detrital compartment, and the results are very high fluxes (approximately double their counterparts in the full model) from these compartments into the bacterial compartment. This in turn leads to a shift in the feeding of the zooplankton (which causes the high summer zooplankton populations observed previously) and the regeneration of material from there. The uptake of detritus by the bacteria, and the relatively high regeneration of material B–Z–N lead to a reduced particulate sinking flux and a lower quantity of entrainment respectively.

Figure 3.49 shows the network of flows for model 5c3. As the explicit form of model 4c3, itself a descen-

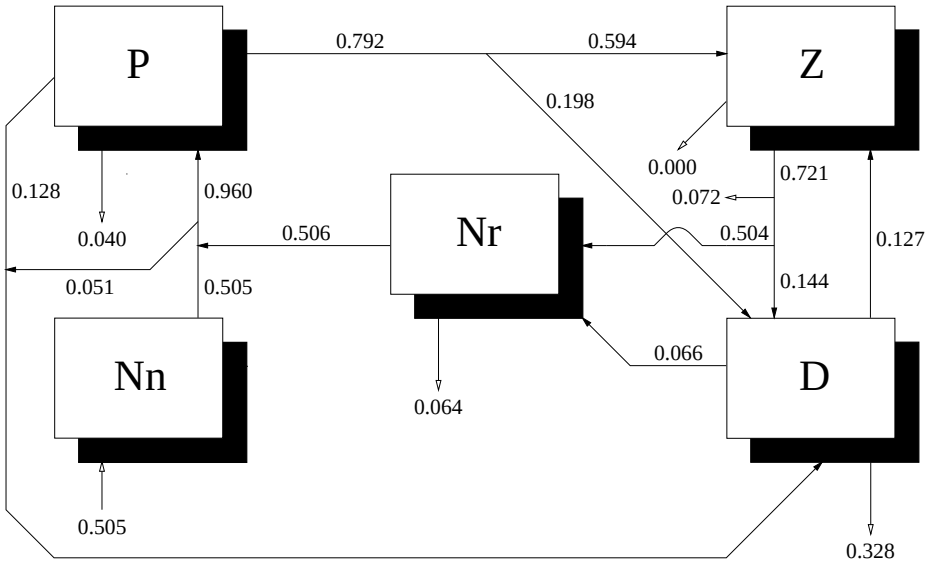

Figure 3.49: Annual nitrogen flows (mol N m^{-2} y^{-1}) at OWS "India" of model 5c3.

dant of model 4c2, this model has flows very similar to both as well as the full model. In common with both of these reduced models, inputs to detritus via DON pathways lead to greater concentrations of detritus and resulting greater sinking and grazing fluxes.

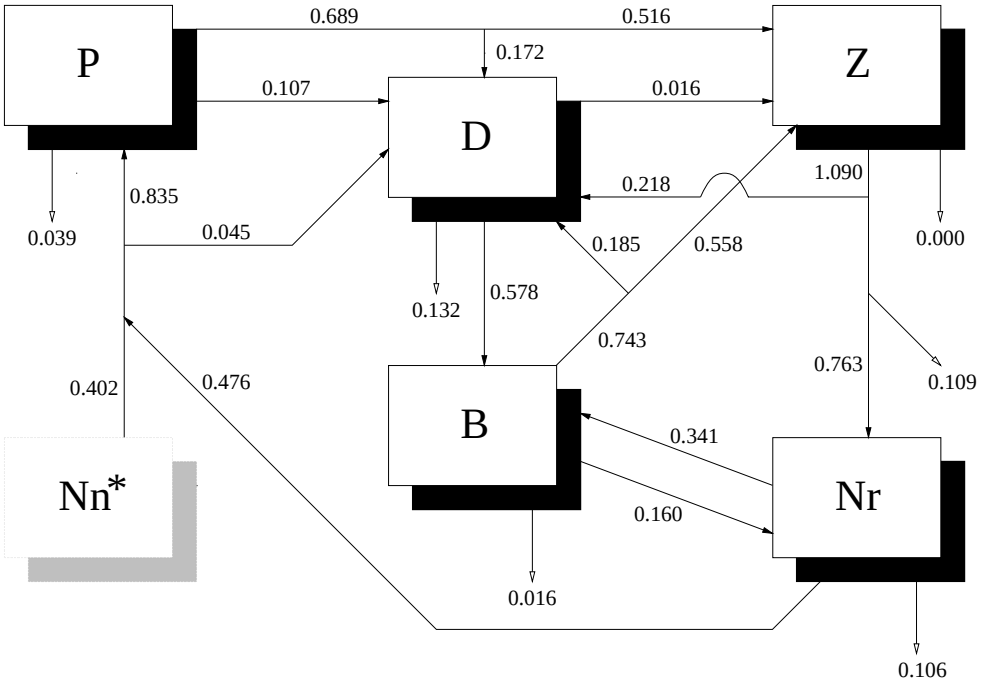

Figure 3.50: Annual nitrogen flows (mol N m^{-2} y^{-1}) at OWS "India" of model 5c4.

Figure 3.50 shows the network of flows for model 5c4. Although this model is more complex in its treatment of nutrients than model 5c2, the fluxes through it remain very similar. Uptake of detritus and ammonium are around double those of the full model. Nitrate entrainment (implicit) and detrital sinking are again lower than that in the full model.

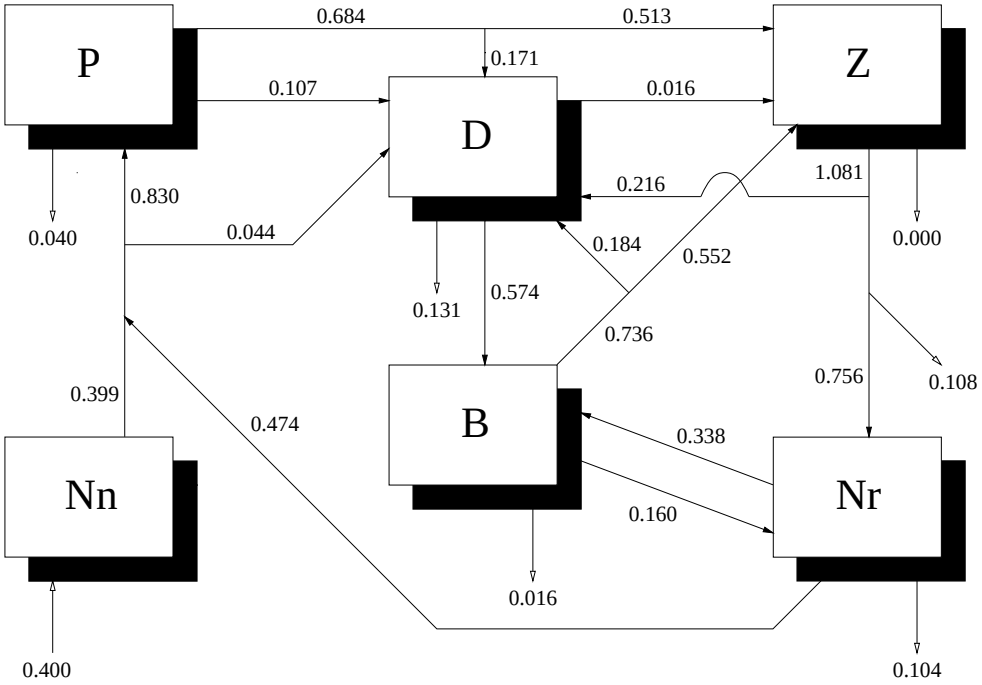

Figure 3.51: Annual nitrogen flows (mol N m^{-2} y^{-1}) at OWS "India" of model 6c.

Figure 3.51 shows the network of flows for model 6c. As a fully realised version of the implicit model 5c4 it has almost identical flows to that model. It shares the high bacterial fluxes of that model and model 5c2 for the same reasons.

Figure 3.52 shows the network of flows for model 6c2. With the single exception of the entrainment flux, almost all of the flows are within 20 mmol N m^{-2} y^{-1} of the full model. Examining the full model flows reveals that the discrepancy in the entrainment flux of model 6c2 is explained exactly by the amount of ammonium detrained in the full model solution.

Figure 3.53 shows the network of flows for model 6c3. As an implicit form of the full model, this model gets the flows almost exactly correct, with only mild differences (principally caused by slightly greater primary production). As observed in the Bermuda Station "S" results though, this model is considerably less successful in a nutrient–limited environment.

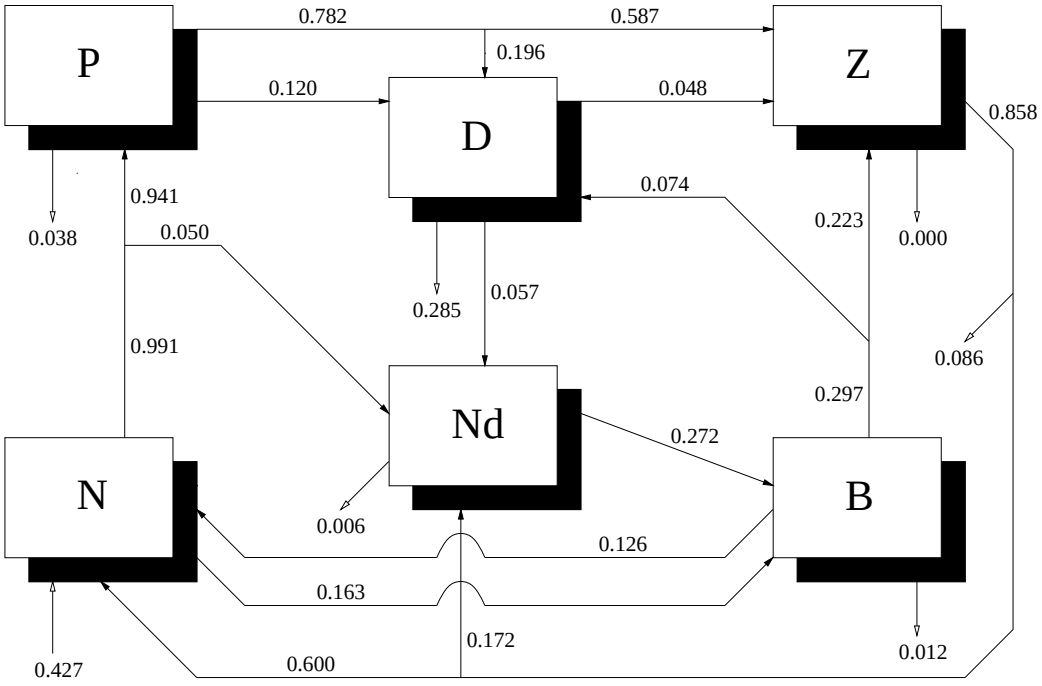

Figure 3.52: Annual nitrogen flows (mol N m^{-2} y^{-1}) at OWS "India" of model 6c2.

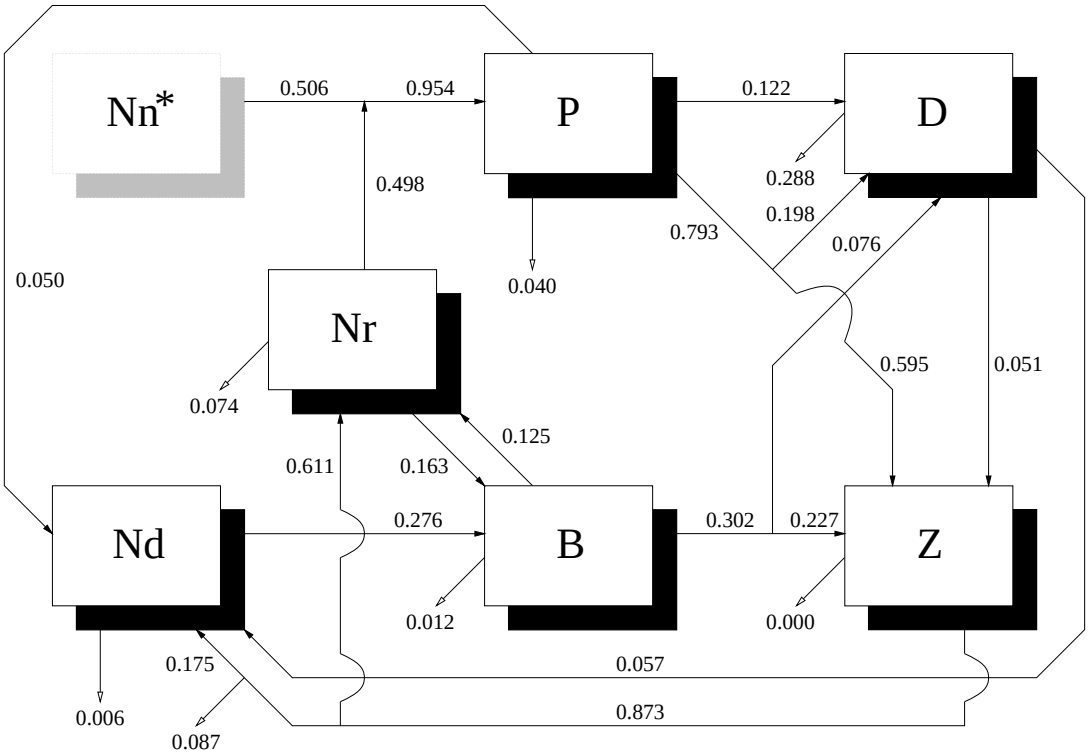

Figure 3.53: Annual nitrogen flows (mol N m^{-2} y^{-1}) at OWS "India" of model 6c3.

Nitrogen flow statistics

Table 3.4 details a series of statistics regarding the nitrogen flow in the full model and its reduced forms.

The f–ratio results agree with those discussed earlier, namely that models 4c3, 5c3 and 6c3 have ratios very similar to that of the full model, whilst models 3c3, 5c4 and 6c produce quite different ratios (particularly model 3c3).

All of the reduced forms (with the exception of model 5c) agree relatively well with the full model in terms of the fraction of phytoplankton nitrogen which is grazed by zooplankton.

The reduced models show more variety in the amount of nitrogen consumed annually by the zooplankton. The smaller models are particularly different from the full model here since they have fewer available prey items. Models 5c2, 5c4 and 6c show higher amounts of zooplankton consumption because of greater bacterial abundance. The remaining larger models with all three prey (6c2 and 6c3) have levels of zooplankton consumption comparable to that of the full model.

The same is true of the proportions of different prey species consumed. The smaller models heavily bias phytoplankton, since it is often the only available prey species. Only the larger models show proportions comparable to those of the full model. Again, models 5c2, 5c4 and 6c show a high bacterial component to the zooplankton diet.

This trend continues with the ratio of bacterial to phytoplankton production. Models 5c2, 5c4 and 6c have ratios more than double that of the full model, whilst models 6c2 and 6c3 have production ratios very close to that of the full model. Model 5c produces a particularly impressive, if thoroughly erroneous, performance.

Detrital sinking fluxes and nutrient entrainment have been discussed previously and are presented here merely to summarise them.

Model	f–ratio	P fate	Z food	P frac	B frac	B/P	D sink	N in
Full I	0.505	0.829	0.854	0.684	0.259	0.459	0.369	0.500
Full B	0.560	0.653	0.308	0.818	0.153	0.459	0.190	0.304
2c		0.874	0.550	1.000				
3c		0.842	0.509	1.000			*0.051*	0.082
3c2		0.841	0.732	0.906			0.305	
3c3	0.622	0.840	0.524	1.000			*0.052*	0.544
4c		0.835	0.655	0.910			0.282	0.319
4c2		0.829	0.721	0.829			0.402	0.442
4c3	0.497	0.822	0.736	0.822			0.406	0.510
5c		0.722	51.319	0.000	0.792	3206.7	6.405	6.741
5c2		0.830	1.155	0.465	0.522	1.155	0.244	0.299
5c3	0.500	0.825	0.721	0.824			0.400	0.505
5c4	0.458	0.825	1.090	0.473	0.512	1.101	0.241	0.402
6c	0.457	0.824	1.081	0.475	0.511	1.099	0.239	0.400
6c2		0.831	0.858	0.684	0.260	0.462	0.371	0.427
6c3	0.502	0.831	0.873	0.682	0.260	0.460	0.375	0.506
NH_4	0.467	0.838	0.919	0.686	0.258	0.454	0.392	0.492

Table 3.4: Model statistics from nitrogen flow data. Full I and Full B refer to flows from runs of the full model at OWS "India" and Bermuda Station "S" respectively. The results presented for the reduced forms are those from OWS "India" runs. **f–ratio** is the ratio of total annual nitrate uptake by phytoplankton to their total annual uptake of nitrogen. **P fate** is the fraction of the annual nitrogen flow into phytoplankton which is consumed by zooplankton. **Z food** is the total annual flow of nitrogen as food into zooplankton (mol N m^{-2} y^{-1}). **P frac** is the fraction of this flow which comes from phytoplankton. **B frac** is the fraction of this flow which comes from bacteria. The remaining fraction of this flow comes from detritus. **B/P** is the ratio of bacterial production to phytoplankton production. **D sink** is the total annual sinking flux of detritus and zooplankton mortality from the mixed layer (mol N m^{-2} y^{-1}). **N in** is the total annual quantity of nitrate or general nutrient entrained into the upper mixed layer. *Italicised* results, whilst correct for that model, are of limited comparative value due to the structure of those models.

3.3.6 Model 6c3 implicit nitrate solutions

As described previously, in the majority of solutions calculated for the implicit nitrate models, N_n^* was set to the mean daily value of N_n obtained from the comparable full model solution.

In order to establish the sensitivity of the implicit models to N_n^*, a series of three solutions using model 6c3 (an implicit form of the full model) were performed for both OWS "India" and Bermuda Station "S" conditions. In the first, N_n^* was assigned the minimum N_n observed during a comparable full model solution, in the second, the mean daily value (as previously), and in the third, the maximum N_n observed.

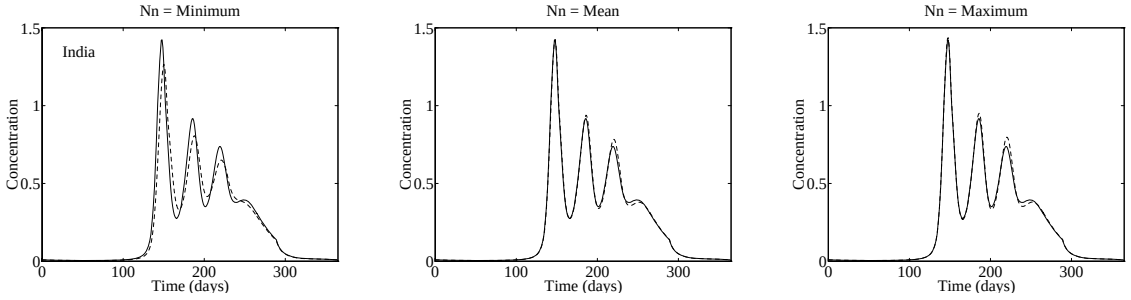

Figure 3.54: Simulated annual cycles of phytoplankton for the full model (solid line) and model 6c3 (dashed line) at OWS "India". N_n^* in model 6c3 set to full model minimum (left), mean (centre) and maximum (right). Concentrations are in mmol N m^{-3}.

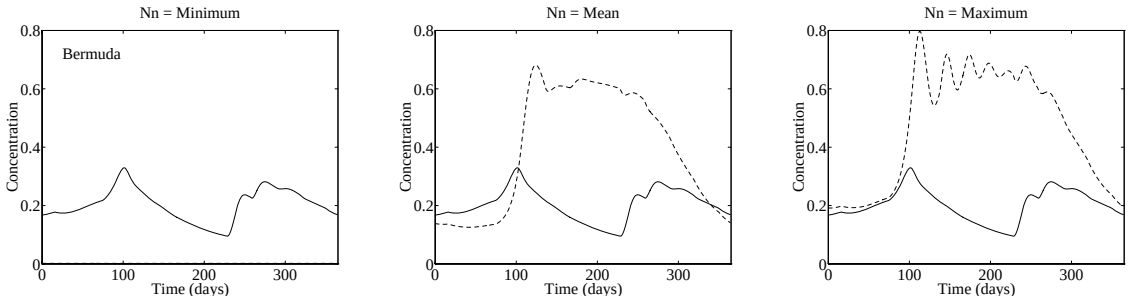

Figure 3.55: Simulated annual cycles of phytoplankton for the full model (solid line) and model 6c3 (dashed line) at Bermuda Station "S". N_n^* in model 6c3 set to full model minimum (left), mean (centre) and maximum (right). Concentrations are in mmol N m^{-3}.

Figure 3.54 shows the results of the solutions performed at OWS "India". As can clearly be seen, in all three cases model 6c3 comes very close to the full model solution. In the $N_n = minimum$ case, the departure from the full model solution is at its greatest. However, this only results in a slightly lower spring bloom maximum and somewhat more damped summer predator–prey oscillations. In the two other cases, the fit is almost perfect with only slightly more extreme predator–prey oscillations in the

summer. These departures coincide with the lowest concentrations of N_n in the full model.

Figure 3.55 shows the results of the solutions performed at Bermuda Station "S". In these cases, the departures from the full model are very extreme. In the minimum case, phytoplankton concentrations are below the minimum recorded by the program performing the solutions (*i.e.* less than 10^{-6} mmol N m^{-3}). In the mean case, winter levels of phytoplankton fall below those of the full model (N_n concentrations in the full model are close to their maximum then), whilst those in the summer exceed those of the full model considerably. Finally, in the maximum case, winter levels of phytoplankton are closer to those found in the full model, but again summer levels are considerably higher.

3.3.7 Ammonium inhibition of nitrate uptake

As discussed earlier, the formulation of ammonium–inhibition of nitrate uptake used in the full model and the reduced forms is by no means the only formulation for nutrient limitation of phytoplankton growth. To this end, the alternative formulation given in Fasham (1995) (and described previously) was put into the full model so that the significance of this particular facet to the model can be explored. This model favourably uptakes ammonium, but with no direct inhibition of nitrate uptake.

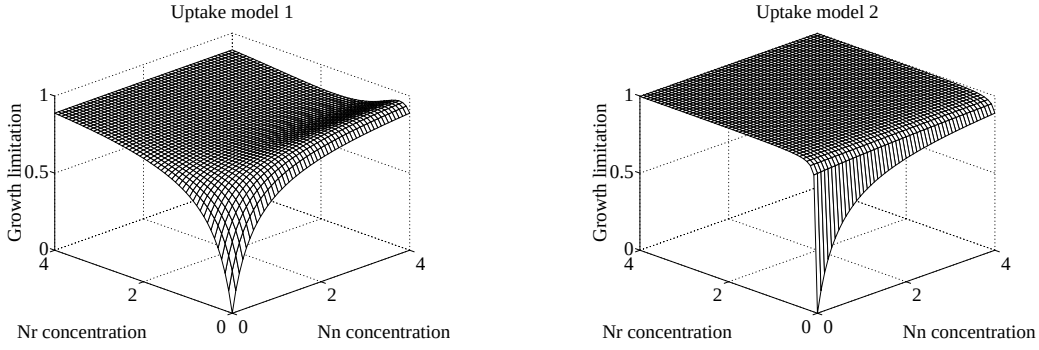

Figure 3.56: Surfaces of phytoplankton growth limitation (model term Q; *i.e.* 0 = totally limited by nutrient availability, 1 = totally unlimited by nutrient availability) produced using different models of nitrate and ammonium uptake. Model 1 is that used in Fasham (1993) and in the majority of the work presented here. Model 2 is that used in Fasham (1995). Concentrations are in mmol N m^{-3}.

Figure 3.56 shows the surfaces of growth limitation produced by the two models of nitrate and ammonium uptake kinetics. Both models cause the greatest limitation at the origin, and in both this falls away as nitrate, ammonium or both increase. Model 1 has relatively shallow increases in uptake as it moves away from the origin since both half–saturation constants have relatively high values. Model 2, on the other hand, has a sharp increase in uptake as soon as ammonium is present since ammonium's half–saturation constant is very much lower than that in model 1. Consequently, the greatest disparity in uptake between the two models occurs at low concentrations of nitrate and ammonium.

Figure 3.57 shows the results of runs performed at OWS "India" and Bermuda Station "S" using full models running both uptake models. The results are presented as a phase portrait in nitrate–ammonium space so that comparison with Figure 3.56 is easier.

The major difference between the two uptake models lies with the concentrations of ammonium they predict. At both OWS "India" and Bermuda Station "S", uptake model 1 predicts ammonium concentrations considerably greater than those of model 2. The seasonal patterns of nitrate concentration, by

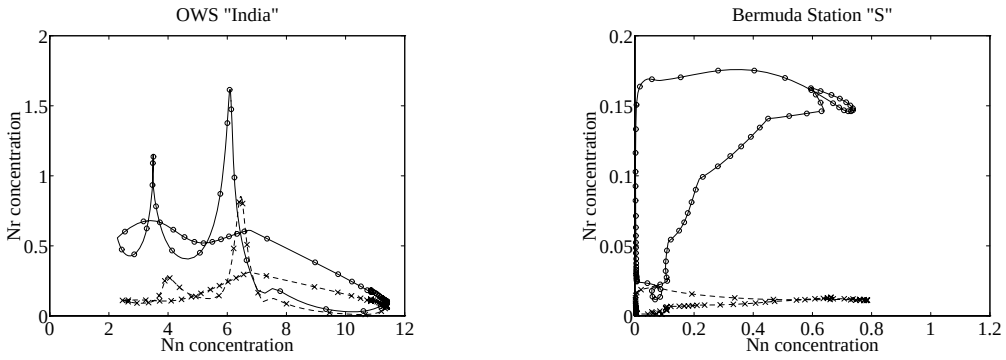

Figure 3.57: Nitrate–Ammonium phase space portraits showing the trajectories of full model running uptake model 1 (circles) and uptake model 2 (crosses) at OWS "India" (left) and Bermuda Station "S" (right). The circles and crosses mark the locations of the trajectories once every 5 days, and are added to convey the rate of movement along the trajectories. Note that the scale of the Bermuda Station "S" plot is one tenth that of the OWS "India" plot. Concentrations are in mmol N m^{-3}.

contrast, are very similar between the two models. This considerable difference conceivably represents a means by which the two models could be distinguished and tested.

In both OWS "India" solutions the lowest nitrate and ammonium concentrations are relatively far away from the region of nitrate–ammonium space in which the disparity between the uptake models is greatest. However, in the case of the Bermuda Station "S" solutions, both models spend the entire annual cycle close to the nitrate–ammonium origin.

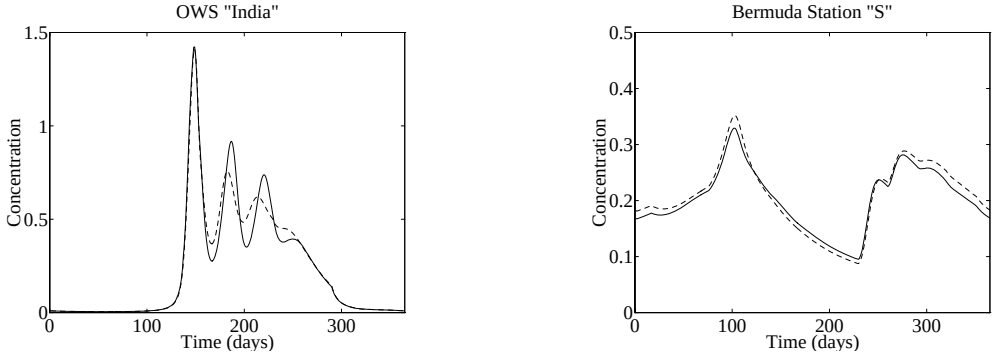

Figure 3.58: Simulated annual cycles of phytoplankton for the full model using uptake model 1 (solid line) and uptake model 2 (dashed line). Concentrations are in mmol N m^{-3}.

Despite the foray of the nitrate–ammonium trajectories into the region close to the origin, figure 3.58 shows relatively little difference in the phytoplankton time series between the different uptake models. The OWS "India" spring bloom is unaffected, although the subsequent summer oscillations are somewhat damped with uptake model 2. At Bermuda Station "S" the differences, although smaller, occur

throughout more of the year. The spring bloom is somewhat higher (phytoplankton growth being higher due to the greater uptake of model 2 close to the origin), and the summer dip somewhat lower (due to the concomitantly lower nutrient levels). This lack of difference in the time series of model compartments is repeated for all of the model compartments except ammonium and DON. In the case of DON, uptake model 2 results in autumn levels of DON around twice those produced in uptake model 1 solutions.

The similarity between the results is not as good as some of the reduced models have shown, but it is considerably better than most of them. The principal differences appear to be slightly higher phytoplankton growth, greater use of ammonium as a growth substrate, and resultant lower concentrations of ammonium (at OWS "India" the maximum ammonium concentration under uptake model 2 is only around a half that when uptake model 1 is used, and around an eighth at Bermuda Station "S").

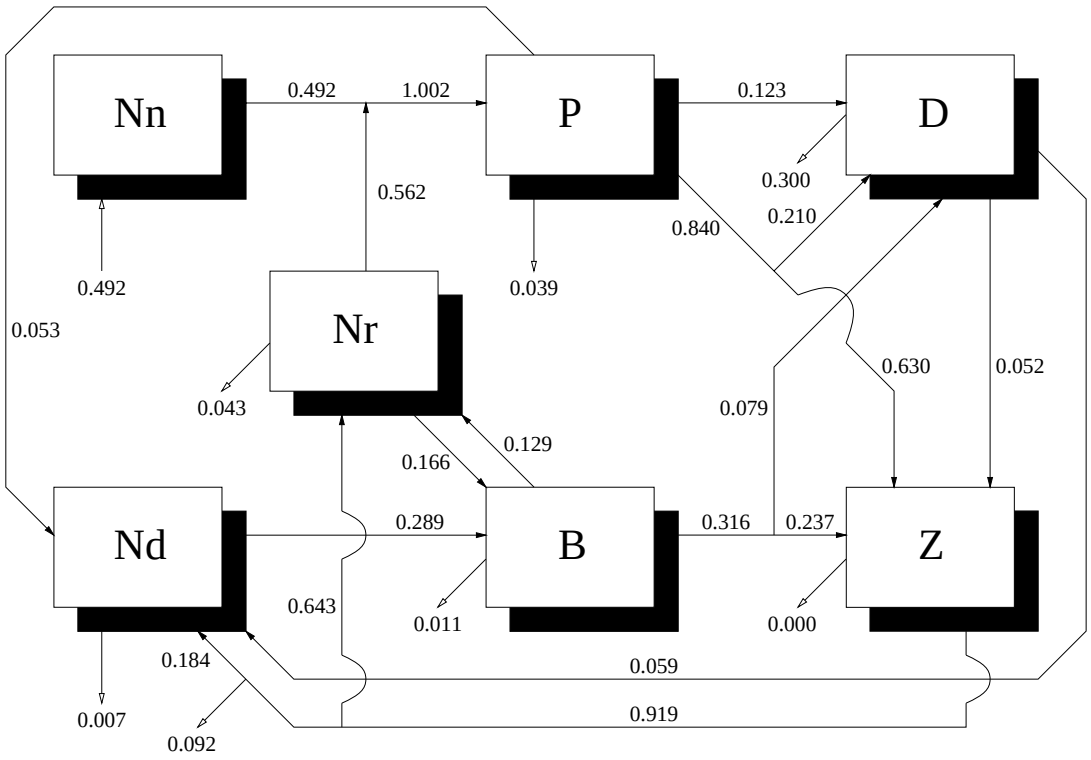

Figure 3.59: Annual nitrogen flows (mol N m^{-2} y^{-1}) of the NH_4 model at OWS "India".

Figure 3.59 shows the network of flows for the NH_4 model. Since the nutrient uptake model used here does not actively limit uptake in the presence of ammonium, uptake of nitrate and ammonium is greater than in the full model solutions using the standard uptake model. Unsurprisingly then, this leads to greater primary production and slightly higher fluxes throughout the network. Since ammonium is now preferred to nitrate there is greater uptake of ammonium and a slightly reduced uptake of nitrate. This leads to lower ammonium detrainment and lower nitrate entrainment. This greater uptake of ammonium is also reflected in the f–ratios calculated across the year at both OWS "India" and Bermuda Station "S" (see figures 3.22 and 3.29, and tables 3.2, 3.3 and 3.4). At both stations both the annual patterns

and averages fall below those produced by the full model with uptake model 1.

3.4 Summary

The primary aim in this chapter was to determine if a "minimum model", which accurately described the behaviour of the full model, could be rebuilt from a naïve deconstruction of the full model. Fourteen reduced models were constructed, ranging in size from a minimal PZ model to a six compartment model with an implicit representation of nitrate. Each model was reconstructed along rational lines, with attention paid to major ecological pathways and to the plausibility and utility of the reduced form. While several models (*e.g.* models 4c, 4c2 and 5c3) were particularly successful in this regard, the failure of the other models also provided insight into the importance of particular ecological pathways included in the full model.

The behaviour of three of the simplest models, 2c, 3c and 3c3, at OWS "India" revealed the first flaw of the reduced models. At OWS "India", nutrient limitation is always less significant than irradiance limitation during full model solutions, and consequently all three reduced models degenerate to rapid PZ cycles. Although these cycles are confined to the summer months, as are the oscillations of the full model, their severity is greater. These results contrast with those of model 3c2, which has no nutrient limitation, but which has a detrital compartment which the zooplankton can graze on. This latter model produces a series of damped summer oscillations, similar to those of the full model.

Another flaw of the simpler reduced models, as well as the implicit nitrate models, was revealed by solutions determined for Bermuda Station "S". At this station, nutrient limitation of the full model is more severe than irradiance limitation for a considerable period of the simulated year. Models 2c and 3c2, which have neither explicit nor implicit nutrient limitation, both produce extreme solutions, with oscillations in the phytoplankton and zooplankton populations which take them to values more than one order of magnitude greater than these populations reach in the full model. In the case of model 3c and the implicit nitrate forms, nutrient limitation is considerably more muted than in the full model (in model 3c, this is because regeneration is so rapid; in the implicit nitrate forms, this is because nitrate cannot be depleted). Consequently, the summer slump in phytoplankton and zooplankton populations found in the full model do not occur in these models, leading to high summer production and even oscillatory behaviour (model 3c3).

As suggested during the original formulation of the reduced models, the reinstatement of the bacterial compartment poses a number of problems. The failure of model 5c, and the difficulties found with models 5c2 and 6c would appear to confirm this. In the case of model 5c, the bacteria utilise only general nutrient for their metabolism. Since they have no seasonal limitations placed on them (unlike the phytoplankton) they make use of general nutrient throughout the year, raising their own populations at the expense of phytoplankton who spend their year considerably more nutrient limited than in the

full model. While the bacterial populations produced across the year by model 5c are never much more than twice the annual maximum found in the full model solutions, these low populations hide bacterial production (annual nitrogen uptake) more than 130 times that found in the full model (for OWS "India"). In model 5c, the N–B–Z pathway almost entirely surplants the N–P–Z pathway.

Models 5c2 and 6c (and, at OWS "India", model 5c4 – the implicit nitrate version of model 6c) also exhibit slightly more active bacterial populations, but nowhere nearly on the scale of model 5c. In both cases, as an alternative to using DON as a growth substrate, bacteria are given access to detritus as a carbon source (note that detritus is also assigned flow inputs which formerly ran to DON). This pathway makes sense since bacteria are known to occur in association with particulate material as well be free–living (Totterdell *et al.*, 1993). However, while ecologically the tying of bacteria to detritus may be unobjectionable, in the context of the Fasham (1993) model it appears that this step is misjudged. In both reduced models, the bacterial populations now have access to a much larger carbon source. Consequently their populations are more pronounced across the year. This leads to a larger zooplankton population, and also to a larger phytoplankton population (supported by regenerated excretion and predation losses from the bacterial and zooplankton populations respectively). Since most detritus becomes regenerated by bacteria, its sinking flux out of the mixed layer is shifted markedly (in both models the flux is lower than the full model flux by at least a third). Note that both models produce very similar results despite differing in the nitrogen source their bacterial utilise (general nutrient in model 5c2, ammonium in model 6c).

Although their results at Bermuda Station "S" have already been singled out as erroneous, the performance the implicit nitrate models 4c3 and 6c3 at OWS "India" is considerably better. This is unsurprising however, since both models are respectively the implicit nitrate forms of reduced model 5c3 and the full model itself. Model 5c3, along with model 4c2, is one of the most successful of the reduced forms (note that 4c2 is the parent model to 5c3). Both of these models accurately caricature the full model's dynamics and flow network, and both predict values of NPP and sinking flux close to those produced by the full model.

In the context of the primary aim of this chapter, the reduced forms known as 4c2 and 5c3 appear to be candidates for the title of "minimum model". The slightly increased complexity of model 5c3 allows it to capture certain facets of the full model that are not addressed by model 4c2 (the f–ratio for instance), and where those facets are required, it is undoubtedly superior.

3.5 Discussion

A key (but unstated) assumption in this chapter has been that the full model represents reality (otherwise why waste time fitting smaller models to a bigger one?). While this assumption is clearly not true, the full model does represent an attempt to capture reality, and makes use of what is known about the pathways between the ecosystem components represented, as well as the parameters which are involved in these pathways. However, since many of the pathways represented are poorly understood, or stand in for a myriad of real ecological processes, there is considerable uncertainty in the full model.

An important part of modelling is the production of models only as complex as demanded by the questions they attempt to answer. The questions the full model attempts to address are mostly concerned with the annual cycle of phytoplankton production, and the annual loss of particulate material to the deep ocean (since answers to these questions will help researchers predict carbon flow to the deep ocean, and ultimately assist in the ongoing race to understand the future impact of the greenhouse effect on earth). Consequently, if simpler models can successfully mimic these important facets of the larger full model, considerable effort can be spared both computationally (should these simpler models be inserted into GCMs) and analytically (usually, the more complex a model, the greater the uncertainty in its formulation, and the harder the interpretation of its results). The approach used here to achieve this (*i.e.* naïve reconstruction) is not obviously inviable, and the success of models 4c2 and 5c3 in reducing the complexity of the full model while behaving very similarly to it, at least lends it empirical support.

In addition to finding that the full model can be reasonably accurately mimiced by a ZPND model, several other interesting results about the importance of parts of the full model were discovered. One of the most significant structural differences between the Fasham (1993) model and simpler models is the inclusion of a relatively complex mechanism for regenerating nitrogen to ammonium. This mechanism includes compartments for both dissolved and particulate organic matter, and additionally a bacterial compartment which both uptakes and regenerates ammonium. Furthermore, numerical solutions of the full model find that these regenerative pathways have a relatively large annual throughput of nitrogen. However, the most successful reduced models with less than 6 compartments were all able to remove these pathways and replace them with either direct flows back to utilisable nutrient, or with decay terms with a constant rate. While this result does not suggest that bacteria are an unnecessary model component in all instances, it does draw into question whether or not they should be explicitly included.

Although explicit bacteria and DON compartments were not found necessary in successful reduced forms, the inclusion of a detrital compartment with similar flows to that in the full model appeared important. In the case of the contrasting results of models 3c and 3c2, the inclusion of such a compartment appears even more important than the addition of a nutrient compartment (at least for the relatively nutrient

replete OWS "India"). As well as providing an alternative food source for zooplankton, the detrital compartment acts as a "halfway house" for dead organic material. This latter role removes the need to instantly regenerate nitrogen back to utilisable nutrient, a pathway which crippled model 3c.

Two other interesting results, both concerning nutrients, also arose from this work. Firstly, the success of the implicit nitrate models (4c3 and 6c3) in mimicing the behaviour of the full model. And secondly, the general success of reduced models in which utilisable nutrients were represented by only a single compartment. Although these models predicted slightly lower values of entrained nutrient (models 4c2 and 6c2 were both within 15% of the full model's annual nitrate entrainment), they were otherwise as successful as those models which divided general nutrient into nitrate and ammonium.

Since numerical solutions were used to examine the reduced models, a large quantity of system information was presented in the results section. While much of this information may appear superfluous, most of it was used to determine the causes of specific model flaws. In the first instance, time series of model state variables or specific processes (limitations, predation, f–ratio) provided a useful first guide to potential model failings. For instance, model 5c's characteristic time series scrawls, and the resemblance of the detritus plots of models 5c2 and 6c to those of DON in the full model provided a useful diagnostic of the (mis)behaviour of these models. The use of flow networks allows comparable pathways between different models to be contrasted aside from the dynamics. In the context of providing estimates of annual photosynthetic uptake of carbon or sinking fluxes to the deep ocean, the flow networks provide crucial information. Particularly so where the reduced forms give the appearance of matching aspects of the time series of the full model while doing so via quite different modelled flows (*e.g.* models 5c2 and 6c). Finally, the summary statistics attempt to quantify aspects of both the time series dynamics and the flows. Some, like **Pmax** and **Ptime**, while not distinguishing the reduced forms at OWS "India" , indicate that despite the wide range of model forms, some results are controlled by forcing or another model feature (*e.g.* the constancy of both **Pmax** and **Ptime** at OWS "India" between models with and without nutrients points to the termination of the spring bloom maxima by zooplankton grazing rather than nutrient starvation).

One of the criteria used in the derivations of the reduced models was that parameter values were to remain at their values assigned in Fasham (1993). This rule was enforced since many model parameters were assigned values from data. However, since parameters are rarely constant in nature, and since the performance of several of the models could probably be improved by parameter manipulation (*e.g.* reduction of the efficiency of regeneration in model 3c; reduction of bacterial growth in models 5c2, 5c4 and 6c), this represents a possible extension to the work. The use of non–linear optimisation techniques (see Fasham & Evans, 1995) with the full model solution as "data" may represent one potential avenue for future research here.

Chapter 4

Oscillatory behaviour at OWS "India"

If we knew what it was we were doing, it would not be called research, would it?

– Albert Einstein (1879–1955)

4.1 Introduction

As has been remarked previously, the OWS "India" simulations of the Fasham (1993) seven compartment ecosystem model (subsequently referred to as the "full model"), as well as the majority of the reduced forms of that model, have marked phytoplankton–zooplankton oscillations in the summer months when the mixed layer is at its shallowest and irradiance at its highest. These oscillations are comparable to the predator–prey cycles seen in simpler models (Lotka, 1925; Volterra, 1926; Truscott & Brindley, 1994), insofar as a predator population (zooplankton) "chasing" a prey population (phytoplankton) leads to a series of overcompensations which result in both populations oscillating between higher and lower values.

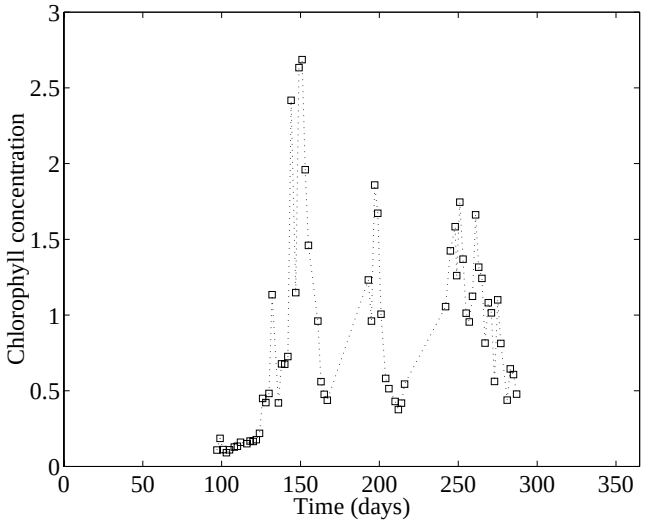

Figure 4.1: Depth–corrected measurements of chlorophyll in the mixed layer at OWS "India" during 1972. Squares represent measurements, dotted line added for clarity. Chlorophyll concentration in mg chl. m^{-3}. (Data courtesy of Bob Williams and Dr. Mike Fasham).

More significantly, chlorophyll data collected at OWS "India" in 1972 and other years shows some evidence for peaks and troughs during the summer months (see figure 4.1[1]), lending the full model some tentative support.

Recent work (Steele & Henderson, 1992; Edwards & Brindley, 1996; Popova *et al.*, 1997) has drawn attention to such oscillations, and in particular to qualitative changes in model behaviour that they may represent. Edwards & Brindley (1996), for instance, examine the 3 compartment ZPN model first proposed by Steele & Henderson (1981), and reveal a rich structure of Hopf bifurcations from stable equilibrium states to stable limit cycles. They also speculatively suggest that the seasonal occurrence of phytoplankton–zooplankton cycles, as perhaps shown in the OWS "India" data, may reflect the move-

[1] Appendix A-1 details the procedure used to convert depth samples to mixed layer concentrations.

ment of the ecosystem from a regime of stable populations to one of limit cycle behaviour.

Furthermore, limit cycle behaviour (or even weakly damped spiral sinks) can have important consequences for models in which spatial structure is included. Parameter fitting is also complicated by any oscillatory behaviour in a model, since most simple statistics assume fixed point behaviour. As the Fasham (1993) model has been both embedded within a spatial GCM (Fasham *et al.*, 1993; Sarmiento *et al.*, 1993), and used in parameter–optimisation studies (Fasham & Evans, 1995), oscillatory behaviour is of interest.

The following chapter describes a probing of the behaviour of the full model at OWS "India" to establish the nature of the summer oscillations observed, and to suggest parameter or forcing regimes under which oscillatory behaviour could be observed. A model prediction of the circumstances under which a plankton ecosystem could shift from a stable equilibrium to limit cycle behaviour would provide a good test of the model's validity.

4.2 Examination of the full model

4.2.1 Forcing functions

A major complicating factor in examining the behaviour of the full model is its use of forcing functions to replicate the annual cycles of mixed–layer depth and solar irradiance. The former driven by an array of daily depth values, the latter by a series of standard astronomical formulae.

In one sense, forcing functions may be regarded as implicit representations of unmodelled processes. Where the exact character of these processes is poorly known, or where they can be accurately characterised by simple equations, this approach can be useful and can reduce model complexity. The seasonal cycle can then be regarded as the limit cycle produced by the full series of equations (those explicitly in the model, and those implicitly incorporated via the forcing functions). This cycle may be examined using Poincaré sections to establish if the model exhibits any behaviour with a periodicity different to that of the forcing (Wiggins, 1990).

In another sense, the forcing functions can be regarded as parameters with continuously changing values. In the actual computer programs used to run the full model, this is essentially how the forcing functions are treated. These parameters create a series of attractors (one for each combination of forcing function values) onto which the model trajectory continually attempts to converge. In this view, unless the model is given sufficient time to converge onto a particular attractor, the resultant trace in the model's phase space will be an unending transient (albeit one which may be repeated regularly with the period of the forcing). Note that "sufficient time" here will be highly dependent on both the forcing functions themselves and the model equations influenced by them.

In the context of elucidating the behaviour of the full model during the oscillations it produces during the summer months of OWS "India" runs, the forcing functions are best treated this latter way. Namely, treated as model parameters and examined to determine whether their range of annual variation includes regions in which the model behaves qualitatively differently.

4.2.2 Fixed forcing studies

To examine its behaviour, runs of the full model were performed under OWS "India" conditions and allowed to equilibrate to the standard annual cycle found in previous work. Then, at specified days of the year the forcing functions were "frozen" to constant values and the model followed to establish the nature of the attractor at those values. Mixed–layer depth (M) was set to a constant value, the rate of change in depth of the mixed layer ($h(t)$) was set to zero, and the daily cycle of irradiance was exactly repeated on subsequent days.

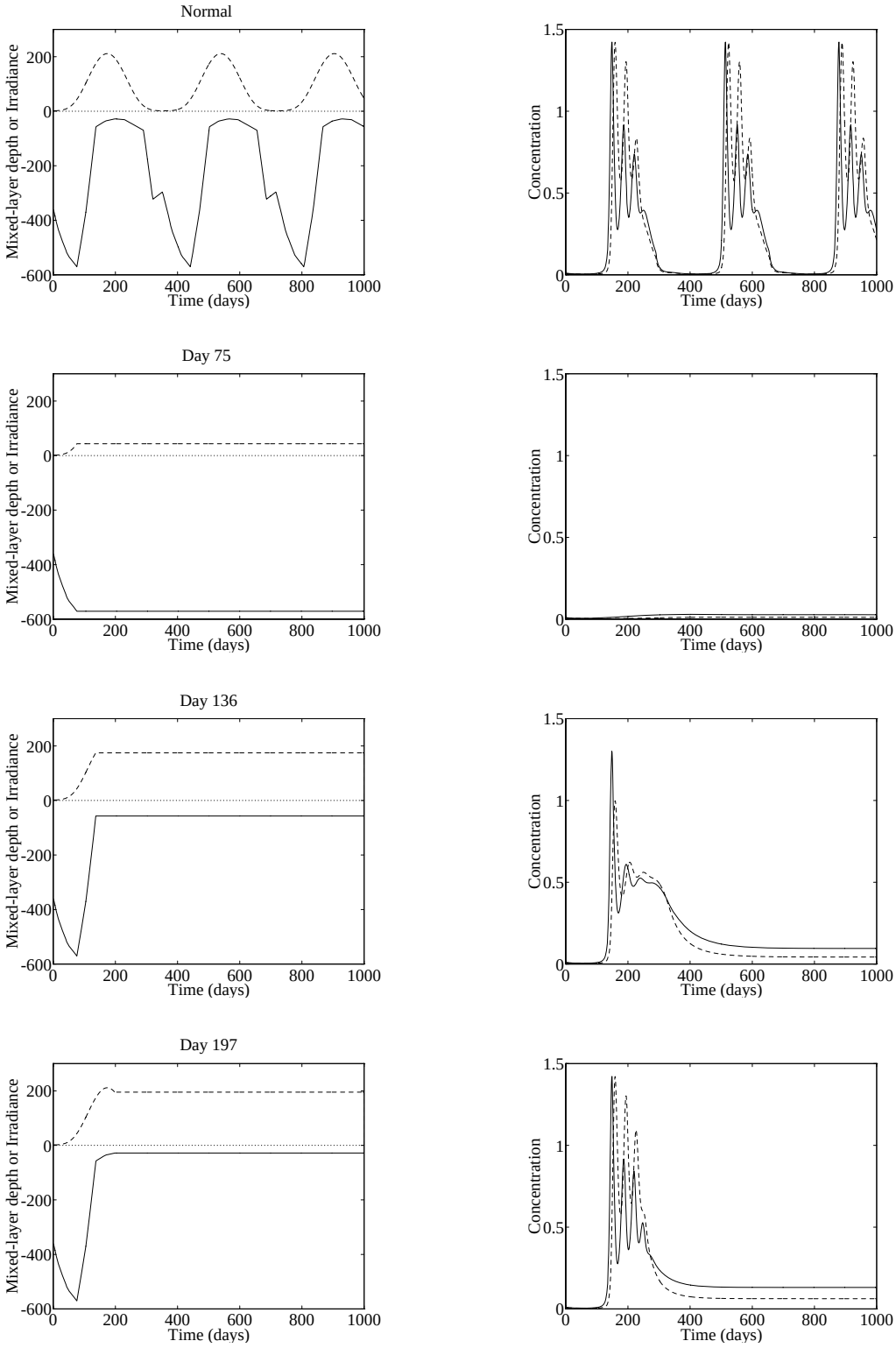

Figure 4.2: Seasonal cycles of forcing functions (left : mixed–layer depth, solid; average daily irradiance, dashed) and plankton (right : phytoplankton, solid; zooplankton, dashed) for simulations in which the forcing functions were locked at the labelled points in the annual cycle (see text for details). Mixed–layer depth in metres, irradiance in W m^{-2}, concentrations in mmol N m^{-3}.

Figure 4.2 shows some of the results obtained. A normal model trace is shown (row 1) plus the traces produced when the forcing functions are frozen at the winter mixed–layer depth maximum (day 75), just prior to the spring phytoplankton bloom (day 136), and at the summer mixed–layer depth minimum (day 197). In each example the values of the forcing functions and the populations of phytoplankton and zooplankton are shown.

In the case where the forcing functions are frozen at the winter mixed–layer depth maximum, the model finally converges on a steady equilibrium solution at low concentrations of all state variables (except nitrate, which converges on a value close to its subthermocline value). It is noticeable that this equilibrium has a phytoplankton concentration approximately 5 times greater than the concentration observed on day 75 during a normal, forced simulation. This supports what was suggested earlier, namely that during forced runs the model solution is not on the attractor, at least not on day 75.

In the remaining cases presented, where the forcing functions are frozen in shallower mixed layer/higher irradiance regimes, stable equilibria are also found. However, unlike the winter case, the equilibria are marked by considerably lower nitrate and somewhat higher concentrations of the other state variables.

When the forcing functions are frozen at pre–bloom levels (day 136) the bloom oscillation is followed by much smaller oscillations than usually observed in the summer. It is likely that the slightly lower phytoplankton growth rate is responsible. Curiously, the phytoplankton and zooplankton oscillations appear to be converging to an equilibrium around 0.5 mmol N m^{-3} by what would be the early winter. However, with the continuing depletion of nitrate (which, because of the high winter levels it rises to, was previously at almost unlimiting concentrations), the phytoplankton and zooplankton concentrations (as well as those of the other state variables) fall to a lower stable equilibrium.

A similar phenomenon occurs when the forcing functions are locked in the height of summer (day 197). However, because of the higher phytoplankton growth rates, nitrate is depleted faster and the "crash" towards lower concentrations occurs earlier. Concomitantly with the higher phytoplankton growth rates though, the summer oscillations observed are more similar to those observed in the forced case. In fact, because the fixed summer minima forcing is even more favourable than the normal variable forcing, the oscillations are slightly more rapid and extreme.

In the winter then, it appears that high nitrate/low phytoplankton–zooplankton stable equilibria exist, whilst in the summer, low nitrate/higher phytoplankton–zooplankton stable equilibria are found. The oscillations observed in the normal simulations would then appear to be transient, and reliant on the high quantities of nitrate entrained during the deep winter mixing. Summer entrainment through cross–thermocline mixing is unable to supply sufficient nitrate to sustain bloom–level phytoplankton populations should summer conditions persist.

4.3 Examining a nitrate–unlimited case

The previous section found that the relatively high summer densities of phytoplankton and zooplankton during normal simulations were supported by the entrainment of nitrate during deep winter mixing, and that a prolonged period of favourable growth conditions led to the exhaustion of this "reservoir" of nitrate and the collapse of phytoplankton densities to much lower stable equilibria. This observation suggests that if nitrate is unlimited (or supplied at a rate greater than or equal to its rate of depletion), phytoplankton densities in favourable conditions may be "buoyed up" to higher densities which may exhibit qualitatively different dynamics.

In Chapter 3, several reduced models were introduced in which nitrate was modelled implicitly by replacing it in equations by a parameter with a constant value. It was found that where nitrate concentrations were not exhausted during a normal seasonal cycle (*e.g.* at OWS "India"), these models were relatively successful at emulating the full model's behaviour.

In order to establish the validity of the suggestion that nitrate replete conditions may exhibit qualitatively different behaviour, model 6c3 was examined in a similar manner to that previously described for the full model. This model is identical to the full model with the single exception that nitrate is modelled implicitly as already described.

As before, the model was run with the forcing functions on until a consistent seasonal cycle was obtained (which, in the case of model 6c3 at OWS "India", is almost identical to that of the full model), then at various points in the annual cycle the forcing functions were fixed and the model behaviour followed.

Figure 4.3 shows the results of locking the forcing functions at the same times in the seasonal cycle as was done previously for the full model. For comparative purposes, row 1 again shows the results from a forced simulation.

As was found with the full model, locking the forcing functions at the winter mixed–layer depth maxima, leads to the state variables converging on a low, stable equilibrium. However, when the forcing functions are locked closer to the more favourable summer values, the behaviour hinted at in the full model simulations becomes much clearer.

When the forcing is fixed at day 136, model 6c3 behaves exactly the same as the full model until approximately day 300. By this point both models show the apparent convergence on an equilibrium at high state values. Beyond this point nitrate becomes limiting in the full model, and the trajectories of the state variables converge on a lower stable equilibrium. However, in model 6c3 the state variables

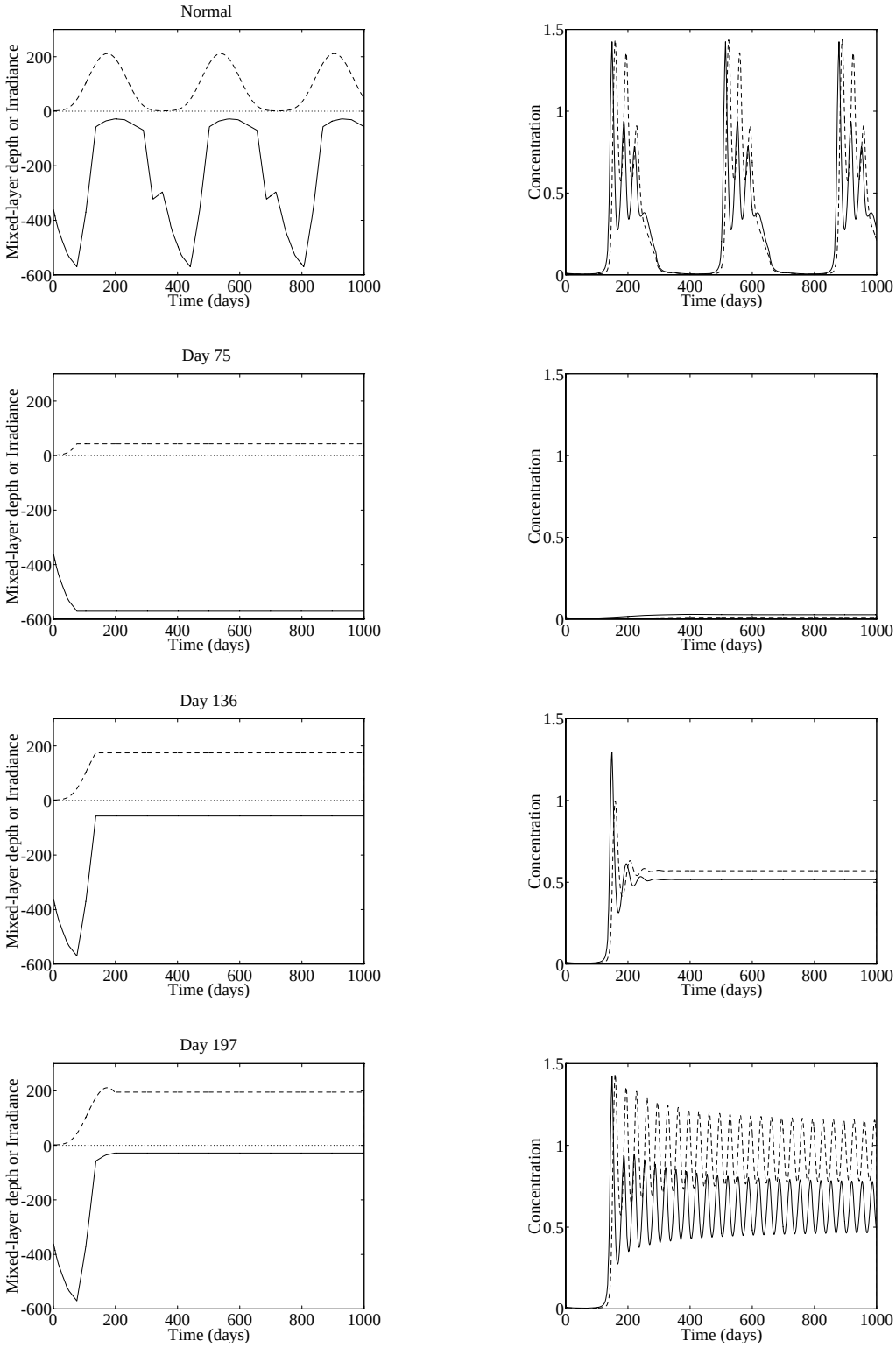

Figure 4.3: Seasonal cycles of forcing functions (left : mixed–layer depth, solid; average daily irradiance, dashed) and plankton (right : phytoplankton, solid; zooplankton, dashed) for simulations of model 6c3 in which the forcing functions were locked at the labelled points in the annual cycle. Mixed–layer depth in metres, irradiance in W m^{-2}, concentrations in mmol N m^{-3}.

continue to converge on a stable equilibrium at these comparatively high values. This confirms the suggestion that a high equilibrium exists and that falling nitrate in the full model prevents this from being a stable equilibrium.

Furthermore, when the forcing is fixed at the summer mixed–layer depth minima, the transient, oscillatory behaviour of the forced simulations collapses not to a stable equilibrium, but to a stable limit cycle. This suggests that the oscillations observed in the summer months of full model runs are transients towards an unstable "limit cycle". This cycle is unstable again because falling nitrate concentrations move the model to the low stable equilibrium.

4.4 Can the full model produce limit cycles?

The conclusion drawn in the previous section from the comparison of numerical solutions of the full model with those of model 6c3, is that depletion of nitrate in simulations of the full model prevents the existence of the the high phytoplankton/high zooplankton stable equilibria and stable limit cycles found in model 6c3.

Given this, is it possible that these solutions become stable in the full model at different parameter values? The most obvious approach is to examine parameters which directly influence nitrate concentrations. If nitrate depletion can be curtailed, it is possible that these more "interesting" behaviours can be attained.

$$\frac{dN_n}{dt} = -J(t, M, P)Q_1(N_n, N_r)P + \frac{(m + h^+(t))}{M}(N_0 - N_n) \tag{4.1}$$

Equation 4.1 above shows the nitrate differential equation from the full model. The equation consists of only two terms, one for nitrate loss due its uptake by phytoplankton, and a second for entrainment/mixing gains.

The former term is unlikely to offer any productive avenues for progress since any reduction in nitrate loss to phytoplankton will reduce phytoplankton growth rates and prevent the rapid, predator–prey oscillations in question (as can be seen in the fixed forcing simulations which halt during the winter).

The latter term, however, presents two obvious routes for reducing nitrate depletion. By increasing the cross–thermocline mixing rate (m), nitrate can be entrained from below the thermocline at a greater rate. Secondly, by increasing the subthermocline nitrate concentration (N_0) itself, more nitrate can be entrained into the mixed layer.

4.4.1 Analysis

Ideally, an analysis of the model equations would determine the stability of steady states of the model and reveal regions of parameter space in which qualitatively different behaviour occurs.

The local stability of the steady states of a model can be determined by constructing the Jacobian matrix from the equations, and then examining the eigenvalues of the resulting linearised equations about the steady states. The Jacobian matrix of, for instance, a ZPN model with three differential equations would take the following form :

$$A = \begin{bmatrix} \frac{\delta}{\delta P}\left[\frac{dP}{dt}\right] & \frac{\delta}{\delta Z}\left[\frac{dP}{dt}\right] & \frac{\delta}{\delta N}\left[\frac{dP}{dt}\right] \\ \frac{\delta}{\delta P}\left[\frac{dZ}{dt}\right] & \frac{\delta}{\delta Z}\left[\frac{dZ}{dt}\right] & \frac{\delta}{\delta N}\left[\frac{dZ}{dt}\right] \\ \frac{\delta}{\delta P}\left[\frac{dN}{dt}\right] & \frac{\delta}{\delta Z}\left[\frac{dN}{dt}\right] & \frac{\delta}{\delta N}\left[\frac{dN}{dt}\right] \end{bmatrix}$$

This matrix is then evaluated at a fixed point, yielding the eigenvalues. When the real parts of all of the eigenvalues are negative, trajectories are attracted inwards from all directions and a stable equilibrium state results. The magnitude of the different eigenvalues will determine just how quickly a trajectory will move towards this stable equilibrium along different directions. By contrast, when the steady state has at least one eigenvalue with a positive real part this implies that the fixed point is unstable and stable limit cycles are a possible outcome (although by no means the only one). Note that eigenvalues contain a real and an imaginary component. When all the imaginary components are zero (and all of the real components are negative), then the stable equilbrium is a "node" and trajectories will converge to it monotonically. However, when the imaginary component of an eigenvalue becomes non–zero (this necessarily happens to pairs of eigenvalues), a spiralling trajectory results. When all of the eigenvalues have negative real parts and some have non–zero imaginary parts, the stable equilibrium is a spiral sink, and trajectories spiral as they collapse towards it.

Real parts	**Imaginary parts**	**Behaviour**
All -ve	All zero	Stable "node"
All -ve	Some non-zero	Stable spiral sink
All zero	–	Neutrally stable
Some +ve	–	Unstable (limit cycles possible)

To determine the behaviour of neutrally stable systems (*e.g.* the Lotka–Volterra equations described in Chapter 1), higher order terms need to be considered.

The complexity of the full model (in particular the complex depth–integral of phytoplankton growth rate, J, and the minimum function in bacterial substrate uptake, S) prevents such an analysis without simplification, and numerical solutions were employed instead to explore the model's behaviour. In the following section, the program written to explore parameter space and to classify the model behaviour found is described.

4.4.2 Numerical approach

A preliminary "manual" exploration of the m and N_0 parameter space encountered both stable equilibria and oscillatory behaviour. To explore parameter spaces more thoroughly, a program was written to automatically move across them and to categorise the behaviour found for different parameter values. Initial versions of the program attempted to distinguish different dynamical behaviours in a crude fashion. However, through examination of the trajectories these versions produced, more robust algorithms were programmed to automatically classify behaviour.

As previously, all numerical solutions were carried out with fixed forcing. Mixed–layer depth remained

unchanged through the entire duration of each run and the same daily cycle of irradiance was repeated on every simulated day. All parameters, other than the one(s) under study, were set to the baseline values from Fasham (1993). The following procedure was followed by the program for each combination of parameter values in the ranges examined :

(i) **Parameter and state variable initialisation**

At the start of each individual simulation the parameter(s) in question was assigned the next value from the range to be explored. Ranges were specified by their minimum and maximum extent, and the actual parameter values used in the simulations were evenly spaced across the range.

Since it is possible that multiple stable attractors may exist for a particular choice of parameter values, the initial conditions of the each of the state variables were assigned randomly. Should such multiple attractors occur within a region of parameter space examined, the results from solutions of consecutive parameter values may be expected to be attracted differently depending on their initial conditions. Such results would (unless the different attractors reside very closely to one another in state space) be very obvious from plots of the parameter space results. The range of initial values assigned to each of the state variables fell with a uniform distribution between 0.001 mmol N m^{-3} and the value of N_0 (for obvious reasons, ordinarily the ranges of state variables never exceed that of the subthermocline nitrate concentration during a simulation).

(ii) **Initial transient phase**

After parameter and state variable values were assigned, the model was simulated for a period of 500 days to attempt to remove transient behaviour. The run was not monitored during this period.

(iii) **Long–term monitoring phase**

After the initial transient phase, the run continued into a monitoring phase which was allowed to persist for up to 50000 days ($>$ 130 years) during which time the behaviour of the state variables was followed by the program. This section sought to eliminate transient behaviour, and to establish whether a stable equilibrium or oscillatory behaviour was occurring.

Since solar–forcing retained its diel cycle, model state variables exhibited a low amplitude diel signal. The effects of this were ignored by sampling state variables constantly at midday of each simulated day. At this time, the values of each of the state variables were compared to that of the previous midday. Where the values were found to be identical to 6 decimal places (machine precision was still considerably greater than this), a counter was incremented by 1. Where the values were different at the same precision, the counter was reset to 0.

A run was deemed to have reached a stable equilibrium state when the values of **all** of the state variables remained constant (by the definition in the last paragraph) for 20 days. At this point the run in question was terminated, the data from it recorded and a new run with a new parameter value started.

(iv) **Averaging phase**

If a run did not reach a stable equilibrium during the long–term monitoring phase, the midday value of the phytoplankton state variable was recorded for 1000 days and its maximum, minimum and mean over this period calculated.

(v) **Oscillations phase**

These calculations were then used in a final phase during which the trajectory of the phytoplankton state variable was used to determine whether oscillations were occurring about the mean value.

Sampling again at midday, a pair of switches in the program monitored the times when the phytoplankton population crossed the mean value which had been obtained for it in the previous phase. One switch recorded the time when the phytoplankton population rose from below the mean to above the mean, the other monitored for the reverse and reset the first switch when it occurred. Whenever the first switch was triggered, the values of all of the state variables at the time of the switch triggering, and the values of the minima and maxima each state variable had recorded since the last switch triggering were stored. These data allowed the calculation of the period of any oscillations found, as well as the "amplitude" of the oscillations in state variable phase space.

Conventionally, the amplitude of a wave is the distance between its mean and either the maximum or minimum value reached in one wavelength. Since the oscillations in this work were often asymmetric about their mean, here the term "amplitude" is used instead to describe the full distance between the maximum and minimum of a given state variable during one orbit of the limit cycle.

This phase ran for a period of 5000 days. At the end of it, the simulation was terminated and data collected during it was examined.

(vi) **Classification**

Runs which were not deemed to have reached a stable equilibrium during the long–term monitoring phase were found (through manual examinations of their trajectories) to fall into one of three distinguishable categories :

- "Long–term transients"
- "Spiral sinks"
- "Stable limit cycles"

Long–term transients were those trajectories which were constantly rising or falling (increasingly slowly with time) apparently towards a stable equilibrium. Since the trajectory of their phytoplankton population (and that of the other state variables) always moved in one direction, they recorded no oscillations during the oscillation phase.

Using the amplitudes of the oscillations recorded for each state variable whenever the oscillation switch was triggered during the final simulation phase, "spiral sinks" were identified as those

trajectories which, while oscillating around the phytoplankton mean, were constantly contracting in all seven state variables. Although possible that the trajectories labelled as "spiral sinks" were actually converging onto stable limit cycles, after the 50000 days of the long–term transient phase, it was usual for the oscillation amplitudes of trajectories labelled spiral sinks to be considerably smaller than the diel signal.

Again using the amplitudes of the oscillations recorded during the final phase, stable limit cycles were identified as those oscillating trajectories which showed no constant reduction in the amplitudes of the oscillations in the seven state variables. Although the algorithm used to establish whether the amplitudes were constantly decreasing could in principle be "fooled" by trajectories which sometimes increased their amplitudes despite a general trend for amplitude shrinkage, no trajectories classified as stable limit cycles were found to show this pattern of behaviour (data output by the program included that which would show such a pattern were it to exist).

While these three categories could be distinguished from the trajectories they recorded, it is still possible that had a particular run not been terminated, the trajectory it was tracing could have changed its behaviour as it approached an unseen attractor. Since *only* trajectories were used to distinguish different behaviours, this possibility cannot be ruled out.

(vii) **Data output**

To safeguard against misclassification of trajectories, pertinent summary data from each simulation was output. This included a time series of the midday values of each of the state variables for each of the last 100 simulated days. Also output were the amplitudes recorded for each of the state variables for each of the oscillations tracked by the program during the oscillation phase.

These data were perused later for anomalies through data handling and presentation software (MATLAB). Although no anomalies were found during runs of the most robust program, the possibility for errors in such work always exists.

While transient behaviour may be important in the seasonal dynamics of forced runs, initial conditions can play an important role in their duration. Therefore, although the program could distinguish long–term transients and spiral sinks, only stable equilibrium and stable oscillatory behaviours were sought and the duration of the long–term transient phase was often increased to allow trajectories time to "settle down" and be classified as stable equilibria.

All of the research described in the remainder of this chapter made use of this program.

4.5 Mixing rate and subthermocline nitrate

As stated previously, the results of simple fixed forcing simulations of the full model and model 6c3 suggest two obvious parameters which may provides routes to stable oscillatory behaviour : the cross–thermocline mixing rate, m, and the subthermocline nitrate concentration, N_0.

4.5.1 OWS "India"

In the first instance, a region of parameter space of both of these parameters was examined. The cross–thermocline mixing rate, m, is assigned a wide range of values in the modelling literature. Fasham (1993) used a low value of 0.01 m d^{-1} to better fit the summer phytoplankton dynamics at Bermuda Station "S". Almost all of the models in the literature surveyed (see Chapter 2) used values below 1.0 m d^{-1}, but values up to 3.0 m d^{-1} have also been used (Evans & Parslow, 1985). The values of subthermocline nitrate, N_0, used in the literature normally reflect the geographical location the model is intended to simulate. Strass & Woods (1991) report mixed layer nitrate concentrations during winter ranging from approximately 2 mmol N m^{-3} at 38° N, to 14 mmol N m^{-3} at 55° N. Since the mixed layer is normally shallower when the majority of phytoplankton production occurs, and since models normally assume that most production is occurring in this shallower mixed layer, the subthermocline nitrate parameter is usually set to the concentration reached in the deeper mixed layer of the winter. Consequently, latitudinal differences in the annual cycles of thermal stratification and wind–mixing mean that the parameter N_0 is usually assigned a value between 2 and 15 mmol N m^{-3} depending on the location in question.

Figure 4.4 shows the results of numerical solutions across a range of m and N_0. The first three rows of plots show surfaces of equilibrium concentrations (left) and limit cycle amplitudes (right) for phytoplankton, zooplankton and nitrate respectively. The seventh plot shows the periods measured for the limit cycles found, and the eighth plot shows the pattern of limit cycle amplitude against period.

The "bulges" which can be seen on the phytoplankton and zooplankton equilibrium surfaces are caused by the limit cycles which occur at those regions of parameter space. In these regions the plots actually show the extent (the maximum and minimum concentrations which occur during a cycle) or *envelope* of the limit cycles found (although not visible in these plots, the "bulges" extend both upwards and downwards – see later figures). The nitrate surface also has this "bulge", but because of the scale on the plot, it cannot easily be seen. The plots of limit cycle amplitude aim to show the extent of limit cycle oscillations more clearly. Combinations of parameters which produce stable equilibria have amplitudes of zero.

In the case of the plot of limit cycle periods, parameter combinations which produce stable equilibria have their periods set from 0 to 30 days for the purpose of clarity in the plot. The plot has also been

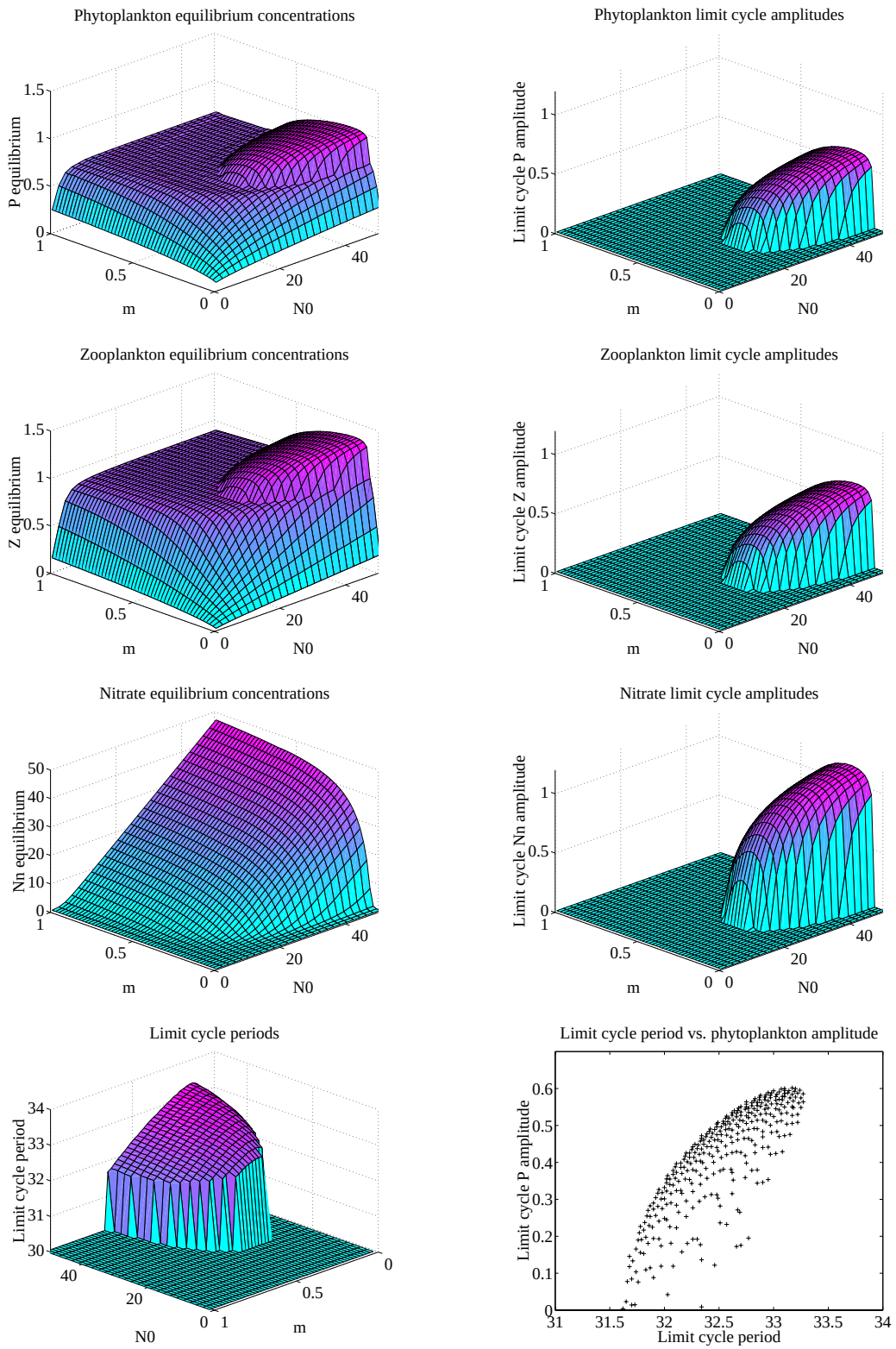

Figure 4.4: The results of numerical solutions performed at OWS "India" on day 197 across a range of cross–thermocline mixing rates (m) and subthermocline nitrate concentrations (N_0). Mixing rates in m d^{-1}, subthermocline nitrate concentrations in mmol N m^{-3}. Equilibrium concentrations and limit cycle amplitudes in mmol N m^{-3}. Limit cycle periods in days. Note that non–limit cycle regions are assigned periods of 30 days in the bottom two plots for the purposes of graphical presentation.

rotated anti–clockwise by 90° to more clearly present its most interesting surface. In subsequent plots of limit cycle period, the value assigned to regions of stable equilibria, and the angle the plot is rotated to, are similarly adjusted to maximise the information presented.

The results show that a region of limit cycle behaviour exists for mixing rates between approximately 0.09 and 0.63 m d^{-1} and for values of subthermocline nitrate greater than approximately 23 mmol N m^{-3}. While mixing rates of this magnitude are not uncommon in the literature, the minimum value of subthermocline nitrate required for such behaviour falls considerably outside the range of deep nitrate observed at OWS "India" or nearby latitudes (Strass & Woods, 1991; Fasham *et al.*, 1993).

The amplitudes of the limit cycles were found to increase with rising N_0, while increases in m at first increased amplitudes, but then decreased them before limit cycle behaviour ceased at values above 0.63 m d^{-1}. This cessation is likely to be related to one of the "side–effects" of increased mixing. While increasing subthermocline nitrate can only add nitrate to the mixed layer, increased mixing adds nitrate but also removes phytoplankton. Above a certain amount of mixing, the phytoplankton gains from enhanced nitrate supply will be outweighed by the losses incurred from cells being mixed out of the mixed layer.

Limit cycle periods ranged between 31.5 and 33.5 days, with the most significant trend being decreasing period with increasing m. The chlorophyll data collected at OWS "India" during 1972 suggests oscillations with a period around 50 days. This clearly contrasts with the shorter periods of the model cycles found here. However, as the periods found here are variable with parameter values, it is still possible that different values of other parameters (excluding the parameters examined here, there are around 25 other parameters) will produce cycles with longer periods. However, the model periods found do agree with several other model studies. In their analysis of the considerably simpler ZPN model of Steele & Henderson (1981), Edwards & Brindley (1996) found limit cycles with periods between approximately 33 and 36 days. Oscillation periods within this range were also found by Popova *et al.* (1997). McCauley & Murdoch (1987) reviewed algae and *Daphnia* data from both experimental and field environments. Cyclic behaviour with periods ranging across 29–54 (algae) and 25–47 (*Daphnia*) days was commonly found (although the work reviewed related exclusively to freshwater habitats).

Aside from the region of limit cycle behaviour, the stable equilibria of phytoplankton and zooplankton rise relatively sharply with increases in both m and N_0. For the majority of the parameter space examined, phytoplankton and zooplankton concentrations plateau to stable equilibria around 0.64 and 0.87 mmol N m^{-3} respectively. Nitrate stable equilibria mostly reached values slightly below the value of N_0 for each given simulation. These results are expected since the phytoplankton are also limited by irradiance, so can only deplete nitrate at some maximum rate. When nitrate is supplied faster than this rate (which it is across most of the parameter space examined) it cannot be depleted and tracks its subthermocline concentration.

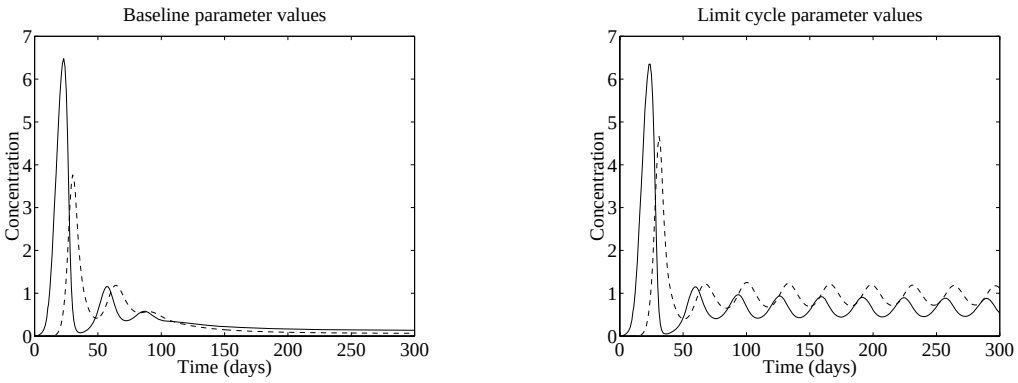

Figure 4.5: Sample time series of phytoplankton (solid) and zooplankton (dashed) for two pairs of m and N_0 values. Baseline (left; $m = 0.01$, $N_0 = 12$) and limit cycle (right; $m = 0.30$, $N_0 = 23$) values of parameters used. Concentrations in mmol N m^{-3}.

Figure 4.5 shows examples of stable equilibrium and limit cycle time series. Identical initial state variable conditions were used in both examples. Although in both cases shown the long term behaviour of the model is quickly approached (in the case of the baseline parameter values, a stable equilibrium state was judged here to have been reached after approximately 1100 days), as parameter values approached those which resulted in limit cycle behaviour, the time taken by the program to judge a trajectory to have reached its stable equilibrium increased sharply. This is entirely expected from bifurcation theory. As a model's behaviour moves from a locally stable equilibrium to an unstable one, the real part of at least one of the eigenvalues which describes the local stability will increase from a negative value to a positive one. As it does so, the time taken for a trajectory to converge to the stable equilibrium increases, since the value of the eigenvalue in question dictates the rate of convergence (in the state space direction it represents). A Hopf bifurcation occurs when the real part of the eigenvalue passes through zero. Fortunately, prohibitively long transient times ($\gg$ 50000 days) were encountered infrequently in the work here (and generally in the simulations presented in this chapter).

4.5.2 Bermuda Station "S"

The results from model runs performed during the OWS "India" summer place a region of limit cycle behaviour at values of m and N_0 quite far from their baseline values. Although simulations performed at Bermuda Station "S" (unlike those at OWS "India") show no evidence of limit cycle behaviour across the seasonal cycle, the irradiance–limitation of phytoplankton growth is considerably reduced (both by greater surface irradiance and a shallower mixed layer) and the baseline maximum phytoplankton growth rate is more than double that at OWS "India" . For these reasons, a second series of runs across m–N_0 parameter space was undertaken with fixed forcing from the Bermuda Station "S" summer. Forcing was locked on the values from day 165, the first day of the shallowest mixed layer depths in the summer.

Figure 4.6 shows the results of these runs. Comparable plots to those already presented for results

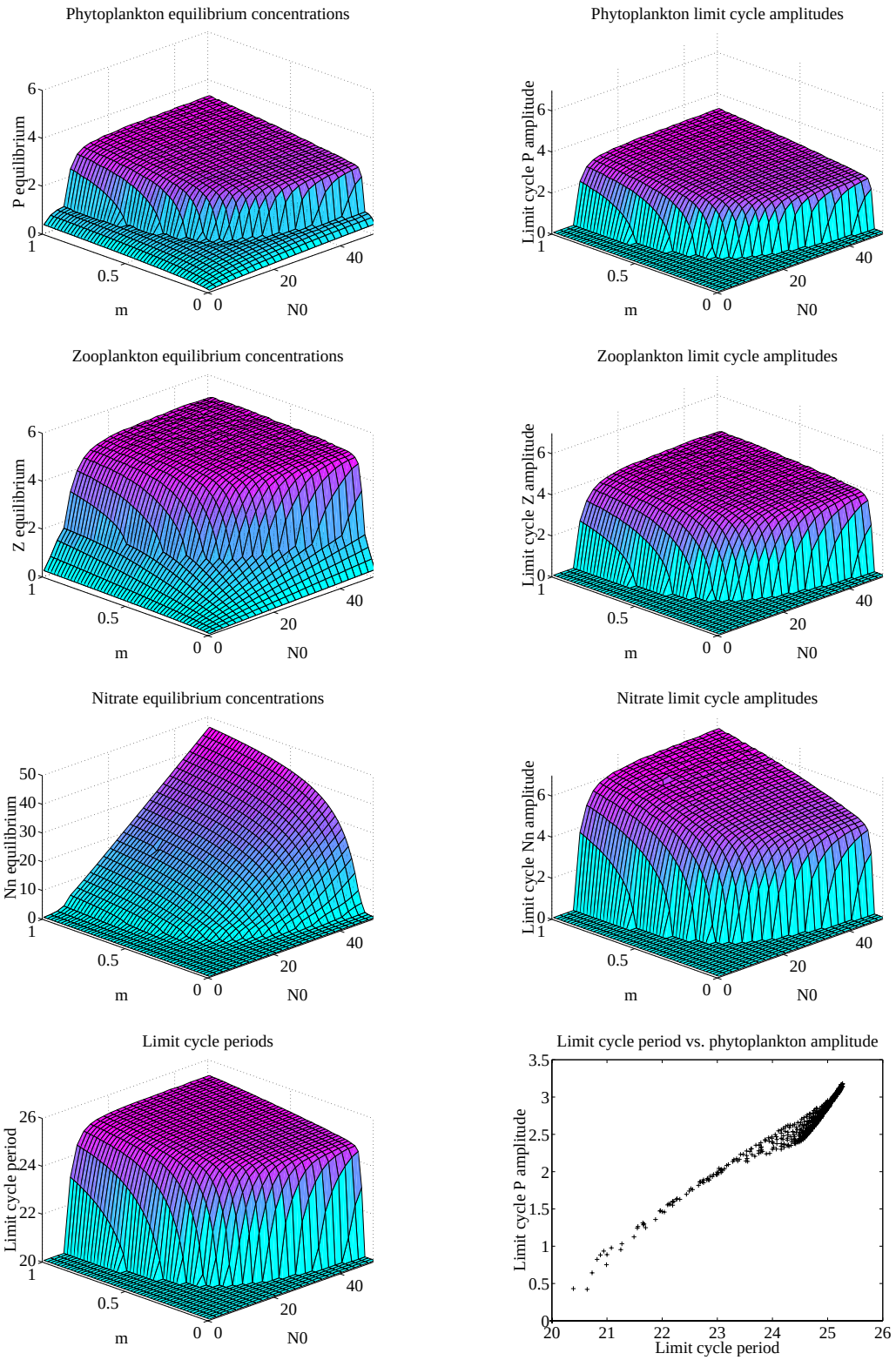

Figure 4.6: The results of numerical solutions performed at Bermuda Station "S" on day 165 across a range of cross–thermocline mixing rates (m) and subthermocline nitrate concentrations (N_0). Mixing rates in m d^{-1}, subthermocline nitrate concentrations in mmol N m^{-3}. Equilibrium concentrations and limit cycle amplitudes in mmol N m^{-3}. Limit cycle periods in days. Note that non–limit cycle regions are assigned periods of 20 days in the bottom two plots for the purposes of graphical presentation.

from OWS "India" are shown. Note that in the case of the plot of limit cycle periods, locations of the parameter space in which only stable equilibria were found are here assigned a period of 20 days for the purposes of clarity.

The pattern of limit cycle behaviour found is quite different from that found under conditions during an OWS "India" summer. The region of limit cycle behaviour is much larger, and although at low m the pattern of occurrence is similar to that at OWS "India", the region of limit cycles does not stop above a certain value of m in the range examined (see also figure 4.7). This is not unexpected since the potential for phytoplankton growth (and thus the growth term of the phytoplankton equation given sufficient nutrient) is much higher at Bermuda Station "S" (*i.e.* higher irradiance, shallower mixed layer, higher maximum phytoplankton growth rate). Furthermore, the minimum values of N_0 at which limit cycles occur are considerably lower than those found at OWS "India". With high m (> 0.60 m d^{-1}), limit cycles are found at subthermocline concentrations of nitrate as low as 9 mmol N m^{-3}. This value is lower than the baseline value used for OWS "India".

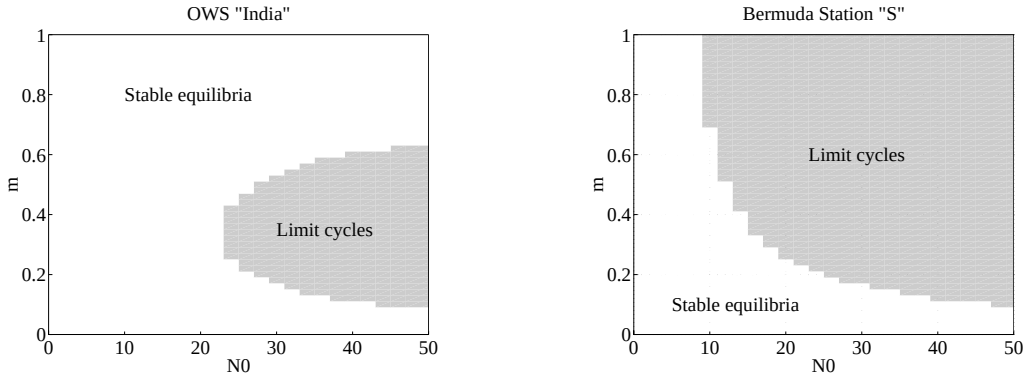

Figure 4.7: Extent of limit cycle regions (shaded grey) for fixed forcing simulations at both stations on days 197 and 165 respectively. OWS "India" baseline values : $m = 0.01$ m d^{-1}, $N_0 = 12$ mmol N m^{-3}. Bermuda Station "S" baseline values : $m = 0.01$ m d^{-1}, $N_0 = 2$ mmol N m^{-3}.

The limit cycles found also differ from those found at OWS "India" in their size and duration. Their amplitudes are up to four times as great and their periods are around 6 to 10 days shorter (ranging from approximately 20.5 to 25.5 days in duration). The pattern of amplitudes reflects the distribution of limit cycles in the parameter space examined, and there is no rise–then–fall of amplitude with increasing m. And unlike OWS "India", where increasing m led to a decrease in the period of the limit cycles found, increasing m here leads to an increase.

These differences are also reflected in the patterns of limit cycle amplitudes against their periods at both stations. While both stations are merely located at different positions in the continuum of multi–parameter space, the differences are quite stark. At OWS "India" the relationship, while positive (*i.e.* limit cycles of longer duration tend to have a larger amplitude), is comparatively loose, with limit cycles

of different periods showing a similar amplitude. The limit cycles at Bermuda Station "S" by contrast show a markedly stronger positive relationship between amplitude and period.

One feature the limit cycle regions at both locations share is their ranking compartments by limit cycle amplitude. In both cases, nitrate amplitudes are greater than zooplankton ones, and zooplankton ones are greater than phytoplankton ones. Commonly in modelled plankton oscillations (*e.g.* Steele & Henderson, 1992; Edwards & Brindley, 1996) the order is instead $N > P > Z$, since transfer inefficiencies at each level bring less to each consumer than they take from the consumed. This is obscured in this model by the multiple prey compartments the zooplankton graze.

As already pointed out, the periods of the oscillatory behaviours found under Bermuda Station "S" conditions were considerably shorter than those found for OWS "India" forcing conditions. The differences between these two situations relate to the irradiance–limitation of phytoplankton growth. At Bermuda Station "S", growth is enhanced by greater irradiance (the station is located at a lower latitude), a shallower mixed layer (phytoplankton growth is integrated across a narrower water column), and a higher maximum specific growth rate for phytoplankton (the station has a higher mixed layer temperature). Since these three factors result in a higher irradiance–limited phytoplankton growth rate, an additional series of numerical solutions across a range of V_p, the maximum specific phytoplankton growth rate, was performed. This aimed to establish that the ranges of limit cycle periodicity observed between the two locations could be bridged by phytoplankton growth rate.

The simulations were performed, as previously, with fixed forcing for OWS "India" during the height of summer (day 197). Baseline values were used for all parameters except m and N_0, which were set to values which produced limit cycle behaviour ($m = 0.30$, $N_0 = 23$). The value of V_p was ranged between 0.1 to 4.0 d^{-1}.

Figure 4.8 shows the limit cycle periods found for the range of V_p across which they were encountered. For the particular forcing and parameter values chosen, no limit cycles were found for values of V_p below 1.2 d^{-1}. Above this value limit cycles were encountered all of the way to the top of the V_p range examined. The period of oscillations found can be seen to fall sharply with faster growth rates. At the OWS "India" baseline value (1.25 d^{-1}), the period is approximately 32.5 days (as was found in the earlier simulations). By the Bermuda Station "S" baseline value (2.9 d^{-1}), the period of the oscillations has fallen to around 27 days, and by the end of the range examined, the oscillation periods have fallen to values below 26 days (these periods are still slightly higher than those recorded during the earlier Bermuda Station "S" results because the irradiance and mixed layer depth conditions are still slightly less favourable at OWS "India" forcing conditions).

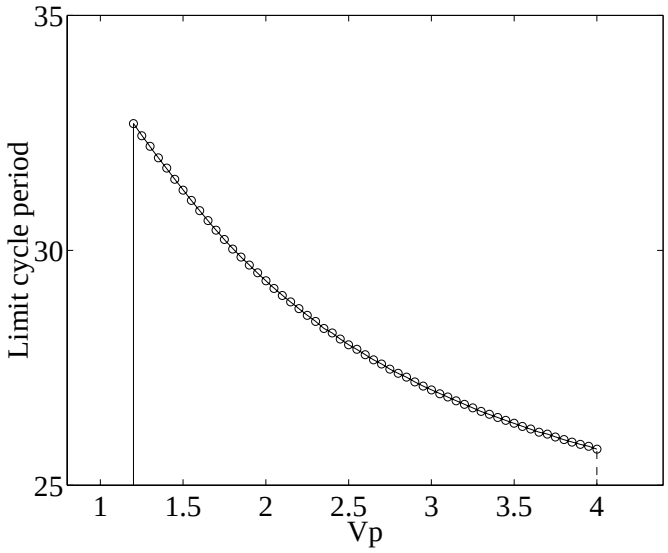

Figure 4.8: Limit cycle period versus phytoplankton maximum growth rate at OWS "India" on day 197. Circles mark values of V_p used. Values of V_p to the left of the solid vertical line did not produce oscillatory behaviour. The dashed vertical line at the right of the plot indicates that values of V_p above this value were not examined (*i.e.* limit cycle behaviour may persist beyond this value). Maximum phytoplankton growth rate in d^{-1}. Limit cycle periods in days.

4.5.3 Conclusions

In this section, limit cycle behaviour was sought across a region of m–N_0 parameter space. While only stable equilibria were found in the area around baseline values of these parameters (both at OWS "India" and Bermuda Station "S"), oscillatory behaviour was found at more extreme values. Although these values were extreme for both stations, they do not fall outside the ranges of both parameters used in the modelling literature. At Bermuda Station "S" for instance, limit cycle behaviour was found in the region $m \geq 0.69$, $N_0 \geq 9.0$. However, such mixing values are still extreme and it is questionable whether the concentration of nitrate just below the seasonal thermocline (here parameterised by the constant N_0) would remain at such a high value in the face of such intense mixing. The resolution of problems such as this one will require the use of more realistic or explicit water column models (*e.g.* the Kraus–Turner turbulent kinetic energy model or the Mellor–Yamada turbulence closure model; see Archer, 1995, for a comprehensive introduction to models of upper ocean physics).

Since both parameters are directly involved in the supply of nitrate to the mixed layer, the occurrence of limit cycles with higher values of both is analogous to a result found by Rosenzweig (1971). His work on simpler ecological models found a "paradox of enrichment", where inputs to an ecological system (in this case, nitrate entrainment) caused instability in the system instead of the naïvely expected increases in productivity.

4.6 Bifurcations in other parameter ranges

In the previous section, the long–term behaviour of the full model was examined across a range of m–N_0 parameter space. While limit cycle behaviour was found within the range of these parameters used within the modelling literature, the values were extreme and questionable (*i.e.* they push at the boundaries of the assumptions made by such a single layer model). Across most of the plausible parameter space, only stable equilibria were found.

As already stated, the variability of certain parameters, like N_0, usually reflects physical or geographical influences. However, as the wide range of parameter values (see table 2.7) indicates, most, if not all, other parameters also exhibit variability in their values. Again, some of this variability may be associated with features of the local physical environment. However, this variability may also be attributed to uncertainties in data collection, lack of data itself, or variability introduced by the biological systems studied (*e.g.* different species compositions will show different composite responses to nutrients or to predators; similar compositions may show different responses where their histories are different; apparently similar compositions may behave differently due to the presence of pathogens which may go undetected).

Therefore, to explore the full model's behaviour across the ranges of parameter variability, a series of runs were performed, one for each parameter. Each parameter was examined over a range which included the maximum and minimum listed in table 2.7. Where groups of parameters shared a common function (*e.g.* half–saturation constants, maximum mortality rates, *et cetera*) they were examined over identical ranges. As previously, the full model was simulated with with fixed forcing (OWS "India", day 197). Runs were initially performed with all parameters, bar the one in question, at their baseline values. They were also performed with a cross–thermocline mixing rate of 0.30 m d^{-1} (a value within the range that was closest to limit cycle activity in previous OWS "India" runs). Both sets produced results which were very similar qualitatively (although unsurprisingly different quantitatively). However, some of the numerical solutions with higher mixing rates also generated plausible limit cycles, so only the results from this latter series are shown and discussed here.

Figures 4.9 to 4.13 show the phytoplankton, zooplankton and nitrate equilibria found across ranges of each of the model parameters. The cloudiness index, C, was excluded because it does not have a continuous range. Figures 4.14 and 4.15 show the equilibria of selected parameters for bacteria and detritus respectively. In the case of most parameters, these two compartments show behaviour qualitatively very similar to the phytoplankton compartment. These latter graphs show the bacterial or detrital equilibria where they differ markedly from those of the phytoplankton compartment.

In each plot shown, a solid line marks a region of stable equilibria across the range of that parameter

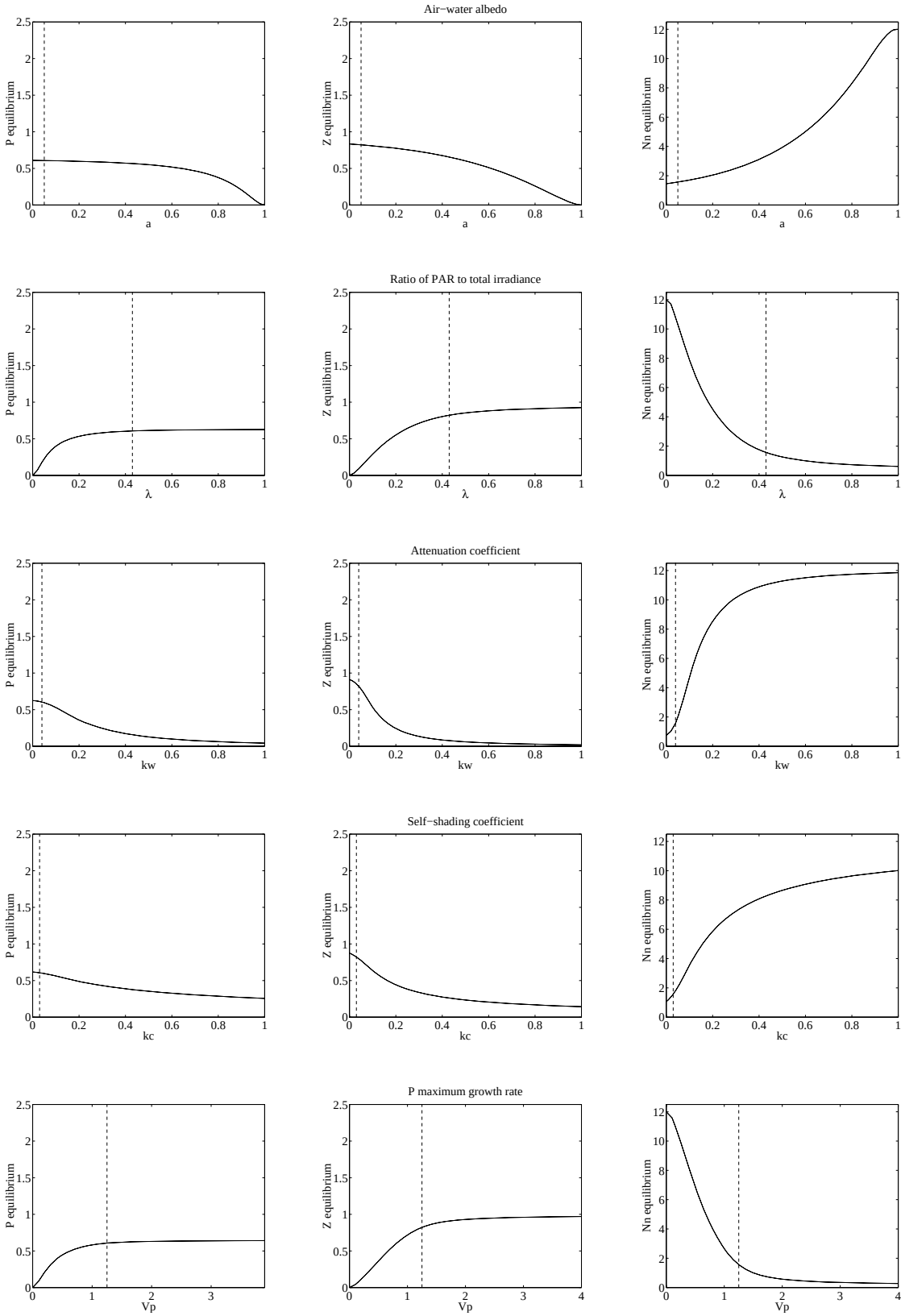

Figure 4.9: Phytoplankton, zooplankton and nitrate equilibria across ranges of parameters a, λ, k_w, k_c and V_p (see text for further details).

value. When dotted lines are shown oscillatory behaviour occurs in the region marked. The extent of the gap between the lines marks the amplitude of the oscillations. A dashed vertical line marks the baseline value of the parameter in question. Note that a constant vertical scale for each compartment is used on each of the plots. The units used on each plot are those listed in table 2.7.

Parameters a (air–water albedo) and λ (PAR fraction) relate to physical constants which are not likely to vary significantly. Both directly affect the amount of irradiance available to phytoplankton. Consequently, increases in the former (more light reflected at the air–sea interface) and decreases in the latter (incoming irradiance shifted to less photosynthetically active parts of the electromagnetic spectrum) both lead to decreased phytoplankton concentrations, and consequently lower zooplankton concentrations and higher nitrate concentrations. Shifts in the reverse direction produce the reverse effects. In both cases, the baseline values of the parameters place the phytoplankton equilibria in relatively flat plateau regions.

The attenuation coefficient, k_w, controls the absorption and reflection of light as it descends the water column. Similarly to a, increases in k_w decrease the amount of irradiance available to phytoplankton. However, as can be clearly seen on the plot, over the literature range of k_w ($0.03 \rightarrow 0.20$ m^{-1}), the equilibria shift much more sharply. Since k_w can, in principle, be influenced by biological activity[2] (*e.g.* by the coccoliths of prymnesiophyte algae), this is a significant parameter.

The self–shading coefficient, k_c, acts similarly to k_w but its effects on downwelling irradiance are dependent on the concentration of phytoplankton. For the equilibrium concentrations of phytoplankton found, the effects of increasing or decreasing its value are very similar to those of k_w but slightly less severe. The reported range for the parameter ($0.03 \rightarrow 0.12$ m^2 (mmol N)$^{-1}$) is also narrower.

The effects of varying the maximum phytoplankton growth rate, V_p are very similar to those with λ. Decreasing the value lowers both phytoplankton and zooplankton equilibria, but raises those of nitrate. Increases only slightly produce the reverse effects. Also similarly to λ, the baseline value of V_p at OWS "India" puts the equilibrium near the summit of a plateau. Although earlier work explored oscillatory behaviour across a range of V_p, there was no evidence of such behaviour here.

The initial slope of the photosynthesis–irradiance (P–I) curve, α, again produces very similar curves of equilibria to V_p and λ. Also again, while decreases in its value decrease the phytoplankton and zooplankton equilibria and increase the nitrate equilibria, increases in its value only slightly reverse these trends, since the baseline value again places the baseline equilibria near the summit of a plateau.

The fraction of phytoplankton photosynthate which is used for growth is controlled by the exudation

[2]The distinction between the ostensibly abiotic k_w, and the biotic k_c, is blurred when non–living or formerly–living organic material is considered. Garver *et al.* (1994) draw attention to the significant role of such material in submarine absorption of radiation.

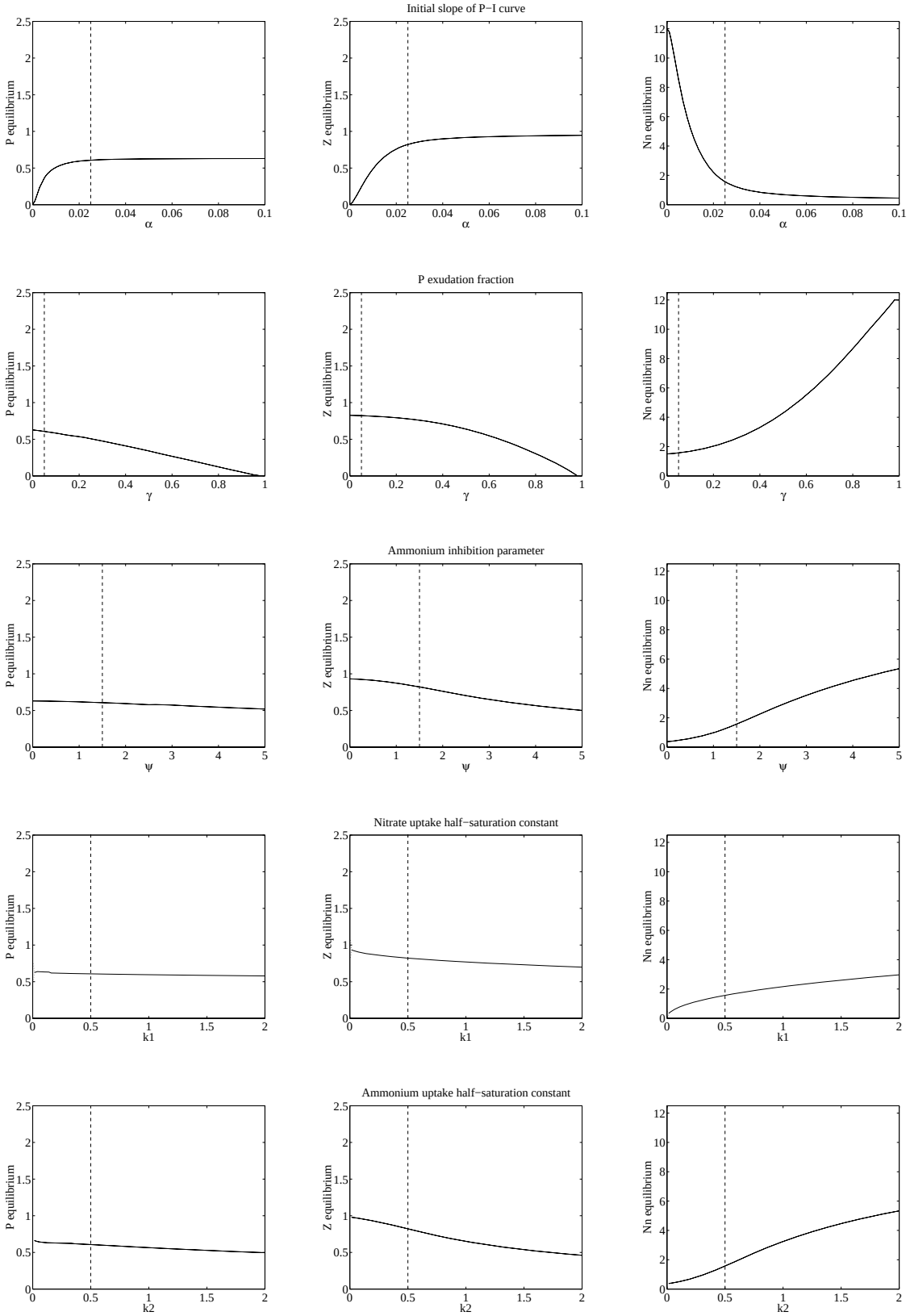

Figure 4.10: Phytoplankton, zooplankton and nitrate equilibria for parameters α, γ, ψ, k_1 and k_2.

fraction parameter, γ. Increases in its value lead to an almost linear decline in phytoplankton equilibria. At a value of 1, the phytoplankton are incapable of growth and their population entirely extinguished. The zooplankton equilibria, while decreasing with rising γ, do so at a lower rate since bacterial equilibria rise with increasing γ (exudation produces DON, a growth substrate for bacteria in the model). Although the fractions used in the modelling literature only range up to 0.15, field estimates range up to 0.70 (Moloney & Field, 1991).

No directly comparable literature estimates were found for the ammonium inhibition parameter, ψ, so an arbitrary range was chosen to examine it over. Although the phytoplankton equilibria fell only slightly as ammonium became more inhibiting, the zooplankton concentration almost halved, and the nitrate concentration rose more than five–fold. However, since no range was known for this parameter, the significance of these results is unclear.

Unexpectedly, the phytoplankton half–saturation constant for nitrate uptake, k_1, produced a series of limit cycles at the extreme low end of the range of values examined. As k_1 was reduced from 0.015 to 0.001 mmol N m^{-3}, a series of limit cycles (all with a period between 30 and 31 days; see Figure 4.16) were found. They were unexpected since the reduction of k_1 from its baseline value towards the literature minimum actually reduced the equilibrium concentrations of nitrate. The values at which the limit cycles occur are not as low as that used by Moloney & Field (1991) for their smallest phytoplankton class (which are actually bacterioplankton), but they do fall at the low end of the range found by Harrison, Harris & Irwin (1996) during their survey in the North Atlantic open ocean.

While the behaviours of the stable equilibria across the range of the ammonium half–saturation constant, k_2, are somewhat similar to those across the range of its sister parameter k_1, no limit cycle behaviour was found. Across the literature range of k_2 ($0.01 \rightarrow 0.5$ mmol N m^{-3}), the phytoplankton and zooplankton equilibria rise only slightly, but the nitrate equilibria more than halve. The shape of the latter curve of equilibria within this range is different from that of parameter k_1. That parameter traces a hyperbolic curve, tending towards zero nitrate concentration, while the equilibria produced by k_2 trace a sigmoid shape, tending toward a positive non–zero equilibrium at $k_2 = 0$.

The half–saturation constant of zooplankton grazing, k_3, traces an interestingly non–linear series of equilibria. Below its baseline value (also the lowest value obtained from the literature), both phytoplankton and zooplankton concentrations rise with increasing k_3 (and decreasing grazing ability on the part of the zooplankton). This is matched by a sharp decrease in the equilibrium concentrations of nitrate. However, almost straight after the baseline value, the zooplankton equilibrium concentrations cease rising and begin to fall as the zooplankton grazing abilities continue to decline. The phytoplankton equilibria continue to rise, and the nitrate equilibria to fall however.

The effect on the phytoplankton, zooplankton and nitrate equilibria across the range of bacterial uptake

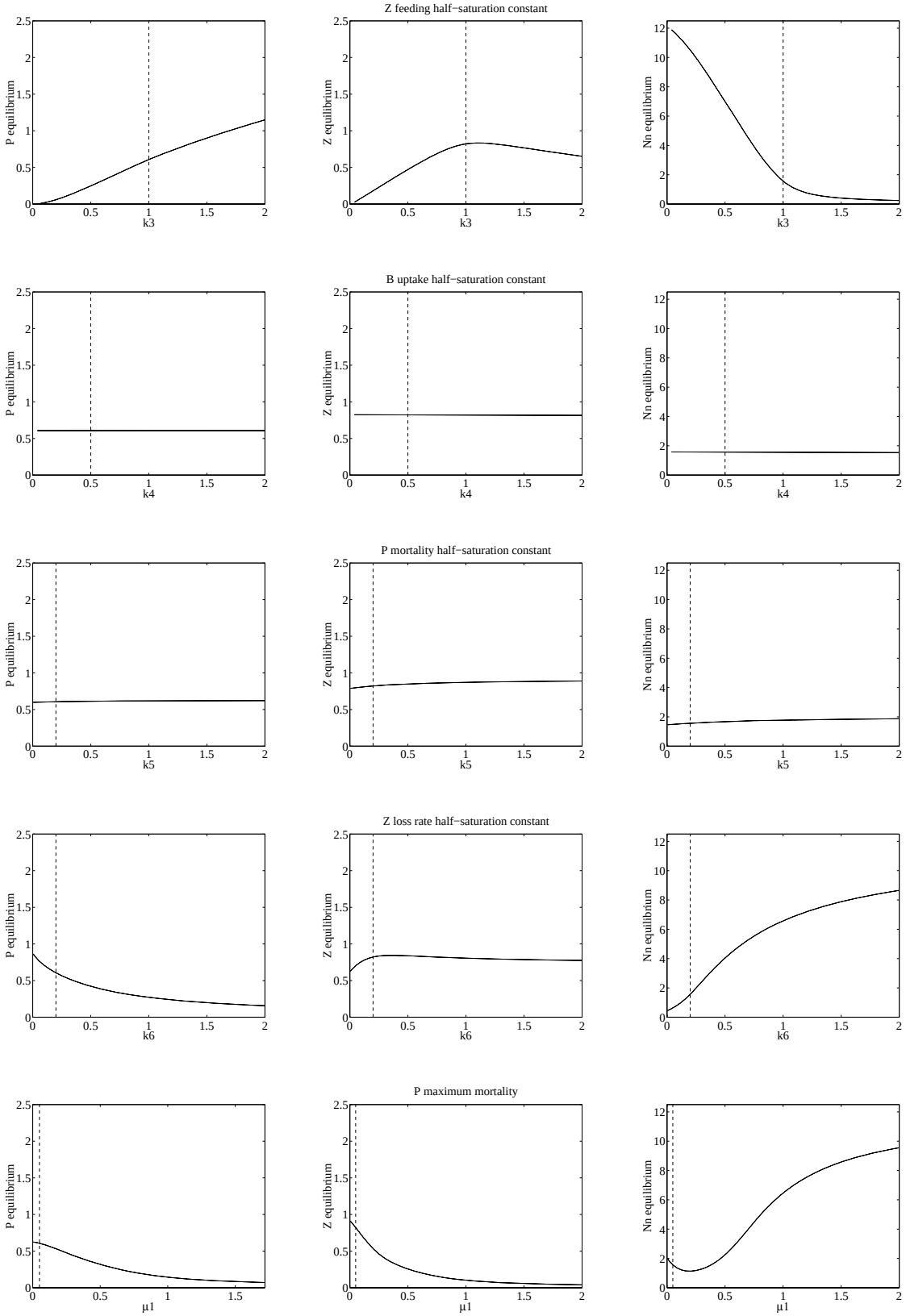

Figure 4.11: Phytoplankton, zooplankton and nitrate equilibria for parameters k_3, k_4, k_5, k_6 and μ_1.

half–saturation constant, k_4, examined was found to be almost negligible. Perhaps surprisingly, the same was found also for the bacterial equilibria. Over the range examined, the bacterial equilibria changed by less than 2%.

The half–saturation constant of phytoplankton mortality, k_5, produced a similarly invariable series of equilibria across the range examined.

By contrast, its zooplankton equivalent, k_6, was found to influence equilibria much more strongly across its range ($0.2 \rightarrow 5.03$ mmol N m^{-3}; the range shown is truncated to match those of the other half–saturation constants). The largest changes in the equilibria were additionally found around the baseline value used by Fasham (1993). The nitrate equilibria were found to be particularly dependent on k_6.

The phytoplankton natural mortality parameter, μ_1, behaved similarly to several other parameters (*e.g.* k_w, k_c). Although a phytoplankton parameter, across its literature range, μ_1 most affected zooplankton and nitrate equilibria. Unexpectedly, the nitrate equilibria initially fell with increasing phytoplankton mortality before rising, as would be expected from reduced phytoplankton concentrations. This anomaly coincides with the rise in the detrital equilibria in the same region of μ_1 space (phytoplankton natural mortality produces detrital material), and may be an effect of shifting zooplankton food preferences (*i.e.* preference for detritus increases, leading to an easing of the grazing pressure on phytoplankton and a resultant increase in nitrate uptake).

Varying the zooplankton maximum mortality rate, μ_2, produced effects on the equilibria found which were similar (but much more extreme) to those produced by the zooplankton parameter k_3. Increasing μ_2 from its literature minimum produced a sharp sigmoidal trend in the phytoplankton equilibria, and an even sharper decline in the nitrate equilibria. Below its baseline value, the zooplankton equilibria rose with the increasing phytoplankton (despite the increasing predation). However, at a value of 0.30 d^{-1}, this trend abruptly changed, with the equilibria falling, most sharply at values close to the baseline. Of the other state variables, both the bacteria and detritus equilibria increase with μ_2 at low values, but both plateau (and the bacteria equilibria actually fall away) above certain values. In the case of bacteria, this decline is caused by a reduction in the availability of ammonium (which they utilise as a growth substrate), which itself is caused by a reduction in the zooplankton equilibrium biomass. In the case of detritus, its major inputs normally come from the feeding inefficiency of zooplankton, and as zooplankton equilibrium populations fall, so do these inputs (however, this is partially offset by a similarly falling grazing pressure on detritus). The significance of this parameter is further examined in a later section of this chapter.

Unlike the two previous "mortality" rates, μ_3 and μ_4 (respectively the bacterial excretion and detrital breakdown rates) are in functional forms which make them constant rates (μ_1 and μ_2 are in hyperbolic forms). Both also share the occurrence of limit cycle behaviour (in a later section in which μ_2 is used in

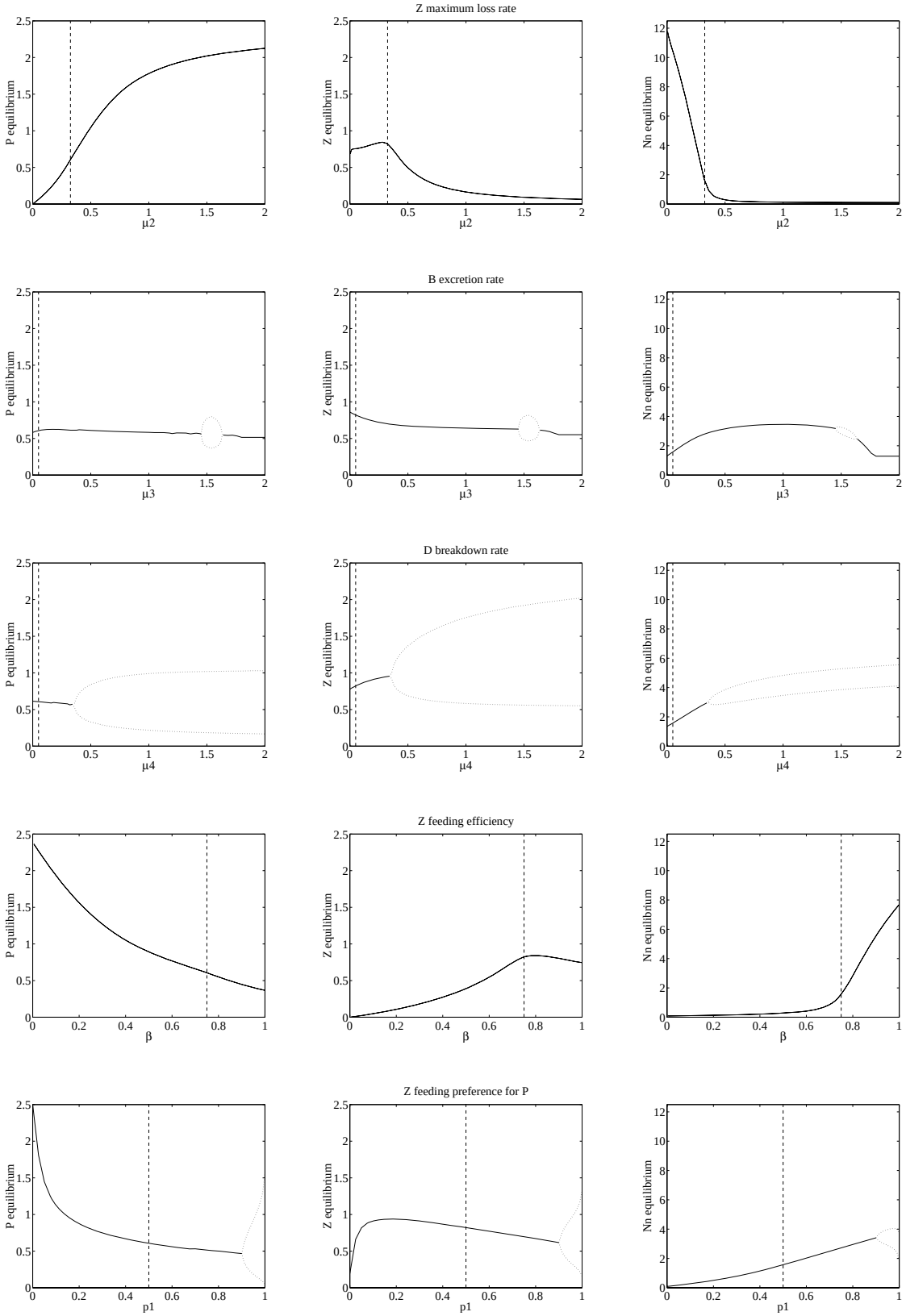

Figure 4.12: Phytoplankton, zooplankton and nitrate equilibria for parameters μ_2, μ_3, μ_4, β and p_1.

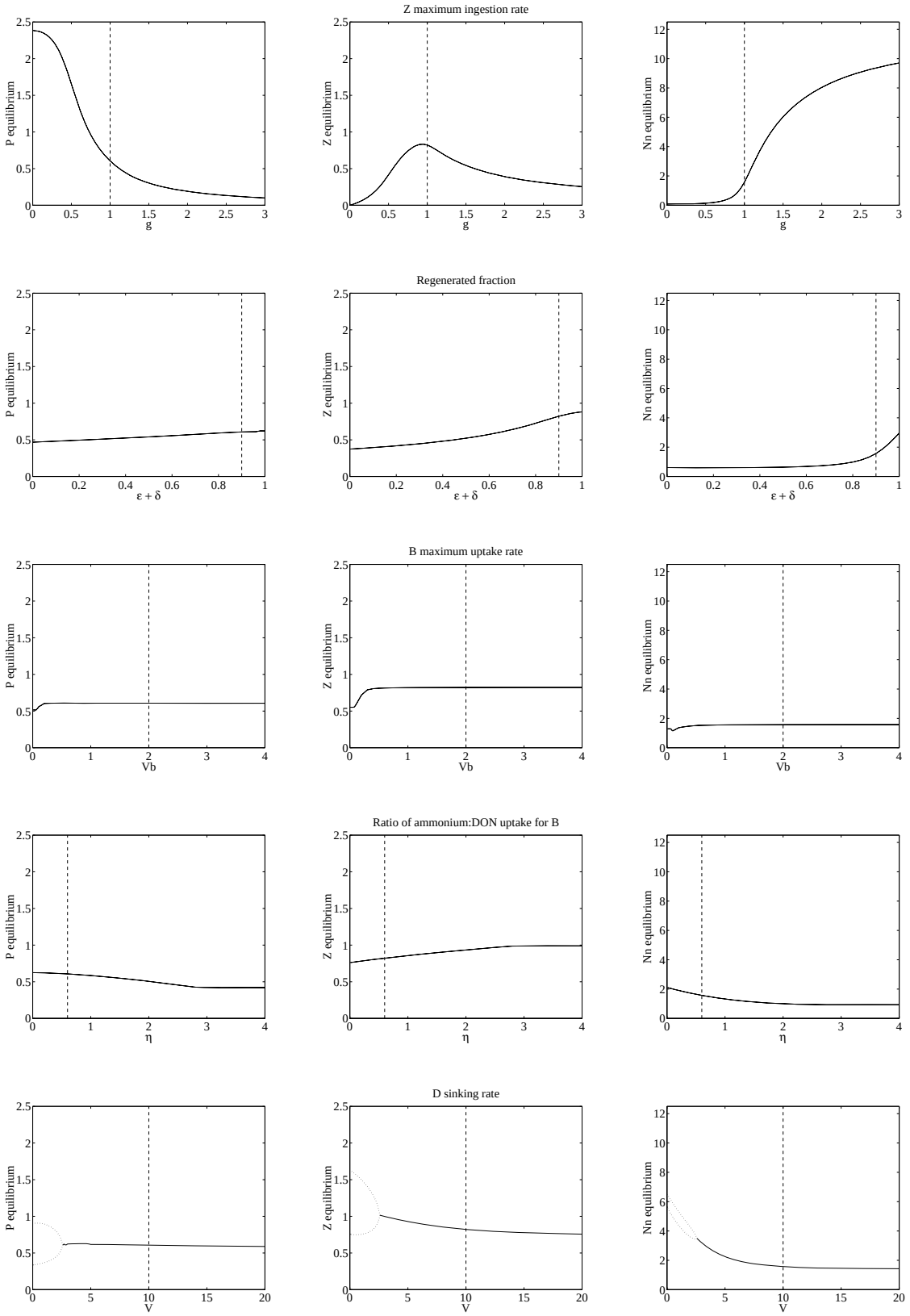

Figure 4.13: Phytoplankton, zooplankton and nitrate equilibria for parameters g, $(\epsilon + \delta)$, V_b, η and V.

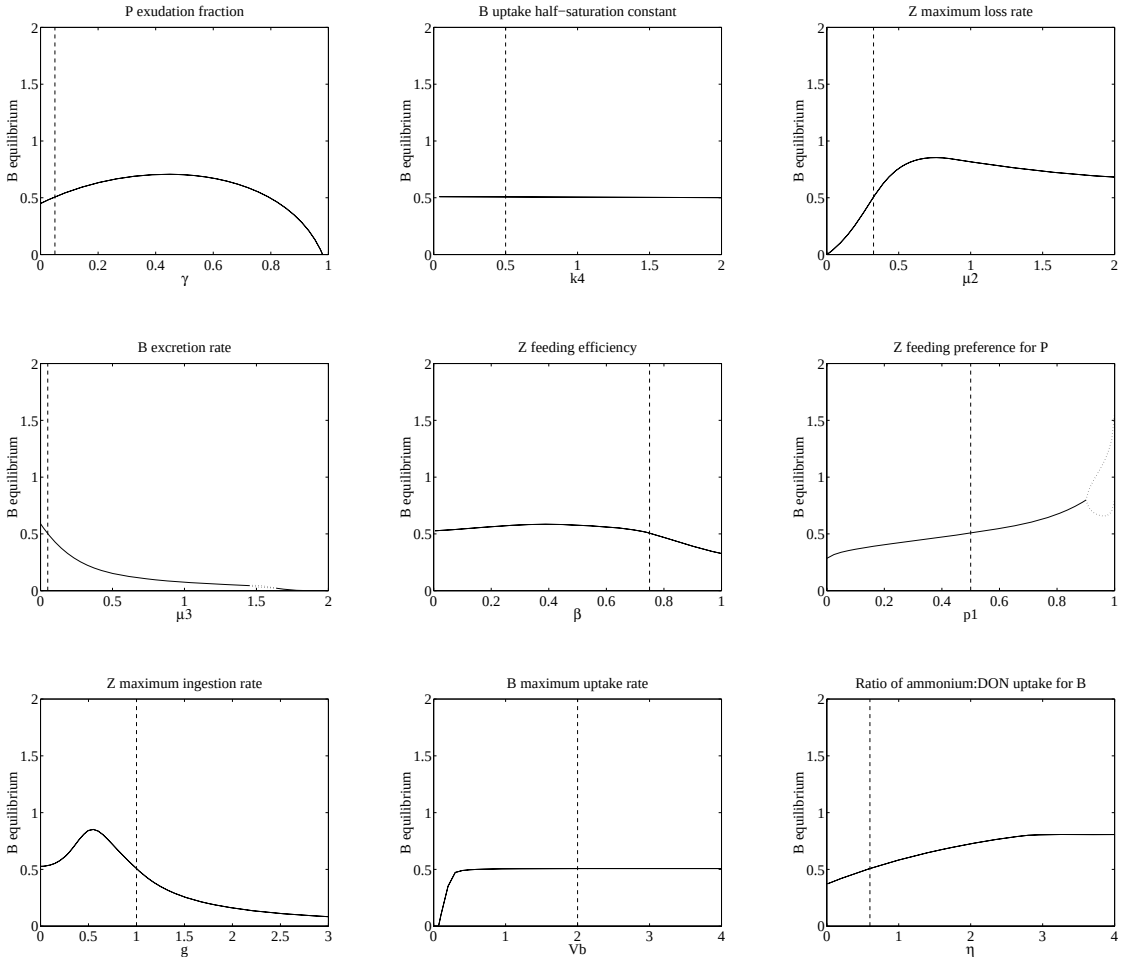

Figure 4.14: Bacterial equilibria for selected parameters.

a similar constant form, the model is also able to exhibit such behaviour). In the case of μ_3, oscillatory behaviour only occurs over a small region of parameter space, already at very high values outside that of the literature range. The oscillations found have a period of around 28 days (see Figure 4.16), and occur across a stretch of parameter space ($1.46 \leq \mu_3 \geq 1.63$) just before the bacterial population goes extinct ($\mu_3 \geq 1.80$). Their extinction can be seen in the equilibria of phytoplankton, zooplankton and nitrate, where they all abruptly become constant. Across the region of parameter space used in the literature, the phytoplankton equilibria mostly decrease slightly. The zooplankton equilibria also decrease with rising μ_3 (bacteria being one of their prey). The nitrate equilibria rise relatively significantly, due both to decreasing phytoplankton (more zooplankton attention), and also to increasing ammonium (which the bacteria excrete).

In contrast with μ_3, oscillatory behaviour is found across a much wider range of μ_4. The limit cycles found occupy almost the whole region of parameter space examined ($\mu_4 \geq 0.36\ \mathrm{d}^{-1}$) and exhibit periods ranging from 34.5 days up to almost 38.5 days. However, although this behaviour begins at a relatively low value, Fasham, Ducklow & McKelvie (1990; citing Jones & Henderson, 1986) report a maximum for

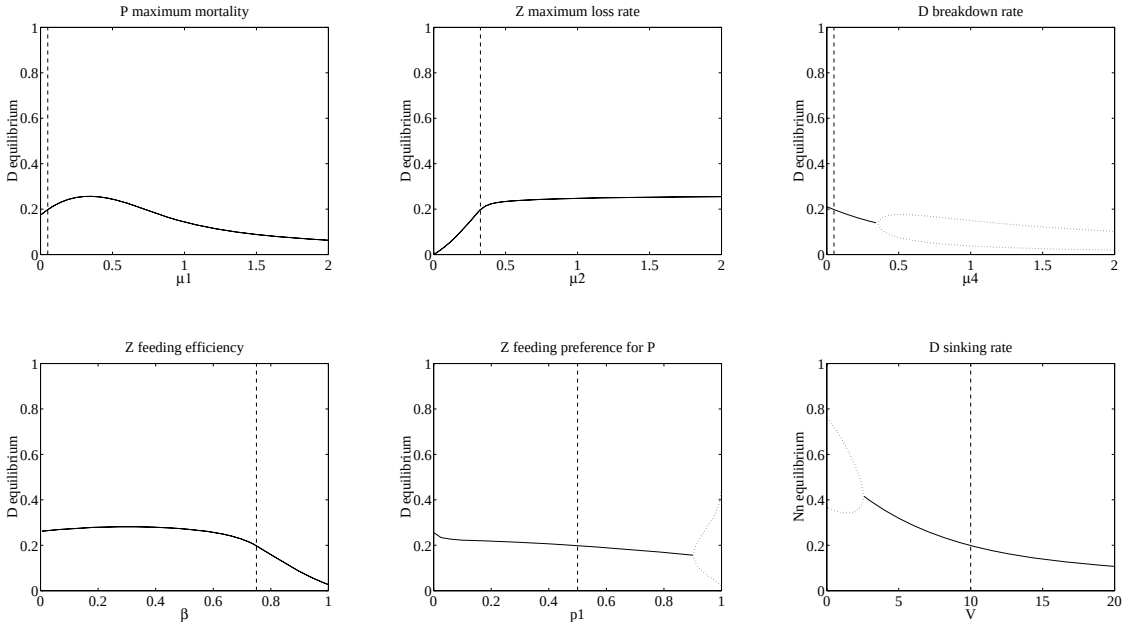

Figure 4.15: Detritus equilibria for selected parameters.

μ_4 of 0.18 d^{-1}.

The zooplankton assimilation efficiency parameter, β, produces a number of unexpected results. The phytoplankton and nitrate equilibria behave as one might expect across the full range from total inefficiency ($\beta = 0$) to total efficiency ($\beta = 1$). At low efficiency, the phytoplankton equilibria are very high, and the nitrate equilibria very low. Increasing efficiency reverses this position. The other two prey compartments, bacteria and detritus, both have their maximum equilibrium points lying inside this range. The zooplankton equilibria, unsurprisingly, rise with increasing efficiency. However, the maximum equilibrium falls before total efficiency ($\beta = 0.80$), very close in fact to the baseline value.

Similarly, the zooplankton feeding preference for phytoplankton, p_1 (p_2 and p_3 are automatically set to values of $(1 - p_1)/2$), produces some unexpected results. Although, of the three zooplankton prey species, phytoplankton normally occur at the highest density, the zooplankton reach their stable equilibrium maximum at a relatively low value ($p_1 = 0.17$). Also, despite sharing a common response to increasing p_1 (*i.e.* being preferred by zooplankton less), the bacteria and detritus equilibria show equilibrium trends in opposite directions. As p_1 increases, the bacteria equilibria rise, while those of the detritus compartment fall. Additionally, at high values of preference for phytoplankton ($p_1 \geq 0.91$), limit cycle behaviour is encountered. Both the amplitude and period of this behaviour increase with p_1. The heterogeneity of the organisms which make up the zooplankton compartment makes choosing a value for p_1 difficult, and consequently the parameter was used originally to fine–tune the behaviour of the full model (Fasham, Ducklow & McKelvie, 1990). As such, it is possible that the oscillatory behaviour encountered may occur at reasonable values for this parameter.

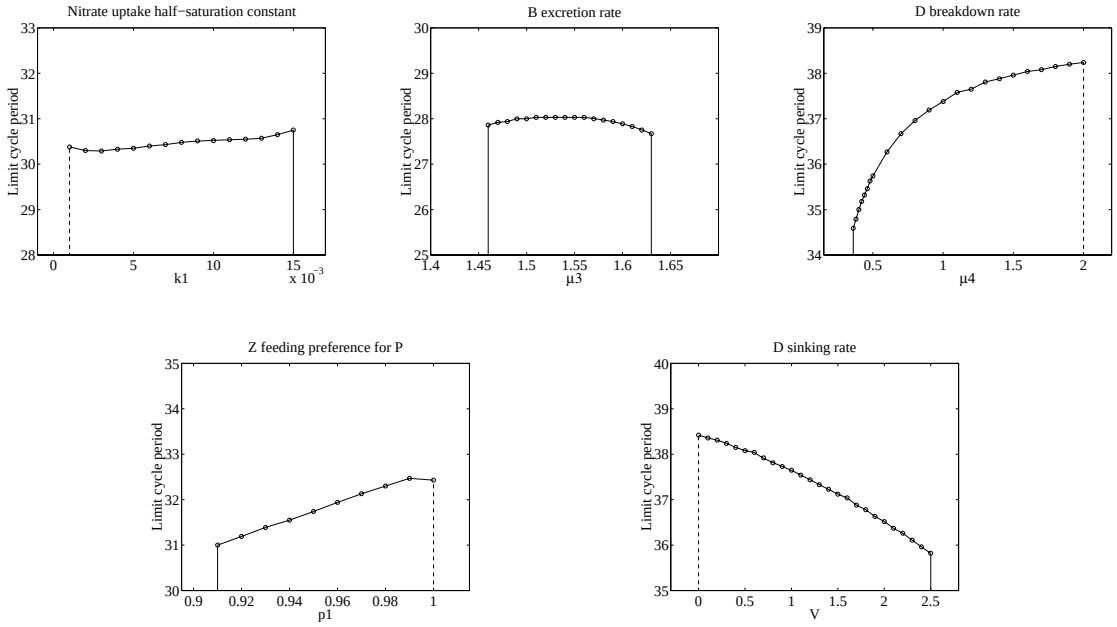

Figure 4.16: Variation in limit cycle period with parameter value for parameters k_1, μ_3, μ_4, p_1 and V. Circles mark parameter values where numerical solutions were obtained. Solid vertical lines mark values above or below which runs were performed but only stable equilibria found. Dashed vertical lines mark values beyond which runs were not performed. Limit cycle activity may still occur beyond these values however. Note that on each plot the vertical scale covers a 5 day range.

The behaviour of the stable equilibria across the examined range of zooplankton maximum ingestion rate, g, is similar to that produced by β. At low values, the phytoplankton equilibria are high, while the nitrate equilibria are low. As g increases, the phytoplankton equilibria fall and the nitrate equilibria rise. Again the zooplankton equilibria reach a maximum at an intermediate value across the range, and again that value almost coincides with the baseline value chosen by Fasham (1993). The bacteria equilibria also reach a maximum at an intermediate value ($g = 0.55$).

Regeneration of zooplankton losses is governed by two terms, ϵ and δ, which respectively are the ratios of the losses returned as ammonium and as DON. In the examination of them here, they were kept at a constant ratio to one another (ϵ:δ of 3.5) and the value of their sum was ranged from total loss from the mixed layer ($\epsilon + \delta = 0$) to total regeneration in the mixed layer ($\epsilon + \delta = 1$). Models in the literature use values across the full range examined here. The stable equilibria of all 7 state variables rose with increasing regeneration, but the magnitude of the change in equilibria differed between state variables (the ammonium equilibria increased more than 60–fold across the range, whereas the DON equilibria only managed to double).

Similarly to its partnered half–saturation constant, k_4, the maximum uptake rate of bacteria, V_b, was

found to produce only very slight changes in stable equilibria of all of the state variables across its literature range. At low values ($V_b \leq 0.20$ d^{-1}; below the literature minimum), the stable equilibria of the bacteria fell significantly (with similar decreases in most other state variables, although DON equilibria increased markedly), and below 0.06 d^{-1} the bacteria compartment went extinct. However, across the majority of its range examined (and the entire region encompassed by the literature) V_b produced almost no change in the values of the model state variables.

Unlike several other bacteria parameters, the ammonium:DON uptake ratio, η, changed stable equilibria across the range examined. As its value was increased (and the bacteria were able to uptake more ammonium per unit DON), the bacteria stable equilibria rose, at the expense of the phytoplankton stable equilibria which fell as more of the available ammonium was utilised by bacteria. The increasing bacteria populations supported a greater zooplankton population, with their stable equilibria also rising. However, above $\eta = 3.2$, no further rises in the bacteria equilibria occurred and the equilibria of all of the state variables remained constant. Unfortunately, no estimates for this parameter were found (Fasham, Ducklow & McKelvie, 1990, examined the parameter at values double and a half that of the baseline), so the significance of these results is unclear.

Examination of a range of the parameter μ_4 found that oscillatory behaviour occurred as the rate of detrital breakdown rose (and the value of the detrital stable equilibria fell). By contrast, when a range of detrital sinking velocities, V, was examined, oscillatory behaviour was found to occur as the rate decreased (and detrital stable equilibria rose). For values ≤ 2.5 m d^{-1}, limit cycle behaviour was found. These cycles were found to increase in period as the rate of sinking was slowed. The range over which the cycles occurred overlapped with the literature range, and fell close to that estimated by Fasham (1993) from measurements of the sinking flux. While the stable equilibria of all the other state variables rose with decreasing V, the equilibria of the phytoplankton population were found to remain fairly constant until oscillatory behaviour occurred.

4.6.1 Conclusions

This section aimed to uncover bifurcations in the ranges of other parameters, and to determine whether any oscillatory behaviour so produced occurred within the parameter ranges reported in the literature.

Five of the parameters examined were found to produce oscillatory behaviour in the ranges across which they were examined. These were the nitrate uptake half–saturation constant (k_1), the bacterial excretion rate (μ_3), the detrital breakdown rate (μ_4), the zooplankton preference for phytoplankton (p_1) and the detrital sinking velocity (V). The region of oscillatory behaviour of k_1, while not outside the literature range, was at the low extreme of values reported (Harrison, Harris & Irwin, 1996). Both μ_3 and μ_4 were found to only produce limit cycles in regions outside those reported in the literature (in the case of μ_4, this region was only slightly beyond that reported). The parameter p_1 affects the feeding preferences of the zooplankton for their three food species. Since most other plankton models do not include multiple

prey for their zooplankton, and since the formulation of the zooplankton compartment in Fasham (1993) attempts to mimic the behaviour of a changing zooplankton species composition (rather than emulate a particular zooplankton species), it is difficult for either the modelling or experimental literature to provide a reasonable range for p_1. So although oscillatory behaviour occurs, it is unclear whether it does so at plausible values. However, the range of detrital sinking velocities examined contains a region of limit cycle behaviour within that of the modelling literature, and within that estimated by Fasham (1993) from a regression of total particulate material and total sinking flux.

Note that in this work, only one dimensional transects through parameter space have been used to look for limit cycle behaviour. Using a bifurcational region of the zooplankton mortality parameter (d), Edwards & Brindley (1996) examined the movement of this region as each of the other model parameters was moved across a range from the literature. This effectively examined two dimensional planes of parameter space for the bifurcation in question. Ideally any searches for qualitative changes in model behaviour would occur across the full parameter space. However, for models with as many parameters as these models this is utterly impractical. The Hopf bifurcations found with the five parameters here are only those found for baseline values of the other parameters. At different parameters values, other model parameters will contain Hopf bifurcations within their literature range.

Aside from the oscillatory behaviour found, several other interesting points arose from observations of the equilibria detected. Curiously, the baseline values of four of the six zooplankton parameters (k_3, μ_2, β and g) all fell very close to the values which produced the highest zooplankton stable equilibria for those parameters. Another unexpected result came with the insensitivity of the equilibria of all the model compartments to the bacterial growth parameters, k_4 and V_b. In both cases, the equilibria found, even for the bacteria themselves, varied only slightly across parameter ranges examined. This is surprising because bacterial production (growth) constitutes a major ecological flow (see the results in Chapter 3).

4.7 Effects of a reduced detrital sinking rate

The previous section established that, in addition to m and N_0, five other model parameters produced limit cycles while baseline values of the other parameters were used (except m, which was set to 0.30 m d^{-1}). Of these, only really the detrital sinking velocity, V, produced limit cycles well within its literature range (and within the range used by both Fasham, Ducklow & McKelvie, 1990, and Fasham, 1993, for "fine–tuning"). Since the original exploration of m–N_0 parameter space found limit cycles at only the extremes of the reasonable range for those parameters, another exploration of m–N_0 space was undertaken to establish the effect of a reduced detrital sinking velocity on the region of limit cycles.

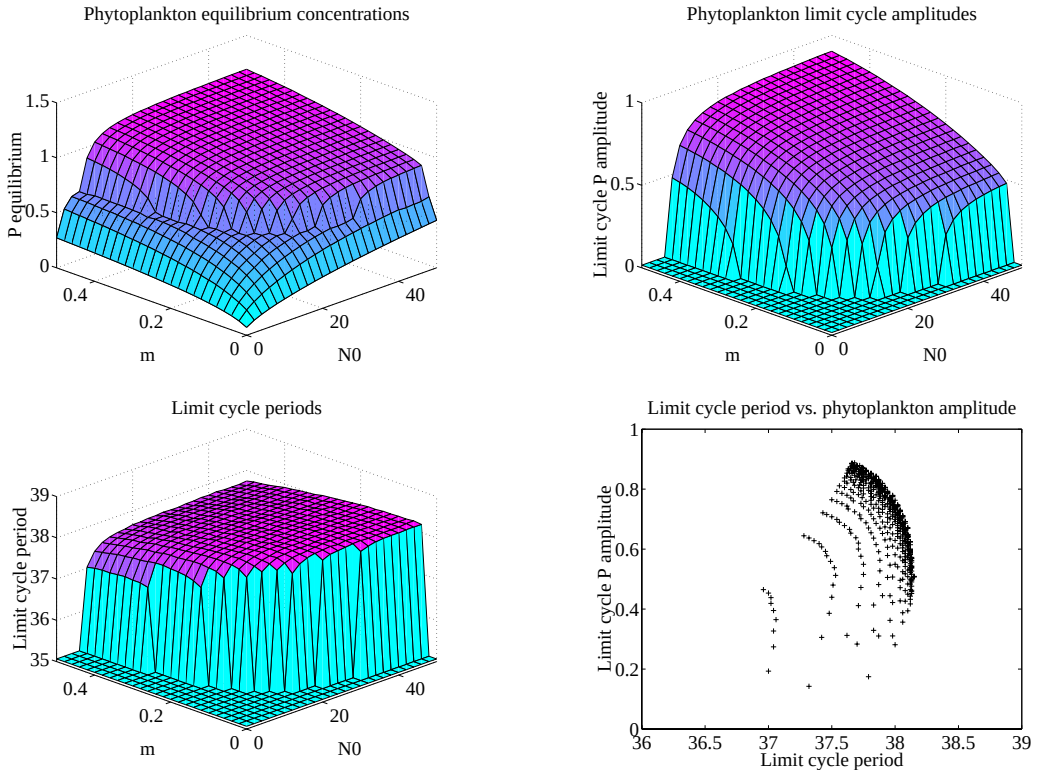

Figure 4.17: The numerical solutions produced from runs performed at OWS "India" on day 197 across a range of cross–thermocline mixing rates (m) and subthermocline nitrate concentrations (N_0). Detrital sinking velocity set to 1 m d^{-1}. Mixing rates in m d^{-1}, subthermocline nitrate concentrations in mmol N m^{-3}. Equilibrium concentrations and limit cycle amplitudes in mmol N m^{-3}. Limit cycle periods in days.

For this analysis, m–N_0 space was explored with all the other model parameters at their baseline values except for V, which was set to 1 m d^{-1} (the low value used by Fasham, 1993; the baseline value is 10 m d^{-1}). Model runs were performed again with OWS "India" forcing from day 197, and Bermuda Station "S" forcing from day 165.

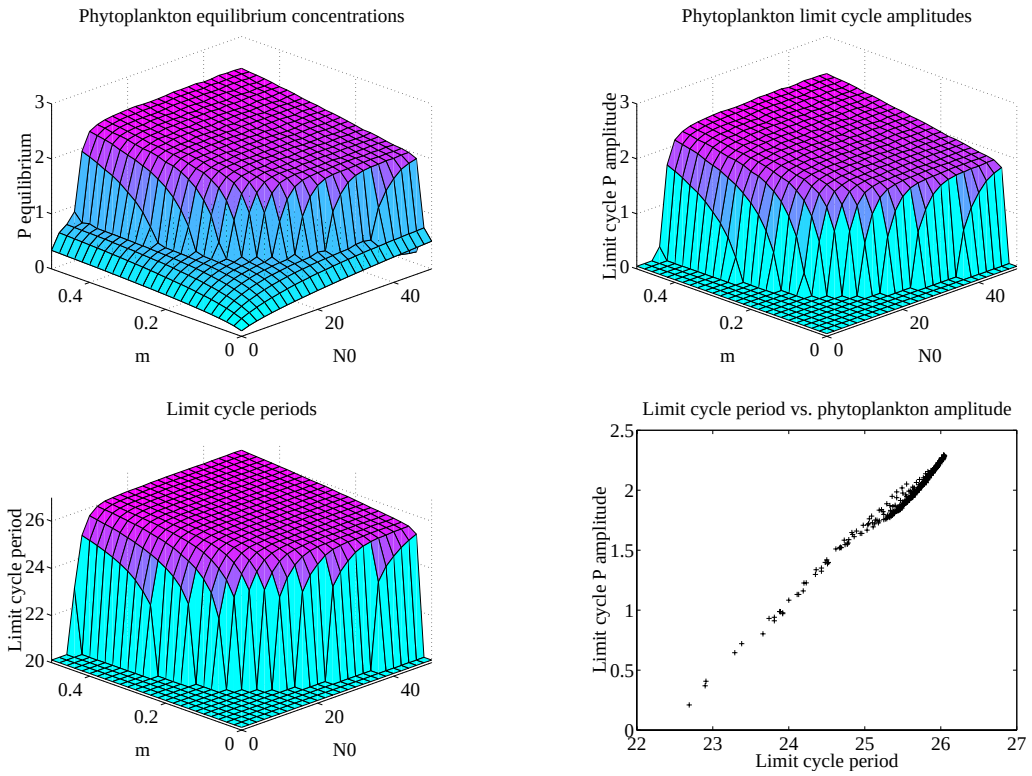

Figure 4.18: The numerical solutions produced from runs performed at Bermuda Station "S" on day 165 across a range of cross–thermocline mixing rates (m) and subthermocline nitrate concentrations (N_0). Detrital sinking velocity set to 1 m d^{-1}. Mixing rates in m d^{-1}, subthermocline nitrate concentrations in mmol N m^{-3}. Equilibrium concentrations and limit cycle amplitudes in mmol N m^{-3}. Limit cycle periods in days.

Figures 4.17 and 4.18 show the results obtained from the OWS "India" and Bermuda Station "S" runs respectively. Since, in both cases, the zooplankton and nitrate results followed the phytoplankton ones in the same manner as before, only the equilibria and amplitudes from the phytoplankton compartment are shown. The limit cycle periods, and the relationships between limit cycle period and phytoplankton amplitude are also shown. Note that the range of m across which results are shown is half that of the previous graphs (the range of m was explored up to values of 1.01 m d^{-1}).

The results from both stations show a marked increase in the size of the region across which limit cycles were found. At OWS "India", at mixing rates as low as 0.25 m d^{-1}, limit cycle behaviour was found at values of $N_0 \leq$ its baseline value. At Bermuda Station "S", limit cycles were still not found at its baseline N_0 value, but they found over an increased region (although not as increased as that at OWS "India"). While previously limit cycles could only be found with mixing rates of 0.09 m d^{-1}, with the reduced detrital sinking velocity, they could be found at values as low as 0.05 m d^{-1} (see also figure 4.19).

Similarly to the solutions found at OWS "India" for higher V, the amplitudes of the cycles increase here with m at first, then fall off after reaching a certain value ($\simeq$ 0.64 m d^{-1}; by which time the maximum

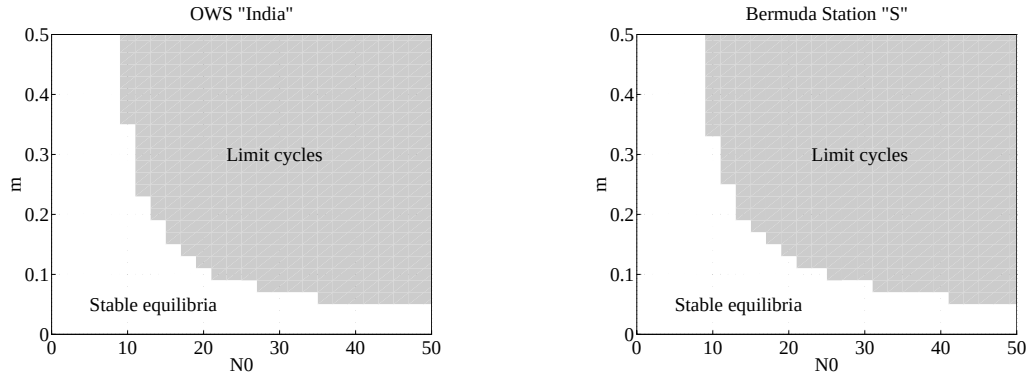

Figure 4.19: Extent of limit cycle regions (shaded grey) for fixed forcing runs at both stations on days 196 and 165 respectively.

amplitudes found are almost double those found for higher V). However, across the range of m examined, limit cycle behaviour did not cease as it had previously with increasing m. Also in common with those earlier solutions, the period of the cycles was found to mostly decrease with rising m. Noticeably, all of the cycles found here are of longer period (the lowest found here was just below 36 days, while the highest found at higher V was below 34 days) than those found in at higher V.

Bermuda Station "S" results show similar patterns of period and amplitude across m–N_0 space as those found previously. Both increase with m and produce a similar, almost linear, relationship with one another across m–N_0 space. In comparison with the earlier work at higher V, the range of periods found (like that at OWS "India") is shifted upwards to longer periods. However, the ranges of limit cycles period found at both values of V mostly overlap (unlike that at OWS "India").

Overall, both sets of results increase the range of m and N_0 over which limit cycle behaviour is found. More importantly, at least for OWS "India", a reduced detrital sinking velocity brings limit cycle behaviour inside a more reasonable range of m and N_0. This makes the possibility that modelled limit cycles may indeed be features which could be searched for in real world data more likely.

4.8 Seasonal forcing

Earlier sections have shown that stable limit cycle behaviour can occur across regions of parameter space for the summer forcing conditions found at OWS "India" and Bermuda Station "S". Although no limit cycles were found at Bermuda Station "S" within a reasonable range of N_0, at OWS "India" (with manipulation of the parameters m and V) such behaviour was found at values of N_0 below the baseline value. In this section, the full range of seasonal forcing is explored to determine the fraction of the year during which limit cycle behaviour occurs given these manipulations.

Two sets of runs were performed to answer this question. Both were performed at OWS "India", and both determined the equilibria produced by fixing the forcing regime on each day of the year. The first set of runs used baseline values for all model parameters, the latter set repeated this procedure, but used values of the cross–thermocline mixing rate, m, and the detrital sinking velocity, V, which produced limit cycle behaviour ($m = 0.30$ m d^{-1}; $V = 1.0$ m d^{-1}). The results from these runs were compared with normal dynamic solutions using these parameter regimes.

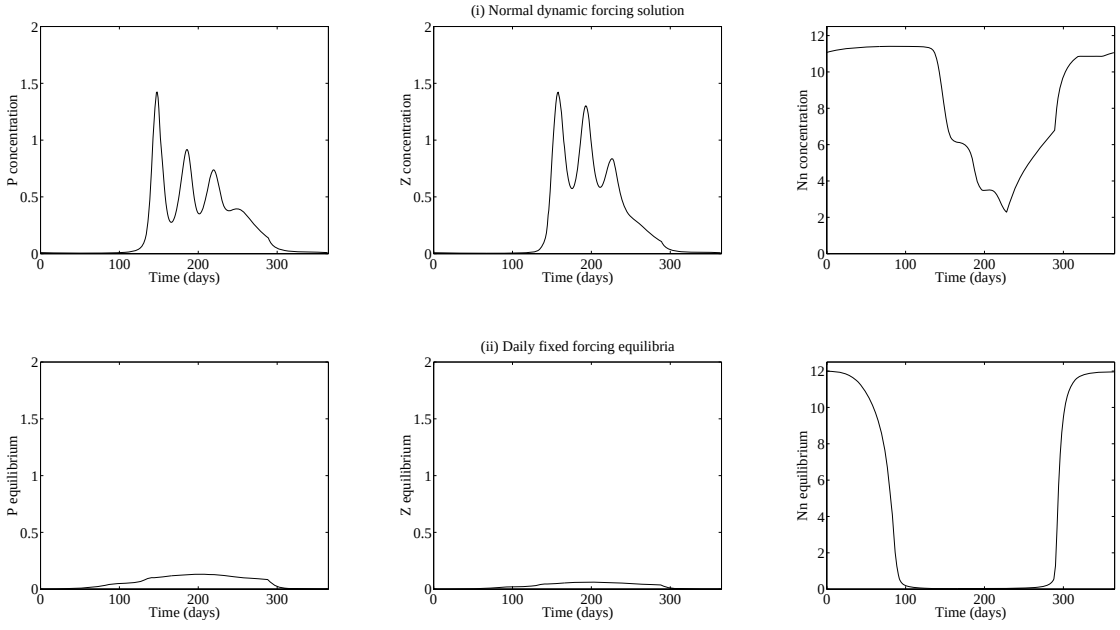

Figure 4.20: Normal dynamic forcing solution (top row) and daily fixed forcing equilibria (bottom row) for OWS "India". Baseline parameter values used. Concentrations and equilibria in mmol N m^{-3}.

Figures 4.20 and 4.21 show the results from these runs. In both cases, the top row of plots shows the normal, forced solutions for the phytoplankton, zooplankton and nitrate compartments. The bottom row of plots shows the equilibria for these compartments found when forcing is fixed on each day of the

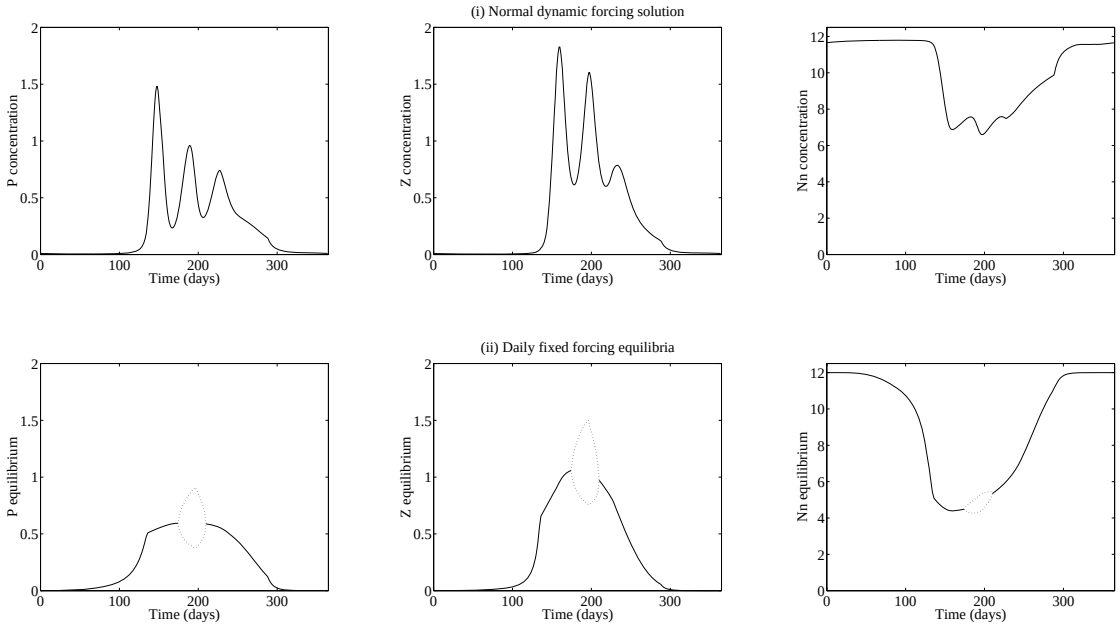

Figure 4.21: Normal dynamic forcing solution (top row) and daily fixed forcing equilibria (bottom row) for OWS "India". High cross–thermocline mixing rates (m = 0.30 m d^{-1}) and low detrital sinking velocities (V = 1.0 m d^{-1}) used. Concentrations and equilibria in mmol N m^{-3}.

year. The plots share the same vertical scale to ease comparison.

As expected from the results presented for the full model at the beginning of this chapter, there are differences between the forced, dynamic solutions and the fixed forcing equilibria. These differences are most obvious in the case of the runs performed at baseline parameter values. The nitrate equilibria found are much lower across most of the year (from the early spring to the late autumn) than their dynamically forced equivalents. Consequently the concentrations of phytoplankton and zooplankton supported are also much lower. Although the nitrate equilibria in the second set of runs are also mostly lower than their equivalents in normally forced solutions, they never reach particularly limiting concentrations. The phytoplankton and zooplankton equilibria then fall at values much closer to those observed during the dynamic solutions.

More importantly though, while in the former set of runs only stable equilibria were found, in the latter set, limit cycle behaviour occurs during the summer between days 176 and 209 (inclusively). The cycles found varied in amplitude (reaching a maximum amplitude on day 197) and period (reaching a minimum on day 191), showing trends which reversed around the centre of the limit cycle region. These results support the suggestion made earlier that seasonal forcing may move the model equilibria from a region of stable fixed points to one of stable limit cycles.

4.9 Functional forms of higher predation

Although the results so far have found oscillatory behaviour occurring in regions of parameter space associated with nitrate supply to the mixed layer (in agreement with Steele & Henderson, 1992, and Popova *et al.*, 1997), Edwards & Brindley (1996) and Steele & Henderson (1992) have examined the occurrence of such behaviour in relation to losses of the zooplankton to higher predation. Edwards & Brindley (1996) found that the rate of this process acted as a bifurcation parameter for their modelled ZPN system, while Steele & Henderson (1992) found that different forms of the loss term had different consequences for system behaviour.

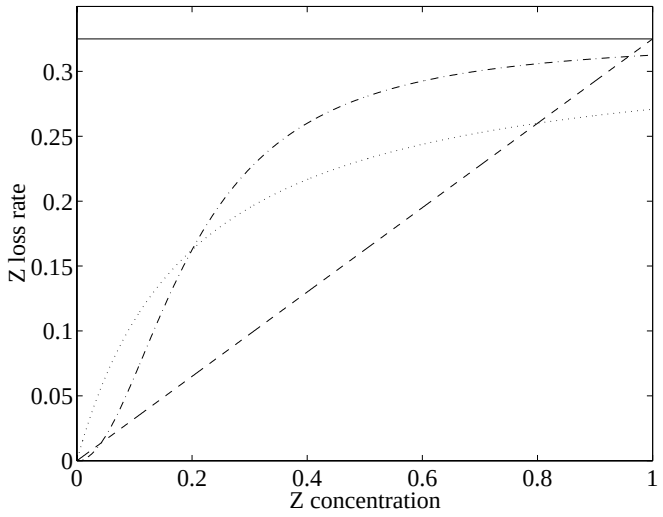

Figure 4.22: Zooplankton loss rate (d^{-1}) versus zooplankton concentration (mmol m^{-3}) for four functional forms of higher predation. The forms shown are *constant* (solid), *linear* (dashed), *hyperbolic* (dotted) and *sigmoid* (dot–dash). The loss rate, μ, in each case is 0.325 d^{-1}. For the hyperbolic and sigmoid cases, the half–saturation constant is 0.2 mmol N m^{-3}.

The full Fasham (1993) model makes use of a hyperbolic, or type II, response curve to determine the loss rate of zooplankton. Edwards & Brindley (1996) and Steele & Henderson (1992) observed limit cycle behaviour in their ZPN models with linear and constant responses respectively. Figure 4.22 shows the shape of these three forms, together with a fourth sigmoidal form, in relation to zooplankton concentration. Table 4.1 lists the functions which specify each of these forms as well as examples of their use in the modelling literature.

The constant form has a specific rate independent of zooplankton concentration, and may be interpreted as representing a predator whose biomass does not fluctuate. Although this is perhaps unrealistic, the constant form is the simplest and is commonly used. The value of the rate constant, μ, may be fine–tuned

Mortality term	**Function**	**Literature examples**
Constant	$\frac{dZ}{dt} = \ldots - (\mu)Z$	5, 9, 10, 14, 17
Linear	$\frac{dZ}{dt} = \ldots - (\mu Z)Z$	3, 18
Hyperbolic	$\frac{dZ}{dt} = \ldots - \left(\frac{\mu Z}{(k+Z)}\right) Z$	7, 1, 16
Sigmoid	$\frac{dZ}{dt} = \ldots - \left(\frac{\mu Z^2}{(k^2+Z^2)}\right) Z$	15

Table 4.1: Zooplankton mortality terms used in the modelling literature. Key to literature examples in Chapter 2.

to produce a model output in agreement with a particular data set (*e.g.* Fasham, Ducklow & McKelvie, 1990).

Note that some researchers (*e.g.* Edwards & Brindley, 1996) prefer to call this form "linear", since the term appears linear in the zooplankton ODE. The "linear" form, as used here, is then defined as "quadratic", again because of the appearance of the term in the ODE.

The linear form has a specific rate dependent on the zooplankton biomass itself. This may be interpreted as representing either cannibalism within the zooplankton compartment, or a predator whose biomass is proportional to that of the zooplankton. As such, this form is perhaps more realistic since predator populations commonly vary with those of their prey. Note that in a bulk model such as the full model, cannibalism in the form above may represent true cannibalism (*i.e.* species X eats species X) or intra-trophic cannibalism (*i.e.* zooplankton species X eats zooplankton species Y). The latter as sometimes known as "functional" cannibalism since it is only cannibalism because all of the zooplankton have been combined into a single compartment where they are assumed to be functionally identical.

The latter two forms, hyperbolic and sigmoid, lie between the constant and linear forms. At lower zooplankton concentrations, both behave somewhat similarly to the linear form (*i.e.* with a specific rate proportional to zooplankton biomass), while at high zooplankton concentration, both plateau and behave similarly to the constant form (*i.e.* with an invariant specific rate). Both may be interpreted as representing satiable predators. This "satiation" may parameterise a number of different ecological processes. Following Holling's original derivation, it may represent *handling time*, the minimum period of time which a predator spends processing each food item before it can catch another one. Alternatively, it may represent a limit on predator density, either caused by some other factor in the environment (*e.g.* availability of suitable mating sites), or by direct interference between the predators themselves (deliberate or accidental).

The sigmoidal form differs from the hyperbolic form in its behaviour at very low zooplankton concentration. At these densities (and with the same half–saturation constant), the sigmoidal response leads to lower rates of predation than the hyperbolic form. However, as zooplankton density increases, the sigmoidal response leads to a more–than–linear increase in predation rate. This is why the form is referred to as sigmoidal or "S–shaped". One of the ways such a response may occur in a biological system is where the predator "switches" between different prey types (Begon, Harper & Townsend, 1986). Alternatively, the lowering of predation rate at low zooplankton density may parameterise a predator with a prey threshold concentration. Below a certain prey concentration the predator reduces its searching efforts to save resources until prey density becomes sufficient to make a net gain for effort expended. Some models (*e.g.* Kremer & Nixon, 1978; Evans & Parslow, 1985; Frost, 1987; Moloney & Field, 1991) utilise a "refuge" concentration, below which predation ceases, to achieve a similar effect.

While these latter two functional forms allow modellers to specify a more complex response, clearly such forms of predation require much more information about the predators they aim to implicitly model. The former models, by contrast, require only that predator numbers are either independent of prey, or increase with them. Steele & Henderson (1992) note that the more complex forms are often used to model situations for which no data for predation is available. The μ and k parameters are then used to fine–tune the model so that it fits the data which is actually available. Since a wide range of response curves are possible from these forms, that these models can be made to fit the available data is perhaps unsurprising.

However, as illustrated by table 4.1, all of the functional forms are used in modelling studies of plankton systems. In their review of predation terms, Steele & Henderson (1992) attempted to summarise the ranges of behaviour different terms produced in simple ZPN models. The following section compares the response of the full model to each of the four terms above, and compares the results found with those of Steele and Henderson (1992) and Edwards & Brindley (1996).

4.9.1 Four closure terms and a nutrient index

Each of the four predation terms was incorporated separately in a version of the full model. In the first instance, simulations were performed for each of the four resulting models over a range of the maximum loss rate, μ_2 (note that in the linear case μ_2 does not represent the *maximum* loss rate, since for values of $Z > 1$, the loss rate is higher than μ_2). In the hyperbolic and sigmoid cases, the half–saturation constants were kept at the baseline value of 0.2 mmol N m^{-3}. As previously, the simulations had constant forcing (OWS "India", day 197) and were run until either a stable equilibrium was reached, or the behaviour could be established from the system trajectory. Aside from the cross–thermocline mixing rate, m, being set to 0.30 m d^{-1} (in accordance with previous simulations), all parameters were set to their baseline values.

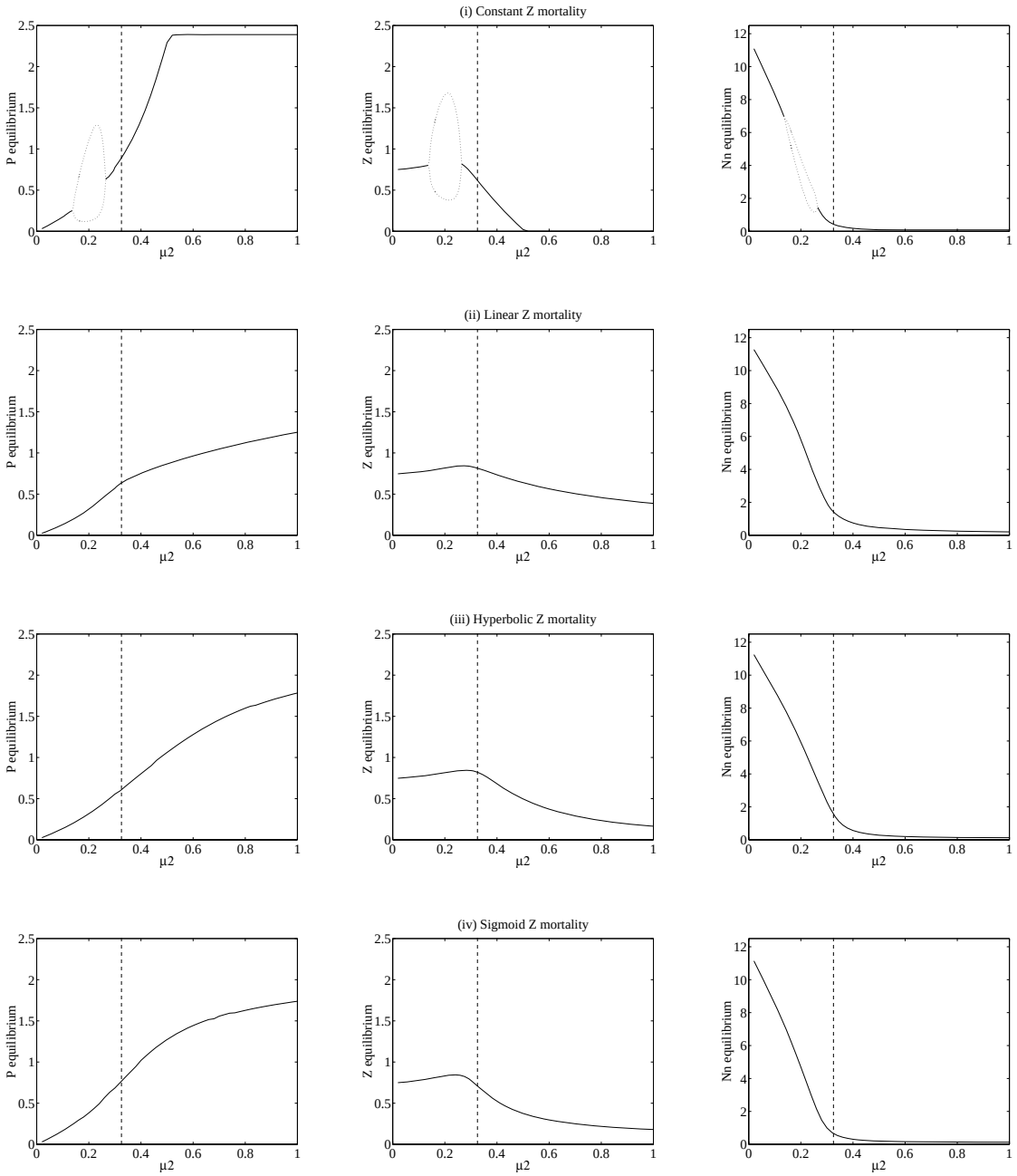

Figure 4.23: Phytoplankton, zooplankton and nitrate equilibria across ranges of maximum zooplankton mortality rate, μ_2, for each of the four functional forms. Solid lines indicate stable equilibrium solutions, dotted lines indicate the range of limit cycle amplitude, and dashed lines mark the baseline value of μ_2 used in Fasham (1993). Concentrations in mmol N m^{-3}.

Figure 4.23 shows the resulting equilibria of these simulations for the phytoplankton, zooplankton and nitrate compartments. The most significant difference between the four rows of plots is the occurrence of limit cycles with the constant mortality term. These cycles occur just below the baseline value of μ_2 ($0.14 \leq \mu_2 \leq 0.26$), and have periods which decrease from 37.5 to 30.8 days as μ_2 is increased.

Aside from the limit cycle behaviour of the constant form, the four terms show somewhat similar behaviour in response to increasing μ_2. In all four forms, the zooplankton equilibria increase with μ_2 to a point just below the baseline value. After this point, the equilibria all decline to lower values. In the case of the constant form this decline is extreme, and for values of $\mu_2 > 0.50$, the zooplankton equilibria fall below 0.0001 mmol N m^{-3}. In the other three cases the equilibria fall, but to a much lesser degree. This shared response to increasing μ_2 is also found with the phytoplankton and nutrient compartments, which show opposite trends to increasing μ_2.

The oscillation results are broadly in agreement with those of Steele & Henderson (1992), whose simulation results suggest that shorter term oscillations (55–60 days) are easily obtained with a constant zooplankton mortality term, while are absent when a linear mortality term is used. The simulations described in Steele and Henderson's (1992) work differ from those presented in this chapter since the ZPN models are forced by a sinusoidal phytoplankton growth rate. This creates repeating ~300 day cycles in a similar fashion to those in the previous chapter. The short term oscillations found are superimposed on these seasonal cycles. However, more recent work by Edwards & Brindley (1996) found the wide occurrence of oscillatory behaviour in the ZPN model of Steele & Henderson (1981), which has a linear mortality term. This work was extended in Edwards (1997) to include a model with a constant mortality term, and this was found to exhibit limit cycle behaviour across a wider range of parameter values. While no limit cycles were found here when the linear term was used, the exploration of parameter space was considerably narrower than that examined by Edwards & Brindley (1996) and Edwards (1997).

In the case of the hyperbolic and sigmoid mortality forms, although no limit cycles were found in the range of μ_2 examined, it is easy to see from the equations themselves that at $k_6 = 0$, both terms collapse to the constant mortality term. To examine the significance of the parameter k_6 on the behaviour of the model, a second pair of simulations exploring ranges of μ_2 and k_6 for both mortality terms were performed. As previously, both pairs of simulations were performed with constant forcing (OWS "India", day 197) and with otherwise baseline parameter values (except cross–thermocline mixing rate, m, which again was set to 0.30 m d^{-1}).

Figure 4.24 shows the phytoplankton, zooplankton and nitrate equilibria found by these simulations. For both terms, as $k_6 \rightarrow 0$, oscillatory behaviour was found. The hyperbolic term only yielded such behaviour at values of $k_6 \leq 0.02$, a value one tenth that of the baseline value use by Fasham (1993). The sigmoid term found oscillations up to values of 0.16, only slightly lower than the baseline.

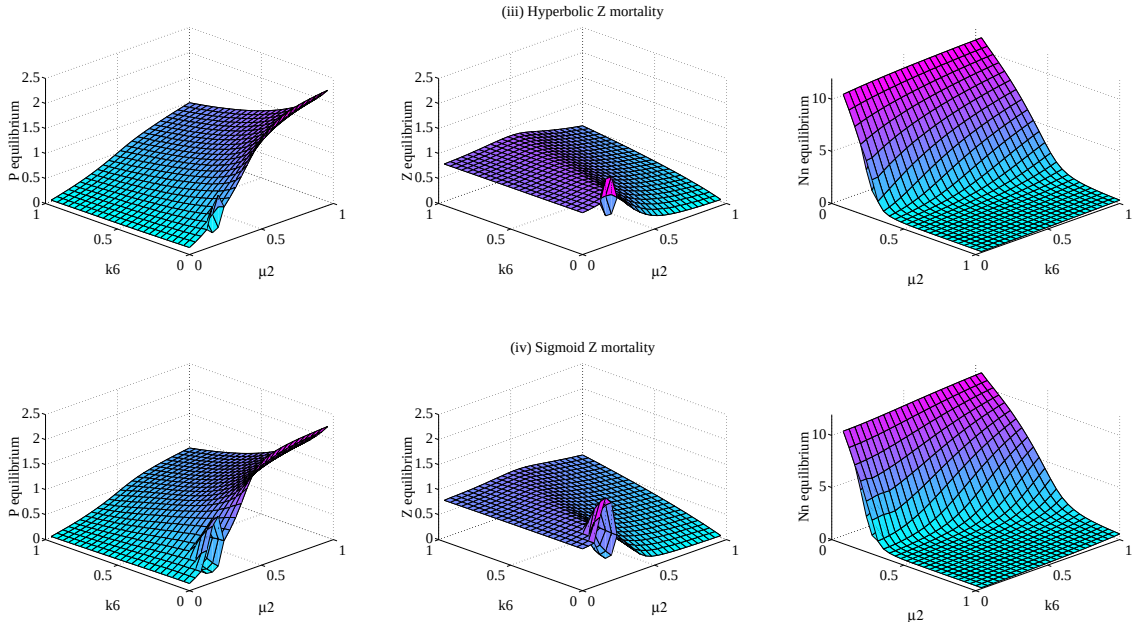

Figure 4.24: Phytoplankton, zooplankton and nitrate equilibria across ranges of maximum zooplankton mortality rate, μ_2, and mortality half–saturation constant, k_6, for the hyperbolic and sigmoid functional forms. Baseline values of predation parameters : $\mu_2 = 0.325$ d^{-1}, $k_6 = 0.2$ mmol N m^{-3}. Note that the plots of nitrate equilibria have been rotated clockwise by 90° for the purposes of clarity. Concentrations in mmol N m^{-3}.

Other than the difference in the range of values over which limit cycles occur, both mortality terms show very similar equilibrium densities across parameter space. As k_6 is increased, predation on the zooplankton decreases leading to greater grazing pressure on the phytoplankton (and other prey species) and consequently reduced nitrate uptake. As suggested already, a relatively wide range of equilibrium densities for the state variables can be obtained by a careful choice of the values of the mortality parameters.

The reason for the difference in extent of limit cycle regions can be seen from the shapes of the two response curves (see figure 4.22). For the same half–saturation constant and for zooplankton concentrations above that constant (which, in the case of this model and its baseline parameter values, is normal for the summer zooplankton population), the sigmoid term results in greater levels of predation on zooplankton (*i.e.* levels of predation closer to those of the constant term) than the hyperbolic term. Resultingly, the region of μ_2–k_6 space in which limit cycle behaviour occurs is larger for the sigmoid than for the hyperbolic form.

One of the general conclusions drawn by Steele & Henderson (1992) regarding different functional forms for zooplankton mortality dealt with the nutrient status of the equilibrium states obtained under different mortality forms. They found that when the ratio of N^* (nutrient equilibrium) to k (the phytoplankton nutrient uptake half–saturation constant, in this case k_1) was considered, the functional forms could be

ranked :

$$\begin{array}{ccccc} constant & < & linear & < & hyperbolic \\ \frac{N^*}{k} < 1 & & \frac{N^*}{k} > 1 & & \frac{N^*}{k} \gg 1 \end{array}$$

The implication of this conclusion is that different functional forms for predation may directly and generically influence the equilibrium state of plankton systems. Table 4.2 shows the values of N^*/k they obtained from their models, and those obtained using from simulations of the full model with the appropriate mortality form. In the case of the full model simulations, the ones obtained at baseline values of μ_2 and k_6 were used.

Mortality term	**Steele & Henderson (1992)**	**This work**
Constant	0.2	0.931
Linear	3.3	3.036
Hyperbolic	6.0	3.403
Sigmoid	–	1.421

Table 4.2: Values of N^*/k for each mortality term. The values estimated by Steele & Henderson (1992) for their models are shown for comparison.

While the value of N^*/k produced by the full model with constant mortality is not quite as low as that found by Steele & Henderson (1992), it does still fall below 1. The values produced by the other forms fall markedly above 1, and rank in the same order as Steele & Henderson (1992) found. The range of N^*/k values found between the different forms of mortality is slightly narrower, but in general the comparison between the results is favourable.

Figure 4.25 shows ranges of N^*/k that were calculated from the nitrate equilibria of each mortality form. Where limit cycle behaviour was encountered, the nitrate equilibrium was set to the midway point between the oscillation maximum and minimum.

These results show how sensitive the N^*/k ratio is to the choice of zooplankton maximum mortality rate. Although at the baseline value of μ_2 the constant mortality form has a ratio slightly less than 1 (and ratios for the other forms are > 1), the ratio sharply increases with falling μ_2 (this occurs with all of the mortality forms, with each one having a slightly differently shaped curve).

Although at the baseline value of μ_2 (and with OWS "India" forcing conditions at the height of summer) the constant form of mortality does predict a N^*/k ratio clearly different from those of the other mortality forms (except perhaps the sigmoid form), when forced simulations are considered, the picture becomes less clear.

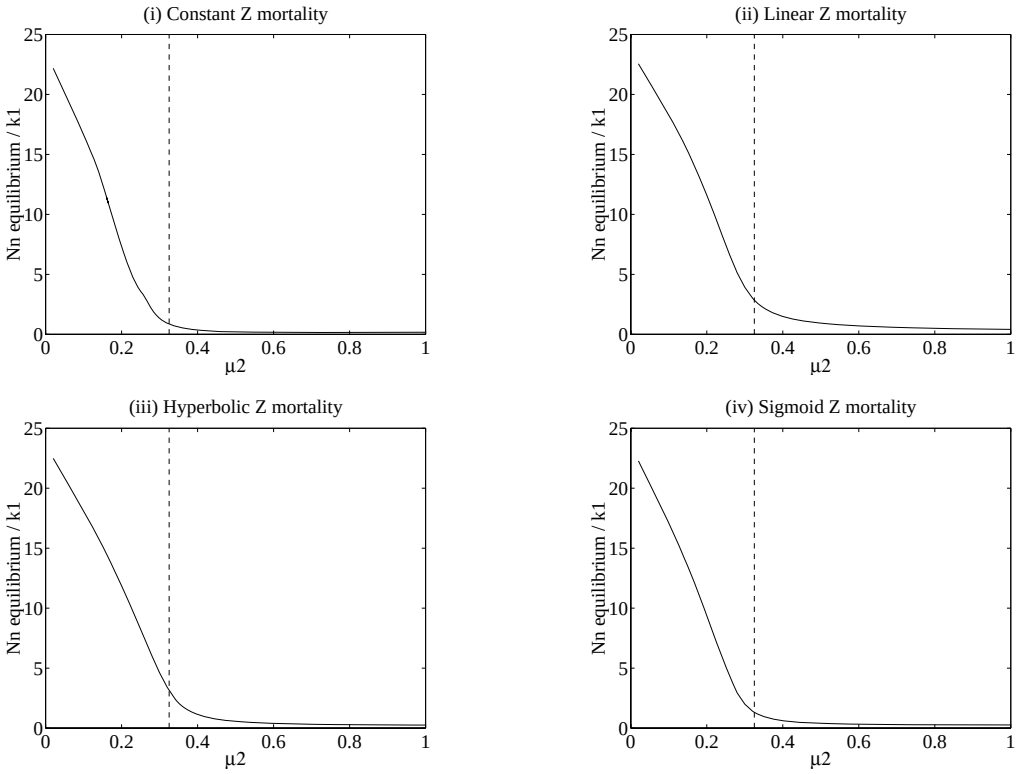

Figure 4.25: Plots of the ratio of N_n^* to k across a range of maximum zooplankton mortality rate for each of the four functional forms. The half–saturation constants of the hyperbolic and sigmoid forms were held constant at 0.2 mmol N m^{-3} (the baseline value).

Figure 4.26 shows the results of normally forced simulations at OWS "India" for each of the four mortality terms. Baseline values for both of the mortality parameters were used. In each case, the annual cycles of phytoplankton, zooplankton and nitrate concentrations are shown.

The most significant difference is (again) with the constant mortality. The constantly high predation on zooplankton almost entirely extinguishes the population during the winter months when there are no prey to consume. This allows an extremely large phytoplankton population to bloom in the spring and causes almost zero nitrate concentrations for a significant fraction of the summer. Even with a constant mortality rate half of the baseline value, sizeable zooplankton populations at OWS "India" only make a brief appearance late in the autumn (results not shown). By contrast, the other three mortality forms produce annual cycles which have considerably lower phytoplankton densities (well within the range of OWS "India" observations) and with more reasonable zooplankton concentrations. The sigmoid form shares the familiar phytoplankton–zooplankton oscillations of the usual hyperbolic form, while the linear form's oscillations are confined to an indistinct spring bloom which merges with the summer population.

These results suggest that for zooplankton mortality to be represented by a constant form in the full Fasham (1993) model, the constant rate needs to be set at a lower value than for comparable simulations with the other three mortality forms (the replacement of the constant mortality term in the model of

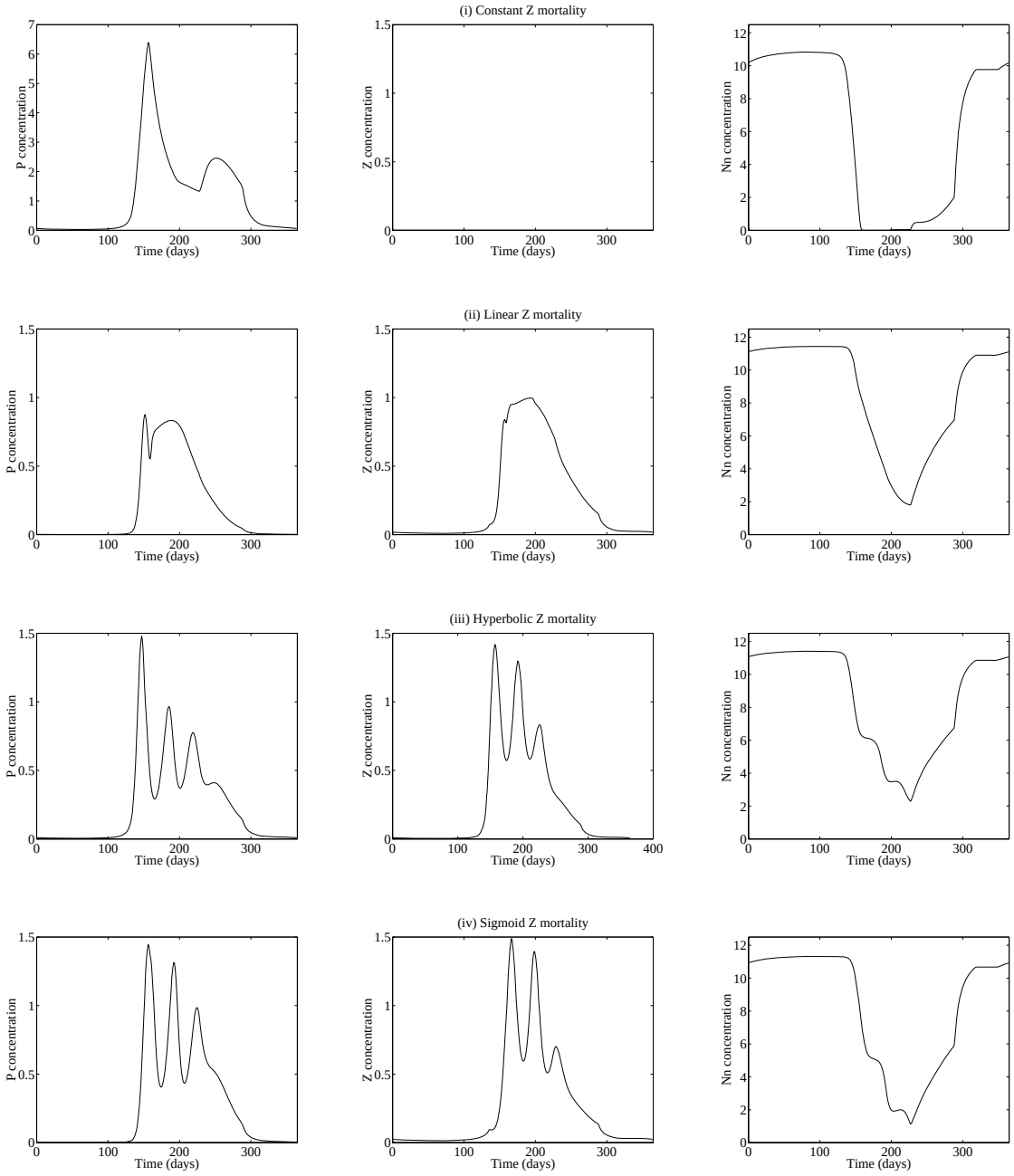

Figure 4.26: Simulated annual cycles of phytoplankton, zooplankton and nitrate at OWS "India" for each of the four zooplankton mortality terms. Note that the scale on the phytoplankton plot of the constant mortality row is more than four times that of the other phytoplankton plots. Concentrations in mmol N m^{-3}.

Fasham, Ducklow and McKelvie, 1990, by the hyperbolic term in the "updated" model of Fasham, 1993, was related to this problem). This may be a problem where the rate has been assigned from measurements. Alternatively, the rate may be treated as yet another forcing function and allowed to vary across the year. However, this would raise both practical (*i.e.* difficult measurements of predation would be required throughout the seasonal cycle) and theoretical (*i.e.* another empirical forcing function would reduce the "robustness" of the model across a geographical range) objections.

Significantly, changing the value of μ_2 for models using the constant mortality term to prevent zooplankton extinction drastically increases the N^*/k ratio, and this contradicts Steele & Henderson's (1992) conclusions about the significance of this ratio.

4.9.2 Conclusions

In this section the effects of varying the form of the higher predation term of zooplankton mortality have been examined through simulations of four versions of the full model which incorporate different forms. While evidence of limit cycle behaviour has been sought in line with the work of Steele & Henderson (1992), Edwards & Brindley (1996) and Edwards (1997), some of the conclusions of Steele & Henderson's (1992) work have also been examined.

In addressing the former question, it was found that only the constant form of mortality exhibited cycles across a range of the maximum zooplankton loss rate. However, by varying the half–saturation constant of mortality, limit cycles could be obtained in both the hyperbolic (the default in Fasham, 1993) and sigmoid forms. Although Edwards & Brindley (1996) found that the use of a linear mortality term in their ZPN model produced a rich structure of Hopf bifurcations to stable limit cycles, no such behaviour was found when the linear term was used in the full model.

Steele & Henderson (1992) found that the nutrient equilibria reached by models using different mortality forms could indicate systems in which phytoplankton are either nutrient– or grazer–limited. The results obtained from the full model simulations support this conclusion, although the equilibria found using different mortality forms were strongly dependent on the actual value of the maximum mortality rate. Fitting models that differ only in the form of their zooplankton loss terms to the same data sets can necessitate choosing maximum loss rates which are very different. This suggests that Steele & Henderson's (1992) conclusions regarding N^*/k ratios should be examined closely when models are formulated to represent the limiting features of specific ecosystems.

4.10 Summary

This chapter set out to determine the nature of the oscillatory behaviour of the full model during the summer months at OWS "India". While oscillations in a model's behaviour may only be a feature or artifact of that model, time–series measurements of chlorophyll from OWS "India" lend support to the notion that such oscillations may actually be occurring in the real world.

The question was tackled in a number of ways. Initially, simple numerical solutions were performed which, after a period of normal forcing, had their forcing "frozen". Their behaviour after this event was then followed to determine whether the oscillations found continued. This turned out not to be the case. Nitrate limitation (which normally is curtailed by the end of the favourable summer conditions) became important and only low, stable equilibria of phytoplankton and zooplankton resulted. The oscillations found in the normal simulations are transients towards a low, stable equilibrium.

However, the repetition of this work with the implicit nitrate model 6c3 (which cannot run out of nitrate) showed that, where nitrate never became limiting, both high, stable equilibria and stable oscillatory behaviour could result. Since two model parameters directly control nitrate supply to the modelled mixed layer, an investigation of these parameters was undertaken.

Because of the complexity of the full model, rigorous analysis proved too difficult, and a numerical approach was used to study the behaviour of the full model across parameter space. A program was written which used the trajectories of numerical solutions to determine the behaviour of the full model under given parameter or forcing regimes. While this is a non–standard approach, the complexity of the problem at hand favoured it. In a similar investigation of Steele & Henderson's (1981) "simple plankton model", Edwards & Brindley (1996) and Edwards (1997) make use of the numerical tools AUTO and LOCBIF (see references within Edwards & Brindley, 1996, for details).

Use of this program established that stable oscillatory behaviour occurred across regions of m–N_0 parameter space. While this behaviour did occur within the literature ranges of these parameters, it did so only at more extreme values. The assumptions these parameters make include some which make extreme values potentially untenable. To this end, explorations of the parameter space of each of the other model parameters (25 of them) were undertaken to determine whether oscillatory behaviour could be more easily found.

The equilibria produced across ranges of these parameters were determined, and five parameters were found to produce oscillatory behaviour. Of those, the detrital sinking velocity, V, produced such behaviour well within its literature range. Repetition of the previous explorations of m–N_0 space, but with

a reduced value of V, extended the size of the region of limit cycle behaviour to much more reasonable values of m and (particularly) N_0.

Examination of the whole seasonal cycle found that, at appropriate non–baseline values of m and V, the forcing functions moved the model's equilibria from low, stable equilibria in the winter to high, stable equilibria and stable oscillatory behaviour in the summer. For the parameter values used here, a 32 day window of limit cycles was produced during the summer months.

Recent work by Steele & Henderson (1992) has drawn attention to the essentially arbitrary use of different zooplankton mortality terms to "close" models, and the consequences for model behaviour of their use. Their results were compared with those from similar work performed using the full model, and their conclusions were re–examined. While some of the results found in work here supported those of Steele & Henderson (1992), the generalisations they drew concerning the mortality form and its role in equilibrium nutrient status appeared quite fragile. As Steele & Henderson's (1992) paper is comparatively well known in the field, it is probably important that researchers are cautious in their application of its findings.

4.11 Discussion

Predator–prey cycles have a long history in ecology stretching back to the neutrally stable oscillations of the Lotka–Volterra model (Lotka, 1925; Volterra, 1926; see Chapter 1 for further details). In the context of the present work, their appearance in the behaviour of a model, particularly when it coincides with apparently similar behaviour in data from the real world, provides an opportunity to use dynamical behaviour, as well as quantitative model output, to test that model. To a degree, limit cycle behaviour in a model constitutes a "risky prediction", which may aid in the model's comparison with the real world.

The work here has predicted such cycles under particular parameter and forcing regimes. Although primarily centred on OWS "India", the predictions are most likely to be testable in an environment with the appropriate forcing, but which remains relatively stable for longer periods of time. The work here has shown that although stable oscillatory behaviour is possible, transient oscillatory behaviour (such as that produced by the baseline parameter values) may obscure stable oscillations. While Bermuda Station "S" provides an example of a more stable forcing environment (mixed layer depth is less than 25 m for 122 days of the year; enough time for more than 4 of the oscillations predicted in Bermuda Station "S" runs), its baseline parameter regime is quite far removed from that required to generate stable oscillations. Regions where mixing with deeper, nutrient–richer water is greater are more likely to supply the necessary regimes (*e.g.* upwelling regions, tidal regions).

In Chapter 3, attention was drawn to the redundancy of the bacteria compartment in reduced models. In an interesting parallel, the work in this chapter which examined the behaviour of model equilibria across ranges of different parameters found that these equilibria (even those of the bacteria compartment itself) were very insensitive to changes in most bacterial parameters.

Although only briefly mentioned during the explorations of parameter space, transient oscillations to a stable equilibrium are a common type of behaviour. Because of the difficulty in quantifying damping times, *et cetera* for such behaviour (due to the importance of initial conditions), only stable equilibria and stable limit cycles have been sought here. A more rigorous study (particularly if it were concerned with the use of dynamical behaviour to test model predictions) would need to examine the importance of such behaviour in the model.

An issue not raised in the work in this chapter is that of the role of space in oscillations. While the OWS "India" chlorophyll data ostensibly represents a time series of phytoplankton density, it is possible that in reality it represents the passage of distinct blooms in space past the measuring station. However, while it is difficult to reject this statement without further data, the work of McCauley & Murdoch (1987) lends a small degree of support to the existence of true limit cycles (albeit ones in a freshwater

environment).

Despite these latter difficulties, it is hoped that the work in this chapter may provide a background to any more serious attempts to compare the Fasham (1993) model with ocean measurements.

Chapter 5

Sensitivity analyses and stochastic parameterisation

God does not play dice.

– Albert Einstein (1879–1955)

5.1 Introduction

In Chapter 4, the behaviour of model equilibria across ranges of each of the model parameters was determined. While the aim was to determine whether any of the parameters produced stable oscillatory behaviour, it was also noted that several of the parameters, noticeably the attenuation coefficient, k_w, caused the stable equilibria found to shift significantly near the baseline values of these parameters. These results suggested that different parameters could be of quite different significance to the model solutions, and that emphasis should perhaps be placed to determining more accurate values for the most "sensitive" model parameters. As most parameters require difficult or time–consuming experiments, knowing which parameters most strongly influence model behaviour can optimise the development of a model.

Fasham, Ducklow & McKelvie (1990) performed such a parameter sensitivity analysis with the original version of the model used in this thesis. In this chapter, their work is reprised together with two stochastic approaches to parameter sensitivity studies. The latter of these two approaches is also explored in depth to examine aspects of its implementation and behaviour.

5.2 Model uncertainties

In models such as Fasham (1993) there are several potential sources of uncertainty in the formulation and solution of the model.

(i) *Model structure*

The representation of the real world included in the structure of the model, and the form of the terms within the model (*e.g.* phytoplankton, zooplankton, nutrients, *et cetera*).

(ii) *Initial conditions*

The values of the state variables used to initialise the model (*e.g.* $P(0) = x$).

(iii) *Forcing functions*

The influence of variable factors not explicitly included as dynamic variables in the structure of the model (*e.g.* daily/seasonal cycles of mixed layer depth and irradiance).

(iv) *Model parameters*

The parameters (or coefficients) which usually quantify the various relationships between the model state variables (*e.g.* rates, half–saturation constants, ingestion fractions, *et cetera*).

(v) *Numerical implementation*

The computational system by which the model is put into effect (*e.g.* numerical integration scheme, iteration step length, accuracy of state variable representation, *et cetera*).

Although the sensitivity of the Fasham (1993) model to its various parameters is the focus of this chapter, the other sources of uncertainty merit brief discussion.

At the very deepest level, there is uncertainty in the actual structure of the model and the forms of the terms within it. Chapter 2 gave a brief overview of the variety in these aspects across the plankton modelling literature, and Chapters 3 and 4 contain versions of the Fasham (1993) model which aim to examine the sensitivity of the model's behaviour to different structures and functional forms. Additionally, as pointed out in Chapter 1, even modelling systems as ODEs (or difference equations, or PDEs, or CMLs, *et cetera*) carries with it assumptions and, therefore, uncertainties.

As raised in Chapter 3, the initial conditions of the state variables are only usually of any consequence in the first 5–10 years of a model solution. By the end of this period the model solution has normally converged onto an annual cycle which is repeated indefinitely. Note though that this repeating cycle is actually transient behaviour, for the state variables are constantly "chasing" the forcing functions. The stable equilibrium values of the state variables for a given day's forcing conditions can consequently be

very different from their actual values on that day for a normally forced solution.

Unlike initial conditions, forcing functions play a strong role in the dynamics of the Fasham (1993) model. This can be seen in the difference in the model behaviour at the forcing locations of OWS "India" and Bermuda Station "S" (see Chapters 3 and 6), and when mixed–layer depth forcing is varied (see Chapter 3).

The numerical integration scheme used in the implementation of the models in this thesis is 4th order Runge–Kutta, a standard one used by many modellers. Other integration methods (3rd order Runge–Kutta, 3rd order Runge–Kutta : Nystrom formulation, 6th order Runge–Kutta : Fehlberg formulation) were examined in the early stages of the work in this thesis, but as they produced indistinguishable results and offered no considerable benefits over the standard Runge–Kutta IV scheme, they were not adopted. Numerical experiments with the integration step length (detailed in Chapter 3) found that hourly integration was more than sufficient to produce a stable solution.

5.3 A sensitivity analysis of the full model

Fasham, Ducklow & McKelvie (1990) performed a parameter sensitivity analysis for 23 of the parameters in the full model. This analysis consisted of performing pairs of deterministic runs for each of these model parameters, one for a low value of the parameter in question, and one for a high value. Each of these runs was then compared to the normal deterministic solution to determine the normalised change in the solution caused by a change in the parameter. For the purposes of this analysis, Fasham, Ducklow & McKelvie (1990) used annual net primary productivity (NPP) and the annual f–ratio (total new primary production divided by NPP) as comparative statistics. Since the authors were interested in the situation at Bermuda Station "S" the numerical solutions were determined for the forcing regime there.

This analysis found that NPP was most strongly influenced by parameters k_w, λ, α, μ_1, N_0 and k_1, while the annual f–ratio was additionally strongly affected by g. The authors acknowledged that other sensitivity techniques could equally have been used, and drew attention to the problem of accounting for interactions between the model parameters in sensitivity studies.

In this chapter, two alternative techniques, Monte Carlo and stochastic parameters, are introduced and applied to a parameter sensitivity study of the full model. Since the analysis of Fasham, Ducklow & McKelvie (1990) dealt with an earlier version of the full model[1], the technique they used in their analysis

[1] The version of the full model used by Fasham, Ducklow & McKelvie (1990) differs from that used by Fasham (1993) primarily in its handling of the mortality terms for phytoplankton and zooplankton. In both cases, constant rates are used for these processes, and in the case of zooplankton mortality, the flows from this process are proportioned slightly

has been re–applied to the full model from Fasham (1993) to provide a comparison. Also, since work in this thesis has focussed more heavily on model behaviour at OWS "India", the initial parameter sensitivity studies have been performed with the forcing regime from this location.

5.4 Techniques for sensitivity analysis

In contrast to the deterministic approach taken by Fasham, Ducklow & McKelvie (1990) in their analysis of the full model's sensitivity to its various parameters, the two additional techniques applied in this chapter employ stochastic approaches. In doing so they incorporate uncertainty into the model parameters, and aim to determine the consequences of this uncertainty on the model's behaviour. With both of the techniques, model parameters are assigned values at random[2] from some specified probability distribution, and then these parameters are used within simulations. As both techniques involve simulating the model, they do not require any simplification of it. This contrasts with other techniques for including parameter uncertainty into a model. First Order Variance Propagation Analysis, for instance, requires that the model be approximated to first order equations (*i.e.* non–linear terms modified or removed). The use of Random Differential Equations is usually similarly confined to simpler models (which are more amenable to rigorous analysis). The two techniques used here differ mechanically in the timing of the parameter stochasticity, but also, and more significantly, in their underlying assumptions about the nature of the model parameters.

5.4.1 Monte Carlo simulations

The technique referred to in this chapter as *Monte Carlo*[3] (MC) is one commonly used in modelling studies (*e.g.* Loehle, 1997). The parameter (or parameters) in question is first assigned a value at random from a known distribution. This distribution may base its mean and variance on measurements of the parameter from field observations or experiments. Next, the model is simulated deterministically, as usual, and the run statistics are collected. The procedure of assigning parameter values at random and then running model simulations is then repeated again and again until, normally, the mean and variance of the Monte Carlo simulations have converged. This procedure may be applied to single parameters or to groups of parameters.

The Monte Carlo technique essentially assumes that parameters in the real world are fundamentally

differently into the ammonium and DON compartments. The version of the full model detailed in Fasham (1993) instead favours density–dependent Michaelis–Menten relationships for these processes.

[2]In the context of computer simulations, the term "random" usually means that a deterministic "random" number–generating algorithm or a look–up table is used to provide numbers for use by the computer program. The work in this thesis makes use of a "non–linear additive feedback random number generator" which returns successive pseudo–random numbers in the range 0 to $((2^{31}) - 1)$, with a period of approximately $16((2^{31}) - 1)$.

[3]Note that the term "Monte Carlo" is applied to many other techniques in modelling where elements of chance enter into analyses or simulations.

constant, but that their values (for whatever reason) are known only poorly.

As an aside, unlike the work in this chapter, the Monte Carlo technique is commonly used in simulations where multiple parameters are allowed to vary. In such cases the volume of parameter space from which the parameters are assigned values can be very large, and the technique is often augmented by a process known as *Latin hypercube sampling*, which aims to minimise the number of model runs required by more systematically exploring the available parameter space.

5.4.2 Stochastic parameter simulations

Kremer (1983) introduced a technique, known as *stochastic parameters*, in which model parameters, instead of remaining constant during a given simulation, are allowed to vary randomly throughout its duration. Similarly to the Monte Carlo technique described above, parameters are initially assigned random values from a known distribution. However, at fixed intervals during the simulation, the stochasticity algorithm is applied again and the model parameter (or parameters) in question is assigned a new value.

In contrast to the Monte Carlo technique, Kremer's stochastic parameters approach assumes that parameters are not constant, and that they may be represented as being variable in time.

Since the biological state variables of many ecological models (and almost all plankton models, including those in this thesis) are intended to cover a diverse and changing mix of species, it is unlikely that the model parameters, which are proxies for physiological and interactive processes, are best modelled as constants[4]. Furthermore, even when only a single species is considered, it is unlikely that all individual members of that species will share a common parameter value. Genetic differences and influences from the life history of each individual are likely to make the modelled population heterogeneous with respect to its parameters, and this heterogeneity is liable to be variable in time (because of shifts in the population genetics, and because of organisms responding to their environments). Consequently, Kremer (1983) argues that, at least empirically, stochastic parameters provide a means of incorporating temporal variability and uncertainty into the parameterisation of ecological models.

5.5 Parameter sensitivity at OWS "India"

In this section the sensitivity of the Fasham (1993) model to 25 of its parameters is assessed. For various reasons, several model parameters have not been included in this analysis, and several others have been handled in particular ways. Because of difficulty in formulating a satisfactory algorithm for assigning values to the parameters δ and ϵ (where $\delta + \epsilon \leq 1$), this pair of parameters has been excluded from this

[4] As Kremer (1983) points out, although this point being well–known among modellers, model parameters are still often anomalously referred to as "rate constants".

analysis. Parameters β_1, β_2 and β_3 are treated as a single parameter, β. Zooplankton feeding preference p_1 is allowed to vary, with p_2 and p_3 each assuming values of $(1 - p_1)/2$. With the exception of these exclusions and treatments, all other model parameters are handled identically in the analysis.

Unlike the results from Chapter 4, in which the equilibrium solution of the model under fixed forcing was calculated across ranges of each of the model parameters, in this chapter the model is simulated with normal forcing, and the consequences of changes to the model parameters assessed over a full simulation year. This approach potentially allows a more accurate assessment of the importance of a given model parameter to the model's predictions.

An important consideration in examining the sensitivity of a model to its various parameters is the criterion by which the effects of the different parameters are assessed. Fasham, Ducklow & McKelvie (1990) use the annual NPP and f–ratio. Fasham (1995) uses the timing and magnitude of the annual spring bloom. Kremer (1983) (though not interested directly in individual parameters) uses final phytoplankton biomass, and time series variance of phytoplankton biomass normalised to that from the baseline deterministic solution. For the majority of this work the approach taken by Fasham, Ducklow & McKelvie (1990) is followed, and the annual NPP and f–ratio used to assess model sensitivity.

5.5.1 Simulation methods

Deterministic techniques

For each parameter four sets of simulations were performed. Two of these followed the deterministic procedure used by Fasham, Ducklow & McKelvie (1990), where parameters were assigned values above and below their baseline value, and then deterministic solutions were calculated for each of those two values. The choice of values for these upper and lower limits is discussed in the following section on the stochastic techniques. As usual for such numerical solutions, the model was allowed to run for 50 years to equilibriate to a constant annual cycle.

Stochastic techniques

Except in the timing of the assignment of parameter values, the two stochastic approaches were handled very similarly. Firstly, a deterministic period of 50 years was allowed to provide initial conditions for January the 1st. These initial conditions were used to start each stochastic run. After this deterministic initialisation period, both Monte Carlo and stochastic parameters approaches assigned the chosen parameter a new random value. The model simulations then proceeded forwards. In the case of Monte Carlo runs, the chosen parameter retained this new value for the duration of the run. In the case of stochastic parameters, a timer changed the parameter's value at fixed intervals throughout the run. Figure 5.1 shows a diagrammatic representation of the two stochastic techniques.

In all of the work presented in this chapter, the distribution of parameter values for stochastic simula-

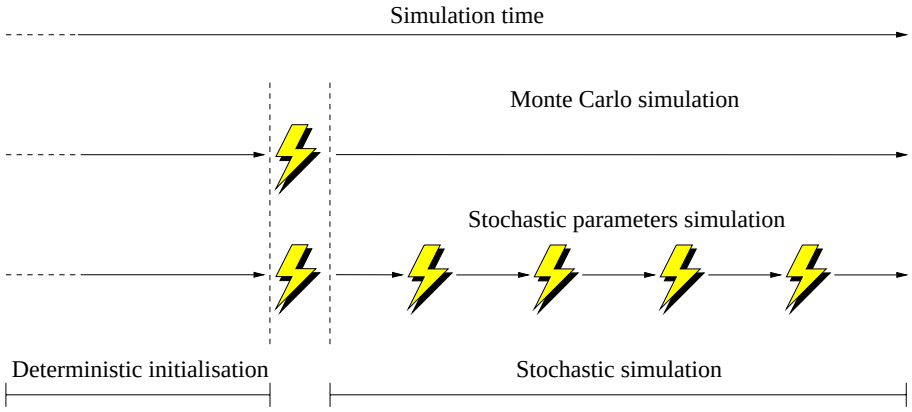

Figure 5.1: Diagrammatic representation of the Monte Carlo and stochastic parameters techniques. Timing of stochastic transformations of parameters indicated by lightning symbols. In both cases, stochastic simulations are preceded by a normal deterministic period (with baseline parameter values) to provide initial conditions for the stochastic simulations.

tions was assumed to be uniform around the baseline value. While a normal distribution may be more intuitively appealing, it was not used since several of the model parameters (λ, $p_{1,2,3}$, $\beta_{1,2,3}$ and γ) are fractions (*i.e.* bounded between 0 and 1), and thus awkward to treat as normally varying quantities. Additionally, in order that the results between different parameters could be directly compared, the range of values for all of the model parameters was fixed at the baseline $\pm$ 30%. Although the range of possible values this permits is not in agreement with all of the ranges of values measured for the model parameters, for most parameters this distribution is fairly congruent with the ranges described by Fasham, Ducklow & McKelvie (1990) (note though that, because of the paucity of data or assumptions made by the model, more than a third of the parameters examined by Fasham, Ducklow and McKelvie were assigned nominal values of double and a half that of the baseline).

As already mentioned, the stochastic parameters technique involves changing the value of the parameter in question throughout a given simulation run. In the real world, variability in the properties which are modelled as parameters is (presumably) continuous, depending upon hundreds of processes occurring across a range of scales (*e.g.* variation in the weather at the large scale, down to variation in the fortunes of individuals within populations). However, as models almost invariably homogenise the populations they study, variability is not normally modelled as precisely as it occurs in nature. As Kremer (1983) observes, models presume some limit in the temporal resolution of variability below which it is ignored. This limit is then the time scale at which uncertainty is allowed to alter the trajectory of the deterministic model. Depending on the nature of the processes modelled, this time scale may vary from minutes to hours to days. Following Kremer's (1983) algal model, in this work the time scale of stochastic periodicity has been set to 1 day (although this choice is examined later in the chapter).

Also related to the periodicity of transformations in the stochastic parameters technique is the actual

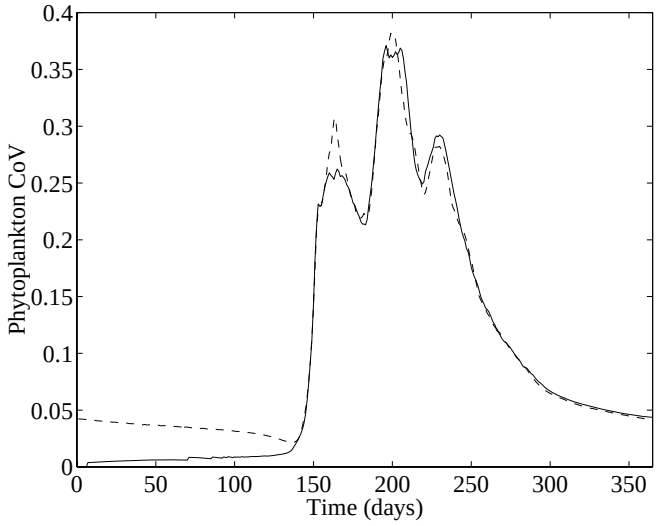

Figure 5.2: The seasonal behaviour of phytoplankton coefficient of variance (CoV) for two stochastic parameters simulations which differ in the number of transient years used prior to sampling (see text for full description). The solid line represents the CoV produced when no transient years are allowed for the simulation, the dashed line that produced when a single transient year is used prior to the sampled simulation year. Note that the former simulations have a much lower CoV in the first four months as the stochastic trajectories slowly diverge from that of the deterministic trajectory. Phytoplankton CoV is dimensionless.

timing during a given day. As indicated above, most of the work presented here has made use of a transformation period of 1 day. In order to ensure that no biasing of results occurs during runs as a consequence of parameters always being assigned a new value at the same time of each simulated day (*e.g.* parameters only change at midday or midnight), in each individual run, the second stochastic transformation is made to occur at a (uniform) random fraction of a day (the transformation period) after the initial transformation. Subsequent transformations are spaced at regular, fixed intervals. Similarly, when the periods of transformations are high (weeks to months), this procedure prevents transformations always occurring on the same days in different simulation runs (*e.g.* parameters only change at the start of each month, or on day 246 of a simulated year).

Since Monte Carlo runs are essentially deterministic (albeit with stochastically assigned parameter values), like normal numerical solutions they move towards an equilibrium annual cycle which is repeated indefinitely. As such, although the initialisation of the state variables aims to place each given simulation closer to its equilibrium cycle than randomly assigned values, several transient years were found to be required to allow each Monte Carlo simulation to equilibriate to its annual cycle. Preliminary work (combined with that described previously for normal deterministic solutions) found that a period of at least 3 years was required after the transformation of the parameter in question for this cycle to be reasonably accurately attained. Ideally periods much longer than this would be used to better

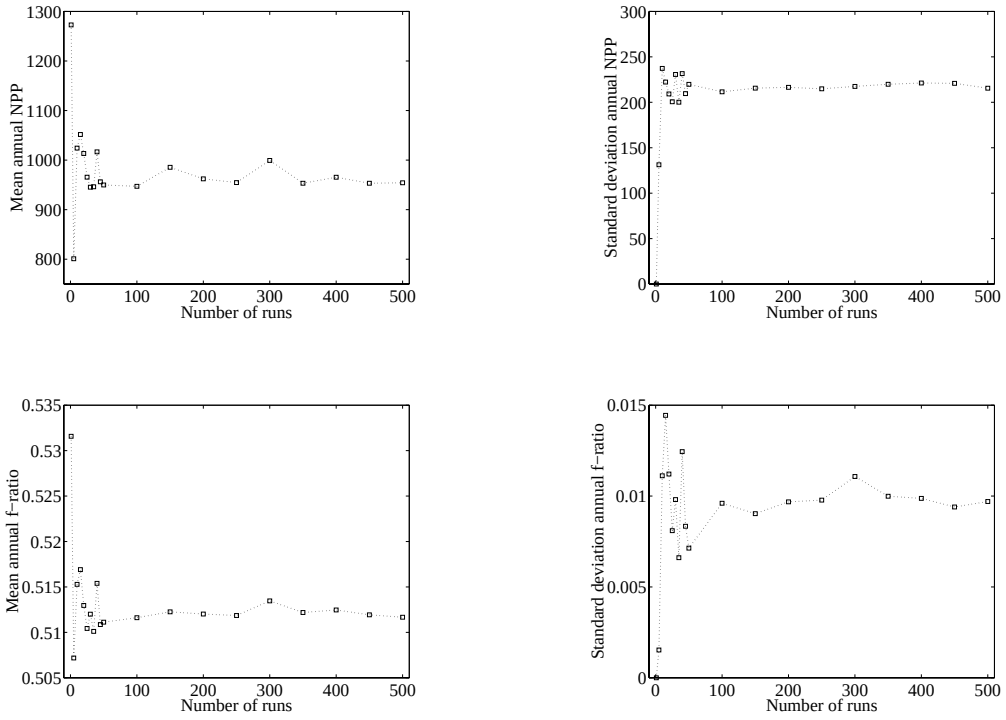

Figure 5.3: The behaviour of annual NPP and f–ratio means and standard deviations as the number of Monte Carlo simulations used to calculate them is increased. Model parameter g (zooplankton maximum ingestion rate) treated stochastically : 1.0 d^{-1} $\pm$ 30%. Annual NPP in mmol N m^{-2} y^{-1}. The annual f–ratio is dimensionless.

characterise the Monte Carlo simulations. However, as many individual Monte Carlo simulations are required to produce consistent estimates of the mean and variance of simulations using the technique, the number of preliminary years allowed before the sampled year weighs heavily on the computational load of a given run. Consequently, only 5 transient years were used prior to sampled years for Monte Carlo simulations.

A similar problem afflicts stochastic parameters simulations. As figure 5.2 shows, for a period shortly after the start of the stochastic simulations, the variability in the simulated phytoplankton population is considerably narrower than that towards the end of the first simulated year. This is an artifact caused by all of the simulations starting with the same initial conditions and then only slowly diverging from them. However, unlike Monte Carlo simulations, preliminary work found than only a single transient year was required before the stochastic parameters technique produced consistent estimates of daily means and variances, and the work presented here made use of simulations in which only a single transient occurred. (Later work in which the period of the stochastic transformations was increased up to 350 days found that a single transient year was often insufficient. Such simulations are identified in the text).

Both Monte Carlo and stochastic parameters techniques are used here to produce distributions of the

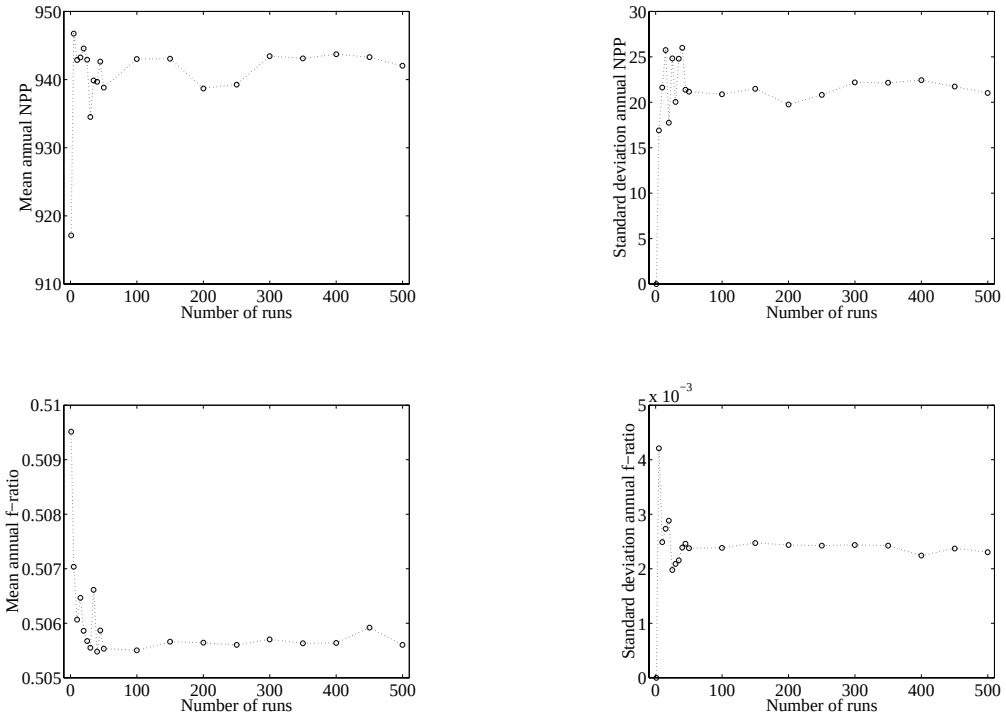

Figure 5.4: The behaviour of annual NPP and f–ratio means and standard deviations as the number of stochastic parameter simulations used to calculate them is increased. Model parameter g (zooplankton maximum ingestion rate) treated stochastically : 1.0 $d^{-1} \pm 30\%$, with transformation period of 1 day. Annual NPP in mmol N m^{-2} y^{-1}. The f–ratio is dimensionless.

outcomes that result when parameters are allowed to vary stochastically. In order that these distributions can be described accurately, multiple runs are required. As each run takes computer time to produce, the fewer runs required the better. Figures 5.3 and 5.4 show the behaviour of the means and standard deviations of annual NPP and the annual f–ratio as the number of runs used to calculate them increases from a single run to 500 runs. For both techniques, the means and standard deviations calculated for both measures are highly variable when less than 100 runs are used. Below 200 runs there is still variability in some of the statistics shown, and consequently 400 runs were used for both Monte Carlo and stochastic parameters techniques to produce distributions of results.

As an aside, figures 5.3 and 5.4 also illustrate the standard graphical format for summary statistic plots in this chapter. Markers (*e.g.* squares, circles, triangles or stars) indicate actual simulations. Dotted lines connecting markers aim to ease interpretation of such plots. Note also that Monte Carlo and stochastic parameters simulations are always indicated by square and circle markers respectively.

5.5.2 Simulation results

Using the methods described above, simulations were run for 25 of the Fasham (1993) model's parameters. The results of these simulations were processed in several ways. In the first instance, the annual NPP and f–ratio calculated from the baseline solution were compared to those calculated for each of the parameters at their upper and lower limits, and to the means produced by the stochastic techniques. The results from the sensitivity techniques were standardised to those from the baseline solution, and the model parameters were ranked in accordance to the deviation from the baseline solution they caused.

Parameter sensitivity ranking

Tables 5.1 and 5.2 show the results of the ranking process for annual NPP and the annual f–ratio respectively. Parameters which produce very little deviation from the baseline solution have a value close to 1.0, while values some distance from 1.0 indicate parameters with a more profound influence over the model's behaviour with respect to the measure in question. The results from the four approaches revealed some interesting agreements and disagreements.

With respect to annual NPP, the four approaches broadly agreed on the importance, or otherwise, of most model parameters. The least important parameter in all four cases was the cross–thermocline mixing rate, m. This result is perhaps surprising considering the prominence given to the parameter in Chapter 4. However, as indicated by the work in Chapter 4, the importance of m to the model lies mostly with situations in which nitrate starvation of the mixed layer occurs. Forced simulations at OWS "India" do not normally reach this situation, and the importance of m is diminished[5]. The four approaches differ on the most important parameter, although they all broadly agree on the importance of phytoplankton and zooplankton parameters in the "top 10". The parameters of greatest importance are those pertaining to phytoplankton photosynthesis (k_w, α, λ and V_p) and zooplankton grazing (g, β, k_3 and p_1). Fasham, Ducklow & McKelvie (1990) found a similar result with the photosynthesis parameters k_w, λ and α, but found the zooplankton parameters less important. Additionally they found that model solutions at Bermuda Station "S" were sensitive to parameters k_1, N_0 and μ_1. The importance of these latter parameters is, however, likely to be reduced in the work here, since OWS "India" (even accounting for the range of possible N_0 values) is considerably further from nitrate starvation than Bermuda Station "S" , and μ_1 is now part of a hyperbolic term rather than the linear one in the model of Fasham, Ducklow & McKelvie (1990) (as the results presented in Fasham, 1993, and in Chapter 3 indicate, this change has more than halved the importance of the P $\rightarrow$ D natural mortality pathway).

Away from the most important parameters, the four approaches also agree on the model's broad insensitivity to bacterial and detrital parameters (*e.g.* V_b, k_4, μ_3, μ_4 and V). From the equilibrium work in

[5]Note also that the range of values permitted to m in this analysis was considerably narrower than that in Chapter 4. This indicates a potential flaw in the results of this parameter sensitivity study. However, as it is difficult to obtain accurate limits for parameter values (Fasham, Ducklow & McKelvie, 1990, used a nominal range for m for instance), the approach here of assuming $\pm$ 30% is defensible as a conservative approach.

Annual NPP							
Param.	**Det. L.**	**Param.**	**Det. U.**	**Param.**	**MC**	**Param.**	**SP**
m	1.000	m	1.000	m	1.000	m	1.000
V_b	1.002	μ_3	1.000	k_4	1.000	η	1.000
k_4	0.998	k_4	1.002	μ_1	1.000	μ_4	1.000
μ_3	0.998	V	1.002	μ_4	1.000	γ	1.000
μ_4	0.995	η	1.004	γ	1.000	μ_3	1.000
V	0.995	μ_4	1.005	k_1	1.000	μ_1	1.000
η	0.994	V_b	0.993	η	1.000	V_b	1.000
k_5	1.006	k_5	0.991	μ_3	1.000	V	1.000
μ_1	0.985	μ_1	1.015	V	1.000	k_4	1.000
k_1	0.984	k_1	1.016	k_5	1.000	N_0	1.000
N_0	1.022	γ	1.029	V_b	0.999	k_1	1.000
γ	0.971	k_c	1.083	k_3	1.002	k_5	0.999
k_c	0.936	k_6	1.112	k_2	0.997	g	0.999
k_6	0.909	N_0	0.879	k_c	1.004	k_c	1.001
k_2	0.905	k_2	1.127	k_6	0.996	β	0.997
ψ	0.903	β	1.130	k_w	1.006	μ_2	0.996
p_1	0.894	ψ	1.132	ψ	1.006	k_6	1.004
k_w	0.822	p_1	1.155	p_1	1.010	p_1	1.004
V_p	1.197	k_w	1.246	N_0	0.986	k_2	1.006
α	1.202	α	0.733	g	1.014	ψ	1.006
λ	1.203	λ	0.731	λ	0.986	k_w	1.009
k_3	1.266	V_p	0.719	V_p	0.984	α	0.990
μ_2	1.303	k_3	0.635	α	0.983	λ	0.989
g	0.643	μ_2	0.629	μ_2	0.980	V_p	0.988
β	0.633	g	1.401	β	0.954	k_3	0.975

Table 5.1: Sensitivity of annual NPP at OWS "India" to model parameters for deterministic, Monte Carlo and stochastic parameters techniques. The baseline deterministic solution (annual NPP = 940.2 mmol N m^{-2} y^{-1}) is compared to solutions produced by deterministic runs at lower (**Det. L.**) and upper (**Det. U.**) ends of parameter range, and to the mean solutions produced by stochastic techniques (**Monte Carlo** and **Stochastic parameters**). This produces a table of relative differences to the baseline solution (= 1.0) which is then ranked. Sensitivity of the model to parameters increases towards the bottom of the table.

f–ratio							
Param.	**Det. L.**	**Param.**	**Det. U.**	**Param.**	**MC**	**Param.**	**SP**
k_4	1.000	k_1	0.999	γ	1.000	μ_4	1.000
k_1	1.000	k_4	0.999	k_1	1.000	N_0	1.000
V_b	0.999	V_b	1.001	ψ	1.000	V_b	1.000
k_6	0.999	m	0.999	V_b	1.000	μ_1	1.000
m	1.001	k_w	0.996	m	1.000	m	1.000
N_0	0.998	γ	0.995	k_4	1.000	k_c	1.000
γ	1.005	k_6	1.006	μ_4	1.000	k_4	1.000
k_5	0.994	μ_4	1.007	k_5	1.000	γ	1.000
μ_4	0.993	ψ	0.993	k_c	1.000	k_1	1.000
ψ	1.007	k_5	1.007	η	1.000	μ_3	1.000
k_c	1.009	k_c	0.990	μ_1	1.000	k_5	1.000
μ_2	1.012	k_3	1.017	μ_3	1.001	p_1	1.000
k_3	1.012	μ_3	1.020	k_6	1.001	η	1.000
g	1.014	N_0	1.020	p_1	0.999	V	1.000
μ_3	0.983	η	0.973	k_2	1.002	k_3	1.001
α	0.982	μ_1	0.973	N_0	1.002	β	0.999
λ	0.982	p_1	0.973	k_w	1.003	k_6	1.001
p_1	1.022	k_2	0.968	V	0.996	ψ	0.999
k_w	1.022	μ_2	1.043	k_3	1.005	k_w	1.001
μ_1	1.027	α	1.043	λ	1.005	μ_2	1.001
V	1.027	λ	1.044	α	1.005	g	1.001
η	1.028	V	0.954	V_p	1.006	k_2	0.999
k_2	1.029	V_p	1.062	μ_2	1.009	α	1.002
V_p	0.969	g	1.105	g	1.017	λ	1.002
β	0.776	β	1.357	β	1.022	V_p	1.002

Table 5.2: Sensitivity of the annual f–ratio at OWS "India" to model parameters for deterministic, Monte Carlo and stochastic parameters techniques. The baseline deterministic solution (annual f–ratio = 0.505) is compared to solutions produced by deterministic runs at lower (**Det. L.**) and upper (**Det. U.**) ends of parameter range, and to the mean solutions produced by stochastic techniques (**Monte Carlo** and **Stochastic parameters**). This produces a table of relative differences to the baseline solution (= 1.0) which is then ranked. Sensitivity of the model to parameters increases towards the bottom of the table.

Chapter 4, this insensitivity is not unexpected.

As table 5.2 shows, the sensitivity of the annual f–ratio to model parameters is very similar to that of annual NPP. The model is most sensitive to phytoplankton photosynthesis and zooplankton grazing parameters, and least sensitive to bacterial and detrital parameters. Contrary to the findings of Fasham, Ducklow & McKelvie (1990)for Bermuda Station "S", but in keeping with the results already found here, the annual f–ratio is fairly insensitive to parameters k_1, N_0 and μ_1.

Sensitivity and stochastic distributions

While the results produced by deterministic solutions at upper and lower parameter limits consist of only a single value for both annual NPP and the annual f–ratio, both stochastic approaches produce many such values, of which only the mean values were used to produce tables 5.1 and 5.2. Figures 5.5 to 5.8 show the distributions of both annual NPP and the annual f–ratio produced for each model parameter by both the Monte Carlo and stochastic parameters techniques. In each case, a histogram of the distribution produced is shown together with the mean of the distribution and the deterministic baseline value of the measure in question. Because of space considerations, the results for parameter k_4 are not shown. The summary results for this relatively minor parameter are still included in all of the relevant tables however.

The most obvious feature of these distributions is the difference between the Monte Carlo and stochastic parameters techniques. The latter produces distributions which are normal in shape, and usually symmetrical about the mean. By contrast, all of the Monte Carlo simulations have non–normal distributions. Most are fairly uniform distributions, usually with a mild slope from one edge of the distribution to the other. However, some parameters (*e.g.* β and N_0 for annual NPP; λ, k_w, μ_2, g and N_0 for the annual f–ratio) have skewed distributions, with relatively narrow regions containing a disproportionate number of simulation results.

Another difference between the two techniques is the range of results produced. While individual Monte Carlo runs have annual NPP ranging from around 600 to 1300 mmol N m^{-2} y^{-1}, stochastic parameter runs only range from around 875 to 1000 mmol N m^{-2} y^{-1}.

Differences in distribution and range between the Monte Carlo and stochastic parameters techniques were similarly reported by Kremer (1983) with his algal model. However, as his work used a two species competition model which, for Monte Carlo simulations, invariably led to the extinction of one of the algal species, it is difficult to discern whether these differences in the distribution of system measures were caused by differences in the techniques used, or by the extinction–prone structure of the model itself.

In the context of parameter sensitivity, the distributions reveal that simple comparisons between simulation means and the deterministic baseline solution can miss the effects of important parameters. For example, the results of Monte Carlo simulations for parameters k_3 and g, and stochastic parameters sim-

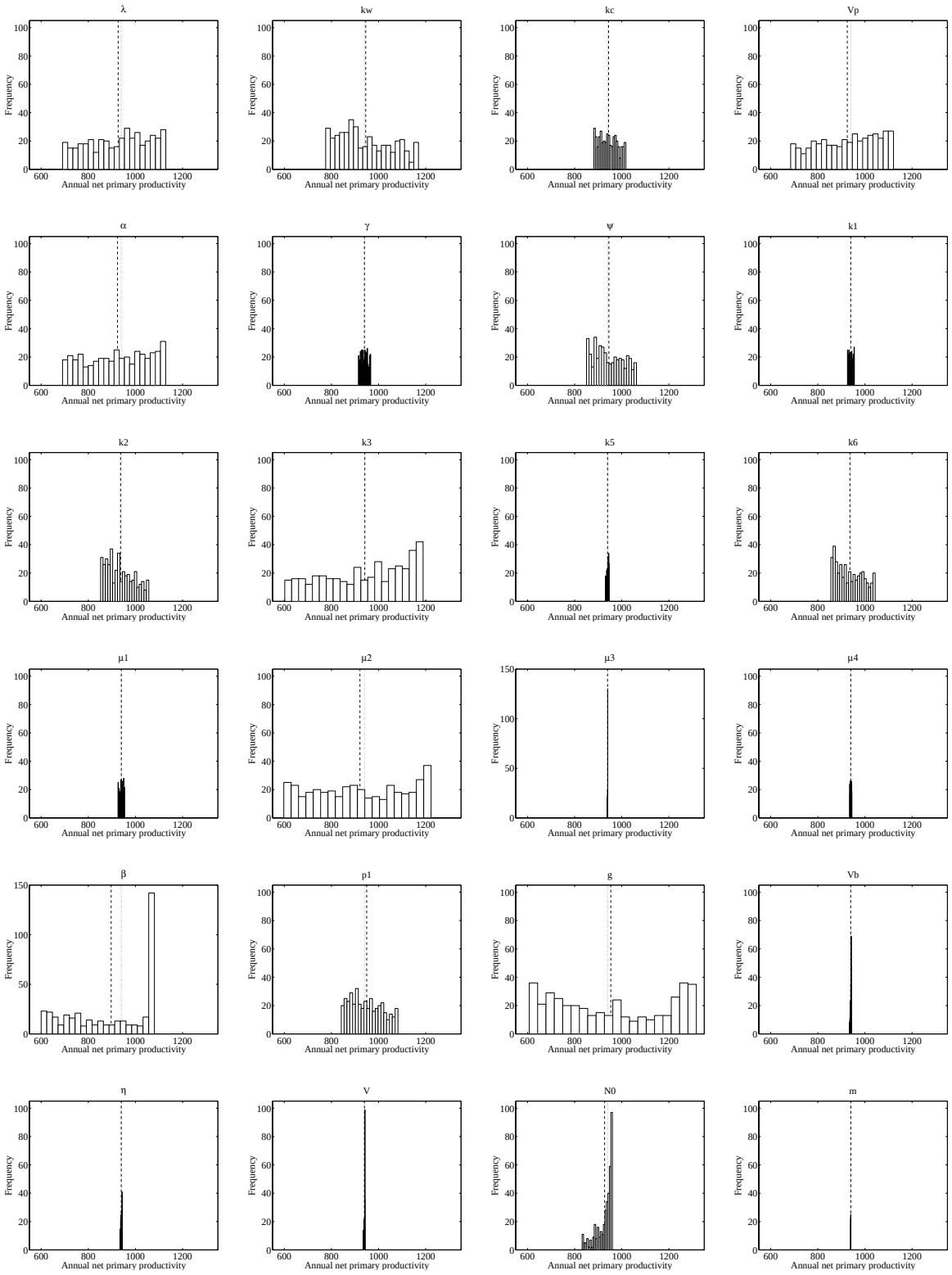

Figure 5.5: Frequency distributions of annual NPP for each model parameter produced by Monte Carlo simulations at OWS "India". The dotted line marks annual NPP for the deterministic solution with baseline parameter values. The dashed line marks mean annual NPP from the stochastic simulations. Note the change in vertical scale on the histograms of model parameters μ_3 and β. Annual NPP in mmol N m^{-2} y^{-1}.

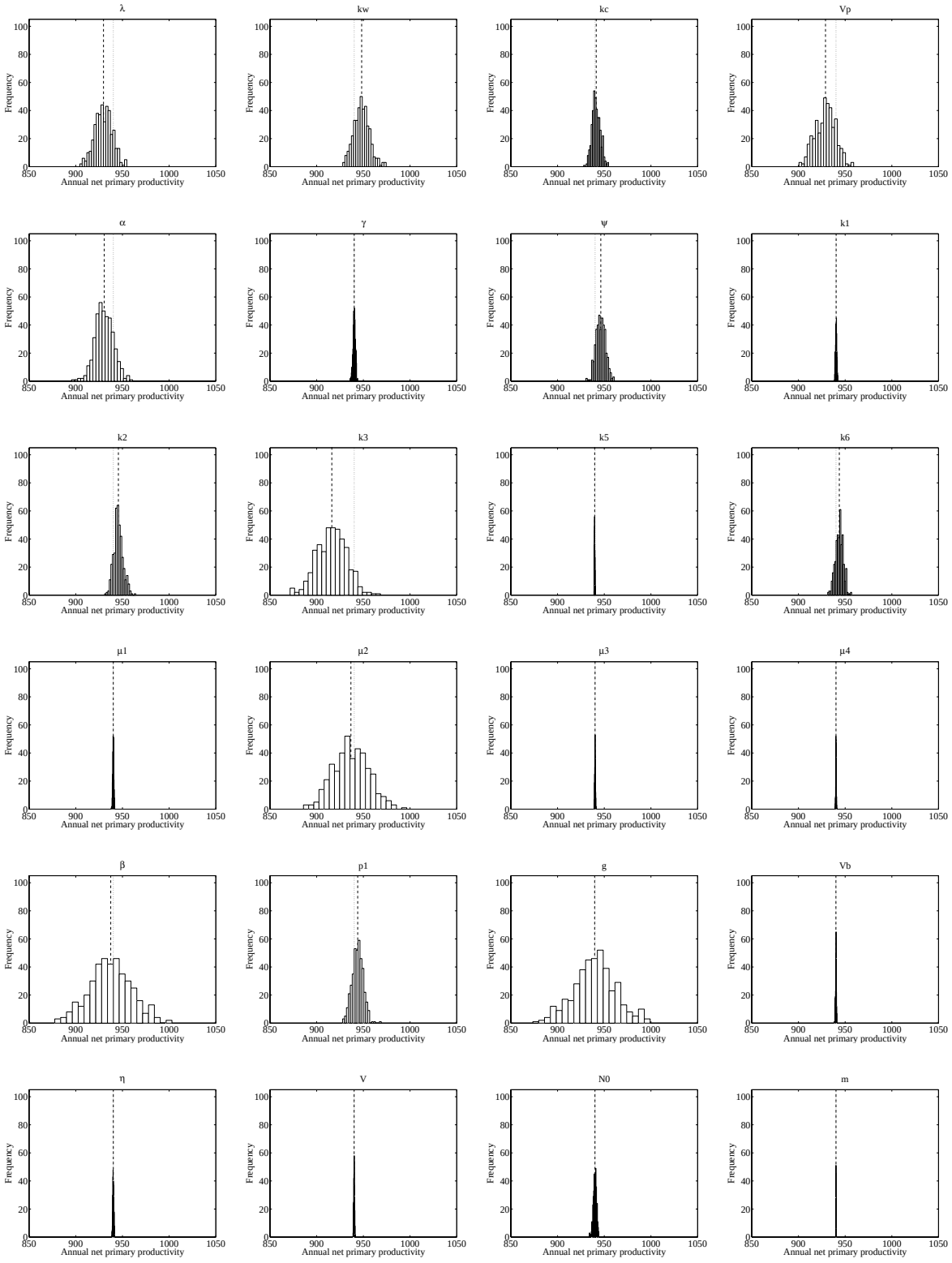

Figure 5.6: Frequency distributions of annual NPP for each model parameter produced by stochastic parameter simulations at OWS "India". The dotted line marks annual NPP for the deterministic solution with baseline parameter values. The dashed line marks mean annual NPP from the stochastic simulations. Annual NPP in mmol N m^{-2} y^{-1}.

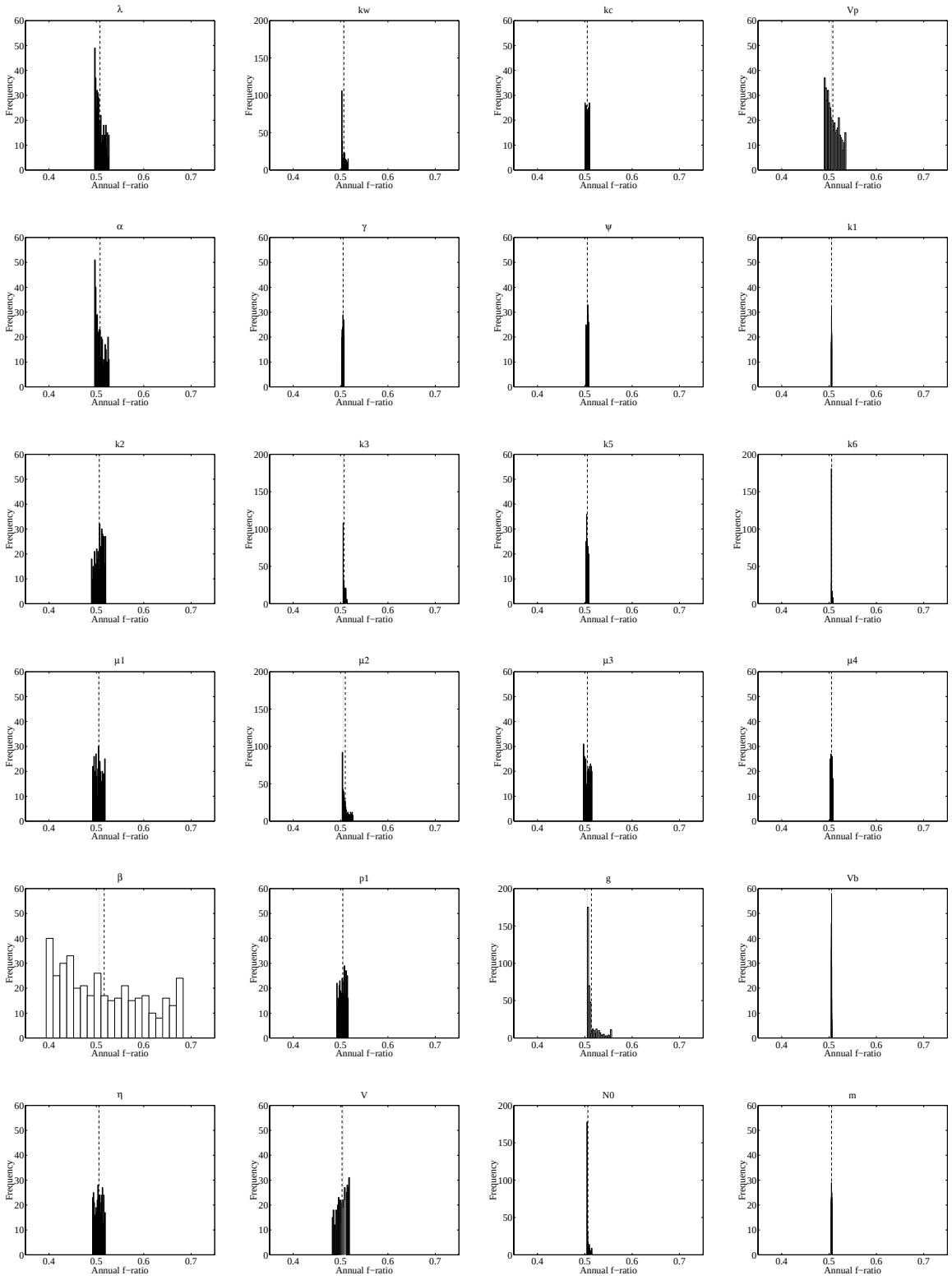

Figure 5.7: Frequency distributions of the annual f–ratio for each model parameter produced by Monte Carlo simulations at OWS "India". The dotted line marks the annual f–ratio for the deterministic solution with baseline parameter values. The dashed line marks mean annual f–ratio from the stochastic simulations. Note the change in vertical scale on the histograms of model parameters k_w, k_3, μ_2, g and N_0. The f–ratio is non–dimensional.

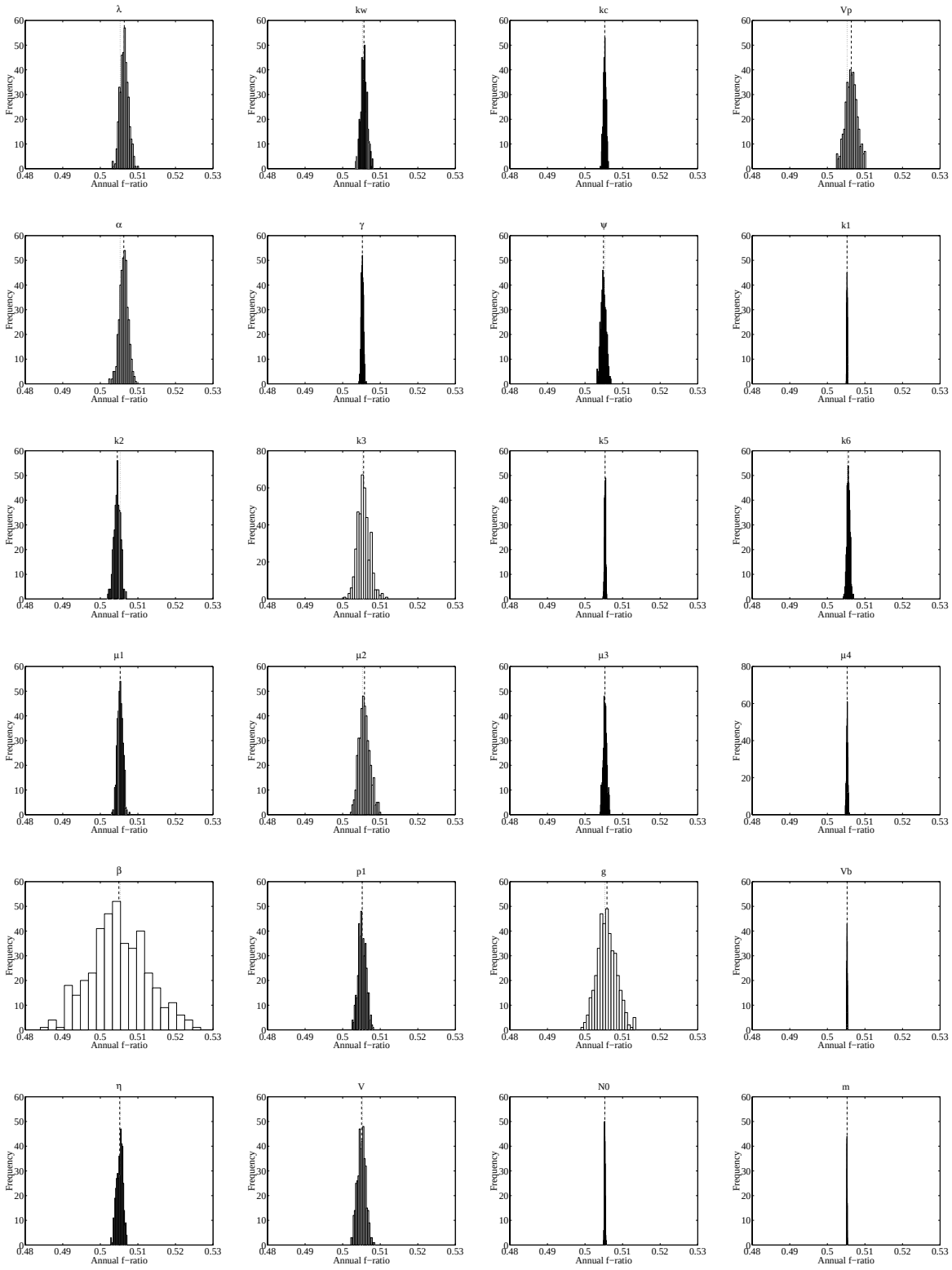

Figure 5.8: Frequency distributions of the annual f–ratio for each model parameter produced by stochastic parameter simulations at OWS "India". The dotted line marks the annual f–ratio for the deterministic solution with baseline parameter values. The dashed line marks mean annual f–ratio from the stochastic simulations. Note the change in vertical scale on the histograms of model parameters k_3 and μ_4. The f–ratio is non–dimensional.

ulations for β and g, show that a parameter can have a strong influence on the range of simulation results but leave little trace of this in the simulation mean. These parameters appear less significant in tables 5.1 and 5.2 but become among the most important when the range of results are considered. Table 5.3 shows an alternative ranking of the results from Monte Carlo and stochastic parameters simulations in which the standard deviations of the distributions are instead used to quantify model sensitivity to parameters.

While these new rankings do not cause any major revisions of the results already discussed (the same photosynthesis and grazing parameters dominate, while the same bacterial and detrital parameters are still of minor importance), they underline the fact that analyses should take account of more than just mean behaviour of simulations. Parameter g, for instance, is ranked 13th in significance when mean annual NPP in stochastic parameters simulations is used for ranking. When its effects on the distribution of annual NPP are considered it becomes the most important parameter. Figure 5.9 shows the comparison between deviation of the stochastic mean from the baseline deterministic solution and stochastic standard deviation. In three of the four cases shown, the parameter which causes the greatest standard deviation is not the same as the parameter which shows the greatest deviation in its stochastic mean from the deterministic solution. As would be expected, parameters which produce deviance from the deterministic solution in their stochastic means tend to have greater standard deviations (since parameters are stochastically assigned values from a *continuous* distribution), but the reverse is clearly not true. Given that the parameters here are assigned stochastic values symmetrically about their baseline value, and that the response of the model equilibrium to changes in the parameter value is not necessarily symmetrical (see figures 4.9 to 4.13 in Chapter 4), then results such as this are not unexpected (although they may be difficult to predict given the complexity of the model).

A marked difference between results for annual NPP and the annual f–ratio, which is reflected in the simulations of both stochastic techniques, is that although different parameters affect these two system measures differently, there is a fairly continuous range of parameter sensitivities with annual NPP, whereas with the annual f–ratio, the model is acutely sensitive to a single parameter (β) and considerably less sensitive to all of the others. Both techniques find that modelled annual NPP is most sensitive to parameter g, but find that it is relatively closely followed by a string of other parameters to which the model is almost as sensitive. In contrast, with the annual f–ratio both techniques find that parameter β is the most influential, but that its rivals lag considerably behind it in importance. In the case of Monte Carlo simulations, its nearest rival, V_p, induces less than a sixth of the variability that β produces (with stochastic parameters, the closest rival, g, induces only slightly more than a third of the variability of β). This extreme sensitivity to β is particularly curious since the parameter has no direct dealings with either nitrate or ammonium (unlike parameters k_1, k_2 or ψ).

Sensitivity of state variables

All of the work so far has focussed on the sensitivity of two major system measures to changes in parameter values. Annual NPP measures the total quantity of nitrogen absorbed by model phytoplankton,

Monte Carlo				Stochastic parameters			
Param.	**NPP**	**Param.**	**f–ratio**	**Param.**	**NPP**	**Param.**	**f–ratio**
m	0.188	k_1	0.128	m	0.022	m	0.027
μ_3	0.850	k_4	0.158	k_4	0.275	k_4	0.036
k_4	1.157	V_b	0.186	k_5	0.276	V_b	0.043
V_b	2.158	m	0.309	μ_4	0.286	k_1	0.086
V	2.190	k_6	1.013	μ_3	0.359	N_0	0.115
η	2.483	γ	1.324	V_b	0.441	k_5	0.162
μ_4	2.607	k_5	1.908	V	0.444	μ_4	0.184
k_5	4.133	μ_4	1.929	η	0.566	γ	0.300
μ_1	8.111	ψ	2.013	μ_1	0.603	k_c	0.389
k_1	8.687	k_3	2.184	k_1	0.718	k_6	0.415
γ	14.946	N_0	2.620	γ	1.324	μ_3	0.509
N_0	34.015	k_c	2.762	N_0	1.774	ψ	0.711
k_c	39.049	k_w	4.291	k_6	4.251	μ_1	0.717
k_6	55.929	μ_3	5.476	k_c	4.438	η	0.842
k_2	57.106	μ_2	6.401	k_2	5.018	k_w	0.871
ψ	61.021	p_1	6.866	ψ	5.110	k_2	0.883
p_1	67.234	η	7.773	p_1	5.955	p_1	1.057
k_w	111.627	μ_1	7.790	k_w	8.343	V	1.109
V_p	126.170	k_2	8.590	λ	9.295	λ	1.118
λ	126.459	λ	8.868	α	9.818	α	1.140
α	130.153	α	9.153	V_p	10.759	μ_2	1.450
β	171.833	V	10.589	k_3	15.913	V_p	1.585
k_3	176.993	g	12.468	μ_2	18.952	k_3	1.630
μ_2	193.203	V_p	13.092	β	22.483	g	2.577
g	234.591	β	86.910	g	22.554	β	7.562

Table 5.3: Sensitivity of annual NPP (**NPP**) and the f–ratio (**f–ratio**) to model parameters at OWS "India" . Stochastic simulations performed using both Monte Carlo and stochastic parameters techniques, and sensitivity assessed by ranking of parameters by standard deviation. Sensitivity of model to parameters increases towards the bottom of the table. Note that both sets of f–ratio standard deviations have been multiplied by a factor of 1000 for clarity. Annual NPP in mmol N m^{-2} y^{-1}. The f–ratio is dimensionless.

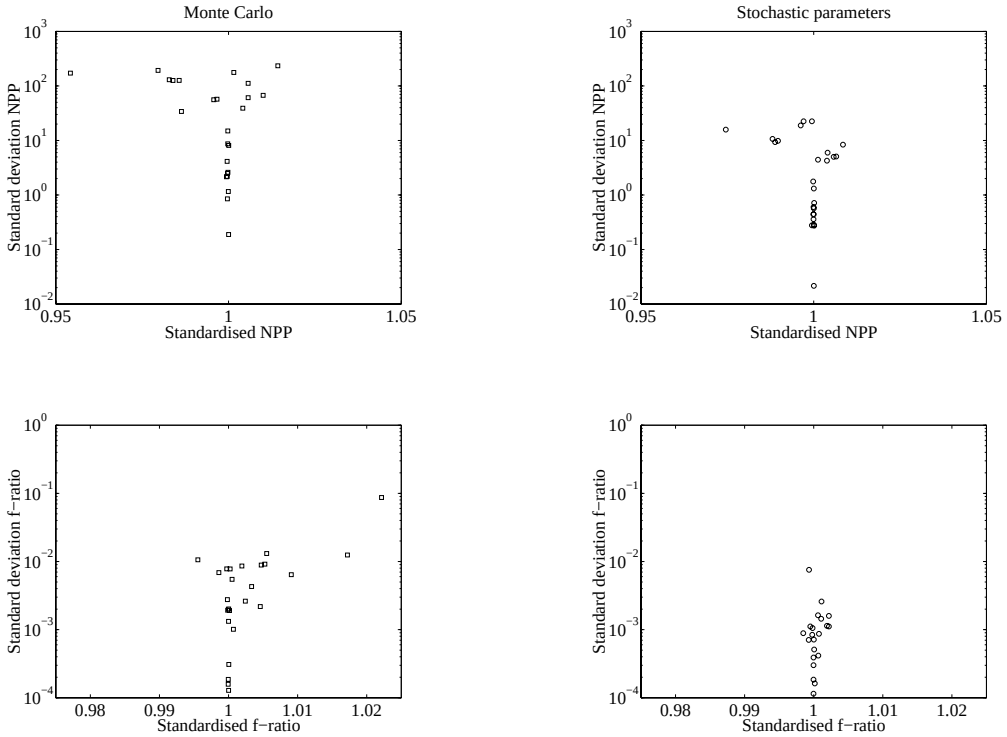

Figure 5.9: Comparing the standardised deviation of stochastic means from the deterministic solution with the standard deviation of the stochastic distributions. Annual NPP (top row) and the annual f–ratio (bottom row) considered for both Monte Carlo (left) and stochastic parameter (right) techniques. Each marker indicates a different model parameter. Note that the scales on each pair of graphs is constant, and that standard deviations are plotted on a logarithmic scale. Means of both measures standardised to those from the deterministic solution (*i.e.* deterministic baseline value = 1.0).

and available for their growth processes (or to those of the zooplankton which graze upon them). The annual f–ratio quantifies the fraction of modelled annual NPP which is supported by nitrate uptake ("new" production), and this fraction of total production is considered important because it is coupled to the transfer of biomass to the deep ocean and, potentially, its burial in sediments on the ocean floor ("regenerated" production involves the use of nitrogen from organic sources recycled in the mixed layer; as it has already been recycled, such organic material clearly cannot be buried on the ocean floor). These system measures are important to the issue of climate change, since they relate to biogeochemical pathways which play an important role in the regulation of carbon dioxide in the earth's atmosphere.

However, in the validation of models where, for instance, the importance of specific model compartments, rather than global measures, may be significant, examining the sensitivity of other measures may be more appropriate. To this end, tables of the sensitivity of each of the model's state variables (plus **Total N**, the total concentration of nitrogen in the modelled mixed layer) to each of its parameters were constructed from the results of the Monte Carlo and stochastic parameters techniques. These tables used

annual means of daily standard deviation for each of the state variables, and then ranked the importance of each parameter to these measures. Tables 5.4 and 5.5 show the results of this procedure. Comparable tables using the deterministic solutions produced at upper and lower parameter limits were not constructed, primarily because the choice of deviation metric (from the baseline solution) was not simple, but also because the previous sensitivity results broadly agreed with those of the stochastic approaches.

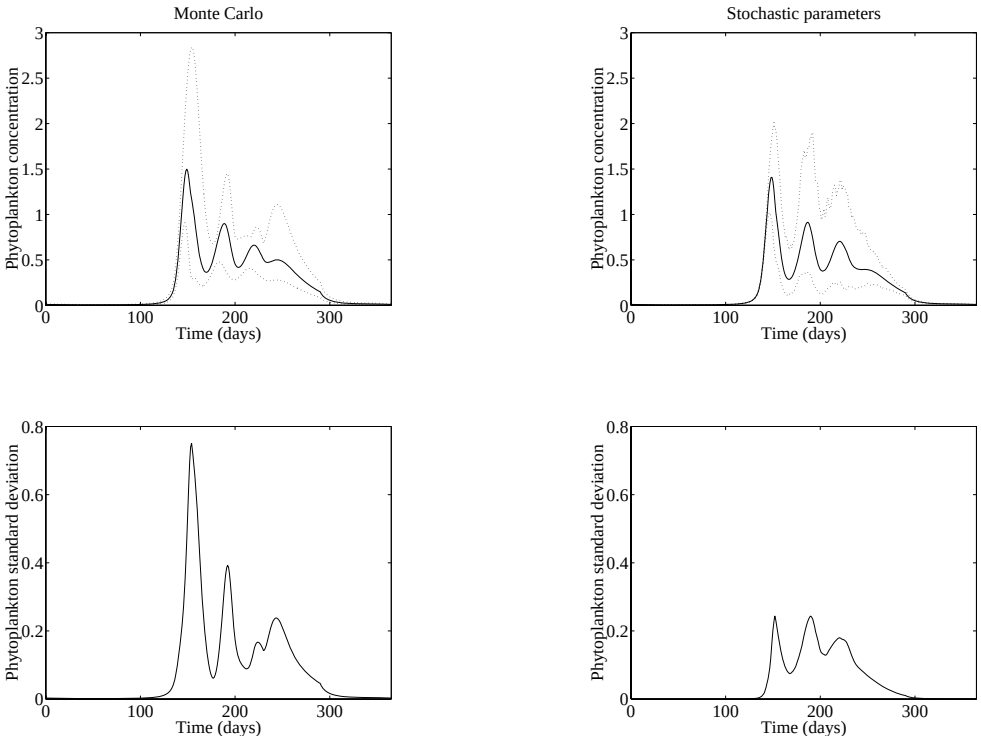

Figure 5.10: Variability in the seasonal cycle of phytoplankton concentration for Monte Carlo (left) and stochastic parameters (right) techniques. Parameter g variable in both cases (1.0 $d^{-1} \pm 30\%$; transformation period of 1 day for stochastic parameters). The top row of plots show the daily mean (solid), and minimum and maximum (dotted) concentrations produced by the two techniques. Concentrations (and standard deviations) in mmol N m^{-3}.

The parameter sensitivity results again show broad agreement with those already presented. Most model compartments (especially phytoplankton and zooplankton) are sensitive to the same parameters as annual NPP and the annual f–ratio. Phytoplankton photosynthesis and zooplankton grazing parameters dominate, but certain compartments show greater sensitivity to other parameters. With both stochastic techniques, nitrate and total nitrogen are very sensitive to N_0, the concentration of subthermocline nitrate. As this parameter is critical in controlling the quantity of nitrogen in the modelled system (most of which remains as nitrate in the short OWS "India" summers) this result is unsurprising. In Monte Carlo simulations, this rise in importance is slightly matched by that of m, the cross–thermocline mixing rate, which also plays a role in supplying nitrate to the mixed layer. However, as entrainment of nitrate from the deep ocean by seasonal wind–mixing is very important at OWS "India", cross–thermocline mixing

Monte Carlo							
P	**Z**	**B**	**D**	$\mathbf{N}_n$	$\mathbf{N}_r$	$\mathbf{N}_d$	**Total N**
m	m	m	m	k_4	m	m	k_4
μ_4	k_4	k_1	k_4	m	μ_4	k_1	V_b
k_1	μ_4	μ_4	k_1	k_5	μ_3	μ_4	m
μ_3	k_1	k_5	μ_3	γ	k_5	N_0	k_5
k_4	μ_3	γ	k_5	V_b	k_4	k_5	γ
η	k_5	V	μ_4	μ_4	k_1	V	k_1
k_5	γ	μ_1	γ	k_1	p_1	η	μ_3
γ	V_b	N_0	η	μ_3	γ	γ	μ_4
V	η	η	V_b	μ_1	η	μ_1	η
V_b	k_6	k_2	μ_1	η	V_b	k_c	μ_1
N_0	V	k_c	N_0	V	μ_1	k_2	k_c
μ_1	μ_1	p_1	p_1	k_c	k_6	ψ	V
ψ	N_0	ψ	ψ	k_2	k_2	p_1	k_2
k_2	ψ	k_4	k_2	k_6	k_3	k_6	ψ
k_c	k_2	k_6	k_6	p_1	V	β	k_6
p_1	p_1	μ_3	k_c	ψ	N_0	μ_2	p_1
k_6	k_c	V_b	V	k_w	ψ	g	k_w
V_p	μ_2	V_p	V_p	λ	k_c	k_3	λ
λ	k_3	λ	λ	α	μ_2	V_p	α
α	k_w	α	α	V_p	V_p	μ_3	V_p
k_w	λ	k_w	k_w	k_3	k_w	k_4	k_3
k_3	α	k_3	k_3	μ_2	λ	λ	μ_2
μ_2	V_p	μ_2	μ_2	g	α	α	g
β	β	β	g	β	g	k_w	β
g	g	g	β	N_0	β	V_b	N_0

Table 5.4: Sensitivity of each of the model compartments at OWS "India" to model parameters for Monte Carlo simulations. Parameters ranked according to the mean annual standard deviation of each compartment. Sensitivity of the compartments to parameters increases towards the bottom of the table.

Stochastic parameters							
P	**Z**	**B**	**D**	**N**$_n$	**N**$_r$	**N**$_d$	**Total N**
m	m	m	m	m	m	m	m
N_0	k_5	N_0	N_0	k_5	k_5	N_0	k_4
μ_4	μ_4	k_5	γ	γ	γ	k_1	γ
k_5	N_0	k_1	k_5	k_4	N_0	k_5	V_b
k_4	γ	μ_1	k_4	μ_4	μ_4	V	k_5
k_1	k_4	μ_4	k_1	V_b	k_4	μ_1	k_1
γ	k_1	γ	V_b	k_1	k_1	η	μ_3
μ_3	V_b	V	μ_3	μ_3	V_b	μ_4	μ_4
V_b	μ_3	μ_3	μ_4	μ_1	μ_3	ψ	η
η	μ_1	k_c	η	η	μ_1	k_2	μ_1
V	V	η	μ_1	V	V	k_c	k_c
μ_1	η	k_6	k_6	k_6	η	μ_3	V
k_c	k_c	k_4	k_c	k_2	k_6	k_6	k_6
k_6	k_6	k_2	k_2	k_c	k_c	γ	k_2
k_2	k_2	ψ	ψ	p_1	k_2	p_1	ψ
ψ	ψ	V_b	V	ψ	ψ	μ_2	k_w
k_w	k_w	p_1	p_1	k_w	k_w	V_p	p_1
p_1	p_1	k_w	k_w	λ	p_1	k_3	λ
α	α	α	α	α	α	β	α
λ	λ	λ	λ	V_p	λ	λ	V_p
V_p	V_p	V_p	V_p	k_3	V_p	α	k_3
k_3	k_3	k_3	k_3	μ_2	k_3	g	μ_2
μ_2	μ_2	μ_2	μ_2	g	μ_2	k_4	g
β	β	β	g	N_0	β	k_w	β
g	g	g	β	β	g	V_b	N_0

Table 5.5: Sensitivity of each of the model compartments to model parameters for stochastic parameter simulations. Parameters ranked according to the mean annual standard deviation of each compartment. Sensitivity of the compartments to parameters increases towards the bottom of the table.

plays a less important role (though its role is likely to be much greater at locations like Bermuda Station "S", where seasonal mixing is less extreme). Another marked shift in the importance of parameters occurs with the DON compartment. Although this compartment is strongly coupled to the phytoplankton and zooplankton compartments because of their inputs to it, bacterial parameters V_b and k_4 (and, in Monte Carlo simulations, μ_3), hitherto considered minor from their annual NPP and annual f–ratio results, become of much greater importance. This result stems from the role bacteria play as the sole sink for DON. In contrast, the bacterial compartment itself is by far most sensitive to the phytoplankton and zooplankton parameters already mentioned (the insensitivity of the bacterial compartment to its own parameters was also remarked upon in Chapter 4).

Aside from the differences already mentioned, the results of the Monte Carlo and stochastic parameters simulations are relatively similar. The Monte Carlo results show more variability in the precise placing of parameters on the sensitivity tables (by contrast, with the stochastic parameters technique, four compartments share exactly the same "top 7" parameters), but aside from this minor difference, it is difficult to distinguish any further shifts in the sensitivity to different parameters between the techniques.

Although the work in this section has focussed on mean variance of the state variables across a simulated annual cycle, variance is not constant across this period. Figure 5.10 shows the results of variability in parameter g (zooplankton maximum ingestion rate; one of the most influential parameters in the earlier analysis) on the daily range and standard deviations of phytoplankton concentrations for both Monte Carlo and stochastic parameters techniques.

Both techniques find that variance around the mean solution is seasonal, with greatest variance during the summer months (this pattern is also reflected in the coefficient of variation, although to a lesser degree; results not shown). Both techniques also produce very similar patterns of mean concentration across the year, both to each other, and to the deterministic solution. In particular, the summer oscillations appear strongly in both the means and variance produced by the two techniques.

The two techniques differ in the magnitude of the variance they produce, with Monte Carlo often producing daily standard deviations more than double those of the stochastic parameters technique. The variance of the Monte Carlo simulations also hints at a slight "fourth oscillation" during the autumn months. The daily ranges of results between the two techniques also differ. The Monte Carlo range is smooth, probably because it represents the solutions produced by values of g at the extremes of the parameter's range. By contrast, the range produced by 400 runs of the stochastic parameters technique is jagged, presumably because of the daily parameter transformation.

5.5.3 Conclusions

This section has detailed an examination of the sensitivity of the Fasham (1993) model to 25 of its parameters under OWS "India" forcing. The deterministic approach outlined in Fasham, Ducklow & McKelvie (1990) and two stochastic approaches were used, principally to determine the sensitivity of two key system measures, annual NPP and the annual f–ratio, to variations in the values of the model parameters under question. In addition to the parameter comparisons themselves, the significance of the choice of measure by which to compare the parameters was also examined.

In performing their deterministic analysis, Fasham, Ducklow & McKelvie (1990) found that parameters k_w, λ, α, μ_1, N_0, g and k_1 strongly influenced the model's behaviour at Bermuda Station "S". Although the analysis here focussed on OWS "India", most of these parameters were still found to be important. The parameter sensitivities of both system measures were dominated by phytoplankton photosynthesis and zooplankton grazing parameters. Parameters dealing with other model compartments (in particular those pertaining to bacteria) were of much lesser importance. Despite the variety in the techniques used to study parameter sensitivity, there was broad agreement on which were the most, and least, significant parameters. When sensitivity studies were extended to variability in model compartments across the year, very similar results were found, although some otherwise low importance parameters were found to be important to particular compartments.

Examination of the distribution of the two system measures in question found that the two stochastic approaches differed greatly in their results. Stochastic parameters produced normal–like curves, while Monte Carlo produced near–uniform or strongly skewed distributions. The variance of these results also illustrated that the results of stochastic techniques should be assessed by their standard deviations as well as their means.

5.6 Parameter sensitivity at Bermuda Station "S"

The previous section examined the sensitivity of the Fasham (1993) model to each of its parameters under the OWS "India" forcing regime. In this section the procedure is repeated, but for the Bermuda Station "S" forcing regime. Since the different approaches to measuring parameter sensitivity in the last section broadly agreed on which parameters the model was most sensitive to, for this section only the stochastic parameters technique is reprised.

Simulations for each of the model parameters were performed as described previously. The baseline parameter values used were those used previously for Bermuda Station "S" simulations (*i.e.* identical to those for OWS "India", with the exception of parameters V_p and N_0). Uniform $\pm$ 30% distributions around the baseline values of each of the parameters were used to generate stochastic values every sim-

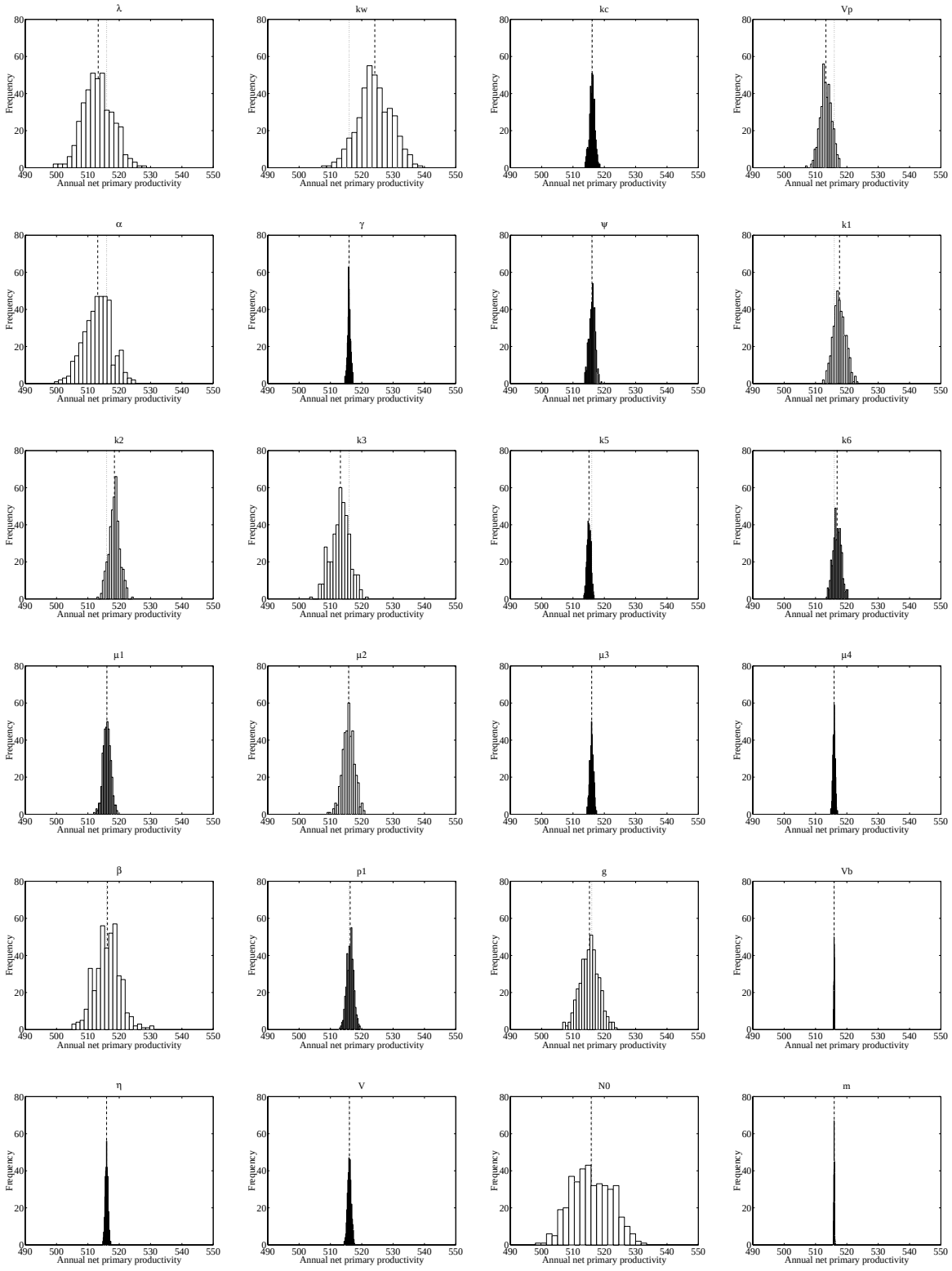

Figure 5.11: Frequency distribution of annual NPP for each model parameter produced by stochastic parameter simulations at Bermuda Station "S". The dotted line marks annual NPP for the deterministic solution with baseline parameter values. The dashed line marks mean annual NPP from the stochastic simulations. Annual NPP in mmol N m^{-2} y^{-1}.

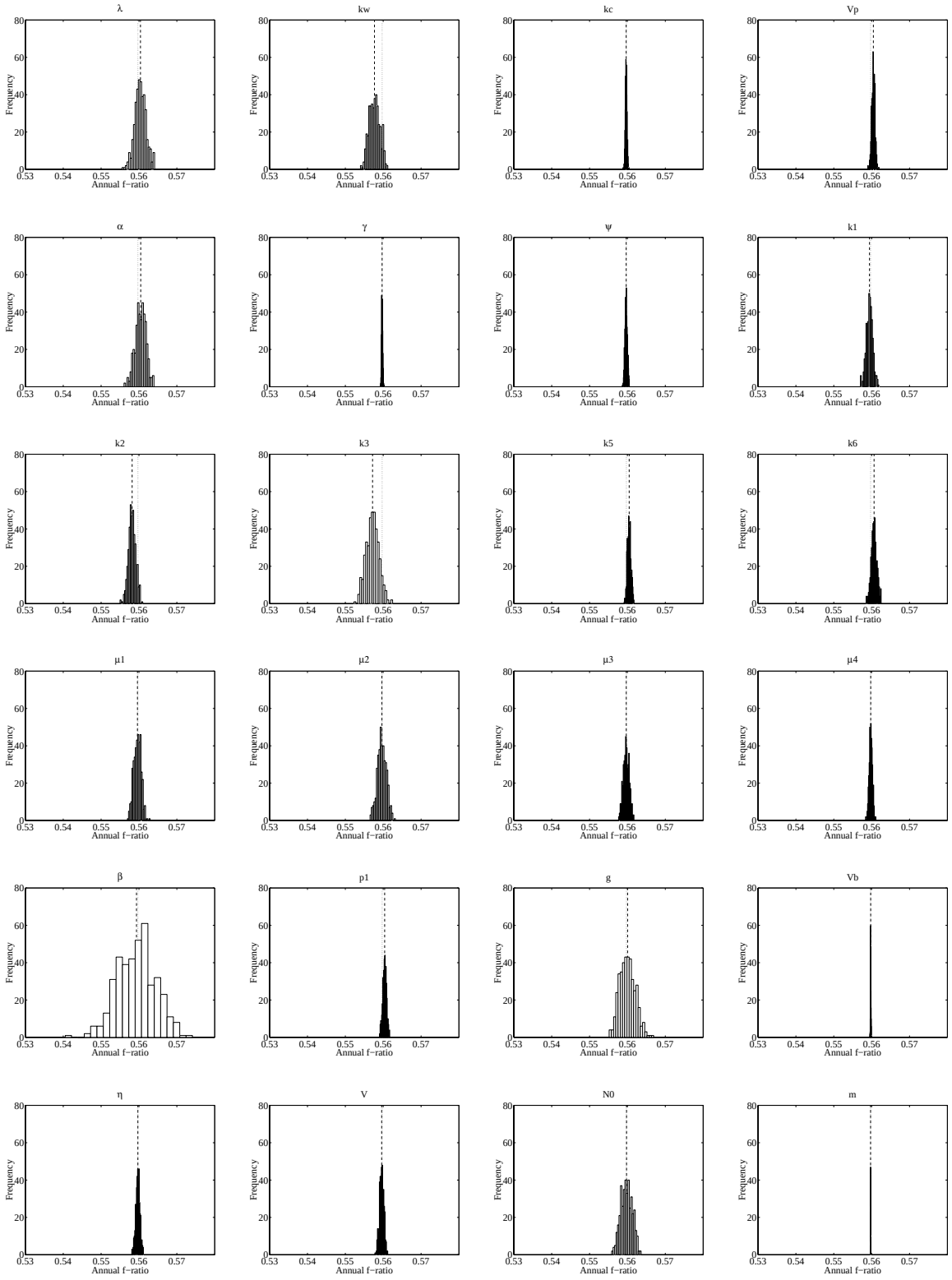

Figure 5.12: Frequency distributions of the annual f–ratio for each model parameter produced by stochastic parameter simulations at Bermuda Station "S". The dotted line marks annual NPP for the deterministic solution with baseline parameter values. The dashed line marks mean annual NPP from the stochastic simulations. The f–ratio is non–dimensional.

Annual NPP				f–ratio			
Param.	**Mean**	**Param.**	**St. dev.**	**Param.**	**Mean**	**Param.**	**St. dev.**
η	515.968	k_4	0.065	m	0.560	m	0.022
μ_3	515.966	V_b	0.066	γ	0.560	k_4	0.068
m	515.958	m	0.097	η	0.560	V_b	0.070
γ	515.952	μ_4	0.370	V_b	0.560	γ	0.147
V_b	515.931	η	0.439	μ_3	0.560	k_c	0.223
k_4	516.043	γ	0.483	μ_4	0.560	ψ	0.330
μ_4	515.920	V	0.586	N_0	0.560	μ_4	0.433
V	516.063	μ_3	0.586	k_c	0.560	V_p	0.446
ψ	516.075	k_5	0.612	ψ	0.560	k_5	0.489
μ_1	516.076	k_c	0.846	μ_2	0.560	p_1	0.515
k_c	516.125	ψ	0.964	k_4	0.560	η	0.564
N_0	515.822	p_1	1.116	V	0.560	V	0.580
μ_2	515.808	μ_1	1.213	μ_1	0.560	k_6	0.760
β	516.242	k_6	1.326	k_1	0.559	μ_3	0.792
p_1	516.309	k_2	1.756	g	0.560	k_1	0.858
g	515.266	V_p	1.839	β	0.559	k_2	0.971
k_5	515.108	μ_2	1.899	p_1	0.560	μ_1	0.973
k_6	516.886	k_1	1.963	λ	0.560	μ_2	1.197
k_1	517.663	k_3	2.988	V_p	0.560	k_w	1.398
k_2	518.468	g	3.050	α	0.560	α	1.421
V_p	513.316	β	4.091	k_5	0.560	λ	1.489
λ	513.299	α	4.410	k_6	0.561	N_0	1.522
k_3	513.185	λ	4.763	k_2	0.558	k_3	1.677
α	513.140	k_w	5.331	k_w	0.558	g	2.028
k_w	524.158	N_0	6.428	k_3	0.557	β	5.073

Table 5.6: Sensitivity of annual NPP and the f-ratio to model parameters at Bermuda Station "S". Stochastic simulations performed using the stochastic parameters technique. Parameters ranked for both system measures by difference of stochastic mean to deterministic solution (**Mean**), and by standard deviation of stochastic simulations (**St. dev.**). Sensitivity of the model to parameters increases towards the bottom of the table. Note that the f–ratio standard deviations have been multiplied by a factor of 1000 for clarity. Annual NPP in mmol N m^{-2} y^{-1}. The f–ratio is dimensionless.

ulated day for 400 separate runs. Each run was initialised with state variable values calculated from a 50 year deterministic solution, and consisted of a single transient year followed by a single sampled year.

Figures 5.11 and 5.12 respectively show the distributions of annual NPP and the annual f–ratio produced by these simulations. Table 5.6 shows the ranked parameter sensitivities of both of these measures. Parameter ranking is both by deviation of the stochastic mean from the baseline solution and by the standard deviation of the stochastic simulations.

With respect to the distributions produced, there are only mostly minor differences between the results from the two locations. As with OWS "India" simulations, parameter sensitivity is dominated by phytoplankton photosynthesis parameters and zooplankton grazing parameters (although, with annual NPP, the photosynthesis parameters are of greater importance than the grazing ones). The largest difference between the locations occurs in the importance of N_0. At OWS "India" N_0 was of relatively minor importance, mostly because the forcing regime includes a long period of deep mixing and a relatively short summer period, the effects of which prevent nitrate starvation. Bermuda Station "S", by contrast, undergoes long periods in the summer during which nitrate is at limiting levels. Consequently, variation in subthermocline nitrate is more liable to affect primary production. Though less so, the annual f–ratio is also more sensitive to N_0 at Bermuda Station "S" than at OWS "India" . As at OWS "India", parameter β dominates variability at Bermuda Station "S".

Fasham, Ducklow & McKelvie (1990) found that parameters μ_1 (utilised slightly differently in their model) and k_1 also strongly affected the model. In the case of the former parameter, its lack of importance in the earlier work at OWS "India" was put down to the change in functional form of the phytoplankton loss term between the models of Fasham, Ducklow & McKelvie (1990) and Fasham (1993). However, as figures 3.38 and 3.39 indicate, the phytoplankton loss term is of considerably greater importance at Bermuda Station "S"and, correspondingly, this is reflected in the rise in importance of μ_1 in the results here. Although only rising from 17th to 13th position in the annual NPP rankings (and 13th to 9th in the annual f–ratio rankings), μ_1 more than doubled its variability between the two stations (noteworthy since the variability of most other important parameters fell substantially between the stations). The same changes occurred with parameter k_1, which both rose in position and absolute variability between OWS "India" and Bermuda Station "S" (in the case of the annual f–ratio, k_1's variability rose by almost an order of magnitude).

The only other major difference between simulations at the two locations is the shift in mean annual f–ratio for parameters k_w and k_3. In both cases Bermuda Station "S" simulations predict lower mean f–ratios than the baseline solution, while at OWS "India" both parameters predict higher means than their corresponding baseline solution. Aside from these (relatively major) shifts, other parameters predict means relative to the baseline solution similarly between the two locations.

5.6.1 Conclusions

This section attempted to determine any differences in the sensitivities of parameters when the model was run under different forcing conditions. The results (from only the stochastic parameters technique in this instance) were similar to those from OWS "India", but additionally found that parameters μ_1, k_1 and (especially) N_0 became more important because of changes in the forcing regime. The promotion of these parameters is partially in line with their status in Fasham, Ducklow & McKelvie (1990).

5.7 Exploring stochastic approaches

In the previous sections, stochastic techniques were used to determine sensitivity rankings for each of the Fasham (1993) model's parameters. In this section the two techniques are explored to determine the behaviour of the model in response to variation in the size of parameter variability and variation in the period of parameter transformations.

5.7.1 Distribution width

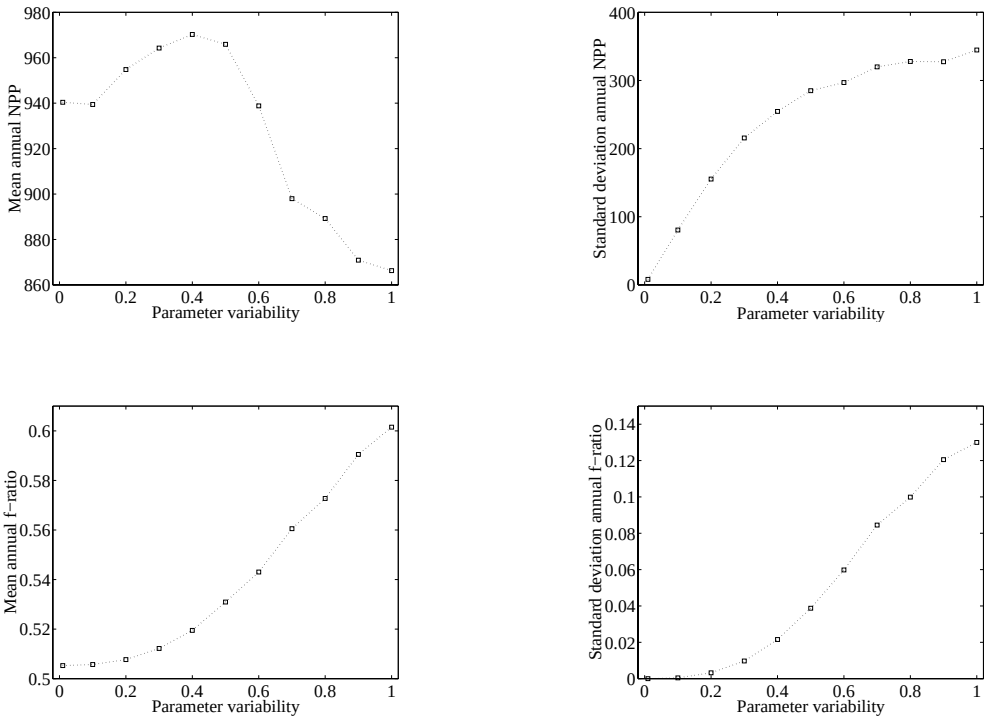

Figure 5.13: The behaviour of annual NPP and f–ratio means and standard deviations as the variability about the parameter mean is increased. Simulations apply Monte Carlo technique to model parameter g (zooplankton maximum ingestion rate). Variability around parameter mean increased from 0.01 ($\pm$ 1%) to 1.0 ($\pm$ 100%). Annual NPP in mmol N m^{-2} y^{-1}. The annual f–ratio is dimensionless.

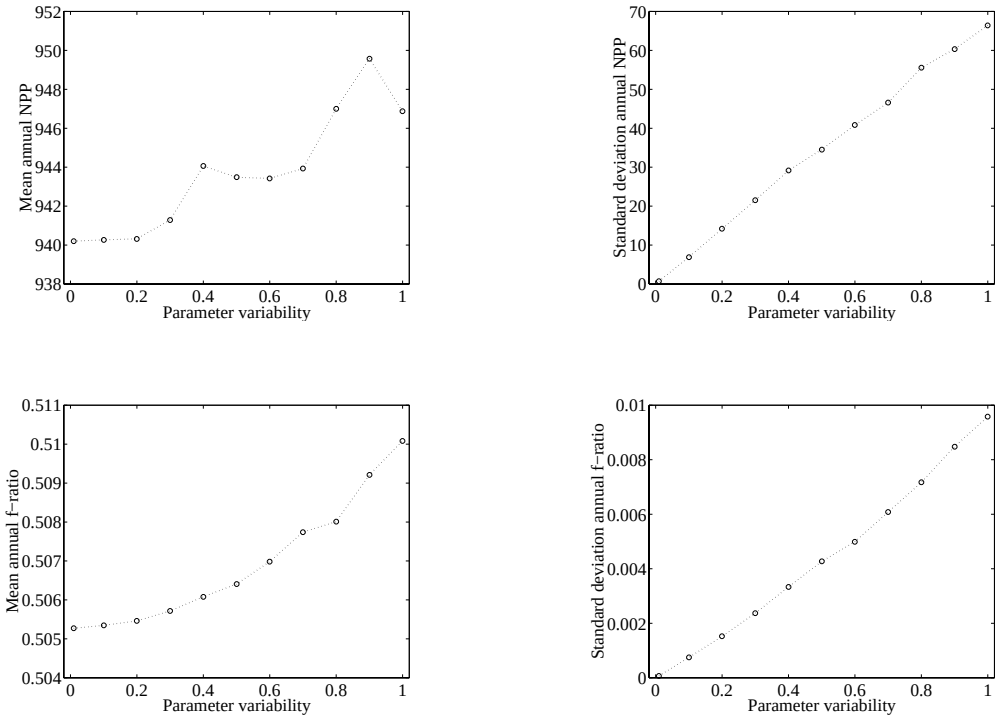

Figure 5.14: The behaviour of annual NPP and f–ratio means and standard deviations as the variability about the parameter mean is increased. Simulations apply stochastic parameters technique to model parameter g (zooplankton maximum ingestion rate). Variability around parameter mean increased from 0.01 ($\pm$ 1%) to 1.0 ($\pm$ 100%). Annual NPP in mmol N m^{-2} y^{-1}. The annual f–ratio is dimensionless.

In the earlier parameter sensitivity studies a constant variability (mean $\pm$ 30%) was used for all parameters examined. In this section simulations were performed in which the variability of g (zooplankton maximum ingestion rate), the model parameter which induced the most variability in annual NPP with both the Monte Carlo and stochastic parameters techniques, was increased from $\pm$ 1% (range : 0.99 to 1.01 d^{-1}) up to $\pm$ 100% (range : 0.0 to 2.0 d^{-1}).

Both Monte Carlo and stochastic parameters techniques were used as previously. Simulations were performed with OWS "India" forcing. All model parameters (except g) were held constant at their baseline values. The distribution of stochastic values of g were uniform around its baseline value. Stochastic parameters simulations transformed the value of g with a period of 1 day. Preliminary simulations found that for extreme parameter variability ($> 75\%$) 400 runs were not sufficient to produce reliable means and standard deviations, and consequently 1000 runs were performed for all simulations in this section. As previously, each simulation run was initialised with state variable values calculated during a 50 year deterministic solution, and consisted of a transient period (Monte Carlo : 5 years; stochastic parameters : 1 year) followed by a single sampled year.

Figures 5.13 and 5.14 show the results of the simulations for Monte Carlo and stochastic parameters techniques respectively. In both cases the behaviour of the means and standard deviations of annual NPP and the annual f–ratio are shown.

The Monte Carlo simulation results show a number of interesting (and unexpected) features. While the mean annual f–ratio shows a fairly constant, curved increase as parameter variability is increased, mean annual NPP rises at first until a parameter variability around ± 50%, then falls sharply as variability is increased to ± 100% (see figure 5.13). Both measures show increasing variability as parameter variability is increased. However, while variability in annual NPP increases in a hyperbolic form with parameter variability, variability in the annual f–ratio increases in a sigmoid fashion, with the greatest increases in variability occurring as parameter variability is increased from around ± 40% to ± 90%.

By contrast, the stochastic parameters simulations produce much simpler results. The mean annual f–ratio increases in a similar fashion to that already found in the Monte Carlo simulations (although the magnitude of increase is considerably smaller). Mean annual NPP, while being somewhat erratic in its trend with increasing parameter variability (possibly an even greater number of simulations are required to smooth this trend), generally increases with parameter variability (although again the magnitude of increase is considerably smaller than that found with Monte Carlo simulations). The variability found in both of these measures increases almost perfectly linearly with increasing parameter variability (see figure 5.14). This contrast with the results of the Monte Carlo simulations is perhaps explained by the significant difference in magnitude of variability between the two stochastic techniques. Although variability in the Monte Carlo simulations takes hyperbolic and sigmoid forms with increasing parameter variability, at values of annual NPP and f–ratio variability comparable in absolute terms with those produced during stochastic parameters simulations, both measures do not have such obviously curved relationships between parameter variability and measure variability. Curved relationships between parameter and measure variability may only occur in stochastic parameters simulations where much greater parameter variability is used (at least for parameter g).

5.7.2 Period of stochastic transformations

The periodical nature of the parameter transformations in stochastic parameters simulations effectively introduces another parameter which otherwise comparable Monte Carlo simulations lack. Kremer (1983) found that as the period of transformations was increased, variability of the system measure studied also increased. His results suggested a non–linear relationship between transformation period and variance, but only simulations using a few different periods were performed.

In this section, the effect of varying the frequency of stochastic transformations is investigated by increasing the period of transformations from 1 to 350 days (*i.e.* from daily to essentially annual parameter variability). As previously, parameter g was used in simulations with stochastic variability ± 30%. Simulations were performed with OWS "India" forcing. Simulation details were otherwise identical to those

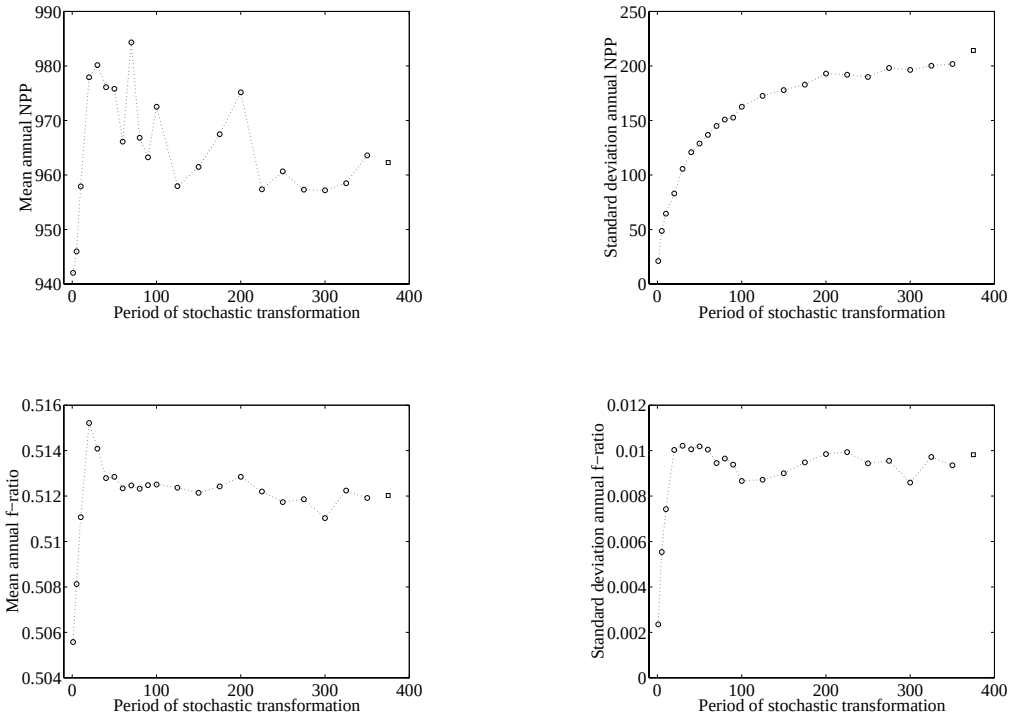

Figure 5.15: The behaviour of annual NPP and f–ratio means and standard deviations as the period of the parameter transformations in stochastic parameter simulation is increased. The circles represent stochastic parameters simulations, the squares represent a comparable Monte Carlo simulation. Annual NPP in mmol N m^{-2} y^{-1}. The annual f–ratio is dimensionless.

in section 5.7.1.

Figure 5.15 shows the annual NPP and annual f–ratio results for these simulations. For the purposes of comparison, the results from a Monte Carlo simulation with the same parameter variability have also been plotted on the graphs (the assignment of 375 days as the period of the Monte Carlo simulation is purely for graphical purposes). In all four cases, as the period of the stochastic transformations is increased (*i.e.* the transformations occur less often), the stochastic parameters results converge towards that of the Monte Carlo simulation. However, the means of both measures begin at values below that of the Monte Carlo simulation, and rise to values above it before falling back towards it. In the case of the mean annual f–ratio, its maximum value is attained at a clearly defined peak with a transformation period of 20 days. The results of mean annual NPP are considerably more variable (as was also found in the previous section), with the maximum value being attained at a transformation period of 70 days. However, barring this value, and another potential outlier at 200 days, the maximum appears to be attained at a much lower period (approximately 30 days).

The standard deviation results of both measures show much clearer, but considerably different, trends.

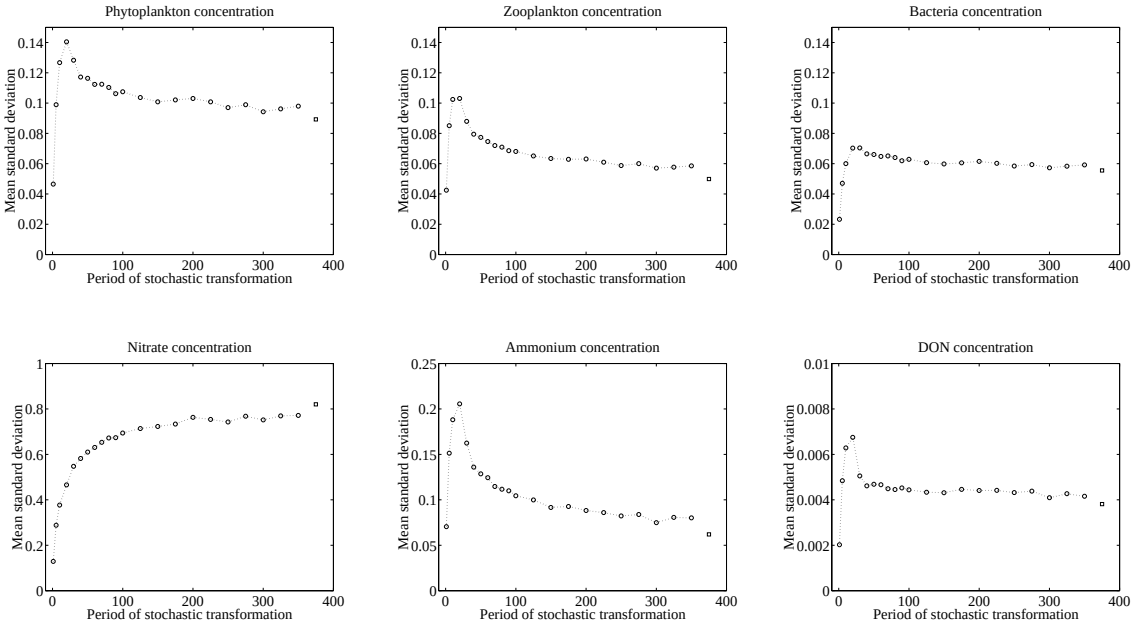

Figure 5.16: Plots of the annual means of the daily standard deviations of each of the model compartments as the period of the parameter transformations is increased. The circles represent stochastic parameters simulations, the squares represent a comparable Monte Carlo simulation. Note that the scale of the vertical axes vary between plots. Standard deviations in mmol N m^{-3}.

While variability in annual NPP rises hyperbolically with increasing transformation period (almost reaching the variability of the Monte Carlo simulation by period 350 days), variability in the annual f–ratio peaks at low period (approximately 30 days) and meanders around a plateau of variability as transformation period increases (Monte Carlo variability is slightly lower than this plateau).

Figure 5.16 shows comparable plots of the annual means of the daily standard deviations of each of the model compartments (except detritus, which produced a plot very similar to that of phytoplankton, zooplankton and bacteria). In all of the compartments bar nitrate, variability peaks when a transformation period of 20 days is used. Variability in the nitrate compartment, by contrast, behaves similarly to annual NPP with increasing transformation period. In all cases, as period is increased beyond 20 days, variability tends towards that found in the comparable Monte Carlo simulation.

Although these results find that the variability in nitrate (when averaged across the entire year) behaves qualitatively differently to that of the other model compartments in response to parameter transformations, when individual days during the year are considered this picture is more complicated. Figure 5.19 shows the results from two significant days during the forced year : day 149 (spring bloom maximum), and day 197 (minimum mixed layer depth). In the case of day 197, the patterns of variability are very similar (if even more exaggerated) to those already shown (figure 5.16). However, in the case of day 149, the patterns of variability of the phytoplankton and zooplankton concentrations are quite different to

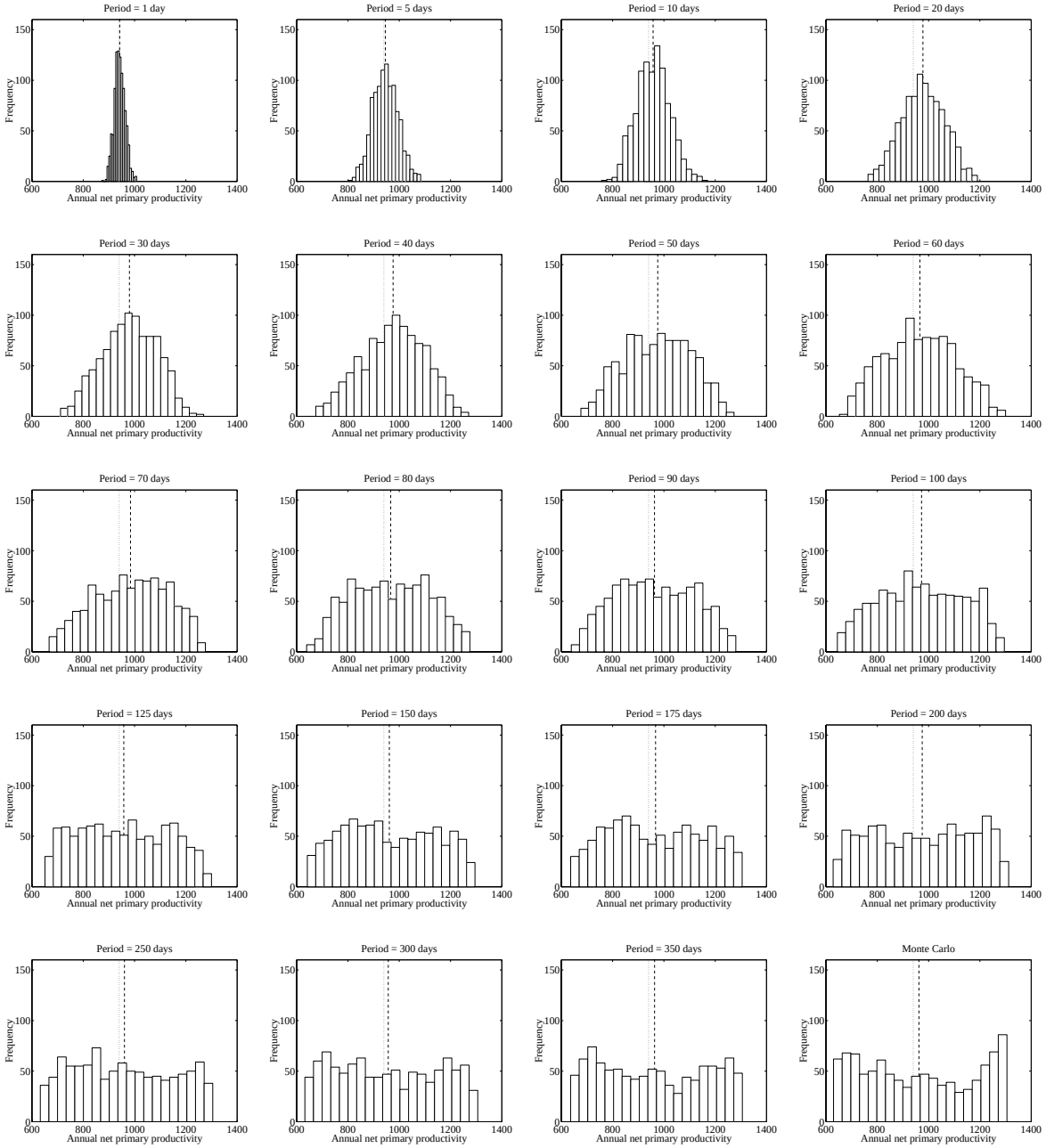

Figure 5.17: Frequency distributions of annual NPP for stochastic parameter simulations with increasing transformation period. The dotted line marks annual NPP for the deterministic solution with baseline parameter values. The dashed line marks mean annual NPP from the stochastic simulations. The final graphs shows the comparable frequency distribution produced by the Monte Carlo technique. Annual NPP in mmol N m^{-2} y^{-1}.

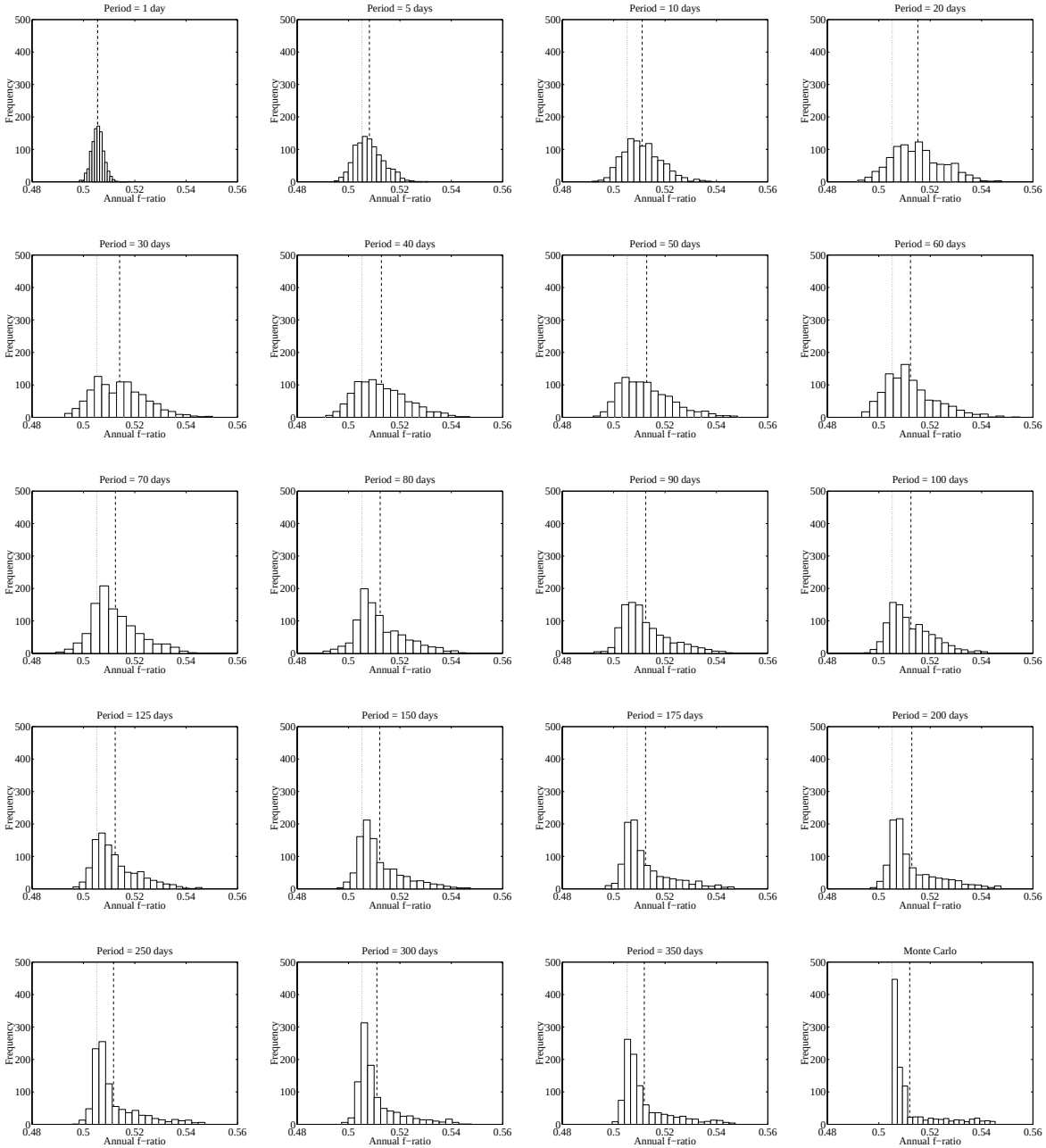

Figure 5.18: Frequency distributions of the annual f–ratio for stochastic parameter simulations with increasing transformation period. The dotted line marks the annual f–ratio for the deterministic solution with baseline parameter values. The dashed line marks mean annual f–ratio from the stochastic simulations. The final graphs shows the comparable frequency distribution produced by the Monte Carlo technique. The annual f–ratio is dimensionless.

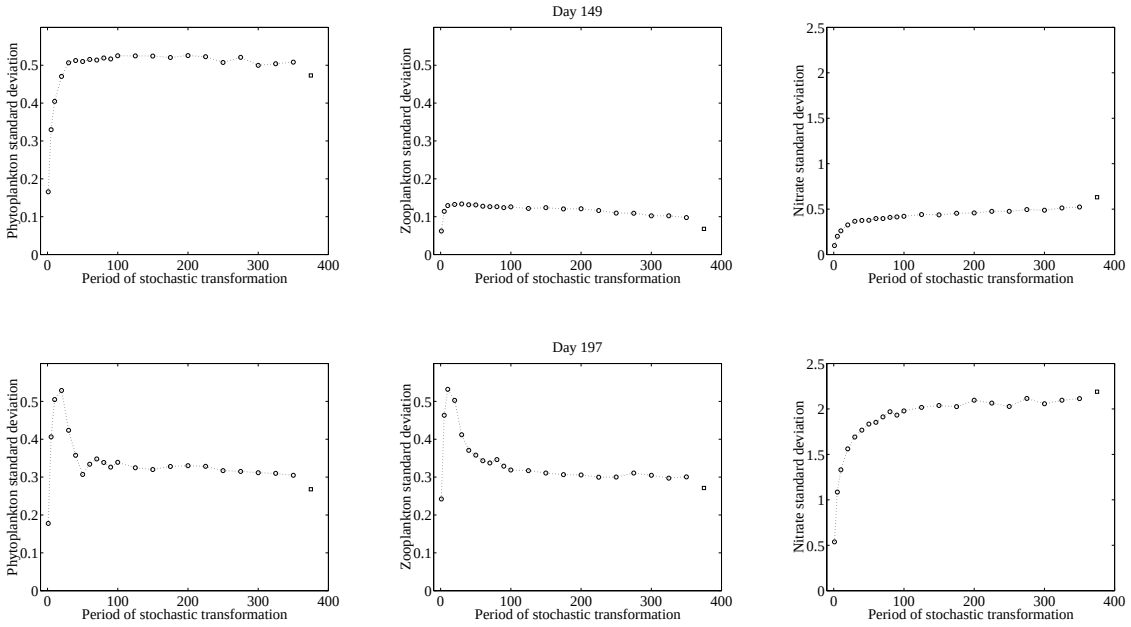

Figure 5.19: Variation in the patterns of standard deviation with stochastic transformation period for the phytoplankton (left), zooplankton (centre) and nitrate (right) compartments. The two rows of plots show standard deviations for each of the three compartments for days 149 (spring bloom maximum) and 197 (minimum mixed layer depth) respectively. The circles represent stochastic parameters simulations, the squares represent a comparable Monte Carlo simulation. Standard deviations in mmol N m^{-3}.

those of both day 197 and the annual average.

Figures 5.17 and 5.18 further illustrate the consistent trend for the results of stochastic parameters simulations to tend towards those of Monte Carlo simulations as the period of transformations is increased. The distributions of both annual NPP and the annual f–ratio shift from near–normal curves at low transformation period, towards the near–uniform (annual NPP) and skewed (annual f–ratio) distributions of Monte Carlo simulations. Since stochastic parameters simulations use a single transient year before the sampled year, simulations with transformation periods of 365 days experience two transformations during an individual simulation (in addition to the transformation at its start), and so are not directly comparable to a Monte Carlo simulation.

5.7.3 Transformation timing of stochastic parameters

As introduced by Kremer (1983), in the stochastic parameters technique, model parameters, when transformed, are allowed to take any value within a given range. However, the timing of the transformation events themselves is rigidly fixed, with a constant period between events. In this section, this aspect of the technique is modified to allow the timing of parameter transformation itself to become a stochastic process.

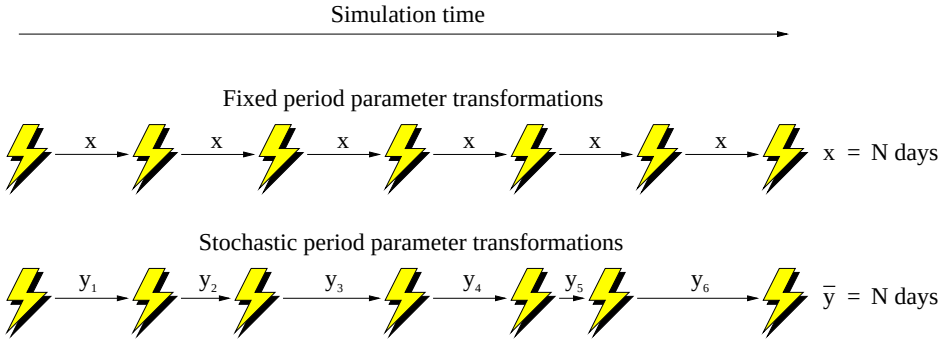

Figure 5.20: Diagrammatic representation of the fixed period and stochastic period approaches to stochastic parameter transformations. In the former case, the time between each parameter transformation is a constant N days. In the latter case, the timing of parameter transformations is a stochastic process itself, with a mean period of N days.

Figure 5.20 shows a diagrammatic representation of both the fixed period and the stochastic period forms of the stochastic parameters technique. In the fixed period form (the one used up until this point), transformation events (indicated by the lightning symbols in the figure) occur with a constant period, x, of N days. In the stochastic period form of the stochastic parameters technique, the time between each parameter transformation, y, is allowed to vary stochastically, but such that it has an *average* period of N days.

Computationally this is achieved by calculating the probability of a stochastic transformation event occurring during a given model iteration, and then "rolling the dice" to decide whether or not the transformation occurs. The probability of a transformation event occurring is (τ/N), where τ is the duration of each iteration (*e.g.* 0.04 days for a simulation using 25 iterations per day), and N is the average period of the stochastic transformations. Since the closer the value of τ (a feature of the model's implementation) to N (a model parameter), the more this approach resembles the fixed period approach (when $\tau \geq N$, the procedure described here triggers a stochastic transformation with a fixed period τ). The effects on simulation results of varying τ were investigated, and figure 5.21 shows the results of three such simulations where different numbers of daily iterations were used. In the three cases shown, the results were very similar, suggesting that 24 iterations per day are sufficient for the stochastic period approach outlined above.

As the stochastic period approach affects the timing of stochastic transformations the work from the previous section was repeated, and a series of simulations were performed across a range of average transformation periods (1 day to 350 days). As previously, parameter g used in simulations with variability $\pm$ 30%. Simulations were performed under OWS "India" forcing. Otherwise, simulation details identical to those in section 5.7.1.

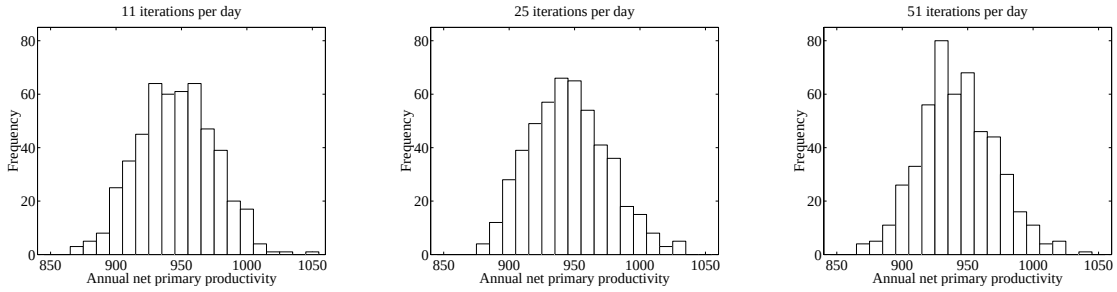

Figure 5.21: Frequency distributions of annual NPP produced by stochastic period stochastic parameters simulations as the number of daily model iterations is increased. Simulations performed with average transformation period of 1 day. Note that the scale on all three plots is identical. Annual NPP in mmol N m^{-2} y^{-1}.

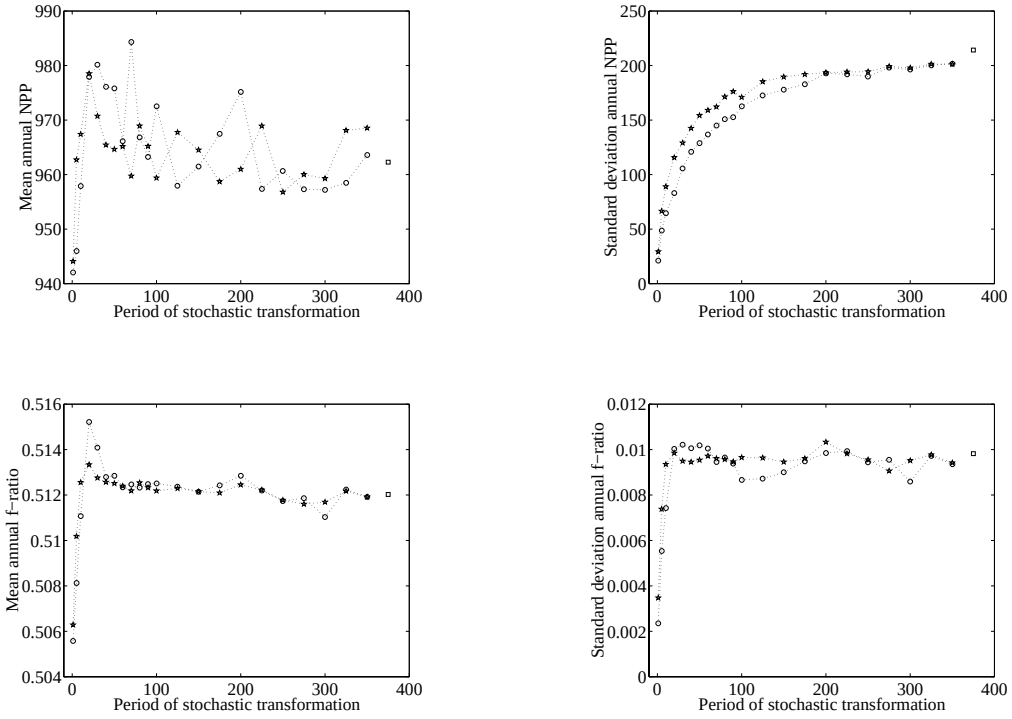

Figure 5.22: The behaviour of annual NPP and f–ratio means and standard deviations as the period of the parameter transformations in stochastic parameter simulations is increased. Plots show the results from both fixed period stochastic parameters (circles) and stochastic period stochastic parameters (stars). Squares represent results from a comparable Monte Carlo simulation. Annual NPP in mmol N m^{-2} y^{-1}. The annual f–ratio is dimensionless.

Figure 5.22 shows the behaviour of the means and standard deviations of annual NPP and the annual f–ratio as mean transformation period is increased. For the purposes of comparison, in each case the results from comparable fixed period simulations are also shown (and, as previously, the result from a Monte Carlo simulation). With the exception of slightly raised values at low transformation period (in stochastic period simulations with periods below around 20 days), it is difficult to discern any difference

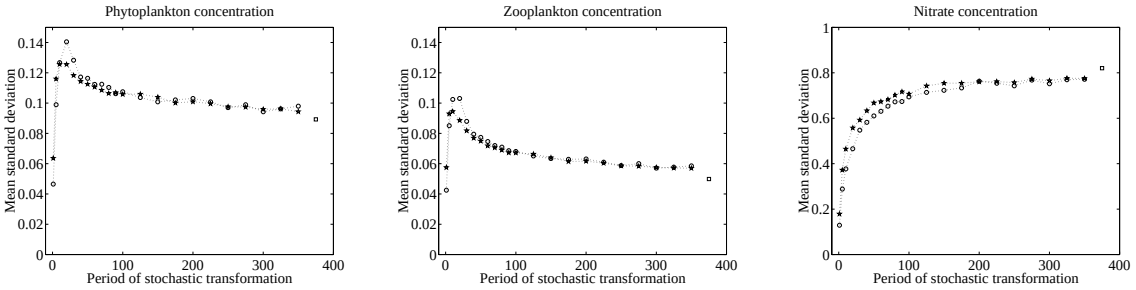

Figure 5.23: The behaviour of the annual means of the daily standard deviations of the phytoplankton (left), zooplankton (centre) and nitrate (right) compartments as the period of the parameter transformations in stochastic parameter simulations is increased. Plots show the results from both fixed period stochastic parameters (circles) and stochastic period stochastic parameters (stars). Squares represent results from a comparable Monte Carlo simulation. Standard deviations in mmol N m^{-3}.

between the behaviour of the means of both measures between stochastic and fixed period simulations. Both types of simulation result in scattered annual NPP at medium to high period. In the case of the annual f–ratio, both approaches produce a slowly declining mean after an initial peak (which is slightly higher with fixed period transformations) as transformation period is increased.

Although the variance of the annual f–ratio repeats this pattern of a slight difference between the two approaches at low period (variance is slightly greater with stochastic period transformations), the difference is noticeably greater when the variance of annual NPP is considered. Until transformation periods of around 200 days, variance of annual NPP in stochastic period simulations is consistently greater than that in fixed period simulations. This difference between the two approaches is repeated in the results of mean annual standard deviation of nitrate concentration, as shown in figure 5.23. However, this is not repeated in the simulations of the other model compartments (phytoplankton and zooplankton shown), although they do find that for periods of less than 10 days, stochastic period simulations again show greater variance than otherwise comparable fixed period ones. This is also shown in the annual cycles of variability of phytoplankton concentration in figure 5.24. Both the range of results observed and the daily standard deviations find that stochastic period simulations are more variable than fixed period simulations (at least for the low transformation period used in these simulations).

5.7.4 Conclusions

In this section, simulations have explored the consequences of changing the variability of a parameter about its mean, increasing the period between parameter transformations in the stochastic parameters technique, and modifying the stochastic parameters technique such that parameter transformations occur at stochastic intervals rather than the fixed intervals.

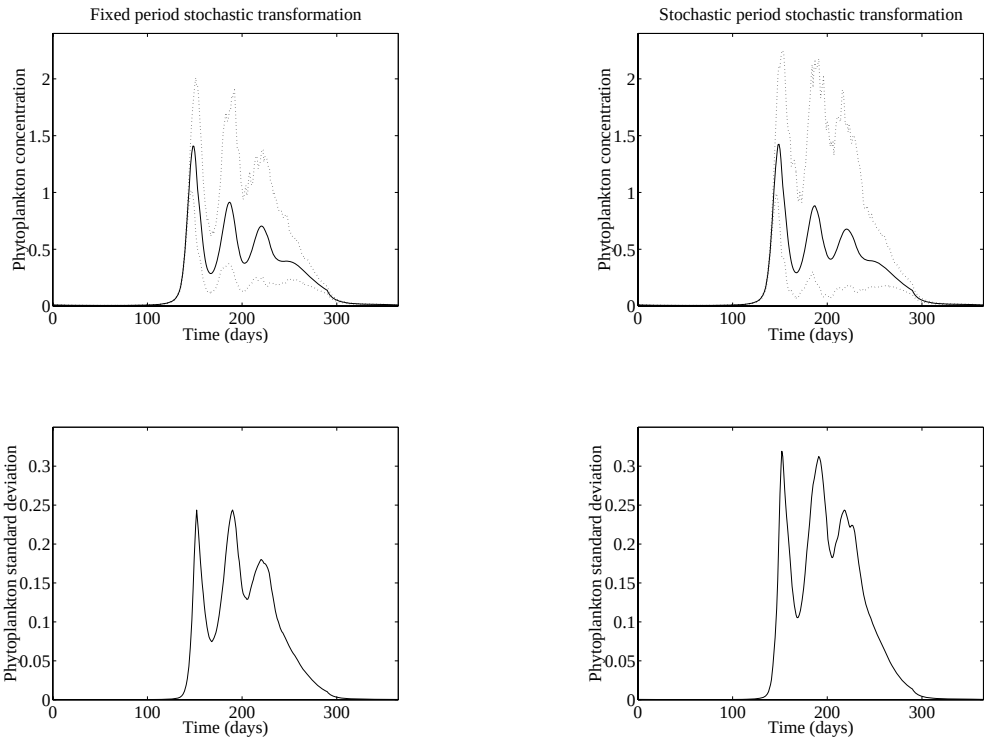

Figure 5.24: Variability in the seasonal cycle of phytoplankton concentration for fixed period (left) and stochastic period (right) approaches to the stochastic parameters technique. The top row of plots show the daily mean (solid), and minimum and maximum (dotted) concentrations produced by the two techniques. Period of stochastic transformations in both cases is 1 day (fixed and average respectively). Concentrations and standard deviations in mmol N m^{-3}.

The first series of simulations increased the variability of parameter g from $\pm$ 1% to $\pm$ 100%, and examined the consequence of this for both the Monte Carlo and stochastic parameters techniques. Both techniques found that (unsurprisingly) the higher the range of possible parameter values, the greater the variability in the model output. In the case of stochastic parameters, a fairly linear correlation between parameter variability and model variability resulted. However, the Monte Carlo results were more complex with the two system measures examined responding differently to different levels of parameter variability.

Section 5.7.2 examined the results of simulations in which the periodicity of the parameter transformations in the stochastic parameters technique was varied between 1 day and 350 days. While this work mostly found that increasing the transformation period increased variability, several of the measures used found that variability either reached a maximum at quite low periods (< 30 days) or peaked at low periods and fell off as periods were further increased. As the period between transformations increased, stochastic parameter simulations were found to increasingly resemble those of Monte Carlo simulations (at least in terms of overall variability).

Finally, an alternative version of the stochastic parameters technique was developed in which the intervals between parameter transformations were themselves allowed to be stochastic processes, rather that the fixed length intervals of the normal technique. This modification to the technique slightly increased variability at low transformation periods (< 20 days) for most measures, but increased the variability in annual NPP noticeably for periods of up to 200 days.

5.8 Multiple parameters and variability

In all of the previous sections, parameter variability has been confined to a single parameter for each simulation. While this procedure allows the sensitivity of the model to each individual parameter to be estimated, variability in the real world processes which the parameters represent is ubiquitous. In this section, the effects on model variability as multiple parameters are allowed to vary are explored using the stochastic parameters technique (with fixed transformation period). Although Kremer (1983) allowed 5 model parameters to vary during the same simulations, he never investigated the effects of either individual parameters or combinations of parameters on model variability.

There are several ways in which multiple parameter simulations could be implemented : parameters associated with the same state variable (*e.g.* phytoplankton or zooplankton physiological parameters) could be co–varied; parameters could be added one–by–one to simulations in a nominal order; or parameters could even be all made stochastic and their contribution to overall variability assessed by making them constant and calculating any reduction (or, conceivably, gain) in variability. In the work here, table 5.3's parameter ranking (which is based upon the variability of annual NPP) was used to provide an order in which parameters could be added. In the first instance, simulations began with the parameter g, which annual NPP is most sensitive to, and then added a parameter at a time to simulations. Parameters were added according to their position on table 5.3, with β then μ_2 following g. This procedure was continued to the 10th most sensitive parameter. A final series of simulations established the variability produced when all 25 parameters were allowed to vary stochastically. The procedure was then reversed, starting from the 10th most important parameter, ψ, and working towards g.

As previously, parameter values were transformed with a uniform distribution of $\pm$ 30% around their baseline values, and with a period of 1 day. All parameters to be transformed were re–assigned values simultaneously. Each simulation run was initialised with state variable values calculated during a 50 year deterministic solution, and consisted of a transient period followed by a single sampled year.

Figures 5.25 and 5.27 show the behaviour of the means and standard deviations of annual NPP and the annual f–ratio as the number of stochastic parameters is increased. On both sets of plots a triangle is used to indicate the results when all 25 parameters of interest are varied stochastically. In both series of

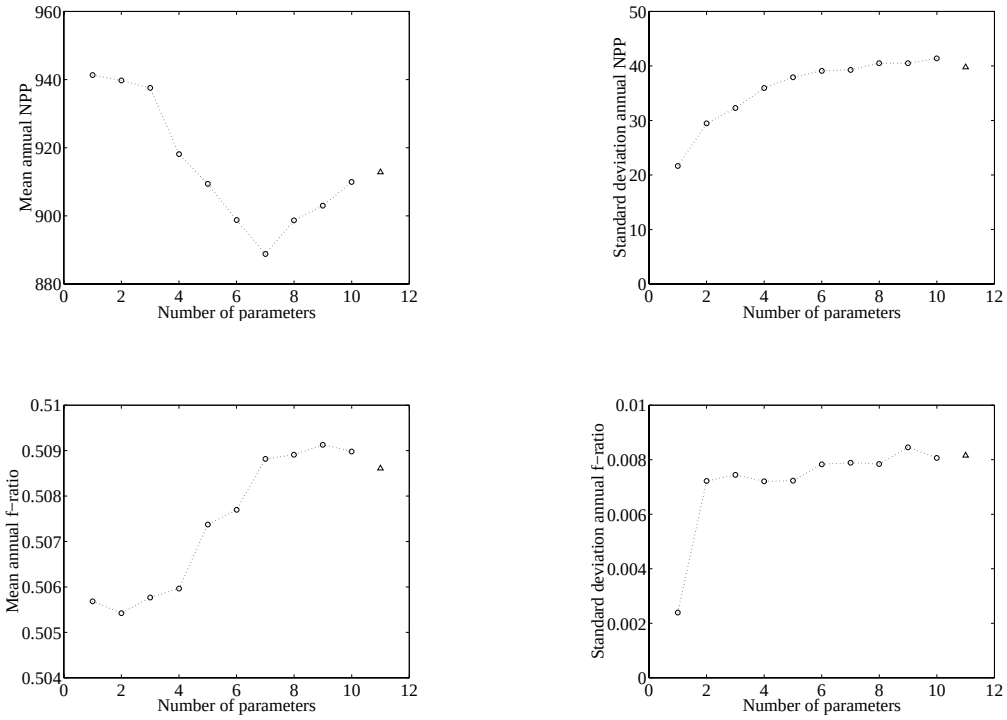

Figure 5.25: The behaviour of annual NPP and f–ratio means and standard deviations as the number of stochastic parameters in each simulation used to calculate them is increased. Parameter g is the first to be treated stochastically. The others are made stochastic in ranked order, from the 2nd (β) to the 10th (ψ) most sensitive. The triangles mark the results when all 25 model parameters are made stochastic. Annual NPP in mmol N m^{-2} y^{-1}. The annual f–ratio is dimensionless.

simulations the means of both measures shift erratically and substantially (considering previous results) in response to the addition of more stochastic parameters. In all cases, the means of these measures are shifted by the bias of each added parameter. For instance, in the case of mean annual NPP in figure 5.25, parameters β and μ_2 (2nd and 3rd) drag mean annual NPP down slightly as they are added. As evidenced in table 5.1, both also individually shift mean annual NPP slightly downwards. Likewise, when parameters k_3, V_p, α and λ(4th, 5th, 6th and 7th) are added, mean annual NPP shifts sharply downwards and, correspondingly, these parameters can also be seen in table 5.1 to cause relatively large downward shifts in mean annual NPP (in fact, these four parameters are the most important in terms of changing mean annual NPP). The rise in mean annual NPP as parameters k_w, p_1 and ψ (8th, 9th and 10th) are turned stochastic reflects the increases in mean annual NPP caused by each of these parameters individually. This influence over mean annual NPP is repeated with the annual f–ratio and also occurs when the parameters are added in reverse order.

With a few minor exceptions, increasing the number of stochastic parameters increases variability in the system measures shown (see also figures 5.26 and 5.28). Variability of annual NPP in figure 5.25 follows

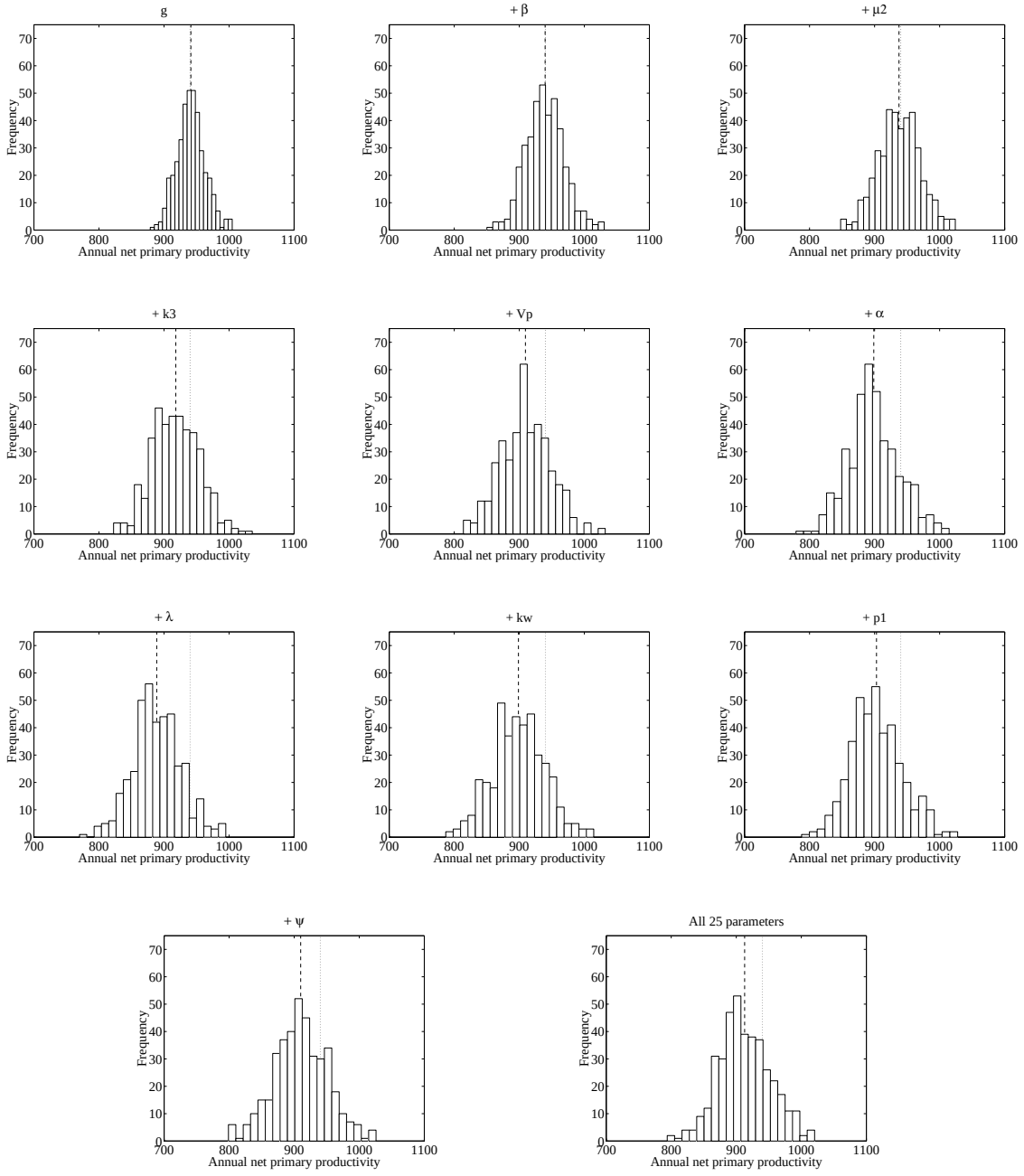

Figure 5.26: Frequency distributions of annual NPP for a series of simulations in which the ten parameters with the greatest effect on annual NPP are made stochastic one by one. Parameter g (the parameter which annual NPP is most sensitive to) is the first to be treated stochastically. The others are made stochastic in ranked order, from the 2nd to the 10th most sensitive. The final graph shows the result when all 25 model parameters are made stochastic. Annual NPP in mmol N m^{-2} y^{-1}.

a hyperbolic course as the number of stochastic parameters rises. Each addition adds progressively less variability to the total. While this might be expected considering the order in which parameters were added, the variability added by successive parameters is usually considerably lower than the variability detailed in table 5.3 (*i.e.* total variability is not additive). The pattern of variability increase is not

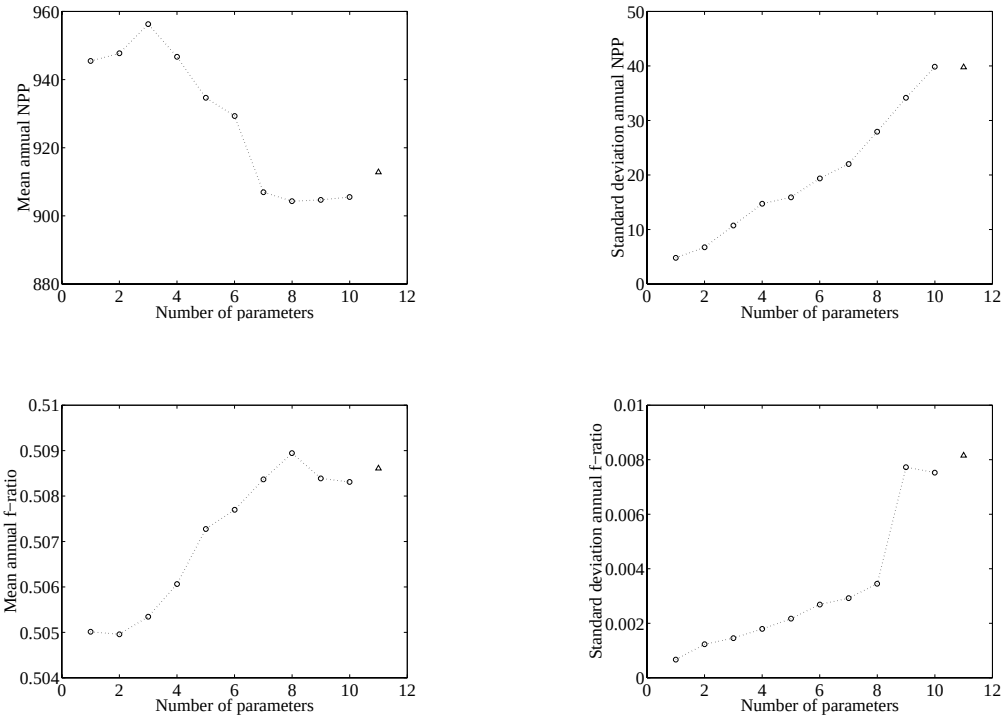

Figure 5.27: The behaviour of annual NPP and f–ratio means and standard deviations as the number of stochastic parameters in each simulation used to calculate them is increased. Parameter ψ is the first to be treated stochastically. The others are made stochastic in ranked order, from the 9th (p_1) to the 1st (g) most sensitive. The triangles mark the results when all 25 model parameters are made stochastic. Annual NPP in mmol N m^{-2} y^{-1}. The annual f–ratio is dimensionless.

repeated in figure 5.27, where the most important parameters are added last. This reversal tends to make each parameter add roughly similar variability to total variability.

Variability in the mean annual f–ratio results of both series of simulations is dominated by parameter β. As remarked previously, while the sensitivity of mean annual NPP to different parameters is fairly continuous, mean annual f–ratio is acutely sensitive to this parameter and, in both figures 5.25 and 5.27, its addition causes a marked rise in total variability. The addition of other model parameters is of minor note by comparison.

5.8.1 Conclusions

While previous sections dealt entirely with situations in which only a single parameter varied during a simulation, this section aimed to determine the consequences to model behaviour of simultaneous variability in multiple parameters. The question was addressed by performing series of simulations in which parameters were added one by one in increasing or decreasing order of model sensitivity.

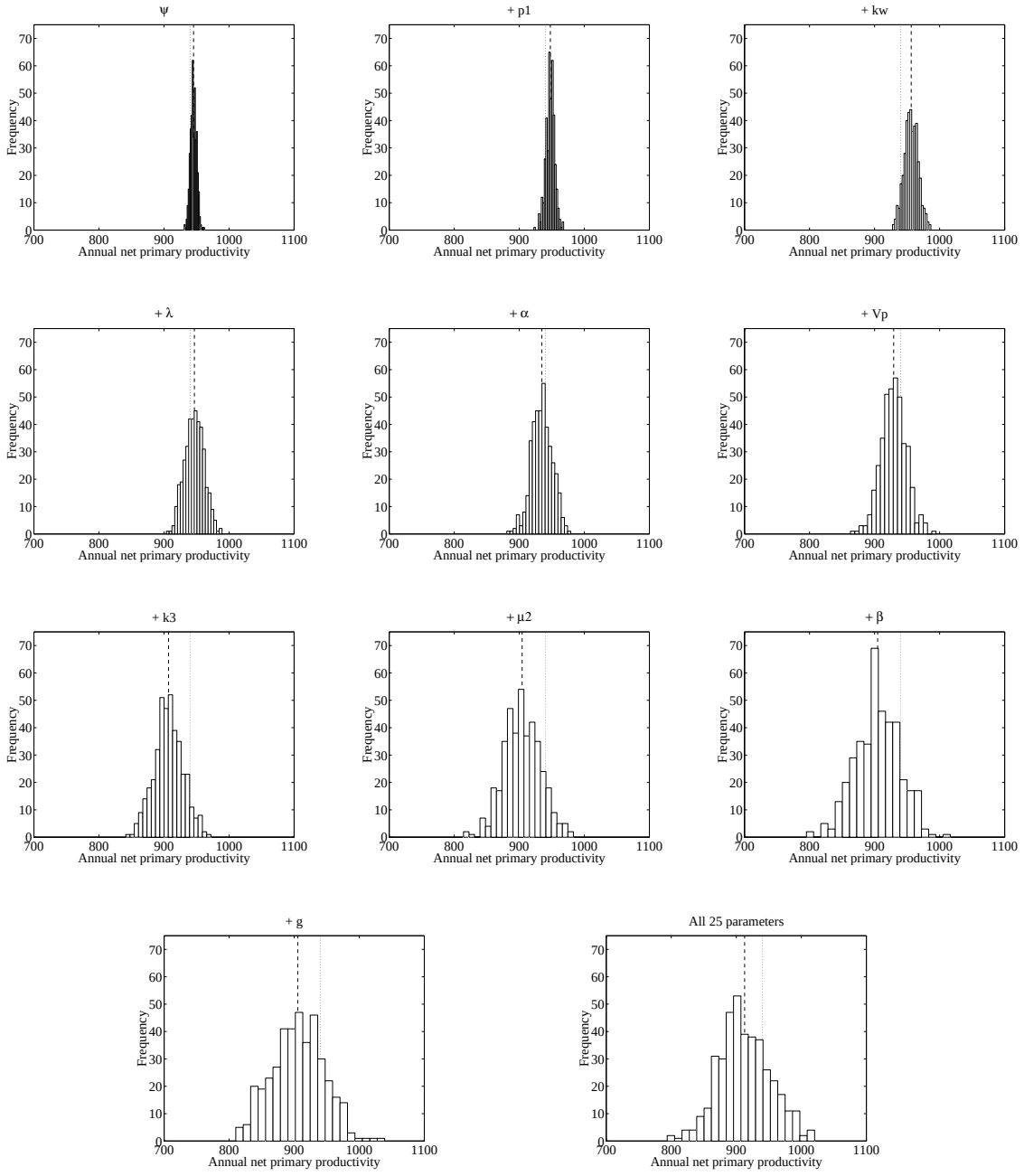

Figure 5.28: Frequency distributions of annual NPP for a series of simulations in which the ten parameters with the greatest effect on annual NPP are made stochastic one by one. Parameter ψ (the parameter which annual NPP is 10th most sensitive to) is the first to be treated stochastically. The others are made stochastic in ranked order, from the 9th to the 1st most sensitive. The final graph shows the result when all 25 model parameters are made stochastic. Annual NPP in mmol N m^{-2} y^{-1}.

While the addition of more stochastic parameters to a simulation almost always increased overall variability, the contribution of each parameter to total variability (*i.e.* the difference in variability between a simulation with that parameter stochastic and one where it was constant) was found to depend on the order of addition. Total variability of annual NPP was found to saturate as parameters were added,

while the annual f–ratio was still dominated by the influence of parameter β.

5.9 Variability and the reduced models

At the start of this chapter it was noted that another source of uncertainty in models was the actual form of the model equations and the terms within them. In Chapter 3 a series of reduced models were introduced that aimed to explore the importance of structural elements in the full model. An important part of this work was examining the response of each of the models to different forcing regimes, to determine whether they shared the response of the full model or deviated from its response, possibly revealing a flaw in doing so. In this section, stochastic parameters simulations of each of the reduced models were performed to determine how each of them responded to the addition of variability to their parameters.

Two series of simulations were performed. In the first series, only parameter g was allowed to vary (since all of the reduced models are at least PZ models, this parameter is used in all of them). The second series allowed the "top eight" parameters (again, as assessed by their impact on mean annual NPP at OWS "India" in the full model) to vary in all of the reduced models. Since the reduced forms exhibit a range in the total number of parameters they possess, this second series of simulations aimed to determine if there were any differences between models in which different fractions of their parameters were varying (*i.e.* model 2c has only 16 parameters, whereas model 6c3 has more than double this number). Models with fewer parameters might be expected to be more affected when a greater proportion of these are varied. Only eight of the "top ten" parameters were used because entries 9 and 10 in the ranking (p_1 and ψ respectively) are not used in several of the reduced models.

As previously, simulations were performed for each of the reduced models at OWS "India". Parameter values were transformed with a uniform distribution of $\pm$ 30% around their baseline values, and with a period of 1 day. Where multiple parameters were varied, all were re–assigned values simultaneously. Each simulation run was initialised with state variable values calculated during a 50 year deterministic solution, and consisted of a transient period followed by a single sampled year.

Figures 5.29 and 5.30, and table 5.7 contain results from the first series of simulations. Table 5.8 summaries the results from the second series of simulations. Figure 5.29 shows the mean daily concentrations of phytoplankton, and the range of concentrations found during the simulations, for each of the reduced models. Results for the full model appear at the top left of the tableau of plots. Figure 5.30 shows the daily standard deviations of phytoplankton concentration found for each of the reduced models. Both tables 5.7 and 5.8 summarise annual NPP and annual f–ratio results for each of the reduced models.

As figure 5.29 shows, in all of the models (including the full model) the seasonal patterns of mean daily

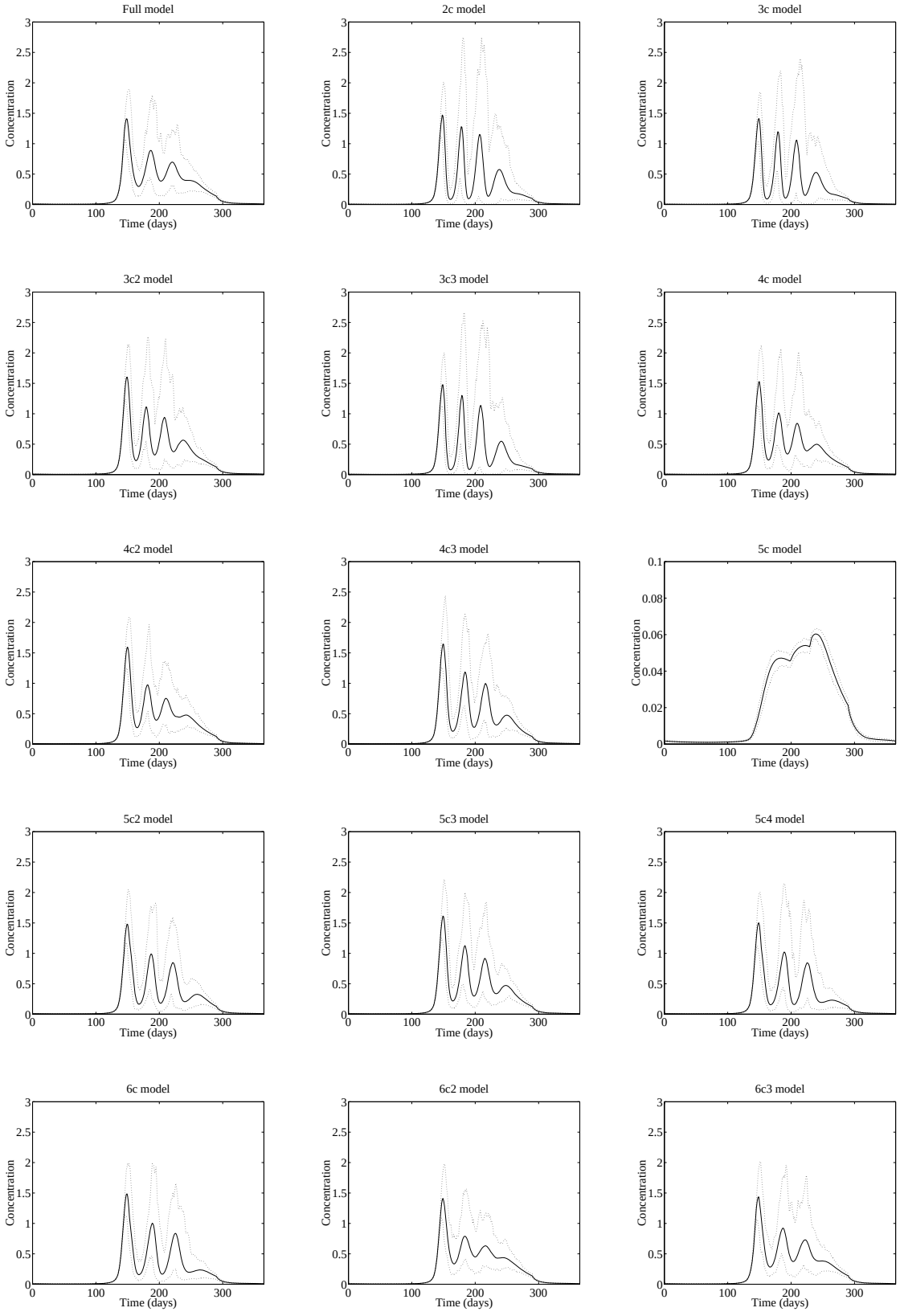

Figure 5.29: Plots of the daily mean (solid line) and range (dotted lines) of phytoplankton concentrations produced by stochastic parameter simulations of each of the reduced models. Simulations stochastic with respect to model parameter g (zooplankton maximum ingestion rate). Note the change of vertical scale on the plot for model 5c. Concentrations in mmol N m^{-3}.

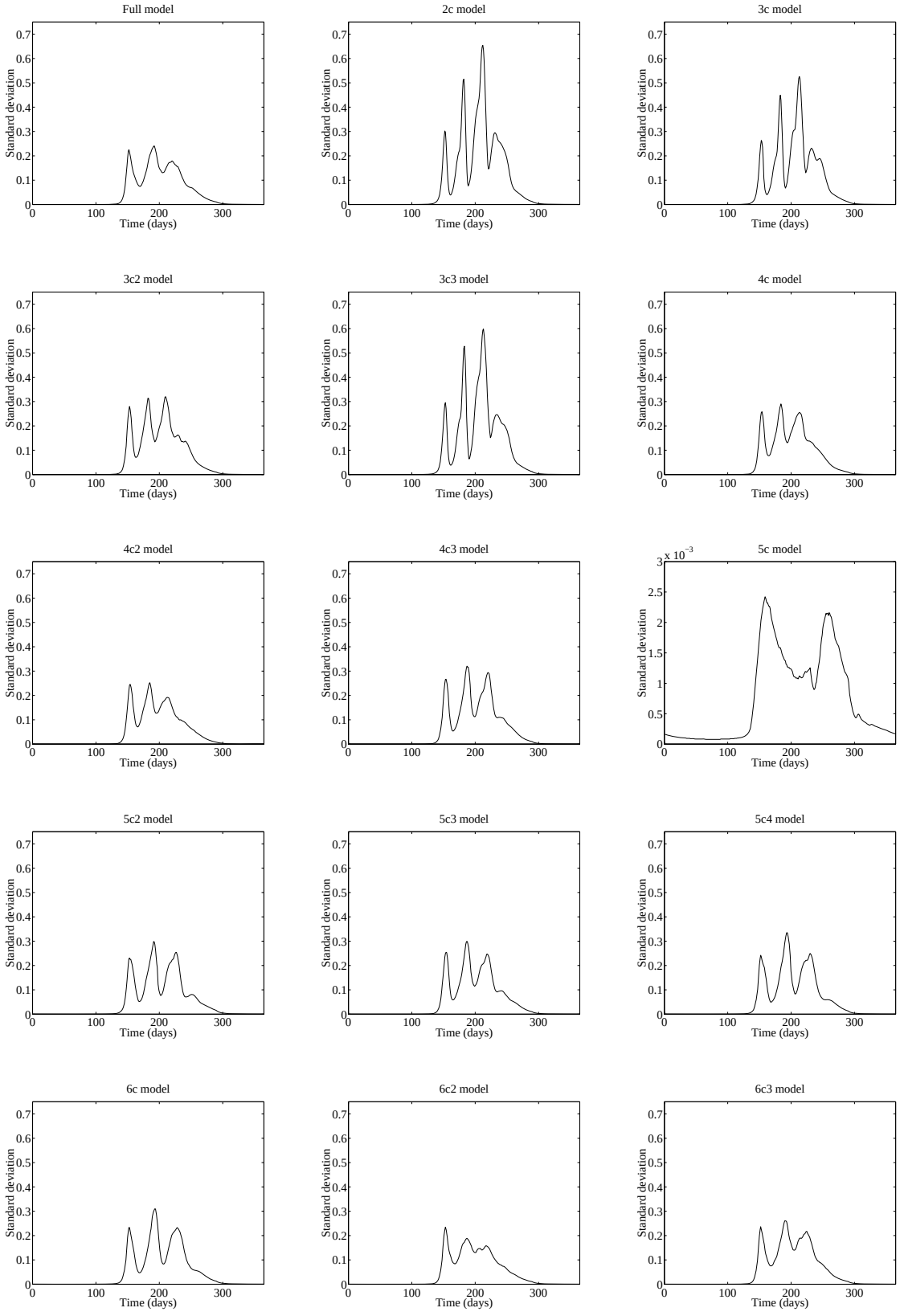

Figure 5.30: Plots of the daily standard deviation of phytoplankton concentrations produced by stochastic parameter simulations of each of the reduced models. Simulations stochastic with respect to model parameter g (zooplankton maximum ingestion rate). Note the change of vertical scale on the plot for model 5c. Standard deviations in mmol N m^{-3}.

	Annual NPP			f–ratio		
Model	**Det.**	**Mean**	**St. dev.**	**Det.**	**Mean**	**St. dev.**
Full	940.179	939.465	20.783	0.505	0.506	2.510
2c	868.860	870.564	25.503	–	–	–
3c	806.278	809.377	22.544	–	–	–
3c2	1051.082	1052.150	25.935	–	–	–
3c3	843.609	843.593	24.176	0.623	0.623	5.630
4c	951.913	953.935	22.811	–	–	–
4c2	963.119	964.640	19.303	–	–	–
4c3	985.531	989.833	23.440	0.498	0.497	2.060
5c	17.541	17.486	0.536	–	–	–
5c2	863.087	868.928	24.149	–	–	–
5c3	960.461	961.528	21.492	0.499	0.499	1.867
5c4	843.422	852.496	28.795	0.458	0.460	8.110
6c	830.146	837.717	26.141	0.457	0.460	6.922
6c2	941.060	941.668	18.804	–	–	–
6c3	964.198	967.072	23.023	0.504	0.505	2.473

Table 5.7: The deterministic values, stochastic means and stochastic standard deviations of the annual NPP and f–ratios of the full model and its reduced forms from Chapter 3. Stochastic parameters technique applied to parameter g (zooplankton maximum ingestion rate). Note that the f–ratio standard deviations have been multiplied by a factor of 1000 for clarity. Annual NPP in mmol N m^{-2} y^{-1}. The f–ratio is dimensionless.

phytoplankton concentration are very similar to the deterministic solutions as shown in figure 3.16. The range of daily results about these means is relatively narrow about the spring bloom produced by each model but broadens during the summer and early autumn. This is particularly noticeable in models 2c, 3c and 3c3, all three of which have a particularly pronounced third bloom in the late summer. In figure 5.30 this is particularly clear, with each bloom showing more variability than the last. Another difference between certain of the reduced models and the full model is the coherence of this third bloom in the variability about the mean. This can be seen in the range of values about the mean, but is again clearer in the daily standard deviations of figure 5.30. Models 3c2, 4c, 4c3, 5c2, 5c3, 5c4 and 6c all show this bloom strongly in their variability, while models 4c2 (one of the favourites from Chapter 3), 6c2 and 6c3 show, in common with the full model, a much less distinct third bloom. This distinction does not follow previously mentioned differences in the models (*e.g.* presence/absence of bacteria compartment, bacterial access to detritus as a growth substrate), nor does it appear to relate to the period of the summer oscillations (see table 3.2).

	Annual NPP			f–ratio		
Model	**Det.**	**Mean**	**St. dev.**	**Det.**	**Mean**	**St. dev.**
Full	940.179	909.965	41.363	0.505	0.509	8.068
2c	868.860	821.184	46.404	–	–	–
3c	806.278	763.763	41.016	–	–	–
3c2	1051.082	1006.734	47.927	–	–	–
3c3	843.609	795.562	44.730	0.623	0.625	10.998
4c	951.913	912.690	40.816	–	–	–
4c2	963.119	933.475	37.565	–	–	–
4c3	985.531	949.869	45.541	0.498	0.500	6.350
5c	17.541	16.352	1.525	–	–	–
5c2	863.087	839.545	41.031	–	–	–
5c3	960.461	925.501	40.438	0.499	0.502	6.017
5c4	843.422	835.869	49.478	0.458	0.470	14.448
6c	830.146	817.535	42.089	0.457	0.468	12.708
6c2	941.060	908.863	36.735	–	–	–
6c3	964.198	929.803	43.440	0.504	0.508	8.395

Table 5.8: The deterministic values, stochastic means and stochastic standard deviations of the annual NPP and f–ratios of the full model and its reduced forms from Chapter 3. Stochastic parameters technique applied to the top 8 model parameters (as defined earlier). Note that the f–ratio standard deviations have been multiplied by a factor of 1000 for clarity. Annual NPP in mmol N m^{-2} y^{-1}. The f–ratio is dimensionless.

Table 5.7 shows a number of interesting results. Variation in parameter g causes, at most, a shift in mean annual NPP of approximately 1% from the deterministic solution (model 5c4). Almost all of the reduced models (except models 3c3, 5c and, notably, the full model), show a very slight increase in mean annual NPP from that in deterministic solutions. Although models 4c2 and 5c3, favourites from Chapter 3, have standard deviations closest to that of the full model, the standard deviations of the other models are mostly fairly similar (between around 18 to 28 mmol N m^{-3}), with no obvious patterns between models. The mean annual f–ratios show similarly small shifts in their mean values from deterministic solutions. However, there are greater differences in the standard deviations calculated. Models 4c3, 5c3 and, particularly, 6c3 have deviations close to that of the full model, but the remaining models (3c3, 5c4 and 6c) have deviations more than double that of the full model.

The results of table 5.8 broadly support those found using only the full model in section 5.8. With the "top eight" parameters varying together, mean annual NPP falls in all models, while the mean annual

f–ratio slightly rises (see figure 5.25 for comparison). The standard deviations of both measures increase for all models. In the case of annual NPP, deviations roughly double. The standard deviations of the annual f–ratios increase by about 5.0×10^{-3}, undoubtedly mostly due to the addition of parameter β. However, contrary to the suggestion made earlier, neither annual NPP nor the annual f–ratio data suggest that smaller models are more greatly affected by having a greater fraction of their parameters varying.

5.9.1 Conclusions

In this section, the reduced models of Chapter 3 were re–introduced, and work performed to determine whether the different structures of the models led to any differences in their response to stochastic parameters. The models were simulated with either a single parameter or the "top eight" parameters stochastically varying.

While there were differences between the outputs of the models, the only major differences between lay in seasonal patterns of variability (most notably with "excitable" models, 2c, 3c and 3c3). Most models exhibited variability close to that of the full model, and no obvious relationships between the complexity of the models and their variability were discerned. Several models (3c3, 5c4 and 6c) were consistently more variable than the others, but with no obvious common structures which could explain this.

5.10 Summary

This chapter initially set out to determine the sensitivity of the Fasham (1993) model to its various parameters. Using an earlier version of the model, Fasham, Ducklow & McKelvie (1990) performed a deterministic analysis of parameter sensitivity at Bermuda Station "S" . The work here supplemented this approach with two stochastic techniques, and initially moved focus to OWS "India" (to complement the research in Chapter 4).

The parameter sensitivity analyses of OWS "India" all agreed on the dominance of phytoplankton photosynthesis (k_w, α, λ and V_p) and zooplankton grazing parameters (g, β, k_3 and p_1). These parameters consistently appeared in the "top ten" rankings produced by all of the sensitivity techniques employed. Several of these were previously identified as important by Fasham, Ducklow & McKelvie (1990) in their analysis, but the analysis here found that N_0, k_1 and μ_1 were considerably less sensitive than found by Fasham, Ducklow & McKelvie (1990). Comparisons of different system measures found that there was mostly agreement about important parameters. However, the analysis also found that rankings of stochastic analyses which used means of measures frequently missed parameters which caused significant variability but no shift in the mean.

This initial analysis was followed by a re–analysis of parameter sensitivity at Bermuda Station "S" to determine if different parameters dominated at this location. The parameters identified as important at OWS "India" were also mostly dominant at Bermuda Station "S". However, parameters k_1, μ_1 and (particularly) N_0, previously identified as important by Fasham, Ducklow & McKelvie (1990), were found to play a more significant role at this location. N_0's dominance reflects the oligotrophic nature of Bermuda Station "S" (*i.e.* the importance of N_0 may vary inversely with its baseline value).

The sensitivity analyses performed at OWS "India" and Bermuda Station "S" made assumptions regarding both variability in the parameters and use of the stochastic techniques. One of these assumptions was that all parameters varied $\pm$ 30% around their baseline (deterministic) values. A series of simulations explored the effects of a range of variability of parameter g (one of the most significant model parameters) on the outputs of both Monte Carlo and stochastic parameters runs. Perhaps unsurprisingly, increased parameter variability was found to induce greater variability in the system measures examined. However, the two stochastic techniques differed in the form of this variability. Stochastic parameters simulations found an almost linear relationship between parameter variability and variability in model output, but Monte Carlo simulations found more complicated hyperbolic and sigmoidal relationships (depending upon the system measure in question). The lack of such these more complex relationships in the results of stochastic parameters is believed to be due to the much lower variability encountered in the system measures of such simulations.

A major (nominal) assumption in the use of the stochastic parameters technique was that parameters varied with a periodicity of 1 day (*i.e.* every day parameters were assigned a new stochastic value). The effects of this assumption were examined in a series of simulations in which the period between transformations was ranged from 1 to 350 days. Variability of annual NPP was (again) found to increase hyperbolically with transformation period. However, variability in the annual f–ratio, plus that in most of the state variables, was found to display a more complex pattern. In the former case, variability reached a plateau at relatively low periodicity, while in the latter cases, variability often peaked at low period (20 days) before falling with increasing transformation period. For all of the measures examined however, increasing transformation period shifted the results of stochastic parameters simulations towards those of Monte Carlo simulations. Since Monte Carlo simulations can be viewed as an extreme case of stochastic parameters (*i.e.* parameters have a transformation period of ∞), this trend is somewhat expected.

A feature of the description of stochastic parameters by Kremer (1983) was the fixed periodicity of parameter transformations. As another exploration of the stochastic parameters technique, the process of timing the transformations was modified such that it became a stochastic process itself. Instead of parameters transforming every N days, they were transformed at stochastic intervals, *on the average* once every N days. To explore any differences between normal stochastic parameters and this modification, a repetition of the last section (varying the periodicity of the stochastic parameters technique)

was performed. This work found that the differences between the two techniques varied between the measures examined. On the whole though, the stochastic period approach resulted in slightly greater variability than the fixed period approach, particularly when transformation periods were low (< 20 days). In the case of annual NPP, this difference continued for periods of up to 200 days. However, the differences between the two approaches were considerably lower than the difference between the Monte Carlo and stochastic parameters techniques.

The effect of multiple stochastic parameters on model variability was then examined. Broadly the results found that variability increased as more and more parameters were added (although the variability added by a given parameter was not simply related its contribution to variability when the only stochastic parameter). However, in both measures examined, variability was found to approach a plateau. Where parameters were added starting with the most important, this plateau was reached relatively quickly. In the case of the annual f–ratio, total variability was still dominated by parameter β, whenever it was added.

The final section in this chapter re–introduced the reduced models from Chapter 3 and aimed to determine whether, a) the different structures of the models resulted in any different or distinguishing patterns of variability, and b) in a multiple parameter simulation, did having a greater or lower fraction of their parameters stochastic result in any differences between the models? While differences between certain of the models and the full model were noted (particularly the more "excitable" models), most of the models shared similar patterns of variability with the full model, and there were no obvious correlations between the performance of a reduced model and its complexity.

5.11 Discussion

Uncertainty and variability play a large role in ecological studies but their incorporation into plankton models is only occasionally addressed (fewer than half of the models discussed in Chapter 2 raise or study such issues). Kremer (1983) introduced one technique by which variability can be introduced into a model, and this chapter has both utilised his approach, and explored variants of it.

An issue which has been treated only lightly in this chapter is whether or not it is reasonable to represent parameters in the manner in which they are treated here. Although attention has been drawn to the potential failings of the Monte Carlo approach[6], its representation of parameters as poorly known but constant makes fewer (and more justifiable) assumptions. The stochastic parameters technique, by contrast, makes a number of assumptions. Firstly it assumes that parameters are variable across time. As already discussed though, this is known to be true (although this is far from saying that the variability of parameters is understood or well–documented). Secondly it assumes that parameter variability

[6]See also the Addendum following this section.

can be reasonably approximated by allowing parameter values to change randomly. This is far from clear, and data sets which may support or reject this assumption are non–existent at present (T. Platt, Bedford Institute of Oceanography, Dartmouth, Canada, pers. comm.). Finally, the technique assumes a characteristic periodicity of parameter changes. Kremer (1983) points out that real variability is likely to be continuous, but the implementation of parameter variability forces periodicity and necessitates a choice for its value.

As noted in the section on multiple parameters, the addition of a further stochastic parameter to a simulation usually contributes much less to total variability than the addition of that parameter when all of the other parameters are constant. Since most of the parameters are variable in real life, an alternative approach to assessing the importance of a parameter would be to note the *decline* in total variability if that parameter were to become the only constant one. Also related to parameters, and touched upon at several points during the thesis, is the significance of relationships between model parameters. This chapter has (as Chapter 4 before it) treated each parameter as if it were independent of all others. At this time, relating parameters is not commonplace among modelling studies, though as knowledge about such relationships increases, studies such as this one will have to account for this.

After the initial parameter sensitivity study, a considerable fraction of the work in this chapter made use of only parameter g to explore the effects of various changes to the techniques used. As this parameter was chosen specifically because of its effects on key system measures, the results of this latter work should not be interpreted as applying across all parameters. Indeed, as the sensitivity study found, the annual f–ratio was much more profoundly influenced by parameter β, and may respond quite differently should this parameter be handled in a similar manner to that of g. Any further studies which use the techniques in this chapter should establish whether or not all parameters behave in a similar manner to that of g.

Section 5.7.1 found marked disparity between the results from Monte Carlo simulations and from those of stochastic parameters. The disparity was suggested to be caused by the considerably lower variability in the stochastic parameters simulations. An avenue, unapproached here, which could test this suggestion would be to increase variability in appropriate stochastic parameters simulations by increasing the period of transformations. Since the periodicity results already suggest a trivial link between the two stochastic techniques, this work may prove fruitful.

In the sections on variation in the periodicity of transformations attention focussed on periods of a day or more. In his work, Kremer (1983) examined situations in which transformations occurred with periods of less than one day. Although, as Kremer (1983) found (and the results reported here suggest), variability is lower for shorter and shorter transformation periods, confirmation of this would complete this facet of the work here.

5.12 Addendum : Response to Annan (1997)

Much of the work in this chapter makes use of the technique used originally by Kremer (1983) to study a two species phytoplankton model. In a recent paper, Annan (1997) presents an re–analysis of this technique and questions the appropriateness of its use. The re–analysis accounts for one of the more significant differences Kremer (1983) found between simulations using the conventional Monte Carlo approach and those using stochastic parameters. As the conclusions of Annan's analysis cast doubt on the applicability of stochastic parameters to ecological problems (*e.g.* the work in this chapter), his analysis and conclusions are examined here.

Kremer (1983) used a simple model in which two algal species with identical parameter values competed with one another for nutrients for growth. Since both species were the same in every respect, the model resulted in both species reaching an identical concentration at equilibrium. However, when stochastic approaches were used, Kremer found quite different results. The stochastic parameters technique produced time series in which both species co–existed at concentrations which shifted stochastically around means close to the deterministic equilibrium. In stark contrast, the Monte Carlo simulations almost always resulted in the extinction[7] of one of the algal species and the dominance of the other.

Annan (1997) focuses on this particular result (that Monte Carlo simulations result in extinction) and presents an argument for its occurrence. Extinctions in the model are a consequence of one of the algal species being "dealt" an inferior set of parameter values at the start of a given Monte Carlo simulation. The other algal species is then able to grow faster than its rival, uptake more of the available nutrient, and ultimately drive its competitor towards extinction. Since the stochastic parameters technique constantly varies parameters (Kremer used a period of 1 day), any advantage (or disadvantage) in its parameter values given to one species is usually short–lived. From simulations of his own, Annan notes that the closer together the parameter values of the two species, the longer it takes for one to become extinct (in both Kremer's and Annan's work, extinction was defined as the point at which an algal species' concentration fell below its initial concentration). Since, in the case of the stochastic parameters technique, parameter values are re–assigned multiple times during a given simulation, they better approximate the mean of the distribution they are chosen from than they do during a Monte Carlo simulation, in which they are only chosen once. As a result, the time–averaged parameter values of both species are likely to be closer to one another during a stochastic parameters simulation, and consequently extinction is liable to take a longer period of time. Annan contests that the absence of extinction in Kremer's work with stochastic parameters is merely a consequence of the simulations proceeding for insufficient time. Annan further proposes that to make Monte Carlo simulations more correctly comparable to those with stochastic parameters, the distribution from which parameters are randomly chosen for a Monte Carlo simulation

[7]Since the model used continuous variables to describe the algal populations, extinction *per se* was not possible (see Chapter 1's discussion of the continuity assumption). However, algal populations often became vanishingly small during Kremer's (1983) Monte Carlo simulations.

should be narrower (*i.e.* have a lower standard deviation) than that used to specify parameter values during an analogous stochastic parameter simulation. The narrowing of the distribution should scale with the number of number of times parameters are re–assigned values during a stochastic parameters simulation. Annan concludes that :

> *By analyzing the behaviour of the model more thoroughly we explain the reasons for* [extinctions], *and show that in fact when* [Monte Carlo] *is carried out correctly, there is little or no difference in model output between the two types of simulation.*
> ...
> *Although there may well be some circumstances when* [stochastic parameters] *would be useful there is no justification for it here.*

This analysis raises and justifies a valid objection to Kremer treating Monte Carlo and stochastic parameter simulations as qualitatively different (as section 5.7.2 already demonstrated, as the period of transformations is increased, stochastic parameters simulations tend towards Monte Carlo simulations). Additionally it proposes an interesting alternate approach to assigning parameter values for Monte Carlo simulations. However, the analysis fails to justify the conclusions drawn by Annan on several levels, and these conclusions should be treated cautiously. This failure to justify the dismissive conclusions stems primarily from Annan's over–simplification of the problem that Kremer was addressing.

In the first instance, Kremer was not primarily interested in the extinctions that resulted during Monte Carlo simulations. One of Kremer's primary concerns was in the time series produced by the different techniques. Whichever technique is used, Kremer argues that the time series of an individual simulation should be an acceptable output (*i.e.* should resemble an observed time series from real world measurements). In the context of Kremer's work, Monte Carlo simulations (even ones corrected in the manner described by Annan) will always tend towards extinction at any given point during the simulation (even if extinction is a long way off in the future). Stochastic parameter simulations, although ultimately ending with the extinction of one of the species, do not tend to that end point throughout a simulation. At a given point during a stochastic parameters simulation it may not be possible to ascertain its end point. This is in direct contrast to a Monte Carlo simulation where its end point can be predicted at any point during a simulation.

Annan's proposed "correction" to Monte Carlo simulations to make them comparable with those of stochastic parameters simulations raises an additional problem for his conclusions. The mean and distribution of parameter values used in stochastic parameters (or Monte Carlo) simulations would normally be drawn from field measurements. The act of "correcting" these distributions for a Monte Carlo simulation (which, in the case of the work here, would involve a sharp constriction of the variability around the mean) puts into question the relevance of such simulations by only permitting a fraction of the variability measured in the field (irrespective of the origin of the parameter variability). Turning the problem on

its head, and increasing the variability of parameters in stochastic parameters simulations instead, then forces these simulations to use values for parameters well outside the measured range. Either way, the purported "correction" would appear to render one or other of the techniques of questionable merit. Furthermore, on a purely methodological basis, Annan's "correction" to parameter variability presupposes a comparison between Monte Carlo and stochastic parameters. If only Monte Carlo simulations are to be performed, just how much should the variability from field measurements be trimmed to accommodate the technique?

Fundamentally, Annan (1997) misconstrues the philosophical underpinnings of Kremer's work. Kremer was not merely proposing stochastic parameters as a rival sensitivity technique to Monte Carlo simulations (although, as evidenced in Kremer, 1983, and within this chapter, it is clearly a contender for use in sensitivity analyses). Stochastic parameters was advanced as a technique to incorporate *real* temporal variability of parameters, rather than presumed uncertainty, into dynamic models.

Although Annan's analysis concisely explains the occurrence of extinctions in Kremer's Monte Carlo simulations and their absence in his stochastic parameters simulation, this latter point nullifies his negative conclusions regarding the potential role of stochastic parameters simulations in ecological modelling. However, it does underline the need for modellers to always clarify the exact nature of any uncertainty introduced into a model.

Chapter 6

Deep chlorophyll maxima, two layer plankton models and Fasham (1993)

Keep on the lookout for novel ideas that others have used successfully. Your idea has to be original only in its adaptation to the problem you're working on.

– Thomas Edison (1847–1931)

6.1 Introduction

One of the simplifications made by all of the models so far discussed is that of a single, vertically–homogenised mixed layer. All of the components of the plankton models are assumed to be at the average concentration down through this mixed layer, and (with the exception of nitrate or general nutrient) at zero concentration in the deeper ocean layers below it.

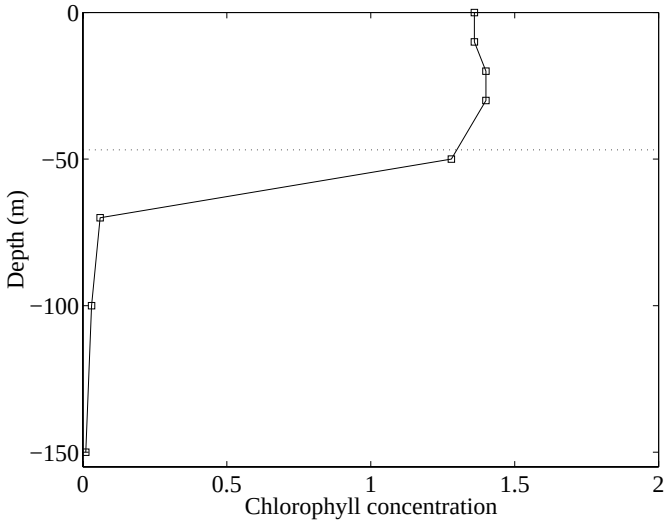

Figure 6.1: A vertical profile of chlorophyll concentration collected at OWS "India" on August the 27th 1972. The squares represent the chlorophyll concentrations measured from water bottles at those depths. The dotted line refers to the mixed–layer depth interpolated from Levitus (1982) on the same day. Chlorophyll concentration in mg chl. m^{-3}, depth in m. (Data courtesy of R. Williams and Dr. Mike Fasham).

Whilst some studies do bear this assumption out for certain locations and for certain times of the year (*e.g.* see figure 6.1), many other studies (Menzel & Ryther, 1960; Hayward, 1991; Brock, Sathyendranath & Platt, 1993; Estrada *et al.*, 1993; Taylor & Stephens, 1993; McManus & Dawson, 1994; Gayoso, 1995; Jochem, 1995; Longhurst, 1995) reveal a common pattern of phytoplankton distribution in which the concentration of phytoplankton (usually inferred from chlorophyll fluorescence) peaks at some subsurface maximum. These regions of relatively greater chlorophyll concentration are referred to as *deep chlorophyll maxima* (DCM). They are also often the regions of highest primary production (Gieskes & Kraay, 1986; Brock, Sathyendranath & Platt, 1993; Jochem, 1995). Figure 6.2 shows a diagrammatic representation of a DCM in relation to the prevailing nutrient and thermal profiles.

DCM are found permanently in oligotrophic, tropical waters, and are observed seasonally in temperate

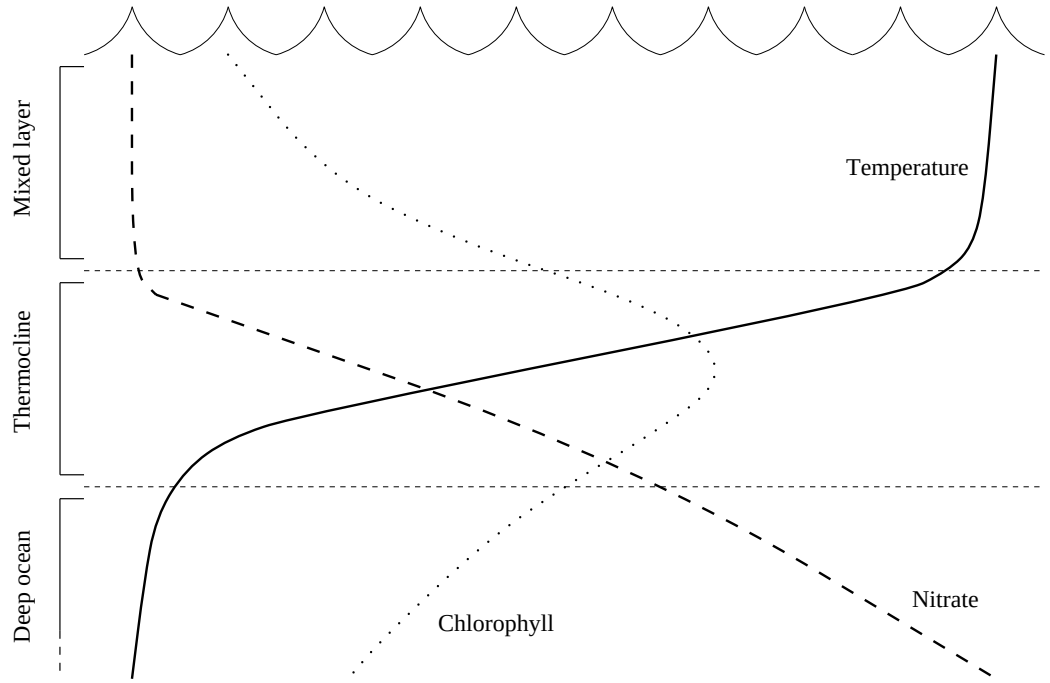

Figure 6.2: Schematic diagram of the typical vertical profiles of temperature, nitrate and chlorophyll in the tropical latitudes. This pattern is usually referred to as the *Typical Trophic Structure* (Banse, 1987). After Mann & Lazier (1991).

waters (Mann & Lazier, 1991). Their appearance in temperate waters usually occurs during the summer months, where a shallow mixed layer, combined with relatively high irradiance, leads to conditions similar to those in the oligotrophic tropics.

It has been proposed (Riley, Stommel & Bumpus, 1949) that the occurrence of a DCM in the summer is the result of phytoplankton cells, produced in the surface waters during the spring bloom, sinking to greater depth. Clearly though, this cannot explain the situation in the tropics, where the DCM persists throughout the year. In their study of community composition and physiological differences between mixed layer and thermocline phytoplankton, Gieskes & Kraay (1986) list several other older (and less favoured) hypotheses of DCM formation. These include the differential degradation of photosynthetic pigments with depth, and the accumulation of cellular debris in the density gradient at the base of the mixed layer. While these hypotheses are not incorrect, they now appear to be less significant processes.

More recently, two hypotheses have been put forward that include processes which may explain the formation of DCM. The first is that the sinking rates of phytoplankton cells are influenced by depth (or irradiance). A decrease in sinking rate with depth, for example, would cause cells to increase in concentration with depth. Experimental work (Bienfang, Syper & Laws, 1983; Lecourt, Muggli & Harrison, 1996) has found that a decrease in irradiance (such as would occur with increasing depth) can result in

decreases in sinking rates in some species, lending support to this hypothesis.

The second hypothesis rests more on the processes of mixing in the upper ocean. As depth increases, turbulent mixing (from wind–driven and convective processes) declines. Together with solar heating of the upper waters of the ocean, this leads to a warmer, more buoyant layer overlying a cooler, less buoyant layer (as described in Chapter 1). The region between these, where the water forms a temperature gradient between the two layers, is known as the thermocline. In tropical locations, or during temperate summers, irradiance is at levels which permit high phytoplankton growth. However, uptake of nutrients from the upper mixed layer to supply this growth, and the subsequent loss of these nutrients from the layer through various pathways (sinking, zooplankton faecal pellets, detrainment, *et cetera*), depletes the layer. Nutrient entry to the upper mixed layer then relies on low mixing and diffusive processes across the thermocline. Given this low rate of nutrient supply and sufficiently high levels of irradiance (even at the depth of the thermocline), populations of phytoplankton can thrive in the thermocline region, giving rise to a DCM.

The structure of the model used in this work essentially assumes the physical processes involved in the latter hypothesis. Several of the results lend support (perhaps unsurprisingly) to the latter hypothesis, but the formulation of sinking processes of phytoplankton here do not permit a fair examination of the former hypothesis.

6.2 Model equations

As in earlier chapters, the full model from Fasham (1993) has been used as the base model.

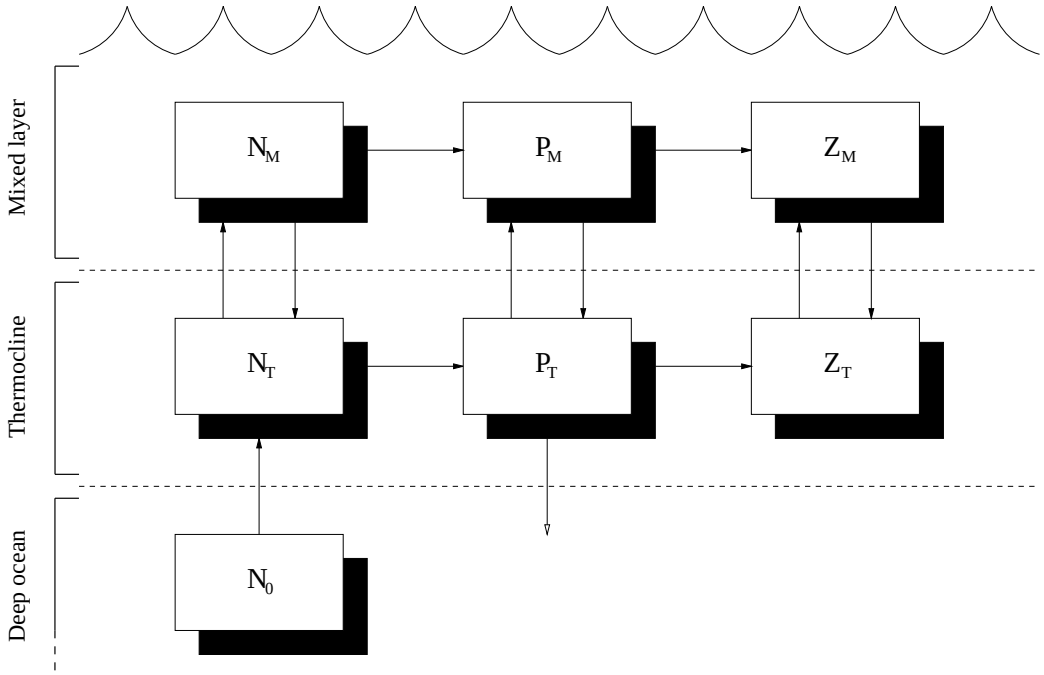

Figure 6.3: Diagrammatic representation of the structure of the two layer model. Only nutrient, phytoplankton and zooplankton are illustrated, but the model contains pairs of each of the full model's compartments.

The new model retains the mixed layer from the base model, but adds a second layer beneath it to represent the thermocline layer. The mixed layer's depth, M, is variable, and is modelled as before by a series of daily values. The thermocline layer, T, is assumed to remain a constant thickness throughout the year. Following Taylor *et al.* (1991), unless stated otherwise this has been set to 40 m. All model compartments are represented separately in both layers (except in the case of one zooplankton model; see later), and both layers are assumed to be well–mixed. As before, all compartments (with the exception of nitrate) are assumed to be at zero concentration below the bottom layer. This arrangement follows the format of several other two layer models (Peng *et al.*, 1987; Taylor, 1988; Taylor *et al.*, 1991; Taylor & Stephens, 1993; Ross *et al.*, 1993; Ross *et al.*, 1994).

Figure 6.3 shows a simplified diagram of the model. Nitrate (shown as nutrient in the diagram) mixes between the layers and from a constant deep ocean supply. Phytoplankton (as well as several of the other model compartments) mix between the layers and can be lost to the deep ocean from the thermocline

layer. As before, the zooplankton are not lost to the deep ocean. Whilst the diagram shows mixing of zooplankton between the two layers, the choice of how to represent them in a two layer model is not entirely clear and this is discussed more fully later.

The model equations remain essentially unchanged, with the exception of the mixing/entrainment terms. These terms now have to account for exchanges between the layers as well as with the deep ocean beneath the modelled system. The equations below detail the necessary changes.

In order to distinguish mixed layer from thermocline populations, compartment notation has been modified with a subscript. M is used for mixed layer populations and T for thermocline populations. For example, phytoplankton, P, are now represented by P_M in the mixed layer, and P_T in the thermocline layer. The notation for the three model compartments, nitrate, ammonium and DON, which already possess subscripts, has been modified similarly to distinguish mixed layer from thermocline layer concentrations. For example, nitrate, N_n, is now represented by $N_{n,M}$ and $N_{n,T}$.

6.2.1 Phytoplankton

Although no additional processes are involved in the phytoplankton mixing/entrainment term, the formulation now has to account for exchange between two layers with non–zero populations of phytoplankton as well as exchange with the empty, deep ocean layer.

In the mixed layer population of phytoplankton, the mixing/entrainment term becomes,

$$\begin{aligned} \frac{dP_M}{dt} &= \ldots + \frac{m_1}{M}(P_T - P_M) + \frac{h^+(t)}{M}(P_T - P_M) \\ &= \ldots + \frac{(m_1 + h^+(t))}{M}(P_T - P_M) \end{aligned} \tag{6.1}$$

where,

$$h(t) = \frac{dM}{dt} \tag{6.2}$$

$$h^+(t) = \max(h(t), 0) \tag{6.3}$$

This term is identical to the comparable one in the single layer model except that now the processes occur between the mixed layer and the thermocline layer rather than the mixed layer and an empty, deep ocean layer.

As in the single layer model, a shallowing of the mixed layer, whilst actually detraining phytoplankton from the layer, does not affect the concentration of cells. A deepening, by contrast, will affect the cell concentration by entraining water from the thermocline layer which may have a different cell concentration. This is incorporated in the definition of $h^+(t)$.

The mixing/entrainment term for the phytoplankton in the thermocline layer becomes,

$$\begin{aligned}\frac{dP_T}{dt} &= \ldots + \frac{m_1}{T}(P_M - P_T) + \frac{m_2}{T}(0 - P_T) + \frac{h_T^+(t)}{T}(P_M - P_T) + \frac{h^+(t)}{T}(0 - P_T) \\ &= \ldots + \frac{(m_1 + h_T^+(t))}{T}(P_M - P_T) - \frac{(m_2 + h^+(t))}{T}P_T \end{aligned} \tag{6.4}$$

where,

$$h_T^+(t) = \max(-h(t), 0) \tag{6.5}$$

This term is more complicated than the previous one since the thermocline layer communicates with both the mixed layer and the deep ocean.

Although the thermocline is assumed to have a fixed thickness (T), shallowing of the mixed layer moves it up the water column and detrains its contents from its lower margin with the deep ocean. Unlike the mixed layer, however, its concentration may change during shallowing since it entrains water from the mixed layer above. This is parameterised by defining $h_T^+(t)$, which takes the value of the rate of mixed layer depth change when it is shallowing, but becomes zero when it is deepening (this is essentially the opposite of $h^+(t)$).

When the mixed layer deepens, the thermocline layer loses phytoplankton which become entrained in the mixed layer, and has its concentration of phytoplankton cells diluted by entrainment of water from the deep ocean. The former loss leads to no change in the concentration of cells, so does not appear in the equation (although it does appear in the equation for mixed layer phytoplankton). The latter process dilutes the cell concentration, and so is parameterised (as in the single layer model) by $h^+(t)$.

In both equations, mixing between layers is parameterised, as normal, by a constant rate, m. Since mixing now occurs across two boundaries (mixed layer to thermocline, thermocline to deep ocean), two parameters have been created, m_1 and m_2. However, unless otherwise stated, both have been assigned the same value in the work presented here.

The photosynthetic processes of phytoplankton in the thermocline layer are modelled in the same way as those in the mixed layer. Equation 6.6 uses Beer's law from chemistry to calculate the amount of irradiance which reaches the top of the thermocline layer after passing through the mixed layer. This equation is the same as the one which is used to provide depth–integrated irradiance in the irradiance–limited portion of phytoplankton growth.

$$I_T = I_0 \exp\{-(k_w + k_c P_M)M\} \tag{6.6}$$

Although the mixing/entrainment terms above deal specifically with the phytoplankton equation, they are also applied to the bacterial, ammonium and DON equations, which comprise similarly passive particles or molecules. Because there are no other changes to the equations of these three compartments, outside of the modifications to the mixing/entrainment terms, they have not been repeated here.

However, the detritus, nitrate and zooplankton equations require different changes to accommodate differences in their mixing/entrainment terms.

6.2.2 Detritus

In addition to the mixing and entrainment changes already described in the phytoplankton terms above, the detritus terms also have to account for sinking of particles. In the mixed layer, this only means sinking loss as before. However in the thermocline layer, this means accounting both for particles sinking out of the layer, and particles sinking into the layer from the mixed layer above.

The equations then become,

$$\begin{aligned}\frac{dD_M}{dt} &= \ldots + \frac{m_1}{M}(D_T - D_M) + \frac{h^+(t)}{M}(D_T - D_M) - \frac{V_1}{M}D_M \\ &= \ldots + \frac{(m_1 + h^+(t))}{M}(D_T - D_M) - \frac{V_1}{M}D_M \end{aligned} \tag{6.7}$$

$$\begin{aligned}\frac{dD_T}{dt} &= \ldots + \frac{m_1}{T}(D_M - D_T) + \frac{m_2}{T}(0 - D_T) + \frac{h_T^+(t)}{T}(D_M - D_T) \\ &\quad + \frac{h^+(t)}{T}(0 - D_T) + \frac{V_1}{T}D_M - \frac{V_2}{T}D_T \\ &= \ldots + \frac{(m_1 + h_T^+(t))}{T}(D_M - D_T) + \frac{V_1}{T}D_M - \frac{(m_2 + h^+(t) + V_2)}{T}D_T \end{aligned} \tag{6.8}$$

As with the mixing constants described earlier, V_1 and V_2 refer to the sinking velocities of particles in the different layers. They have been assigned the same value in all of the work presented here.

6.2.3 Nitrate

The mixing/entrainment terms used in the equations for the two layers are almost identical to those described earlier for phytoplankton. The only difference is that the term for nitrate concentration in the thermocline layer includes exchanges with a non–zero concentration of nitrate (N_0) in the deep ocean.

$$\begin{aligned}\frac{dN_{n,M}}{dt} &= \ldots + \frac{m_1}{M}(N_{n,T} - N_{n,M}) + \frac{h^+(t)}{M}(N_{n,T} - N_{n,M}) \\ &= \ldots + \frac{(m_1 + h^+(t))}{M}(N_{n,T} - N_{n,M}) \end{aligned} \tag{6.9}$$

$$\begin{aligned}\frac{dN_{n,T}}{dt} &= \ldots + \frac{m_1}{T}(N_{n,M} - N_{n,T}) + \frac{m_2}{T}(N_0 - N_{n,T}) \\ &\quad + \frac{h_T^+(t)}{T}(N_{n,M} - N_{n,T}) + \frac{h^+(t)}{T}(N_0 - N_{n,T}) \\ &= \ldots + \frac{(m_1 + h_T^+(t))}{T}(N_{n,M} - N_{n,T}) + \frac{(m_2 + h^+(t))}{T}(N_0 - N_{n,T}) \end{aligned} \tag{6.10}$$

6.2.4 Zooplankton

In the single layer model presented in Fasham (1993), the zooplankton are assumed to be motile organisms and are neither mixed nor detrained from the mixed layer. When the layer shallows they concentrate

into a smaller volume, and when the layer deepens they are diluted across a larger volume.

Given these assumptions, the modification of the zooplankton equation to accommodate a two layer model structure presents several problems :

- When the mixed layer shallows, do mixed layer zooplankton remain within the mixed layer, or do they allow themselves to be detrained into the thermocline layer?
- Similarly, when the mixed layer deepens, do thermocline zooplankton remain within the thermocline, or do they allow themselves to be entrained into the mixed layer?
- And, since they are motile, is their any communication of zooplankton between the two layers independent of mixed layer movement?

Four different formulations of zooplankton movement were derived to address these points. All four preserve the assumption that the zooplankton do not allow themselves to be detrained into the "abiotic" deep ocean, but differ in their treatment of exchange between the two upper layers. They are :

(i) **"Faithful", non–mixing zooplankton compartments**

The zooplankton in this formulation remain "faithful" to the layer in which they originate. There is no mixing between the layers.

$$\frac{dZ_M}{dt} = \ldots - \frac{h(t)}{M} Z_M \tag{6.11}$$

$$\frac{dZ_T}{dt} = \ldots + 0.0 \tag{6.12}$$

This formulation treats both zooplankton equations as if they were still in single layer models. The mixed layer zooplankton are concentrated and diluted in exactly the same way as the zooplankton in the single layer model are. The thermocline zooplankton are entirely unaffected by changes in mixed layer depth since T is constant and the organisms track the movement of their layer.

(ii) **"Faithful", mixing zooplankton compartments**

As above, but the zooplankton are slightly less "faithful" and mix between the layers.

$$\frac{dZ_M}{dt} = \ldots + \frac{m_1}{M}(Z_T - Z_M) - \frac{h(t)}{M} Z_M \tag{6.13}$$

$$\frac{dZ_T}{dt} = \ldots + \frac{m_1}{T}(Z_M - Z_T) \tag{6.14}$$

This formulation is the same as above, except that it permits mixing between the two upper layers. The mixing takes the same form as in the passive model compartments.

(iii) **"Unfaithful", mixing zooplankton compartments**

As the depth of the mixed layer rises and falls, the zooplankton lag behind and are transferred

between the two layers. However, they still cannot be detrained from the two layer system.

$$\begin{aligned}\frac{dZ_M}{dt} &= \ldots + \frac{m_1}{M}(Z_T - Z_M) + \frac{h^+(t)}{M}(Z_T - Z_M) \\ &= \ldots + \frac{(m_1 + h^+(t))}{M}(Z_T - Z_M) \end{aligned} \tag{6.15}$$

$$\begin{aligned}\frac{dZ_T}{dt} &= \ldots + \frac{m_1}{T}(Z_M - Z_T) + \frac{h^+_T(t)}{T}(Z_M - Z_T) + \frac{h^+(t)}{T}(0 - Z_T) \\ &= \ldots + \frac{(m_1 + h^+_T(t))}{T}(Z_M - Z_T) - \frac{h^+(t)}{T}Z_T \end{aligned} \tag{6.16}$$

The zooplankton in the mixed layer behave here in the same way as passive compartments in the mixed layer. They are detrained by its shallowing, mixed across its margin with the thermocline layer and absorb entrained thermocline zooplankton when it deepens. The thermocline zooplankton mix with and absorb detrained mixed layer zooplankton, and are diluted (as well as detrained to the mixed layer) when the mixed layer deepens.

(iv) **Single zooplankton compartment**

Whilst the previous three formulations split the total zooplankton population between the two modelled layers, the zooplankton in this formulation remain in a single population which spans both modelled layers.

$$\frac{dZ}{dt} = \ldots - \frac{h(t)}{(M+T)}Z \tag{6.17}$$

The single zooplankton compartment here is concentrated and diluted in the same way as in the single layer model. The only difference is that the layer is now thicker because it includes the thermocline.

In the first three formulations above, the remaining portions of the zooplankton equations (grazing and mortality) take the same form as in the single layer model (albeit that the zooplankton in a given layer graze only on phytoplankton, bacteria and detritus from that same layer).

However, the final formulation requires that the zooplankton graze on compartments in both layers. This involves directing flows from two layers into a single layer. Since the layers are usually of different thicknesses, and since all of the terms deal in concentrations rather than absolute quantities, this means that the grazing inputs to the single zooplankton compartment need to be scaled according to the different layer thicknesses. The following (grossly) simplified example provides an illustration.

Considering only the (evaluated) phytoplankton losses to zooplankton grazing :

$$\begin{aligned} \frac{dP_M}{dt} &= -0.5\,\text{mmol N m}^{-3}\,\text{d}^{-1}, \quad M = 30\,\text{m}, & \int_0^M \frac{dP_M}{dt}\,dz &= -15\,\text{mmol N d}^{-1} \\ \frac{dP_T}{dt} &= -0.3\,\text{mmol N m}^{-3}\,\text{d}^{-1}, \quad T = 40\,\text{m}, & \int_M^{M+T} \frac{dP_T}{dt}\,dz &= -12\,\text{mmol N d}^{-1} \end{aligned}$$

Therefore, ignoring transfer inefficiencies between compartments, the zooplankton compartment's gains

are :

$$\begin{aligned}\int_0^{M+T} \frac{dZ}{dt}\,dz &= 15 + 12\,\text{mmol N d}^{-1} \\ &= 27\,\text{mmol N d}^{-1}\end{aligned}$$

The concentration change required for such an absolute change in zooplankton is then :

$$27\,\text{mmol N d}^{-1} = \frac{27}{70}\text{mmol N m}^{-3}\text{ d}^{-1}$$

This change is obtained by re–scaling the grazing rates on the phytoplankton populations in the two layers by the thicknesses of their respective layers :

$$\begin{aligned}\frac{dZ}{dt} &= 0.5\frac{M}{M+T} + 0.3\frac{T}{M+T}\text{mmol N m}^{-3}\text{ d}^{-1} \\ &= 0.5\frac{30}{(30+40)} + 0.3\frac{40}{(30+40)}\text{mmol N m}^{-3}\text{ d}^{-1} \\ &= \mathbf{\frac{27}{70}}\text{mmol N m}^{-3}\text{ d}^{-1}\end{aligned}$$

The grazing terms in the phytoplankton equations (as well as those in the bacterial and detrital equations), and their scaled forms in the single zooplankton equation then look as follows :

$$\frac{dP_M}{dt} = \ldots - G_{1,M} + \ldots \tag{6.18}$$

$$\frac{dP_T}{dt} = \ldots - G_{1,T} + \ldots \tag{6.19}$$

$$\frac{dZ}{dt} = \frac{M}{(M+T)}\beta_1 G_{1,M} + \frac{T}{(M+T)}\beta_1 G_{1,T} + \ldots \tag{6.20}$$

Inputs to the detritus compartments of the two layers due to zooplankton feeding inefficiencies remain unscaled since the losses are assumed to occur at the time of feeding. Thus, in a given layer, material consumed by zooplankton which is lost in this fashion, is lost to the detritus compartment in the same layer.

$$\frac{dD_M}{dt} = \ldots + (1-\beta_1)G_{1,M} + \ldots \tag{6.21}$$

$$\frac{dD_T}{dt} = \ldots + (1-\beta_1)G_{1,T} + \ldots \tag{6.22}$$

In studying the diel migratory behaviour of sub–Antarctic copepods, Atkinson, Ward & Murphy (1996) found two species which underwent daily migrations which took them across the thermocline, *Metridia lucens* and *Pleuromamma robusta*. Since these species only fed at night in the upper mixed–layer, their food intake had a diel signal. However, their gut evacuation did not show diel periodicity, allowing these species to export material from the upper mixed–layer. This is contrary to the assumption of synchronicity made here. However, in the geographical area examined, the authors found that these two species were too scarce for this export pathway to be significant.

Note that zooplankton mortality (essentially the reverse of grazing, since the losses from the single zooplankton compartment flow into sets of compartments in two layers), does not require any re–scaling since it is assumed to occur at a constant, homogeneous rate down the water column.

6.2.5 Assigning parameter values between the layers

In this work, where a parameter is meaningful in both modelled layers, that parameter has been assigned the same value in both. There are several good reasons to suspect this is not likely to be the case for biological parameters, and studies have found differences between the surface and DCM phytoplankton communities (Murphy & Haugen, 1985; Gieskes & Kraay, 1986). However, because of the problems of trading–off biological parameters against one another, this work has not explored this particular avenue. In a later section of this chapter though, independent ranges of the two mixing parameters, m_1 and m_2 are examined.

6.3 Choosing a zooplankton model

Since all four of the zooplankton formulations are plausible given the assumptions made about zooplankton, models incorporating each of them were simulated at OWS "India" and Bermuda Station "S" to establish if the choice of formulation led to any significant differences in the behaviour of the modelled system.

Figures 6.4 and 6.5, and tables 6.1 and 6.2 show the results of simulations for each of the four zooplankton models. The figures show the annual patterns of the major model compartments, and the tables present major summary statistics from the simulations.

Statistic	**Model (i)**	**Model (ii)**	**Model (iii)**	**Model (iv)**
P_M max	1.410	1.412	2.372	2.829
P_M time	148	149	149	155
P_T max	0.490	0.476	0.365	0.221
P_T time	170	170	152	157
NPP_M	0.933	0.934	0.990	1.022
NPP_T	0.129	0.127	0.096	0.051
NPP ratio	0.879	0.880	0.912	0.953
f–ratio$_M$	0.520	0.520	0.508	0.423
f–ratio$_T$	0.678	0.677	0.635	0.482

Table 6.1: Model statistics from simulations performed at OWS "India" for the four zooplankton models. Mixed layer statistics are denoted by a subscripted M, thermocline statistics by a subscripted T. **P max** is the maximum concentration of phytoplankton predicted during the simulated year (mmol N m^{-3}). **P time** is the day of the year this maximum occurs on. **NPP** is the annual net primary production in each layer (mol m^{-2} y^{-1}). **NPP ratio** is the ratio of annual net primary production in the mixed layer to total net primary production in both layers. **f–ratio** is the mean annual f–ratio.

At Bermuda Station "S", all four models show the same "double–peaked" mixed layer phytoplankton pattern, and similar annual patterns of abundance of thermocline phytoplankton. All four models exhaust nitrate in almost exactly the same fashion during the summer months, and have zooplankton abundances which peak just behind the spring bloom.

At OWS "India" by contrast, whilst models (i) and (ii) show very similar behaviour (and mixed layer

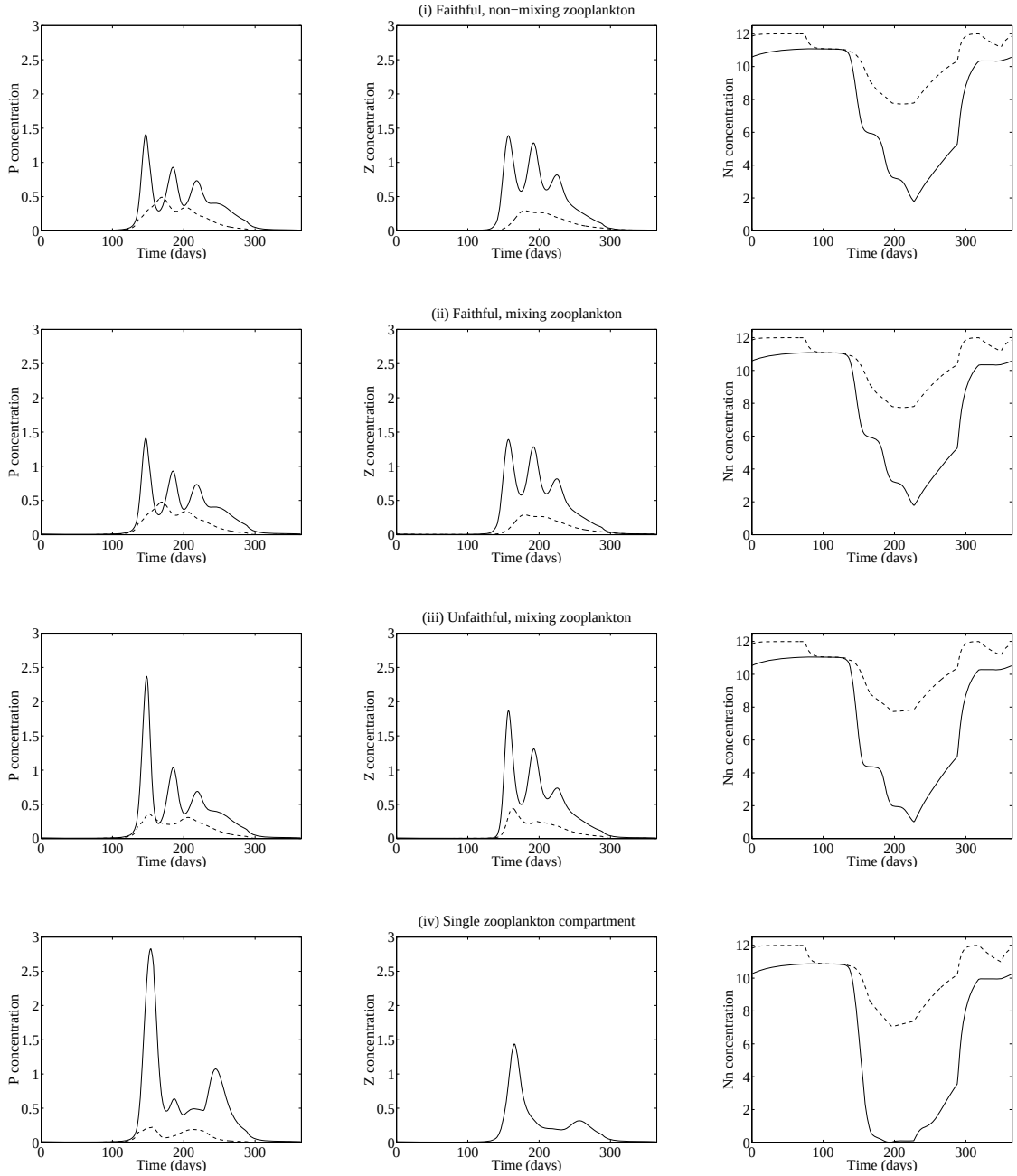

Figure 6.4: Simulated annual cycles of phytoplankton, zooplankton and nitrate concentration at OWS "India" for each of the formulations of zooplankton two–layer behaviour. Mixed layer concentrations are represented by a solid line, thermocline layer concentrations by a dashed line. In the case of formulation (iv) (the bottom set of diagrams), zooplankton are represented by single compartment spanning both model layers so no thermocline layer is plotted. Concentrations are in mmol N m^{-3}.

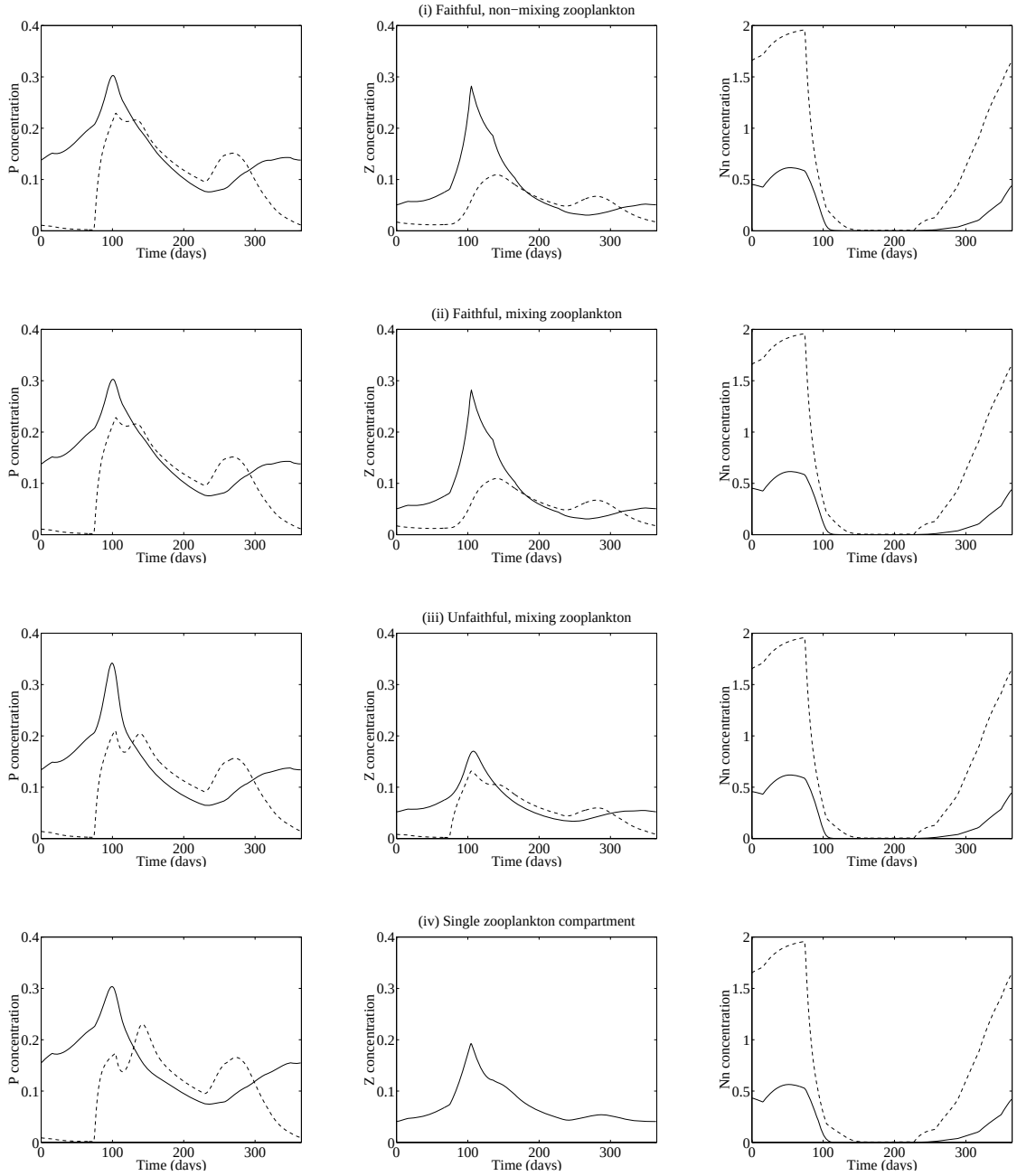

Figure 6.5: Simulated annual cycles of phytoplankton, zooplankton and nitrate concentration at Bermuda Station "S" for each of the formulations of zooplankton two–layer behaviour. Mixed layer concentrations are represented by a solid line, thermocline layer concentrations by a dashed line. In the case of formulation (iv) (the bottom set of diagrams), zooplankton are represented by single compartment spanning both model layers so no thermocline layer is plotted. Concentrations are in mmol N m^{-3}.

Statistic	Model (i)	Model (ii)	Model (iii)	Model (iv)
P_M max	0.303	0.303	0.342	0.304
P_M time	102	102	100	100
P_T max	0.229	0.228	0.211	0.230
P_T time	106	106	105	143
NPP_M	0.360	0.360	0.332	0.343
NPP_T	0.083	0.084	0.081	0.088
NPP ratio	0.812	0.812	0.804	0.796
f–ratio$_M$	0.394	0.393	0.392	0.385
f–ratio$_T$	0.559	0.559	0.574	0.537

Table 6.2: Model statistics from simulations performed at Bermuda Station "S" for the four zooplankton models. Mixed layer statistics are denoted by a subscripted M, thermocline statistics by a subscripted T. **P max** is the maximum concentration of phytoplankton predicted during the simulated year (mmol N m^{-3}). **P time** is the day of the year this maximum occurs on. **NPP** is the annual net primary production in each layer (mol m^{-2} y^{-1}). **NPP ratio** is the ratio of annual net primary production in the mixed layer to total net primary production in both layers. **f–ratio** is the mean annual f–ratio.

behaviour very similar to that from single layer model simulations), models (iii) and (iv) show considerably larger spring blooms of phytoplankton. After this larger spring bloom, model (iii) falls into the normal (with respect to the single layer model) pattern of damped predator–prey oscillations during the summer. Model (iv), instead, has a much larger and longer spring bloom, followed by very small summer oscillations (noticeably only observed in the phytoplankton abundances), and then a relatively large autumn bloom before the system falls to low winter abundances. The reasons for these two patterns are discussed below.

During the shallowing of the mixed layer in springtime, model (iii)'s zooplankton are detrained from the mixed layer and entrained into the thermocline layer. This can be seen in the zooplankton plot of figure 6.4, and more clearly in the detailed time series of figure 6.6. This latter plot shows the fraction of total, depth–integrated zooplankton biomass which is in the mixed layer. As the mixed layer shallows, zooplankton are transferred into the deeper thermocline layer. This contrasts with model (i) (also shown in the figure) where the zooplankton remain "faithful" to the layer they find themselves in, and track its shallowing and deepening. The reduction of zooplankton in the mixed layer in model (iii) allows the phytoplankton population there to escape grazing for longer and consequently have a much larger spring bloom maximum (see table 6.1). Once the mixed layer zooplankton population has recovered though, model (iii) behaves very similarly to models (i) and (ii) through the remainder of the summer.

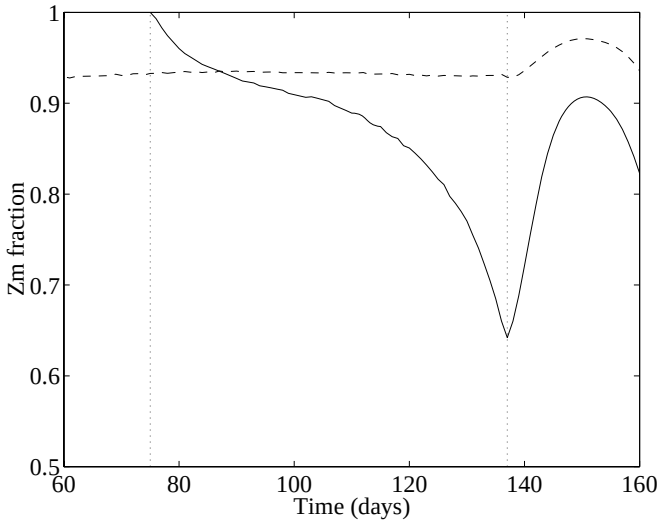

Figure 6.6: A detail showing the fraction of total mixed layer and thermocline zooplankton biomass in the mixed layer during the shallowing of the mixed layer in springtime (the dotted vertical lines mark the start and finish of the shallowing period). The simulated results of models (i) (dashed line) and (iii) (solid line) are shown.

Model (iv) behaves somewhat similarly to model (iii) insofar as a reduced zooplankton population in the spring is unable to control an escaping phytoplankton bloom. However, the reason for the reduced population is quite different. Unlike the other models, where the zooplankton population is divided into two subpopulations which are treated separately, zooplankton in model (iv) are assumed to be distributed homogeneously through the entire depth of the mixed and thermocline layers. In the case of OWS "India", where the prey concentration in the mixed layer is considerably higher than in the thermocline layer, the formulation of model (iv) reduces the ability of the zooplankton population to "keep up with" the phytoplankton population in two ways. Firstly, higher gains to the zooplankton from grazing in the mixed layer are distributed through both layers, effectively reducing the population growth rate of the zooplankton in the mixed layer. Secondly, the "buoying–up" of zooplankton concentrations in the thermocline layer by inputs from their brethren in the mixed layer, exposes this fraction of the zooplankton population to a greater rate of loss than the lower concentrations of thermocline zooplankton in the other three models experience. These two consequences of the model (iv) formulation effectively burden the whole zooplankton compartment with a lower population growth rate, whereas the mixed layer gains and thermocline layer losses are partitioned in the models with two zooplankton compartments. Figure 6.7 shows the difference in the balance of zooplankton grazing and predation fluxes between model (iv) and the mixed layer zooplankton of model (i). The smaller positive balance of model (iv) at the start of the spring bloom prevents it from controlling the bloom as effectively as the zooplankton in model (i). As a result, the mixed layer phytoplankton bloom is much greater and lasts much longer.

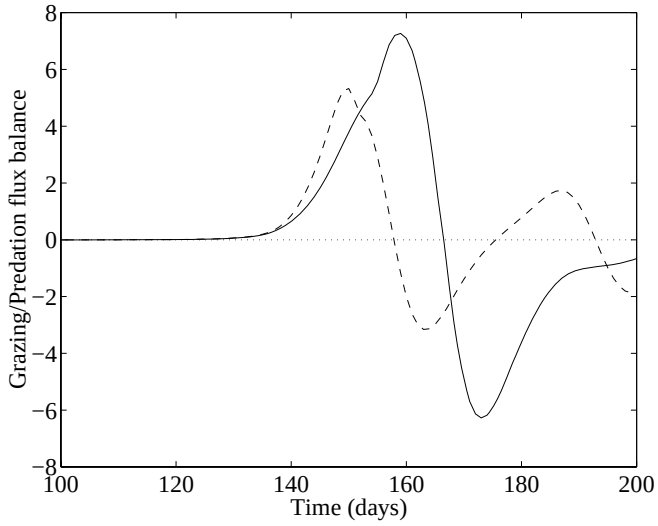

Figure 6.7: A detail showing the balance of zooplankton fluxes coming from grazing and going to predation during the spring bloom. The simulated results of Z_M from model (i) (dashed line) and Z from model (iv) (solid line) are shown. Fluxes in mmol N m^{-2} d^{-1}.

In addition to the greater mixed layer phytoplankton blooms found with models (iii) and (iv), the thermocline layers have much lower and much earlier phytoplankton maxima. In the case of model (iii), this occurs because zooplankton entrained in the thermocline layer from the mixed layer are able to control the phytoplankton there more easily. In model (iv), the higher mixed layer phytoplankton concentrations reduce the availability of light in the thermocline and "stunt" growth there. In both cases, these processes lead to primary productivity in the mixed layer being even more significant than that in the thermocline layer (see tables 6.1 and 6.2).

Another consequence of the single zooplankton compartment in model (iv) is that ammonium levels become significantly higher in the thermocline layer where phytoplankton grow too slowly to fully exploit it. This is then reflected in a much lower f–ratio in the thermocline layer (the exhaustion of nitrate in the mixed layer during the high spring bloom shifts the mixed layer f–ratio similarly downwards).

The different models of zooplankton therefore differ dynamically in several ways. These differences are fairly minor at Bermuda Station "S" , where the change of mixed–layer depth across the year is lower, but they become significant at OWS "India". Models (i) and (ii) behave almost identically, and produce seasonal patterns of abundance similar to those observed at OWS "India". Models (iii) and (iv), by contrast, behave quite differently, both from the other two models, from the single layer model and from the observations at OWS "India".

For these reasons, models (iii) and (iv) were discarded in favour of models (i) and (ii). Since zooplankton are well known to move vertically in the water column, the less "faithful" zooplankton of model (ii) were

chosen over their rigidly "faithful" model (i) counterparts. For the rest of the work detailed in this chapter, model (ii) was used to represent the zooplankton.

6.3.1 Evolutionary considerations

The decision to choose model (ii) to represent the zooplankton in this chapter was based on the greater congruence of this model with observations at OWS "India". Another potentially reasonable way to decide could have been to run the models in competition against one another. Whichever model produced the higher annual biomass could then be chosen as the "victor".

However, as with "evolving" values for model parameters, this technique suffers from a lack of knowledge of the various feedbacks and links between different model terms. A motility strategy in this model which may maximise consumption of phytoplankton, may ignore the effects on predation losses the same strategy may have in the real world. The most successful model strategy is likely (in the absence of good knowledge about the full effects of different strategies in the real world) to be precisely that, the most successful *model* strategy. Hence success here has been restricted to the greatest agreement with data.

6.4 Latitudinal variation in the importance of DCM

As could be seen previously with the simulations performed at OWS "India" and Bermuda Station "S", the importance of the thermocline layer (in terms of primary production) is not constant. At OWS "India" , the layer contributed about 12% of total net primary productivity, whereas at Bermuda Station "S", the layer produces almost 20% of the total (tables 6.1 and 6.2).

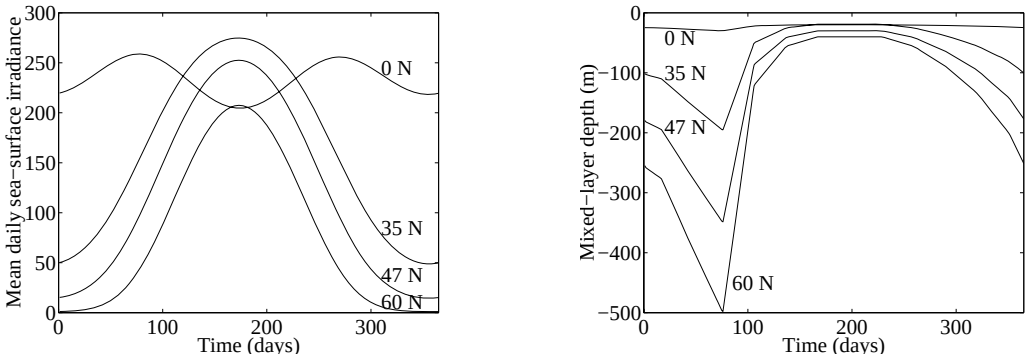

Figure 6.8: Annual cycles of mean daily sea–surface irradiance (left) and mixed–layer depth (right) at each of the four simulated latitudes. The Smith & Dobson (1984) model of atmospheric transmittance of irradiance was used, with a cloud cover of 4 oktas. Mixed–layer depth data re–scaled from Bermuda Station "S" data using limits in Taylor *et al.* (1991). Irradiance in W m^{-2}. Mixed–layer depth in m.

However, OWS "India" and Bermuda Station "S" only represent two locations. In order to simulate plankton dynamics at other latitudes, the approach from Taylor *et al.* (1991) was used. Taylor and his co–workers ran their two layer model (a considerably simpler phytoplankton–nutrient model) with the mixed–layer depth data for Bermuda Station "S", but re–scaled it to the maximum and minimum depths found at four different latitudes (0°, 35°, 47° and 60° N). Several other model parameters were also given latitude–specific values. Their resulting simulations reproduced most of the significant features of phytoplankton abundance at the latitudes examined.

Figure 6.8 shows the seasonal cycles of sea–surface irradiance and mixed–layer depth at the four simulated latitudes. Table 6.3 lists the latitude–specific parameter values (from tables 1a and 1b in Taylor *et al.*, 1991). With the exception of these changes, the two layer model simulations were run as normal.

6.4.1 Comparison with Taylor *et al.* (1991)

The simulated annual cycles of phytoplankton, zooplankton and nitrate at each of the four latitudes are shown in figure 6.9. Since both this two layer model and Taylor *et al.*'s phytoplankton–nutrient model

Parameter	Symbol	Unit	0° N	35° N	47° N	60° N
Minimum mixed–layer depth	M_{min}	m	20.0	19.0	30.0	40.0
Maximum mixed–layer depth	M_{max}	m	30.0	196.0	350.0	500.0
Thermocline thickness	T	m	40.0	40.0	40.0	40.0
Mixing rates	m_1, m_2	m d^{-1}	0.20	0.40	0.45	0.60
Attenuation coefficient	k_w	m^{-1}	0.03	0.03	0.05	0.08
P maximum growth rate	V_p	d^{-1}	2.00	2.00	2.00	2.00
Subthermocline nitrate	N_0	mmol N m^{-3}	2.00	3.00	9.00	6.00

Table 6.3: Parameter value changes used for simulations performed at the four latitudes (following Taylor *et al.*, 1991). The listed phytoplankton maximum growth rate applies to the phytoplankton populations in both modelled layers. All other model parameters remained at the standard values listed in Fasham (1993).

produce similar kinds of output, their simulation results can be compared with one another, as well as with real data from the appropriate latitudes.

60° N

At 60° N, the model shows similar behaviour to that already shown for OWS "India". The seasonal cycle shows high phytoplankton concentrations in the summer and very low concentrations during the winter. The annual phytoplankton maximum occurs during the spring bloom, and the phytoplankton in the mixed layer are entirely dominant across the year. This pattern of activity is broadly in agreement with the data collected from OWS "India" (recounted in : Fasham, 1993; Taylor *et al.*, 1991). The maximum chlorophyll concentration predicted is 1.9 mg chl. m^{-3}, which is slightly lower than the 2.7 mg chl. m^{-3} observed at OWS "India" in 1972[1]. Total annual primary production is predicted at 54.6 g C m^{-2} y^{-1}, slightly less than the maximum, 63.6 g C m^{-2} y^{-1}, recorded at OWS "India". These agreements are somewhat closer than those with Taylor *et al.*'s model, which over–estimates the magnitude of the spring bloom (5.0 mg chl. m^{-3}) and the total annual production (89.0 g C m^{-2} y^{-1}). Taylor *et al.*'s model also predicts much lower summer nutrient levels than are commonly found at OWS "India" (Fasham, 1993).

47° N

As latitude falls through 47° to 35 ° N, the spring bloom is predicted to arrive earlier and earlier. This pattern was found by Strass & Woods (1991) in their analysis of the horizontal variation of mixed–layer chlorophyll. The predicted importance of the thermocline layer also rises, and this prediction is somewhat supported by Strass & Woods' (1991) finding that the depth of the DCM increases (*i.e.* the

[1] The conversion of mmol N m^{-3} to mg chl. m^{-3} uses the standard Redfield C:N molar ratio of 6.625 and a C:chlorophyll mass ratio of 50; this equates 1.0 mmol N m^{-3} with 1.59 mg chl. m^{-3}.

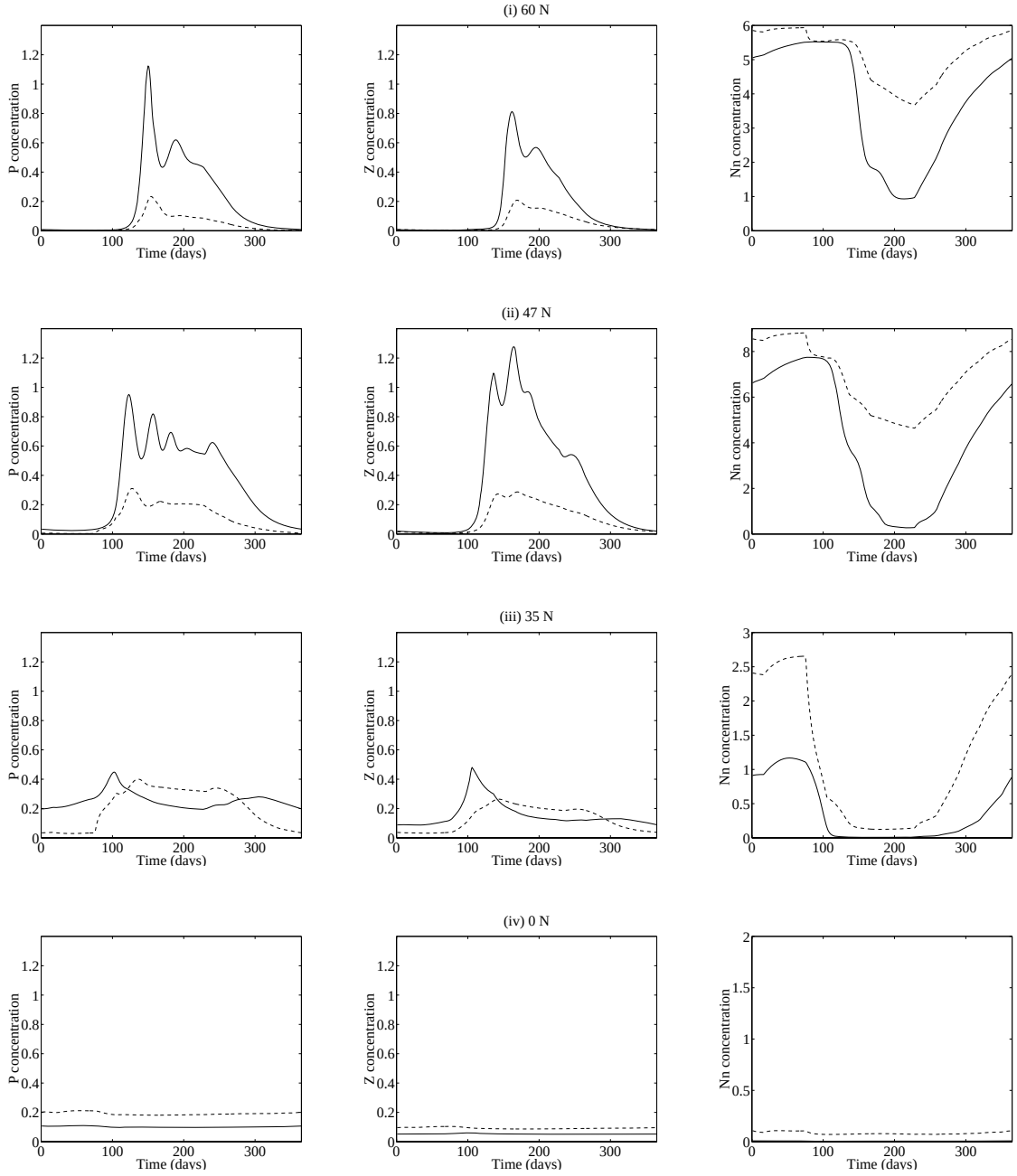

Figure 6.9: Annual cycles of phytoplankton, zooplankton and nitrate concentration at each of the simulated latitudes. Mixed layer concentrations are represented by a solid line, thermocline layer concentrations by a dashed line. The nitrate plots are scaled such that the top of the graph marks the concentration of the subthermocline nitrate level (N_0). Concentrations are in mmol N m^{-3}.

DCM gets deeper) at lower latitudes. However, the importance of the thermocline layer in the late summer (0.5–1.0 mg chl. m^{-3}) is under–estimated by the model (0.3 mg chl. m^{-3}). Taylor *et al.*'s model more accurately predicts the late summer importance of the thermocline at 47° N (although it again over–estimates the significance of the spring bloom).

35° N

By 35° N both models predict that the thermocline layer dominates the summer months. This agrees with Menzel & Ryther's (1960) findings. However, both models disagree with the magnitude of phytoplankton concentration at different times of the year. Again, Taylor *et al.*'s model over–estimates the magnitude of the spring "bloom". Menzel & Ryther (1960) found concentrations between 0.5 and 1.0 mg chl. m^{-3} (as did the two layer version of Fasham, 1993), while Taylor *et al.* predicted concentrations of almost 2.5 mg chl. m^{-3}. During the summer months, the accuracy of the models was reversed, with the two layer version of Fasham (1993) predicting considerably higher phytoplankton concentrations (> 0.3 mg chl. m^{-3}) in both layers than were found by Menzel & Ryther (< 0.2 mg chl. m^{-3}), and predicted by Taylor *et al.*.

These higher summer concentrations are partially explained by the markedly higher mixing rates assumed in this work. Whilst Fasham (1993) assumed a cross–thermocline mixing rate of 0.01 m d^{-1}, Taylor *et al.* chose a rate of 0.40 m d^{-1}, which allows much more nitrate to enter the modelled system from below the thermocline. However, even at this much reduced mixing rate, mixed layer phytoplankton remain at relatively high concentrations (0.15–0.30 mg chl. m^{-3}; results not shown).

Despite these discrepancies in phytoplankton concentration, the two layer version of Fasham (1993) predicts a pattern of production (see figure 6.10) very similar to that found by Menzel and Ryther (1960), and estimates a total annual production of 88.2 g C m^{-2} y^{-1}. This compares very favourably with the value of 90 g C m^{-2} y^{-1} reported by Smith, Jickells & Knap (1987; as cited in Fasham, Ducklow & McKelvie, 1990).

0° N

The predicted community structure at 0° N was agreed upon by both models. The thermocline phytoplankton entirely dominate the whole year, although both populations exist at very low, almost unchanging concentrations. This pattern is referred to as the *Typical Trophic Structure* (Banse, 1987). Whilst the models predict different phytoplankton concentrations, both predictions fall within the range found by Banse (1987) for the equatorial Gulf of Guinea (0.1–0.4 mg chl. m^{-3}).

6.4.2 Patterns of biological production

Figure 6.10 and table 6.4 respectively show the annual patterns of production and the major statistics from the four latitude simulations.

As before, with decreasing latitude the spring production maximum comes earlier and earlier, and the significance of the thermocline layer becomes greater and greater. Between 60° and 35° N, the timing of the spring bloom advances almost 50 days. Across the same range of latitude, the fraction of total production which occurs in the thermocline layer rises from less than 1% to almost 35%, and at the equator this fraction almost reaches 90%. Another trend with decreasing latitude is the increasing reliance on regenerated nutrient for production. This occurs in both layers, although it is a particularly strong trend in the mixed layer.

Statistic	**0° N**	**35° N**	**47° N**	**60° N**
P_M max	0.110	0.448	0.951	1.124
P_M time	51	102	123	150
P_T max	0.212	0.400	0.310	0.234
P_T time	53	136	128	154
NPP_M	0.039	0.725	1.412	0.683
NPP_T	0.261	0.385	0.085	0.004
NPP ratio	0.131	0.654	0.943	0.994
f–ratio$_M$	0.157	0.388	0.486	0.573
f–ratio$_T$	0.555	0.633	0.578	0.705

Table 6.4: Model statistics from simulations performed at the four latitudes. Mixed layer statistics are denoted by a subscripted M, thermocline statistics by a subscripted T. **P max** is the maximum concentration of phytoplankton predicted during the simulated year (mmol N m^{-3}). **P time** is the day of the year this maximum occurs on. **NPP** is the annual net primary productivity in each layer (mol m^{-2} y^{-1}). **NPP ratio** is the ratio of annual net primary production in the mixed layer to total net primary production in both layers. **f–ratio** is the mean annual f–ratio.

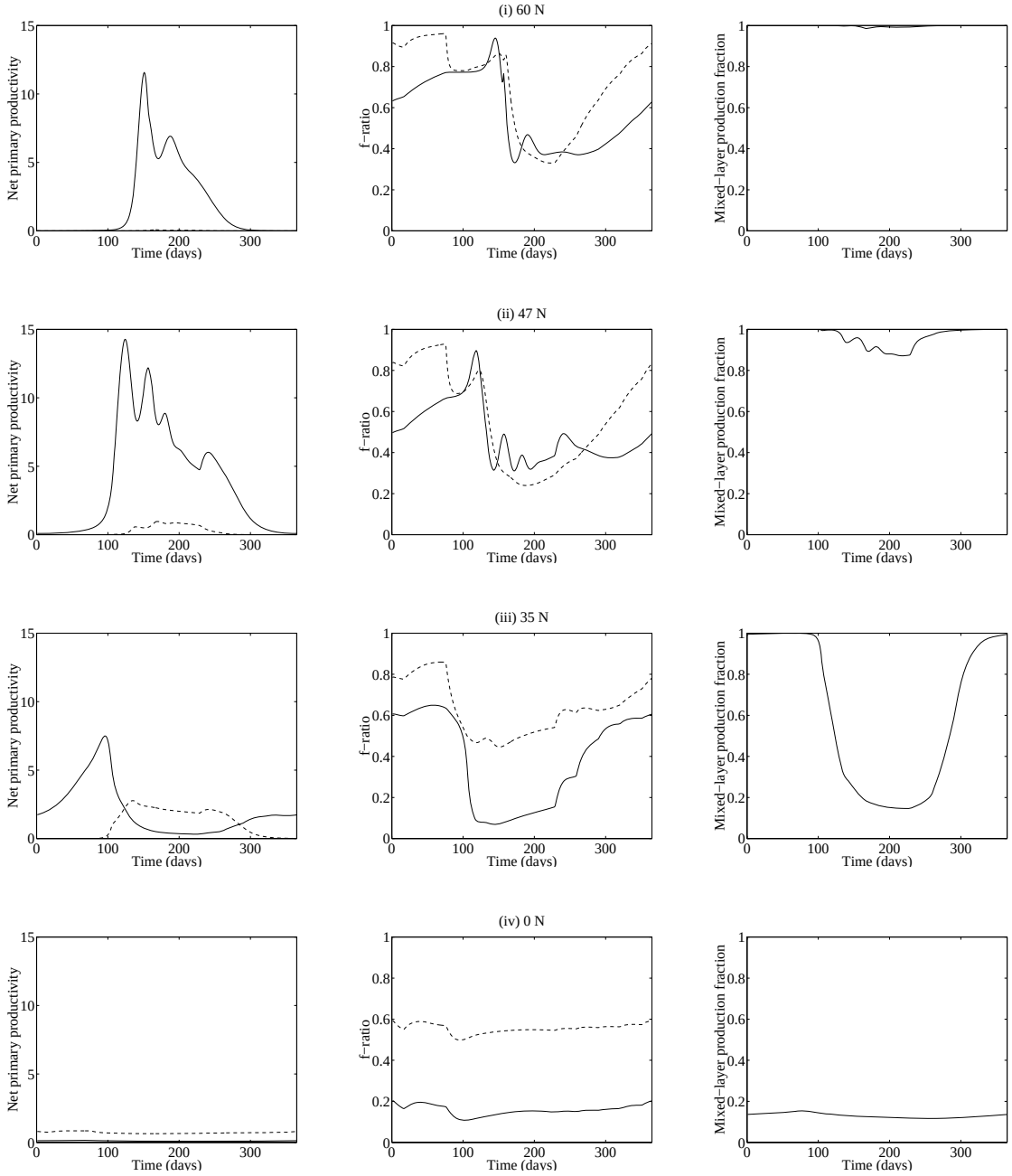

Figure 6.10: Annual cycles of net primary productivity, the f–ratio and the proportioning of net, depth–integrated production in the two modelled layers at each of the simulated latitudes. Mixed layer results are represented by a solid line, thermocline results by a dashed line. Since the latter column of results represents a proportion between the two layers only a single solid line is shown. Net primary productivity is in mmol N m^{-2} d^{-1}. The f–ratio and the production ratio are dimensionless.

6.5 Taylor's common model properties

Taylor (1988) defined a simple two–layer, two component plankton model to explore the general properties of such vertically structured models. This model's two–layer structure is identical to that detailed previously in the modified form of Fasham (1993), but consists only of phytoplankton and a general nutrient. The model equations are detailed below. Several of the terms and parameters used have been renamed here to give greater parity with the Fasham (1993) model.

$$\frac{dP_M}{dt} = [J(I_0)Q(N_M) - \mu - \frac{v}{M}]P_M + \frac{m_1}{M}(P_T - P_M) \quad (6.23)$$

$$\frac{dN_M}{dt} = -\gamma[J(I_0)Q(N_M) - \epsilon\mu]P_M + \frac{m_1}{M}(N_T - N_M) \quad (6.24)$$

$$\frac{dP_T}{dt} = [J(I_M)Q(N_T) - \mu]P_T - \frac{v}{T}(P_T - P_M) - \frac{m_2}{T}P_T + \frac{m_1}{M}(P_M - P_T) \quad (6.25)$$

$$\frac{dN_T}{dt} = -\gamma[J(I_M)Q(N_T) - \epsilon\mu]P_T + \frac{m_2}{T}(N_0 - N_T) + \frac{m_1}{T}(N_M - N_T) \quad (6.26)$$

As before, the mixed layer is denoted by the M subscript, and the thermocline layer by the T subscript; these are also the parameters representing the thicknesses of the two layers. Sea–surface irradiance, I_0, is attenuated down the water column to the top of the thermocline layer, to I_M, in the same manner as before.

Phytoplankton growth is defined by the product of light–limited, $J(I)$, and nutrient–limited, $Q(N)$, functions. A single constant loss rate, μ, represents grazing and other mortality. The phytoplankton cells sink out of the modelled system at a constant rate v, and are transferred between the modelled layers and the deep ocean by the mixing rates m_1 and m_2.

Nutrient concentrations are depleted by phytoplankton growth (the modifier γ is the nutrient concentration of the cells), replenished by recycling (where ϵ is the recycling efficiency), and mixed between the two modelled layers (in the same way as the phytoplankton cells). A deep–ocean reservoir of nutrient at a constant concentration, N_0, communicates with the thermocline layer.

To determine general properties, Taylor further simplified the model to allow it to be examined algebraically. It was assumed that the nutrient concentration in the mixed layer is sufficiently low that the phytoplankton growth function in the layer could be rewritten as $\beta_M N_M$, where β_M is a constant which depends solely on irradiance at the sea surface. Additionally, it was assumed that vertical stratification is sufficiently weak that nutrient concentration in the thermocline layer is never limiting for the phytoplankton cells there, and that their growth function could be rewritten as a constant, θ_T, which depends only on irradiance at the sea surface. Seasonal variation in irradiance and mixed–layer depth forcing was also ignored. These simplifications were used to help derive algebraic expressions relating various terms in the model.

Similar work with a more complicated three compartment model (phytoplankton, nitrate and ammonium) and a more detailed ecosystem model (the **M**ixed **U**pper–**L**ayer **E**cosystem **S**imulation, or MULES, model of Parsons & Kessler, 1987), supported the results of the initial analysis of Taylor's two compartment system.

The results of the analysis and simulation of these three model systems indicated several common features in the behaviour of these models which could, in principle, be searched for in observational data. Taylor (1988) proposed four such properties, but to simplify later discussion, his final property is divided into the latter two here. The five properties are then :

(i) The nutrient concentration of the mixed layer is independent of the efficiency of recycling and the concentration of nutrient below the thermocline, whilst the abundance of phytoplankton increases with both of these

(ii) The phytoplankton concentrations in each of the two vertical layers show a common response to changes in : efficiency of recycling, subthermocline nutrient concentration, the Michaelis–Menten parameters, and the loss term rates

(iii) Raising the growth of phytoplankton in the thermocline (*e.g.* by increasing the surface irradiance) results in a decrease in growth of phytoplankton in the upper mixed layer

(iv) The ratio of upper mixed layer to thermocline production, and the ratio of "new" nutrient entering the layer to nutrient recycled back into it, do not depend on the concentration of nutrient below the thermocline

(v) The ratio of the production in the two layers also does not depend on the efficiency of recycling

Although the two layer version of Fasham (1993) lacks several of the processes present in the models Taylor examined (*e.g.* respiratory losses, phytoplankton sinking, variable cell quota; some of which are modelled implicitly in Fasham's model), it does model several others more explicitly (*e.g.* grazing loss, nitrogen regeneration processes), and overall permits examination for the five properties, since it shares the same foundation as the models examined by Taylor.

However, the complexity of the two layer form of Fasham (1993) prevents any similar algebraic analysis of these common model properties unless sacrifices of model complexity are made. Since Taylor's work has dealt with comparatively simpler models already, and to maximise the use of existing computer programs, the full complexity of the two layer form of Fasham (1993) has been retained. So numerical solutions were used instead to examine whether Taylor's properties could be found.

Since Taylor assumes a situation for his analysis in which the mixed layer is nutrient–limited and the thermocline layer irradiance–limited, simulations were run with constant forcing from Bermuda Station "S" on day 173. At this latitude, and at this time of year, these conditions are closely met. Mixed layer

nitrate is at near–zero concentrations, and thermocline phytoplankton have a light–limited maximum growth rate about half that of mixed layer phytoplankton.

When a range of a parameter was examined, the parameter's value was changed in both layers unless otherwise stated. Several parameters (*e.g.* N_0, mixed–layer depth, thermocline thickness) are only important to a single layer, but most are involved in the model equations in both layers.

6.5.1 Testing the predicted properties

Property (i)

> *The nutrient concentration of the mixed layer is independent of the efficiency of recycling and the concentration of nutrient below the thermocline, whilst the abundance of phytoplankton increases with both of these.*

Property (i) was examined by simulating the model across ranges of N_0, the subthermocline nitrate concentration, and $(\epsilon + \delta)$, the regenerative terms of zooplankton loss processes. In Fasham (1993), ϵ and δ refer to the fractions of zooplankton losses which are returned to the modelled system as ammonium and DON respectively (assigned the values 0.7 and 0.2 in the normal parameter set). Here they were kept in constant proportion to one another (ϵ:δ ratio of 3.5) whilst the fraction of zooplankton losses which were lost from the system altogether was ranged from total loss (= 1.0) to total retention (= 0.0).

In these simulations (as well as the others in this section), the equilibrium–finding program from Chapter 4 was used to find the equilibrium solutions. Only stable equilibrium solutions were found during this work however. As already stated, forcing functions were held constant at those for midsummer at Bermuda Station "S".

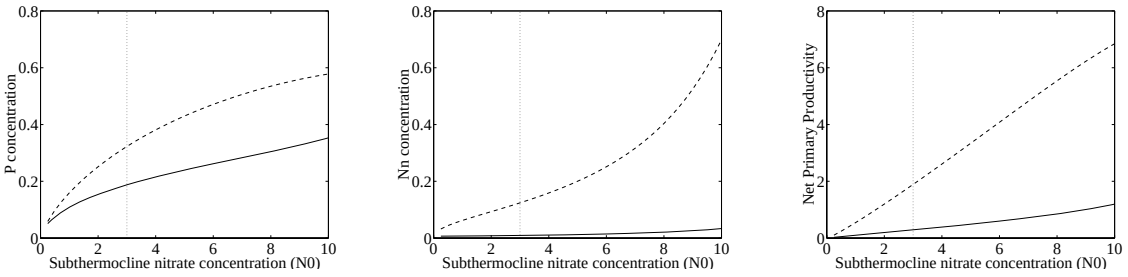

Figure 6.11: Simulated model equilibria of phytoplankton (left), nitrate (centre) and daily net primary productivity (right) across a range of subthermocline nitrate concentrations (model parameter N_0). The mixed layer is represented by a solid line and the thermocline layer by a dashed line. The dotted line indicates the baseline value for N_0 at Bermuda Station "S". Concentrations are in mmol N m^{-3}. Net primary productivity is integrated down each layer and is measured in mol N m^{-2} d^{-1}.

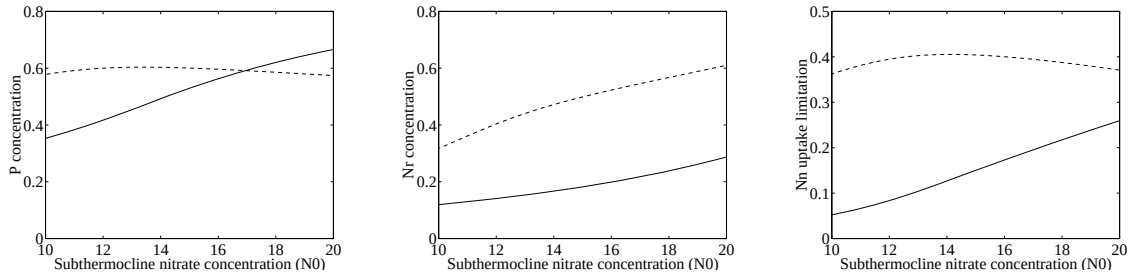

Figure 6.12: Simulated model equilibria of phytoplankton (left), nitrate (centre) and phytoplankton nitrate uptake limitation (right) across a more extreme range of subthermocline nitrate concentrations. The mixed layer is represented by a solid line and the thermocline layer by a dashed line. Concentrations are in mmol N m^{-3}. Nitrate limitation is dimensionless.

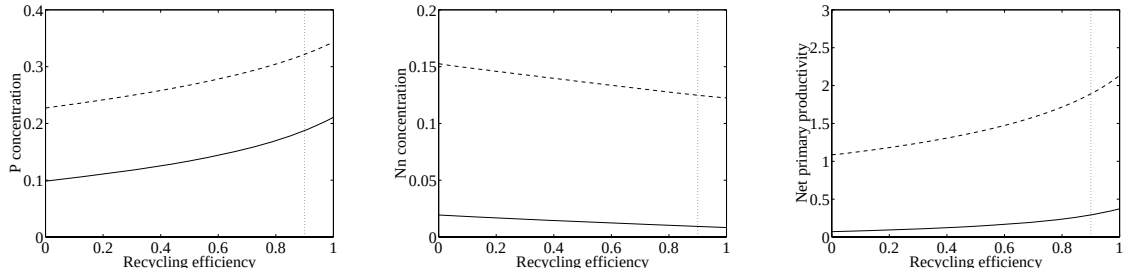

Figure 6.13: Simulated model equilibria of phytoplankton (left), nitrate (centre) and daily net primary productivity (right) across a range of recycling efficiency (model parameters ϵ and δ). The mixed layer is represented by a solid line and the thermocline layer by a dashed line. The dotted line indicates the baseline value of $(\epsilon + \delta)$. Concentrations are in mmol N m^{-3}. Net primary productivity is integrated down each layer and is measured in mol N m^{-3} d^{-1}.

Figure 6.11 shows the results of simulations in which N_0 was ranged from 0.1 to 10.0 mmol N m^{-3}. This range encompasses the full range of values from different latitudes given in table 6.3.

In accordance with Taylor's findings, the phytoplankton concentrations in both layers rise with increasing N_0. However, as do the equilibrium levels of nitrate in the two layers. By contrast, Taylor found that nitrate in the mixed layer was independent of N_0. However, the rise in mixed layer nitrate is very slight across a relatively wide range of N_0.

As an aside, figure 6.12 shows the results from simulations across a more extreme (and somewhat unrealistic) range of N_0. The graphs show that while phytoplankton concentrations in both layers increase at first, above N_0 concentrations of around 12 mmol N m^{-3}, the thermocline layer phytoplankton concentrations begin to fall. Although this is partially due to increased phytoplankton in the mixed layer

blocking the penetration of light to the thermocline layer, it is also caused by a build up of ammonium in the thermocline layer (see centre graph). This leads to an actual reduction in nitrate uptake (see right right) due to the inhibitory effects of ammonium. However, this result does occur at less realistic subthermocline nitrate concentrations (and will also depend on the choice of ammonium uptake model – see Chapter 3).

Figure 6.13 shows the results of simulations in which $(\epsilon + \delta)$ was ranged from 0.0 to 1.0. The phytoplankton results are in agreement with Taylor. As recycling efficiency is increased, the phytoplankton concentration in both layers increases. As with the results for the N_0 simulations, mixed layer nitrate is not entirely independent of $(\epsilon + \delta)$. Similarly though, the change in mixed layer nitrate across the range examined is relatively slight.

Property (ii)

> *The phytoplankton concentrations in each of the two layers show a common response to changes in : efficiency of recycling, subthermocline nutrient concentration, the Michaelis–Menten parameters, and the loss term rates.*

Property (ii) was examined by simulating the two layer model over ranges of phytoplankton nutrient uptake and loss process parameters. Since phytoplankton in Fasham (1993) can uptake both nitrate and ammonium there are two nutrient uptake half–saturation constants, k_1 and k_2. Similarly, the loss processes are more complicated in Fasham (1993) than in Taylor's work. Phytoplankton suffer grazing as well as naturality mortality processes, both of which have maximum rates (g and μ_1 respectively) as well as half–saturation constants (k_3 and k_5 respectively). However, the different equations of Fasham (1993) and Taylor (1988) do still attempt to model the same processes and should be comparable. The ranges of these six parameters examined included the extremes listed for the parameters in Fasham, Ducklow & McKelvie (1990).

The simulations already described for property (i) found that the phytoplankton concentrations in each layer showed a common response to changes in N_0 and $(\epsilon + \delta)$.

Figure 6.14 shows the results of the simulations across the ranges of the six parameters. The equilibrium phytoplankton concentrations in both layers are shown, and the baseline value of each parameter is marked to facilitate analysis.

All of the parameters involved in phytoplankton loss processes produce similar responses in the equilibrium concentrations of phytoplankton in both layers. Increasing the zooplankton maximum ingestion rate (g) causes both phytoplankton equilibria to fall. Similarly, the maximum phytoplankton natural mortality rate (μ_1). Both the zooplankton ingestion and phytoplankton natural mortality half–saturation constants (k_3 and k_5 respectively) induce rises in both phytoplankton equilibria as they increase.

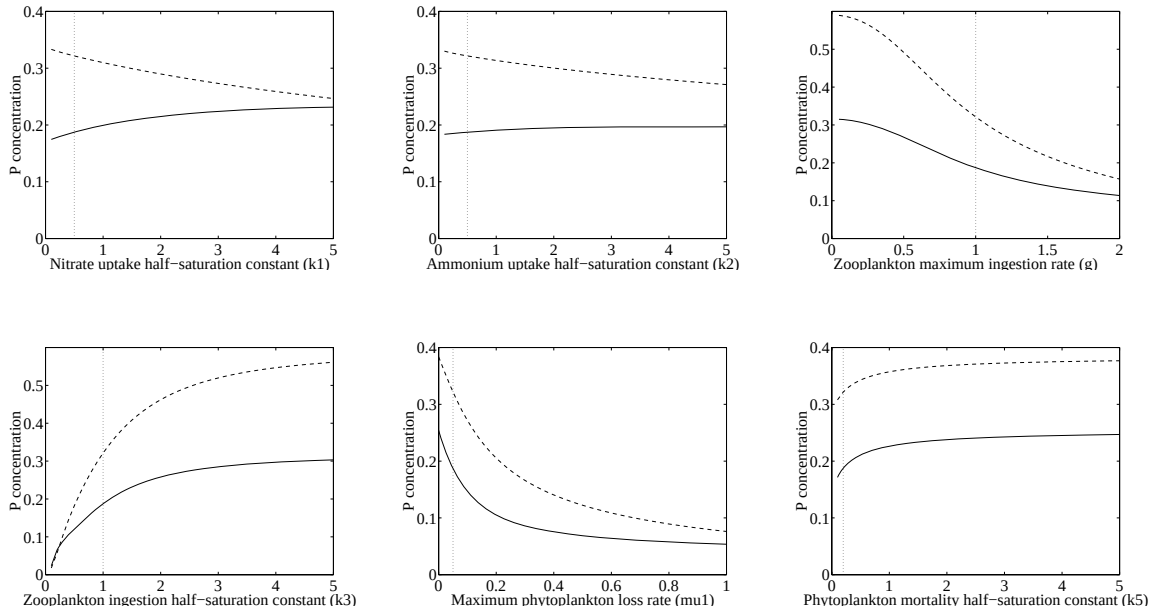

Figure 6.14: Simulated model equilibria of phytoplankton across ranges of nitrogen uptake and loss parameters. The mixed layer is represented by a solid line and the thermocline layer by a dashed line. Concentrations are in mmol N m^{-3}. Parameter units have been described previously.

However, the responses of the two phytoplankton equilibria differ when nutrient uptake half–saturation constants are considered. In both cases (more noticeably with k_1, the nitrate parameter) increases in the half–saturation constants lead to decreases in the equilibrium concentration of thermocline phytoplankton but increases in the equilibrium concentration of mixed layer phytoplankton. Since a decrease in the uptake of nitrate by thermocline phytoplankton is likely to make more available for mixed layer phytoplankton, this is perhaps not surprising. However, it differs from the property found by Taylor in the models he examined. The reason for this difference probably stems from the assumption Taylor made of zero nutrient limitation in the thermocline layer. In the work here, nutrient limitation is still modelled explicitly in both layers, so changes in the uptake kinetics of the model can still filter through to affect the phytoplankton in both layers.

Property (iii)

Raising the growth of phytoplankton in the thermocline (e.g. by increasing the surface irradiance) results in a decrease in growth of phytoplankton in the upper mixed layer.

Since there are several feedbacks in the two layer version of Fasham (1993), property (iii) can be examined in a number of different ways. In the first instance, and following Taylor's own work, it was examined by raising sea–surface irradiance. The parameters k_w and k_c, which are involved in the attenuation of irradiance down the water column, were also studied. As were the phytoplankton growth parameters V_p, the maximum possible phytoplankton growth rate, and α, the initial slope of the photosynthesis–irradiance curve. Finally, the thicknesses of both modelled layers were examined. A shallower mixed

layer should increase the fraction of sea–surface irradiance which makes it to top of the thermocline. A thinner thermocline layer (by means of the assumption that the thermocline layer is homogeneous) should have a higher depth–integrated phytoplankton growth rate since the cells are mixed down through a shallower layer.

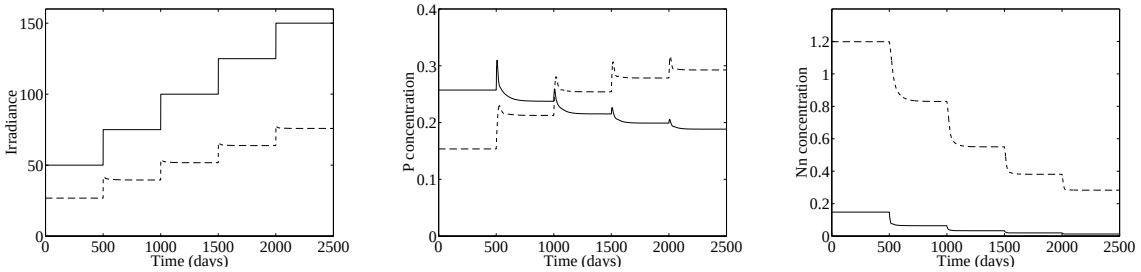

Figure 6.15: Time series showing the concentrations of phytoplankton (centre) and nitrate (right) across a period during which surface irradiance (left) is increasing stepwise every 500 days. The mixed layer is represented by a solid line and the thermocline layer by a dashed line. The dashed line on the irradiance plot is the amount of irradiance reaching the top of the thermocline layer. Concentrations are in mmol N m^{-3}. Irradiance in W m^{-2}.

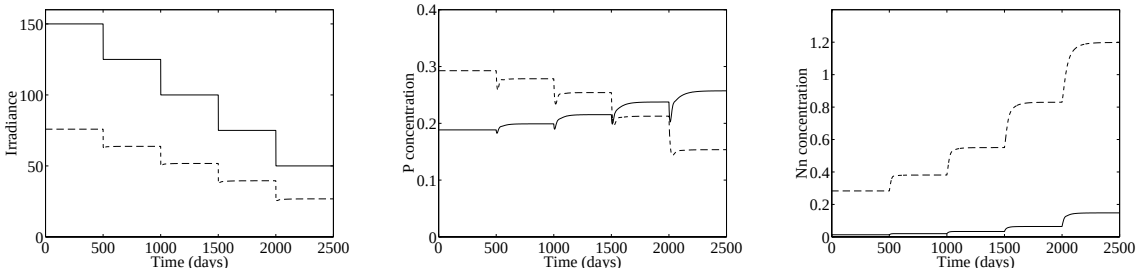

Figure 6.16: As figure 6.15 except for stepwise decreasing surface irradiance.

Figure 6.15 shows the time series of a single simulation in which sea–surface irradiance was increased stepwise every 500 days. As can clearly be seen, each increase in irradiance leads to an increase in the equilibrium concentration of thermocline phytoplankton, and a concommitant decline in that of the mixed layer phytoplankton (centre graph), although in the short term, this trend is hidden by transient behaviour which sees concentrations in both layers rise before the new equilibria are reached. In both layers, nitrate can be seen to fall with each successive rise in irradiance. As an aside, figure 6.16 shows the process in reverse, as irradiance is decreased every 500 days.

This result confirms that found by Taylor, and lends support to the hypothesis known as the "light effect" (A. H. Taylor, Plymouth Marine Laboratory, pers. comm.). This hypothesis suggests that whenever more light reaches the thermocline layer, the phytoplankton there are able to grow slightly more

and deprive the mixed layer phytoplankton of slightly more nutrient. This system has the capacity for slight positive feedback, since any reduction of nutrient influx to the mixed layer leads to a decline in the phytoplankton concentration there, which leads to a rise in the amount of irradiance reaching the top of the thermocline, which ... However, since irradiance is mostly attenuated by seawater itself and not by photosynthetic pigments, it would be difficult for runaway positive feedback to occur.

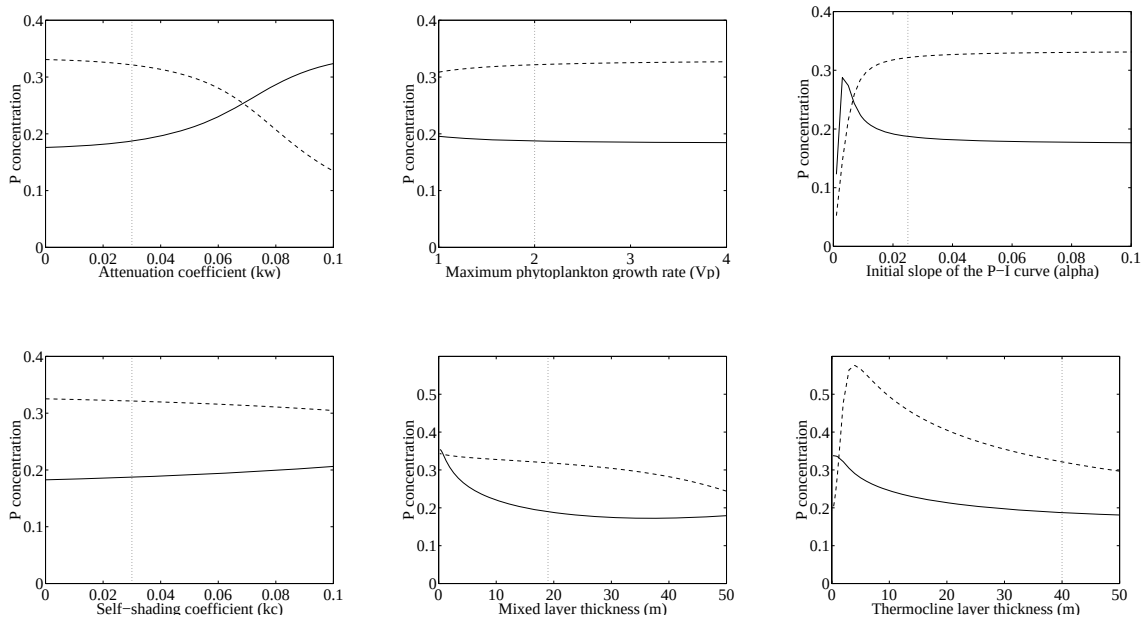

Figure 6.17: Simulated model equilibria of phytoplankton across ranges of k_w, V_p, α, k_c, mixed–layer depth and thermocline thickness. The mixed layer is represented by a solid line and the thermocline layer by a dashed line. Concentrations are in mmol N m^{-3}. Parameter units have been described previously.

Figure 6.17 shows the results of the simulations across ranges of the other six parameters. In each case, the equilibrium phytoplankton concentrations and the baseline value of the parameter are shown.

Decreases in the attenuation coefficient, k_w, of the surrounding seawater (which could be caused by a reduction in the quantities of suspended particles), increases in the maximum phytoplankton growth rate, V_p, increases in the initial slope of the P–I curve, α, and decreases in the absorption coefficient of chlorophyll, k_c (which could be caused by an increase in the nitrogen:chlorophyll ratio in the phytoplankton cells) all lead to rises in the thermocline phytoplankton at the expense of mixed layer phytoplankton. These results are in agreement with Taylor's findings for property (iii) (although none are of particularly large magnitude).

An increase in the nitrogen:chlorophyll ratio could occur, one might imagine, in mixed layer phytoplankton cells when nitrogen stress was beginning. Being in competition for nitrogen with other mixed layer cells, any cell which diverted its nitrogen from chlorophyll (which it would need less of anyway because

of the low irradiance stress) to the synthesis of uptake proteins (which would enable the cell to increase its share of the remaining nitrogen), would be at an advantage to its neighbours, and would increase in number at their expense. However, whilst winning this competition in the mixed layer, the cell (and its line of descendants) would also be "tightening the noose" around its own neck by increasing the irradiance to the thermocline layer and further starving the mixed layer of nitrogen.

Moving the values of k_w, k_c, V_p and α in the reverse direction produces the expected results. Mixed layer phytoplankton become more important, whilst thermocline phytoplankton decrease in importance. With parameters V_p and k_c, the changes are still of low magnitude. However, even comparatively small changes in k_w and α can shift the balance between mixed layer and thermocline phytoplankton significantly. In the case of α, such a change is unlikely to occur in nature since thermocline phytoplankton are, if anything, only likely to *increase* α to make the most of their lower irradiance. The attenuation coefficient k_w, however, is more variable (see table 6.3) and can be influenced by biological activity (Balch, Kilpatrick & Trees, 1996; Balch *et al.*, 1996). Coccolithophore algae, for instance, can strongly influence the local optical environment through the production and release of coccoliths. These are organic scales produced by all Prymnesiophyte algae, but covered in a layer of calcite (a form of $CaCO_3$) in the coccolithophorids. This layer causes the coccoliths to scatter light, and this phenomenon has been known to change the ocean's colour so that it appears a milky turquoise (Balch *et al.*, 1996). This scattering of light effectively increases the attenuation coefficient and reduces the amount of light available to phytoplankton in the thermocline layer. It is possible to imagine that this could serve as a strategy to deal with the "nutrient stranglehold" placed on the mixed layer phytoplankton by those in the thermocline. However, until the trade–offs of producing coccoliths are fully understood, it is unwise to speculate on their significance in this context.

The results for shallowing mixed–layer depth and a thinning thermocline layer however, whilst showing an increase in thermocline phytoplankton, also show an increase in mixed layer phytoplankton, contrary to the decrease found with the other four parameters.

In the case of the shallowing mixed layer this is caused by an increase in the proportion of the mixed layer which is mixed with the thermocline layer. This tends to homogenise the concentrations of phytoplankton and nitrate in the layers more. This is bolstered by the general increase in phytoplankton in the thermocline layer due to greater quantities of irradiance which reach the top of it.

Where the thermocline's thickness is decreasing, several processes lead to rises in both layers. The thermocline phytoplankton increase their growth rate mostly through an increase in depth–integrated light–limited growth (see the light–limited growth plot of figure 6.18), though the narrower thickness of the layer means that the mixing in of nitrate from the deep ocean is more important (see the nutrient limitation plot of figure 6.18). In the mixed layer, the phytoplankton concentration is raised mostly by the mixing in of phytoplankton from the thermocline layer, but also by a decrease in nutrient limitation

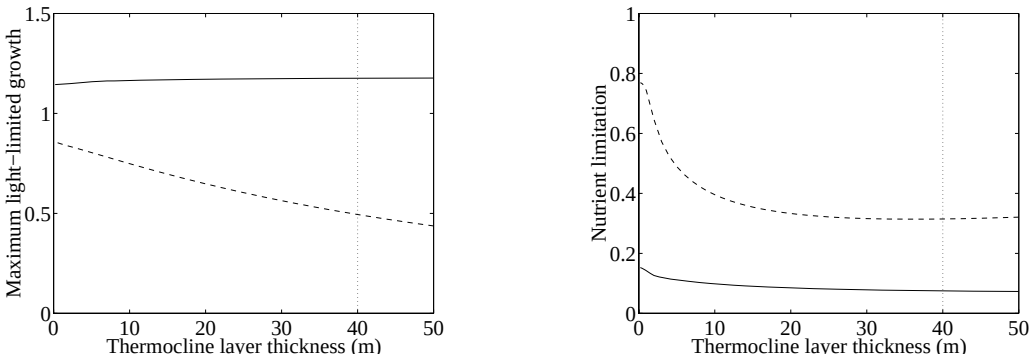

Figure 6.18: Maximum light–limited growth rate and nutrient limitation for phytoplankton across a range of thermocline thicknesses. The mixed layer is represented by a solid line and the thermocline layer by a dashed line. Maximum growth rate is in d^{-1}, nutrient limitation is non–dimensional.

caused by more nitrate diffusing in from the thermocline layer (see the nutrient limitation plot of figure 6.18).

Whilst the results from increasing sea–surface irradiance and the former four model parameters support Taylor's property (iii), changes to the latter two parameters suggest that phytoplankton growth in the thermocline layer *can* be increased without a concommitant decrease in the mixed layer.

Property (iv)

> *The ratio of upper mixed layer to thermocline production, and the ratio of "new" nutrient entering the layer to nutrient recycled back into it, do not depend on the concentration of nutrient below the thermocline.*

Property (iv) was examined by simulating the two layer version of Fasham (1993) across a range of subthermocline nitrate concentrations (as with property (i)). The net primary productivity (NPP) ratio between the two layers was calculated by dividing the integrated production of the mixed layer by that of the thermocline layer. The ratio of "new" nutrient entering a layer to nutrient "recycled" into the layer was calculated by dividing the quantity of nitrate entering the layer from below by the quantity of ammonium and DON regenerated through zooplankton loss processes. The role of the bacterial compartment in the cycling of nitrogen via ammonium was ignored here since it is of quantitatively minor importance in the model, and is complicated by the uptake of ammonium by bacteria.

Figure 6.19 shows the results these calculations together with the calculated f–ratio. As before, the a range of N_0 values including all those from table 6.3 was examined. The baseline value of N_0 at Bermuda Station "S" is marked by a vertical dotted line.

Although the NPP ratio is clearly not independent of N_0, the ratio changes only slightly across most of the range examined. It is only at the extreme lows and extreme highs (not shown here) that the ratio

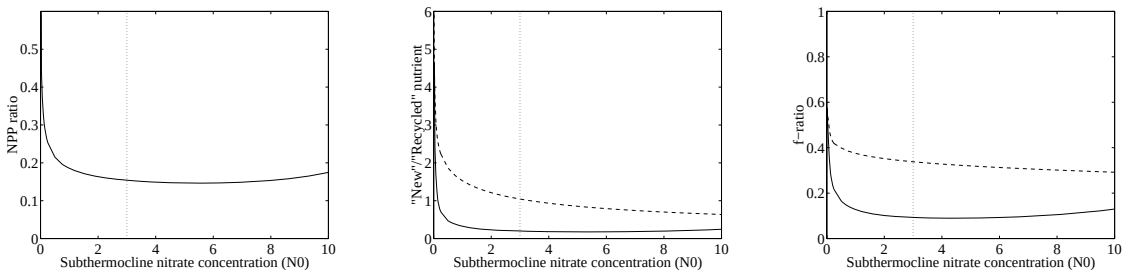

Figure 6.19: Simulated NPP mixed layer/thermocline layer ratio (left), "new"/"recycled" nutrient ratio (centre) and the f–ratio (right) across a range of subthermocline nitrate concentrations (model parameter N_0). In the latter two graphs, the mixed layer is represented by a solid line and the thermocline layer by a dashed line. The dotted line indicates the baseline value of N_0. Concentrations are in mmol N m^{-3}. All three ratios are dimensionless.

shifts markedly towards mixed layer production.

This result is also found with the "new"/"recycled" nutrient ratio in the mixed layer. Only the extremes of the range examined show large shifts in the ratio (in this case, towards "new" production). In the thermocline layer though, this ratio decreases with increasing N_0 across the full range of N_0.

The f–ratio results show some trivially counter–intuitive results. In the mixed layer, the f–ratio is at its highest at extremely low N_0, when nitrate is at its most limiting. Whilst in the thermocline layer, the f–ratio falls across the full range of N_0 values examined despite rising nitrate in the layer. However, in both instances, these apparently odd results are easily explicable.

Property (v)

> *The ratio of the production in the two layers also does not depend on the efficiency of recycling.*

Property (v) was examined by simulating the two layer version of Fasham (1993) across a range of $(\epsilon + \delta)$, the regenerative terms of zooplankton loss processes (as with property (i)). Although Taylor's property (v) dealt only with the NPP ratio, the "new"/"recycled" nutrient ratio and the f–ratio were also calculated.

As figure 6.20 shows, the ratio of NPP between the two layers was found to vary across the whole range of $(\epsilon + \delta)$, with the steepest changes occurring near the baseline value. Increasing efficiency was found to increase the fraction of production which occurred in the mixed layer.

Unsurprisingly, increasing recycling efficiency decreased both the "new"/"recycled" nutrient ratio and the f–ratio as more nitrogen was returned to the useable nutrient pool as ammonium.

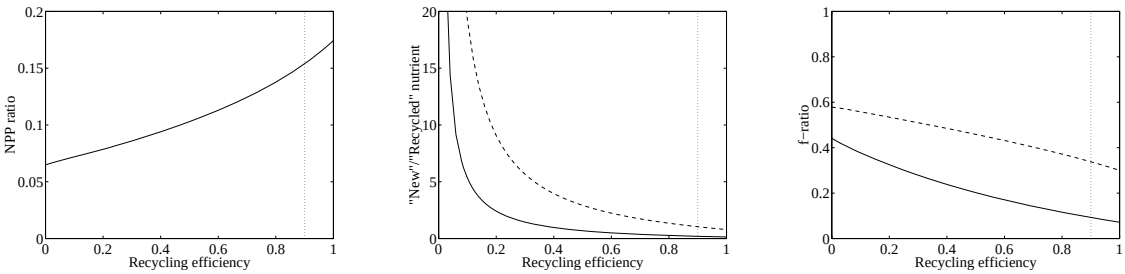

Figure 6.20: Simulated NPP mixed layer/thermocline layer ratio (left), "new"/"recycled" nutrient ratio (centre) and the f–ratio (right) across a range of recycling efficiency (model parameters ϵ and δ). In the latter two graphs, the mixed layer is represented by a solid line and the thermocline layer by a dashed line. The dotted line indicates the baseline value of $(\epsilon + \delta)$. Recycling efficiency is dimensionless. All three ratios are dimensionless.

6.5.2 Latitudinal differences

The assumptions made in Taylor's original analysis constrained the application of the derived properties to a relatively restricted subset of ocean environments. The choice of Bermuda Station "S" as the location to examine the properties for the two layer version of Fasham (1993) was made with these assumptions in mind. However, to establish whether or not the properties could be sought in data from other environments, each of the properties above was examined additionally at 0°, 47° and 60° N. The forcing and parameter values detailed previously were used for each set of simulations.

Figure 6.21 shows a selected subsample of the results from these simulations. The columns refer to each of the three latitudes, the rows to each of the five properties. As previously, the baseline values of the parameters in question are indicated by dotted lines.

The results from 0° N agree well with those found for Bermuda Station "S". The only exception is with property (iv). At Bermuda Station "S" it was found that the NPP ratio only changed significantly at extremely low N_0. At 0° N, the baseline value of N_0 falls within the region where significant changes to the ratio are occurring. This aside, it is not surprising that the results are similar to those from Bermuda Station "S" since both locations find the phytoplankton in the mixed layer considerably more nutrient limited than those in the thermocline layer, as per Taylor's assumptions.

By contrast, at 47° and 60° N there is little difference in the nutrient–limitation status between the two layers (both because of the higher baseline N_0, and the lower lighted–limited growth rates). Consequently, Taylor's properties almost completely cease to be found. The mixed–layer nitrate levels do remain almost constant across the full range of $(\epsilon + \delta)$, and the phytoplankton in both locations do show a common response to changes in the nutrient uptake Michaelis–Menten and loss process parameters. However, aside from these minor agreements, all of the other properties fail to be met. Mixed–layer

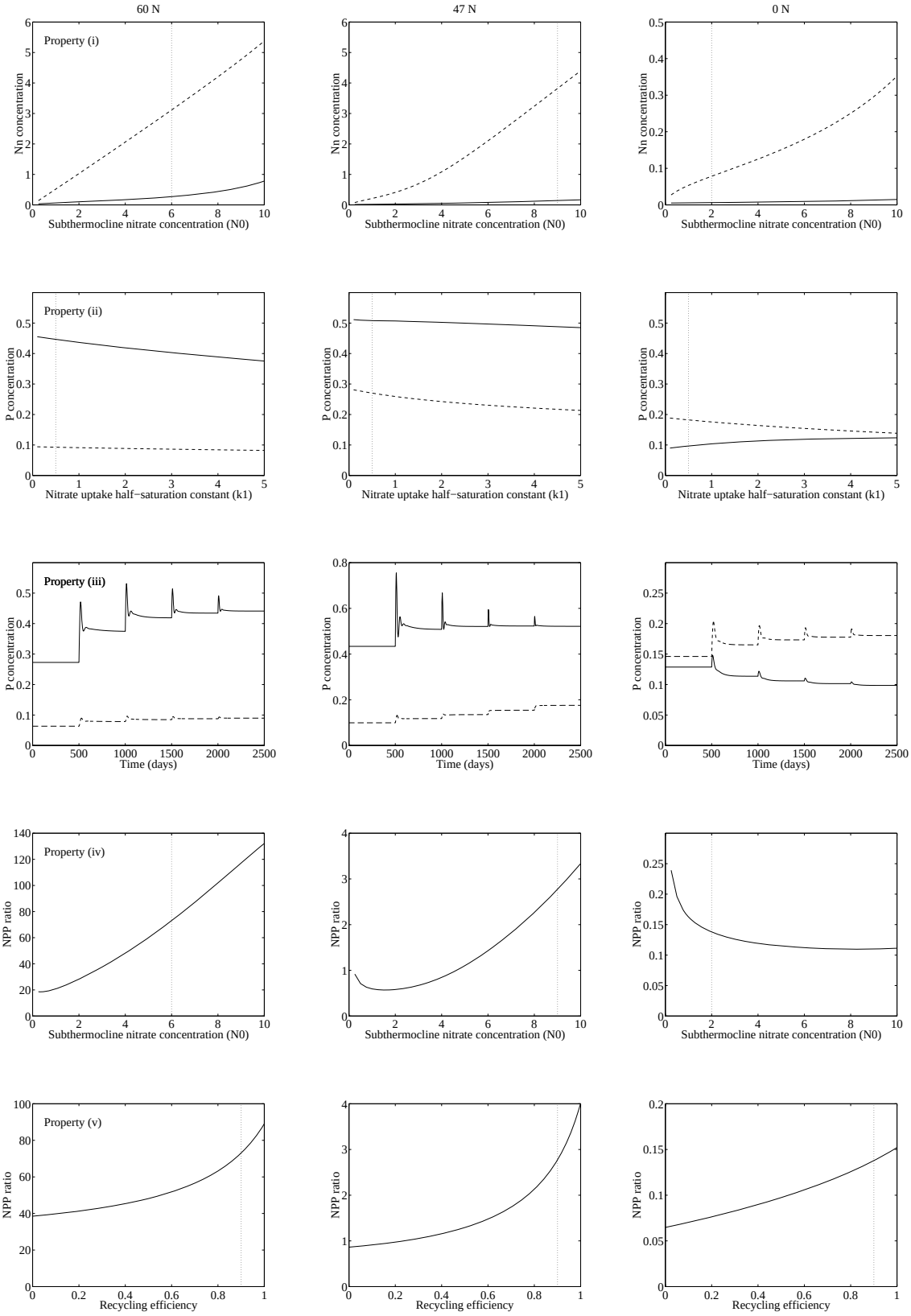

Figure 6.21: Latitudinal differences in the response of the two layer version of Fasham (1993) to Taylor's five properties. The columns refer to each of the three latitudes, the rows to each of the five properties. Concentrations are in mmol N m^{-3}. All three ratios are dimensionless. Parameter units have been described previously.

nitrate rises with increasing N_0, increases in the growth rate of thermocline phytoplankton lead to rises in the equilibrium concentrations of phytoplankton in both layers, and the NPP ratio is strongly affected by changes in both N_0 and $(\epsilon + \delta)$. Again, this is not surprising, since the assumptions used by Taylor to derive the common properties are not compatible with the conditions found at 47° and 60° N.

These results suggest that any attempt to find Taylor's properties in observational data needs to be constrained to only those regions in which his major assumptions apply. Only in the tropics and sub–tropics are there regions where mixed–layer phytoplankton experience considerably greater nutrient limitation than those in the thermocline layer for prolonged periods of time.

As an aside, in the simulations performed here, parameter changes which increased the growth rate of thermocline phytoplankton happened to the value of the parameter in both layers. No simulations were performed in which, for example, the values of V_p or α were raised *only* for the thermocline phytoplankton. Such changes would undoubtedly favour thermocline over mixed–layer phytoplankton. However, they would imply that the two populations were somehow different (community structure; different acclimation to ambient conditions; *et cetera*). Whilst this can be the case in nature (Gieskes & Kraay, 1986), it is beyond the scope of this work.

6.5.3 Summary

Each of the five properties Taylor found in the models he studied have been looked for in the two layer version of Fasham (1993). With relatively minor discrepancies, the simulations of the two layer version of Fasham (1993) (at an appropriate latitude) share properties (i) to (iv) with Taylor's work. The following list summarises the agreement between the properties Taylor found with his models, and those at an appropriate latitude.

- **Property (i)**

  It was found that phytoplankton concentrations in both layers correlated positively with increasing N_0 and $(\epsilon + \delta)$, and that mixed layer nitrate changed only slightly across the ranges of these parameters. These results agree mostly with those found by Taylor.

- **Property (ii)**

  In agreement with Taylor, it was found that the phytoplankton in both layers showed a common response to changes in the phytoplankton loss parameters, g, k_3, μ_1 and k_5. However, in the case of the Michaelis–Menten terms for nutrient uptake, k_1 and k_2, changes which reduced the uptake rates in both layers led to a decrease in thermocline phytoplankton, but an *increase* in mixed layer phytoplankton.

- **Property (iii)**

  Once again in agreement with Taylor, increases in the growth rate of phytoplankton in the thermocline layer, mediated by the parameters k_w, V_p, α, k_c and sea–surface irradiance, lead to rises

in the thermocline phytoplankton with concommitant decreases in the mixed layer phytoplankton.

Although not examined by Taylor, decreases in both the mixed–layer depth and thermocline thickness also led to increases in the thermocline phytoplankton growth rate and, consequently, concentration. However, unlike the previous parameters, these changes also led to *increases* in the mixed layer phytoplankton.

- **Property (iv)**

  Whilst neither the NPP ratio nor the "new"/"recycled" nutrient ratio were found to be independent of N_0, in both cases the ratios were found to be fairly constant in the most interesting range. This is broadly in agreement with Taylor's results.

- **Property (v)**

  In the case of the NPP ratio and recycling efficiency, it was found that the ratio increased significantly with increasing efficiency. The steepest portion of this increase was found around the baseline value of recycling efficiency. This disagrees with the comparable result obtained by Taylor.

Despite differences in both model complexity and analytical approach (Taylor's rigorous analysis versus numerical simulation used here), it is clear from this list that the two layer version of Fasham (1993) lends support to the majority of Taylor's properties. It is particularly significant that agreement was reached without any of the linearising assumptions made by Taylor to simplify analysis. Non–linear forms in the two layer version of Fasham (1993) were retained in full.

Whether or not these properties could be looked for in data though is not clear. For properties (i) and (iv) to be examined, a region in which there was considerable variability in N_0 would need to be found. Because of differences in the maximum depth of winter mixing, N_0 essentially increases with latitude (table 6.3; Figure 4 of Strass & Woods, 1991). However, as already discussed, increasing latitude has several other effects which make comparison between different latitudes difficult or impossible. A possibility may exist along the equator where near constant upwelling (caused by the divergence of the Trade winds of the northern and southern hemispheres) brings nutrient rich waters to shallower depths. As these waters spread from the equator and mix with more nutrient–depleted waters, it is possible that enough of a range of deep nitrate would persist to make examining properties (i) and (iv) possible.

The majority of nitrogen which is regenerated in the Fasham (1993) model does so via the zooplankton mortality pathway. The ecological processes which this pathway represents include direct excretion of ammonium by the zooplankton, as well as the more complex routes through higher predators and regenerative bacteria. As such, it is not obvious how properties (i) and (v) could reasonably be studied. It is conceivable that regeneration efficiency could be estimated based on knowledge of the regenerative processes of particular species compositions or perhaps the results of experiments tracing the fate of labelled nitrogen. Variation in species composition through space and time could then provide a range of efficiency across which properties (i) and (v) could be examined. However, the ecological uncertainties

involved in such an effort might entirely swamp its aims.

Similar comparisons between species compositions at different locations and studies which track seasonal succession patterns may offer some avenues for investigating property (ii). However, since phytoplankton uptake and mortality parameters relate to somewhat more tangible ecological processes than nutrient regeneration, it may be easier to find appropriate data. Many studies have examined the uptake kinetics of phytoplankton (see Dortch, 1990, for an excellent review of the interplay between ammonium and nitrate uptake), the grazing rates of zooplankton (Evans & Paranjape, 1992; Peters, 1994; Paffenhöfer *et al.*, 1995) and the significance of viruses in phytoplankton mortality (Beltrami & Carroll, 1994; Bratbak *et al.*, 1995). However, once again, the uncertainties involved may obscure the processes under study.

Property (iii) probably presents the best chance for confirming Taylor's predictions. Although, as Banse (1987) has pointed out, very transient fluctuations in sea–surface irradiance (*e.g.* by the movement of passing clouds) occur on far too short a time scale for any noticeable effect of reducing irradiance, it is still possible that events over a longer period (*e.g.* diel cycle of sunlight; a prolonged period of cloudiness) may reveal the patterns found by Taylor and in the two layer version of Fasham (1993). It is worth noting though, that the simulations of varying sea–surface irradiance here found that changes in incident irradiance have transient periods at first where the phytoplankton do not behave as predicted. In the simulations here, these transient periods were up to 50 days long. However, this transient was not observed in the nitrate results.

The attenuation coefficient, k_w, and the thicknesses of the mixed and thermocline layers, M and T, also present possibilities for confirming Taylor's predictions against data. As already mentioned, some algae are capable of significantly altering the optical properties of sea water (Balch, Kilpatrick & Trees, 1996; Balch *et al.*, 1996). During blooms of these organisms, it may be possible to examine property (iii) across a range of k_w. Alternatively, and somewhat speculatively, following the example set by the IronEx experiments in the Pacific (Behrenfeld *et al.*, 1996), experiments in which the optical properties of the mixed layer were altered artificially could be performed. Taylor & Stephens (1993) describe work in which accurate depth profiles of temperature and chlorophyll (measured by the Undulating Oceanographic Recorder) were used to predict the timing and onset of the spring phytoplankton bloom. Similar measurements recording shifts in the thicknesses of the mixed and thermocline layers could provide data to confirm or refute the simulation results presented here for these parameters.

6.6 Limit cycle behaviour of the two layer model

In Chapter 4 the normal single layer version of Fasham (1993) was examined for limit cycle behaviour. Such cycles were found in certain regions of parameter space, and their implications for the model were discussed. In this section, the two layer version of Fasham (1993) was similarly examined to establish whether or not it shared the behaviour of the single layer model.

6.6.1 Mixing rate and subthermocline nitrate

Studies of the full model, and the reduced model 6c3, found that preventing the exhaustion of nitrate in the modelled system allowed the persistence of predator–prey cycles between the phytoplankton and zooplankton. In the first instance then, the parameter space of mixing rate, m, and subthermocline nitrate, N_0, was examined.

As previously, the equilibrium–finding program from Chapter 4 was used to find the equilibrium solutions at each combination of parameter values. In keeping with the previous work, numerical solutions were determined at both OWS "India" and Bermuda Station "S" with the forcing functions from days 197 and 165 respectively. All of the plots use the same graphical format that was described originally in Chapter 4.

For comparative purposes, figures 6.22 and 6.23 show the results that were found when the single layer model was examined. OWS "India" has a pattern of limit cycles which persist only at intermediate mixing rates. Bermuda Station "S" has limit cycles across almost the full range of the parameters examined (although none at values of N_0 close to the baseline value). The two stations also differ significantly in the periods of the limit cycles found. The cycles at OWS "India" all have periods between 31 and 34 days, whilst at Bermuda Station "S", all of the cycles have periods between 20 and 26 days. The relationships between cycle period and amplitude also differ significantly between the stations.

Figures 6.24 and 6.25 show the results obtained from simulations of the two layer model at the two stations. In both cases the stations show somewhat similar patterns of mixed layer phytoplankton behaviour to their single layer equivalents. However, both of these patterns are similarly "retracted" from the patterns found in the single layer model. While in the single layer model at OWS "India" limit cycles could be found at values of N_0 around 20 mmol N m^{-3}, in the two layer model they are only found at values over 45 mmol N m^{-3}. A similar reduction in the area of parameter space in which limit cycles occur was found at Bermuda Station "S".

For the same parameter values, this "retraction" has also reduced the amplitude of the mixed layer limit cycles between the two models. This has also happened, although to a less obvious degree, with the limit cycle periods. Overall, the addition of the thermocline layer to Fasham (1993) has "pushed back"

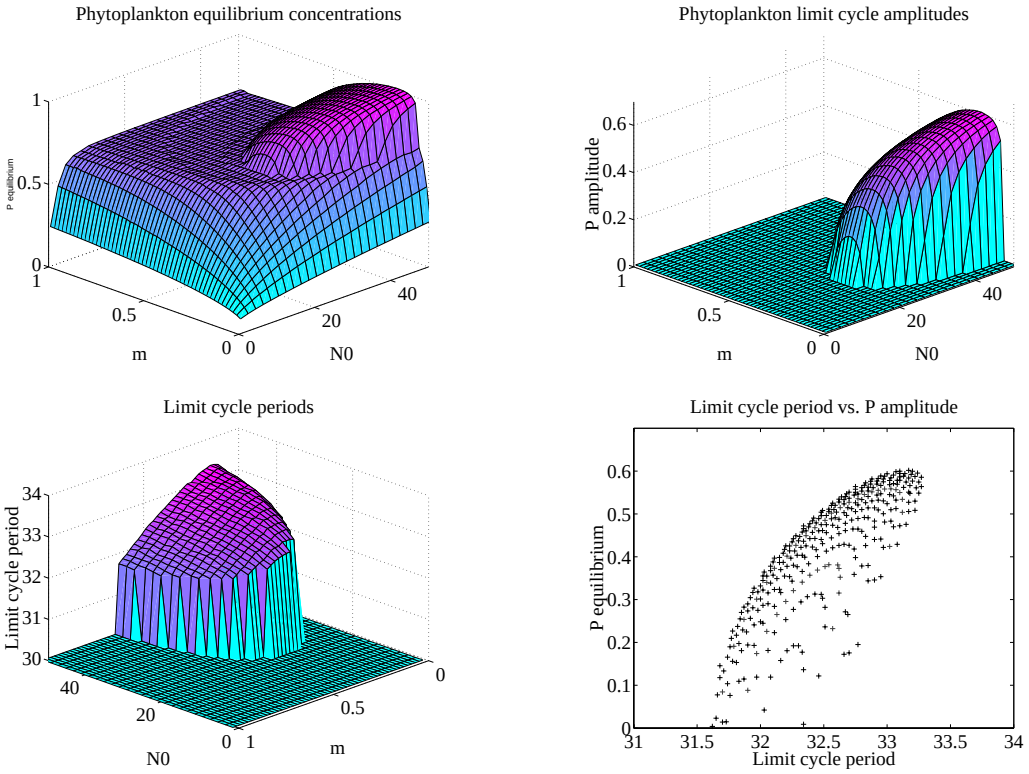

Figure 6.22: The results of simulations of the normal, 7 compartment version of Fasham (1993) performed at OWS "India" on day 197 across a range of cross–thermocline mixing rates (m) and subthermocline nitrate concentrations (N_0). Mixing rates in m d^{-1}, subthermocline nitrate concentrations in mmol N m^{-3}. Phytoplankton equilibrium concentrations and limit cycle amplitudes in mmol N m^{-3}. Limit cycle periods in days. Limit cycle amplitude set to 0 and period to 30 days (for clarity) where only stable equilibrium solutions found.

the region of stable oscillatory behaviour so that it occurs at more extreme values of N_0 and m.

The area of m–N_0 space in which limit cycle behaviour occurs in the two layer model can be increased by decreasing the detrital sinking rate in the same manner as was done with the single layer model in Chapter 4 (results not shown here). Setting detrital sinking rate, V, to 1 m d^{-1} permitted limit cycle behaviour at subthermocline nitrate concentrations as low as 14 mmol N m^{-3} (with $m = 0.30$ m d^{-1}).

In the thermocline layer, the patterns of phytoplankton behaviour are different. At both OWS "India" and Bermuda Station "S", increases from both low N_0 and m lead to increases in the equilibrium concentration of phytoplankton (for low values of both parameters at Bermuda Station "S", the thermocline phytoplankton equilibriate at higher concentrations than in the mixed layer). However, as the concentration of phytoplankton in the mixed layer also rises, this quickly leads to the thermocline layer equilibria falling away again as the phytoplankton there are "starved" of light.

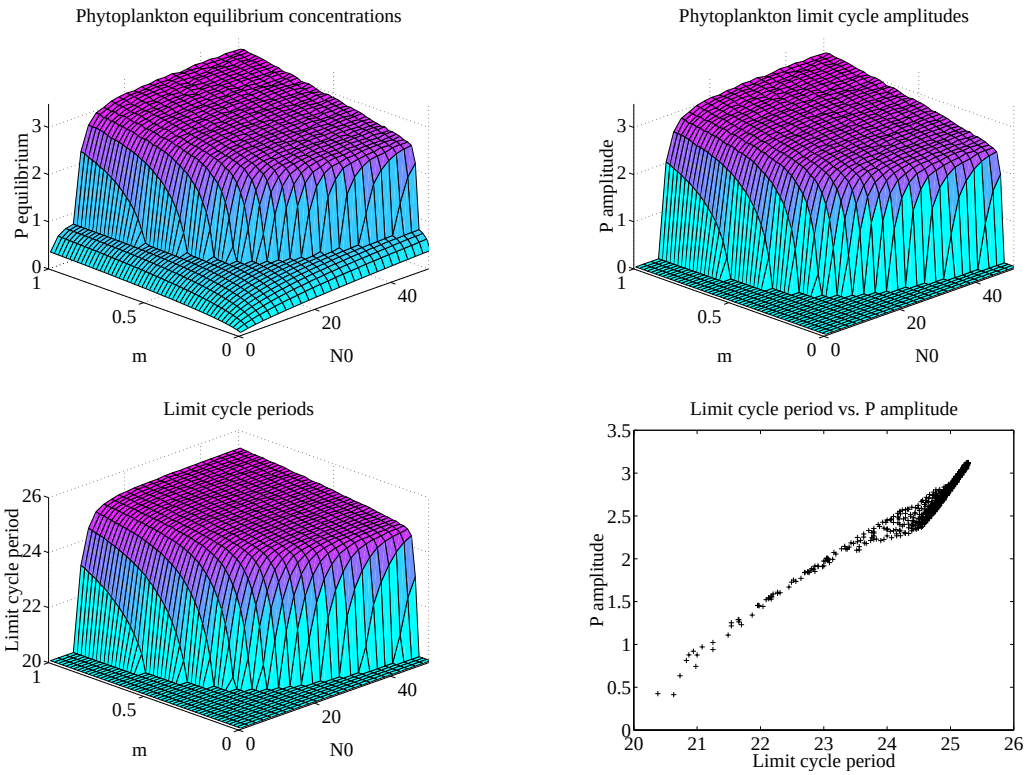

Figure 6.23: The results of simulations of the normal, 7 compartment version of Fasham (1993) performed at Bermuda Station "S" on day 165 across a range of cross–thermocline mixing rates (m) and subthermocline nitrate concentrations (N_0). Mixing rates in m d^{-1}, subthermocline nitrate concentrations in mmol N m^{-3}. Phytoplankton equilibrium concentrations and limit cycle amplitudes in mmol N m^{-3}. Limit cycle periods in days. Limit cycle amplitude set to 0 and period to 20 days (for clarity) where only stable equilibrium solutions found.

At both locations, the amplitudes of the phytoplankton oscillations are comparable to those in the mixed layer. In the case of OWS "India", the pattern of amplitudes in the thermocline layer is almost identical to that in the mixed layer, with both populations showing small "humps" at high N_0. Figure 6.26 shows a sample time series from an OWS "India" simulation. The phytoplankton oscillations in the thermocline layer are 20.4 days out of phase (peak to peak) with those in the mixed layer.

At Bermuda Station "S" however, the pattern of amplitudes is much more complicated. The highest amplitudes in the parameter region examined occur at high N_0 but low m, then fall off at first with increasing m. However, above $m = 0.5$ m d^{-1}, the amplitude of the oscillations rises again. This can be seen in the phytoplankton plots of figure 6.27. The oscillation amplitude of the mixed layer phytoplankton increases with m, but the thermocline phytoplankton fall then rise again. Noticeably, however, the amplitudes of the thermocline zooplankton and nitrate limit cycles do not show this trend. In both cases, amplitude increases with increasing m. Attempts to determine the reason for this pattern of behaviour failed to establish a cause.

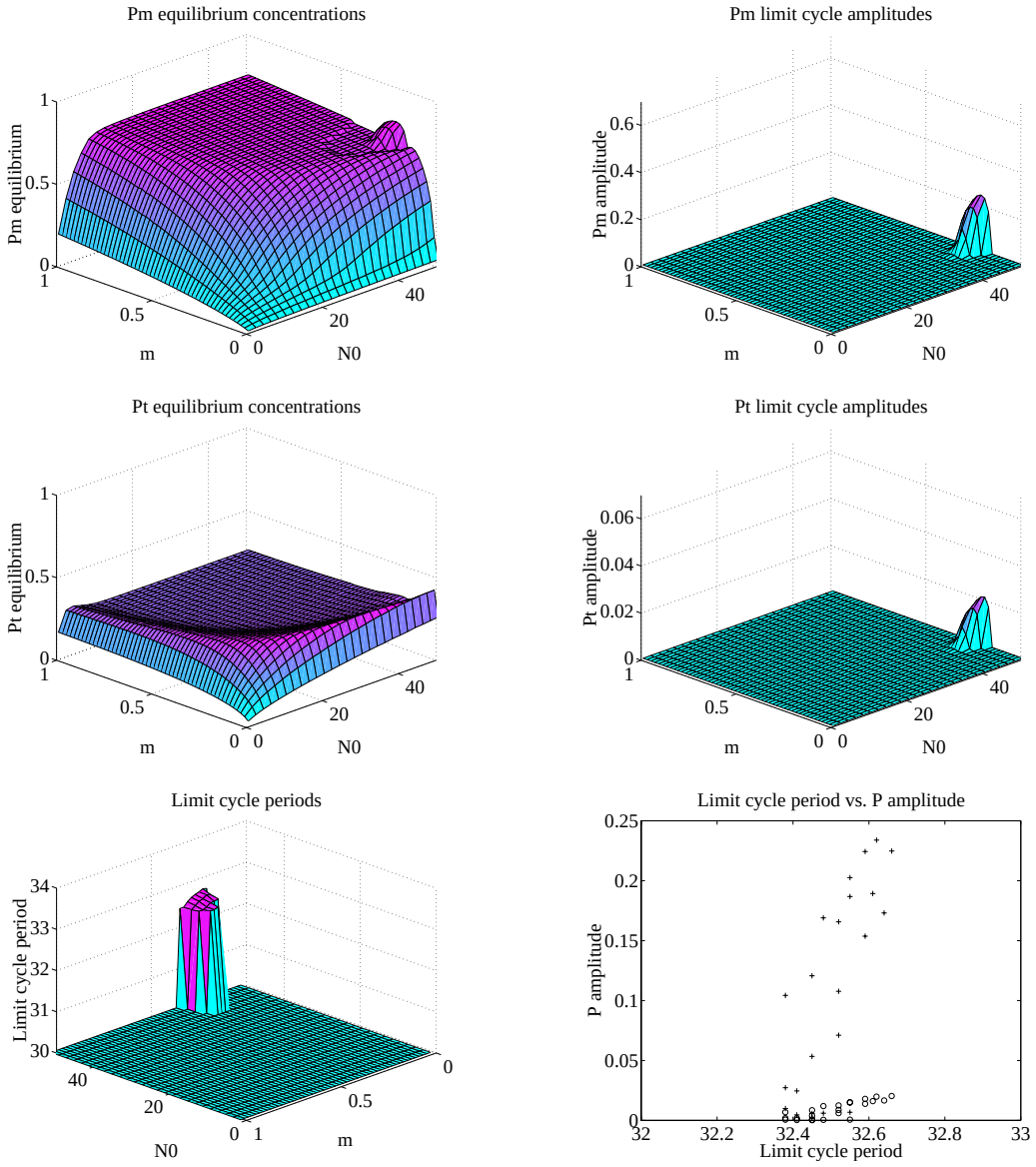

Figure 6.24: The results of simulations of the two layer version of Fasham (1993) performed at OWS "India" on day 197 across a range of cross–thermocline mixing rates (m) and subthermocline nitrate concentrations (N_0). Mixing rates in m d^{-1}, subthermocline nitrate concentrations in mmol N m^{-3}. Phytoplankton equilibrium concentrations and limit cycle amplitudes in mmol N m^{-3}. Limit cycle periods in days. Limit cycle amplitude set to 0 and period to 30 days (for clarity) where only stable equilibrium solutions found. On the limit cycle period vs. amplitude plot, mixed layer phytoplankton represented by "+" and thermocline phytoplankton by "o".

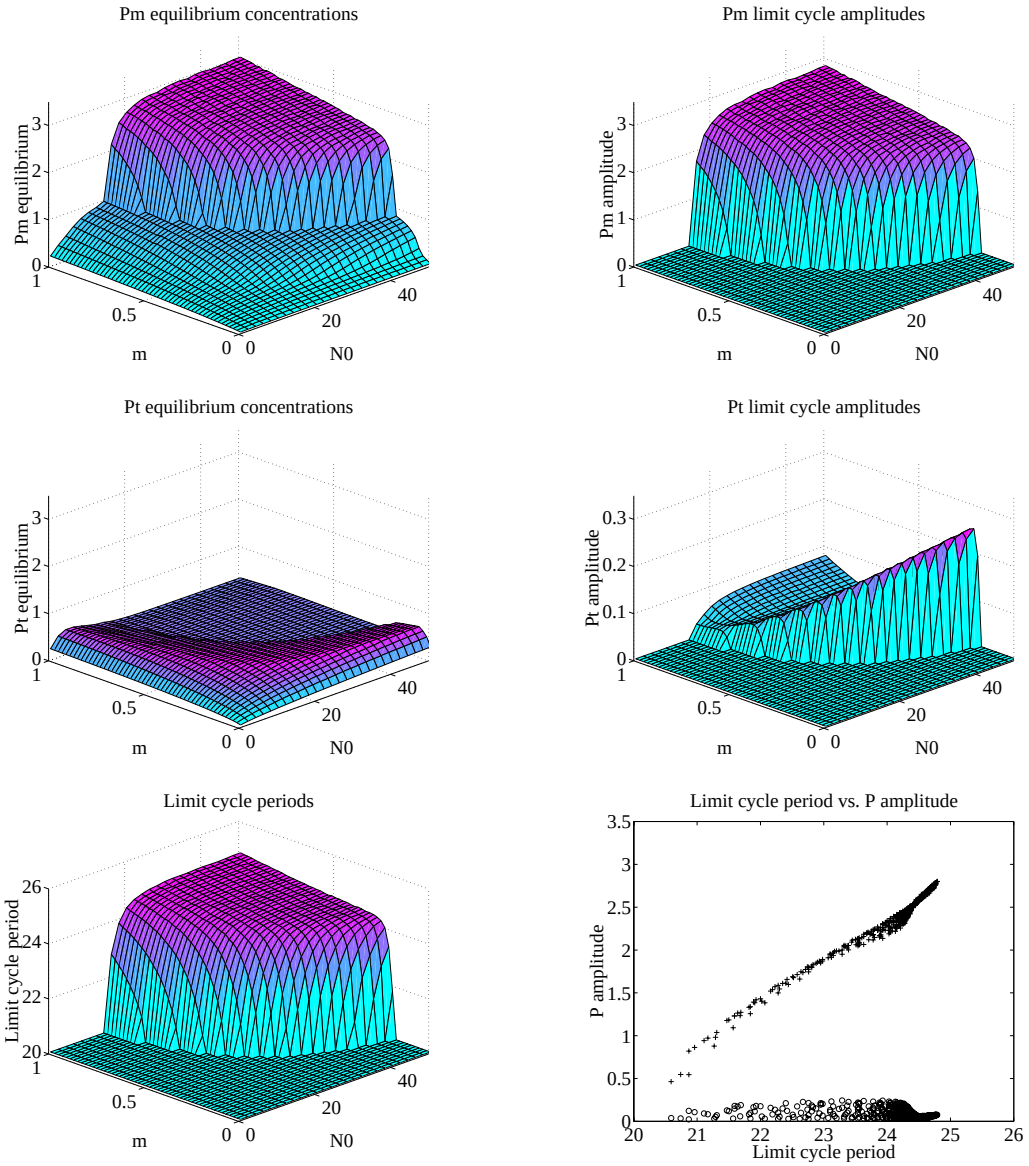

Figure 6.25: The results of simulations of the two layer version of Fasham (1993) performed at Bermuda Station "S" on day 165 across a range of cross–thermocline mixing rates (m) and subthermocline nitrate concentrations (N_0). Mixing rates in m d^{-1}, subthermocline nitrate concentrations in mmol N m^{-3}. Phytoplankton equilibrium concentrations and limit cycle amplitudes in mmol N m^{-3}. Limit cycle periods in days. Limit cycle amplitude set to 0 and period to 20 days (for clarity) where only stable equilibrium solutions found. On the limit cycle period vs. amplitude plot, mixed layer phytoplankton represented by "+" and thermocline phytoplankton by "o".

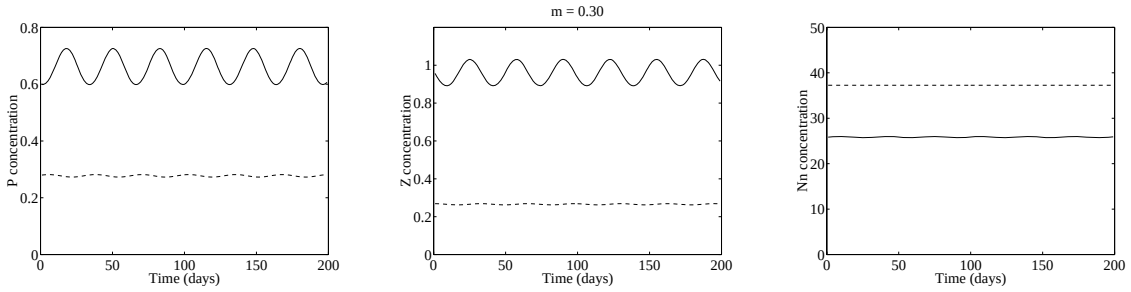

Figure 6.26: Time series results of a two layer model simulation performed at OWS "India" . Phytoplankton (left), zooplankton (centre) and nitrate (right) shown. Mixed layer concentrations are represented by a solid line, thermocline layer concentrations by a dashed line. Concentrations are in mmol N m^{-3}.

The abundances in the mixed and thermocline layers of all three of these major model components all become more in phase as the mixing rate rises (in the graphs shown the phytoplankton in the two layers are out of phase by approximately 14, 7 and 5 days respectively). The higher the mixing, the more homogenised the populations become, so this is not surprising.

6.6.2 Thermocline thickness

The results in the previous section illustrate the effects that the addition of a thermocline layer has to the limit cycle dynamics of the model. Although many different parameter ranges could be examined for other differences in model behaviour, one of the most obvious parameters to vary is that of the thermocline thickness itself, since the quantity of nitrate from the deep ocean which reaches the upper mixed layer is liable to be strongly tied to this.

Thermocline thickness was examined by performing simulations across a range of T and N_0 under the standard conditions of OWS "India" on day 197. Mixing was fixed at 0.30 m d^{-1}, the value at which limit cycles were previously found. The thermocline thickness was ranged from 1 m to 101 m. The ranges of the two parameters included the region already examined for limit cycle behaviour.

Figure 6.28 shows the results from these simulations. Equilibrium concentrations and limit cycle amplitudes of phytoplankton in both layers are shown. The periods of the limit cycles are also shown, together with a plot showing the relationship between the limit cycle periods and their amplitudes.

Mixed layer phytoplankton equilibrium concentrations rise (as before) with increasing N_0, and the bifurcation found previously for a 40 m thermocline can be seen on the plot. Thermocline phytoplankton, rise at first with N_0, but their concentration falls away as mixed layer phytoplankton increasingly starve them of light.

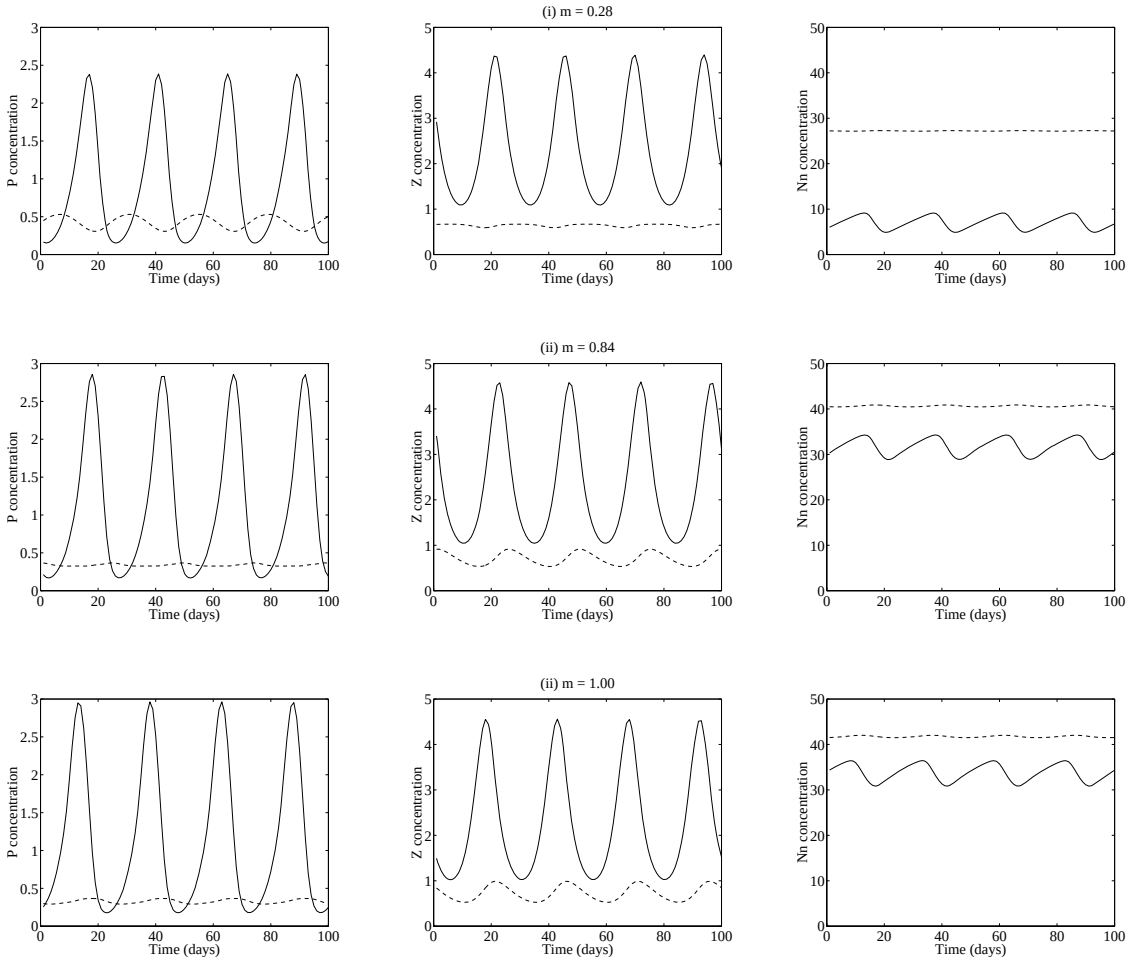

Figure 6.27: Time series results of two layer model simulations performed at Bermuda Station "S" for three values of mixing rate, m. Phytoplankton (left), zooplankton (centre) and nitrate (right) shown. Mixed layer concentrations are represented by a solid line, thermocline layer concentrations by a dashed line. Concentrations are in mmol N m^{-3}.

For values of N_0 in the normal range ($\leq$ 15 mmol N m^{-3}), the mixed layer phytoplankton are almost unchanged by increasing thermocline thickness. In contrast, the thermocline phytoplankton equilibria across the same region fall as increasing thermocline thickness reduces their depth–integrated, light–limited growth.

However, above around 30 mmol N m^{-3}, the system bifurcates at low values of thermocline thickness, and limit cycles occur. The amplitudes of the mixed layer phytoplankton cycles are much higher than those previously found for the two layer model, and very close to those which were found at comparable m and N_0 values with the single layer model. The phytoplankton cycles in the two layers are also almost perfectly in phase with one another ($<$ 1 day out of phase). These results are not surprising, since as the thermocline's thickness shallows, the two layer system comes closer and closer to being a single layer system. The thermocline layer phytoplankton have a depth–integrated light–limited growth closer to that of the mixed layer phytoplankton, and the narrow thermocline allows much greater homogenisation

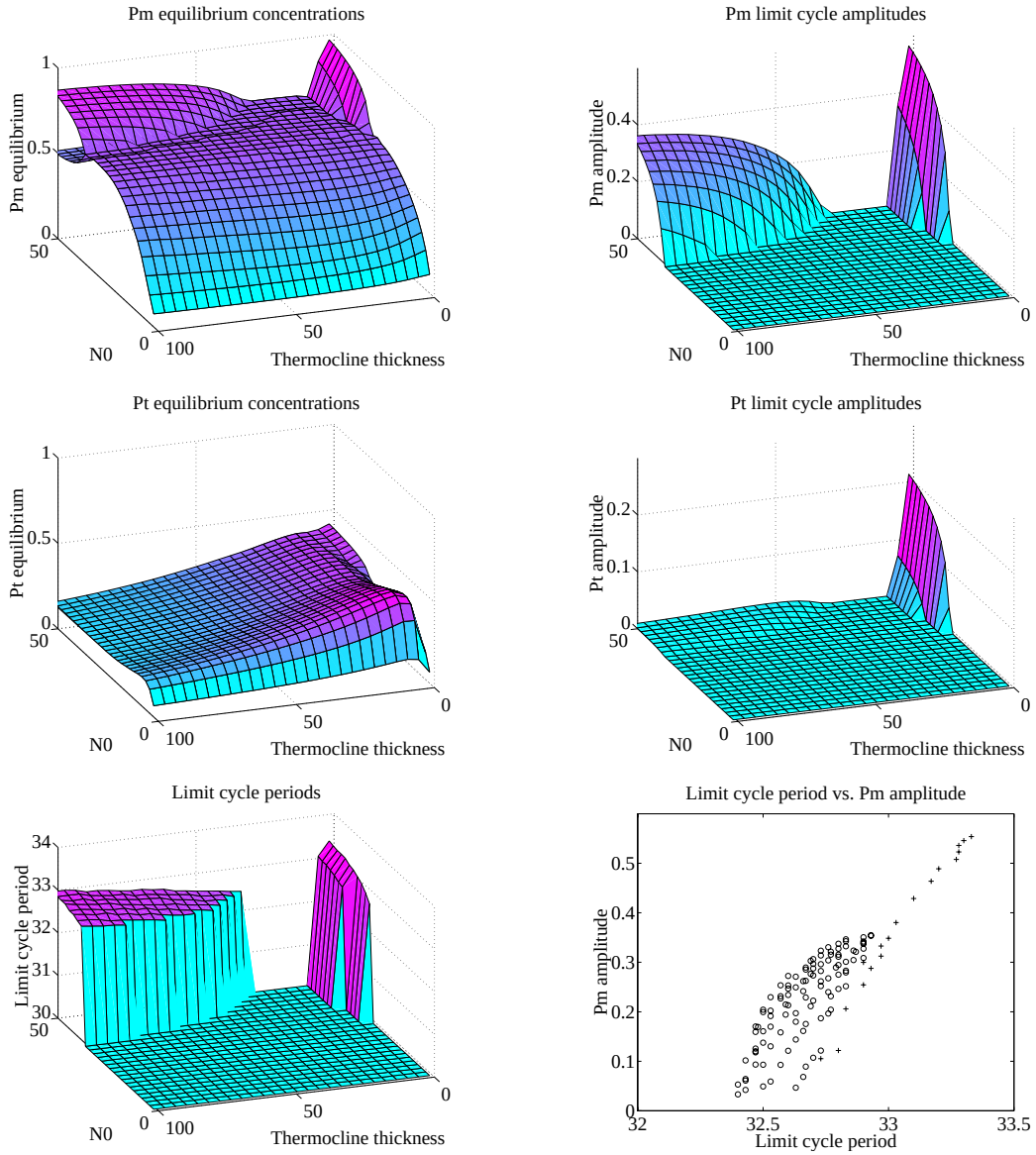

Figure 6.28: The results of simulations of the two layer version of Fasham (1993) performed at OWS "India" on day 197 across a range of thermocline thickness and subthermocline nitrate concentrations (N_0). Thermocline thickness in m, subthermocline nitrate concentrations in mmol N m^{-3}. Phytoplankton equilibrium concentrations and limit cycle amplitudes in mmol N m^{-3}. Limit cycle periods in days. Limit cycle amplitude set to 0 and period to 30 days (for clarity) where only stable equilibrium solutions found. On the limit cycle period vs. amplitude plot, thinner–thermocline limit cycles represented by "+" and thicker–thermocline limit cycles by "o".

of the two layers. This homogenisation mixes more phytoplankton into the thermocline layer from the mixed layer, but also permits a much greater nitrate influx into the mixed layer.

However, as the thermocline thickness increases, whilst the limit cycle behaviour at first ceases, a second series of limit cycles are found. In the range of N_0 examined, these limit cycles begin at thermocline thicknesses above 35 m. This thickness is comparable to the thickness of the mixed layer itself, and the limit cycles are not caused purely by diffusion of phytoplankton into the thermocline layer from the mixed layer. This is evidenced by the thermocline phytoplankton peaks trailing the mixed layer ones by around 20 days. These limit cycles are caused by the increase of nitrate flux to the mixed layer, which is in turn caused by the reduced light–limited growth of the thermocline phytoplankton.

The limit cycles found in these simulations (particularly those which occur with thicker thermoclines) all occur at values of N_0 well outside the normal range. As has been done previously, a second series of simulations, where detrital sinking rate, V, was reduced to 1 m d^{-1}, were performed to establish whether or not limit cycles could occur at parameter values likely to be encountered in the real world.

Figure 6.29 shows the results of these simulations. The most obvious difference from the results shown in figure 6.28 is the extension of the area of parameter space in which limit cycles occur. While the extent of the area in which limit cycles occur ($\approx$ 17 mmol N m^{-3} and upwards) does not quite reach the normal range ($\leq$ 15 mmol N m^{-3}), the gap is small and may be quite easily bridged by changes in other parameters.

Note that, although the two "types" of bifurcation with thermocline thickness previously mentioned have merged into a single region, they can still be easily discerned by the increases in limit cycle amplitude (especially with thermocline phytoplankton) and period as the thermocline thins.

As was found previously with low detrital sinking rates, the limit cycle periods are slightly higher, and across the range examined here, show much less variation than was found for the same range with high sinking rates.

The model simulations here assume that the thermocline phytoplankton are at a homogeneous concentration through their layer in the same manner as the mixed layer phytoplankton. However, while the mixed layer phytoplankton are mostly passively mixed in their layer, the thermocline phytoplankton distribute themselves more actively (swimming, sinking, buoyancy control). As such, a homogeneous distribution through a particularly thick thermocline (which would considerably reduce light–limited growth) is unlikely. Consequently, the more extreme thermocline thicknesses examined previously are liable to produce results quite different from those which would be found in comparable real–life situations.

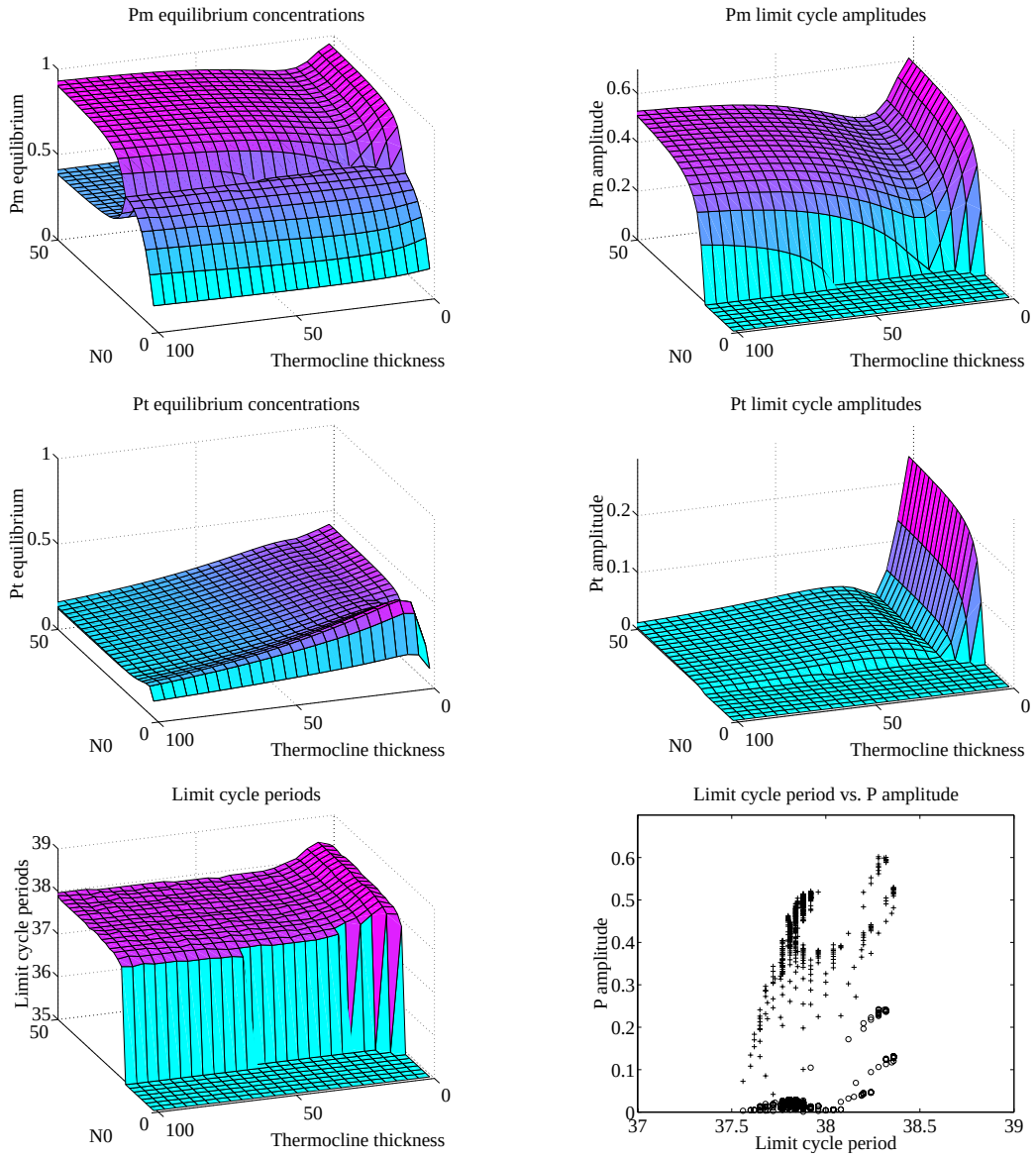

Figure 6.29: The results of simulations of the two layer version of Fasham (1993) performed at OWS "India" on day 197 across a range of thermocline thickness and subthermocline nitrate concentrations (N_0). In these simulations, detrital sinking rate, V, was set to the lower value of 1 m d^{-1}. Thermocline thickness in m, subthermocline nitrate concentrations in mmol N m^{-3}. Phytoplankton equilibrium concentrations and limit cycle amplitudes in mmol N m^{-3}. Limit cycle periods in days. Limit cycle amplitude set to 0 and period to 35 days (for clarity) where only stable equilibrium solutions found. On the limit cycle period vs. amplitude plot, mixed layer phytoplankton represented by "+" and thermocline phytoplankton by "o".

6.6.3 Mixing inputs

As has already been established, the inter–layer mixing rates, m_1 and m_2, can have a profound influence on the dynamics of the system by affecting the rate at which nitrate influxes to the modelled system. In the work described so far, whenever a range of mixing rates has been examined, the two mixing parameters have been assigned the same value. However, the factors affecting mixing processes at the mixed layer–thermocline and thermocline–deep ocean margins are not the same and it is likely that in real life the two parameters have a degree of independence. Wind will strongly affect mixed layer–thermocline mixing, whilst currents in the deep ocean will affect the mixing processes between the thermocline and the deep ocean.

To examine the significance of varying m_1 and m_2 independently, simulations were performed across ranges of both. As usual, simulations were performed for both OWS "India" and Bermuda Station "S" situations.

Figures 6.30 and 6.31 show the results of these simulations. In the ranges examined, only stable equilibria were found, and the phytoplankton, nitrate and net primary productivity equilibria are shown.

The simulations at both latitudes share several features. Nitrate and phytoplankton concentrations in the thermocline layer are strongly related to the value of m_2 (the thermocline–deep ocean mixing rate), whilst concentrations of nitrate and phytoplankton in the mixed layer increase most significantly in response to increases of both m_1 and m_2. This is not surprising since increasing m_1 on it own cannot directly increase the flux of nitrate into the modelled system (though, by decreasing $N_{n,T}$ even further, increasing m_1 slightly increases the influx of nitrate into the thermocline layer from the deep ocean).

At OWS "India" the potential for the thermocline phytoplankton to dominate is curbed by the less favourable light environment there, and P_T only really dominates where m_2 is high but m_1 is low. In fact, as both rise, P_T begins to fall away as shading from the prospering mixed layer phytoplankton reduces light–limited growth even further. However, near the baseline values of m_1 and m_2, even small increases in m_2 lead to the significant rises in total primary productivity.

At Bermuda Station "S" the thermocline phytoplankton almost entirely dominate the full range of m_1 and m_2. This control is most visible on the plot of mixed layer nitrate. Although the equilibrium values of this do increase with m_1 and m_2, the absolute quantity of nitrate in the mixed layer is held very low by the productivity of the thermocline phytoplankton. This result is analogous to Taylor's property (i) ($N_{n,M}$ is independent of N_0). Both relate to the powerful control on nitrate flux exerted by thermocline phytoplankton. Because of the low importance of mixed layer phytoplankton, increases in primary productivity are almost entirely reliant on increases in the mixing between the thermocline and the deep ocean. The more light–limited environment of OWS "India" finds total primary productivity reliant on

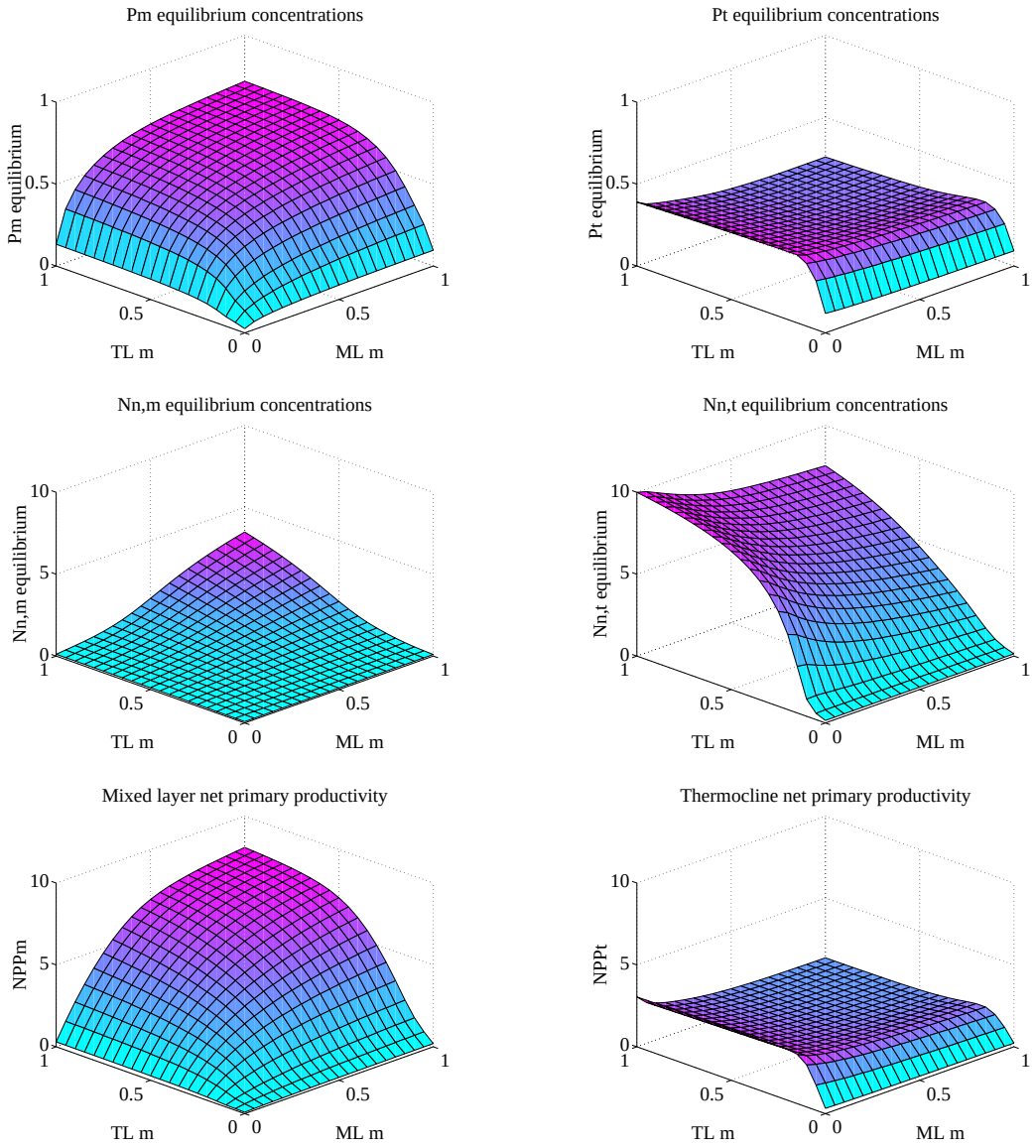

Figure 6.30: The results of simulations of the two layer version of Fasham (1993) performed at OWS "India" on day 197 across a range of mixed layer–thermocline (m_1; ML m) and thermocline–deep ocean (m_2; TL m). The figures show the equilibrium concentrations of phytoplankton (top) and nitrate (middle), and the equilibrium net primary productivity (bottom) in the two modelled layers. Mixing rates are in m d^{-1}, concentrations in mmol N m^{-3} and net primary productivity is in mmol N m^{-2} d^{-1}.

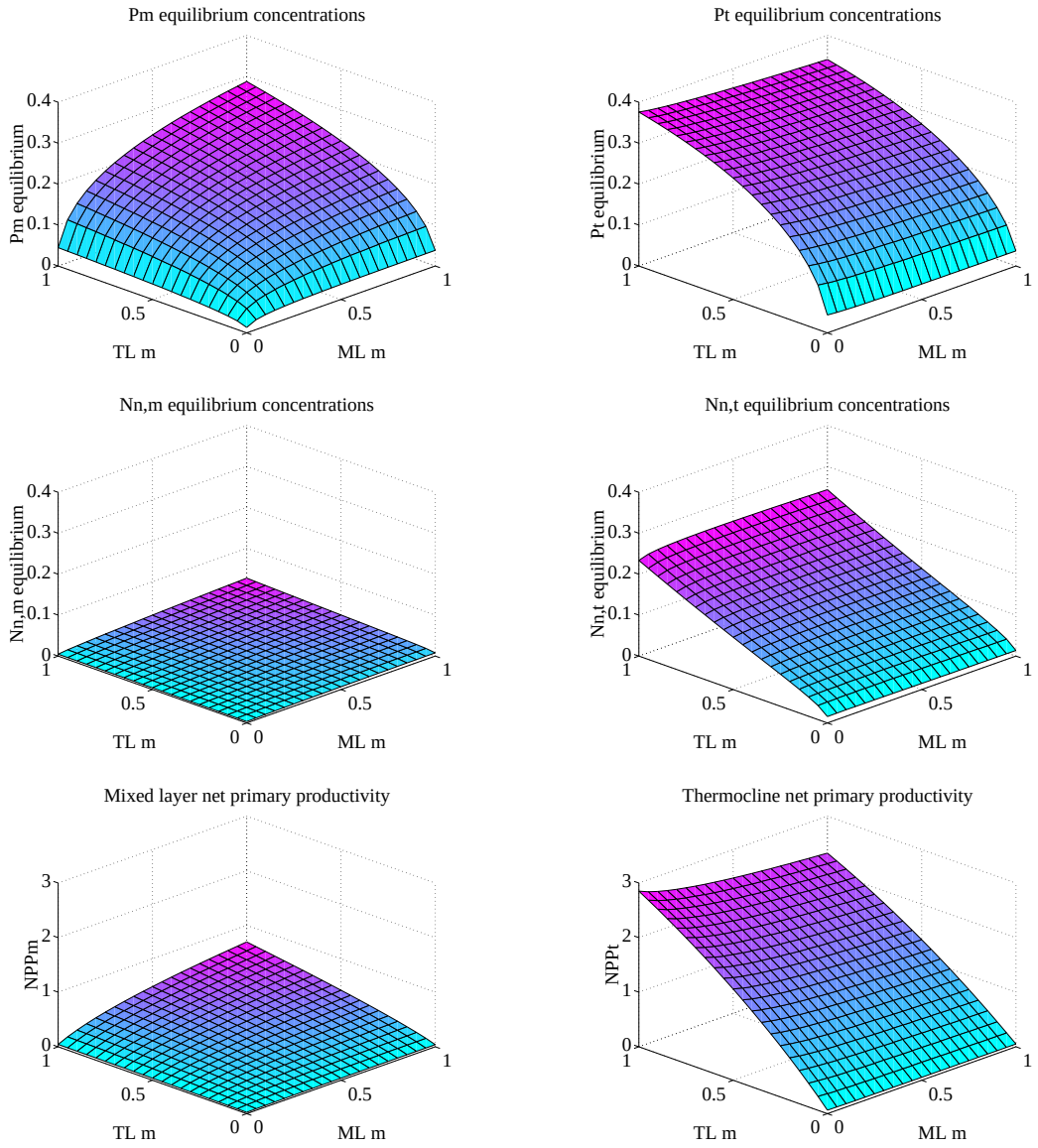

Figure 6.31: The results of simulations of the two layer version of Fasham (1993) performed at Bermuda Station "S" on day 165 across a range of mixed layer–thermocline (m_1; ML m) and thermocline–deep ocean (m_2; TL m). The figures show the equilibrium concentrations of phytoplankton (top) and nitrate (middle), and the equilibrium net primary productivity (bottom) in the two modelled layers. Mixing rates are in m d^{-1}, concentrations in mmol N m^{-3} and net primary productivity is in mmol N m^{-2} d^{-1}.

mixing at both layer margins.

At both locations, increasing m_2 leads to rises in both $N_{n,T}$ and P_T, but very much lower changes to $N_{n,M}$ and P_M. This is not unexpected, since nitrate is ordinarily limiting at both locations during the summer (see the values of $N_{n,M}$ and $N_{n,T}$ at the baseline values of m_1 and m_2), and any increase of nitrate influx to the modelled system is likely to be taken advantage of by the thermocline phytoplankton.

6.7 Summary

This chapter has explored the features and behaviour of a two layer version of Fasham's (1993) model. Previously, other researchers have examined such models (Taylor, 1988; Taylor *et al.*, 1991) and the work presented here is intended to complement that work.

The form of the two layered model used is essentially a simple extension of the single layer system, with a second set of thermocline ODEs which interact with their mixed layer partners. These interactions mostly take the form of mixing, diffusion and de/entraining, although the thermocline phytoplankton are further affected by the amount of light which penetrates the mixed layer, and the zooplankton compartments are complicated by the assumed mobility of the organisms they contain.

This latter complication permits the construction of several reasonable formulations for zooplankton behaviour. However, examination of four of these revealed some significant differences in their behaviour, leading to the adoption of a form with two separate, but communicating, compartments. Other authors (Kremer & Nixon, 1978; Ross, Gurney & Heath, 1993, 1994) have used more complicated functions, in some of which the zooplankton are capable of tracking their prey. However, such forms are usually confined to studies in which the nature of the zooplankton in question is well understood and fairly narrow. In the Fasham (1993) model, the compartment is assumed to be a broad mixture of many different zooplankton types and is less well suited to such specific behaviour.

The primary reason for the construction of a two layer model was to attempt to capture the phenomenon of DCM observed in many locations (Menzel & Ryther, 1960; Brock, Sathyendranath & Platt, 1993; Estrada *et al.*, 1993). Since latitude is an important factor, a series of simulations were performed where latitudinal differences in forcing functions and parameter values were accounted for. These simulations broadly agreed with data, and predicted DCM at tropical and sub–tropical latitudes.

In an attempt to create testable predictions from two layer models, Taylor (1988) deduced a series of general properties from several models which could be looked for in data from appropriate ocean regions. An examination of the two layer version of Fasham (1993) found that most of these properties applied to it, and suggested a few additional avenues which could be looked for in data. The prospects of finding support for these properties in data were also discussed.

Following on from the work in Chapter 4, the two layer model was similarly examined for limit cycle behaviour. Simulations found that while the model did exhibit limit cycles, the parameter range in which they occurred was smaller than that found for the single layer model. The thickness of the thermocline was examined as a possible bifurcation parameter, and it was found that increasing it from zero

caused two "types" of bifurcation. Simulations with very shallow thermoclines behaved very similarly to the single layer model, whilst thicker thermoclines reduced phytoplankton growth there sufficiently that nitrate influx to the mixed layer permitted limit cycles. However, the significance of these latter results is reduced by the less realistic assumptions they make about the thermocline, and the behaviour of the compartments within it. Finally, independent differences in the mixing rates between the two layers were examined. Simulations here found that for mixed layer production to increase significantly, mixing between both the thermocline and the deep ocean, and the mixed layer and the thermocline had to increase, whereas thermocline production (unsurprisingly) only required greater thermocline to deep ocean mixing. The significance of these results was examined at both OWS "India" and Bermuda Station "S".

6.8 Discussion

The assumption that the physics of the plankton ecosystem can be modelled as single, well–mixed surface layer has been a key one throughout this thesis (and in the majority of plankton models). In this chapter, the assumption has been challenged by making a second assumption of a deeper ocean layer overlain by this well–mixed surface layer. This deeper layer was created to represent the thermocline, the region of the water column across which the thermal (and haline, and nutrient) change between the homogenised surface waters and the deep ocean occurs.

This addition to the model was made in an attempt to capture the uneven vertical distribution of phytoplankton and primary production which is often observed in the ocean. Although the addition of a second vertical layer could not fail to improve the modelled distribution of phytoplankton, the resulting model was found to be more successful than the single layer model in predicting total primary productivity for certain geographical locales. However, several of the assumptions used in the construction of the model (*e.g.* perfect mixing within both layers, restricted mixing between the two layers) do favour such agreement, and are probably not entirely consistent with reality. Archer (1995) provides an overview of more realistic (and complex) physical ocean models.

In summary, modelling the oceanic plankton ecosystem as two layers allows the resulting model to more accurately capture the patterns of production in oligotrophic ocean regions (the tropics and sub–tropics).

Chapter 7

Conclusions and future work

Big whorls have little whorls
that feed on their vorticity,
and little whorls have lesser whorls
and so on to viscosity

– Lewis Fry Richardson (1922)

Thought for the day:
If you see a light at the end of the tunnel, it is probably a train.

– Anonymous

7.1 Summary

The chapters of this thesis describe four different investigations of the Fasham (1993) model. While the final of these explores the consequences of an extension to the original model, the first three each address uncertainty in the structure or parameterisation of it. Because of the relative complexity of the model, throughout the thesis a numerical approach to the problems tackled was adopted.

Chapter 3 aimed (somewhat naïvely) to determine a minimum model which captured the behaviour of the full Fasham (1993) model at both OWS "India" and Bermuda Station "S". The full model was "stripped" to what were considered its bare essentials, a PZ form, and then the model was rationally reconstructed to the full form. At each step, consideration was given to the pathways reinstated and the forms that they took (*e.g.* the zooplankton grazing term). To retain mechanistic integrity, neither the functional forms nor the parameter values were changed from those used in the full model. The simulations found that models only became successful once they possessed a detrital compartment. In contrast, the bacteria compartment was found to be fairly redundant, with several models (*e.g.* 4c, 4c2, 5c3) successfully managing without it. OWS "India" simulation results found that when nutrients were not limiting through most of the year, models which ignored them or demoted them to a single parameter were surprisingly successful.

The summer months of simulations at OWS "India" are distinguished by oscillations in the concentration of phytoplankton. These oscillations are interesting since data sets from OWS "India" also appear to exhibit such cycles, while they are entirely absent from both data and model simulations at Bermuda Station "S". Chapter 4 sought to characterise the nature of these oscillations in the modelled phytoplankton and zooplankton populations. Numerical studies of the full model using "fixed forcing" revealed that they are transient behaviour towards a stable equilibrium which is never normally reached because of the forced annual cycle. An intensive numerical study of parameter space around the baseline parameter values did, however, uncover regions of parameter space in which stable oscillatory behaviour was found to occur (parameters m, N_0 and V were particularly important in this regard). From the ranges of parameters in the literature, plausible combinations of values were found which would make the oscillations stable, and potentially observable in data. Work investigating parameter ranges also suggested potentially sensitive parameters (those where model equilibria were particularly sensitive near baseline values), and also particularly insensitive parameters (somewhat in agreement with Chapter 3, bacterial parameters were found to elicit almost no changes in model equilibria). Because of recent interest in the literature, the role of the zooplankton loss term in such behaviour was also investigated. The findings from this latter work suggested caution in applying the conclusions of a well–known study by Steele & Henderson (1992).

While Chapter 4 studied parameters with a view to the dynamical behaviour they could elicit, Chapter 5 instead aimed to establish the sensitivity of the forced model to variation in each of the parameters. The work built upon a similar analysis by Fasham, Ducklow & McKelvie (1990), and introduced stochastic approaches to study parameter sensitivity. One of these techniques was that described by Kremer (1983). After initial parameter sensitivity studies at both OWS "India" and Bermuda Station "S"(which found parameter sensitivity dominated by photosynthesis and grazing parameters), the techniques themselves were examined to study issues such as model sensitivity to multiple variable parameters, the quantitative relationship between variability in a parameter and corresponding variability in the model, and the periodicity of variability in parameters. Finally, the reduced models from Chapter 3 were re–introduced to study the effects of parameter variability on models varying in their complexity. While certain differences between the simpler "excitable" model and the full model were discerned, there did not appear to be a strong relationship between model size and susceptibility to parameter variability.

A key assumption running through all of the earlier models in the thesis was that of a homogeneous mixed layer in which all of the modelled biology resided. Chapter 6 altered the vertical structure of the full model by adding a second, deeper layer to represent the thermocline. Such models have been examined in the literature since they can better capture the vertical distribution of phytoplankton in tropical and sub–tropical waters. The assumed motility of zooplankton in such a model caused difficulty in constructing the model, but it was found that they were best treated as "faithful" to the layer in which they originated. The effect of latitudinal differences in seasonal cycle, and the generality of several propositions of Taylor (1988) concerning such models were examined, and the results were compared (often favourably) with appropriate measurements where available. The equilibrium behaviour of the two layer model was also examined in a manner similar to that in Chapter 4. While oscillatory behaviour was found in the two layer model, the parameter ranges over which it occurred were found to be much reduced.

7.2 Conclusions

Several major conclusions can be drawn from the four research chapters :

- Detritus plays a key role in the success of the reduced models, while bacteria are mostly redundant.
- Models in which nitrate (the "fuel" of the ecosystem) is represented by a static parameter rather than a dynamic variable can be successful under certain conditions.
- Predator–prey oscillations during normally forced OWS "India" solutions are transients toward a stable fixed point.
- Stable limit cycles exist in reasonable regions of parameter space (parameters m, N_0 and V were found to be important).

- At both OWS "India" and Bermuda Station "S", model solutions are sensitive to phytoplankton photosynthesis (k_w, α, λ and V_p) and zooplankton grazing parameters (g, β, k_3 and p_1).

- The two layer version of Fasham (1993) can improve estimates of NPP, and better capture the dynamics in subtropical and equatorial regions.

7.3 Future work

There are a number of directions in which the work in this thesis could be extended. A particular limitation of the work common to all of the research chapters has been its focus on the geographical locations of OWS "India" and Bermuda Station "S". While these stations differ substantially in their forcing and the values of certain key parameters (particularly N_0), they still only represent a fraction of the variability in the world ocean. For instance, although mentioning the potential significance of equatorial upwelling regions for oscillatory behaviour, Chapter 4 does not explore this avenue (Fasham *et al.*, 1993, citing Toggweiler, 1990, report such behaviour in simulations at this location).

Focusing on individual chapters, several lines of further research suggest themselves. As noted in Chapter 3, one of the restrictions placed on the reduced models was that their parameters were fixed at the values from the full model. Using the kind of non–linear optimisation technique described in Fasham & Evans (1995) (and the full model as a "perfect" data set), the parameters of reduced models could be optimised to establish whether a given reduced model could, in principle, be reasonably made to "fit" the full model (*i.e.* those models whose optimised parameters fall close to those of the full model). Although the success of bacteria–less models such as 4c2 and 5c3 was well–received, further work to establish the effects of this subtraction, and possibly new implicit representations of heterotrophic bacteria, would be interesting. As already suggested, extension of the comparison of models could be extended to other forcing regimes. The differential success of the implicit nitrate models between the two locations studied suggests choosing different reduced models for different locations (possibly to ease computation burden in spatially–extended GCMs).

A weakness of Chapter 4's analysis of oscillatory behaviour was its reliance on a relatively crude numerical approach to explore parameter space. While the complexity of the model favoured this, the investigation of more powerful numerical utilities (such as those described in Edwards, 1997) would ideally precede any future studies of model behaviour. Tying the results of Chapters 3 and 4, the behaviour of the reduced models could systematically be probed[1] to establish if any patterns of behaviour between the models occurred. Edwards (1997) found that the addition of a detritus compartment to the ZPN ecology of Steele & Henderson (1981) resulted in very similar patterns of bifurcation. The lack of

[1] A preliminary analysis of model 4c2 along these lines has already been performed using the programs from Chapter 4. While the behaviour of the stable equilibria across parameter ranges was very similar to that of the full model, no limit cycle behaviour was uncovered. However, as with the study of the full model, the analysis examined only a fraction of parameter space.

success of 3 compartment models (compared to 4 compartment ones) in Chapter 3 suggests a contrary result with the reduced forms of the Fasham (1993) model. Furthermore, the bifurcations already found should be re–examined from a more mathematical standpoint to establish any relationships between the oscillatory behaviour here and the menagerie of bifurcations found in the analysis of Edwards (1997).

Aside from consideration of the range and nature of variability of the parameters used in the analysis of Chapter 5 (already mentioned in Chapter 5's discussion), there are several paths for future research. Sensitivity work in Chapter 5 assessed parameters over the full annual cycle. In the case of Bermuda Station "S", where the concentrations of plankton are relatively high throughout the year, such an approach may suit an analysis. By contrast, at OWS "India", where plankton only occur at high concentrations from the late spring to early autumn, attention to parameter sensitivities should perhaps only focus on this period (however, the choice of system measure used may negate such concerns). As stated in Chapter 2, many of the terms in the Fasham (1993) model (and in all plankton models) represent a composite of many different ecological processes. A possible extension to the work of Chapter 5 would be to explore the consequences to model sensitivity of de–compositing such processes. For example, although bacterial losses are represented as :

$$\begin{aligned} \frac{dB}{dt} &= \ldots - \mu_3 B - \ldots \\ &= \ldots - excretion - \ldots \end{aligned}$$

they may be more accurately modelled as :

$$\begin{aligned} \frac{dB}{dt} &= \ldots - \mu_{3a} B - \mu_{3b} B - \mu_{3c} B - \mu_{3d} B - \ldots \\ &= \ldots - excretion - starvation - phage\,infection - senescence - \ldots \end{aligned}$$

where each process is modelled (and parameterised) separately, and usually approximated to the term above. However, since each of the separate parameters which would then make up bacterial losses would likely command only a fraction of the model sensitivity of the "lumped" term (since $\mu_{3x} < \mu_3$), the effect of this, even where all of the sub–parameters are allowed to vary stochastically together, is likely to be a reduction in importance of the total pathway (*e.g. excretion*) these sub–pathways model[2]. This reduction in importance may profoundly affect the conclusions of such work (and may misdirect ventures to sample "sensitive" parameters).

The work of Chapter 6 made several major assumptions about the modelled biology and physics, each of which presents a potential agenda for extending the work. The assumption of identical populations of plankton in the two modelled layers could be replaced by parameterisations based upon observations

[2]Annan's (1997) comparison of the Monte Carlo and stochastic parameters techniques has some bearing here. His analysis suggested that stochastic parameters simulations show lower variance than those of Monte Carlo simulations because multiple re–sampling of a parameter narrows the "real" variance around its mean. Similarly, where a parameter, x, is broken down into n sub–parameters (where, for instance, $x_1 + x_2 + \ldots + x_n = x$), and then these sub–parameters are allowed to vary stochastically together, then for every single re–sampling of x in the normal model, there are n re–samplings in the de–composited model.

of the assemblages dominating the different layers (*e.g.* surface layer cyanobacteria versus deep layer eukaryotes; Gieskes & Kraay, 1986). Alternatively, competition models with multiple phytoplankton species (each with their own parameterisation) could be used to establish whether any succession patterns (which could be sought in observational data) occurred. As stated in Chapter 6, the formulation of the zooplankton compartment is far from clear depending upon the assumptions made about their behaviour. Although this aspect of the model could be extended by further variants of the zooplankton compartment (*e.g.* migration to the most phytoplankton–rich layer; introduction of migrating and non–migrating zooplankton species; DVM zooplankton), any behaviour which distinguished between the modelled layers should also examine whether the effects of processes such as predation should be similarly different between the layers. With respect to the physics, more realistic representations of vertical space and mixing (*e.g.* see Archer, 1995; Taylor & Stephens, 1993) could be used, although any adaptation in this direction may entirely alter the basic two layer structure of the model and complicate comparisons.

7.4 "Robust" models

The context of many attempts to model plankton systems is to establish a single model (a "robust" model) which, when given the appropriate physical forcing with respect to a location in question (or inserted into a GCM), will produce annual patterns of biological activity in agreement with data. Fasham (1993) and Fasham (1995) explicitly spell out this "goal" of plankton ecosystem modelling.

Since data, on the whole, has tended to be poor in either overall spatio–temporal coverage (*e.g.* cruise data), or bandwidth (*e.g.* satellite data), models have tended to be relatively simple. Researchers are not necessarily using ZPN models simply because they are easy to use, but often because the available data is restricted to only chlorophyll or DIN concentrations. The success of such simple models in reproducing phenomena such as the spring phytoplankton bloom has additionally led to their persistence in the plankton modelling literature.

However, it is likely that for a robust model to be generated, more than simple ZPN models will be required. Work such as Kremer & Nixon (1978), Andersen, Nival & Harris (1987), Frost (1987), and Taylor *et al.* (1993) has drawn attention to the need to include multiple ZPN "species" (*e.g.* copepods versus microzooplankton; diatoms versus phytoflagellates; nitrogen nutrients versus silicate, phosphate or iron) to model specific data sets, and it is likely that any model which aims to be applicable to the entire world ocean will need to be similarly structured.

The work in this thesis, although utilising a model with some degree of complexity (*e.g.* multiple nitrogen nutrients, representations of both DON and PON), still ignores almost all of the other distinctions made above. However, following Einstein's dictum (see Chapter 3), simple models should still ideally be preferred, and analyses similar to that of Chapter 3 should always be borne in mind.

7.5 Closing remarks

Although considerable work still remains to be done in the development of models which accurately, and robustly, predict plankton behaviour across the world ocean, it is hoped that the work in this thesis, by suggesting important state variables, functional forms and parameters, can play a small part in their realisation.

References

Every day, approximately 20 million words of technical information are recorded. A reader capable of reading 1,000 words per minute would require 1.5 months, reading eight hours a day, to get through one day's output, and at the end of that period he would have fallen 5.5 years behind in his reading.

– Hubert Murray Jr.

The secret to creativity is knowing how to hide your sources.

– Albert Einstein (1879–1955)

Adams, J. M., Fauré, H., Fauré–Denard, L., McGlade, J. M. and Woodward, F. I. (1990)
Increases in terrestrial carbon storage from the last glacial maximum to the present.
Nature **348** : 711–714.

Alexander, R. M. (1995)
Leg design and jumping technique for humans, other vertebrates and insects.
Philosophical Transactions of the Royal Society of London B **347** : 235–248.

Anderson, D. M. (1997)
Turning back the harmful red tide.
Nature **388** : 513–514.

Anderson, R. M. and May, R. M. (1991)
Infectious Diseases of Humans : Dynamics and Control.
Oxford University Press, Oxford, U.K.

Andersen, V., Nival, P. and Harris, R. P. (1987)
Modelling of a planktonic ecosystem in an enclosed water column.
Journal of the Marine Biological Association of the U.K. **67** : 407–430.

Annan, J. D. (1997)
On repeated parameter sampling in Monte Carlo simulations.
Ecological Modelling **97** : 111–115.

Archer, D. (1995)
Upper ocean physics as relevant to ecosystem dynamics : a tutorial.
Ecological Applications **5** : 724–739.

Arenovski, A. L., Lin Lim, E. and Caron, D. A. (1995)
Mixotrophic nanoplankton in oligotrophic surface waters of the Sargasso Sea may employ phagotrophy to obtain major nutrients.
Journal of Plankton Research **17** : 801–820.

Atkinson, A., Ward, P. and Murphy, E. J. (1996)
Diel periodicity of sub–Antarctic copepods – relationships between vertical migration, gut fullness and gut evacuation rate.
Journal of Plankton Research **18** : 1387–1405.

Azam, F., Fenchel, T., Field, J. G., Gray, J. S., Meyer–Reil, L. A. and Thingstad, F. (1983)
The ecological role of water–column microbes in the sea.
Marine Ecology Progress Series **10** : 257–263.

Balch, W. M., Kilpatrick, K. A. and Trees, C. C. (1996)
The 1991 coccolithophore bloom in the central North Atlantic. 1. Optical properties and factors affecting their distribution.
Limnology and Oceanography **41** : 1669–1683.

Balch, W. M., Kilpatrick, K. A., Holligan, P., Harbour, D. and Fernandez, E. (1996)
The 1991 coccolithophore bloom in the central North Atlantic. 2. Relating optics to coccolith concentration.
Limnology and Oceanography **41** : 1684–1696.

Banse, K. (1987)
Clouds, deep chlorophyll maxima and the nutrient supply to the mixed layer of stratified water bodies.
Journal of Plankton Research **9** : 1031–1036.

Barnes, R. D. B. (1986)
Invertebrate Zoology (Fifth edition).
Saunders College Publishing, Philadelphia, U.S.A.

Barstow, S. F. (1983)
The ecology of Langmuir circulation – a review.
Marine Environmental Research **9** : 211–236.

Bascompte, J., Solé, R. V. and Valls, J. (1992)
Chaotic behaviour in simulated planktonic successions, I : discrete temporal map.
Scientia Marina **56** : 285–292.

Bauer, P., Gaito, S., McGlade, J. M. and Winter, D. (1993)
Estimation of net photosynthetically available radiation over oceans from satellite data – application to a dynamic model of a plankton bloom in the Atlantic Ocean.
Photogrammetric Engineering and Remote Sensing **59** : 323–329.

Bees, M. A. and Hill, N. A. (1997)
Wavelengths of bioconvection patterns.
Journal of Experimental Biology **200** : 1515–1526.

Bees, M. A., Mezić, I. and McGlade, J. M. (1997)
Planktonic interactions and chaotic advection in Langmuir circulation.
IMACS Journal of Mathematics and Computers in Simulation (in press)

Begon, M., Harper, J. L. and Townsend, C. R. (1986)
Ecology : Individuals, Populations and Communities.
Blackwell Scientific Publications Inc., Oxford, U.K.

Behrenfeld, M. J., Bale, A. J., Kolber, Z. S., Aiken, J. and Falkowski, P. G. (1996)
Confirmation of iron limitation of phytoplankton photosynthesis in the equatorial Pacific Ocean.
Nature **383** : 508–511.

Beltrami, E. and Carroll, T. O. (1994)
Modelling the role of viral disease in recurrent phytoplankton blooms.
Journal of Mathematical Biology **32** : 857–963.

Bienfang, P. K., Syper, J. and Laws, E. (1983)
Sinking rate and pigment responses to light–limitation of a marine diatom : implications to dynamics of chlorophyll maximum layers.
Oceanologica Acta **6** : 55–62.

Bralewska, J. M. and Witek, Z. (1995)
Heterotrophic dinoflagellates in the ecosystem of the Gulf of Gdansk.
Marine Ecology Progress Series **117** : 241–248.

Bratbak, G., Levasseur, M., Michaud, S., Cantin, G., Fernandez, E., Heimdal, B. R. and Heldal, M. (1995)
Viral activity in relation to *Emiliania huxleyi* blooms – a mechanism of DMSP release.
Marine Ecology Progress Series **128** : 133–142.

Brock, J., Sathyendranath, S. and Platt, T. (1993)
Modelling the seasonality of subsurface light and primary production in the Arabian Sea.
Marine Ecology Progress Series **101** : 209–221.

Brock, T. D. (1981)
Calculating solar radiation for ecological studies.
Ecological Modelling **14** : 1–19.

Burkill, P. H., Edwards, E. S., John, A. W. G. and Sleigh, M. A. (1993)
Microzooplankton and their herbivorous activity in the northeastern Atlantic ocean.
Deep–Sea Research II **40** : 479–493.

Campbell, L., Nolla, H. A. and Vaulot, D. (1994)
The importance of *Prochlorococcus* to community structure in the Central North Pacific–Ocean.
Limnology and Oceanography **39** : 954–961.

Cole, J. F. T. (1997)
The surface dynamics of the Northern Benguela upwelling system and its relationship to patterns of clupeoid production.
Ph.D. Thesis, University of Warwick, Coventry, U.K.

Crocker, K. M. and Passow, U. (1995)

Differential aggregation of diatoms.

Marine Ecology Progress Series **117** : 249–257.

Dadou, I., Garcon, V., Andersen, V., Flierl, G. R. and Davis, C. S. (1996)

Impact of the north equatorial current meandering on a pelagic ecosystem – a modelling approach.

Journal of Marine Research **54** : 311–342.

Dahms, H.–U. (1995)

Dormancy in the Copepoda – an overview.

Hydrobiologia **306** : 199–211.

Davidson, K. and Cunningham, A. (1996)

Accounting for nutrient processing time in mathematical models of phytoplankton growth.

Limnology and Oceanography **41** : 779–783.

Davidson, K., Cunningham, A. and Flynn, K. J. (1993)

Modelling temporal decoupling between biomass and numbers during the transient nitrogen–limited growth of a marine phytoflagellate.

Journal of Plankton Research **15** : 351–359.

Davidson, K., Cunningham, A. and Flynn, K. J. (1995)

Predator–prey interactions between *Isochrysis galbana* and *Oxyrrhis marina* .3. Mathematical–modelling of predation and nutrient regeneration.

Journal of Plankton Research **17** : 465–492.

DeLong, E. F., Wu, K. Y., Prézelin, B. B. and Jovine, R. V. M. (1994)

High abundance of Archaea in Antarctic marine picoplankton.

Nature **371** : 695–697.

DeMeester, L., Weider, L. J. and Tollrian, R. (1995)

Alternative antipredator defences and genetic–polymorphism in a pelagic predator–prey system.

Nature **378** : 483–485.

Dobson, F. W. and Smith, S. D. (1988)

Bulk models of solar radiation at sea.

Quarterly Journal of the Royal Meteorological Society **114** : 165–182.

Dortch, Q. (1990)

The interaction between ammonium and nitrate uptake in phytoplankton.

Marine Ecology Progress Series **61** : 183–201.

Dugdale, R. C. and Wilkerson, F. P. (1998)

Silicate regulation of new production in the equatorial Pacific upwelling.

Nature **391** : 270–273.

Dugdale, R. C., Wilkerson, F. P. and Minas, H. J. (1995)
The role of a silicate pump in driving new production.
Deep–Sea Research I **42** : 697–719.

Eccleston–Parry, J. D. and Leadbeater, B. S. C. (1994)
A comparison of the growth–kinetics of 6 marine heterotrophic nanoflagellates fed with one bacterial species.
Marine Ecology Progress Series **105** : 167–177.

Edwards, A. M. (1997)
A rational dynamical systems approach to plankton population modelling.
Ph.D. Thesis, University of Leeds, Leeds, U.K.

Edwards, A. M. and Brindley, J. (1996)
Oscillatory behaviour in a three–component plankton model.
Dynamics and Stability of Systems **11** : 347–370.

Egge, J. K. and Aksnes, D. L. (1992)
Silicate as regulating nutrient in phytoplankton competition.
Marine Ecology Progress Series **83** : 281–289.

Estrada, M., Marrasé, C., Latasa, M., Berdalet, E., Delgado, M. and Riera, T. (1993)
Variability of deep chlorophyll maximum characteristics in the Northwestern Mediterranean.
Marine Ecology Progress Series **92** : 289–300.

Evans, G. T. and Paranjape, M. A. (1992)
Precision of estimates of phytoplankton growth and microzooplankton grazing when the functional–response of grazers may be non–linear.
Marine Ecology Progress Series **80** : 285–290.

Evans, G. T. and Parslow, J. S. (1985)
A model of annual plankton cycles.
Biological Oceanography **3** : 327–347.

Fasham, M. J. R. (1993)
Modelling the marine biota.
In : *The Global Carbon Cycle*, (ed. M. Heimann), pp. 457–504.
Springer–Verlag, New York, U.S.A.

Fasham, M. J. R. (1995)
Variations in the seasonal cycle of biological production in subarctic oceans : A model sensitivity analysis.
Deep–Sea Research I **42** : 1111–1149.

Fasham, M. J. R., Ducklow, H. W. and McKelvie, S. M. (1990)

A nitrogen–based model of plankton dynamics in the oceanic mixed layer.

Journal of Marine Research **48** : 591–639.

Fasham, M. J. R. and Evans, G. T. (1995)

The use of optimisation technique to model marine ecosystem dynamics at the JGOFS station at 47° N 20° W.

Philosophical Transactions of the Royal Society of London B **348** : 203–209.

Fasham, M. J. R., Sarmiento, J. L., Slater, R. D., Ducklow, H. W. and Williams, R. (1993)

Ecosystem behaviour at Bermuda Station "S" and Ocean Weather Station "India" : a general circulation model and observational analysis.

Global Biogeochemical Cycles **7** : 379–415.

Flynn, K. J., Fasham, M. J. R. and Hipkin, C. R. (1997)

Modelling the interactions between ammonium and nitrate uptake in marine phytoplankton.

Philosophical Transactions of the Royal Society of London B **352** : 1625–1645.

Frost, B. W. (1987)

Grazing control of phytoplankton stock in the open subarctic Pacific Ocean : a model assessing the role of mesozooplankton, particularly the large calanoid copepods *Neocalanus* spp.

Marine Ecology Progress Series **39** : 49–68.

Fuhrman, J. A. and Capone, D. G. (1991)

Possible biogeochemical consequences of ocean fertilisation.

Limnology and Oceanography **36** : 1951–1959.

Garver, S. A., Siegel, D. A. and Mitchell, B. G. (1994)

Variability in near–surface particulate absorption–spectra – what can a satellite ocean color imager see?

Limnology and Oceanography **39** : 1349–1367.

Gayoso, A. M. (1995)

Bloom of *Emiliania huxleyi* (Prymnesiophyceae) in the western South Atlantic Ocean.

Journal of Plankton Research **17** : 1717–1722.

Geider, R. J. and LaRoche, J. (1994)

The role of iron in phytoplankton photosynthesis, and the potential for iron–limitation of primary productivity in the sea.

Photosynthesis Research **39** : 275–301.

Gieskes, W. W. and Kraay, G. W. (1986)

Floristic and physiological differences between the shallow and the deep nanophytoplankton community in the euphotic zone of the open tropical Atlantic revealed by HPLC analysis of pigments.

Marine Biology **91** : 567–576.

Guckenheimer, J., Meyers, M. R., Wicklin, F. J. and Worfolk, P. A. (1991)

DSTool : a dynamical system toolkit with an interactive graphical interface.

Center for Applied Mathematics, Cornell University, New York, U.S.A.

Hairston, N. G. and Hairston, N. G. (1993)

Cause–effect relationships in energy–flow, trophic structure, and interspecific interactions.

American Naturalist **142** : 379–411.

Haney, J. D. and Jackson, G. A. (1996)

Modelling phytoplankton growth–rates.

Journal of Plankton Research **18** : 63–85.

Haney, J. F., Sasner, J. J. and Ikawa, M. (1995)

Effects of products released by *Aphanizomenon flos–aquae* and purified saxitoxin on the movements of *Daphnia carinata* feeding appendages.

Limnology and Oceanography **40** : 263–272.

Hardin, G. (1968)

The Tragedy of the Commons.

Science **162** : 1243–1248.

Hardin, G. (1985)

Filters Against Folly.

Viking Penguin Inc., New York, U.S.A.

Hardin, G. (1993)

Living within Limits : Ecology, Economics, and Population Taboos.

Oxford University Press, Oxford, U.K.

Harrison, W. G., Harris, L. R. and Irwin, B. D. (1996)

The kinetics of nitrogen utilisation in the oceanic mixed layer : nitrate and ammonium interactions at nanomolar concentrations.

Limnology and Oceanography **41** : 16–32.

Hays, G. C., Warner, A. J. and LeFevre, D. (1996)

Long–term changes in the diel vertical migration behaviour of zooplankton.

Marine Ecology Progress Series **141** : 149–159.

Hayward, T. L. (1991)

Primary production in the North Pacific Central Gyre : a controversy with important implications.

Trends in Ecology and Evolution **6** : 281–284.

Hein, M. and Sand–Jensen, K. (1997)

CO_2 increases oceanic primary production.

Nature **388** : 526–527.

Henderson–Sellers, A. and Robinson, P. J. (1986)

Contemporary Climatology.

Longman Scientific & Technical, Harlow, U.K.

Hendry, R. J. and McGlade, J. M. (1995)

The role of memory in ecological systems.

Proceedings of the Royal Society of London B **259** : 153–159.

Hoek, C. van den, Mann, D. G. and Jahns, H. M. (1995)

Algae : An Introduction to Phycology.

Cambridge University Press, Cambridge, U.K.

Hoepffner, N., Barker, T., Nykjaer, L., Estrada, M. and Schlittenhardt, P. (1994)

Use of an analytical model to determine the primary production from satellite data in a coastal upwelling environment.

Oceanologica Acta **17** : 431–442.

Hofmann, E. E. and Ambler, J. W (1988)

Plankton dynamics on the outer southeastern U.S. continental shelf. Part II : a time dependent biological model.

Journal of Marine Research **46** : 883–917.

Huntley, M. E., Zhou, M. and Nordhausen, W. (1995)

Mesoscale distribution of zooplankton in the California Current in late spring, observed by Optical Plankton Counter.

Journal of Marine Research **53** : 647–674.

Hutchins, D. A. and Bruland, K. W. (1994)

Grazer–mediated regeneration and assimilation of Fe, Zn and Mn from planktonic prey.

Marine Ecology Progress Series **110** : 259–269.

Jeong, H. J. (1994)

Predation by heterotrophic dinoflagellate *Protoperidinium* cf. *divergens* on copepod eggs and early naupliar stages.

Marine Ecology Progress Series **114** : 203–208.

Jochem, F. J. (1995)

Phototrophic picoplankton community structure in three different pelagic regimes in the Arabian Sea.

Marine Ecology Progress Series **117** : 307–314.

Jones, R. and Henderson, E. W. (1986)

The dynamics of nutrient regeneration and simulation studies of the nutrient cycle.

Journal du Conseil **43** : 216–236.

Jurgens, K. and Gude, H. (1994)

The potential importance of grazing–resistant bacteria in planktonic systems.

Marine Ecology Progress Series **112** : 169–188.

Kahru, M., Leppanen, J. M. and Rud, O. (1993)

Cyanobacterial blooms cause heating of the sea–surface.

Marine Ecology Progress Series **101** : 1–7.

Keeling, M. J. (1995)

The Ecology and Evolution of Spatial Host–Parasite Systems.

Ph.D. Thesis, University of Warwick, Coventry, U.K.

Keeling, M. J. and Grenfell, B. T. (1997)

Disease extinction and community size: modelling the persistence of measles.

Science **275** : 65–67.

Keeling, M. J. and Rand, D. A. (1995)

A spatial mechanism for the evolution and maintenance of sexual reproduction.

Oikos **74** : 414–424.

Kremer, J. N. (1983)

Ecological implications of parameter uncertainty in stochastic simulation.

Ecological Modelling **18** : 187–207.

Kremer, J. N. and Nixon, S. W. (1978)

A Coastal Marine Ecosystem.

Springer–Verlag, New York, U.S.A.

Lamport, L. (1986)

LaTeX: A document preparation system.

Addison–Wesley Publishing Inc., Wokingham, U.K.

Lashof, D. A. (1991)

Gaia on the brink : Biogeochemical feedback processes in global warming.

In : *Scientists on Gaia*, (ed. S. H. Schneider and P. J. Boston), pp. 393–404.

The MIT Press, Cambridge, MA, U.S.A.

Lecourt, M., Muggli, D. L. and Harrison, P. J. (1996)

Comparison of growth and sinking rates of non–coccolith–forming and coccolith–forming strains of *Emiliania huxleyi* (Prymnesiophyceae) grown under different irradiances and nitrogen–sources.

Journal of Phycology **32** : 17–21.

Lee, B. G. and Fisher, N. S. (1994)

Effects of sinking and zooplankton grazing on the release of elements from planktonic debris.

Marine Ecology Progress Series **110** : 271–281.

Levitus, S. (1982)

Climatological atlas of the world ocean.

US Government Printing Office, Washington : NOAA Professional Paper 13.

Liss, P. S., Hatton, A. D., Malin, G., Nightingale, P. D. and Turner, S. M. (1997)

Marine sulphur emissions.

Philosophical Transactions of the Royal Society of London B **352** : 159–168.

Littler, M. M., Littler, D. S., Blair, S. M. and Norris, J. N. (1985)

Deepest known plant life discovered on an uncharted seamount.

Science **227** : 57–59.

Loehle, C. (1997)

A hypothesis testing framework for evaluating ecosystem model performance.

Ecological Modelling **97** : 153–165.

Longhurst, A. (1995)

Seasonal cycles of pelagic production and consumption.

Progress in Oceanography **36** : 77–167.

Loose, C. J. and Dawidowicz, P. (1994)

Trade–offs in diel vertical migration by zooplankton : the costs of predator avoidance.

Ecology **75** : 2255–2263.

Lotka, A. J. (1925)

The Elements of Physical Biology.

Williams & Williams Co., Baltimore, U.S.A.

Lovelock, J. E. (1989)

The Ages of Gaia.

Oxford University Press, Oxford, U.K.

Lowry, R. K., Machin, P. and Cramer, R. N. (1994)

Users' guide to the BOFS North Atlantic data set.

Natural Environment Research Council, Swindon, U.K.

Malchow, H. (1993)

Spatio–temporal pattern in non–linear non–equilibrium plankton dynamics

Proceedings of the Royal Society of London B **251** : 103–109.

Malchow, H. (1994)

Non–equilibrium structures in plankton dynamics.

Ecological modelling **75** : 123-134.

Malthus, T. (1798)

An Essay on the Principle of Population.

`http://socserv2.socsci.mcmaster.ca/~econ/ugcm/3ll3/malthus/popu.txt`

Mann, K. H. and Lazier, J. R. N. (1991)

Dynamics of Marine Ecosystems.

Blackwell Scientific Publications Inc., Oxford, U.K.

Martin, J. H. and Fitzwater, S. E. (1988)

Iron–deficiency limits phytoplankton growth in the northeast Pacific subarctic.

Nature **331** : 341–343.

May, R. M. (1974)

Stability and Complexity in Model Ecosystems.

Princeton University Press, Princeton, U.S.A.

McCauley, E. and Murdoch, W. W. (1987)

Cyclic and stable populations : plankton as paradigm.

American Naturalist **129** : 97–121.

McGlade, J. M. (1990)

The impact of global climate change on marine ecosystems.

In : *Global Climate and Ecosystem Change*, (ed. G. J. MacDonald and L. Sertorio), pp. 165–184.

Plenum Press, New York, U.S.A.

McManus, G. B. and Dawson, R. (1994)

Phytoplankton pigments in the deep chlorophyll maximum of the Caribbean Sea and the western tropical Atlantic Ocean.

Marine Ecology Progress Series **113** : 199–206.

Menzel, D. W. and Ryther, J. H. (1960)

The annual cycle of primary production in the Sargasso Sea off Bermuda.

Deep–Sea Research **6** : 351–367.

Mogie, M. (1996)

Malthus and Darwin : world views apart.

Evolution **50** : 2086–2088.

Moloney, C. L. and Field, J. G. (1991)

The size–based dynamics of plankton food webs. I. A simulation model of carbon and nitrogen flows.

Journal of Plankton Research **13** : 1003–1038.

Morris, A. J. (1997)

Representing Spatial Interactions in Simple Ecological Models.

Ph.D. Thesis, University of Warwick, Coventry, U.K.

Mosekilde, E. (1996)

Topics in Nonlinear Dynamics : Applications to Physics, Biology and Economic Systems.

World Scientific Publishing Co. Pte. Ltd., London, U.K.

Murphy, L. S. and Haugen, E. M. (1985)

The distribution and abundance of phototrophic ultraplankton in the North Atlantic.

Limnology and Oceanography **30** : 47–58.

Murray, A. G. (1995)

Phytoplankton exudation : exploitation of the microbial loop as a defence against algal viruses.

Journal of Plankton Research **17** : 1079–1094.

Murray, J. D. (1989)

Mathematical Biology.

Springer–Verlag, Berlin, Germany.

Newell, G. E. and Newell, R. C. (1973)

Marine Plankton (Third edition).

Hutchinson Educational Ltd., London, U.K.

Oberhuber, J. M. (1988)

An atlas based on the COADS data set : The budgets of heat, buoyancy and turbulent kinetic energy at the surface of the global ocean.

Max–Planck–Institut für Meteorologie : Report no. 15.

Omori, M. and Ikeda, T. (1992)

Methods in Marine Zooplankton Ecology.

Krieger Publishing Company, Malabar, U.S.A.

O'Neill, R. V., Angelis, D. L., Pastor, J. J., Jackson, B. J. and Post, W. M. (1989)

Multiple nutrient limitation in ecological models.

Ecological Modelling **46** : 147–163.

Paffenhöfer, G. A., Bundy, M. H., Lewis, K. D. and Metz, C. (1995)

Rates of ingestion and their variability between individual calanoid copepods – direct observations.

Journal of Plankton Research **17** : 1573–1585.

Parsons, T. R. and Kessler, T. A. (1987)

An ecosystem model for the assessment of plankton production in relation to the survival of young fish.

Journal of Plankton Research **9** : 125–137.

Pascual, M. (1993)

Diffusion–induced chaos in a spatial predator–prey system.

Proceedings of the Royal Society of London B **251** : 1–7.

PENG, T.–H. AND BROECKER, W. S. (1991)

Factors limiting the reduction of atmospheric CO_2 by iron fertilisation.

Limnology and Oceanography **36** : 1919–1927.

PENG, T. –H., TAKAHASHI, T., BROECKER, W. S. AND OLAFSSON, J. (1987)

Seasonal variability of carbon dioxide, nutrients and oxygen in the northern North Atlantic surface water : Observations and a model.

Tellus **39B** : 227–229.

PETERS, F. (1994)

Prediction of planktonic protistan grazing rates

Limnology and Oceanography **39** : 195–206.

PIERCE, R. W. AND TURNER, J. T. (1994a)

Plankton studies in Buzzards Bay, Massachusetts, USA. III. Dinoflagellates, 1987 to 1988.

Marine Ecology Progress Series **112** : 225–234.

PIERCE, R. W. AND TURNER, J. T. (1994b)

Plankton studies in Buzzards Bay, Massachusetts, USA. IV. Tintinnids, 1987 to 1988.

Marine Ecology Progress Series **112** : 235–240.

PLATT, T., SATHYENDRANATH, S. AND LONGHURST, A. (1995)

Remote sensing of primary production in the ocean : promise and fulfilment.

Philosophical Transactions of the Royal Society B **348** : 191–202.

POPOVA, E. E., FASHAM, M. J. R., OSIPOV, A. V. AND RYABCHENKO, V. A.[3] (1997)

Chaotic behaviour of an ocean ecosystem model under seasonal external forcing.

Journal of Plankton Research **19** : 1495–1515.

POULET, S. A., IANORA, A., MIRALTO, A. AND MEIJER, L. (1994)

Do diatoms arrest embryonic–development in copepods?

Marine Ecology Progress Series **111** : 79–86.

RAVEN, J. A. (1994)

Carbon fixation and carbon availability in marine–phytoplankton.

Photosynthesis Research **39** : 259–273.

RAVEN, J. A. (1995)

Scaling the seas.

Plant, Cell and Environment **18** : 1090–1100.

RAVEN, J. A. (1997)

Phagotrophy in phototrophs.

Limnology and Oceanography **42** : 198–205.

[3]Reference to this paper is based upon recollections of its content during a presentation at the "*Mathematical Modelling of Plankton Population Dynamics*" symposium in Cambridge, 1996.

Reed, R. K. (1977)
On estimating insolation over the ocean.
Journal of Physical Oceanography **7** : 482–485.

Riebesell, U., Wolf–Gladrow, D. A. and Smetacek, V. (1993)
Carbon dioxide limitation of marine phytoplankton growth–rates.
Nature **361** : 249–251.

Riley, G. A., Stommel, H. and Bumpus, D. F. (1949)
Quantitative ecology of the plankton of the western North Atlantic.
Bulletin of Bingham Oceanographic College **12** : 1–169.

Ring Group, The (1981)
Gulf Stream cold–core rings : their physics, chemistry, and biology.
Science **212** : 1091–1100.

Roemmich, D. and McGowan, J. (1995)
Climatic warming and the decline of zooplankton in the California Current.
Science **267** : 1324–1326.

Rose, I. D. (1998, in preparation)
The Spatial Dynamics of the BS Model and Variants.
Ph.D. Thesis, University of Warwick, Coventry, U.K.

Rosenzweig, M. L. (1971)
Paradox of enrichment : destabilisation of exploitation ecosystems in ecological time.
Science **171** : 385–387.

Ross, A. H., Gurney, W. S. C. and Heath, M. R. (1993)
Ecosystem models of Scottish sea lochs for assessing the impact of nutrient enrichment.
ICES Journal of Marine Science **50** : 359–367.

Ross, A. H., Gurney, W. S. C. and Heath, M. R. (1994)
A comparative study of the ecosystem dynamics of four fjords.
Limnology and Oceanography **39** : 318–343.

Rothschild, B. J. and Osborn, T. R. (1988)
Small–scale turbulence and plankton contact rates.
Journal of Plankton Research **10** : 465–474.

Russell, R. W. and Wilson, J. W. (1996)
Aerial plankton detected by radar.
Nature **381** : 200–201.

Sarmiento, J. L. and Orr, J. C. (1991)

3-dimensional simulations of the impact of Southern–ocean nutrient depletion on atmospheric CO_2 and ocean chemistry.

Limnology and Oceanography **36** : 1928–1950.

Sarmiento, J. L. and Sundquist, E. T. (1992)

Revised budget for the oceanic uptake of anthropogenic carbon dioxide.

Nature **356** : 589–593.

Sarmiento, J. L., Slater, R. D., Fasham, M. J. R., Ducklow, H. W., Toggweiler, J. R. and Evans, G. T. (1993)

A seasonal three–dimensional ecosystem model of nitrogen cycling in the North Atlantic euphotic zone.

Global Biogeochemical Cycles **7** : 417–450.

Sathyendranath, S., Gouveia, A. D., Shetye, S. R., Ravindran, P. and Platt, T. (1991)

Biological control of surface temperature in the Arabian Sea.

Nature **349** : 54–56.

Sigmund, K. (1993)

Games of Life : Explorations in Ecology, Evolution, and Behaviour.

Oxford University Press, Oxford, U.K.

Smith, S. D. and Dobson, F. W. (1984)

The heat budget at Ocean Weather Station Bravo.

Ocean–Atmosphere **22** : 1–22.

Smith, S. R., Jickells, T. D. and Knap, A. H. (1987)

Primary production in the Sargasso Sea : concurrent oxygen and carbon fluxes and an estimate of new production.

Unpublished manuscript.

Steele, J. H. and Henderson, E. W. (1981)

A simple plankton model.

American Naturalist **117** : 676–691.

Steele, J. H. and Henderson, E. W. (1992)

The role of predation in plankton models.

Journal of Plankton Research **14** : 157–172.

Stein, J. (editor) (1973)

Handbook of Phycological Methods.

Cambridge University Press, Cambridge, U.K.

Strass, V. H. and Woods, J. D. (1991)

New production in the summer revealed by the meridional slope of the deep chlorophyll maximum.

Deep–Sea Research **38** : 35–56.

Suttle, C. A. (1994)

The significance of viruses to mortality in aquatic microbial communities.

Microbial Ecology **28** : 237–243.

Suttle, C. A. and Chan, A. M. (1994)

Dynamics and distribution of cyanophages and their effect on marine *Synechococcus* spp.

Applied and Environmental Microbiology **60** : 3167–3174.

Sverdrup, H. U. (1953)

On conditions for the vernal blooming of phytoplankton.

Journal du Conseil International pour l'Exploration de la Mer **18** : 287–295.

Tang, E. P. Y. (1996)

Why do dinoflagellates have lower growth rates?

Journal of Phycology **32** : 80–84.

Taylor, A. H. (1988)

Characteristic properties of models for the vertical distribution of phytoplankton under stratification.

Ecological Modelling **40** : 175–199.

Taylor, A. H., Harbour, D. S., Harris, R. P., Burkill, P. H. and Edwards, E. S. (1993)

Seasonal succession in the pelagic ecosystem of the North Atlantic and the utilisation of nitrogen.

Journal of Plankton Research **15** : 875–891.

Taylor, A. H. and Stephens, J. A. (1993)

Diurnal variations of convective mixing and the spring bloom of phytoplankton.

Deep–Sea Research II **40** : 389–408.

Taylor, A. H., Watson, A. J., Ainsworth, M., Robertson, J. E. and Turner, D. R. (1991)

A modelling investigation of the role of phytoplankton in the balance of carbon at the surface of the North Alantic.

Global Biogeochemical Cycles **5** : 151–171.

Thain, M. and Hickman, M. (1994)

Dictionary of Biology (Ninth edition).

Penguin Books Ltd., London, U.K.

Thomas, W. H., Vernet M. and Gibson, C. H. (1995)

Effects of small–scale turbulence on photosynthesis, pigmentation, cell–division, and cell–size in the marine dinoflagellate *Gonyaulax polyedra* (Dinophyceae).

Journal of Phycology **31** : 50–59.

Tilstone, G. H., Figueiras, F. G. and Fraga, F. (1994)

Upwelling–downwelling sequences in the generation of red tides in a coastal upwelling system.

Marine Ecology Progress Series **112** : 241–253.

Toggweiler, J. R. (1990)

Modelling workshop offers first look at new simulation of the Equatorial Pacific.

U.S. JGOFS News **2** : 1 and 11.

Totterdell, I. J., Armstrong, R. A., Drange, H., Parslow, J. S., Powell, T. M. and Taylor, A. H. (1993)

Trophic resolution.

In : *Towards a Model of Ocean Biogeochemical Processes*, (ed. G. T. Evans and M. J. R. Fasham), pp. 71–92.

Springer–Verlag, New York, U.S.A.

Turner, J. T. and Borkman, D. G. (1993)

Plankton studies in Buzzards Bay, Massachusetts, USA. I. Hydrography and bacterioplankton, 1987 to 1990.

Marine Ecology Progress Series **100** : 17–26.

Tyrrell, T. and Taylor, A. H. (1995)

Latitudinal and seasonal–variations in carbon–dioxide and oxygen in the Northeast Atlantic and the effects on *Emiliania huxleyi* and other phytoplankton.

Global Biogeochemical Cycles **9** : 585–604.

Truscott, J. E. and Brindley, J. (1994)

Equilibria, stability and excitability in a general class of plankton population models.

Philosophical Transactions of the Royal Society of London A **347** : 703–718.

Volterra, V. (1926)

Fluctuations in the abundance of a species considered mathematically.

Nature **118** : 558–560.

Waterbury, J. B., Watson, S. W., Valois, F. W. and Franks, D. G. (1986)

Biological and ecological characterization of the marine unicellular cyanobacterium *Synechococcus*.

In : *Photoynthetic Picoplankton*, (ed. T. Platt and W. K. W. Li), pp. 71–120.

Department of Fisheries and Oceans, Ottowa, Canada

Watson, A. J. and Maddock, L. (1991)

A geophysiological model for glacial–interglacial oscillations in the carbon and phosphorus cycles.

In : *Scientists on Gaia*, (ed. S. H. Schneider and P. J. Boston), pp. 240–246.

The MIT Press, Cambridge, MA, U.S.A.

Weinbauer, M. G. and Peduzzi, P. (1995)
Significance of viruses versus heterotrophic nanoflagellates for controlling bacterial abundance in the northern Adriatic Sea.
Journal of Plankton Research **17** : 1851–1856.

Wells, M. L., Price, N. M. and Bruland, K. W. (1994)
Iron limitation and the cyanobacterium *Synechococcus* in equatorial Pacific waters.
Limnology and Oceanography **39** : 1481–1486.

Wiggins, S. (1990)
Introduction to Applied Non–linear Dynamical Systems and Chaos.
Springer–Verlag, New York, U.S.A.

Williams, W. T., Bunt, J. S., John, R. D. and Abel, D. J. (1981)
The community concept and the phytoplankton.
Marine Ecology Progress Series **6** : 115–121.

Williamson, C. E., Sanders, R. W., Moeller, R. E. and Stutzman, P. L. (1996)
Utilization of subsurface food resources for zooplankton reproduction : Implications for diel vertical migration theory.
Limnology and Oceanography **41** : 224–233.

Wilsey, B. J. (1996)
Plant–responses to elevated atmospheric CO_2 among terrestrial biomes.
Oikos **76** : 201–206.

Woods, J. D. and Barkmann, W. (1995)
Modelling oligotrophic zooplankton production : seasonal oligotrophy off the Azores.
ICES Journal of Marine Science **52** : 723–734.

Worsley, T. R., Nance, R. D. and Moody, J. B. (1991)
Tectonics, carbon, life, and climate for the last three billion years : A unified system?
In : *Scientists on Gaia*, (ed. S. H. Schneider and P. J. Boston), pp. 200–210.
The MIT Press, Cambridge, MA, U.S.A.

Wroblewski, J. S. (1977)
A model of phytoplankton plume formation during variable Oregon upwelling.
Journal of Marine Research **35** : 357–394.

Wroblewski, J. S. (1989)
A model of the spring bloom in the North Atlantic and its impact on ocean optics.
Limnology and Oceanography **34** : 1563–1571.

Yool, A. (1994)

Malthus was right.

New Scientist **143** : 45.

Zweifel, U. L., Norrman, B. and Hagström, Å (1993)

Consumption of dissolved organic carbon by marine bacteria and demand for inorganic nutrients.

Marine Ecology Progress Series **101** : 23–32.

Martin Q. Blank *I'm a professional killer.*

Paul Sericki *Do you have to do post–graduate work for that?*

– "Grosse Point Blank" (1997)

Appendices

God does not care about our mathematical difficulties. He integrates empirically.

– Albert Einstein (1879-1955)

A computer lets you make more mistakes faster than any other invention in human history, with the possible exception of handguns and tequila.

– Mitch Radcliffe (Digital Media)

A-1 Correction of the 1972 OWS "India" data

In several chapters in this thesis, use is made of data collected by Bob Williams at OWS "India" in 1972. The data consists of chlorophyll (0–200 metres) and nitrate (0–70 metres) measurements made at a series of fixed depths during the period from the spring through to the autumn of 1972.

In order to compare this data with model output, it was necessary to depth–integrate it to get an average value across the mixed layer, since the models used in this thesis assume a homogeneous mixed layer. However, in order to depth–integrate the data, the depth of the mixed layer when the samples were taken needs to be known. Unfortunately, this data was not available.

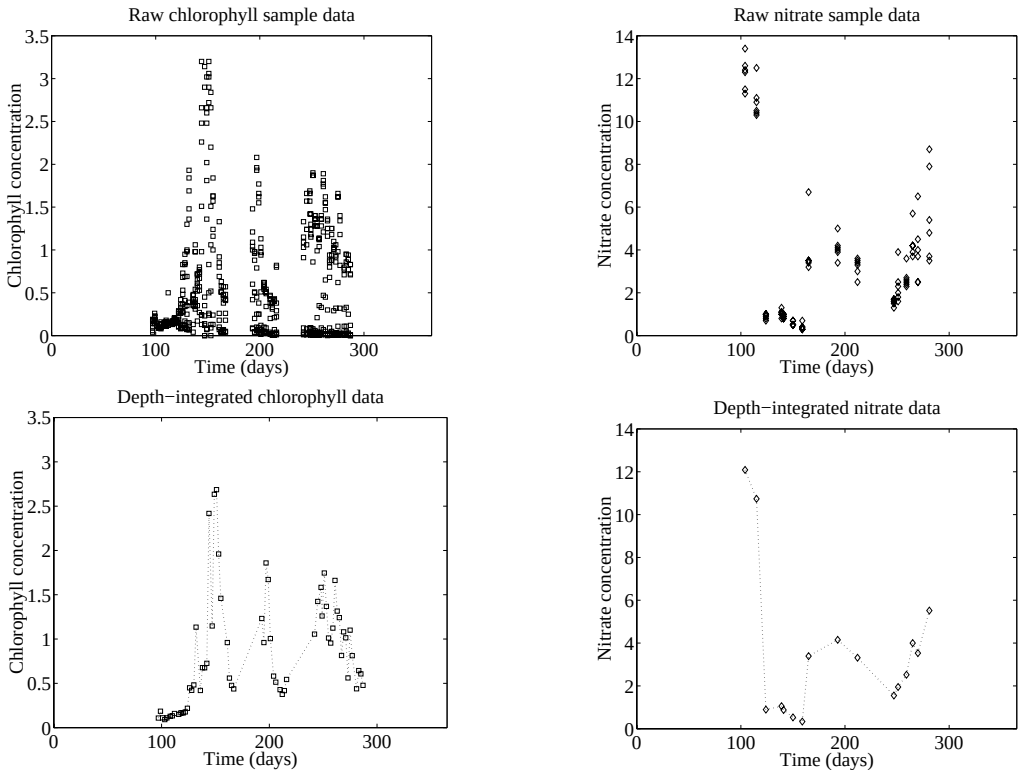

Figure A.1: Plots of the raw chlorophyll and nitrate samples (top row), and the depth–integrated concentrations after the data have been corrected for mixed–layer depth (bottom row). In the raw plots, there are 8 chlorophyll and 6 nitrate data points for each sampling day, where each point refers to a different sampling depth. Chlorophyll concentration in mg chl. m^{-3}, nitrate concentration in mmol N m^{-3}.

To get around this problem, the mixed–layer depth data interpolated from Levitus' (1982) monthly averages was used to provide an estimate of mixed–layer depth on each of the sampling days. As remarked in Fasham (1993) though, in 1972 the seasonal thermocline shallowed to less than 50 metres in April, whilst in the interpolated depth data this only happens in May. Since the appearance of the spring

phytoplankton bloom is highly dependent on the shallowing of the mixed layer, it is important that this difference in the timing of mixed layer shallowing is accounted for. In the absence of guiding observations, this was done by time–shifting the data by 14 days so that the spring chlorophyll maximum in the measured data coincided with that of the model (which uses the interpolated Levitus data). While this does give the modelled spring bloom possibly undeserved credibility, it probably makes the estimated mixed–layer depth a more accurate reflection of the true state of affairs.

The depth–integration assumed linear distribution of chlorophyll or nitrate between each sample depth, and where the mixed layer was estimated to be deeper than the deepest sample, the corrected value was that calculated by depth–integrating to that deepest sample. Figure A.1 shows the raw and processed data for both chlorophyll and nitrate. All of the measurements made from samples taken at different depths are shown in the plots of raw data. The depth–integrated values calculated are linked by a dotted line to make the time series clearer.

Data courtesy of Bob Williams and Dr. Mike Fasham.

A-2 Program code

The majority of the work presented in this thesis was produced using author–written programs (all in the language C). Because of the reliance on such code, this appendix contains one of the programs used. For ease of reading, the program is listed here in several pieces.

Software was compiled and run on Sun SPARC stations (IPX, 10 and 20) using SunOS 4.1.3 or SunOS 5.4. Compilation was performed using `gcc` version 2.7.2. Standard mathematics libraries included in executable code.

A-2.1 Main program

The program shown is a version which distinguishes limit cycle behaviour from stable equilibria (as used in Chapter 4). The program is annotated to clarify its operation. Note that the functions which read information (*e.g.* parameter values, forcing data) in from files are not shown.

```
/* Libraries
   --------- */
#include <stdlib.h>   /* Need this for the rand function */
#include <stdio.h>
#include <math.h>
#include <time.h>     /* Need this to seed the rand function */
#include "string.h"

/* #defined parameters
   ------------------- */
/* Replacement variables */
#define PI        3.141592654 /* Duh */
#define YEAR      365         /* Length of simulation year in days */
#define REGIME    4           /* Order of Runge-Kutta regime */
#define ORDER     7           /* Order of ODEs */
#define PARAMS    38          /* Number of model parameters */
#define FLOWS     43          /* Number of flows monitored */
#define OUTPUTS   20          /* Number of model outputs */
#define NUTRIENT  4           /* Nutrient compartment */
#define BIGNUMB   1073741824  /* Two to the power of thirty */

/* Define globals
   -------------- */
/* Control parameters */
double const_mld, trans_step, trans_dist, latitude, lat, const_Iss;
double ll_param, ul_param, ll_param2, ul_param2;
int    triangle, location, stat_mld, det_years, stoch_years, stat_Iss;
int    cmodel, oktas, dummy, day_cycle, stoch_on, fix_force, fix_day;
int    fix_trigger, decimals, cyc_days, avg_days, rand_init;
int    param, param2, trans_days, data_days, steps, steps2, z_pred;
int    lock1, lock2, sim_type, z_mixing;
char   savedata[100], load_MLD[100];

/* Model parameters array */
double MLD[YEAR], irrad[YEAR], MLDiff[YEAR], cover[6][9];
double base[PARAMS], trans[PARAMS], upplim[PARAMS], lowlim[PARAMS];
double base2[PARAMS], trans2[PARAMS];
int    compartment[ORDER+6], output_comp, constant[PARAMS], iters;

/* Flow monitoring parameters */
double flow[FLOWS], v_flow[REGIME][FLOWS], flow_array[FLOWS][YEAR];

/* State variables */
double state[ORDER+1], v[ORDER];
```

```
/* Runge-Kutta parameters */
double a[REGIME][REGIME], b[REGIME], c[REGIME];

/* Declare functions
   ----------------- */
/* Initialisation functions */
void   init_control();
void   init_param();
void   init_MLD_forcing();
void   init_cloud_data();
void   init_RK4();

/* Runge-Kutta functions */
void   runge_kutta(double, double);
void   add_to_v(double, double *);
void   set_v_to(double *);

/* Fasham model functions */
double light_equation(double, double, double);
double full_fasham(double *, double *, double, int, int);
void   model_outputs(double *);

/* Transmogrifying functions */
void   transform();

/* Fasham MLD forcing functions */
double mixed_layer_depth(double);

/* Fasham irradiance functions */
double I0_now(double);
double declination(int);
double rad_vector(int);
double sunrise_ha(double, double);
double daylength(double);
double integrated(double, double, double, double, double);
double hour_angle(double);
double zenith_angle(double, double, double);
double ir_top_atmos(double, double, double);
double sea_surface(double, double);

/* Output functions */
void   output_param();
void   output_flows();

/* Standard maths functions */
double min(double, double);
double max(double, double);
double power(double, int);
double divide(double, double);
double rolling_mean(double, double, int);
double rolling_variance(double, double, double, double, int);
int    same_number(double, double, int);

/* Main program
   ------------ */
main()
{
  /* [Program changed : 24th June 1997]

     Simulation types :

     This version of the Fasham programs allows the user 4 different
     simulation types for runs.

     0. Normally forced simulations
        These simulations use the daily mixed layer data and irradiance
        equations to generate diel and annual forcing patterns.

        A typical run has several transient years followed by a final
        year during which data is collected from the simulation.

     1. Diel forced simulations
        These simulations have diel forcing locked on a particular day
        of the year.  Irradiance changes across the day but MLD remains
        the same.

        A typical simulation runs the model for a long period of time
        during which the dynamical behaviour is "determined" before
```

```
      a final (usually short) period during which the simulation is
      sampled.

   2. Fixed forcing simulations
      These simulations have no time-dependent forcing at all.  Both
      irradiance and MLD are locked on constant, user-defined values.

      As for the diel forced simulations.

   3. Fixed forcing simulations
      As for the fixed forcing simulations.

      A typical simulation runs the model once for a continuous and long
      period of time.  Periodically, a model parameter is changed.  The
      model is sampled for data during the entire run.

      (This latter type of simulation was devised solely to facilitate
       a probe of the so-called "light-effect".)
   */

/* ============================================================ */

/* Variable Initialisation
   ----------------------- */
/* MinMax arrays */
double baseline[OUTPUTS][ARRAY], clock[ARRAY];
double mod_outs[OUTPUTS];
double average[OUTPUTS][ARRAY], variance[OUTPUTS][ARRAY];
double minimum[OUTPUTS][ARRAY], maximum[OUTPUTS][ARRAY];
double store_check[OUTPUTS+1][10000];

/* Net primary productivity and f-ratio arrays and storage variables */
double fratio[400], npp[400], nnpp[400], nrpp[400];
double now_fr, now_npp, now_nnpp, now_nrpp;

/* Other run statistics */
double box_max[ORDER + 1], box_min[ORDER + 1];

/* Sim type 3 variables */
double sim3timer;
int    sim3_flag;

/* Stable equilibrium checking variables */
double stable_equil[ORDER][2], mintimer, mintime;
int    stab_flag, stab_flag2, decicheck, same_days;

/* Averaging variables */
double averagetimer;
int    avgtime;

/* Collapsing limit cycle variables */
int    collapse_flag;

/* Limit cycle variables */
double cyctimer, cyctime, cycles[ORDER+2][10000], cycles2[ORDER+2][10000];
double cyccorrect;
int    cycle, cycflag, cycflag2;

/* Output statistics */
double avg_cyc, min_cyc, max_cyc, tot_cyc, now_cyc;
int    behaviour;

/* Storing initial conditions for runs */
double p1store[ORDER], p2store[ORDER], shove;

/* Housekeeping variables */
double simtime, transtimer, datatimer, dt, flowtimer, fixtimer;
double initials[ORDER], step_size, step_size2;
double sum, stoch, old_mean, old_var, dummy_end;
int    runs, inttime, timeup, poincare;
char   savenpp[110], savepoincare[110], savesummary[110], savecycles[110];
double x, y, z;
int    a, b, c, i, j, k, l, m;
int    count1, count2, count3, output_array[1000];

/* Filing variables */
FILE   *Send_out, *Send_out2, *Send_out3, *Send_out4;

/* ============================================================ */
```

```
/* Initialise control, model, and forcing parameters
   ------------------------------------------------- */
init_control();
printf("Control parameters\n"); /* Program control parameters */
init_param();
printf("Model parameters\n");   /* Model parameters */
init_MLD_forcing();
printf("MLD forcing\n");        /* MLD forcing data */
init_cloud_data();
printf("Cloud data\n");         /* Cloud cover arrays */
init_RK4();
printf("Runge-Kutta IV\n");     /* Runge-Kutta weights */

/* ============================================================ */

/* Output procedures
   ----------------- */
/* Output model parameter values to file*/
output_param();

/* Open up main data output file */
if((Send_out = fopen(savedata,"w"))==NULL)
  {
    printf("*** Cannot open parameters output file ***\n",savedata);
    exit(1);
  }

/* Open up Poincare section output file */
sprintf(savepoincare,"%s_poincare",savedata);
if((Send_out2 = fopen(savepoincare,"w"))==NULL)
  {
    printf("*** Cannot open raw stream output file ***\n",savedata);
    exit(1);
  }

/* Open up summary data output file */
sprintf(savesummary,"%s_summary",savedata);
if((Send_out3 = fopen(savesummary,"w"))==NULL)
  {
    printf("*** Cannot open summary output file ***\n",savedata);
    exit(1);
  }

/* Open up limit cycles output file */
sprintf(savecycles,"%s_limitcycle",savedata);
if((Send_out4 = fopen(savecycles,"w"))==NULL)
  {
    printf("*** Cannot open limit cycles output file ***\n",savedata);
    exit(1);
  }

/* ============================================================ */

/* Setting up initial conditions
   ----------------------------- */
if (sim_type<2)
  stat_mld=stat_Iss=0;
else
  stat_mld=stat_Iss=1;

srandom(((time(NULL))%1024));

same_days=20;   /* the number of days required for a stable equilibrium
                   to be declared */
dt=(1.0/iters); /* duration of a single model iteration */
mintimer=500.0; /* minimum time before a run can be declared a stable
                   equilibrium */
decicheck=(int)(power(10.0, decimals));

if(steps>1)
  step_size=(ul_param - ll_param)/((double)(steps - 1));
else
  step_size=0.0;
if(steps2>1)
  step_size2=(ul_param2 - ll_param2)/((double)(steps2 - 1));
else
```

```
    step_size2=0.0;

  if (sim_type==3)
    {
      steps=((int)(trans_days/avg_days)) - 1;
      step_size=(ul_param - ll_param)/((double)steps);
    }

  if (sim_type==0)
    poincare=YEAR;
  else
    poincare=1000;

  /* Clear flows storage array */
  for(i=0;i<YEAR;i++)
    {
      for(j=0;j<FLOWS;j++)
flow_array[j][i]=0.0;
    }

  /* ============================================================ */

  /* Do initial deterministic runs
     ---------------------------- */
  /* Parameter 2 loop */
  m=0;
  do
    {
      /* Assign parameter 2's new value */
      trans[param2]=ll_param2 + m*step_size2;

      /* Parameter 1 loop */
      l=0;
      do
{
  /* Assign parameter 1's new value */
  trans[param]=ll_param + l*step_size;

  /* Is parameter one of the special ones? */
  if(param==19)
    {
      /* Zooplankton feeding efficiency */
      trans[20]=trans[21]=trans[param];
    }
  if(param==22)
    {
      /* Zooplankton grazing preference */
      x=1 - trans[param];
      trans[23]=trans[24]=(x/2.0);
    }
  if(param==25)
    {
      /* Zooplankton grazing preference (2 prey models only) */
      trans[26]=1 - trans[param];
    }
  if(param==28)
    {
      /* Recycling efficiency of zooplankton losses */
      x=trans[param];
      trans[param]=(base[28]/(base[28] + base[29]))*x;
      trans[29]=(base[29]/(base[28] + base[29]))*x;
    }

  /* State variable initial conditions */
  for(i=0;i<ORDER;i++)
    {
      do
{
  stoch=((double)((random()%BIGNUMB))/BIGNUMB);
  state[i]=stoch*base[33];
}
      while(state[i]>(base[33]*0.5) || state[i]<0.0);
    }
  state[NUTRIENT]=base[33];

  /* Simulation type 3 initial conditions */
  if (sim_type==3)
    {
```

```
      for(i=0;i<ORDER;i++)
state[i]=0.01;
    }

  /* Reset storage arrays */
  for(i=0;i<ORDER;i++)
    {
      minimum[i][0]=1000.0;
      maximum[i][0]=0.0;
    }

  /* Reset program clocks and event timers */
  i=0;
  timeup=0;
  inttime=0;
  avgtime=0;
  cycflag=0;
  simtime=0.0;
  stab_flag=0;
  sim3_flag=0;
  mintimer=1.0 + 0.5 - (0.5*dt);
  if (sim_type>0)
    datatimer=(trans_days + avg_days + cyc_days) + 0.5 - (0.5*dt);
  else
    datatimer=((trans_days - 1)*YEAR) + 0.5 - (0.5*dt);
  if (sim_type==3)
    datatimer=cyc_days - (0.5*dt);
  if (sim_type==1 || sim_type==2)
    flowtimer=mintimer;
  else
    flowtimer=datatimer - 1.0;
  cyctimer=(trans_days + avg_days) + 0.5 - (0.5*dt);
  mintime=mintimer;
  cyctime=cyctimer;
  averagetimer=trans_days + 0.5 - (0.5*dt);
  sim3timer=avg_days + cyc_days - (0.5*dt);

  do
    {
      simtime+=dt;

      runge_kutta(simtime, dt);

      model_outputs(mod_outs);

      /* Poincare section output */
      j=(i%(iters*poincare));
      if(j==0)
{
  fprintf(Send_out2,"%.1lf ",simtime);
  for(k=0;k<ORDER;k++)
    {
      fprintf(Send_out2,"%.3lf ",state[k]);
    }
  fprintf(Send_out2,"\n");
  fflush(Send_out2);
}

      /* Sort out flows for non-forced simulations */
      if ((sim_type==1 || sim_type==2) && simtime>flowtimer)
{
  for(j=0;j<FLOWS;j++)
    {
      flow[j]=0.0;
    }
  flowtimer++;
}

      /* Store state variables for later output */
      if ((sim_type==0 || sim_type==3) && simtime>flowtimer)
{
  for(j=0;j<FLOWS;j++)
    {
      flow[j]=0.0;
    }
  flowtimer+=50000;
}
      if (simtime>datatimer)
```

```
{
  for(j=0;j<OUTPUTS;j++)
    {
      store_check[j][inttime]=mod_outs[j];
      /* if(j==4 || j==11)
 printf("%.6lf %.6lf\n",state[j],mod_outs[j]); */
    }
  store_check[OUTPUTS][inttime]=simtime -
    (trans_days + avg_days + cyc_days + 0.5);

  /* Store parameter value for sim_type 3 simulations */
  if (sim_type==3)
    store_check[OUTPUTS][inttime]=trans[param];

  /* Correct nutrient limitation and f-ratio values */
  store_check[20][inttime]=store_check[20][inttime]/
    store_check[24][inttime];
  store_check[18][inttime]=store_check[18][inttime]/
    store_check[24][inttime];
  store_check[30][inttime]=store_check[30][inttime]/
    store_check[34][inttime];
  store_check[28][inttime]=store_check[28][inttime]/
    store_check[34][inttime];
  if (sim_type==0 || sim_type==3)
    {
      for(j=0;j<FLOWS;j++)
{
  flow[j]=0.0;
}
    }

  inttime++;
  datatimer++;
  /* This line outputs midday and midnight values instead
     datatimer=datatimer + 0.5; */
}

      /* For type 3 simulations */
      if (sim_type==3 && simtime>sim3timer)
{
  /* Increase parameter under question */
  trans[param]=trans[param] + step_size;
  sim3timer=sim3timer + avg_days;
}

      /* For fixed day or fixed forcing functions simulations */
      if (sim_type>0 && sim_type<3)
{
  /* Check to establish if stable equilibrium reached */
  if(simtime>mintimer)
    {
      /* Store today's state variable values */
      for(j=0;j<ORDER;j++)
{
  stable_equil[j][1]=mod_outs[j];
}
      j=0;
      stab_flag2=0;

      /* Check today's states to yesterday's */
      do
{
  a=same_number(stable_equil[j][0],
stable_equil[j][1],decimals);
  if(a==0)
    j++;          /* They're the same! */
  else
    stab_flag2=1; /* They're different */
}
      while(j<ORDER && stab_flag2==0);

      /* If today==yesterday trigger stable equilibrium flag */
      if(stab_flag2==0)
stab_flag++;
      else
stab_flag=0;
```

```
      /* Move today's states ready for tomorrow */
      for(j=0;j<ORDER;j++)
stable_equil[j][0]=stable_equil[j][1];

      mintimer++;
    }

  /* Average results for limit cycle calculations */
  if(simtime>averagetimer && simtime<cyctimer)
    {
      for(j=0;j<ORDER;j++)
{
  if(mod_outs[j]<minimum[j][0])
    minimum[j][0]=mod_outs[j];
  if(mod_outs[j]>maximum[j][0])
    maximum[j][0]=mod_outs[j];
  old_mean=average[j][0];
  average[j][0]=rolling_mean(old_mean,
     mod_outs[j],
     avgtime);
}
      averagetimer++;
      avgtime++;
    }

  /* Limit cycle period calculations
     ------------------------------ */
  if(simtime>cyctimer && cycflag==0)
    {
      /* Setting up for first limit cycle */
      average[0][0]=((maximum[0][0]
      - minimum[0][0])/5.0) + minimum[0][0];
      cycle=0;
      for(j=0;j<ORDER;j++)
{
  minimum[j][0]=1000.0;
  maximum[j][0]=0.0;
}
      if(mod_outs[0]<average[0][0])
cycflag=1;
      else
cycflag=2;
    }
  if(simtime>cyctime)
    {
      /* Minima and maxima for this limit cycle */
      for(j=0;j<ORDER;j++)
{
  if(mod_outs[j]<minimum[j][0])
    minimum[j][0]=mod_outs[j];
  if(mod_outs[j]>maximum[j][0])
    maximum[j][0]=mod_outs[j];
}
    }
  if(simtime>cyctime)
    {
      if(cycflag==2 && mod_outs[0]<average[0][0])
{
  /* Lap completed - store data */
  cycles[0][cycle]=simtime;
  cycles2[0][cycle]=simtime;
  for(j=0;j<ORDER;j++)
    {
      cycles[j+1][cycle]=mod_outs[j];
      cycles2[j+1][cycle]=maximum[j][0]
- minimum[j][0];
      minimum[j][1]=minimum[j][0];
      maximum[j][1]=maximum[j][0];
      minimum[j][0]=1000.0;
      maximum[j][0]=0.0;
    }
  cycle++;
  cycflag=1;
```

```
}
      if(cycflag==1 && mod_outs[0]>average[0][0])
{
  /* Half-lap completed - set trap to catch cycle */
  cycflag=2;
}
      cyctime++;
    }
  if (i<((trans_days+avg_days+cyc_days+data_days-1)*iters))
    timeup=0;
  else
    timeup=1;
}
      else
{
  /* For normal or fixed forcing simulations */
  if (sim_type==0)
    {
      /* Normal simulations */
      if (i<((trans_days*YEAR)*iters))
timeup=0;
      else
timeup=1;
    }
  else
    {
      /* Fixed forcing simulations */
      if (i<((trans_days + cyc_days)*iters))
timeup=0;
      else
timeup=1;
    }
}

      /* Increment loop counter */
      i++;
    }
  while(timeup<1 && stab_flag<same_days);

  /* ============================================================ */

  /* Output routines
     --------------- */
  if (sim_type==0)
    {
      /* Normal annually forced simulations */
      fprintf(Send_out,"%.2lf %.2lf ",trans[param2],trans[param]);
      for(k=3;k<OUTPUTS;k++)
{
  fprintf(Send_out,"0 ");
}
      fprintf(Send_out,"\n");
      for(k=0;k<inttime;k++)
{
  fprintf(Send_out,"%d ",k);
  for(j=0;j<OUTPUTS;j++)
    fprintf(Send_out,"%.6lf ",store_check[j][k]);
  fprintf(Send_out,"\n");
}
    }
  if (sim_type==3)
    {
      /* Constant forcing simulations */
      for(k=1;k<inttime;k=k+data_days)
{
  fprintf(Send_out,"%d %.2lf ",k,store_check[OUTPUTS][k]);
  for(j=0;j<output_comp;j++)
    fprintf(Send_out,"%.6lf ",store_check[compartment[j]][k]);
  fprintf(Send_out,"\n");
}
      sim3_flag=1;
    }
  if (sim_type==1 || sim_type==2)
    {
      /* Fixed day or constant forcing simulations */

      /* Stable equilibrium data
```

```
 ----------------------- */
      if(stab_flag==same_days)
{
  /* This run ended with a stable equilibrium point */
  avg_cyc=min_cyc=max_cyc=0.0;
  behaviour=1;

  /* Main data output */
  fprintf(Send_out,"%.1lf %.2lf %.2lf ",
  simtime,trans[param2],trans[param]);
  for(j=0;j<output_comp;j++)
    fprintf(Send_out,"%.6lf ",mod_outs[compartment[j]]);
  fprintf(Send_out,"%d 1\n",behaviour);

  /* Summary data output */
  fprintf(Send_out3,"%.1lf %.3lf %.3lf ",
  simtime,trans[param2],trans[param]);
  for(j=0;j<ORDER;j++)
    fprintf(Send_out3,"%.4lf %.4lf 0 0 ",
    mod_outs[j],mod_outs[j]);
  for(j=ORDER;j<OUTPUTS;j++)
    fprintf(Send_out3,"%.4lf ",mod_outs[j]);
  fprintf(Send_out3,"0 0 0 %d\n",behaviour);

  /* Limit cycles data output */
  fprintf(Send_out4,"%.1lf %.2lf %.2lf ",
  simtime,trans[param2],trans[param]);
  for(j=0;j<ORDER;j++)
    fprintf(Send_out4,"%.4lf ",mod_outs[j]);
  fprintf(Send_out4,"0.000 %d 1\n",behaviour);
}
      else
{
  /* Transient or limit cycle data
     ---------------------------- */
  if(cycle==0)
    {
      /* No stable equilibrium or cycles found */
      avg_cyc=min_cyc=max_cyc=0.0;
      behaviour=2;
      for(j=0;j<ORDER;j++)
{
  minimum[j][1]=minimum[j][0];
  maximum[j][1]=maximum[j][0];
}
    }
  else
    {
      /* Cycling behaviour found! */

      /* Are cycles collapsing? */
      collapse_flag=0;
      k=2;
      do
{
  for(j=0;j<ORDER;j++)
    {
      a=same_number(cycles2[j+1][k-1],
    cycles2[j+1][k],6);
      if(a==-1)
collapse_flag=1;
    }
  k++;
}
      while(collapse_flag==0 && k<cycle);
      if(collapse_flag==0)
{
  /* System appears to be collapsing */
  behaviour=3;
}
      else
{
  /* System oscillations appear to be stable */
  behaviour=4;
}
```

```
      avg_cyc=0.0;
      min_cyc=cyc_days - 1.0;
      max_cyc=0.0;
      for(j=2;j<cycle;j++)
{
  now_cyc=cycles[0][j] - cycles[0][j-1];
  avg_cyc=avg_cyc + now_cyc;
  if(now_cyc<min_cyc)
    min_cyc=now_cyc;
  if(now_cyc>max_cyc)
    max_cyc=now_cyc;
}
      avg_cyc=avg_cyc/(cycle - 2);
    }

  /* Main data output */
  for(k=0;k<inttime;k++)
    {
      if(k==0)
fprintf(Send_out,"%.1lf %.2lf %.2lf ",
store_check[ORDER][k],trans[param2],
trans[param]);
      else
fprintf(Send_out,"%.1lf 0 0 ",store_check[ORDER][k]);
      for(j=0;j<output_comp;j++)
fprintf(Send_out,"%.6lf ",
store_check[compartment[j]][k]);
      if(k==0)
fprintf(Send_out,"%d %d\n",behaviour,inttime);
      else
fprintf(Send_out,"0 0\n");
    }

  /* Summary data output */
  fprintf(Send_out3,"%.1lf %.3lf %.3lf ",
  simtime,trans[param2],trans[param]);
  for(j=0;j<ORDER;j++)
    fprintf(Send_out3,"%.4lf %.4lf %.4lf %.4lf ",
    minimum[j][1],maximum[j][1],cycles2[j+1][1],
    cycles2[j+1][cycle-1]);
  for(j=ORDER;j<OUTPUTS;j++)
    fprintf(Send_out3,"%.4lf ",mod_outs[j]);
  fprintf(Send_out3,"%.2lf %.2lf %.2lf %d\n",
  avg_cyc,min_cyc,max_cyc,behaviour);

  /* Limit cycles data output */
  if(cycle>0)
    {
      cyccorrect=trans_days + avg_days + 0.5;
      for(k=0;k<cycle;k++)
{
  if(k==0)
    fprintf(Send_out4,"%.1lf %.2lf %.2lf ",
    (cycles[0][k]-cyccorrect),trans[param2],
    trans[param]);
  else
    fprintf(Send_out4,"%.1lf 0 0 ",
    (cycles[0][k]-cyccorrect));
  cyccorrect=cycles[0][k];
  for(j=0;j<ORDER;j++)
    fprintf(Send_out4,"%.4lf ",cycles[j+1][k]);
  if(k==0)
    fprintf(Send_out4,"%d %d\n",behaviour,cycle);
  else
    fprintf(Send_out4,"0 0\n");
}
    }
  else
    {
      fprintf(Send_out4,"%.1lf %.2lf %.2lf ",
      simtime,trans[param2],trans[param]);
      for(j=0;j<ORDER;j++)
fprintf(Send_out4,"%.4lf ",mod_outs[j]);
      fprintf(Send_out4,"0.000 %d 1\n",behaviour);
```

```
    }
}
    }

  /* Flush data to output files */
  fflush(Send_out);
  fflush(Send_out3);
  fflush(Send_out4);
  l++;
}
      while(l<steps && sim3_flag==0);
      m++;
    }
  while(m<steps2 && sim3_flag==0);

  /* Close data streams */
  fclose(Send_out);
  fclose(Send_out2);
  fclose(Send_out3);
  fclose(Send_out4);
}

/* ============================================================ */

void   model_outputs(double array[OUTPUTS])
{
  /* This function organises the outputs array
     ---------------------------------------- */
  double sum;
  int    i;

  for(i=0;i<OUTPUTS;i++)
    array[i]=0.0;

  /* Assign states to array */
  sum=0.0;
  for(i=0;i<ORDER;i++)
    {
      array[i]=state[i];
      sum+=state[i];
    }
  array[ORDER]=sum;

  /* Assign miscellaneous flows to array */
  /* Mixed layer statistics */
  array[15]=flow[0];  /* net primary production */
  array[16]=flow[39]; /* net new primary production */
  array[17]=flow[40]; /* net recycled primary production */
  array[18]=flow[41]; /* daily f-ratio */
  array[19]=flow[35]; /* light limitation term */
  array[20]=flow[33]; /* nutrient limitation term */
  array[21]=flow[36]; /* zooplankton loss rate */
  array[22]=flow[42]; /* mixed-layer depth */
  array[23]=flow[37]; /* solar irradiance at the top of the atmosphere */
  array[24]=flow[34]; /* day length */
  for(i=0;i<6;i++)
    array[35+i]=flow[compartment[output_comp+i]];
}
```

A-2.2 Runge–Kutta integrating engine

These functions integrate the model ODEs using a Runge–Kutta IV engine. Since versions of this program were used with models of differing size, the functions are written to allow models with different numbers of ODEs to be easily incorporated. This code was jointly written by Andrew J. Morris (University of Warwick) and the author.

```
void runge_kutta(double t, double h)
{
  /* This suite of functions performs the numerical integration
     ---------------------------------------------------------- */
  double k[REGIME][ORDER]; /* REGIMEth order RK, ORDERth order ODEs */
  double diffs[ORDER];     /* blank array to store differentials*/
  int    i,j,l;

  for(i=0;i<REGIME;i++)
    {
      for(j=0;j<FLOWS;j++)
        {
          v_flow[i][j]=0.0;
        }
    }

  for(i=0;i<REGIME;i++)
    {
      set_v_to(state);

      for(j=0;j<i;j++)
        {
          add_to_v(h*a[i][j],k[j]);
        }

      for(l=0;l<ORDER;l++)
        {
          diffs[l]=0.0;
        }

      /* Run model equations */
      full_fasham(v,diffs,t+h*c[i],l,i);

      for(l=0;l<ORDER;l++)
        {
          k[i][l]=diffs[l];
        }
    }

  for(i=0;i<REGIME;i++)
    {
      for(j=0;j<ORDER;j++)
        {
          state[j]+=h*b[i]*k[i][j];
        }
      for(l=0;l<FLOWS;l++)
        {
          flow[l]+=h*b[i]*v_flow[i][l];
        }
    }
}

/* ============================================================ */

void   add_to_v(double scalar, double in[ORDER])
{
  /* Adds values from other steps according to RK routine employed */

  int   i;
  for(i=0;i<ORDER;i++) {v[i]+=scalar*in[i];}
}

/* ============================================================ */

void   set_v_to(double in[ORDER])
{
  /* Puts values of states into a temporary array */
```

```
  int   i;
  for(i=0;i<ORDER;i++) {v[i]=in[i];}
}

/* ============================================================ */

void   init_RK4()
{
  /* This function sets up the 4th order Runge-Kutta regime
     ------------------------------------------------------ */

  int    i;

  /* clear Runge_Kutta tableau */
  for(i=0;i<(REGIME*REGIME);i++) {a[i/REGIME][i%REGIME]=0.0;}

  /* 4th order Explicit Runge-Kutta scheme */
  a[1][0]=0.5;
  a[2][1]=0.5;
  a[3][2]=1.0;

  b[0]=1.0/6;
  b[1]=1.0/3;
  b[2]=1.0/3;
  b[3]=1.0/6;

  c[0]=0.0;
  c[1]=0.5;
  c[2]=0.5;
  c[3]=1.0;

  printf("Done ");
}
```

A-2.3 Fasham (1993) model function

These functions specify the ODEs used in the full model. The first function includes the model ODEs and the nitrogen flows produced by modelled ecological processes. All of the reduced forms of this model, as well as the expanded two layer model, are simple modifications of this function. The second function is used by the first to calculate depth–integrated phytoplankton growth (see Chapter 3).

```
double full_fasham(double In[ORDER], double Out[ORDER], double t,
                   int component, int rkstep)
{
  /* Fasham full model equations
     -------------------------- */

  /* 0   Phytoplankton
     1   Zooplankton
     2   Bacteria
     3   Detritus
     4   Nitrate
     5   Ammonium
     6   Dissolved organic nitrogen */

  double functime;
  double J, Q, Q1, Q2, sigma, P_mort, hplus, P_mix;
  double f, f2, G1, G2, G3, Z_mort, Z_mix;
  double S, U1, U2, B_excr, B_mix;
  double D_degr, D_mix;
  double Nn_mix;
  double Nr_mix;
  double Nd_mix;
  double I_ss, I_now, MLD_now, MLDiff_now, store[ORDER];

  /* Calculate forcing functions at this time */
  if(sim_type==0)
    {
      /* Forcing functions vary across the year */
      MLD_now=mixed_layer_depth(t);
      I_ss=I0_now(t);
      MLDiff_now=(-1*MLDiff[(((int)(t))%365)]);
      hplus=max((MLDiff_now),0);
    }
  if(sim_type==1)
    {
      /* Forcing functions locked on a single day */
      functime=fix_day + (t - ((int)(t)));
      MLD_now=mixed_layer_depth(functime);
      I_ss=I0_now(functime);
      MLDiff_now=0.0;
      hplus=0.0;
    }
  if(sim_type==2)
    {
      /* Forcing functions locked on constant values */
      MLD_now=trans[37];
      I_ss=trans[39];
      MLDiff_now=0.0;
      hplus=0.0;
    }
  if(sim_type==3)
    {
      /* Special type of simulation which outputs time series data */
      functime=fix_day + (t - ((int)(t)));
      MLD_now=mixed_layer_depth(functime);
      I_ss=trans[39];
      MLDiff_now=0.0;
      hplus=0.0;
    }

  /* Correct irradiance for albedo and PAR fraction */
  I_now=I_ss*(1 - trans[0])*trans[1];

  /* Phytoplankton */
  if(I_now>0) /* daytime */
```

```
  {
    J=light_equation(In[0],I_now,(MLD_now));
    Q1=(In[4]*exp(-trans[8]*In[5]))/(trans[9] + In[4]);
    Q2=In[5]/(trans[10] + In[5]);
    Q=(Q1 + Q2);
    sigma=(J*Q);
    v_flow[rkstep][34]=1;
  }
else        /* nighttime */
  {
    J=0.0;
    Q=Q1=Q2=0.0;
    sigma=0.0;
    v_flow[rkstep][34]=0;
  }
f=trans[11]*((trans[22]*In[0]) + (trans[23]*In[2]) + (trans[24]*In[3]));
f2=((trans[22]*In[0]*In[0]) + (trans[23]*In[2]*In[2]) +
    (trans[24]*In[3]*In[3]));
G1=(trans[27]*trans[22]*In[0]*In[0]*In[1])/(f + f2);
P_mort=(trans[15]*In[0]*In[0])/(trans[13] + In[0]);
P_mix=((trans[34] + hplus)*In[0])/(MLD_now);
Out[0]=(((1 - trans[7])*sigma*In[0]) - G1 - P_mort - P_mix);

/* Zooplankton */
G2=(trans[27]*trans[23]*In[2]*In[2]*In[1])/(f + f2);
G3=(trans[27]*trans[24]*In[3]*In[3]*In[1])/(f + f2);
if(z_pred==0) /* constant mortality */
  Z_mort=(trans[16])*In[1];
if(z_pred==1) /* linear mortality */
  Z_mort=(trans[16]*In[1])*In[1];
if(z_pred==2) /* hyperbolic mortality */
  Z_mort=((trans[16]*In[1])/(trans[14] + In[1]))*In[1];
if(z_pred==3) /* sigmoid mortality */
  Z_mort=((trans[16]*In[1]*In[1])/
  ((trans[14]*trans[14]) + (In[1]*In[1])))*In[1];
Z_mix=((MLDiff_now)*In[1])/(MLD_now);
Out[1]=((trans[19]*G1) + (trans[20]*G2) + (trans[21]*G3) - Z_mort - Z_mix);

/* Bacteria */
S=min(In[5], (trans[31]*In[6]));
U1=(trans[30]*In[2]*In[6])/(trans[12] + S + In[6]);
U2=(trans[30]*In[2]*S)/(trans[12] + S + In[6]);
B_excr=trans[17]*In[2];
B_mix=((trans[34] + hplus)*In[2])/(MLD_now);
Out[2]=(U1 + U2 - G2 - B_excr - B_mix);

/* Detritus */
D_degr=trans[18]*In[3];
D_mix=((trans[34] + hplus + trans[32])*In[3])/(MLD_now);
Out[3]=(((1 - trans[19])*G1) + ((1 - trans[20])*G2)
          - (trans[21]*G3) - D_degr + P_mort - D_mix);

/* Nitrate */
Nn_mix=((trans[34] + hplus)/(MLD_now))*(trans[33] - In[4]);
Out[4]=((-1*J*Q1*In[0]) + Nn_mix);

/* Ammonium */
Nr_mix=((trans[34] + hplus)*In[5])/(MLD_now);
Out[5]=((-1*J*Q2*In[0]) - U2 + B_excr + (trans[28]*Z_mort) - Nr_mix);

/* Dissolved Organic Nitrogen (DON) */
Nd_mix=((trans[34] + hplus)*In[6])/(MLD_now);
Out[6]=((trans[7]*sigma*In[0]) + D_degr + (trans[29]*Z_mort) - U1 - Nd_mix);

/* Output data for calculation of model flows */
v_flow[rkstep][0]=(((1 - trans[7])*sigma*In[0])*MLD_now);
v_flow[rkstep][1]=-G1*MLD_now;
v_flow[rkstep][2]=-P_mort*MLD_now;
v_flow[rkstep][3]=-((fabs(min(MLDiff_now, 0.0))) + trans[34])*In[0];
v_flow[rkstep][4]=(trans[19]*G1)*MLD_now;
v_flow[rkstep][5]=(trans[20]*G2)*MLD_now;
v_flow[rkstep][6]=(trans[21]*G3)*MLD_now;
v_flow[rkstep][7]=-Z_mort*MLD_now;
v_flow[rkstep][8]=0.0;
v_flow[rkstep][9]=U1*MLD_now;
v_flow[rkstep][10]=U2*MLD_now;
```

```
  v_flow[rkstep][11]=-G2*MLD_now;
  v_flow[rkstep][12]=-B_excr*MLD_now;
  v_flow[rkstep][13]=-((fabs(min(MLDiff_now, 0.0))) + trans[34])*In[2];
  v_flow[rkstep][14]=(1 - trans[19])*G1*MLD_now;
  v_flow[rkstep][15]=(1 - trans[20])*G2*MLD_now;
  v_flow[rkstep][16]=P_mort*MLD_now;
  v_flow[rkstep][17]=-(trans[21]*G3)*MLD_now;
  v_flow[rkstep][18]=-D_degr*MLD_now;
  v_flow[rkstep][19]=-((fabs(min(MLDiff_now, 0.0))) + trans[34]
                       + trans[32])*In[3];
  if (MLDiff_now<0.0)
    v_flow[rkstep][20]=(MLDiff_now*In[4]);
  else
    v_flow[rkstep][20]=(MLDiff_now*trans[33]);
  v_flow[rkstep][20]+=(trans[34]*(trans[33] - In[4]));
  v_flow[rkstep][21]=(-1*J*Q1*In[0])*MLD_now;
  v_flow[rkstep][22]=(trans[28]*Z_mort)*MLD_now;
  v_flow[rkstep][23]=B_excr*MLD_now;
  v_flow[rkstep][24]=(-1*J*Q2*In[0])*MLD_now;
  v_flow[rkstep][25]=-U2*MLD_now;
  v_flow[rkstep][26]=-((fabs(min(MLDiff_now, 0.0))) + trans[34])*In[5];
  v_flow[rkstep][27]=(trans[7]*sigma*In[0])*MLD_now;
  v_flow[rkstep][28]=D_degr*MLD_now;
  v_flow[rkstep][29]=(trans[29]*Z_mort)*MLD_now;
  v_flow[rkstep][30]=-U1*MLD_now;
  v_flow[rkstep][31]=-((fabs(min(MLDiff_now, 0.0))) + trans[34])*In[6];
  v_flow[rkstep][32]=(1 - (trans[28] + trans[29]))*Z_mort*MLD_now;
  v_flow[rkstep][33]=Q;
  v_flow[rkstep][35]=J;
  v_flow[rkstep][36]=(Z_mort/In[1]);
  v_flow[rkstep][37]=I_ss;
  v_flow[rkstep][39]=(((1 - trans[7])*(J*Q1)*In[0])*MLD_now);
  v_flow[rkstep][40]=(((1 - trans[7])*(J*Q2)*In[0])*MLD_now);
  v_flow[rkstep][41]=divide(Q1, (Q1 + Q2));
  v_flow[rkstep][42]=MLD_now;
}

/* ============================================================ */

double light_equation(double P, double I, double M)
{
  /* This routine calculates the depth-integrated light field
     ------------------------------------------------------- */
  double part[9];

  part[1]=power(I,2)*power(trans[6],2);
  part[2]=exp(-1*(trans[2] + (trans[3]*P))*M);
  part[3]=power(trans[4],2);
  part[4]=(trans[4]*trans[6]*I);
  part[5]=(trans[2] + (trans[3]*P));
  part[6]=(log((pow(part[1],0.5)) +
       (pow((part[3]+part[1]),0.5)))*part[4])/
 ((pow(part[1], 0.5))*part[5]);
  part[7]=(log((pow(part[1],0.5)*part[2]) +
       (pow((part[3]+(part[1]*(part[2]*part[2]))),0.5)))*part[4])/
 ((pow(part[1], 0.5))*part[5]);
  part[8]=((part[6] - part[7])/M);

  return part[8];
}
```

A-2.4 Forcing functions

These functions are used to provide the program with forcing data. All bar the last of these are involved in the calculation of solar forcing. The last function is a simple one to determine the current mixed–layer depth from the daily data.

The cloud cover function is based upon a FORTRAN version supplied to the author by Dr. Mike Fasham. In incorporates four different algorithms to estimate sea–surface irradiance from irradiance at the top of the atmosphere.

```
double I0_now(double t)
{
  /* This function calculates sea surface irradiance
     ---------------------------------------------- */
  /* Model variables */
  double D1, R1, W1, L1, W2, Z, I1, I2, I6;
  double I0, I0_hour, time, SE, Iss, cfrac;
  int    day;

  /* Is irradiance constant across the day? */
  if(triangle==0)
    {
      /* Yes!  Return single 24 hour averaged irradiance */
      return(irrad[fix_day]);
    }
  else
    {
      /* No!  Calculate instantaneous irradiance */

      /* Initialise variables */
      I0=1353.0;
      I0_hour=3600.0*I0;
      day=(((int)(t))%365);
      time=(t - ((int)(t)));

      /* These calculations are performed only once per day */
      D1=declination(day);
      R1=rad_vector(day);
      W1=sunrise_ha(lat, D1);
      /* L1=daylength(W1);
 I6=integrated(I0_hour, R1, W1, lat, D1); */

      time=(time*24.0); /* convert time into hours */
      W2=hour_angle(time);
      Z=zenith_angle(D1, lat, W2);
      I1=ir_top_atmos(I0, R1, Z);
      SE=(PI/2) - Z;
      if(SE>0.0)
{
  cfrac=sea_surface(I1, (sin(SE)));
  Iss=(I1*cfrac);
}
      else
{
  cfrac=0.0;
  Iss=0.0;
}
      return(Iss);
    }
}

/* ============================================================ */

double declination(int day)
{
  /* Calculates the Earth's declination
     This is the angle at solar noon between the equator and the Sun */

  double answer;
```

```
  answer=0.409230*(sin((2*PI)*((double)(284 + day)/YEAR)));

  return answer;
}

/* ============================================================ */

double rad_vector(int day)
{
  /* Calculates the radius vector of the Earth
     This expresses the ellipticity of the Earth's orbit */

  double answer, answer1, answer2;

  answer1=((1 + (0.033*cos((2*PI)*((double)day/YEAR)))));
  answer2=pow(answer1, 0.5);
  answer=1.0/answer2;

  return answer;
}

/* ============================================================ */

double sunrise_ha(double latitude, double declination)
{
  /* Calculates the sunset (or sunrise) hour-angle
     This is the angle between the south point and the setting Sun */

  double answer;

  answer=acos(-1*(tan(latitude)*tan(declination)));

  return answer;
}

/* ============================================================ */

double daylength(double sunset_ha)
{
  /* Calculates the daylength in hours
     This is the time between sunrise and sunset */

  double answer;

  answer=((sunset_ha/(PI/12))*2);

  return answer;
}

/* ============================================================ */

double integrated(double sol_const_hour, double rad_vect, double sunset_ha,
  double latitude, double declination)
{
  /* Calculates integrated daily solar irradiance
     Integrates irradiance across the day to give a single value */

  double answer, answer1, answer2, answer3;

  answer1=(24/PI)*(sol_const_hour/(power(rad_vect, 2)));
  answer2=(sunset_ha*sin(latitude)*sin(declination));
  answer3=(sin(sunset_ha)*cos(latitude)*cos(declination));
  answer=answer1*(answer2 + answer3);

  return answer;
}

/* ============================================================ */

double hour_angle(double time_now)
{
  /* Calculates the hour-angle
     This is the angle between the Sun and the south point */

  double answer;

  answer=(time_now - 12.0)*(PI/12);

  return answer;
}
```

```
/* ============================================================ */

double zenith_angle(double declination, double latitude, double hour_angle)
{
  /* Calculates the zenith angle
     This is the angle between the point directly above the current location
     and the Sun - it is this which is related to the incidence of irradiance
     on a flat surface */

  double answer, answer1;

  answer1=(sin(declination)*sin(latitude)) +
    (cos(declination)*cos(latitude)*cos(hour_angle));
  answer=acos(answer1);

  return answer;
}

/* ============================================================ */

double ir_top_atmos(double sol_const, double rad_vect, double zenith)
{
  /* Calculates the solar irradiance at the top of the atmosphere
     This is the instantaneous irradiance flux at the top of the Earth's
     atmosphere */

  double answer;

  answer=(sol_const/(power(rad_vect, 2)))*cos(zenith);

  if(answer<0.0)
    {
      answer=0.0; /* removes negative answers */
    }

  return answer;
}

/* ============================================================ */

double sea_surface(double Itop, double S)
{
  /* This routine determines sea surface irradiance
     That is, irradiance at the top of the atmosphere is corrected to
     account for atmospheric conditions so that a value of irradiance
     at the sea surface can be derived

     The routine returns a fraction which the the fraction of solar
     irradiance which MAKES IT to the surface.  Althought the variable
     is called cloud absorbance in Fasham's code, he uses it as if it
     were cloud transmittance.  I have used it here as cloud transmittance.

     NOTE : this value must subsequently be corrected to account for sea
     surface albedo and the PAR:total radiation ratio */

  double c, cfrac, sdeg;

  /* Smith & Dobson (1984) model
     ---------------------------
     Atmosphere-Oceans 22:1-22 */
  if(cmodel==1)
    {
      if(oktas>5)
        {
          cfrac=S*(cover[0][oktas] + (cover[1][oktas]*S));
        }
      else
        {
          c=(oktas/8.0);
          cfrac=(cover[3][oktas] + (S*exp(-cover[2][0]/S))
                 *(c*exp(-cover[2][oktas]/S) + 1.0 - c));
        }
    }
  else
    /* Evans & Parslow (1985) model
       ----------------------------
       Biol. Oceanogr. 3:327-347 */
    if(cmodel==2)
      {
        cfrac=1.0 - 0.7*(oktas/8.0);
```

```
      }
    else
      /* Dobson & Smith (1988) model
         --------------------------
         Q. J. Roy. Met. Soc. 114:165-182 */
      if(cmodel==3)
        {
          cfrac=S*(cover[4][oktas] + (S*cover[5][oktas]));
        }
      else
        /* Reed (1977) model
           -----------------
           J. Phys. Oceanogr. 7:482-485 */
        if(cmodel==4)
          {
            sdeg=180.0*(asin(S)/PI);
            cfrac=1.0 - (0.62*(oktas/8.0)) + 0.0019*sdeg;
          }

  return cfrac;
}

/* ============================================================ */

double mixed_layer_depth(double t)
{
  /* This function calculates current mixed-layer depth
     ------------------------------------------------- */
  double mld_now, day2;
  int    day;

  day=(((int)(t))%365);
  day2=(t - ((int)(t)));
  mld_now=-1*(MLD[day] - ((1 - day2)*MLDiff[day]));

  return(mld_now);
}
```

A-2.5 Miscellaneous mathematical functions

These functions are used throughout the program to perform simple calculations.

```
double min(double x, double y)
{
  /* This routine calculates the lesser of two numbers
     ------------------------------------------------ */
  if (x>y)
    return y;
  else
    return x;
}

/* ============================================================= */

double max(double x, double y)
{
  /* This routine calculates the greater of two numbers
     ------------------------------------------------ */
  if (x>y)
    return x;
  else
    return y;
}

/* ============================================================= */

double power(double x, int y)
{
  /* This routine is a faster way of raising to integer powers
     ------------------------------------------------------- */
  int    i;
  double z;
  z=x;
  for(i=1;i<y;i++)
    z=z * x;
  return z;
}

/* ============================================================= */

double divide(double topline, double bottomline)
{
  /* This routine evaluates fractions - making sure the bottom line is not 0
     ---------------------------------------------------------------------- */
  if (bottomline==0 || topline==0)
    return 0.0;
  else
    return (topline/bottomline);
}

/* ============================================================= */

double rolling_mean(double old_mean, double new_value, int n)
{
  /* This routine calculates a "rolling" mean of the daily data
     ---------------------------------------------------------- */
  if (n==0)
    {
      /* First value, therefore mean=current state */
      return new_value;
    }
  else
    {
      return (((n*old_mean) + new_value)/((double)(n+1)));
    }
}

/* ============================================================= */

double rolling_variance(double old_variance, double old_mean,
double new_value, double new_mean, int n)
{
  /* This routine calculates a "rolling" variance of the daily data
     ------------------------------------------------------------ */
  double x1, x2, x3;
```

```
  if (n==0)
    {
      /* First value, therefore variance=0 */
      return 0.0;
    }
  else
    {
      x1=((double)n)/((double)(n + 1));
      x2=old_variance + power(old_mean,2) +
(power(new_value,2))/((double)n);
      x3=power(new_mean,2);

      return ((x1*x2) - x3);
    }
}

/* ============================================================ */

double more_than_zero(double number)
{
  /* This routine ensures that numbers are above zero
     ---------------------------------------------- */
  if (number<0.0)
    return 0.0;
  else
    return number;

}

/* ============================================================ */

double less_than_one(double number)
{
  /* This routine ensures that numbers (mostly fractions) are below one
     ------------------------------------------------------------------ */
  if (number>1.0)
    return 1.0;
  else
    return number;

}

/* ============================================================ */

int    same_number(double one, double two, int places)
{
  /* This routine checks if two numbers are the same to x decimal places
     ------------------------------------------------------------------- */
  double decicheck;
  int    a, b, flag;

  decicheck=(int)(power(10.0, places));
  a=(int)(one*decicheck);
  b=(int)(two*decicheck);

  if(a<b)
    flag=-1;
  if(a>b)
    flag=1;
  if(a==b)
    flag=0;

  return flag;
}
```

A-3 Software used

In addition to the software written by the author, several commercially available and shareware utilities were used to perform the research described within this thesis, as well as in the production of the thesis itself.

All simulation output was handled by the visualisation software, MATLAB (The MathWorks, Inc., Massachusetts, USA), for processing, analysis and interpretation. Additionally, MATLAB was used to generate all of the graphs used in this thesis.

Although none of the results presented in this thesis relied upon it directly, the dynamical systems toolkit, DSTool (Guckenheimer, Meyers, Wicklin and Worfolk, 1991), played an important role in the early stages of model development and implementation.

Thesis typesetting was handled by LaTeX 2_ε, and extensive use was made of Lamport (1986) in the presentation of the work here. All diagrams were produced using the shareware applications XFig and XV (John Bradley).

The timing of this thesis has coincided with the expansion of the world wide web. Consequently, parts of this thesis have made use of facilities or information available on the web. Three web sites have been explicitly referenced in this thesis.

(i) `http://www.aquarius.geomar.de/omc`

"Online Map Creation", by Martin Weinelt.

(ii) `http://wood.jhuapl.edu/`

"World Ocean Optics Database", administered by Jeffrey Smart.

(iii) `http://socserv2.socsci.mcmaster.ca/~econ/ugcm/3ll3/malthus/popu.txt`

"An Essay on the Principle of Population", by Thomas Malthus (1798).